BLANKET COMPARISON AND SELECTION STUDY. VOLUME I

ARGONNE NATIONAL LAB., IL

OCT 1983

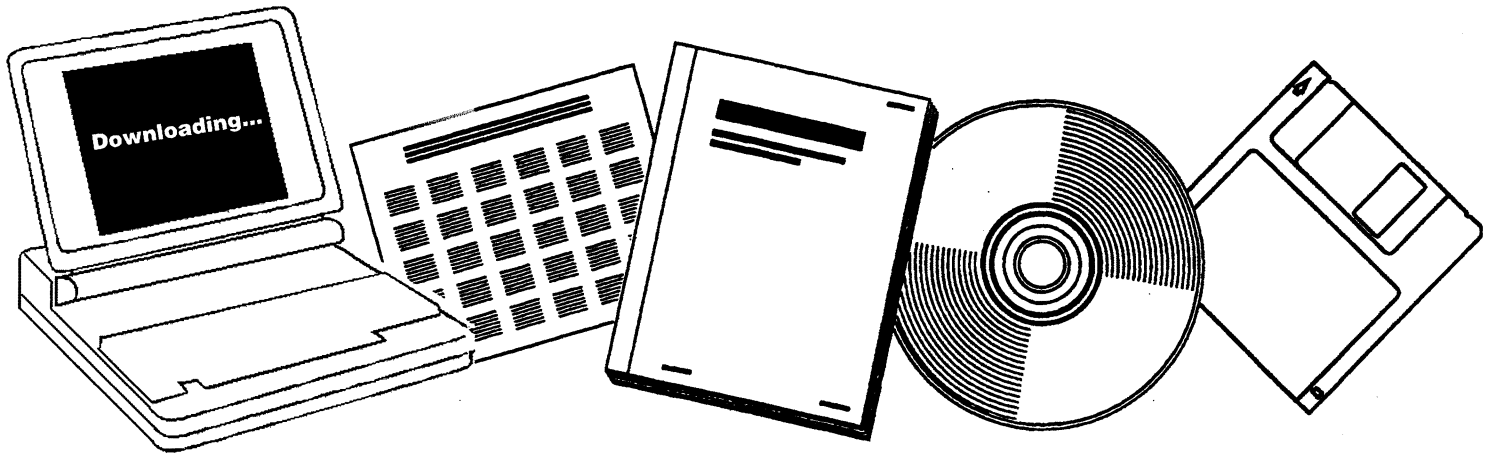

U.S. Department of Commerce
National Technical Information Service

BLANKET COMPARISON AND SELECTION STUDY. VOLUME I

ARGONNE NATIONAL LAB., IL

OCT 1983

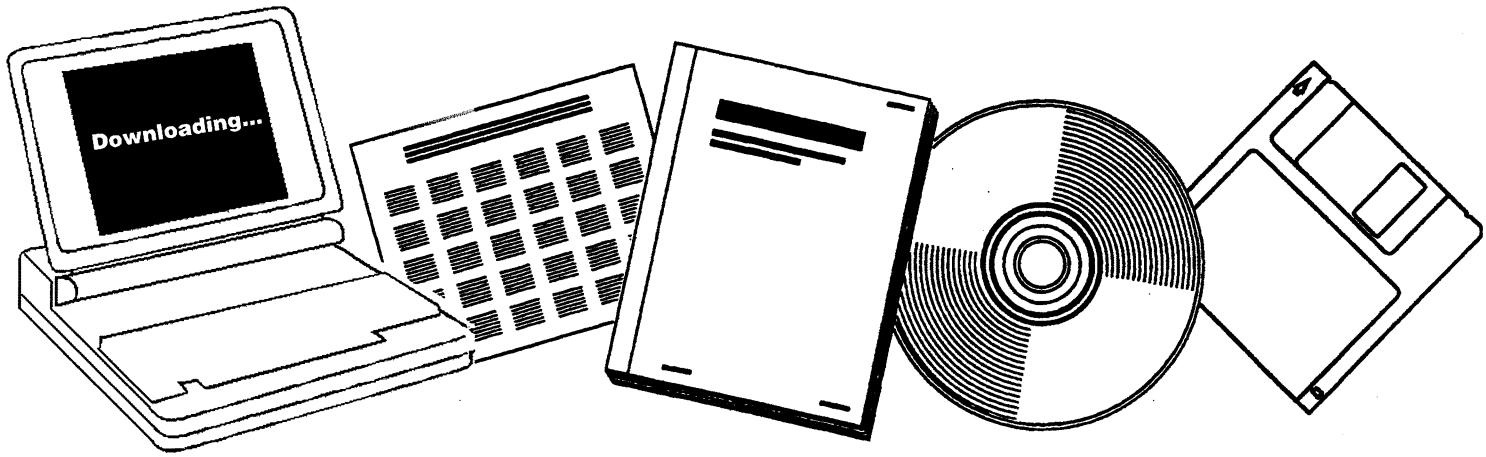

U.S. Department of Commerce
National Technical Information Service

One Source. One Search. One Solution.

NTIS

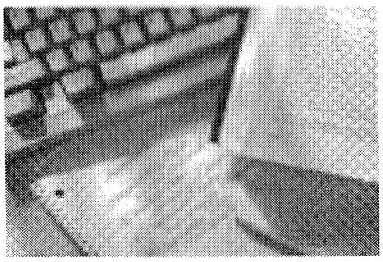

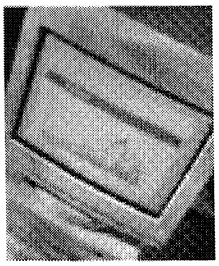

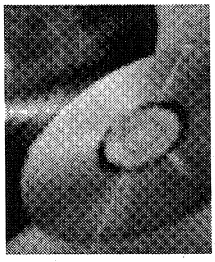

Providing Permanent, Easy Access to U.S. Government Information

The National Technical Information Service is the Nation's largest repository and disseminator of government-initiated scientific, technical, engineering, and related business information. The NTIS collection includes almost 3 million information products in a variety of formats: electronic download, online access, DVD, CD-ROM, magnetic tape, diskette, multimedia, microfiche and paper.

Search the NTIS Database from 1990 forward

More than 600,000 government research information products have been added to the NTIS collection since 1990. All bibliographic entries for those products are searchable on the NTIS Web site at www.ntis.gov.

Download Publications (1997 - Present)

NTIS provides the full text of many reports received since 1997 as downloadable PDF files. When an agency stops maintaining a report on its Web site, NTIS still offers a downloadable version. There is a fee for each download of most publications.

For more information visit our website:

www.ntis.gov

U.S. DEPARTMENT OF COMMERCE
Technology Administration
National Technical Information Service
Springfield, VA 22161

ANL/FPP-83-1
Volume I

DE84003657
ANL/FPP-83-1 VOL 1 10

BLANKET COMPARISON AND SELECTION STUDY

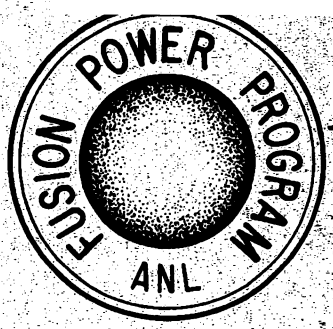

FUSION POWER PROGRAM

Argonne National Laboratory
9700 South Cass Avenue
Argonne, Illinois 60439

Operated by
The University of Chicago
for the U. S. Department of Energy
under Contract W-31-109-Eng-38

DISCLAIMER

Printed in the United States of America
Available from
National Technical Information Service
U. S. Department of Commerce
5285 Port Royal Road
Springfield, VA 22161

NTIS price codes
Printed copy: A21
Microfiche copy: A01

Distribution Categories:
Magnetic Fusion Energy (UC-20)
MFE—Fusion Systems (UC-20d)

ANL/FPP-83-1
Volume I

ARGONNE NATIONAL LABORATORY
9700 South Cass Avenue
Argonne, Illinois 60439

BLANKET COMPARISON AND SELECTION STUDY

Contributors

M. Abdou, ANL
P. Adler, Grumman
C. Baker, ANL
D. Berwald, TRW
J. Bethin, Grumman
W. Bjorndahl, TRW
R. Bourque, GA
W. Brehm, HEDL
Y. Cha, ANL
E. Cheng, GA
O. Chopra, ANL
L. Creedon, GA
J. Davis, MDAC
G. Deis, EG&G
A. Fischer, ANL
J. Garner, TRW
J. Gordon, TRW
R. Gold, W
Y. Gohar, ANL
T. Hellwig, MDAC
N. Hoffman, ETEC
G. Hollenberg, HEDL
C. Johnson, ANL
J. Jung, ANL
T. Lechtenberg, GA
R. Leonard, ANL
H. Levine, GA
W. Lewis, MDAC
Y. Liu, ANL
S. Majumdar, ANL
H. Mantz, MDAC
I. Maya, GA
T. McCarville, TRW
R. Micich, Grumman
B. Misra, ANL
G. D. Morgan, MDAC
S. Mortenson, TRW
B. Picologlou, ANL
S. Piet, EG&G
C. Reed, ANL
D. Ruester, MDAC
K. Schultz, GA
J. Shearer, ANL
D. Smith, ANL
D. Steiner, RPI
D.-K. Sze, U of WI
A. Tobin, Grumman
P. Tortorelli, ORNL
L. Turner, ANL
S. Vogler, ANL
L. Waganer, MDAC
W. Wiffen, ORNL
C. Wong, GA

October 1983

Study supported by
Office of Fusion Energy
U. S. Department of Energy

BLANKET COMPARISON AND SELECTION STUDY

Project Manager: **M. A. Abdou (ANL)**
Deputy Manager: **G. D. Morgan (MDAC)**

TASK LEADERS

Design Guidelines:	M. Abdou (ANL)
Evaluation Criteria:	C. Baker (ANL)
Material Assessment:	D. Smith (ANL)
Safety:	S. Piet (EG&G)
Alternative Concept Screening:	D. Berwald (TRW)
Solid Breeder Designs:	G. D. Morgan (MDAC)
Helium-Cooled Designs:	C. Wong (GA)
Tritium Recovery Issues:	C. Johnson (ANL)
Special Materials:	Y. Liu (ANL)
Liquid Metal Designs:	D. Smith (ANL)
Self-Cooled Liquid Metal Design:	Y. Cha (ANL)
Ternary Solid Breeder Design:	J. Gordon (TRW)
Lithium-Lead Concepts:	D.-K. Sze (U of WI)
Material Resources:	D. Berwald (TRW)
Economic Analysis:	L. Waganer (MDAC)
High Wall Load Study:	D. Steiner (RPI)
Gaseous Corrosion:	R. Micich (Grumman)
Liquid Metal Corrosion:	O. Chopra (ANL)
Power Conversion System:	R. Bourque (GA)
Intermediate Heat Exchanger:	I. Maya (GA)

TABLE OF CONTENTS

BLANKET COMPARISON AND SELECTION STUDY

APPENDIX E - MOLTEN SALT SAFETY STUDIES

LIST OF FIGURES FOR CHAPTER I

LIST OF TABLES FOR CHAPTER I

I. INTRODUCTION

The blanket is one of the most important components of a fusion reactor because it deals directly with the issues of energy extraction and fuel breeding, which represent major technical feasibility questions for the practical development of fusion power. In addition, the blanket substantially influences the reactor economics and safety. Demonstrating the engineering feasibility of the blanket will require extensive research and development.

Numerous studies carried out worldwide over the past fifteen years proposed a large number of design concepts. Many of these concepts vary in material choices and major design features, and they pose widely different types of critical issues. Ideally, R&D programs should seek to develop a broad data base sufficient for resolving the critical issues for all promising design options in order to select with absolute confidence the most attractive blanket for fusion reactors. Realistically, however, a resource-limited R&D program inevitably must select and focus on only a very limited number of options. An exceedingly important concern with this inevitable approach is the decision-making process to identify the fewest low-risk, high pay-off options. One great difficulty is that the information required for complete technical evaluation of all possible options is often not available. There is no unique scientific formula for dealing with this situation; there are only guidelines based on expert judgement. The two-year Blanket Comparison and Selection Study was initiated by the U.S. Department of Energy/Office of Fusion Energy in October 1982 to develop these guidelines and to utilize them in identifying a very limited number ($\sim$ 3) of blanket concepts that should receive the highest R&D priority over the next several years.

The objectives of the Blanket Comparison and Selection Study (BCSS) can be stated as follows:

1) Define a small number ($\sim$ 3) of blanket design concepts that should be the focus of the blanket R&D program. A design concept is defined by the selection of all materials (e.g., breeder, coolant, structure and multiplier) and other major characteristics that significantly influence the R&D requirements.

2) Identify and prioritize the critical issues for the leading blanket concepts.

3) Provide the technical input necessary to develop a blanket R&D program plan. Guidelines for prioritizing the R&D requirements include: a) critical feasibility issues for the leading blanket concepts will receive the highest priority, and b) for equally important feasibility issues, higher R&D priority will be given to those that require minimum cost and short time.

The BCSS is focused on the mainline approach for fusion reactor development. Thus, the study is limited to the deuterium-tritium fuel cycle, tokamak and tandem mirror reactors, and the reactor parameter space of each that is generally believed to have a reasonable probability of being achievable. Alternate confinement concepts that may require a totally different blanket approach are not considered. Likewise, exotic blanket concepts with no data base for meaningful technical evaluation are not included in the the study.

The BCSS is being carried out by a multidisciplinary team with personnel from national laboratories, industry and universities (see Table I-1). The team is led by Argonne National Laboratory. The major industrial organizations are McDonnell Douglas Astronautics Company, GA Technologies, Inc. and TRW. Smaller but significant efforts are provided by EG&G Idaho, Inc., Hanford Engineering and Development Laboratory, Grumman Aerospace Corporation, University of Wisconsin, Rensselaer Polytechnic Institute, University of California - Los Angeles, and Energy Technology Engineering Center. In addition, the study has benefited from consulting with a number of experts in other organizations such as Oak Ridge National Laboratory, the Fusion Engineering Design Center and Westinghouse. A review committee was appointed by DOE's Office of Fusion Energy to provide periodic evaluation of the progress and direction of the study. The membership of this review committee is shown in Table I-2.

The objectives and scope of the BCSS are substantially different from past reactor studies. Previous studies were generally concerned with developing conceptual designs but the focus of the BCSS is on concept selection. Therefore, the project organization and emphasis were carefully

TABLE I-1. BLANKET COMPARISON AND SELECTION STUDY TEAM

ARGONNE NATIONAL LABORATORY
McDonnell Douglas Astronautics Company
GA Technologies, Inc.
TRW, Inc.
Grumman Aerospace Corporation
Rensselaer Polytechnic Institute
University of Wisconsin
University of California - Los Angeles
Energy Technology Engineering Center
Hanford Engineering Development Laboratory
EG&G Idaho, Inc.
Oak Ridge National Laboratory

TABLE I-2. BCSS REVIEW COMMITTEE

R. Krakowski (Chairman) - LANL
C. Flanagan, W/FEDC
C. Henning, LLL
D. Cohn, MIT
G. Kulcinski, U of WI
R. Gold, W
R. Little, PPPL
J. Scott, ORNL

planned at the initial stage to best serve the purpose of the study. A few examples illustrate the point. Blanket designs are developed in the project to serve as a tool (not a goal) for identifying the issues and facilitating comparison of blanket options. Therefore, while the blanket designs are pursued in sufficient depth to make meaningful comparisons, minor details that do not represent significant issues are not considered. In contrast, key issues related to the feasibility and performance of blanket concepts are evaluated to the maximum possible extent permitted by the resources of the project. Wherever possible, key feasibility issues that are relatively independent of the design were evaluated prior to pursuing the design details. In some cases, the results of the key issues evaluation were negative and the resources required for developing designs of the affected blanket concept were conserved.

It was recognized from the outset of the study that considerable effort had to be devoted to developing a comparison methodology and a set of evalua-

tion criteria which would facilitate the primary goal of the study; namely, the selection of a limited number of promising blanket concepts that should be the focus of blanket R&D. This effort is described in Chapter III. Developing this comparison methodology and evaluation criteria required a relatively long time and carrying out the actual process of the comparison of blanket concepts involves considerable effort. Therefore, a less systematic approach was used for screening blanket concepts during FY 1983. The more detailed comparison methodology and evaluation criteria will be utilized during FY 1984 to compare the smaller number of blanket concepts that passed the screening evaluation of FY 1983.

At the beginning of the study, blanket concepts were divided into mainline and alternate concepts. Mainline concepts offer higher potential and were evaluated in considerably more detail than the alternate concepts. The classification of a concept as mainline or alternate was based on expert judgement utilizing the results from previous studies. Figure I-1 shows the blanket options that were considered during FY 1983. The mainline concepts are designated by the choice of the breeder (top item in each box) and coolant (bottom line) while all alternate concepts are referred to in the box designated "concept screening". Designs were developed for each of the mainline concepts by a number of groups. The alternate concepts were evaluated only briefly to ensure that no potentially attractive concept is left out of the mainline concepts. The results of the alternate concept screening evaluation confirmed the initial judgement with one exception. It was recommended that the molten salt coolant option be included for evaluation as a mainline concept. Work was recently begun on the key issues for the molten salt coolant options and, provided the results are positive, design and analysis will be initiated on these options soon.

There are 10 mainline concept classifications designated by the breeder and coolant in Fig. I-1. Each classification actually includes a number of concepts depending on the choice of the neutron multiplier (if required) and the structural material. Since achieving adequate tritium breeding cannot be assured for any of the breeders considered, except for LiPb, the need for a neutron multiplier had to be evaluated. In addition, the resource limitations of beryllium and the practical difficulties with lead had to be addressed since these are the only two attractive non-fissionable neutron multipliers available.

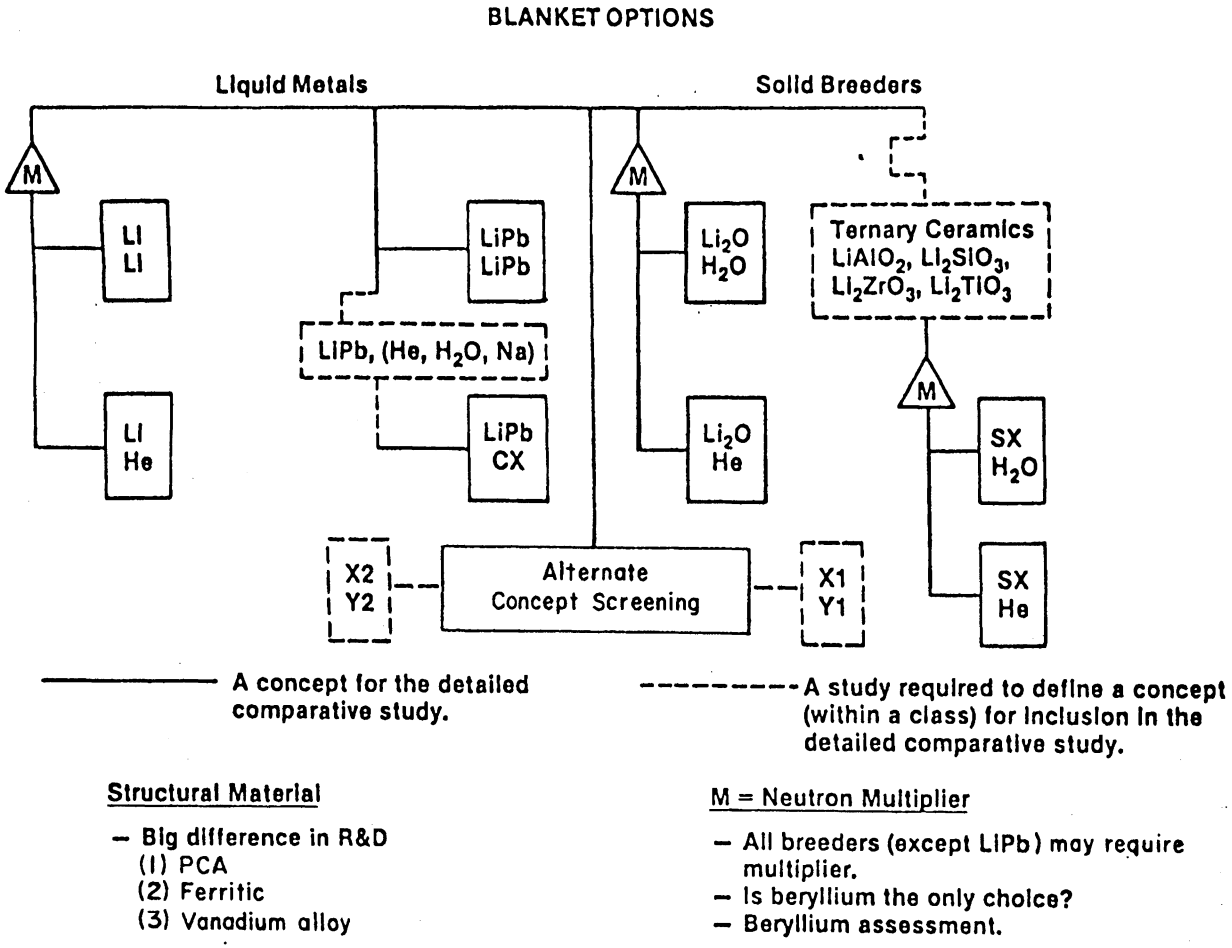

Figure I-1. Blanket options evaluated in FY 1983

Three classes of structural materials were selected for evaluation in the study: 1) austenitic stainless steel represented by PCA (Primary Candidate Alloy), 2) ferritic steels represented by HT-9, and 3) vanadium alloys represented by V-15Cr-5Ti. In addition, low activation variants of the austenitic and ferritic steels will be considered. The BCSS project selected to evaluate all mainline concepts with PCA at the early stages of the study for several reasons. First, a large data base exists for austenitic stainless steel and, at present, PCA is the focus of the alloy development program in the U.S.; and therefore, it is important to determine the relative performance of each blanket concept using PCA. Second, the results for blanket designs with PCA provide a benchmark against which the designs with advanced alloys can be compared, and the benefits of developing advanced alloys can then be assessed. During FY 1983, nearly all initial blanket concept evaluations with PCA have been completed and work on concepts with other structural materials is presently underway.

Figure I-2 shows the BCSS project organization and the tasks emphasized during FY 1983. Each of the mainline concepts was evaluated by one design and analysis group. All the alternate concepts were evaluated by one group. A number of groups were formed to address critical issues such as tritium recovery from solid breeders, liquid metal corrosion, tritium breeding, resources and waste disposal. Two groups were also assigned responsibilities for critical project tasks. The first is developing design guidelines for key parameters such as neutron wall load, surface heat flux, erosion rates, maximum allowable temperatures and stresses. These design guidelines ensure consistency among the designs for various blanket concepts. The second is developing the comparison methodology and evaluation criteria.

The BCSS started in October 1982 and is scheduled for completion in September 1984. This document is an interim report on the results obtained during the first year of the study. The purpose of this interim report is to provide members of the fusion community with sufficient information that enables them to make meaningful feedback at approximately the mid-point of the study. Since a complete documentation of the effort will be made in a final formal report at the end of the study, no attempt was made to make this report a thorough documentation of all the results obtained to date. Furthermore, the time-consuming aspects normally associated with issuing a formal report

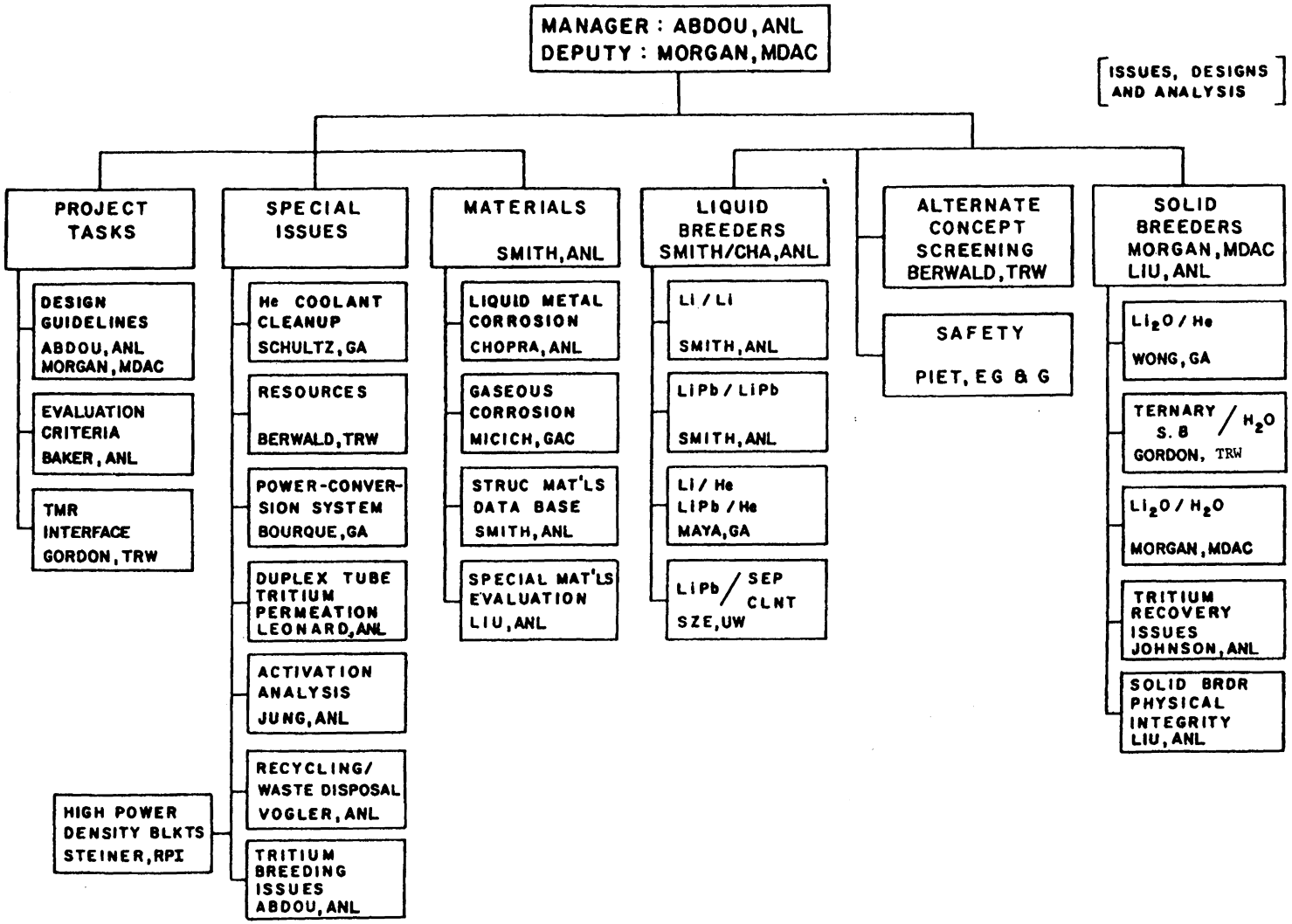

Figure I-2. BCSS project organizations and tasks.

such as making rigorous editing, listing complete references and providing good quality figures have been avoided in order to conserve the resources of the project and to provide for speedy issuance of the report.

TABLE OF CONTENTS

CHAPTER II - OVERVIEW AND SUMMARY

LIST OF FIGURES FOR CHAPTER II

LIST OF TABLES FOR CHAPTER II

II. OVERVIEW AND SUMMARY

II.1 Introduction

The purpose of this chapter is to provide a summary of the work of the Blanket Comparison and Selection Study (BCSS) carried out during FY 1983. The chapter is kept relatively brief to enable all readers to get a clear perspective of all the key results and activities of the project prior to studying the details of the many technical areas that are presented in the rest of the report.

Section II.2 summarizes the design guidelines that have been used in the design and analysis of all blanket concepts. Section II.3 highlights the status of the work on developing a comparison methodology and a set of evaluation criteria to facilitate comparison, selection and ranking of blanket concepts. A number of key issues that are common to many blanket concepts have received considerable attention in the study. Most of these issues are related to structural and special materials, liquid metal, gaseous and water corrosion and solid breeder tritium recovery and are summarized in Sections II.4, II.5 and II.6, respectively.

As mentioned in the previous chapter, all candidate blanket concepts were classified early in the study into mainline and alternative concepts. The mainline concepts are those that were judged, based on previous studies, to be potentially more attractive than alternative concepts. Section II.7 summarizes the results of the alternative concept screening effort. The results of design and analysis and key issues evaluation for the mainline concepts are summarized in Section II.8 for liquid metal breeder concepts and in Section II.9 for solid breeder concepts. An overview of the present status of ranking the candidate blanket concepts is presented in Section II.10.

II.2 Design Guidelines

One of the special project tasks has been the development of Design Guidelines. The purposes of these guidelines are:

- To establish the value (or range of values) of parameters and to state assumptions that require consistency in treating all (or most) blanket concepts.

- To provide guidance on the approach to handling issues of broad interest in all concepts.

A set of design guidelines were issued at the beginning of the study. These guidelines have been updated periodically to provide clarifications and additions as the need arised. The present version of the design guidelines is provided in Appendix A. Some of the key guidelines are briefly reviewed below.

While the focus of BCSS is on the first wall and blanket, there is a need to define a reference reactor to facilitate the definition of boundary conditions and comparison of blanket concepts in terms of the impact on the overall reactor performance, safety and economics. For tandem mirrors, the MARS reactor design is adopted. For tokamaks, STARFIRE with limited modifications is utilized as the reference reactor design. These modifications include increasing the neutron wall load from 3.6 to 5 MW/m^2, reducing the peak toroidal field from 11.1 T to 10 T and reducing the number of TF coils and the number of blanket/shield sectors to 10.

The reference neutron wall load is 5 MW/m^2. This is presently believed to be near the upper end of the optimum range of wall loading for tandem mirrors and tokamaks. While all the mainline and alternative concepts have been evaluated at 5 MW/m^2, a small effort was devoted to evaluating first wall/blanket concepts at higher wall loadings. This effort is summarized in Appendix D. The preliminary results indicate that for the present candidate materials and reactor design concepts, no clear benefits can be identified in terms of the cost of energy for operating at wall loads > 5 MW/m^2.

The design of the first wall is greatly influenced by the value of the surface heat load and the rate of the wall erosion. There are considerable differences in this area between tandem mirrors and tokamaks. In the MARS design, the surface heat flux is ~ 10 W/cm^2 and the charged and neutral fluxes at the first wall are so low that the resulting erosion is insignificant. In contrast, tokamak designs have shown high surface heat fluxes and in some cases high erosion rate at the first wall. There is a trade-off between the heat load on the first wall and that transported to the limiter or divertor plates. Since limiters and divertor plates have limited surface area, the results of the tradeoff generally favor that a large fraction of the α-power

be radiated to the larger surface area of the first wall. If STARFIRE is operated at a neutron wall load of 5 MW/m^2 the total α-power is 970 MW. With a limiter located at the bottom (INTOR type) one can assume one of two cases:

Case A

40% of the α-power is radiated to the first wall
Surface Heat Flux at the first wall = 0.5 MW/m^2
Peak Heat Flux at the limiter = 13 MW/m^2

Case B

80% of the α-power is radiated to the first wall
Surface Heat Flux at the first wall = 1 MW/m^2
Peak Heat Flux at the limiter = 4.3 MW/m^2

Following INTOR, we assumed in the above two cases that the peak-to-average heat flux ratio at the limiter is 1.5.

The erosion rate is determined primarily by the magnitude of the flux and energy of the charge-exchange neutrals at the first wall. Previous reactor studies predicted erosion rates at the first wall as high as 10 mm/y. More comprehensive modeling performed for the recent Phase II of INTOR indicate that the charge exchange flux is very low, hence the erosion rate on the first wall will be low (~ 1 mm/y) except for localized areas near the limiter tips and divertor throat.

The BCSS decided to emphasize in FY 1983 the more demanding parameters that are typical of tokamak conditions. The reference values adopted for the first wall surface heat flux and erosion rate are 0.5 MW/m^2 and 1 mm/y, respectively. In addition, parametric studies were carried out to determine the performance of the candidate first wall/blanket concepts in the ranges of 0.1 to 1 MW/m^2 and 1 to 10 mm/y. As described in Chapter III, first wall/blanket concepts are given higher points for their capabilities to accommodate higher surface heat load and erosion rate. Since the reference value of 0.5 MW/m^2 at the first wall implies a very high heat load (13 MW/m^2) at the limiter and divertor, one needs to carefully evaluate the important aspects of the

design, lifetime and energy recovery for the limiter and divertor because they can considerably affect the comparison of various first wall/blanket concepts. For example, if the results from recent studies that have shown that only a very limited number of materials, e.g., copper, can withstand heat fluxes > 4 MW/m^2 under the many constraints of a limiter design are confirmed, then water may be the only viable limiter/divertor coolant. This would probably affect significantly the safety ranking of some of the liquid metal blanket concepts. Furthermore, the energy deposited on the limiter/divertor is a significant fraction of the fusion power and the ability to usefully recover this energy will be a factor in comparison of concepts.

The maximum structure bulk temperature limits were determined by the material evaluation group as described in Section II.4. The adopted temperature limits are 550°C, 550°C, 750°C for PCA, HT-9 and V-15Cr-5Ti, respectively. The allowable stresses for these structural materials in both the irradiated and unirradiated conditions are given in Chapter IV and Appendix A. These temperature and stress limits proved to be key constraints on the maximum surface heat flux and/or thickness of the first wall. In particular, these constraints limit considerably the attractiveness of PCA first wall designs.

Evaluation of liquid metal corrosion (see Section II.5) provided structure temperature limits at the liquid metal interface. Depending on the velocity of the liquid metals, these interface temperature limits for austenitic steels are in the range of 430°C to 460°C for lithium and 370°C to 400°C for 17Li-83Pb. The interface temperature limits are higher by approximately 50°C and 200°C for ferritic steels and vanadium alloys, respectively. These corrosion temperature limits proved to be among the most critical drivers on liquid metal designs with PCA. Actually, all the 17Li-83Pb designs with PCA appear unattractive when these temperature limits are imposed.

The lower and upper temperature limits for solid breeders were evaluated by the Tritium Recovery Issues group as discussed in Section II.6 and Chapter VIII. The specified temperature limits are given in Appendix A. Recent experimental and analytical results led to specifying temperature limits for solid breeders that result, in general, in wider temperature windows than those assumed in previous studies. Wider temperature windows provide needed flexibility in solid breeder designs.

The specifications for plasma disruptions in the case of tokamaks were examined. The first wall is required to withstand only a few (~ 5) major disruptions during the lifetime. Thus, the first wall erosion resulting from the thermal energy deposition is not significant. However, the requirement to withstand the electromagnetic forces induced in the first wall is an important constraint that has to be satisfied by all design concepts. There are other electromagnetic requirements on all blanket concepts as stated in Appendix A.

II.3 Evaluation Criteria

The evaluation criteria and methodogy are described in detail in Chapter III. The basic approach has been to use a three stage process as follows:

- Separation of blanket concepts into "mainline" and "alternative" categories at the beginning of the study.
- Development of initial screening criteria which have been used, together with expert judgement, to screen the alternative concepts and to provide a framework to evaluate the mainline concepts during the first year of the study.
- Development of a detailed evaluation procedure which will be used during the second year of the study to systematically evaluate and rank the blanket concepts selected during the first year of the study. Blankets will be evaluated with respect to the following areas:

  - safety and environment
  - economics
  - engineering feasibility
  - R&D requirements.

The designation of mainline concepts was shown previously in Fig. I-1. The initial screening criteria are listed in Table II.3-1. These items were selected because they represent major feasibility issues, generally have either maximum or minimum threshold values, and can be quantified to some degree during the initial phase of the study.

With respect to the detailed evaluation criteria, the most readily quantified item, at least in principle, is economics. Here we use the cost of energy (COE) as the overall figure of merit. COE will be determined for each blanket concept, which passes the initial evaluation process of the first year of the study, in the context of both a STARFIRE and MARS reactor. The evaluation will include factors such as the capital cost of the first wall/blanket/

TABLE II.3-1. INITIAL SCREENING CRITERIA

Criteria	Min./Max. Value	Comments
• Breeding Ratio	> 1.05 > 1.20	3-D Calculation 1-D Calculation
• Thermal Efficiency	> 25%	$\frac{\text{(Gross Electric - Pumping) Power}^{b}}{\text{Total Thermal Power}}$
• Blanket Steady-State Tritium Inventory	< 10 g/MW_{th}	Based Primarily on Startup and Tritium Decay Considerations
• Lifetime	> 5 MW-yr/m^2	
• Tritium Loss Rates (Routine Operation)	< 100 Ci/d[a]	Overall Blanket/Power Conversion System (for Plant)
• Compatible Blanket Materials Combination	No Materials Combination Resulting in Large Rate of Energy Released	
• Total Neutron Wall Loading	> 3 MW/m^2	
• "Engineering Feasibility"	No Unduly Complex Configurations or Fabrication Procedures	

[a] For ~ 4000 MW_{th} power plant.

[b] Includes effect of blanket multiplication.

shield components, changes in capital cost of other components affected by the blanket (e.g., magnets), power conversion efficiency and pumping power requirements, total power output including blanket multiplication, and reactor availability. Availability will include consideration of blanket lifetime, failure rates, mean-time-to-failure, and replacement times. (See Sec. III.2.2.2 for a more detailed description.)

The approach taken in "safety and environment" and "engineering feasibility" was to develop a set of indices for each, which were then combined into an overall figure of merit for each by calculating a weighted sum. Each figure of merit for safety and environment (Sec. III.2.2.1 and Chapter XI) and engineering feasibility (Sec. III.2.2.3) has a maximum value of 100. The indices and weighting values are given in Tables II.3-2 and II.3-3.

The R&D requirements for a particular blanket concept will be considered in the latter portion of FY 1984. This evaluation along with the ranking of various concepts with respect to engineering feasibility, safety and environment, and economics will constitute the overall evaluation of blanket concepts. It is anticipated that blankets will be placed in the following categories:

- Potentially attractive, recommended for further near-term development. The goal of the study is to identify only a very limited number of such blankets to receive the highest R&D priority over the next several years. Those blankets that are suitable for both tokamaks and mirrors will be given higher priority than those useful for only one concept.

- Set aside for possible future consideration. This will include those blankets judged to be potentially acceptable or perhaps attractive but they appear at present to be less promising than the recommended blanket concepts. These would generally be viewed as backups to the recommended blanket options.

- Rejected. These blankets are judged to be clearly inferior to those identified above and should not be further pursued.

These rankings are discussed further in Section II.10.

TABLE II.3-2. SAFETY EVALUATION INDICES

Index Name	Weighting Value
1. Structure source term characterization	10
2. Breeder[a] source term characterization	10
3. Coolant source term characterization	10
4. Fault tolerance to breeder-coolant mixing	6
5. Fault tolerance to LOCA, LOFA, and LOSP[b]	6
6. Fault tolerance to external forces[c]	6
7. Fault tolerance to near-blanket system interactions[d]	6
8. Fault tolerance of containment integrity	6
9. Radioactive emission rate	20
10. Occupational exposure	10
11. Waste disposal	10

[a]Breeder index includes neutron multiplier when applicable.

[b]Loss of coolant, loss of flow, and loss of site power.

[c]E.g., plasma disruptions, seismic events, and off-normal magnet behavior.

[d]E.g., blanket-shield or blanket-limiter interactions and response to loss of vacuum integrity.

TABLE II.3-3 ENGINEERING EVALUATION INDICES

Index Name	Weighting Value (W_i)
1. Tritium Breeding and Inventory	23
2. Engineering Complexity and Fabrication	23
3. Resources	9
4. Power Variation	9
5. Ability to Increase Neutron Power Loading	9
6. Higher Surface Heat Flux With Higher Erosion	9
7. Startup/Shutdown	9
8. Maintenance and Repair	9
	100

II.4 Structural and Special Materials

II.4.1 Structural Materials

Three classes of alloys are currently considered as leading candidates for the first wall/blanket structure of a commercial fusion reactor, viz., austenitic stainless steels, ferritic (martensitic) steels and vanadium-base alloys. A representative alloy from each class has been selected for analysis in the present study. Austenitic stainless steels have been used extensively in fission reactor applications, and therefore possess the most developed data base for nuclear applications. For this reason the austenitic steels are generally regarded as a reference with which other candidate alloys are compared. The primary candidate alloy (PCA), which is under development in the U.S. alloy development program, is selected as the reference austenitic steel. This alloy in the 20-25% cold-worked condition is the product of several years of development to provide a radiation damage resistant alloy for fusion reactor applications.

The ferritic steels offer possible advantages over the austenitic steels in the areas of radiation swelling resistance, lower thermally-induced stresses, and better compatibility with liquid lithium and Li-Pb alloy. The HT-9 (Fe-12Cr1MoVW) alloy in the normalized and tempered condition is selected as the reference ferritic alloy primarily on the basis of the extensive nonir-radiation data base and high temperature strength. Although this alloy exhibits good radiation swelling resistance, the composition and thermomechanical treatment has not been optimized for radiation damage resistance as in the case of the PCA alloy.

Vanadium-base alloys represent an advanced alloy that offers advantage with respect to higher temperature operation, better corrosion resistance in lithium (and probably Li-Pb) and possibly better radiation damage resistance. The V-15Cr-5Ti alloy, which was originally developed as part of the fast breeder reactor program, is selected as the reference alloy. The titanium provides improved radiation damage resistance and the chromium provides improved mechanical properties. Although this alloy was developed partially on the basis of good radiation damage resistance, it does not necessarily represent an optimized alloy composition.

Modifications to these reference alloys to reduce residual radioactivity will be considered in later stages of this study. A high manganese austenitic steel and a modified ferritic steel with no nickel or molybdenum will be evaluated in the second year of this study. The reference vanadium alloy composition (VCrTi) offers the potential for low long-term activation.

The materials assessment conducted as part of this study included (1) a compilation of available materials properties data, (2) specification of limiting criteria for materials performance, and (3) determination of design allowable parameters. Where possible, established design rules or codes, e.g., ASME Boiler and Pressure Vessel Code, were applied. Critical design issues associated with each of the three reference alloys are identified.

A review of the critical thermophysical and mechanical proerties of the three reference alloys and the effects of radiation on the properties is presented in Chapter IV. Table II.4-1 gives a summary of the materials data base assessment. Corrosion/compatibility data are presented in Chapter VI. For cases where insufficient data exist for a reliable assessment, best estimates are provided for use in the design studies. The thermophysical properties of PCA and HT-9 alloys are well defined and those of VCrTi are adequately defined for the present study. The temperature dependent tensile and creep properties of the three alloys in the unirradiated condition are given in Chapter IV. For the VCrTi alloy, moderate strain hardening was projected to slightly enhance (~ 20%) the tensile properties compared to the limited data presented for annealed material.

The design stress limits, the maximum allowable operating temperature and the lifetime are set primarily by radiation damage considerations. Representative design stress limits are given in Table II.4-1. The S_m values for HT-9 and VCrTi are based on unirradiated property data since these alloys harden under irradiation. Significant softening of cold-worked PCA occurs above ~ 400°C. The S_t values are based on a general code thermal creep limit of 1% and a radiation creep limit of 5%. The radiation creep limit, which is not well established, is set at a higher limit since radiation creep is generally classified as not damaging. It is important to note that the radiation creep responses of these alloys are not well established. However, radiation creep is projected to be limiting under certain conditions. The maximum design temperature for structural applications is based on helium embrittlement. Severe

TABLE II.4-1. STRUCTURAL MATERIALS ASSESSMENT

Candidate Alloys	Austenitic Steel PCA-CW	Ferritic Steel HT-9	Vanadium V-15Cr-5Ti
Status of Data Base	Extensive	Extensive - Unirrad. Limited - Irrad.	Limited
Thermal Stress Factor $\frac{\alpha E}{K(1-\upsilon)}$ @ 400°C	0.22	0.11	0.055
Design Stress Limit S_m (Irrad.) (>10 dpa)	190 MPa (500°C) 175 MPa (550°C)	175 MPa (500°C) 160 MPa (550°C)	230 MPa (500°C) 230 MPa (700°C)
Maximum Allowable Temperature, °C (Irrad. Embrit.)	550	550	750
Radiation Lifetime (Swelling) (5%)	100 DPA (500°C) 150 DPA (400°C)	~ 200 DPA	> 200 DPA
Critical Design Issues	• Limited Lifetime (swelling) • High Thermal Stress Factor • Liquid Metal Corrosion • Radiation Creep • Operating Temp. Limit	• Weld Procedure (PWHT) • DBTT above RT • Operating Temp. Limit • Liquid Metal Embrittlement • Ferromagnetic Properties	• R&D Requirements • Weld Procedure (inert environment) • Oxidation Character. • High T Permeation Rates • Costs

loss of ductility is observed in most alloys at ~ 0.5 T_m. A margin of ~ 50°C is provided for in the temperature limits listed in the table. The swelling response of the alloys under irradiation has been approximated by a bilinear swelling curve. The curves given in Chapter IV are based on peak swelling temperatures. For PCA a higher swelling lifetime is allowable for temperatures below 400°C. All swelling curves require extrapolation of existing data to fusion reactor conditions; however, the uncertainties associated with swelling of HT-9 and VCrTi are much greater than those for PCA.

Critical limiting or unresolved design issues associated with each of the reference alloys are summarized in Table II.4-1. Although the data base for PCA (or autstenitic steels) is greater than for the other two alloys, the lifetime for swelling, the high thermal stress factor and the radiation creep limits are more limiting than those for HT-9 and VCrTi. The most critical issues associated with HT-9 relate to the more severe weld procedure requirements (post weld heat treatment) and the increase in the ductile -- brittle transition temperature (DBTT) during irradiation. Adequate data for HT-9 at the most critical temperatures (200 - 350°C) have not been generated; however, some ferritic pressure vessel steels exhibit severe embrittlement (DBTT > 250°C) at irradiation temperatures of ~ 300°C. The data base for the VCrTi alloy is much more limited than for the other two alloys. Very limited data have led to a high degree of optimism regarding the potential performance of this alloy class. In addition to these relatively large uncertainties, concerns regarding higher cost and the reactivity of vanadium with various chemical environment, e.g., air, have been identified.

II.4.2 Special Materials

Three areas, tritium breeding materials, neutron multipliers and electrical insulators, were addressed during the first year of the Blanket Comparison and Selection Study. The assessment of solid breeder materials is given in Chapter VIII and is summarized in Section II.6. The effort on liquid metal breeder materials has primarily been focused on the collection, compilation and limited assessment of properties for liquid lithium (Li) and liquid lithium-lead (17Li-83Pb). The purpose is to provide a data base on these two materials so that consistent property values can be used for design within the study. A rather complete set of Li properties is now available, though

several properties for 17Li-83Pb are still lacking (see Table V.1-5). For those unavailable properties, estimates based on separate properties of Pb and Li are recommended for interim use.

With the possible exceptions of Li_2O and Li_8ZrO_6, neutron multipliers are required to achieve an acceptable tritium breeding performance for virtually all other solid breeders. Two neutron multipliers, beryllium and lead, are considered for the solid breeder blanket designs in this study. The main concerns for beryllium are the irradiation swelling caused by helium generation and the resource limitation. With regard to the swelling problem, there is little concern over the loss of beryllium physical integrity as long as it is contained by the surrounding structural material. Swelling needs to be accommodated, however, such that the induced stresses in the structural material are minimized. Two methods for swelling accommodation were investigated. The first method uses high-density beryllium and relies on high irradiation temperature (> 750°C) for helium release. Swelling should be less than the geometrical limit of 30%, but the exact value is not known at the present time. The second method, recommended in the STARFIRE study, is to use a beryllium with 70% theoretical density and interconnected porosity to accommodate swelling. If the added beryllium thickness (due to the low density) does not impose significant penalty on the overall tritium breeding of a fixed-size blanket, the proposed method should be sufficient to solve the swelling problem. An added assurance can be gained when the irradiation temperature is kept below 600°C such that the interconnected porosity will remain open. The degradation of thermal conductivity of such a porous beryllium should not represent a significant heat transfer problem. Calculations using well established formulae for the porosity correction of thermal conductivity showed that the thermal conductivity of a 70% TD beryllium remains high compared to those of the other fusion blanket materials.

The assessment of beryllium resources for fusion neutron multiplier application has resulted in the following conclusion. It appears reasonable to consider beryllium as a neutron multiplier for the first and second generations (~ 1800 and 3000 GWe-y, respectively) of fusion reactor service, but close attention to beryllium recycle losses will be required. Since beryllium will activate in the fusion environment (primarily due to impurities), a remote fabrication technology will be required. Without recycle, beryllium

neutron multiplier should only be considered for use in the first generation of fusion reactors.

Because of its low melting point (327°C), the lead neutron multiplier will most likely be used in liquid form. The primary consideration is the compatibility of liquid lead with the structural materials. Volume expansion/contraction of lead upon melting/freezing is another design aspect that should be taken into consideration.

Electrical insulators are important to liquid metal blankets because they can significantly reduce the magnetohydrodynamic pressure losses. Preliminary work done to date has been to identify potential candidates. Based on limited information, several oxides (Y_2O_3, Sc_2O_3, CaO) were identified. Based on a slightly greater data base, Y_2O_3 is currently suggested as the reference for the present study. However, viability is not considered sufficiently proven to include it in liquid breeder blanket designs. More detailed evaluation of the electrical insulators issue is planned next year.

II.5 Liquid Metal, Gaseous and Water Corrosion/Compatibility

Critical aspects of liquid metal, gaseous and water corrosion/compatibility with candidate structural materials are presented in Chapter VI and summarized in this section. The present study included the following assessments:

- Liquid Metal Corrosion/Compatibility
  - Lithium
  - 17Li-83Pb

- Gaseous Corrosion/Compatibility of Vanadium
  - Helium With Impurities
  - Air or Oxygen Characteristic of Accident Conditions
  - Hydrogen Plasma Environment

- Water (200 - 350°C)
  - Vanadium Alloys
  - Cold-Worked Austenitic Steel

II.5.1 Liquid Metal Corrosion/Compatibility

II.5.1.1 Liquid Metal Corrosion/Compatibility Data Base

Corrosion and compatibility issues are a major consideration in assessing the viability of the different liquid-metal blanket designs. The corrosion and mass transfer problem varies for the many combinations of containment material and liquid metals that can be considered in a fusion reactor blanket system and depends on several variables. This section identifies the possible mechanisms and provides a qualitative assessment of the corrosion problem. The existing data are reviewed to evaluate the influence of the critical material and system variables on corrosion and to establish preliminary temperature limits for circulating or semistagnant liquid metal systems. Emphasis is on the corrosion behavior of austenitic PCA, ferritic HT-9, and vanadium V-15Cr-5Ti alloys in liquid lithium and eutectic 17Li-83Pb environments.

The most important compatibility concerns in any application of liquid metals are corrosion and the effect on mechanical properties of the containment material. Corrosion can lead to significant wall thinning/wastage and deposition of corrosion products in cooler areas of the circuit. Deterioration of mechanical strength of structural materials can result from the influence of the environment itself and the effects of microstructural and compositional changes that occur in the material during long-term exposure to the liquid metal.

The basis for a temperature limit from corrosion considerations can be radioactive mass transport, wall thinning/wastage, or mass transfer and deposition. Data indicate that a temperature limit based on radioactive mass transport, at least for PCA and HT-9, would be too low for blanket systems using liquid lithium or 17Li-83Pb. The problem of radioactive material transport would have to be solved by means other than limiting the temperature. The allowance for wall thinning is not likely to be important for section thicknesses > 3 mm during a service life of 2 to 3 y. The most important consideration in establishing the operating temperature limits for fusion reactor blankets is mass transfer and deposition.

Corrosion mass transfer seems to be the limiting factor for austenitic PCA alloy in circulating lithium systems. Table II.5-1 provides preliminary design temperature limits for the three structural alloys. At flow velocities

between 1.5-0.05 m/s, the use of PCA alloy is probably limited to temperatures below 430-460°C. However, additional data on the effects of various system parameters are needed to accurately establish the operating temperature limits. The ferritic HT-9 alloy is more resistant to corrosion in lithium than the austenitic stainless steels. Mass transfer/deposition effects are not likely to be the limiting factor at temperatures below 530-570°C. Limited data indicate that vanadium alloys have good corrosion resistance in lithium at temperatures up to 750°C. However, nonmetallic element (such as O, N, and C) transfer would dominate corrosion limits. Although the importance of these nonmetallic interactions are reasonably well understood, the purification requirements are not well defined.

Preliminary data in 17Li-83Pb indicate that the use of austenitic stainless steels may be prohibitive for practical applications. The high corrosion rates of austenitic stainless steels in flowing 17Li-83Pb would probably limit the operating temperatures below 370-400°C. The corrosion behavior of ferritic HT-9 alloy in 17Li-83Pb at temperatures up to 440°C is similar to that of the austenitic stainless steels in lithium. Additional data are required to accurately establish the operating temperature limits. Furthermore, low-temperature embrittlement of ferritic steels in Pb-17Li environment is a major concern and needs to be resolved. Information on the corrosion of vanadium alloys in flowing Pb-17Li environment is not available. Based on limited data for corrosion of refractory metals by lithium and lead, an estimated temperature limit of 650°C is recommended for the present study.

II.5.1.2 Liquid Metal Corrosion Product Transfer

A mathematical code for corrosion products transport has been developed. The code uses the results from corrosion experiments as the source term to predict corrosion product deposition in various regions of the primary loop. From the mass deposition, the radiation environment around different components of the primary loop can be calculated. The predicted contact dose rate around a MARS type steam generator (Li-Pb in HT-9) is ~ .2 Rem/hr. Therefore, remote maintenance of the steam generator appears essential.

TABLE II.5-1. PRELIMINARY DESIGN TEMPERATURE LIMITS (°C)[a]

System	Flow Velocity m/s	Austenitic Steel (PCA)[b]	Ferritic Steel (HT-9)	Vanadium Alloy[c] (V-15Cr-5Ti)
Lithium				
Circulating	1.5	430 (470)	535	750
	0.5	445 (480)	550	
	0.05	455 (495)	565	
Static	-	525 (575)	565	750
Pb-17Li				
Circulating	1.5	375 (410)	415 (450)	> 650[d]
	0.5	385 (420)	425 (465)	
	0.05	395 (430)	435 (475)	
Static	-	395 (430)	435 (475)	> 650[d]

[a] Limits based on a uniform dissolution rate of 5 μm/y (or ~ 5.5 mg/m^2.h). The values within brackets correspond to a rate of 20 μm/h.

[b] Temperature limits for Pb-17Li system are for 20% cold worked Type 316 SS.

[c] Nonmetallic element transfer are expected to dominate corrosion limits.

[d] Estimates based on low solubility of refractory metals in Li and Pb.

A corrosion product cleanup scheme has been developed. The principle of the scheme is based on the use of a cold trap to maintain the concentration of the corrosion product under saturation throughout the main loop. If such a corrosion product cleanup system is programmed into the corrosion product transport code, the calculated deposition rate is reduced by a factor of 50.

II.5.2 Gaseous Corrosion/Compatibility

The thermodynamic and kinetic processes for vanadium and VCrTi exposed to helium with low impurity concentrations have been evaluated. Since data are very limited, unalloyed vanadium has been evaluated and extrapolations to VCrTi have been made. For purposes of the present design study, it is concluded that oxidation will be excessive (unacceptable) if VCrTi is exposed to helium with greater than ~ 0.1 ppm moisture at temperatures above ~ 550°C. At temperatures below 500°C, kinetic mechanisms become controlling and may permit

limited use of VCrTi in high purity (< 1 ppm H_2O) helium. This alloy is significantly more resistant to oxidation than unalloyed vanadium. An evaluation of the helium coolant cleanup indicates that the purities required here are extremely difficult to attain economically in practical systems.

The potential effects of short term exposure of VCrTi to air and/or oxygen has been investigated to evaluate potential effects of accident conditions. No severe effects are predicted for exposures to air for a few hours at temperatures $\leq$ 650°C. As in the case of moisture in helium, the alloy is much more resistant to oxidation than unalloyed vanadium.

The potential for hydrogen pickup in VCrTi exposed to the hydrogenous plasma environment was evaluated. The tritium inventory in vanadium exposed to projected hydrogen pressures is predicted to be sufficiently low that hydrogen embrittlement is not projected to be a problem.

II.5.3 Water Corrosion

Most earlier studies have concluded that vanadium alloys could not be used in pressurized water-cooled systems because of excessive corrosion. An evaluation of recent scoping data concludes that selected alloys such as VCrTi may be acceptable for use in pressurized water. Observed corrosion rates in 250-300°C water for relatively short times ($\leq$ 100 h) indicate corrosion rates less than an order of magnitude greater than those typically observed for austenitic stainless steels.

Although austenitic stainless steels have been used extensively in pressurized water systems, stress corrosion problems have frequently been observed under certain conditions. The combination of cold-work and reduced ductility under irradiation may exacerbate this problem. Further investigations should be conducted to more thoroughly evaluate the seriousness of this problem. For the present study, it is assumed that this problem will not prevent the use of cold-worked PCA in pressurized water systems.

II.6 Solid Breeder Tritium Recovery

II.6.1 Introduction

The use of solid tritium breeder materials in fusion blankets demands that attention be given to those technical issues that govern tritium recovery. Significant effort was devoted in BCSS to evaluating these issues. This section provides a summary of the results. The details are given in Chapter VIII. Topics discussed include operating temperature limits, tritium solubility, tritium transport, irradiation behavior, fabrication, and mechanical properties.

II.6.2 Temperature Limits

The tritium inventory in a candidate breeder material, which is characterized by transport (diffusion rates) and solubility constraints, is predicted to possess a strong temperature dependence and to be sensitive to diffusion path length. Bulk diffusion is considered to be the primary contributor to setting the lower temperature limit. As diffusion slows, residence time increases as does the tritium inventory. The recommended lower temperature ranges from 300°C to 410°C for the candidate materials (see Table II.6-1). While the selection of an inventory limit cannot be precisely specified, it is clear that candidate materials exhibiting low inventory are more desirable.

Except for Li_2O, the upper temperature limit for solid breeders is based on experimental determination of the temperature at which closed porosity is apparent which occurs at approximately 90% of the theoretical density. In general, the thermal sintering characteristics of stable ceramic oxides are quite similar. Temperatures in excess of 0.8 T_m (the absolute melting point) are required before significant thermal sintering occurs. However, for some ceramic oxides, neutron irradiation is known to decrease the temperature at which sintering occurs. The effects of radiation may, therefore, close porosity at temperatures lower than 0.8 T_m, suggesting that lower maximum operating temperatures than indicated in Table II.6-1.

There are important conclusions to be drawn from the thermomechanical studies on Li_2O. It is evident that the solubility of LiOH in Li_2O is very low and the phases are nearly immiscible. Consideration of this factor is important because the blanket must not operate in a regime where LiOH is the

TABLE II.6-1. PROPERTY VALUES AND RECOMMEND TEMPERATURE LIMITS FOR CANDIDATE SOLID BREEDER MATERIALS[a]

	Properties			Recommended Temperature Limits		
	MP, °C	ρ_{Li}, g/cm^3	K,[b] W/mk	T_{min}, °C	T_{max}, °C	ΔT, °C
Li_2O	1433	0.93	3.4	410[d]	800[c,h]	390
γ-$LiAlO_2$	1610	0.28	2.2	300[d]	1200[f]	900
Li_5AlO_4	1047	0.61	2.3	350[d]	780[g]	430
Li_2SiO_3	1200	0.36	1.5	410[d]	1000[f]	590
Li_4SiO_4	1250	0.54	1.5	320[d]	950[f]	630
Li_2ZrO_3	1616	0.33	1.3	400[e]	1400[f]	1000
Li_8ZrO_6	1295	0.68	1.5	350[e]	980[g]	630
Li_2TiO_3	1550	0.33	2.0	400[e]	1185[g]	785

[a]Effects of radiation on tem perature limits are not reflected in this table.

[b]Estimated for 85% smeared density and temperature of 1000 K.

[c]Established from chemical considerations, i.e., reaction with moisture to form LiOT. $\log P(LiOH,g)(atm) = -8635/T + \frac{1}{2}\log p(H_2O,g) + 4.57$.

[d]Established from diffusion/inventory considerations (~ 1 μm grain size).

[e]Estimated assuming similar properties (nonirradiated).

[f]Established experimentally from onset of closed porosity.

[g]Estimated assuming $T_{max} = 0.8\ T_m$, K.

[h]1000°C for design approaches with helium purge gas flow directed only to the "cold" region of the breeder.

stable phase. At high temperatures LiOT vaporization could present some design challenges in managing potential blanket transport. However, higher temperatures are very attractive from a thermal hydraulic design point of view. Thus, designs which take advantage of the higher operating temperature limit must have purge gas flow directed only to the "cold" region (< 700°C) of the breeder.

II.6.3 Tritium Solubility

Currently, only Li_2O has received considerable attention in laboratory studies of candidate lithium containing ceramics. These studies have shown Li_2O to have extremely low moisture solubility (parts per million) for the operating temperature range of interest. The solubility is related to the partial pressure of H_2O in the gas phase over the sample (see Fig. II.6-1). If the H_2O partial pressure is large enough, a separate LiOH phase will form. To avoid second phase formation at 700 K, the partial pressure of H_2O must be maintained below 7×10^{-4} atm. Less stringent conditions prevail at higher temperatures. Thus these solubility studies have scoped out the two phase regions in addition to defining the vaporization behavior of LiOH (g); LiOH (g) being the product of reaction between H_2O (g) and Li_2O (s). At 800 K, the partial pressure of H_2O is 5.8×10^{-3} atm while at 900 K, it is 2.4×10^{-2} atm. An assessment of vapor transport is a design-specific issue involving other factors because the amount of material transported depends not only on its vapor pressure but also on the flow rate of the carrier gas. Further, if transport is expected, the system design must allow space to receive the condensate.

The Li-O-H system has been studied in detail thermodynamically and calculations of activity coefficients for LiOH as a solute were derived from the solubility data of LiOH as a function of temperature and pressure, and thermochemical data for LiOH(1), LiOH(g), and Li_2O(s). The activity coefficient is a rather large value (10^3) at low temperature. Over the concentration regime studied, the activity coefficients are greater than unity, indicative of positive deviation from ideality. Such deviations from ideality are interpreted to result from repulsive interactions between LiOH and Li_2O, suggestive of solubility of LiOH that is lower than would be predicted from ideal solution behavior. This condition is favorable from a blanket performance perspective since it indicates that tritium should be easily recoverable.

II.6.4 Tritium Transport

The modeling of tritium escape from solid tritium breeders must recognize the relative importance of mass transfer in the gas phase as well as solid state diffusion. Experimental investigations on oxygen containing compounds have produced considerable uncertainty in the absolute value of the tritium

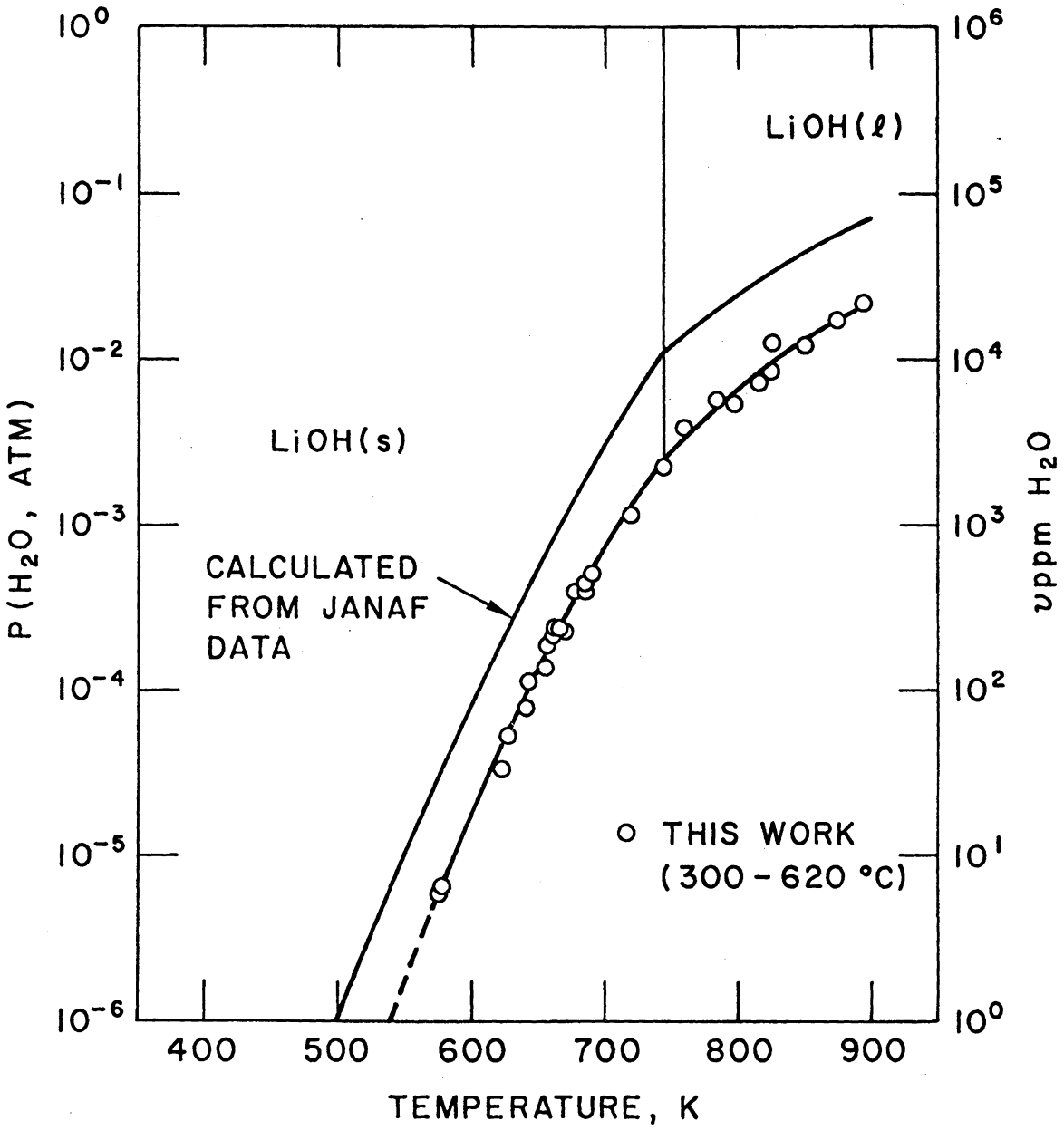

Figure II.6-1. Calculated and measured partial pressure of water as a function of temperature for the Li-O-H system.

diffusion coefficient. Only limited data exist for characterizing the transfer of tritium from the gas-solid interface into the gas stream. Considerations of this latter aspect indicate important consequences for tritium recovery, tritium inventory, and blanket design.

A model for tritium transport in Li_2O has been developed consistent with available diffusion data. Neutron irradiation converts the Li^6 components in Li_2O into tritium and helium creating at the same time (among other defects) a Li vacancy (V_{Li}). The origin of the V_{Li} can arise from several sources: (1) the extrinsic impurity induced defects that control Li diffusion below 1000°C, (2) the $^6Li(n,\alpha)T$ reaction that generates many defects in transforming Li into ^3H and ^4He atoms, and (3) defects generated via displacement damage, i.e., recoil of the energetic ^3H and ^4He atoms. Subsequently the following defect reaction takes place:

$$V_{Li} + T \rightleftarrows V_{Li}/T \qquad [II.6-1]$$

The notation V_{Li}/T denotes a stable defect complex comprising a V_{Li} and a tritium atom bound together in a certain geometrical configuration.

At low temperatures (< 400°C) one can interpret existing diffusion data to suggest that the V_{Li}/T complex migrates as a unit. Above 400°C we expect the complex to be less stable allowing the T atom to move more freely; probably interstitially within the Li_2O lattice. This hypothesis is consistent with the data, however, more detailed studies are needed to affirm this two stage mechanism. If the mechanism has merit, it supports the previously developed thermodynamic ideas that tritium is available for extraction.

II.6.5 Irradiation Effects

Recent EBR-II irradiation tests on solid breeder materials tend to substantiate the selection of the upper temperature limits presented in this report. Available data indicate that tritium retention is low and pellet integrity is reasonably good. For Li_2O, vaporization and swelling introduce potential upper temperature and lifetime limiting phenomena, whereas, other materials (e.g., γ-$LiAlO_2$, Li_4SiO_4, Li_2ZrO_3) do not appear to be as limited. Vaporization and redeposition of approximately 3% of the Li_2O was observed in-reactor at 900°C. The actual transport was probably as LiOT.

In fission reactor applications, material swelling during irradiation has provided lifetime limiting criteria for some materials, e.g., graphite, stainless steel, etc. In other situations, however, swelling does not limit the lifetime because it can be restrained by structural components. In a recent irradiation, Li_2O swelled in an inhomogeneous manner rather than densifying. If Li_2O can plastically deform at blanket operating temperatures, swelling could be restrained and thus not constitute a life limiting phenomena. If restraint is not successful, designs must either accommodate this behavior or accept lower lifetimes. Other ceramics, such as γ-$LiAlO_2$, Li_4SiO_4, and Li_2ZrO_3, do not appear to swell.

A complementary experiment to that cited above is being conducted in the Oak Ridge Reactor. The primary purpose of this experiment is to test in-situ tritium recovery from miniaturized solid breeder blanket (γ-$LiAlO_2$) assembly. Using a 0.1% H_2/He purge stream, tritium was recovered primarily in the HT form, HT/HTO $\tilde{=}$ 10^3/1. Tests suggested tritium recovery is possible at temperatures as low as 500°C.

II.6.6 Blanket Fabrication

There are two possible blanket configurations for solid breeders: pressed and sintered pellets and sphere-pac (spherical form) material. The pressed and sintered technique has been used successfully for preparing Li_2O, Li_4SiO_4, γ-$LiAlO_2$ and Li_2ZrO_3. Excellent experience was gained recently in preparing large pellets, about 2.5 cm diameter by 2.6 cm in length for the lithium breeder module program for TFTR. Li_2O pellets of 70 to 93% theoretical density have been prepared by standard methods while dense pellets up to 99% TD were prepared using hot isostatic pressing methods. The latter technique is preferred when grain size is to be preserved to high density. The sphere-pac technique has been developed for LWR and fast reactor fuel rods and is considered attractive for solid breeders. Compared to the pressed and sintered technique, breeder material in sphere-pac configuration could potentially minimize the effect of variability in breeder-to-structure interface heat conductance. For optimum performance the sphere-pac configuration requires three sizes of spheres to achieve about 88% smear density. These sizes have diametral ratios of about 40:10:1. The actual diameters currently favored are 1200, 300, and 30 μm.

The major advantage of the sphere-pac fuel over pressed and sintered pellets is the improvement in predictability of breeder-to-structure interface heat conductance, which in turn improves the predictability of breeder temperatures. The quantification of this improvement and the reduction in the effective thermal conductivity for a particular solid breeder material requires experiments. The fabrication of microspheres for the selected breeder material needs to be investigated and demonstrated and can be aided by the technology base that exists for sphere-pace fuel for fission reactors.

II.6.7 Mechanical Properties

Experimental data on the mechanical properties of solid breeder materials are nonexistent at the present time. Baseline information on such properties is essential to the design of solid breeder blankets and is necessary to understand the irradiation behavior of solid breeders. Elastic properties are needed to determine the thermoelastic mechanical behavior of materials, i.e., Young's modulus (E) and Poisson's ratio (ν). Thermal stresses in the solid breeder are directly proportional to E and are affected by ν, depending on the solid breeder configuration, i.e., whether the configuration approaches a plane-strain or plane-stress condition. Since thermal stresses typically vary from tensile to compressive in the solid breeder under a temperature gradient or during temperature cycling, the possibility of tensile-stress-induced cracking must be considered. The cracks can represent sources for localized stress and strain concentrations in the cladding if cladding is used to contain the solid breeder. In the event of solid breeder swelling and/or ratchetting during blanket operation, the localized stress and strain concentration is a potential failure cause for the cladding materials. Similarly, ceramic brittle materials are often observed to fracture at a critical uniaxial tensile stress. This maximum stress (σ_f) can be used as a fracture criterion to determine whether or not cracking will occur.

II.7 Alternative Blanket Concept Screening

The alternative concept screening task has the principal objectives of recommending whether any alternative blanket concepts should be added to the mainline concepts being considered in the study. To achieve this objective, a four step process was implemented. First, a literature search compiled a bibliography of fusion-electric blanket designs that were characterized by the

breeding material, coolant, structural material and presence or absence of a multiplier. Second, from this list, twelve alternative concepts were identified. The third step in the process was the comparison of the design parameters for these concepts against the screening criteria established for the project. Fourth, for concepts that were judged to have the potential to be attractive candidates for commercial application, additional design work was performed to enable an improved evaluation to be made.

The alternative concepts can be segmented into six groups. These are molten salt breeders (FLIBE), molten salt coolants, lithium-lead intermetallic breeder (Li_7Pb_2), solid microsphere breeder/coolant, phase change breeders, and slurries. Designs for only the first five groups were evaluated. For the slurry concepts, designs have not been developed to the point where a meaningful evaluation could be performed. Many of these concepts used structural materials such as Inconel, graphite, TZM or titanium/aluminum that are not being included in the BCSS. In our evaluation of these concepts, we have discussed their applicability with austenitic and ferritic steels and with vanadium alloys. None of the identified alternative concepts have a separate neutron multiplier region. Because the ability to achieve an adequate tritium breeding ratio is vital for fusion, we have considered adding neutron multipliers to the design as part of the evaluation.

The FLIBE molten salt breeder blanket that is helium cooled fails to meet the tritium breeding criterion. Analysis has shown that insufficient breeding is an inherent characteristic of this breeder. Therefore, we have modified this concept by adding a lead multiplier zone. In addition, we modified the configuration to be more compatible with present design practice. The results of this work showed an adequate TBR, a preference for a ferritic steel structure, a very simple tritium removal system, and an inherently fault tolerant design. The key concern associated with design is the maximum wall loading that can be accommodated. This wall loading is influenced both by the ability to cool the first wall with helium and the lead/structure interface temperature. We have presently baselined the concept for a neutron wall loading of 3 MW/m^2; however, we believe that this can be extended to 5 MW/m^2 with the most recent corrosion design guidelines. All problems associated with gas cooling of the first wall and blanket (heat flux/erosion capability, blanket/shield thickness, etc.) are also present in this design. One feature of this concept

is that the method of tritium removal is through slip streaming the primary coolant loop. This allows a significant simplification of the mechanical design but increases problems in tritium containment. However, analysis has shown that the concept meets the initial screening criteria on tritium loss. On balance, the helium cooled, lead multiplier, FLIBE breeder concept is considered very similar to the helium cooled, lithium-lead breeder mainline concept. We recommend that this concept be studied further, however, with a lower priority than that for the HTS-cooled blanket discussed below.

Designs of blankets with Li_7Pb_2 as the breeder and helium, water and molten salt coolants have been evaluated. The water cooled designs have been eliminated because of high rate of energy release reactions between the coolant and breeder. A similar conclusion can be reached for Li_7Pb_2 and the nitrate-nitrite molten salt HTS. Helium cooled Li_7Pb_2 designs should pass the screening criteria. However, we judged that problems in oxygen control in the coolant, tritium containment and separation, phase change in the breeder that decreased tritium diffusion and a restricted temperature of operation window for the breeder make the concept unattractive for eventual commercial application. We recommend no further work.

The phase change blanket with 62Li-38Pb breeder and boiling water coolant was developed for application to a pulsed device. There is much less motivation for the concept for steady-state tokamaks or mirrors. In addition, the chemical compatibility of the breeder and coolant may cause excessive rates of energy release in the event of a tube failure. No further work is recommended.

The use of solid microsphere coolant/breeder was proposed for an ICF reactor but could, with modification, be carried over to tokamaks or mirrors. The graphite first wall and blanket structure would have to be replaced with silicon carbide because of radiation damage. This design passes the screening criteria. However, we do not recommend this concept for further work because of the need for a ceramic structure, potential radiation and self-erosion damage to the breeder, and development of the heat transport system.

The final alternative concept that was sufficiently developed to be evaluated was molten salt cooled blankets. The concepts that appeared in the literature are HTS cooled lithium, HTS cooled Li_7Pb_2, and FLIBE cooled lithium. The two HTS designs suffer from chemical compatibility problems that can

result in high rates of energy release. The FLIBE cooled blanket requires a high temperature refractory structure such as TZM because of the high melting point of FLIBE. The concept is not compatible with the structural materials being considered in the BCSS.

Our evaluation of these molten salt designs showed that they failed to meet the project initial screening criteria. However, the HTS coolant has several properties that make it advantageous for fusion blankets. The principal feature is low pressure; other features include low melting point, relatively low viscosity and compatibility with a large range of breeders. Therefore, we developed designs for an HTS cooled lithium breeder (17Li-83Pb) and a solid breeder ($LiAlO_2$ with a lead multiplier). Both of these designs showed adequate tritium breeding. HTS shows good compatibility with both austenitic and ferritic steels over a wide temperature range. Also, this salt has the unusual property of containing tritium by conversion to T_2O, which is easily removed by vacuum degassing. Thus, HTS does not require either a double walled heat exchanger nor an intermediate loop. The potential problems with HTS are radiolytic decomposition which is unknown, the maximum operating temperature based on thermal decomposition, induced radioactivity which presents safety concerns, and voltage enhanced corrosion which restricts flow velocity and tube size in regions of high magnetic field. However, the advantages associated with this concept are sufficiently attractive to recommend its inclusion as a mainline concept.

In summary, the principal recommendation of the alternative concepts task is the addition of HTS as a coolant for lithium-lead and solid breeders as the highest priority. In addition, we recommend that a helium cooled FLIBE breeder with a lead multiplier be considered as a backup to the helium cooled 83Pb-17Li design. All other concepts that were identified have identified problems that make them unsuitable for the BCSS or have significant development uncertainties.

II.8 Liquid Metal Blanket Designs

The viability of blanket concepts based on the use of liquid metals, either lithium or 17Li-83Pb, as the tritium breeding material has been evaluated in the present study. The blanket concepts considered for both tokamak

and mirror reactors represent two classes: (1) self-cooled systems in which the liquid metal serves as both breeder and coolant, and (2) separately-cooled liquid metal blanket concepts. The six concepts evaluated include:

- Self-cooled Systems (Breeder/Coolant)
  - Lithium/Lithium
  - 17Li-83Pb/17Li-83Pb

- Separately-Cooled Systems (Breeder/Coolant)
  - 17Li-83Pb/Sodium
  - 17Li-83Pb/Water
  - Lithium/Helium
  - 17Li-83Pb/Helium

In addition, for tokamak reactors, a preliminary evaluation of a non-breeding inboard blanket with a self-cooled outboard blanket has been conducted. Results of the liquid metal blanket study are presented in Section VII.

II.8.1 Self-Cooled Blanket Concepts

The key feature of the self-cooled blanket concepts relate to the use of the same liquid metal as both tritium breeder and coolant. This factor simplifies both materials and design considerations since the blanket requires only a structure and a breeder-coolant. Coolant-breeder compatibility/reactivity is not a factor. Heat transfer requirements are also reduced because most of the nuclear heating is deposited directly in the breeder-coolant. Lithium and Li-Pb both provide relatively high tritium breeding capability and tritium recovery with relatively low tritium inventory is feasible. The liquid metals are good heat transfer fluids with high thermal conductivities and heat capacities, which are beneficial for normal and transient operation.

Critical feasibility issues and design constraints for full coverage self-cooled liquid metal blanket concepts are summarized in Table II.8-1. Viable self-cooled liquid metal blanket designs are driven primarily by magnetohydrodynamic (MHD) considerations and for some structural materials by corrosion temperature limits. The MHD considerations involve:

TABLE II.8-1. CRITICAL FEASIBILITY ISSUES AND DESIGN CONSTRAINTS FOR SELF-COOLED LIQUID METAL BLANKET CONCEPTS

- Most Critical Feasibility Issues
  - Liquid Metal Corrosion/Compatibility
    - Acceptable Materials Combinations
    - Maximum Structural Interface Temperature
  - Liquid Metal MHD
    - Pressure Losses/Structure Stresses
    - Heat Transfer/Recovery

      First-Wall Heat Flux (Tokamak)
      Temperature Distribution (Laminar Flow)

- Critical Design Constraints
  - Thermal Hydraulics
    - First-Wall Heat Recovery
    - Manifolding
    - Startup/Shutdown Procedure
  - Stress Limitations
    - First-Wall Thermal Stresses
    - MHD Pressure Stresses
    - Weight Loads (Lithium-Lead)
  - Neutronics
    - Neutron Absorption/Shielding (Lithium)
    - Tritium Breeding (Lithium)
  - Tritium Recovery
    - High Tritium Pressure (Lithium-Lead)

- Incorporation of manifolds into blanket modules to minimize flow velocities perpendicular to the primary magnetic field (tokamak-toroidal field; mirror-axial field).

- Some method of flow enhancement is required to provide adequate cooling for the first wall of a tokamak.

Generic blanket concepts considered include:

- Poloidal Flow Manifold/Module
  - Large Straight Channels
  - Induced Helical Flow

- Poloidal Flow Manifold/Module with Toroidal/Axial Flow First Wall

- Poloidal Flow Manifold/Module with Radial Flow First Wall

The second option, i.e., the poloidal flow manifold/module with a toroidal/axial flow first wall, was selected as a reference for the comparison study. Figure II.8-1 is a schematic diagram of the reference design concept for the tokamak configuration. The manifold/module flow circulates at a slight angle to the poloidal direction. Each channel in the manifold serves a bank of first-wall channels and then reenters the manifold at the opposite side of the sector. Table II.8-2 summarizes the key features of the reference design concept, which is used for both lithium and Li-Pb. For the case of the high density Li-Pb, flow would be in the opposite direction, i.e., top to bottom to reduce the effect of the head pressure.

The initial focus of the study has been on the austenitic stainless steel PCA structural material. The Li-Pb breeder-coolant with a PCA structure is not considered viable primarily on the basis of excessive corrosion of PCA by the Li-Pb. As indicated in Section VI and II.5, the maximum interface temperature that meets the corrosion criteria of 5 μm per year is $< 400°C$ for recirculating systems with velocities of ~ 1 m/s.

For the case of the lithium breeder/coolant, corrosion considerations limit the interface temperature for PCA to $\sim 430°C$. This temperature is acceptable for a viable design; however, the energy conversion efficiency will be limited to ~ 33-34%. Table II.8-3 summarizes the design parameters for the PCA/Li design based on the tokamak configuration. This design meets all the initial screening criteria. The major problem relates to the MHD pressure losses. The most critical region is the inboard region and the critical stress region is the webs between the poloidal manifolds. The maximum calcu-

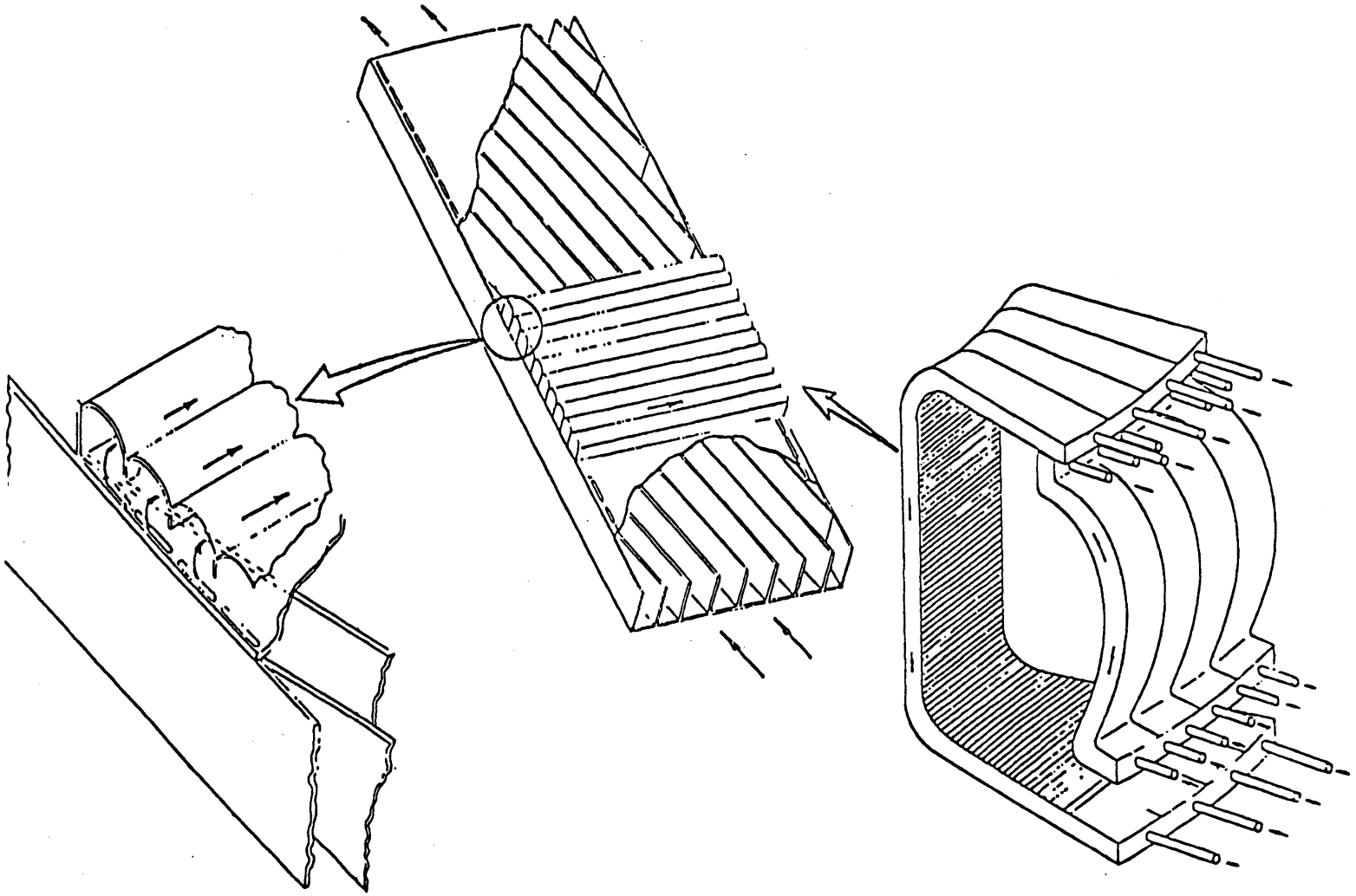

Figure II.8-1. Schematic diagram of reference self-cooled liquid metal blanket concept.

TABLE II.8-2. FEATURES OF TOROIDAL (AXIAL FLOW) FIRST WALL CONCEPT

- Blanket Module Serves as Manifold.
  - Minimizes Velocity Perpendicular to Field.
  - Adjoining Channels Provide MHD Benefit.
  - Maximum Pressure (Inlet) Occurs in Low Temperature Region; Maximum Temperature Occurs in Low Pressure Region (Outlet).
- Toroidal (Axial) Flow First Wall Permits High Coolant Velocity for Effective First Wall Heat Removal.
  - Low MHD Pressure Drop in High Velocity Region.
  - Can be Parallel to Effective Field if Necessary.
  - No Major Effect on MHD Pressure Drop.
- Minimal Number of Bends Reduces MHD Effects.
- Small First-Wall Channel Reduces Primary Stress Effect on First Wall.
- Primary Stress Maximum in Web of Module.
  - Lower Fluence Region Results in Reduced Radiation Creep.
  - Separates Maximum Primary Stress From Maximum Thermal Stress and Maximum Membrane Temperature.
  - Maximum Pressure/Stress at Low Temperature (Inlet).
- Smooth First Wall Maximizes Effective Blanket Density.
  - First Wall Can Easily Conform to Plasma Contour.
- Flow Geometry Provides for Ease of Filling and Draining of Blanket.

lated stress in the webs is 160 MPa, which is 30% less than the maximum allowable design stress. Uncertainties in the MHD pressure loss calculations are estimated to be less than 25%. Tapered thickness webs as described in Section VII are necessary to obtain these allowable stresses. The corrosion temperature limits can be designed for but with very little margin. The breeding ratio exceeds the design specifications for the blanket thickness recommended provided that blanket coverage is high.

TABLE II.8-3. SUMMARY OF Li/PCA TOKAMAK BLANKET PARAMETERS

Materials	
Coolant	Li
Breeder	Li
Structure	PCA
Design Concept	Poloidal Flow Manifold with Integrated Toroidal Flow First Wall
Inboard Blanket/Reflector Thickness	65 cm
Outboard (Top and Bottom) Blanket/ Reflector Thickness	85 cm
Thermal Hydraulics	
Flow Requirements	
Inboard Manifold (Avg).	0.42 m/s
First Wall	1.6 m/s
Maximum Interface Temperature	
Manifold	380°C
First Wall	420°C
Coolant Temperature	
T_{in}	230°C
T_{out}	380°C
System Efficiency	33-34%
MHD/Stress	
System ΔP	Inbd: 3.0 MPa, Outbd: - 1.4 MPa
Pumping Power Requirements	~ 2%
Primary Stress (Web)	160 MPa (30% Margin)
First Wall Thickness	3.5 mm for 50 W/cm^2 flux
Neutronics	
Breeding Ratio (1D)	1.32
Energy Multiplication	17.9 MeV/DTn (1.27)
Fraction of Energy Deposited in Blanket	> 97%
Tritium Recovery	
Y-Getter or Gas Permeation/Recovery	
T-Concentration Li	1 wppm (< 400 g blanket inventory)
T-Processing Rate	~ 0.1% Coolant Flow Rate

A preliminary evaluation of this design has been conducted for a vanadium alloy structure with Li as the coolant/breeder. Because of the projected higher corrosion resistance of vanadium alloys, a higher allowable interface temperature (750°C) and a higher system ΔT (200°C) are acceptable. The critical MHD pressure problem for the V/Li system is approximately the same as that for the PCA/Li system since the higher allowable system ΔT (lower velocity) compensates for the higher electrical conductivity of vanadium. Because of the lower thermal stress factor associated with VCrTi, surface heating of 100 W/cm^2 can be accommodated with a 5-6 mm wall. Replacing PCA with VCrTi results in improved tritium breeding performance by ~ 10%; however, the energy multiplication is reduced by a similar amount. The higher system temperatures allowable with the VCrTi structure provide for an energy conversion efficiency of ~ 40%.

Preliminary analyses of some of the critical aspects of a Li-Pb/self-cooled system have been evaluated. The MHD pressure loss in Li-Pb is only slightly higher than that for lithium. The corrosion limits for VCrTi in Li-Pb are not well defined but are projected to be adequate for acceptable design performance. Based on limited analyses and a relative comparison with the PCA/Li and VCrTi/Li systems, a viable VCrTi/Li-Pb design appears feasible. The energy conversion efficiency may be compromised somewhat compared to the VCrTi/Li system because of the lower temperature limits specified by the corrosion criteria. It is assumed that an intermediate heat exchanger (IHX) and loop are required for both Li and Li-Pb systems.

The major uncertainties regarding MHD effects relate to flow profiles in the channels. The preliminary evaluations conclude that fully developed flow is unlikely for the current design. Undeveloped flow characteristics are expected to enhance heat transfer, but to have limited effect on the pressure losses. A better understanding of MHD effects is required to ensure proper flow distribution and to eliminate unacceptable stagnation regions.

II.8.2 Separately-Cooled Liquid Metal Blanket Concepts

Blanket concepts that incorporate lithium or 17Li-83Pb as breeding materials with a separate coolant have been included in the present study. Separate coolants considered in the initial screening include helium, pressurized water and liquid sodium. Section II.8.2.1 presents a summary of the helium-

cooled blanket concepts with either lithium or Li-Pb as the breeder. Section II.8.2.2 summarizes the evaluation of the water-cooled Li-Pb blanket. Because of the high reactivity of lithium with water, this concept was not included in the evaluation. Section II.8.2.3 summarizes the evaluation of the sodium-cooled Li-Pb concept. Because of the similarity of sodium and lithium, a sodium-cooled lithium-breeder concept was not considered. In addition to these concepts, a preliminary analysis was initiated to evaluate the feasibility/desirability of a separate coolant for the inboard region (non-breeding) of a tokamak reactor.

II.8.2.1 Helium-Cooled Liquid Metal Blanket Concepts

A blanket design concept has been developed for detailed investigation of the critical issues of the liquid breeder, helium-cooled blanket concept. The corrosion temperature limits make a helium-cooled design with lithium or Li-Pb as the breeder unattractive if PCA is used throughout the structure. Therefore, the design effort has focused on the evaluation of concepts that incorporate a combination of PCA and HT-9 as structural materials. Shown in Fig. II.8-2 with Li as the breeder, the design offers a mechanically simple configuration and features a PCA lobed first wall of the bellows type, HT-9 tube fuel elements containing either static (17Li-83Pb) or very slowly circulating (Li) liquid breeder, and a plate-type PCA reflector/shield region. Helium coolant entering the blanket at 275°C is directed initially to the first wall region by a flow baffle and subsequently cross flowed through the tube bank and reflector plates. The helium outlet temperatures are 525°C and 500°C with Li and 17Li-83Pb breeder, respectively, providing a net power conversion system efficiency of 36.5%. The advantages and disadvantages of helium-cooling are summarized in Section II.9. The key features and parameters of the design are presented in Table II.8-4 and summarized below.

The 7.0 mm first wall is designed to handle a neutron wall loading of 5 MW/m^2, and is capable of accommodating a surface heat flux of over 0.5 MW/m^2. The unique bellows configuration of the lobed wall allows it to accommodate the pressure load, thermal stresses, and radiation-induced swelling without relying upon creep for stress relief, although it does accommodate radiation-induced creep. Its maximum temperature is 550°C with a design life of two years set by wall erosion at the rate of 1 mm per year. The first wall design is summarized in more detail in Section II.9. In the breeder zone, the maximum tube diameter and pitch could be 6.2 cm and 6.75 cm with Li and 2.0 cm

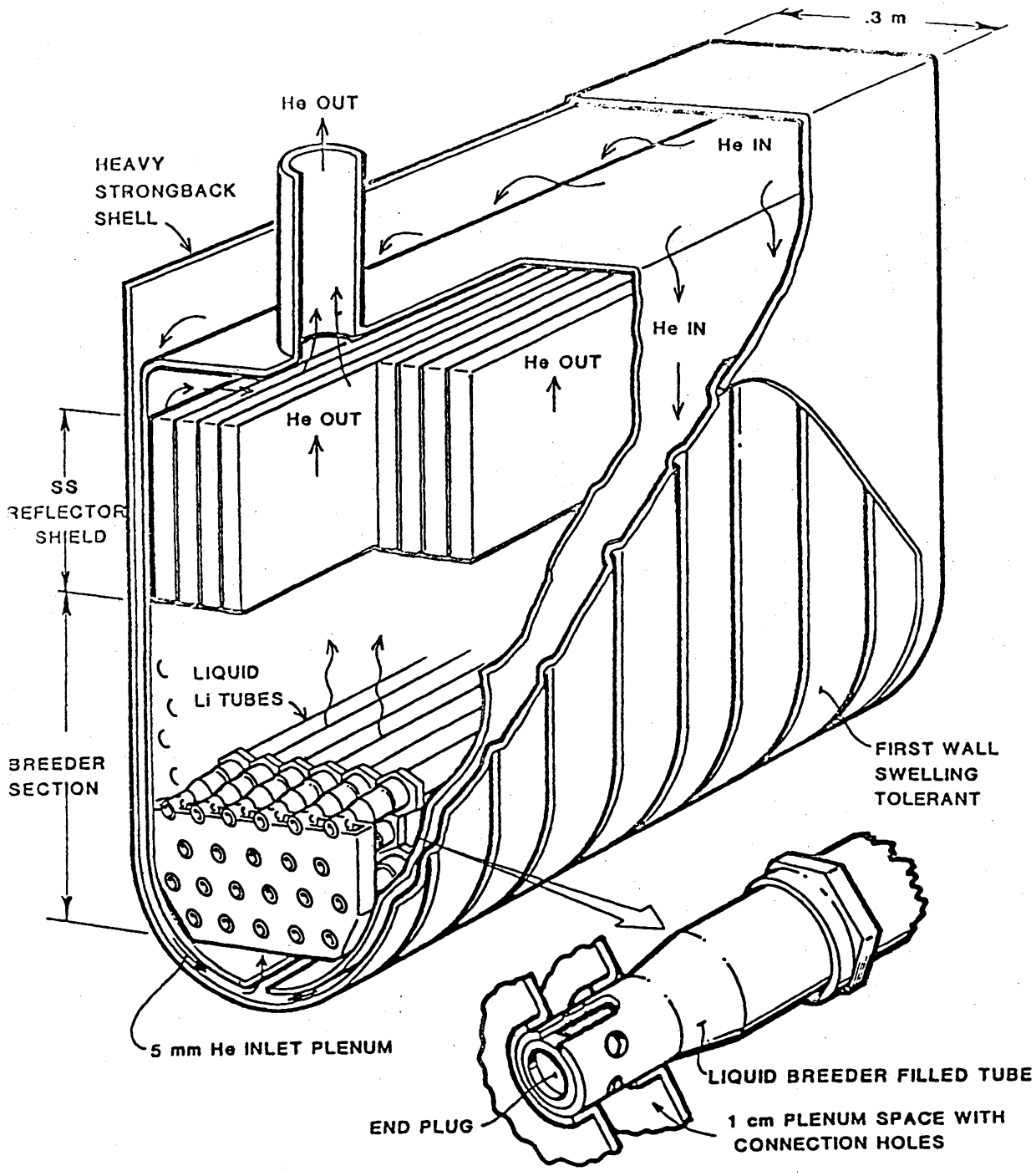

Figure II.8-2. Helium cooled/liquid lithium breeder blanket module.

TABLE II.8-4. KEY FEATURES AND PARAMETERS FOR LIQUID BREEDER/HELIUM-COOLED BLANKET CONCEPTS

Materials		
Breeder	Li	17Li-83Pb
Structure	PCA	PCA
Breeder containment tubes	HT-9	HT-9
Coolant	He, 50 atm	He, 50 atm
First Wall		
Bellows-type; accommodates thermal strains & radiation damage		
Design surface heat flux, MW/m^2	0.6	0.6
Maximum temperature, °C	550	550
Bellows height, (BOL/EOL), mm	9/7	9/7
Equivalent thickness, (BOL/EOL), mm	6.3/5.0	6.3/5.0
Erosion thickness allowance, mm	2.0	2.0
Erosion life at 1 mm/y erosion rate, y	2	2
Coolant		
Inlet/outlet temperature, °C	275/525	275/500
Inlet pressure, MPa	5.1	5.1
Total pressure drop, kPa	61.0	61.0
Net power conversion efficiency, %	36.5	36.5
Breeder		
Liquid breeder contained in tubes	Slow circulation	Static
Tube inner radius, cm	3.1	1.0
Tube wall thickness, cm	0.078	0.025
Pitch	6.75	2.25
Maximum interface temperature, °C	541	487
Blanket thickness, cm	90	66
Tritium Breeding Ratio (1-D)	1.23	1.20
Energy Deposit in Blanket, MeV/DT neutron (multiplication)	16.4 (1.16)	16.8 (1.19)
Blanket Tritium Inventory, kg	0.25	0.6
Tritium Leakage, Ci/d	<1.0	0.02

and 2.25 cm with 17Li-83Pb. In fact, a practical tube size would be smaller for Li. The maximum breeder/HT-9 interface temperature of 541°C with Li satisfies the limits established from compatibility concerns. With 17Li-83Pb breeder and HT-9 tubes, the calculated interface temperature of 487°C exceeds the recommended corrosion temperature limit because the thermal hydraulics design was based on a preliminary temperature limit of 500°C. It is expected that the most recent limit of 435°C might be met by design modifications of the tube diameter and pitch and/or lowering the helium outlet temperature.

The composition and thicknesses of the breeder and reflector zones are determined from neutronics considerations. With Li breeder, a 52 cm breeder zone with a 15 cm reflector provides a 1-D tritium breeding ratio (TBR) of 1.23 and a nuetron energy multiplication factor of 1.16. With 17Li-83Pb, a 27 cm breeder zone with a 15 cm reflector provides a 1-D TBR of 1.20 and a neutron energy multiplication factor of 1.19.

With Li breeder, satisfactory tritium recovery can be accomplished by circulation and reprocessing of the Li at the rate of 0.15 m^3/sec. The maximum Li flow velocity would be 2.7 cm/sec in the header regions of the blanket. The tritium inventory would be ~ 250 grams in the breeder and negligible in the helium coolant. Tritium leak rate through the steam generator at the above conditions would be < 10 Ci/day. This leak rate was calculated assuming a factor of ten reduction in tritium permeation due to an oxide barrier on the steam side of the heat exchanger. Factors of a few hundred have been observed under certain conditions. Thus the leak rate may be significantly lower if increased effectiveness of the oxide barrier is possible. The leak rate could also be reduced with oxygen partial pressure control and tritium cleanup of the helium coolant. With 17Li-83Pb, tritium is permeated into the helium coolant and recovered by slipstream processing of 1.0% of the main helium flow. The helium is controlled to 100 Pa oxygen partial pressure and the 17Li-83Pb is static. The resultant tritium inventory is 560 grams in the breeder and 41 grams in the helium, for a total of 0.6 kg. Tritium leakage through the steam generator is predicted to be ~ 0.02 Ci/day.

The present design offers many inherent safety features. It incorporates a multiple containment approach to liquid breeder release, and since the coolant is helium, the inventory of liquid breeder is minimized to that required only from neutronics considerations. There is no appreciable potential for breeder-coolant chemical interaction due to the low level of impurities in the

helium. The eutectic 17Li-83Pb is significantly less reactive with air or water than is lithium. In a depressurization event, the design allows for rapid communication between submodules. The design is projected to withstand the maximum forces expected without propagation to adjacent submodules. With gas coolant, the capability exists to circulate the depressurized coolant for heat removal during accident conditions, which may prevent module failure from excessive temperatures. The capability also exists to provide a redundant and diverse auxiliary cooling circuit via recirculation of the liquid breeder. Under complete loss of cooling events, the blanket has a large heat capacity (Li) and offers good heat conduction through the blanket for heat removal from the first wall region. Finally, the thin first wall and low structure volume fraction, together with the low tritium inventory and loss rate, would result in low radioactive waste generation levels.

The critical feasibility issues and design constraints of the He-cooled liquid breeder blankets are listed in Table II.8.5. Primary problems/concerns associated with these designs relate to the complexity and limitations of the bellows first wall (see Section II.9.4 for discussion) and corrosion/compatibility of the structural material. As discussed earlier, PCA as the breeder containment is not acceptable because of the corrosion temperature limits. Therefore, HT-9 is suggested for the Li and Li-Pb containment tubes. Even so, the Li-Pb/HT-9 system design needs to be modified to meet the specified corrosion temperature limits. For the case of the Li-Pb breeder, tritium recovery from the helium is required. Uncertainties regarding tritium permeation and reaction kinetics make this a critical design constraint.

II.8.2.2 Water-Cooled Li-Pb Blanket Concept

A blanket concept based on pressurized water as the coolant and 17Li-83Pb as the breeder material is being evaluated in the study. The Li-Pb alloy is much less reactive with water than lithium; however, breeder-coolant compatibility remains an issue. Corrosion criteria for PCA in noncirculating Li-Pb systems require interface temperatures below 400°C. This would be marginal for an acceptable system, particularly when the tritium recovery issues are considered. HT-9 will permit higher operating temperatures, however, embrittlement (liquid metal and irradiation) are primary concerns.

TABLE II.8-5. CRITICAL FEASIBILITY ISSUES AND DESIGN CONSTRAINTS FOR HELIUM-COOLED LIQUID METAL BLANKET CONCEPTS

Most Critical Feasibility Issues

- Temperature/heat flux limits on first wall
- Liquid metal corrosion/compatibility
  - Acceptable materials combinations
  - Maximum structural interface temperature

Critical Design Constraints

- Thermal-hydraulics: breeder zone tube dimensions/pitch; manifolding
- Neutronics: refelction/shield energy distribution and inboard/outboard tradeoff
- Tritium recovery from primary helium coolant (17Li-83Pb)

Adequate tritium breeding is attainable with this system. The major concern relates to tritium recovery. The main difficulty arises from the low tritium solubility, which results in a high tritium partial pressure. To reduce tritium migration into the water coolant to acceptable levels, a double-walled tubing concept is being evaluated. Effective tritium barriers appear to be needed. Preliminary calculations indicate that the Li-Pb must be circulated for tritium recovery. Because of the low tritium solubility in Li-Pb (new data indicate the solubility is a factor of three lower than previously assumed), relatively large flowrates of Li-Pb must be processed to maintain acceptable tritium partial pressures. Mass flowrates equivalent to several percent of those required for self-cooled Li-Pb systems are projected. Further analyses and preconceptual design development are required to assess this concept.

II.8.2.3 Sodium-Cooled Li-Pb Blanket Concept

A sodium-cooled Li-Pb blanket was evaluated in this study. Attractive features of this system relate to (1) lower corrosion rates for sodium in austenitic steel compared to lithium, (2) sodium is a good coolant with a lower melting temperature than lithium, (3) Li-Pb provides excellent breeding capa-

bility, (4) sodium is less reactive with Li-Pb than some other coolants considered, and (5) tritium recovery from sodium by cold trapping appears attractive.

However, preliminary analyses indicated major design problems, particularly compared to other blanket options, and thus a detailed design was not developed in this study. Three considerations have lead to the elimination of this concept as a primary candidate. The added complexity of a separate coolant (when both breeder and coolant are liquid metals) compared to the self-cooled lithium or Li-Pb concepts tends to offset for some of the favorable characteristics. The most critical problem relates to MHD considerations. Excessive pressure losses predicted for a sodium-cooled system relate to:

- The lower heat capacity of sodium requires approximately twice the volumetric flowrate of Li or Li-Pb for equivalent heat removal.

- Since sodium serves only as coolant, only a small volume fraction of the blanket (< 20%) is allowable, therefore, requiring about 5 times higher flowrates.

- Predicted MHD pressure losses are at least 5-10 times those predicted for Li or Li-Pb.

The high MHD pressure losses appear to be prohibitive. Also, activation of ^{23}Na to ^{22}Na and ^{24}Na is projected to have serious safety implications.

II.8.2.4. Dual Coolant Concepts

A blanket design based on a dual coolant concept is being investigated. The outer blanket which is cooled by 17Li-83Pb provides adequate breeding. The inner blanket, which does not breed, is cooled by helium to provide high temperature heat. The Li-Pb is used in the preheater and boiler portion of the steam generator and helium is used in the superheater part. Since Li-Pb is only used in the low temperature operation, an exit temperature of 425°C is sufficient, thereby reducing the corrosion problem. No liquid metal in the inner blanket reduces the overall MHD problem. However, very high temperature steam may be obtainable (538°C, 16.6 MPa) by the use of insulating refractories in the blanket. A power conversion efficiency of > 40% may be feasible.

II.9 Solid Breeder Blanket Designs

This section summarizes the work accomplished by the study in analysis, design development and evaluation of three separate blanket concepts:

- Li_2O solid breeder with pressurized water coolant (Li_2O/H_2O)
- Li_2O solid breeder with helium gas coolant (Li_2O/He)
- Ternary oxide solid breeder (e.g., $LiAlO_2$) with pressurized water coolant and a neutron multiplier ($TO/H_2O/NM$); lead was selected initially to evaluate whether a multiplier other than beryllium was viable.

Analyses performed to enable prediction of solid breeder lifetime and performance are also summarized.

II.9.1 Selection of Concepts

The three blanket concepts listed above were selected at the outset of the project for analysis and development. The specific solid tritium breeder and coolant choices were made largely on the basis of recent blanket studies. The results of those studies and others indicate that of all solid breeder blanket concepts, these three represent those generic concepts that are likely to have the highest overall potential for successful use in magnetic confinement fusion power reactors.

Breeders - Lithium oxide is generally considered today to be the best candidate solid breeder. Its principal attribute is the potential for achieving attractive tritium breeding ratios--significantly higher than unity--without a neutron multiplier. All other candidate solid breeders, with the probable exception of Li_8ZrO_6, will require a neutron multiplier to achieve the required tritium breeding ratio. Other attractive features of Li_2O include a high melting point (~ 1427°C) and very low activation. The primary disadvantages are associated with its hygroscopic nature. The effects of irradiation on the thermophysical properties and tritium release characteristics of Li_2O and all other solid breeders are not well defined.

Coolants - Pressurized high-temperature water and gaseous helium have been the coolants most often proposed for use with solid breeders. Water coolant has excellent heat transfer characteristics, and enjoys a well-developed technology from fission reactor experience for use in power

conversion systems. Its primary disadvantages are lower thermal energy conversion efficiency and the high pressures required for containment. The primary advantage of helium is that it can be operated at high temperatures without an absolute need for very high pressures. It is chemically inert. The principal disadvantages of helium relate to its low volumetric heat capacity.

Neutron Multiplier - Beryllium and lead have been most often proposed as neutron multipliers. Concerns have been expressed in past studies about beryllium's toxicity, its resource usage rate for commercial reactors, and radiation damage. Lead is an excellent multiplier of neutrons, has no resource or radiation damage concerns and only minor toxicity concerns, but its low melting point (327°C) and the relatively low temperature limit, imposed by corrosion considerations, at the interface between liquid lead and structural material are major drawbacks for this application. The combination of these limitations and the relatively high threshold for the (n,2n) reaction (about 6.8 MeV compared to ~ 1.8 MeV for beryllium) result in a lower tritium breeding potential with lead, as compared to beryllium, in most blanket designs. Since beryllium's use in solid breeder power reactor blankets has been previously studied in some depth, the project elected to examine a blanket concept using lead neutron multiplier with a ternary oxide solid breeder. The objective of studying lead is to establish whether an attractive alternative to beryllium as a neutron multiplier exists. Pressurized water was selected as the coolant. The possible benefits to the concept of using Li_2O instead of the ternary oxide, and of using helium coolant instead of water, may be evaluated later if considered appropriate.

Structure - The structural material considered thus far for these concepts is PCA (Prime Candidate Alloy) austenitic stainless steel, which is basically a titanium-modified Type 316 steel. Ferritic steels (principally HT-9 alloy) and vanadium alloys (principally V-15Cr-5Ti) will be examined later.

All three concepts use in-situ recovery of tritium by circulating helium purge gas through the blanket breeder zone. Other tritium recovery methods, such as breeder recirculation or batch recovery, were evaluated as part of the Alternative Concepts Screening task (Chapter X).

II.9.2 Performance and Lifetime Evaluation

Issues of generic importance to the performance and lifetime of solid breeder blankets include solid breeder physical integrity, thermal conductance between solid breeder and structural material, and the irradiation behavior (i.e., sintering, grain growth, creep and swelling) of solid breeders. Analytical results were determined for physical integrity (Sec. IX.2.1) and thermal conductance (Sec. IX.2.2). The evaluation of solid breeder configuration/confinement requirements (Sec. IX.2.3) is germane to all three blanket concepts, and specifically provides a basis for selecting the reference and backup designs for the Li_2O/H_2O concept.

Solid Breeder Physical Integrity - Previous thermal stress analysis for the DEMO blanket design showed that with a monolithic Li_2O solid breeder block, the temperature-gradient induced thermal stresses can reach very high magnitudes, well beyond the estimated solid-breeder fracture strength. The analysis also showed that for thin disc geometry (instead of a long cylinder), thermal stresses can be reduced somewhat, but the propensity for cracking is still very high. Cracking and any resulting cracked fragment relocation will create problems in controlling the gap between solid breeder and coolant tube. Therefore, design solutions have been proposed that entail breeder segmentation both axially (planes normal to the direction of coolant flow) and radially (planes which include from the tube axis). Depending on the degree of segmentation, solid-breeder cracking, in principle, can be avoided, but fabrication may represent a difficult task.

A one-dimensional, first order method for thermal stress analysis of Li_2O solid breeder in plate or beam geometry was developed. Equations were developed which provide the two criteria necessary for sizing the breeder plate or beam thickness: (1) $T_{max} - T_{min} \leq$ allowable ΔT; (2) maximum tensile principal stress $\leq$ fracture stress (σ_f). These equations were used to estimate Li_2O solid-breeder plate and beam thickness requirements established from the temperature window (ΔT) and fracture strength constraints (see Table II.9-1). Of these two criteria, the fracture strength (σ_f) criterion always results in a smaller half-thickness (h) than does the temperature window (ΔT) criterion. To avoid cracking, the plate or beam thickness should be determined from the σ_f criterion, which, if satisfied, automatically satisfies the temperature window constraint.

TABLE II.9-1 PLATE- AND BEAM-TYPE SOLID BREEDER HALF-THICKNESS (h) REQUIREMENTS

Criterion	Half-thickness, h (cm) Region[a]		
	1	2	3
ΔT (T_{max}-T_{min}) $\leq$ 390°C	0.73	1.45	3.64
Max. tensile stress (plate) $\leq \sigma_f$ (23.7 MPa)	0.15	0.30	0.74
Max. tensile stress (beam) $\leq \sigma_f$ (23.7 MPa)	0.17	0.34	0.85

[a]Nuclear heating: Region 1, $Q = Q_{max}$ = 59 W/cc; Region 2, $Q = 0.25\ Q_{max}$; Region 3, $Q = 0.04\ Q_{max}$.

Thermal Conductance - Thermal Conductance (h_I) across the solid breeder/structural materials interface is a key issue in the development of solid breeder blanket technology. Previous analyses showed that the sensitivities of the solid breeder temperatures to variations in h_I and other parameters (e.g., solid breeder thermal conductivity, neutron wall load) are comparable, but the uncertainty range (in percent) of h_I may be considerably larger than for other parameters. The interface between solid breeder and structural materials can be classified into two broad categories: (1) a gap (vacuum or gas-filled), of width d ranging from sintered breeder surface roughness values to $\geq$ 1 mm; and (2) a solid material, which may be metallurgically bonded to the solid breeder and structure.

A general approach to the overall conductance problem for a gap interface was developed (Sec. IX.2.2) based on theoretical considerations. The bulk of the analysis has been for gas-phase conductance only; radiation transport and solid-solid contact will be treated in the future. A theoretical equation was determined for helium gas thermal conductivity as a function of temperature. The results for 1-atm pressure were compared to a correlation derived from experimental data, with good agreement indicated over the interface temperature range (573 - 773 K) of interest.

The gas phase conductance equations were solved for d = 1 to 4 mm. For the same heat flux (q") at the solid breeder surface, the temperature drop (ΔT) will double for doubling gap size according to $\Delta T = q"/h_g$. Assuming the coolant conditions remain the same, the solid breeder temperature must

increase substantially. The other extreme case for h_g occurs when d is very small, of the order of breeder surface roughness ($d = 10^{-7}$ m). The calculation results show that h_g is a factor of roughly 10x to 40x higher than for d = 1 to 4 mm. The implication for blanket design is that the interface ΔT, and its uncertainty range, are greatly reduced for a given set of conditions if close breeder/structure contact is maintained, as compared to gap widths $\gtrsim$ 0.1 mm.

Solid Breeder Configuration/Confinement - The differences in the breeder-outside-tube (BOT) and breeder-in-tube (BIT) approaches (Fig. II.9-1) to breeder configuration were evaluated. Breeder temperature control for the BOT is of relatively far greater concern than for the BIT. Numerous factors will operate to change the gap distance in the BOT approach. The deformation processes not related to radiation effects are driven by solid breeder temperature and stress, and thus are of an iterative nature, requiring continuous tracking of the two surfaces. Additional complicating phenomena are cracked fragment relocation, asymmetric gaps, and development of breeder crack surfaces normal to the radial heat flow direction.

Several potential methods to alleviate these problems were reviewed. Segmentation of the breeder is the equivalent of pre-cracking, so that the thermal gradient is insufficient to cause further cracking. This approach also implies other breeder forms, such as the sphere-pac configuration. For sphere-pac, the interface conductance variation is potentially much less than for the breeder segment approach, and an effective (bulk) breeder thermal conductivity should be adequate in determining solid breeder temperatures. A solid material interface, metallurgically bonded to the solid breeder and structure, could virtually eliminate interface conductance uncertainties during operation if the bond stayed intact. However, braze tests conducted at McDonnell Douglas using metallic felt and Ti-Cu-Ag brazing material indicate that, although the bond itself survives the cooldown phase from braze temperatures, the Li_2O test pellets developed cracks both parallel and near parallel to the interface. Dispersion toughening of the breeder, by introducing second-phase materials such as BeO to increase toughness (or reduce brittleness) of the breeder, is a method established in ceramic engineering. However, little or no work in this area has been done to date using solid breeders.

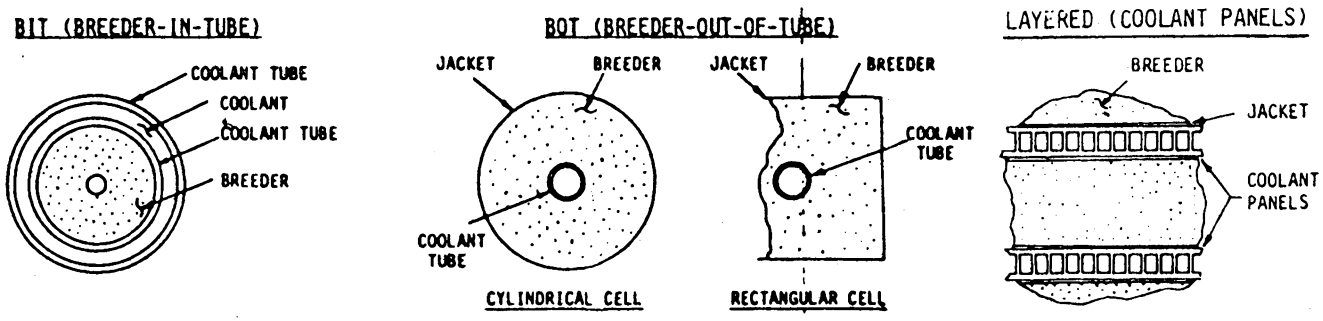

Figure II.9-1. Blanket design approaches selected for evaluation.

Among these three alternatives, the sphere-pac configuration appears most attractive and has been chosen as the reference solid breeder configuration for the Li_2O/H_2O system. The sintered beam-type solid breeder is suitable for the backup design of the Li_2O/H_2O coolant panel concept, and has been chosen as the reference configuration for the Li_2O/He concept.

II.9.3 Li_2O/H_2O Blanket Concept

The development of the design approach for this concept used the major conclusions from recent blanket studies as a starting point. Three basic approaches to blanket general arrangement were considered: (1) BOT (breeder-outside-tube), (2) BIT (breeder-in-tube), (3) layered (breeder between flat coolant panels). These approaches were evaluated from the standpoints of mechanical and structural design, fabrication, thermal-hydraulics requirements, and neutronics.

The preliminary reference design for the blanket concept has adopted the BOT approach for the breeder zone, and the sphere-pac approach for Li_2O fabrication. This is a significant departure from previous designs (e.g., STARFIRE, DEMO) which used the sintered product form for the breeder. A second major difference is the first wall design, which uses a welded coolant panel with flat skins joined by vertical ribs to form rectangular-cross-section coolant channels, whereas STARFIRE and DEMO used corrugated panels with channels die-stamped into the skins.

Conclusions from Previous Studies - The results of previous design studies for water cooled solid breeder blankets have led to a number of important major conclusions, which were used as a starting point for the present work. These conclusions are briefly summarized below:

- Maintenance: Use sector-removal-and-replacement; no in-situ repairs.
- Tritium recovery: In-situ via helium purge gas.
- Water coolant conditions: ~ Same as LWR's.
- Coolant containment: In small-cross-section flow passages.
- Coolant flow direction: Primarily toroidal or poloidal through breeder zone, not radial.
- First wall/blanket integration: Full structural/mechanical integration is strongly preferred.

Evaluation and Comparison of Design Approaches - The major differences among the BOT, BIT and layered approaches to breeding zone arrangement (Fig. II.9-1) affecting the design approach selection are briefly discussed below.

The BIT approach is presently considered not acceptable for use with high-pressure water coolant on the basis of insufficient tritium breeding (less than unity) without the use of a neutron multiplier. This results primarily from the high volume fractions of neutron-absorbing steel for the relatively thick tubes needed to contain the high-pressure water coolant. The BIT approach was therefore not considered further in the comparison.

Tritium Breeding is one of the two most important engineering feasibility evaluation criteria (Section II.3). One-dimensional neutronics analyses indicated that the BOT approach should yield a tritium breeding ratio approximately the same as for the layered approach, i.e., ~ 1.15. The same relative results may also be expected if a beryllium neutron multiplier is added.

Reliability of water-cooled blankets against leaks that result in reactor shutdown is expected to receive major emphasis in the study as the designs are developed further. For the BOT approach, double wall tubes can be used inside the breeder zone, with the ends independently welded at or behind the rear wall such that both pressure boundaries at any given tube must be breached before water/breeder contact can occur. However, similarly providing two barriers at the welded panel/plenum joints for the layered approach could be very difficult.

The major difference in Accident Safety is that the BOT approach permits the incorporation of dual independent coolant loops for the first wall and blanket, to enable safe removal of afterheat from all blanket sectors in the event of a shutdown due to a failure in one of the loops. To incorporate two loops into the layered design would be very difficult; an emergency cooling system would likely be the preferred option.

The Blanket Fabrication complexities for the BOT approach are judged to be less than for the layered approach, mainly because the end plenums and their connections to the first wall and blanket panels are eliminated. The principal complication for the coolant tubes is the welding of the tube ends to the manifold. The use of the sphere-pac breeder fabrication approach will greatly simplify the final blanket assembly for either approach.

The selected approach should preferably have the Design Flexibility to accommodate changes in the blanket concept itself or in design details without requiring major modification. The two most important possible changes to the Li_2O/H_2O blanket reference design would be (1) use of the sintered product breeder instead of the sphere-pac approach, and (2) the addition of a slab-type beryllium neutron multiplier. The layered approach can accept either or both changes with relatively small impact. The re-adoption of the sintered product breeder fabrication approach for this concept would likely require major changes to the BOT approach, however, to assure acceptable breeder/tube interface heat transfer characteristics.

The principal Development Risk for the BOT approach is considered to be the difficulties involved with incorporation of the sintered product breeder, if the sphere-pac approach to Li_2O fabrication does not prove to be workable. For the layered approach, development of highly reliable plenum/panel seals and weld methods is the area of most concern.

The BOT approach was selected for the Li_2O/H_2O concept reference design, on the basis of its relative advantages over the layered approach when coupled with the sphere-pac breeder fabrication method. The layered approach is presently considered a back-up option.

Reference Design Description - The preliminary reference design for the Li_2O/H_2O blanket concept is illustrated schematically in Fig. II.9-2. Key features and major parameters are listed in Table II.9-2.

The blanket design uses individual first-wall/blanket modules, configured as parallelepipeds. These modules are assembled into ten blanket sectors. The first wall is an actively cooled ribbed panel made of PCA. Three millimeters of steel are added to the plasma-facing side of the panel as an erosion allowance, permitting a 3-year life at the assumed 1 mm/y erosion rate. (This is approximately the same as the 3-year PCA first wall life anticipated on the basis of radiation-induced swelling (T ~ 400°C). Over 5 mm of erosion thickness can actually be applied, for the nominal 50 W/cm^2 surface heat flux.) The first wall is mechanically and structurally integrated with the blanket. Actively cooled support frames within the breeding zone are welded to the back side of the first wall and to the rear wall of the breeding zone to provide structural rigidity to the module.

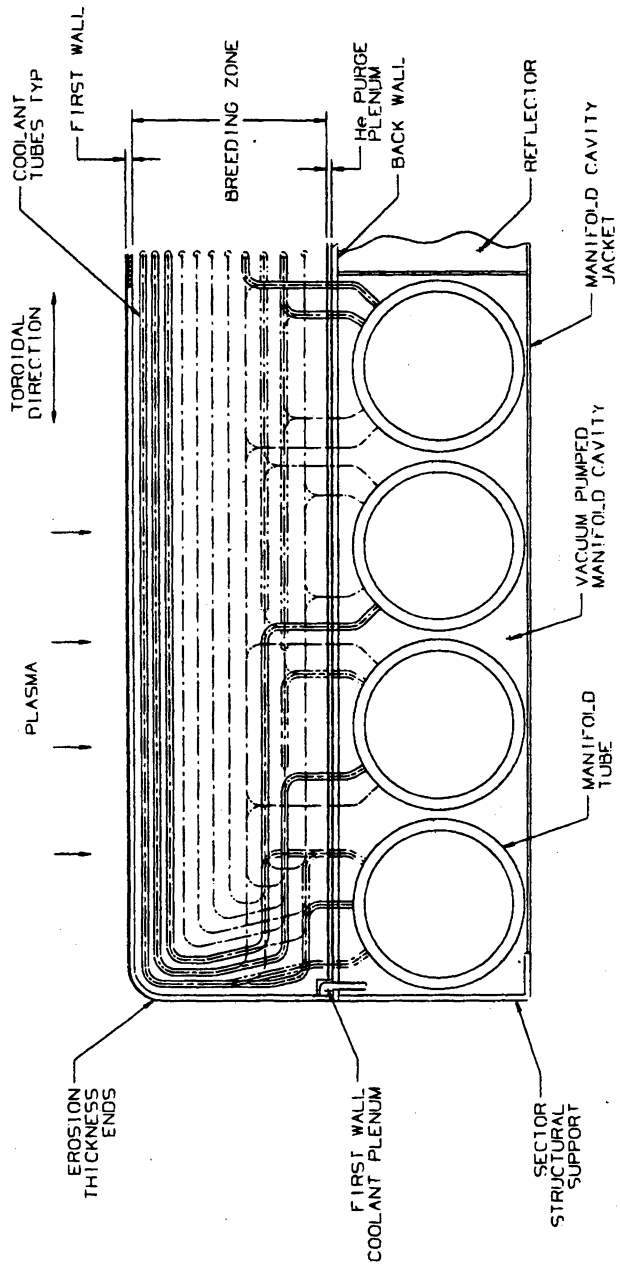

Figure II.9-2. Li_2O/H_2O blanket concept preliminary reference design.

TABLE II.9-2. KEY FEATURES AND MAJOR PARAMETERS FOR Li_2O/H_2O BLANKET REFERENCE DESIGN

Parameter	Value
• Materials	
- Coolant	H_2O
- Breeder	Li_2O
- Neutron Multiplier	(none)
- Structure	PCA Aust. St. Stl.
- Purge Gas	Helium
• First Wall:	
- Coolant panel with rectangular-cross-section channels - Cools part of Li_2O Breeder	
- Fully integrated with blanket	
- Maximum surface temperature	550°C
- Maximum structural thickness	8.9 mm
- Erosion thickness allowance	3.0 mm
- Erosion life at 1 mm/y erosion rate	3.0 y
• Breeder Zone:	
- Li_2O breeder fabricated with sphere-pac method	
- U-bend Coolant Tubes, flow in toroidal direction	
- Coolant Inlet/Outlet temperature	280/320°C
- Coolant pressure	15.2 MPa
- Breeder minimum/maximum temperature	410/800°C
- Purge Gas Pressure	0.1 MPa
• Tritium Breeding Ratio	~ 1.10[a]

[a]3-D Monte Carlo analysis, assuming water cooled outboard belt limiter and rf waveguides.

The Li_2O sphere-pac breeder is contained by the six sides of the module. The toroidally-oriented coolant tubes in the breeder zone are arrayed in banks; each tube makes a single pass through the breeder. Each tube is fabricated from seamless PCA tubing in the cold worked (CW) condition. Inside diameter is 10 mm for each tube, and wall thickness is 0.75 mm. Tube spacing radially and poloidally through the breeding zone is graded in proportion to the local nuclear heating rate, to maintain the Li_2O breeder within the design basis minimum and maximum temperature limits of 410°C and 800°C respectively at all points for normal operating conditions. For each tube, coolant

temperature is increased from 280°C at the inlet to 320°C at the outlet by orificing at the tube entrances to produce the proper flow rate/flow velocity combination. The breeder coolant tubes are U-shaped and terminate in the inlet and outlet manifolds located immediately behind the back wall. A double weld method is proposed for the the tube ends which should sharply increase the reliability of the blanket against water leaks into the breeder.

The tubular manifolds connect all modules within a sector. The present manifold scheme uses four inlet and outlet manifolds, two of each for each of the two separate cooling circuits. The first wall and all even-numbered coolant tube banks are connected to the first circuit; the first coolant tube bank and all other odd-numbered banks are connected to the second circuit. For the inboard blanket, the large manifold tubes end in headers behind the modules above and below the vertical inboard module. The coolant tubes in this module extend through it vertically (poloidally) and terminate in the manifold headers. Thus there are no large-diameter manifold tubes in the inboard module, sharply reducing the inboard wall/blanket/shield thickness which results in very significant capital cost savings for the reactor. Helium purge gas is used to remove tritium from the breeder zone.

Key Issues and Concerns - The work thus far has indicated a number of key issues and areas where significant concern exists regarding the eventual success of the Li_2O/H_2O concept development; these are listed in Table II.9-3.

The ribbed panel first wall design requires further analysis to determine the effects of radiation, primarily creep and swelling. Design detail options to accommodate these effects without degrading blanket performance must be investigated. Methods to increase reliability against leaks in the breeding zone will be pursued, including the use of double wall tubes and double welded tube ends at the rear wall. The key area of the behavior of sphere-pac Li_2O will be pursued, principally as part of the Solid Breeder Tritium Recovery Issues task. Reducing the thickness of the manifold zone can result in possible economic (capital cost) advantages, if the use of thinner blankets leads to a reduced reactor envelope. Manifolds with rectangular flow channels, spanning the rear of each module, could significantly reduce manifold thicknesses compared to tubular manifolds, and will be investigated.

TABLE II.9-3. KEY ISSUES AND CONCERNS FOR Li_2O/H_2O BLANKET CONCEPT

Area	Issue/Concern	Comment
• First Wall	• Reliability against leaks - Basic panel - Panel connections	• Modify to use double skins on both sides • Investigate detail options for connections
	• Irradiation effects	• Find detail options for strain and deformation accommodation
• Breeding Zone	• Reliability against leaks	• Investigate options - Double weld tubes - Double weld tube ends
	• Li_2O sphere-pac - Fabrication - Long term effects	• Continue investigation of sphere-pac fabrication, and behavior under blanket conditions
	• Purge gas flow paths • Accommodation of Be neutron multiplier	
• Manifold	• Thickness requirements	• Evaluate integral rectangular channel option
	• Module removal/replacement	• Investigate options to allow manifold separation/reweld at module interface locations

Conclusions and Recommendations - Some of the most important study conclusions affecting the Li_2O/H_2O concept and the selection of the reference design are summarized in Table III.9-4. The Li_2O/H_2O blanket concept meets all initial screening criteria, and appears to be an attractive choice. It is recommended that this concept be retained for further evaluation and design development during the second year of the project.

TABLE II.9-4. PRELIMINARY STUDY CONCLUSIONS FOR Li_2O/H_2O BLANKET CONCEPT

- Large-scale breeder cracking, if present, will probably result in unacceptably large uncertainties in blanket performance.
- The breeder-in-tube (BIT) approach results in an unacceptable TBR. With a neutron multiplier, TBR is perhaps acceptable but is probably high-risk.
- Tritium breeding ratios for the BOT and layered approaches are estimated as follows:

Approach	Without Multiplier	With Be Multiplier
BOT	~ 1.10-1.15	>> 1.20
Layered	~ 1.10-1.15	>> 1.20

- Coolant panels with rectangular cross section channels are feasible for first wall and breeder zone applications, and meet non-irradiated stress criteria.
- The sphere-pac breeder fabrication method is attractive for the BOT and layered blanket design approaches. The sintered product breeder fabrication approach is less attractive for the layered approach, and leads to major design difficulties for the BOT approach in assuring desired breeder/structure interface characteristics.

II.9.4 Li_2O/He Blanket Concept

The task of selecting and evaluating a helium-cooled, Li_2O breeder blanket design was performed in three phases. Phase 1 was to review existing blanket designs applicable to helium-cooled solid breeder blankets and to make design selections based upon design approaches and configurations. In Phase 2, technical evaluations were performed on the selected designs by identifying and considering critical issues with the aim of selecting a reference blanket design. Conceptual design of the selected blanket approach was then performed in Phase 3. First wall, mechanical, breeder element, thermal hydraulics, and neutronics design aspects were considered, as well as blanket tritium handling and safety-related issues.

Blanket Concepts Evaluation and Selection - Twenty existing blanket designs were reviewed and grouped into four general classifications. The design advantages for a canister design were determined to be covered by the other blanket concepts. In addition, the potential reliability against leaks of large number of joints and connections could be a problem for pressurized module designs. The pressurized tubular module was judged less attractive

than the pressurized lobular module on the basis of design complexity and reduced neutronics performance. The pressurized breeder-outside-tube design was judged to have a potential availability problem because of possible high failure rates resulting from the large number of tubes. Thus, major efforts were devoted to the evaluation and design of the lobular pressurized-module concept and reduced efforts were given to pressurized-tube concepts.

Reference Design Description - The present reference Li_2O/He blanket design is illustrated in Fig. II.9-3. Table II.9-5 lists some of the blanket's key features and parameters. An integral first wall is used with full flow of the inlet helium directed to the first wall. The bellows first wall can withstand a surface heat flux of ~ 0.6 MW/m^2 at a neutron wall loading of 5 MW/m^2. A sacrificial layer of 2 mm of PCA is included on the plasma side of the first wall to give a blanket lifetime of two years. The bellows configuration of the first wall is designed to accommodate neutron-induced swelling without creating large stresses, while maintaining a thin structural member with extended (fin-like) heat transfer surfaces.

The helium coolant at 50 atm pressure enters the module at the rear and flows along the module sides to the first wall. The helium then turns and flows radially outward between adjacent Li_2O fuel elements. To achieve the maximum Li_2O density in the blanket, a flat plate fuel element geometry was adopted. Li_2O "pellets" are clad in PCA to form plates. The coolant flows through the 1 mm coolant gaps between the wire-wrapped breeder plates and maintains the Li_2O temperature distribution within its specified temperature limits.

The clad fuel design has three functions. First, the clad contains the solid breeder and minimizes the potential effects of fuel cracking due to thermal stresses or irradiation. Second, it separates the main coolant from the purge helium extraction flow in order to maintain positive control of coolant impurities. Third, it permits a pressure differential between the purge and main coolant streams in order to minimize the effect of contact resistance between the clad and the breeder.

Based upon three-dimensinal Monte Carlo neutronics analyses, the tritium breeding ratio of the 0.7 m thick blanket was calculated to be 1.09. The analysis assumed STARFIRE-type water cooled outboard belt limiter and rf waveguides, as for the Li_2O/H_2O blanket. Net blanket power conversion efficiency was calculated to be 36.5%. Using the experimentally determined activity

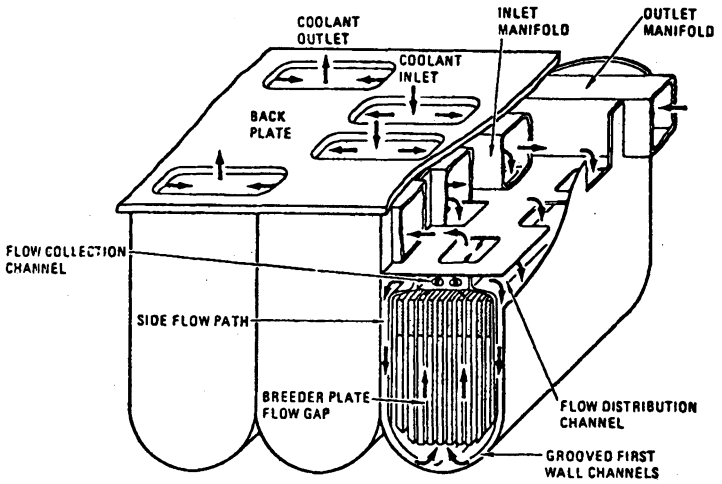

a) Helium coolant flow paths in module and manifold.

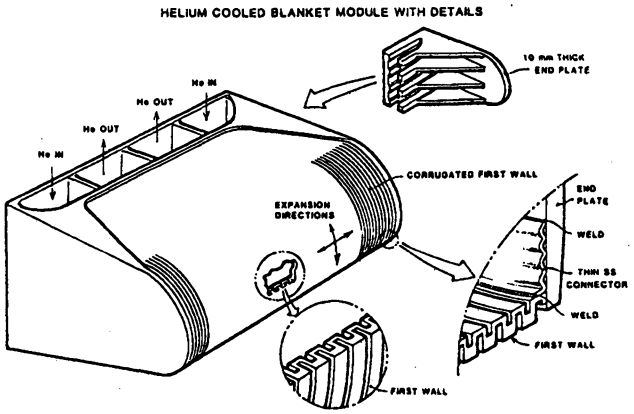

b) Module details.

Figure II.9-3. Li_2O blanket concept reference design.

TABLE II.9-5. KEY FEATURES AND PARAMETERS FOR Li_2O/He BLANKET CONCEPT

• Materials	
- Breeder	Li_2O
- Structure, clad	PCA Austenitic St. Stl.
- Coolant	Gaseous helium (50 atm)
- Purge gas	Gaseous helium (1 atm)
• First Wall	
- Bellows-type; accommodates thermal/mechanical strains & radiation damage	
- Design surface heat flux	0.6 MW/m^2
- Maximum temperature	550°C
- Maximum thickness	9 mm
- Equivalent structural thickness	5 mm
- Erosion thickness allowance	2.0 mm
- Erosion life @ 1 mm/y erosion rate	2 y
• Coolant	
- Inlet/outlet temperature	275°C/500°C
- Inlet pressure	5.1 MPa
- Total pressure drop	122 kPa
• Breeder	
- Clad Li_2O sintered product in plates	
- Plate thickness	17 mm
- Clad thickness	0.25 mm
- Minimum/maximum breeder temperature	508°C/986°C
• Tritium breeding ratio	~ 1.09[a]
• Blanket tritium inventory (estimated)	1.8 kg/GWth

[a] 3-D Monte Carlo analysis, assuming water cooled outboard belt limiter and rf waveguides.

coefficient of T_2O in Li_2O, the normalized blanket tritium inventory was calculated to be 1.8 kg/GW_{th}.

The present design offers numerous inherent safety features. In a depressurization event, the design allows for rapid communication between submodules and can withstand the maximum forces expected without propagation to adjacent units. Under complete loss of cooling events, the blanket offers large heat capacity. Also, the capability exists to circulate the depressurized gas coolant for heat removal during accident conditions and thus prevent module failure. From environmental impact considerations, the thin first wall and low structure volume fractions, together with the low tritium inventory and loss rate, are expected to result in relatively low radioactive waste generation levels.

Key Issues and Concerns - Some of the more important concerns for the present design are listed in Table II.9-6. The majority ultimately relate to economic attractiveness, and the remainder to engineering feasibility. These will be addressed as necessary, as the design is further developed in the second year of the study.

The blanket design approach, presently a pressurized lobular module (pod), was selected--and alternatives rejected--on the assumption that the solid breeder would be a sintered product, with the breeder containment and interface conductance problems asso;ciated with some design approaches (Section II.9.2). The use of the sphere-pac fabrication method may relieve those potential problems, and a reevaluation of the candidate approaches potentially could result in a different choice.

The first wall design approach has a number of advantages for this blanket concept. However, the present study guidelines of a 1 mm/y erosion rate and a 550°C maximum surface temperature for PCA or HT-9 limit the first wall erosion lifetime to 2 y at 0.6 MW/m^2 surface heat flux. At a flux of 1.0 MW/m^2, no erosion allowance is available. Further quantification of first wall capabilities for tokamaks or TMR's is necessary. Optimization of the bellows design for specific conditions is needed. Areas noted in Table II.9-6, such as bellows side wall erosion and effects of grooving the erodable layer, will be investigated.

Thermal-hydraulics concerns for the concept center mainly on the breeding zone and manifolding. The low volumetric heat capacity of helium makes analyses of sensitivity to changes in flow conditions (e.g., flow gap sizes) especially important. The requirements for expansion/contraction zone depths at top and bottom of the breeder plate region will directly affect the blanket thickness requirements. The manifold flow pattern selected for the sector, and the manifold flow passage requirements, will also directly affect blanket thickness. These should be verified and optimized, because of the importance of the inboard blanket thickness in tokamaks.

Conclusion and Recommendation - The Li_2O/He blanket concept meets all initial project screening criteria and appears to be attractive in many areas, particularly those that are safety-related. It is recommended that the concept be carried forward into the second year of the study for further evaluation and design development as well as detailed comparisons with other concepts.

TABLE II.9-6. KEY ISSUES AND CONCERNS TO BE ADDRESSED FOR Li_2O/He BLANKET CONCEPT

Area	Issue/Concern	Comment
Blanket General Design	• Consideration of sphere-pac breeder form as alternate to sintered product	• Sphere-pac may relieve most relative disadvantages of pressurized breeder-in-tube approach
First Wall	• Fabrication effects on strains, material properties	• Stresses built-in during forming may be very high
	• Non-uniform erosion in grooves	
	• Erosion life-time	• Evaluate options to increase allowable erosion thickness
	• Module side/first wall joint	• Demonstrate design details to meet stress limits
	• Time constant for disruptions	• Determine if L/r = 200 ms criteria met
Breeding Zone	• Expansion, contraction regions	• Calculate depth requirements
	• Thermal-hydraulics sensitivity	• Show gap flow uniformity, design sensitivity to gap variations
	• Purge system leaks	• Determine effects of coolant in-leakage on breeder and on purge system reliability
	• Accommodation of Be neutron multiplier	
	• Structural adequacy of thin clad	
Manifolds	• Sector flow pattern and related manifold thickness	• Verify thickness requirements for selected flow pattern

II.9.5 TO/H_2O/Pb Blanket Concept

The purposes of the design feasibility study conducted for this concept are (1) to attempt to determine if water cooled, lead multiplier, ternary oxide (TO) breeder fusion blankets are technologically attractive and if so, (2) to provide enough design definition to adequately compare the resulting blanket with other candidates. The approach has been to address the major issues and to create a design that resolves all of them as nearly as possible, with the intent of providing a basis for comparison with other blanket concepts and for judging the desirability (if not the feasibility) of this blanket. Major design goals are: adequate tritium breeding (full coverage TBR > 1.2), good thermal to electrical conversion (compatible with LWR power cycles), a credible mechanical design, and safe containment of high pressure (2200 psi) water. The issues and the design options examined are discussed below.

Reference Design Description - The basic configuration of the TO/H_2O/Pb blanket is shown schematically in Fig. II.9-4. Some of the major features and parameters are listed in Table II.9-7. The configuration consists of PCA stainless steel pods filled with liquid lead, cooling tubes, and tubes containing $LiAlO_2$ breeder. The front of the pods is screened from the plasma by a row of cooling tubes brazed together to comprise the first wall. The first wall and the half sector configuration shown schematically apply to the tokamak geometry.

The purpose of the pods is to contain the pressure in the event of a coolant tube break or leak. A structure designed to contain only the static pressure of lead (~ 1 MPa) would fail if a tube (~ 15 MPa) leaked, possibly damaging adjacent structures and ejecting missiles which would damage other parts of the structure. A single point failure that could potentially cause failures in other sectors would be very serious. Since high pressure tube failures could occur fairly frequently (as discussed below), catastrophic consequences should be eliminated.

The pods are similar to those conceived in Sections VII.2.1 and IX.4 for helium cooled fusion blankets, but have a smaller nose radius because the pressure is higher for water coolant than for helium coolant. They are constructed of 3 mm thick PCA and are 10 cm wide and 70 cm deep. The length varies around the sector from ~ 1.6 m inboard to ~ 3.5 m outboard. The

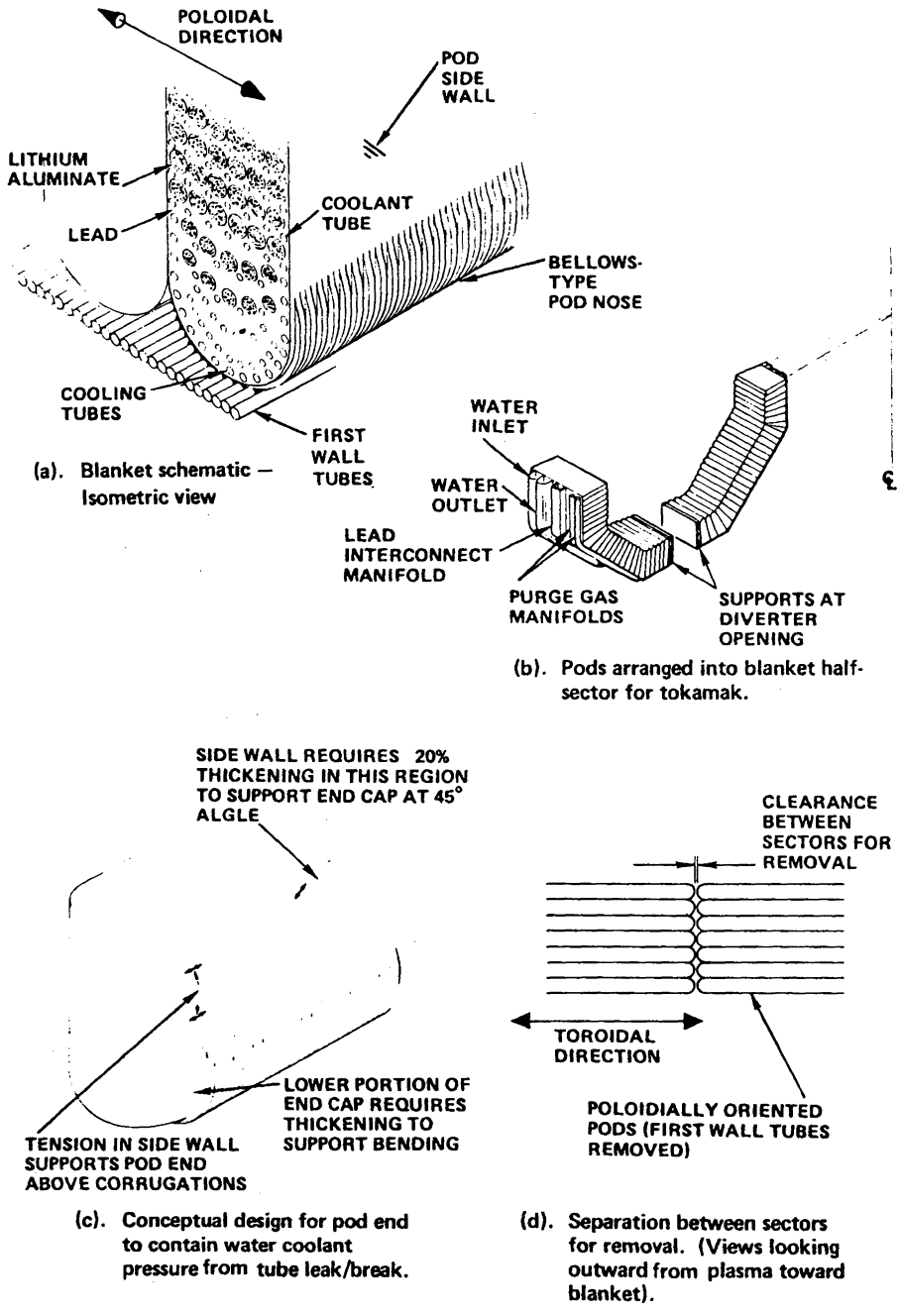

Figure II.9-4. $Pb/LiAlO_2/H_2O$ blanket concept design description.

rounded pod ends form the sector boundaries. The front portion of the pods are corrugated to relieve bending stresses caused by thermal and swelling gradients. Because of these corrugations, extra reinforcement is required at the ends of the pods to contain the pressure and prevent an accordion-like expansion. The pods are balanced across adjacent pod walls. The pods see only the static lead pressure unless a tube failure occurs, and are not intended for reuse after a tube failure. The blanket contains approximately 60,000 separate high pressure tubes.

TABLE II.9-7. KEY FEATURES AND PARAMETERS FOR TO/H_2O/Pb BLANKET CONCEPT

• Materials	
- Breeder	γ-$LiAlO_2$
- Structure	PCA Aust. St. Stl.
- Coolant	H_2O
- Purge gas	Helium (~ 1 atm)
• First Wall	
- Coolant tubes brazed together side-by-side (conceptual)	
• Blanket Module	
- Pod design; bellows-type first wall; 10-cm nose radius; lead-filled	
- Liquid lead manifolded among pods	
• Breeding Zone	
- Coolant contained in 1-cm-dia. tubes, 0.5 mm walls	
- Breeder contained in 1.5-cm-dia. tubes	
- Coolant inlet/outlet temperature	300/320°C
- Coolant pressure	14.9 MPa
- Coolant maximum velocity	8.4 m/s
- Maximum lead/PCA interface temperature (corrosion-limited)	450°C
- Breeder minimum/maximum temperature	320/755°C
- Lead minimum/maximum temperature	300/450°C
• Tritium breeding ratio (2-D, 100% coverage)	~ 1.22

The U-shaped cooling tubes are routed toward the first wall from the back of the blanket, along the forward portion of the blanket for a distance of 1 to 2 m and back out of the blanket, or along a back portion of the blanket and then out, depending on the heat deposition near the particular tube. The $LiAlO_2$-filled tubes are also U-shaped, with the ends connected at the pod rear wall to the helium purge gas plenum.

Heat transfer and thermal hydraulics analyses have been performed to determine tube spacing, film drop temperatures and maximum and minimum temperatures in the lead, lithium aluminate, and structure. The maximum heat generation rate in the lithium aluminate is 170 W/cm^3, and the resulting maximum centerline temperature is 755°C. The pumping power at the 8.4 m/s operating velocity is approximately 0.5% of the blanket energy. A fluid Δt higher than the current 20°C would allow proportionally longer tubes or slower velocity and lower pumping power, but difficulties with freezing lead would become more severe and no great benefits are apparent. Lead freeze up must be prevented by the operator during shutdowns to avoid damage to the blanket.

Possible water coolant inlet and outlet temperatures are restricted by thermal to electric conversion efficiency, the lead melting point (327°C) and the critical point of water (374°C). Two possible inlet/outlet temperature combinations were examined: 330-350°C and 300-320°C. The higher temperature (330-350°C) operating point has the advantage of keeping all the lead in the blanket molten during operation. The major disadvantages are higher temperatures (480°C steel/lead interface) and much higher pressure (21.3 MPa) versus 14.4 MPa for the 320°C outlet temperature). The major advantages of the lower pressure are thinner pods and lower cooling tube stresses.

Operational difficulties, caused by the necessity of preventing solidification of the lead, appear to be generic to the combination of lead and water. The higher temperature operating point (330-350°C) avoids the necessity of raising the coolant temperature at shut down, but operator action is required to make sure that flow rates are reduced at the steam generators or the coolant temperature will drop rapidly. The lower temperature operating point was chosen as the baseline because of the advantages of lower pressure.

One- and two-dimensional neutronics analyses were performed to establish the TBR. The two-dimensional analyses, performed using the TARTNP Monte Carlo code, give results which when reduced to a full coverage case are considered

to produce a minimum TBR of 1.22. The addition of 2 mm of erodable steel to the first wall surface would reduce the TBR by about 0.01.

Key Issues and Concerns - The four most important issues for this concept are liquid metal embrittlement, corrosion of the structure by molten lead, the choice of structural material, and tube reliability. The first three relate to the low melting point of lead (327°C) and the range of feasible operating temperatures possible with water coolant (~ 280-350°C).

Liquid metal embrittlement (LME) of the PCA structure by lead is a major issue in this design. Water temperatures must be in the vicinity of the 327°C melting point of lead. The point of minimum ductility for steels subject to LME occurs near the melting point of the liquid metal. Experiments are required to determine whether PCA is significantly embrittled by lead at temperatures of interest. Corrosion of PCA by liquid lead at the 450°C maximum interface temperature may require corrosion inhibitors in the lead or coatings on the steel. Ferritics such as HT-9 are more corrosion resistant, but the ductile to brittle transition temperature of irradiated ferritic steels could be in the range of the operating temperature at the 300°C water inlet temperature. Reliability of the ~ 60,000 coolant tubes against leaks may be a serious concern because of the potential impact on availability.

Conclusions - Several issues exist for the TO/H_2O/Pb concept compared with other mainline blanket concepts, most of which arise from the lead-water combination. Using another coolant such as HTS molten salt or helium could eliminate problems with LME, lead freezing, and high coolant pressure, and should result in a higher TBR. Corrosion of the structure by liquid lead may limit the upper temperatures regardless of the coolant, but corrosion in this static system should be controllable.

On balance, it is recommended that this concept be pursued further only if no other water cooled solid breeder design looks better and the study wishes to retain a water cooled option.

II.10 Concept Ranking System Status

As discussed in section II.3 a detailed comparative evaluation methodology has been developed and will be used during the second year of the study to systematically evaluate, compare and rank the blanket concepts

selected during the first year of the study. A brief description of the procedure is given below followed by the status of concept ranking as of September 1983.

Blankets selected for detailed comparison will be evaluated and assigned a figure of merit for each of the following four areas:

a) Safety and Environment
b) Economics
c) Engineering Feasibility
d) R&D Requirements.

The methodology to derive a figure of merit in each of these four areas is described in Section II.3 and Chapter III. Based on the ranking in these four areas, a judgement will be made on the final overall ranking of the concepts. This procedure will be used to place concepts in one of the three categories described in Table II.10-1. The number of concepts ranked M=1 at the end of the study will be limited (~ 3-4), in keeping with the study objectives outlined in Chapter I.

TABLE II.10-1. CONCEPT RANKING SYSTEM TO BE USED AT THE STUDY'S COMPLETION

M = 1	Potentially Attractive Recommended for the highest R&D priority.
M = 2	Set Aside for Future Consideration R&D priority is lower than for the concepts in the M=1 category.
M = 3	Reject

Within each of the above M categories, little incentive is foreseen for further ranking of the concepts themselves. However, ranking the R&D items is considered very important and is planned. R&D items to resolve issues for blanket concepts within the M=1 category will be in the highest priority category. For equally important R&D issues, higher priority will be given to those that require minimum cost and short time.

As mentioned earlier, it was not possible to apply the detailed comparison methodology to the very large number of blanket concepts considered during FY 1983. Therefore, a less rigorous methodology was used to classify concepts into a (temporary) ranking status (R) system. This R classification is described in Table II.10-2. Concepts considered during FY 1983 have been classified into one of the following R categories: 1, 2A, 2B and 3. Concepts in the R=1 category are promising candidates for inclusion in the M=1 category at the end of the study. There are numerically more concepts presently categorized R=1 than will be finally included in the M=1 category. Other concepts now being evaluated may also be classified in the R=1 category. During the second year of the study, detailed comparative evaluation will be performed for all blanket concepts within the R=1 category. The results of this detailed comparative evaluation will be used to select those potentially attractive concepts that will be included in the M=1 category at the end of the study. The remaining concepts from the R=1 category will be included in the M=2 (set aside for future consideration) category.

Some concepts have been rejected during the FY 1983 effort and have been assigned an R=3 category. Unless drastically different new findings (probably only new experimental results) are obtained during FY 1984, these concepts will be classified in the M=3 (reject) category without further work.

Those blanket concepts considered during FY 1983 which did not appear attractive enough for the R=1 category and which did not have sufficiently serious critical problems to be included in the R=3 category are included in the R=2A or 2B categories. Concepts in both the R=2A or 2B categories are candidates for inclusion in the M=2 category at the end of the study. There are some differences, however, between the R=2A and 2B categories. Concepts in the R=2A category have no identified critical problems but they are judged to be less attractive than those concepts presently in the R=1 (attractive) category. Further work on the R=2A concepts will be limited to addressing

TABLE II.10-2. DEFINITION OF THE RANKING SYSTEM USED IN TABLES II.10-3 AND II.10-4

R = 1	Potentially Attractive Candidate for the final BCSS M=1 category Continue development Include in the detailed comparison evaluation
R = 2A	No identified critical problems. However, the concept appears less attractive than some other concept(s). Further work in BCSS will be limited to addressing only key issues for the concept. It may be elevated to category R=1 if resolution of key issues on the concept improves its performance or other concepts in R=1 category become less attractive. Otherwise, the concept will be placed in the final BCSS M=2 category.
R = 2B	Candidate for the final BCSS M=2 (set aside) category. Concept has potentially serious problems that cannot be resolved during the study, or the concept is clearly much less attractive than other concepts. Concept not likely to be considered again in the project.
R = 3	Candidate for the final BCSS M=3 (reject) category.
NY	Evaluation incomplete. Ranking will be developed soon.

only key issues. A concept in the R=2A category may be elevated to category R=1 if resolution of key issues improves its performance or if other concepts in the R=1 category become less attractive. Otherwise, the concept will be placed in the M=2 category. Concepts in the R=2B category either have potentially serious problems that cannot be resolved during the study, or they are clearly less attractive than other concepts. The R=2B concepts are not likely to be considered again in the project, and hence they are likely to be placed in the M=2 (set aside) category at the end of the study.

The evaluation of some blanket concepts is still in progress and the results obtained to-date are not sufficient to assign the concepts to an R category. These concepts are designated in the ranking system by R=NY. Many

of the concepts in this R=NY category are based on a molten salt coolant. All molten salt concepts were treated early in the study as only alternative concepts. However, the results of the alternative concept screening task suggested evaluating blanket concepts based on the molten salt coolant option as mainline. This evaluation is now in progress.

Tables II.10-3 and II.10-4 provide the present R ranking category for each of the blanket concepts considered during FY 1983.A brief oversimplified summary of the bases for the current rankings of the various blanket concepts is given in Table II.10-5.

TABLE II.10-3. STATUS OF TEMPORARY RANKING SYSTEM (SEPTEMBER 1983) FOR LIQUID METAL BLANKET CONCEPTS

Concept	PCA	Ferritics	Vanadium
A. Outboard Blanket Same as Inboard			
Li/Li	1	NY	1
LiPb/LiPb	3	NY	1
Li/H_2O	3	3	3
Li/He	2B	NY	2B
Li/Na	3	3	3
Li/HTS	3	3	3
$LiPb/H_2O$	2B	2A	2A
LiPb/He	2B	NY	2B
LiPb/Na	3	3	3
LiPb/HTS	NY	NY	NY
B. LM Outboard Blanket Different Inboard Blanket			
All Concepts	NY	NY	NY
C. Either A or B but using more than one structural material in the same blanket: Evaluation Not Complete (NY)			

TABLE II.10-4. STATUS OF TEMPORARY RANKING SYSTEM (SEPTEMBER 1983) FOR SOLID BREEDER BLANKET CONCEPTS

Concept	PCA	Ferritics	Vanadium
Li_2O/H_2O	1	NY	2A
Li_2O/He	1	NY	2B
[a]Li_2O/HTS	NY	NY	NY
Li_2O/H_2O/Be	2A	NY	2A
Li_2O/He/Be	2A	NY	2B
[a]Li_8ZrO_6/H_2O	2A	NY	2A
[a]Li_8ZrO_6/He	2A	NY	2B
Li_2O/H_2O/Pb	2B	2B	2B
Li_2O/He/Pb	2A	NY	2B
Li_2O/HTS/Pb	2A	NY	NY
Ternary Ceramics (TC) with all coolants and no multiplier	3	3	3
TC/H_2O/Be	2A	NY	2A
TC/He/Be	2A	NY	2B
TC/HTS/Be	NY	NY	NY
TC/H_2O/Pb	2B	2B	2B
TC/He/Pb	2A	NY	2B
TC/HTS/Pb	NY	NY	NY

[a]With and without beryllium.

TABLE II.10-5. BRIEF (OVERSIMPLIFIED) SUMMARY OF PRIMARY REASONS FOR PRESENT RANKING OF BLANKET CONCEPTS

LiPb/LiPb/PCA (R=3, Reject)

- Unacceptable stresses due to large MHD pressure drop. This is a consequence of the allowable coolant temperature rise being too narrow (~ 100°C or more lower than for Li/PCA, Li/V, LiPb/V).
  - Maximum Coolant Temperature Limit
    Interface corrosion limit: 370-400°C
    (Corrosion limit is ~ 50°C lower than for PCA/Li, and > 200°C lower than for LiPb/V or Li/V)
  - Minimum Coolant Temperature Limit
    Melting point ~ 235°C
    (compared to 181°C for Li)
  - Maximum ΔT is ~ 90°C to 120°C
    (compared to 150°C) for Li)
    Increase in coolant velocity eliminates the narrow margin obtained with Li/PCA
- Significantly inferior to Li/PCA, Li/V, LiPb/V

Li/H_2O and Li/HTS (R=3, Reject)

- Relatively high likelihood of and potentially serious consequences from lithium reactivity with water and HTS.

LiPb/Na and Li/Na (R=3, Reject)

- Unacceptable stresses due to very large pressure drop
  - ~ 5-10 times that of self-cooled Li or LiPb
  - Heat capacity of Na requires twice the volumetric flow rate for equivalent heat removal
  - Coolant is restricted to 20% of blanket volume (tritium breeding consideration), therefore Na coolant velocity is ~ 5 times higher
- Na is not substantially different from Li from safety standpoint with the exception of very high activation of Na (^{22}Na and ^{24}Na)

TABLE II.10-5. BRIEF (OVERSIMPLIFIED) SUMMARY OF PRIMARY REASONS FOR PRESENT RANKING OF BLANKET CONCEPTS (CONTINUED)

All Ternary Ceramics (except Li_8ZrO_6) with all Coolants and no Multiplier (R=3, Reject)

- Maximum obtainable tritium breeding ratio is < 1

$LiPb/H_2O$/PCA (R=2B, Set Aside)

- Low tritium solubility results in high tritium pressure, which leads to high tritium permeation. Problem can be eased if double-walled tubes are used in the blanket, but design complexity and additional temperature gradient make the concept marginal.

- Tritium recovery requires circulation of LiPb at large flow rates to attain acceptable tritium pressure.

- Corrosion temperature limit for PCA/LiPb is low.

Li/He/PCA and LiPb/He/PCA (R=2B, Set Aside)

- Liquid metal/PCA interface temperature limits set by corrosion result in unattractive coolant outlet temperatures.

All Breeders (liquid or solid) with He/V (R=2B, Set Aside)

- The moisture level required in helium ($\leq$ 0.1 ppm) to avoid excessive oxidation of vanadium alloys appears to be extremely difficult to attain economically in practical systems.

All Solid Breeders/H_2O/Pb/All Structural Materials (R=2B)

- The operating temperature of water (~ 320°C) and the melting point of lead (327°C) lead to a number of generic problems. The point of minimum ductility for the structure occurs near the melting point of the liquid metal.

- Freezing of lead and module following shutdown and in pipes during startup and operation will be a major design problem.

- The maximum lead at high temperature is limited by liquid metal/structure corrosion to ~ 450°C.

- The combination of the above problems, the relatively low thermal conductivity of lead, high nuclear heating rate, and high (n, 2n) threshold result in a marginal design.

TABLE II.10-5. BRIEF (OVERSIMPLIFIED) SUMMARY OF PRIMARY REASONS FOR PRESENT RANKING OF BLANKET CONCEPTS (CONTINUED)

$LiPb/H_2O/HT-9$ and $LiPb/H_2O/V$ (R=2A)

- Corrosion temperature limit is ~ 50°C higher with HT-9 and ~ 200°C higher with V than with PCA. Operation temperature problem is substantially reduced (compared to $LiPb/H_2O/PCA$).

- Tritium permeation and recovery problems are as discussed before the $LiPb/H_2O/PCA$ but the design problems are eased by the increase in the allowable interface temperature (e.g., temperature drop penalty in double-walled designs is less critical).

$Li_8ZrO_6/H_2O/PCA$, $Li_8ZrO_6/He/PCA$ (R=2A)

- Attractive features similar to other concepts with Li_2O. Concept is not ranked R=1 because its tritium breeding potential (without multiplier) involves higher risk than with Li_2O.

- Cannot be classified with other ternary ceramics (R=3) because the probability of achieving TBR > 1 is reasonable for Li_8ZrO_6 (but zero for other ternary ceramics).

- Limited data base for Li_8ZrO_6.

- Activation of Zr.

$Li_2O/He/Pb/PCA$, $Li_2O/HTS/Pb/PCA$, $TC/He/Pb/PCA$ (R=2A)

- Relative to similar concepts with water coolant (R=2B).
  - Problem of coolant operating temperature coinciding with melting point of lead is eliminated.

- Coolant maximum temperature is still limited by liquid lead/PCA corrosion considerations.

TABLE II.10-5. BRIEF (OVERSIMPLIFIED) SUMMARY OF PRIMARY REASONS FOR PRESENT RANKING OF BLANKET CONCEPTS (CONTINUED)

$Li_2O/H_2O/V$ (R=2A)

- Attractive but was not given R=1 because:
  - V/H_2O compatibility issue is unresolved
  - Li_2O/V compatibility may also be a problem

$Li_2O/H_2O/Be/PCA$, $Li_2O/He/Be/PCA$ (R=2A)

- Attractive as Li_2O/H_2O and Li_2O/He but concept is not ranked R=1 because of limitations on beryllium resources for long term utilization.

$TC/H_2O/Be/PCA$, TC/He/Be/PCA (R=2A)

- Acceptable and attractive in many respects but concepts are not ranked R=1 because of limitations on beryllium resources for long term utilization.

TABLE OF CONTENTS

CHAPTER 3 - EVALUATION CRITERIA

LIST OF FIGURES FOR CHAPTER III

LIST OF TABLES FOR CHAPTER III

III. EVALUATION CRITERIA

III.1 Introduction

The Blanket Comparison and Selection Study (BCSS) has devoted considerable effort to developing a comparison methodogy and set of evaluation criteria which would facilitate the primary goal of the study, i.e., the selection of a limited number of blanket concepts for further research and development. The evaluation and comparison process was developed as a three stage process as follows:

Stage 1. At the beginning of the study in the fall of 1982, blanket concepts were divided into mainline and alternate concepts. The determination of "mainline" designation was the judgement of the project based on previous fusion reactor and blanket design studies. Figure III.1-1 shows the various categories of mainline concepts which are designated by liquid (Li and LiPb) or solid (Li_2O and ternary oxides) tritium breeding materials, various coolants (self-cooled liquid metals, He and H_2O) and the possible need for a neutron multiplier (M). The reference structural material for the initial phase of the study was PCA. Design and special issue groups were then established to begin a careful evaluation of these mainline concepts. In addition to the mainline concepts, an alternate concept screening group was established to examine all blanket concepts not included in the mainline category (see Chapter X).

Stage 2. In order to provide a set of guidelines for the alternate concept screening process and to provide a framework for the initial evaluation of the mainline concepts, a set of initial screening criteria were established (see Sec. III.2.1). The combined judgement of the BCSS team has been used during the first year of the study to reduce the large number of possible blanket options down to a more limited number that will be evaluated in detail during the second year of the study, i.e., Stage 3.

Stage 3. During FY 1984 Stage 3 will employ four types of ratings (safety and environment, economics, engineering feasibility, and R&D require-

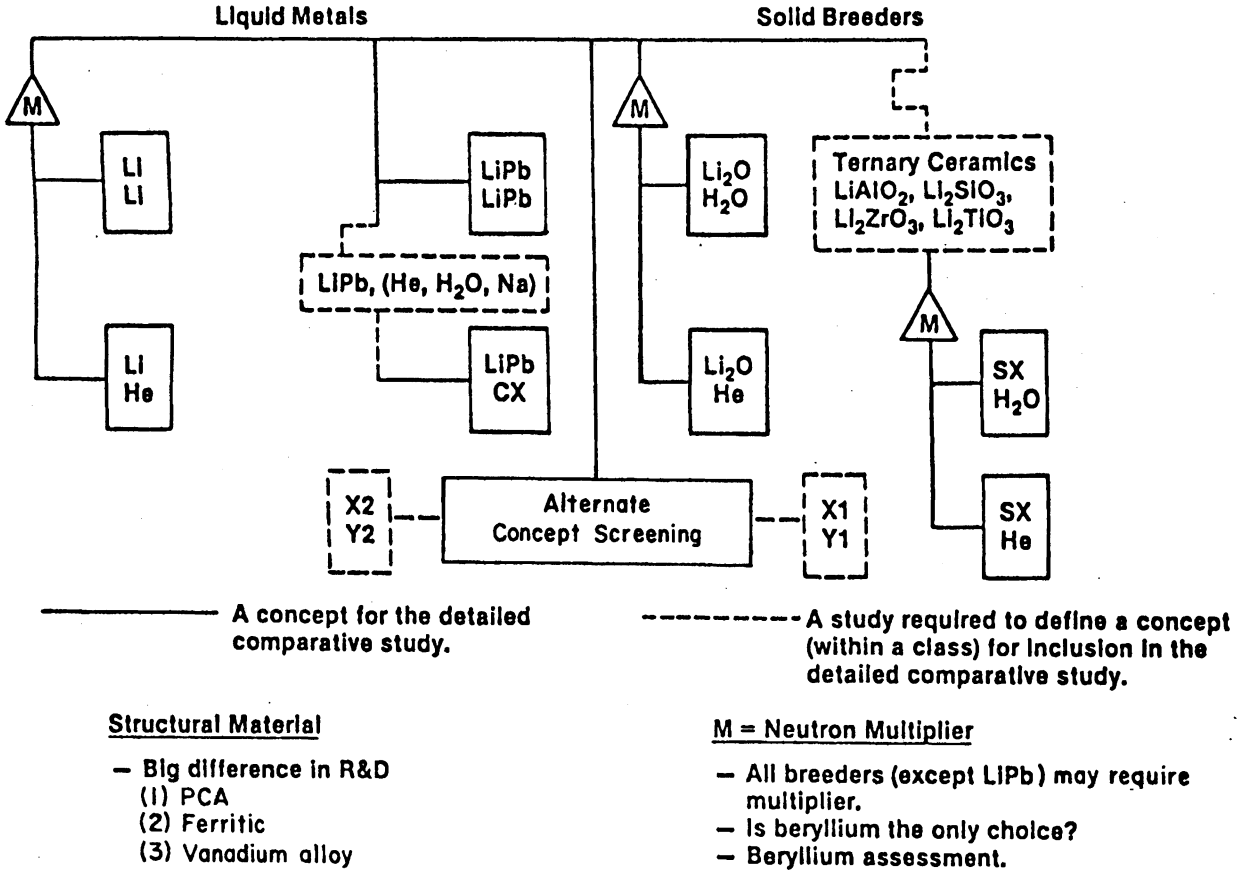

Figure III.1-1. Blanket Options

ments) which will be the result of a quantified, systematic evaluation process as described in Sec. III.2.2. The output of the study will then be a rating of a selected number of blanket concepts (those which pass the initial screening criteria and first year evaluation) with respect to safety and environment, economic and engineering feasibility as well as R&D requirements. With this information an overall recommendation will be made regarding those blanket concepts which should receive priority in future R&D efforts.

III.2 Evaluation Criteria Methodogy

The methodogy used in this study was to designate mainline and alternate concepts based on previous work, establish initial screening criteria and then develop a detailed evaluation procedure using a systematic, comprehensive set of criteria.

III.2.1 Initial Screening Criteria

The first step in developing initial screening criteria was to review a large number of possible criteria as listed in Table III.2-1. It is clear that "economics" and "safety" are broad categories that implicitly include many of the items of Table III.2-1 and are thus not suitable for initial screening criteria. Furthermore, for the initial screening criteria to be useful in the early phases of the study, they should be few in number, be quantifiable with limited analytical/design effort, represent threshold (either minimum or maximum values) values, and represent major feasibility issues. With this in mind, the initial screening criteria were selected as shown in Table III.2-2.

There are eight criteria, six of which have numerical threshold values; these include the breeding ratio, thermal efficiency, steady-state tritium blanket inventory, lifetime, normal tritium loss rate and total first wall neutron power loading. Two others of a qualitive nature have been added which includes no materials combination which could lead to obvious large releases of energy (e.g., H_2O and lithium) and a judgement about the overall engineering and fabrication complexity of the blanket. The numbers were intentionally selected as not being very restrictive in order to avoid eliminating concepts prematurely in the early stages of the study.

TABLE III.2-1. CANDIDATE CRITERIA

Breeding Ratio
Economics
Fabrication
Fault-Tolerant Design
Impact on Blanket/Shield Thickness
Lifetime
Maintenance
Material Resource Demands
Maximum Wall Loading
Module Simplicity
Need for IHX
R&D Requirements
Safety
Startup/Shutdown Requirements
Steady-State Tritium Inventory
Thermal Efficiency
Tritium Loss Rate
Variation in Wall Loading
Waste Management

Two breeding ratio minimum values are specified depending on whether the supporting neutronic analysis is one or three dimensional. (The breeding ratio criteria is discussed in more detail in Sec. III.2.2.3.1) The minimum value of thermal efficiency (25%) includes the effect of energy multiplication in the blanket, efficiency of the heat transport system (including effects of intermediate and double wall heat exchangers or steam generators if required) and pumping power for the blanket coolant. Additional auxiliary power requirements (e.g., plasma heating/current drive systems, refrigeration systems, etc.) are not included here but are included in the detailed evaluation discussed in Sec. III.2.2.2 under Economics.

The maximum blanket steady-state tritium inventory (~ 40 kg for a 4000 MW_{th} plant) was set based primarily on startup and tritium decay issues. Clearly lower inventories are highly desirable as are lower tritium loss rates than the maximum value of 100 Ci/day. These items are primarily related to safety and are considered in Sec. III.2.2.1 and Chapter XI.

The minimum values of wall loading and blanket lifetime are 3 MW/m^2 and 5 $MW-yr/m^2$ respectively. The neutron wall loading is the average loading on the first wall and the lifetime includes radiation damage limitations and overall reliability considerations. Note that the nominal design guideline values are 5 MW/m^2 and 10 $MW-yr/m^2$ (see Sec. II.2).

TABLE III.2-2. INITIAL SCREENING CRITERIA

Criteria	Min./Max Value	Comments
• Breeding Ratio	> 1.05 > 1.20	3-D Calculation 1-D Calculation
• Thermal Efficiency	> 25%	Net Power (Gross Electric - Pumping)[b]
• Blanket Steady-State Tritium Inventory	< 10 g/MW_{th}[a]	Based Primarily on Startup and Tritium Decay Considerations
• Lifetime	> 5 $MW\text{-}yr/m^2$	
• Tritium Loss Rates (Routine Operation)	< 100 Ci/d[a]	Overall Blanket/Power Conversion System (for Plant)
• Compatible Blanket Materials Combination	No Materials Combination Resulting in Large Rate of Energy Released	
• Total Neutron Wall Loading	> 3 MW/m^2	
• Engineering Feasibility	No Unduly Complex Configurations or Fabrication Procedures	

[a]For ~ 4000 MW_{th} power plant.

[b]Includes effect of blanket multiplication.

III.2.2 Evaluation Criteria

In order to carry out a systematic and comprehensive comparison of the leading blanket concepts during the second year of the study, an evaluation methodogy has been adopted which will result in a quantified ranking of blanket concepts in four major areas:

- safety and environment
- economics
- engineering feasibility
- R&D requirements.

A system for quantifying a large number of criteria which fall into the first three areas has been developed along with appropriate weighting factors so that an overall score can be obtained for each area. This system is described in the next three subsections. The fourth area, R&D requiements, will not be treated in detail until the last phase of the study; some initial considerations are presented in Sec. III.2.2.4.

In carrying out some of the analysis to support the evaluation process (e.g., economic comparisons and tritium breeding), it is necessary to place a blanket design into the context of an overall reactor and plant design concept. When this is necessary, the reference concept for tokamaks will be STARFIRE[1] while MARS[2] will serve as the reference for tandem mirrors.

III.2.2.1 Safety and Environment

Ideally, a complete probabilistic risk assessment comprising the entire fuel and facility cycle would be conducted for each blanket concept. Such an analysis would allow a complete comparison among concepts in the area of safety and environment. However, restrictions on study resources and knowledge necessitate a more modest approach. Thus, eleven specific evaluation indices have been established to compare blanket concepts. Individual indices are mixtures of quantitative and qualitative information. This comparison is intended to approximate a relative risk assessment comparison to the extent possible by focusing on various specific areas of possible difference among concepts.

Each concept will receive a score for each index (I_i) between 0.0 and 1.0. Each index also has a weighting value (W_i) indicating its relative importance. The sum of the weighting values equals 100. An overall safety figure of merit (SFM) is defined as the weighted sum of index scores:

$$SFM = \sum_i I_i W_i .$$

Thus, the highest possible safety score would be 100.

The specific indices are listed in Table III.2-3. A full, detailed description of the indices and their origin is provided in Sec. XI.2. There are three categories: source term characterization, fault tolerance, and non-accident concerns. The first category (1 to 3) relate to the component of accident risk from the radioactive and chemical source term common to accident initiators. Thus, issues such as the induced radioactivity and relative volatility and releasibility of the structure, coolant, and breeder/multiplier comprise the source term characterization indices 1 to 3. The response of a blanket concept to specific initiators (and their likelihood) such as loss of coolant, loss of site power, and coolant tube failures comprise the second category, fault tolerance indices 4 to 8. It is emphasized that the accident-related indices (1 to 8) incorporate consequence and probability. These indices are comparative, hence the concepts which best meet the concerns indicated will get the best score of 1.0.

The final three indices (9 to 11) relate to non-accident issues. Again, more details are given in Sec. XI.2. The radioactivity emission rate during normal operation is likely dominated by tritium losses. The molten salt HTS may be an exception because of possible ^{14}C, ^{22}Na, and ^{39}Ar losses (Appendix E). Occupational exposure for the various concepts will be compared via data such as module lifetime/changeout frequency, activity/dose levels near serviced components, and time required for maintenance activities. Waste disposal will be compared via measures such as waste burial options per 10 CFR 61 and radiation exposure from waste processing.

The weighting values were determined by first establishing balance (60-40%) between accidents (indices 1 to 8) and non-accidents (indices 9 to 11). This balance was a compromise between the general public perception that accidents should be weighted high as compared to the actual low weighting for

TABLE III.2-3. SAFETY EVALUATION INDICES

Index Name	Weighting Value
1. Structure source term characterization	10
2. Breeder source term characterization[a]	10
3. Coolant source term characterization	10
4. Fault tolerance to breeder-coolant mixing	6
5. Fault tolerance to LOCA, LOFA, and LOSP[b]	6
6. Fault tolerance to external forces[c]	6
7. Fault tolerance to near-blanket system interactions[d]	6
8. Fault tolerance of containment integrity	6
9. Radioactive emission rate	20
10. Occupational exposure	10
11. Waste disposal	10

[a]Breeder index includes neutron multiplier when applicable.

[b]Loss of coolant, loss of flow, and loss of site power.

[c]E.g., plasma disruptions, seismic events, and off-normal magnet behavior.

[d]E.g., blanket-shield or blanket-limiter interactions and response to loss of vacuum integrity.

accidents that result from total fuel/facility cycle risk studies for other energy technologies. Within the accident relevant indices, a 30-30% split was determined for the source term and fault tolerance indices. The individual source term indices were given equal weighting within their group as were the individual fault tolerance indices. The 40% weighting for non-accident issues was split 20% for normal emissions, 10% for occupational exposure and 10% for waste disposal. The higher relative weighting for normal emissions reflects the substantial concern for adequate reduction of tritium losses. To date, the safety rank ordering of concepts in first stage comparisons (Sec. XI.3) has not been highly sensitive to the exact weighting values.

III.2.2.2 Economics

The economic evaluation criteria are important factors with regard to selection of the blanket concepts to be developed for commercial applications of magnetically-confined fusion. This subsection describes the methodology to be used in the relative economic evaluation of the proposed blanket concepts. Technical and economic groundrules are formulated in the study to provide a

uniform basis of comparison. The final economic criterion will be the estimated cost of electricity.

A key factor in this cost estimate includes the direct cost of the blanket and shield components and components influenced by the blanket choice (magnets, heat transfer, power conversion, etc.). Other major factors directly influenced by the blanket and its performance are the reactor thermal power, shield power loss, power conversion efficiency, recirculating power and reactor availability. Assessment of the above factors (both performance and economic) in a consistent manner requires the blanket be evaluated in the context of a rather detailed and comprehensive conceptual reactor design. Thus, STARFIRE[1] and MARS[2] were adopted as technical and economic baselines for the blanket comparison. Blanket concepts will be evaluated in both reactor types in order to assess the influence of the inherent magnetic and configurational differences on the blanket selection. The various factors which contribute to the cost of electricity are intrinsically weighted due to their influence on the cost of electricity.

During the first year of this study, the methodology and data on blanket concepts have been developed and some initial comparisons have been made. However, the detailed economic comparison will be carried out in FY 1984. The groundrules, data bases, and techniques for evaluation will be discussed in detail in the next subsection.

III.2.2.2.1 Economic Evaluation Methodology

The cost of electricity was adopted as the sole criterion for the economic evaluation of the proposed blanket concepts. When evaluating competing blankets, comparison of only the direct capital costs of the blanket components is an insufficient evaluation technique and may lead to erroneous conclusions. A direct cost comparison will favor the lower cost options and slight the more expensive but higher performance blankets. Use of the cost of electricity criterion integrates the weighted effects of capital and operating costs, replacement time and frequency, thermal power, thermal power conversion and recirculating power requirements.

The "first year" cost of electricity in then-year dollars is defined by the following equation:

$$COE = \frac{(DC+SPR+CTGY+ID+INT+ESCL)FCR+(O\&M+SCR+FUEL)(1+ESC\ RATE)^{YRS}}{(\text{thermal Power} \times \text{Gross Effcny} - \text{Recirc. Power})(\text{Availability})\ (\text{hrs/y})}$$

where

COE	= Cost of Electricity
DC	= Direct Capital Costs
SPR	= Spare Parts Allowance (2 to 4%)
CTGY	= Contingency Allowance (15% of Direct Costs)
ID	= Indirect Costs
INT	= Interest During Construction (Based on 10% cost of money over construction period)
ESCL	= Escalation During Construction (Based on 5% escalation over construction period)
FCR	= Fixed Charge Rate (Nominally 15%)
O&M	= Operations and Maintenance Cost
SCR	= Scheduled Component Replacement Cost
FUEL	= Annual Fuel Cost
ESC RATE	= Annual Escalation Rate (5% per year)
YRS	= Construction Period

The cost of electricity is the total bus bar energy cost for the first year of operation. The total capital investment is equally divided and charged to the annual operating periods through the use of a fixed charge rate. Annual operating costs are also included with appropriate escalation from the year of the estimate (start of construction) to the initial operation date.

Table III.2-4 lists all the major factors which influence the economics. In this evaluation, the direct costs of the blanket (including first wall, multiplier, breeder, reflector and manifolding) and shield are calculated. Additionally, if the blanket design influences the cost of other ancillary systems (such as magnets, heat transport, power conversion, etc.), these costs are estimated and included in the assessment. Unit Material Costs are applied to estimated material and fabrication requirements plus unit costs for discrete components. All other direct costs are adopted from the STARFIRE or MARS economic analyses. Allowances for spare parts, contingency and indirect costs are applied to the direct costs. Interest and escalation costs incurred during construction are levied to transform the estimated costs at start of

construction to initial year of operation. A fixed charge rate (usually 15 percent) is applied to amortize total capital debt and to provide for insurance, taxes and other annual capital-related costs.

TABLE III.2-4. FACTORS WHICH INFLUENCE ECONOMICS

Direct Costs	Annual Costs
Blanket Shield Magnets Heat Transport & Steam Generator Systems	Scheduled Component Replacement: - Blanket Replacement Cost - Blanket Replacement (Life)
Power Output	**Availability**
Blanket Energy Multiplication Power Loss to Shield Gross Efficiency Coolant Pumping Power	Blanket Replacement Time Blanket Replacement Frequency Blanket In-Service Failure Rate Blanket Mean Time to Repair/Replace
Invariant Support Data[a]	
Other Reactor & Plant Direct Costs Spares Allowances Contingency Allowances Indirect Cost Allowances Construction Time Interest and Escalation Rates Fixed Charge Rate	Basic Reactor Geometry Direct Convertor Efficiency Other Recirculating Power Requirements Scheduled and Unscheduled Outages Unit Material Costs Operations and Maintenance Costs

[a]Data obtained from STARFIRE and MARS conceptual design studies.

The annual operations and maintenance costs from the reference conceptual reactor designs were adopted. The scheduled component replacement cost is the cost associated with the regular replacement of the blanket and limiter or divertor modules. This cost is related to the component costs and the frequency of replacement.

A non-cost factor which significantly contributes to the cost of electricity is the power output of the plant. The blanket concept design approach, material choices and performance capabilities have a profound influence on the power output. The blanket energy multiplication determines the total thermal power available. The percentage of the power recovered in the blanket versus how much is lost as non-useful energy in the shield is also important. The temperatures of the coolant media (both primary and secondary, if required) determine the gross power conversion efficiency. The choice of coolant media and their operating pressures determines the pumping power requirements which reduce the plant's net power output.

The final set of factors deal with the availability of the power plant. Availability is the percent of time the power plant is available for services, whether operated or not. It is equal to available hours divided by the total hours in the period under consideration. The time required to replace blanket modules and the frequency of replacement (which is related to the blanket lifetime) influences the reactor availability. The design life of blankets, as estimated in this and previous studies, contains a fairly large amount of uncertainty. Likewise, removal and replacement of blanket modules are estimated with a large uncertainty. Real unknowns remain in the areas of in-service failure rates and mean-time-to-repair or replace these components. This study has not estimated these data; thus the availability values of the baseline reactors have been adopted for this analysis.

All of the above influences and data will be gathered and analyzed for this economic evaluation task. Figure III.2-1 illustrates some blanket tasks, the economic subtasks, and data flow between the tasks. The blanket analysis task computes the blanket performance parameters (e.g., maximum coolant temperature, heat loss to the shield, energy multiplication, blanket and shield thicknesses and blanket design lifetime) and the estimated material requirements for the blanket and shield. The power conversion task computes the power conversion efficiency and the overall pumping power required. Using the STARFIRE and MARS reactor baselines, the net power is calculated and the magnets are resized to conform to the thinner or thicker blanket and shield combinations. These data are used to estimate the direct and annual costs. All of these are used to generate the COE values for the two reactor configurations for each blanket concept evaluated.

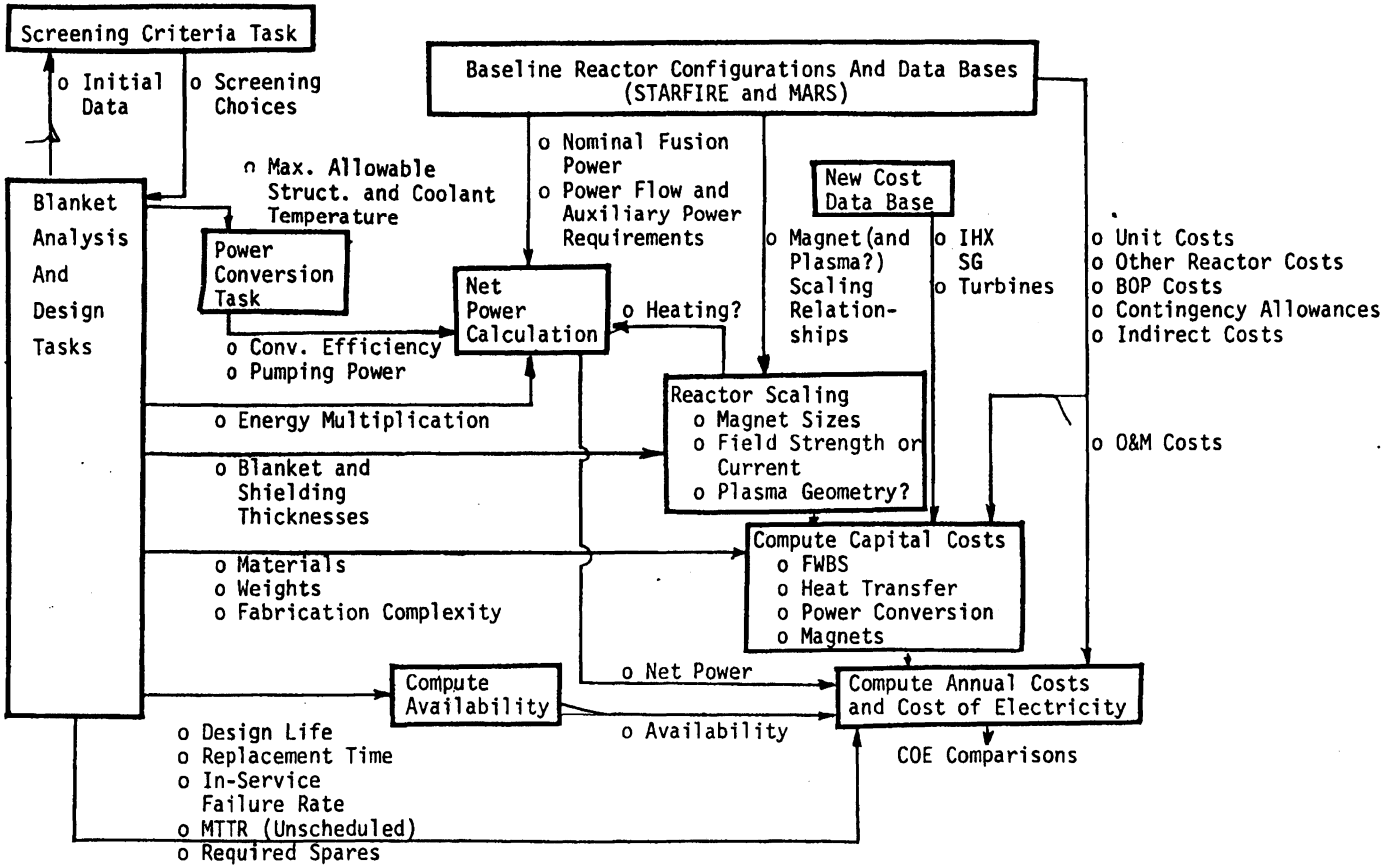

Figure III.2-1. The logic flow for the blanket economic comparison task illustrates the influence of performance data on the cost of electricity.

III.2.2.2.2 Economic Groundrules

To provide a consistent comparison, performance and economic groundrules were established. As mentioned earlier, the blanket comparisons were conducted within the framework of the conceptual designs of STARFIRE and MARS. This allowed realistic geometry constraints, auxiliary power requirements and economic burdens. Some modifications were required to achieve the 5 MW/m^2 neutron wall loading adopted as a blanket design basis. The tandem mirror design adopted the plasma geometry of MARS with a minor variation in beta to achieve 5 MW/m^2 from a nominal value of 4.25 MW/m^2 (β increased to 0.30 from 0.28). Alternatively, the plasma radius could be increased from 0.49 to 0.53 m. The approach for the tokamak utilized the STARFIRE geometry but increased the fusion power from 3510 MW to 4875 MW by allowing the average toroidal beta to increase from 0.067 to 0.097, assuming a maximum field strength of 10 T as opposed to 11.1 T for the STARFIRE baseline. Given a set of thicknesses for a particular blanket and shield combination, a new magnet geometry is calculated. This geometry coupled with a maximum field of 10 T at the magnet yields a new field at the plasma center (B_o). The new tokamak fusion power is related to the plasma center field by the equation:

$$P_{f(new)} = P_{f(ref)} \times \left(\frac{B_{o(new)}}{B_{o(ref)}}\right)^4 \qquad [III.2\text{-}1]$$

The approach adopted holds the first wall geometry and maximum magnetic field constant while varying the wall loading. An alternative approach could have held the fusion power and the wall loading (and wall area) constant, but would have required determining a new plasma and reactor geometry, which was deemed too extensive for this study. This is not a difficulty in the tandem mirror analysis as the plasma geometry is not as affected by the change in blanket and shielding thicknesses. The installed costs of the materials used in the blanket and shield are calculated using the weight of the materials and the unit material costs shown in Table III.2-5. These values will be used unless the complexity of fabrication requires use of adjusted unit material costs. These unit values have been scaled from data suggested for use as standard unit costs in a handbook[6] prepared by Pacific Northwest Laboratory and from data used in recent conceptual designs.[1,3-5,7] The magnet costs will be scaled from the STARFIRE[1] and MARS[2] economic analyses.

TABLE III.2-5. UNIT COST FOR BLANKET AND SHIELDING MATERIALS

Material	Description	Theoretical Density (kg/m^3)	Installed Cost (1983$)	References
PCASS	Complex Fabrication	8020	43	1,3,4,5,6
	Moderate Fabrication	8020	33	1,3,4,5,6
HT-9	Complex Fabrication	8020	39	
	Moderate Fabrication	8020	29	
	Bulk Material	8020	12	7
FE-1422	Complex Fabrication	8020	35	
			25	1,3,4,5
			12	1,3
Graphite	Block Form	1600	15	1,6
Lithium	Natural	530	37	6,8
	90% Enriched ^6Li	530	1200	7
$LiAlO_2$	Natural in Cans	3400	50	6
	60% Enriched	3400	100	1,4
	90% Enriched	3400	200	6
Li_2O	Natural in Cans	2010	40	3,6
	90% Enriched	2010	600	6
17Li-83Pb	Natural	8805	4	7
	35% Enriched	8805	7	7
	90% Enriched	8805	12	7,8
Pb	Liquid	10500[a]	4	3,6
Be	Coating	1850	300	1,4,6
	Bulk	1850	400	4,6
B_4C	Blocks	2540	43	1,3,6
Ti-6Al-4V	Moderate Fabrication	4850	80	1
Ti-6Al-2V-4Sn-2Mo	Moderate Fabrication	4850	---	---

[a]Density at 300°C.

The application of the blanket concepts into a reactor design required several engineering groundrules be imposed, e.g., maximum fluence limit of 5×10^9 rads at the magnet insulation, common vacuum gaps, insulation layers and

dewar thicknesses. Tables III.2-6 and III.2-7 define the various materials and gaps required along with their respective thicknesses for the tokamak and tandem mirror, respectively. These data allowed usage of varying thickness blankets and shields. The shielding thickness is adjusted to achieve the identical damage limit in the insulation of the superconducting coils for all blanket concepts.

The remaining economic factors, which are largely invariant with respect to the blanket concept, are adopted from the STARFIRE and MARS economic analyses. These factors are other reactor and balance of plant costs, indirects, allowances, operating expenses and availability. The economic life of the plant is assumed to be 30 y.

III.2.2.3 Engineering Feasibility Criteria

The items included under "Engineering Feasibility" include important, even vital, blanket criteria that either deserve separate consideration or do not readily fit under the categories of safety and economics. These items include the following:

- tritium breeding and inventory
- engineering complexity and fabrication
- resources
- ability to operate at different power levels (power variation)
- ability to increase neutron power loading
- ability to increase surface heat flux and erosion
- startup/shutdown operations
- maintenance and repair

The basic approach to be followed is similar to that used for safety criteria as described in Sec. III.2.2.1. The overall engineering figure of merit (EFM) is defined as the weighted (W_i) sum of an index (I_i has a value of 0 to 1) for each item listed above:

$$EFM = \sum_i I_i W_i \qquad [III.2-2]$$

where the maximum score would be 100. The weighting values are given in Table III.2.-8.

TABLE III.2-6. TOKAMAK BLANKET AND SHIELD GEOMETRY ASSUMED IN ECONOMIC ANALYSES (STARFIRE IS REFERENCE)

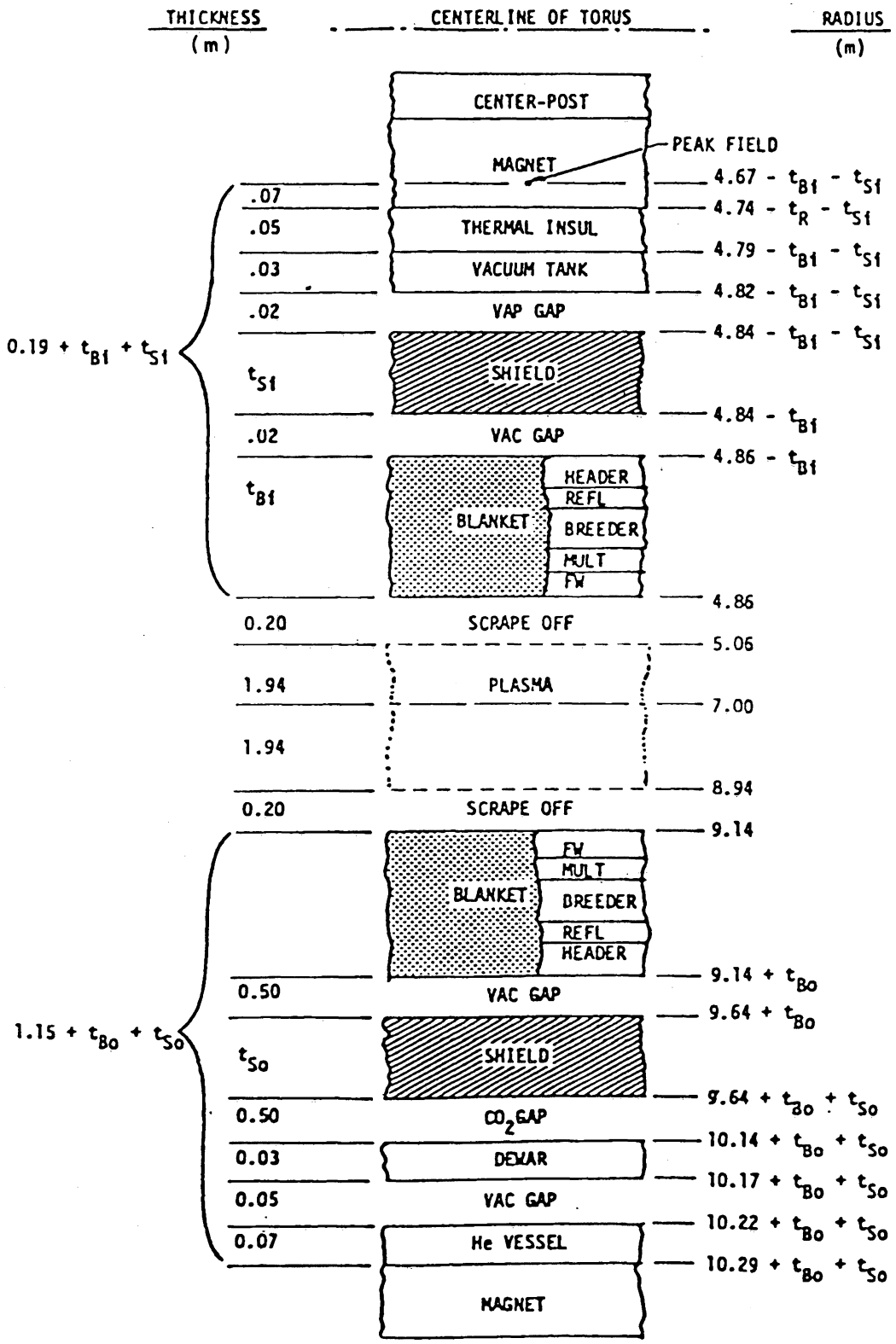

TABLE III.2-7. TANDEM MIRROR BLANKET AND SHIELD GEOMETRY ASSUMED IN ANALYSES (MARS IS REFERENCE)

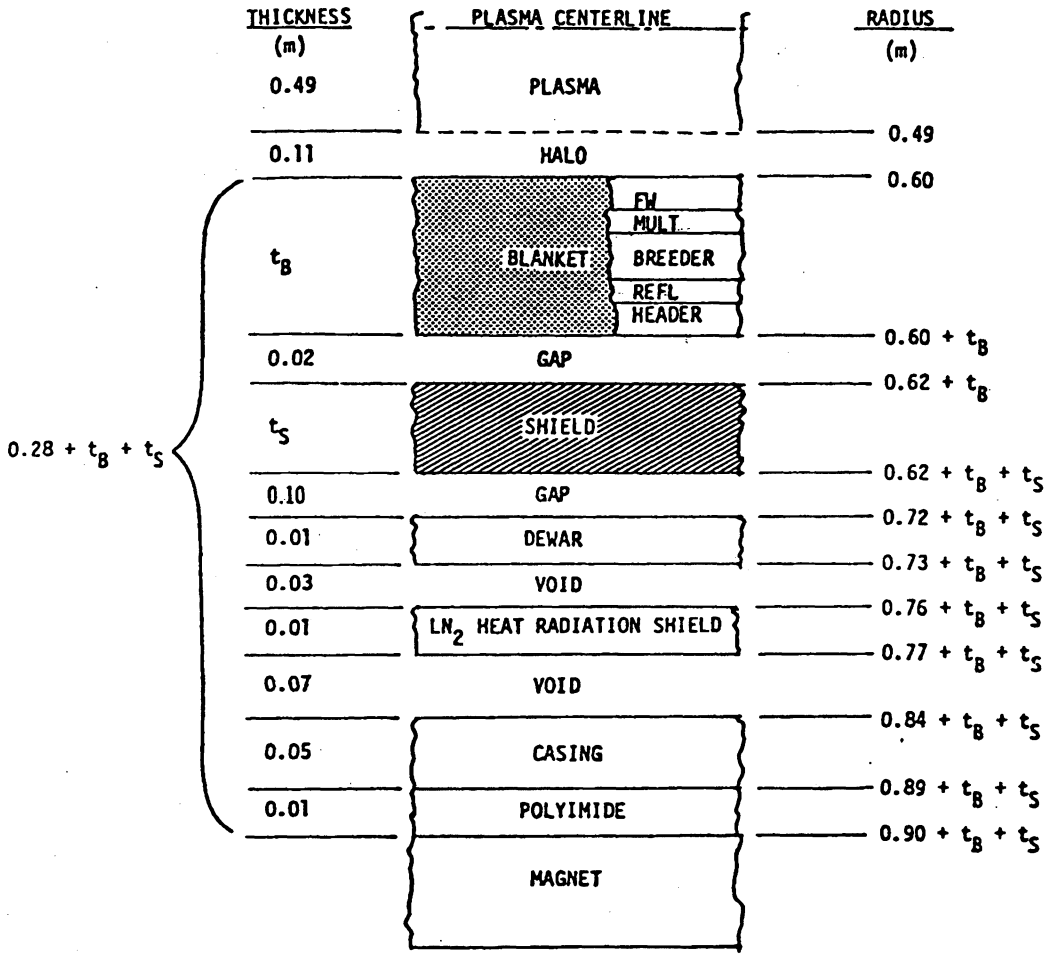

TABLE III.2-8. ENGINEERING EVALUATION INDICES

Index Name	Weighting Value (W_i)
1. Tritium Breeding and Inventory	23
2. Engineering Complexity and Fabrication	23
3. Resources	9
4. Power Variation	9
5. Ability to Increase Neutron Power Loading	9
6. Higher Surface Heat Flux with High Erosion	9
7. Startup/Shutdown	9
8. Maintenance and Repair	9
	100

Because the method outlined above uses weighted sums rather than weighted products, a zero in one of the indices of Table III.2-8 would not result in an overall value of the EFM of zero. If the reason for assigning a zero value for a particular index is judged to be so serious that it is a fatal flow for that particular blanket concept, then the concept will not be further considered in the evaluation process. This is not expected to be a problem because initial screening and selection process of the first year of the study should eliminate most blankets with fatal flaws.

III.2.2.3.1 Tritium Breeding and Inventory

Obtaining an adequate tritium breeding ratio is clearly a major feasibility issue[9] and has been given the highest weighting value. This subsection describes the technical basis for the tritium breeding index developed in the study.

The required tritium breeding ratio (T_r) in a self-sustained fusion power economy must exceed unity by a margin (G) to cover 1) losses and radioactive decay during the period between production and use, and 2) supplying inventory for startup of other fusion reactors. G is often called "doubling time margin". T_r can be written as:

$$T_r = 1 + G_o + \Delta_G \qquad [III.2-3]$$

where G_o is the breeding margin for a reference conceptual design. G_o is a function[10] of the reactor tritium inventory (I) and the doubling time (t_d), and can be written as

$$G_p = \frac{I}{\tau \bar{N}} \times F(t_d) \qquad [III.2-4]$$

where τ is the mean decay time of tritium, $\bar{N}$ is the rate of tritium consumption and $F(t_d)$ is a function of t_d. G_o increases rapidly as I increases and t_d decreases. I includes the tritium inventory in the blanket, fueling and exhaust systems, other reactor components, and the storage inventory for use in off-normal conditions and to start up a new reactor. At present, there are large uncertainties in estimating I. For example, the magnitude of the tritium inventory retained in a solid breeder blanket is uncertain by at least an order of magnitude. Similar uncertainties exist for the fueling and exhaust system because of lack of information on the achievable tritium fractional burnup in the plasma. Therefore, the magnitude of the required tritium breeding ratio (T_r) is uncertain. We designate such uncertainty by the parameter Δ_G in Eq. [III.2-3]. An estimate of Δ_G can be evaluated for various fusion reactor design options and technology choices by a combination of analytical estimates and experimental data on the tritium inventories in the various reactor components.

Figure III.2-2 shows the minimum breeding margin (G) as a function of the reactor tritium inventory for various values of the doubling time. For the hypothetical case of a tritium inventory usually of 1 kg, G is very small. Present estimates of the reactor tritium inventory vary in the range of 10 kg to 50 kg. Many uncertainties such as those due to uncertainties in the magnitude of the tritium fractional burnup in the plasma and the storage inventory needed for off-normal situations are common to all blanket concepts. However, the portion of the tritium inventory related to tritium retained in the blanket, first wall and limiter/divertor varies considerably from one blanket concept to another depending on the type of breeder and structural materials. Therefore, the required tritium breeding margin will vary from one concept to another.

As shown in Fig. III.2-2 the required tritium breeding margin is quite dependent on the doubling time. For example, for I = 30 kg, the required margin is 0.18, 0.10 and 0.05, for t_d = 1 y, 2 y and 5 y, respectively.

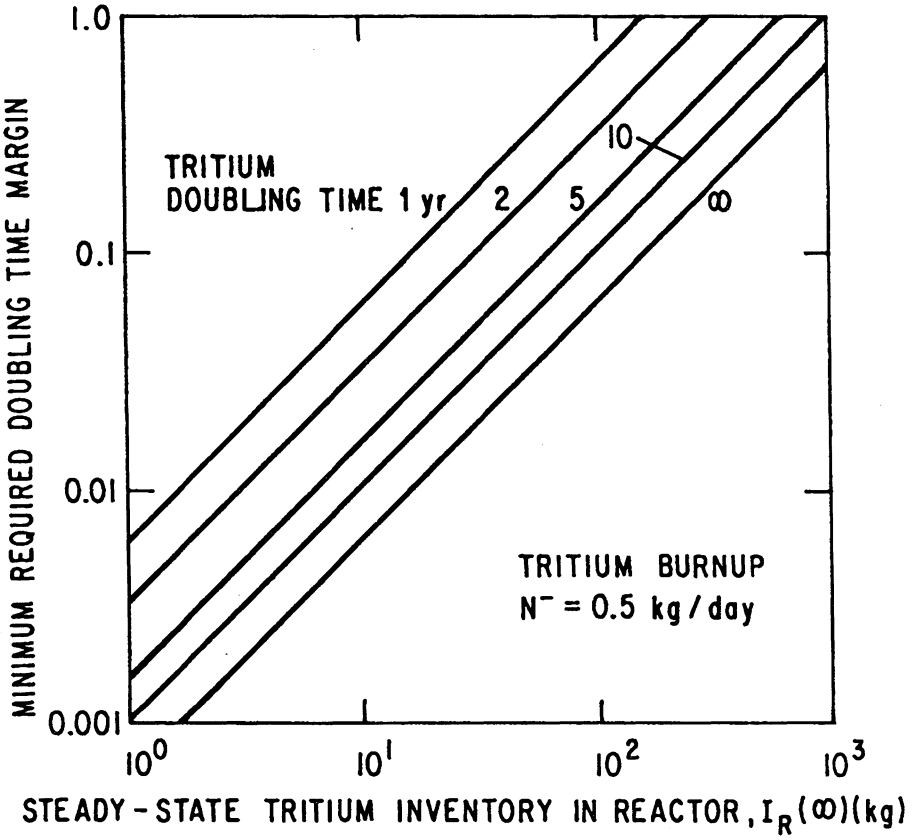

Figure III.2-2. Minimum required doubling time margin as a function reactor tritium inventory at several values of the doubling time.

For a blanket concept to be feasible, the achievable tritium breeding ratio (T_a) must be equal to or greater than the required tritium breeding ratio, i.e.,

$$T_a \geq T_r. \qquad \text{[III.2-5]}$$

Prior to the construction of an actual fusion reactor, the only means to evaluate the breeding potential of a given blanket concept in a preliminary fusion reactor design is to calculate, using present codes and data, a tritium breeding ratio (T_c). The calculated and achievable breeding ratio can be related as follows:

$$T_a = T_c - \Delta_c \qquad \text{[III.2-6]}$$

where Δ_c is the uncertainty in the calculated breeding ratio. The sources of uncertainties that contribute to Δ_c are numerous but can be broadly classified into three areas: 1) reactor design definition, 2) neutronics calculations, and 3) nuclear data.

The tritium breeding ratio is sensitive to many of the design features of the fusion reactor. Some of the important features are: 1) the materials, geometry and size of the in-vessel components (e.g., limiter or divertor for impurity control) that intercept the fusion neutrons before entering the blanket; 2) materials, volume fraction and distributions of structural materials and coolants in the first wall and blanket; 3) size and locations of the many void regions that penetrate the blanket and serve important functions such as plasma heating, plasma-current drive, vacuum pumping and fueling; 4) the presence of non-breeding regions in the blanket, which are reserved for presently ill-defined requirements such as passive coils for plasma stabilization; and 5) overall plasma characteristics and reactor configuration, including fusion neutron source distribution, shape of first wall, modularity of components, etc.

Fusion is still in a somewhat early stage of research and development with active conceptualization of reactor designs. Technology choices and design concept selections have not been made for many of the reactor systems. Moreover, these selections will not be made for a number of years to come because a number of issues are yet to be resolved experimentally and

analytically. The achievable tritium breeding ratio is certainly one of the key considerations in the selection among concepts.

The dependence of the tritium breeding ratio on technology and design concept choices can be quite large, 50% in some instances. Obviously, one cannot design a breeding blanket with a breeding potential that accommodates these large variations. Since the analysis to assess the breeding potential for candidate breeding materials will be (and is already being) performed for various technology and design concept choices (e.g., the differences between tokamaks and tandem mirrors), we will require that Δ_c includes an allowance of only a few percent for design definition. This is merely enough to account for those additional design details that cannot be developed at present for a given conceptual reactor design.

Neutronics calculations of the breeding ratio in a given system are subject to a number of uncertainties. Assuming that the designer uses the best methods and codes available, there are two sources of errors. First, geometrical modeling of the fusion reactor configuration entails some approximations that are necessary to make the problem practical from computer storage and computing-time viewpoints. Second, there are errors that are inherent in all calculational methods and codes for a variety of reasons such as those related to numerical techniques, averaging, and/or discrete treatment of continuous variables.

The third source of uncertainty in estimating the breeding ratio comes from errors in nuclear data (e.g., cross sections and energy and angular distribution of secondary neutrons). These include errors arising from the accuracy of measurements, representation of parameters in data files, and processing of the data into a form suitable for use in radiation transport codes.

For a candidate blanket concept to be judged feasible, one needs to show that:

$$T_c > 1 + G_o + \Delta_G + \Delta_c. \qquad \text{[III.2-7]}$$

The key issue now is evaluating the terms G_o, Δ_G, Δ_c and providing a methodology to combine the uncertainty terms Δ_G and Δ_c. Strictly speaking, both Δ_G and Δ_c are dependent on the particular blanket and reactor concepts being considered. The BCSS project plans to carry out during FY 1984 sensi-

tivity and uncertainty analyses to provide reliable estimates for the terms in Eq. 7 above. This effort is time-consuming and will be performed only for the smaller number of blanket concepts that will be the focus of BCSS during FY 1984. For the larger number of concepts considered in FY 1983, we developed a simple figure of merit to be applied to all concepts.

We select a reference value for the doubling time margin, G_o, of 0.05. This corresponds to (see Fig. III.2-2) that required for I = 30 kg and t_d = 5 y; or alternatively to I ~ 20 kg and t_d ~ 2.5 y. If one considers the likely range of I to be ~ 10 kg to 50 kg and the desired t_d to be in the range of one year to 15 y, then Δ_G is in the range of -0.04 to +0.25 (see Fig. III.2-2). The results of the neutronics analysis discussed later in this report show that it will be impossible for most concepts to satisfy the breeding requirements implied by such a large Δ_G. The problem comes from the need for the first generation of fusion reactors to have a short doubling time (~ 1 y). We assume here that the problem of generating tritium for the first generation reactors will be addressed as a separate issue and we will limit ourselves here to $t_d > 5$ y. In this case, the maximum Δ_G is ~ 0.08.

The calculational and data uncertainties have not been evaluated yet. These vary from one concept to another. We assume here that the best detailed 3-D calculations will be made for each concept to eliminate some of the modeling uncertainties. The reference reactor designs for BCSS, MARS and STARFIRE, are based on minimum penetrations (e.g., limiter and high power density rf). The effects of other types of penetrations (e.g., divertor) will be evaluated and included in Δ_c estimate in the future. For the present, we assume Δ_c is in the range of ~ 0.05 to 0.15.

Based on the above assumptions, one can classify concepts based on the calculated tritium breeding ratio T_c (notice that T_c is the net breeding ratio obtained from 3-D calculations for the detailed reference design) as follows:

$T_c > 1.2$	Low Risk
$1.1 < T_c < 1.2$	Medium Risk
$1.05 < T_c < 1.1$	High Risk
$T_c < 1.05$	Reject

For concepts that have T = 1.05, we assign a figure of merit of zero. For concepts, with T > 1.2, the figure of merit is 1. Thus, a simple index for tritium breeding is given as follows:

$$I_i = \frac{T_c - 1.05}{0.15} \begin{cases} I_i = 0 & T_c < 1.05 \\ I_i = 1 & T_c > 1.20 \end{cases} \qquad \text{[III.2-8]}$$

III.2.2.3.2 Engineering Complexity and Fabrication

The basic engineering design and required fabrication procedures for the blanket are clearly important considerations and have been accorded the same weighting value as tritium breeding. This index is much more difficult to quantify than the breeding ratio and thus dictates a different approach. The approach that we have selected is to identify eight important features (see Table III.2-9) which if realized in a blanket would reduce the engineering and fabrication complexity of the blanket. Each feature can score a maximum of three points for a total maximum score of 24. While it is possible to consider some weighting factors between these eight features, this was not done in order to keep the procedure from becoming too complex. The index is obtained by dividing the score by 24 so the maximum value of the index is 1.0.

It should be noted that aspects of engineering complexity will also appear in the other evaluation categories. For example estimates of capital cost which will include consideration of fabrication difficulties will be considered under economics. In addition, issues related to failure frequency and mode, which are intimately related to engineering complexity, will be considered in the safety and economic evaluation.

III.2.2.3.3 Resources

Another important consideration is the use of possible limited resources for certain blanket concepts, e.g., the use of Be as a neutron multiplier. We also consider lithium resources but do not consider tritium resources required for startup; this is a factor in the tritium breeding item discussed in Section II.2.2.3.1. The approach is to consider the most limiting material (s) in the overall blanket design as a fraction of U.S. and world resources, where a total fusion economy of 1000 Gw(e) (or about 830 STARFIRE size

Table III.2-9. FEATURES FOR ENGINEERING COMPLEXITY AND FABRICATION

(1)	First Wall* (FW)	
	- Requires Stand-Alone FW	0
	- Integral FW, Separate Coolant Loop	1
	- Integral FW, Separate or Successive Flow Path With Blanket	2
	- Completely Integrated FW/Blanket	3
(2)	Neutron Multiplier* (NM)	
	- Separate NM, Complex Requirements	0
	- Separate NM, Simple Requirements	1
	- NM Fully Integrated with Breeder	2
	- No NM Required	3
(3)	Breeder Fabrication*	
	- Many Pieces and/or Containment Required	0
	- Some Pieces and/or No Containment	1
	- Simple Module Fill Operations	2
	- Combined Breeder and Coolant	3
(4)	Coolant Containment/Flow Path Requirements+ [3 Parts]	
	- Module Walls: • High Pressure Confined	0
	• Low Pressure Confined	1
	- Coolant Flow Path Requirements: • Many Paths, Balancing Required	0
	• Few or Single Path, Little or No Balancing	1
	- Containment Fabrication: • High Complexity, Many Pieces	0
	• Low Complexity, Few Pieces	1
(5)	Tritium Removal*	
	- Many Connections, He Purge	0
	- Few Connections, He Purge	1
	- Breeder/Coolant Circulation	2
	- Passive System (e.g., Permeation)	3
(6)	Manifolding*	
	- Separate From Blanket, Many Connections	0
	- Separate From Blanket, Few Connections	1
	- Structurally Integrated; Connections to Blanket	2
	- Fully Integrated, No Connections	3

TABLE III.2-9. FEATURES FOR ENGINEERING COMPLEXITY AND FABRICATION (CONTD.)

(7)	Inboard/Outboard Blanket*	
	- Different inboard blanket coolant with different breeder	0
	- Different inboard blanket coolant with same breeder	1
	- Inboard blanket coolant and breeder same as outboard but with different configuration	2
	- Inboard blanket same as outboard blanket	3
	[NOTE: Tandem mirror would score 3 points on this feature.]	
(8)	Manufacturing Operations+ [3 parts]	
	- Coatings: • Separate Material Applied	0
	• None or "Natural" Oxides	1
	- Welding: • Many Operations and/or Restrictive Requirements (e.g., special atmosphere)	0
	• Few Operations and/or Relaxed Requirements	1
	- Machining: • Many Operations, High Tolerances	0
	• Few Operations, Low Tolerances	1

* Select one value of 0, 1, 2 or 3.
\+ Select one value of 0 or 1 for each of three parts.

reactors with a 40 year lifetime) is assumed. The values of the index are given in Table III.2-10 where one selects the largest index for either U.S. or world resources. If a blanket uses more than one limited material (n), then the overall index will be given by

$$I_i = \prod_{j=1}^{n} I_{ij} \qquad \text{[III.2-9]}$$

where I_{ij} is the index score for the jth material.

TABLE III.2-10. RESOURCES INDEX

Requirements	I_i	
	U.S. Resources	World Resources
< 1%	1.0	0.5
1 - 10%	0.5	0.3
10% - 50%	0.2	0
> 50%	0	0

III.2.2.3.4 Power Variation

While fusion power plants, particularly those based on tokamaks and tandem mirrors, are generally viewed as being base-load plants, there is still the need to operate at reduced power for extended periods of time (ranging from hours to months) to accommodate standard utility practices for startup procedures. Such operation at reduced power levels may be required in order to operate the plant with a failed component until a convenient or scheduled replacement time. In addition, it is generally necessary to operate at low power during startup. Thus we are interested in the ability of a given reference blanket concept, designed for a nominal wall loading of 5 MW/m^2, to operate over a range of power loading from as low as 5% to as much as 120%. Typically the coolant temperature might remain constant while the flow rate is changed to accommodate power changes. The higher percentage is to accommodate spatial variations (e.g., poloidal variation in tokamaks) at nominal conditions as well as possible modest power surges above the nominal operating point. A blanket that cannot operate 10% to 20% above the nominal value for at least short periods of time will not be considered further. The index values are given below:

Power Variation

Variation	I_i
5% - 120%	1.0
25% - 120%	0.8
50% - 120%	0.5
90% - 110%	0.2
No Variation	0

An important consideration is the ratio of surface heat flux to neutron flux over the possible range of neutron wall load variation. It will be assumed that the surface heat flux is proportional to the neutron wall load.

Another important consideration is whether it will be necessary to recover tritium from the blanket during low power operation; this will be a particularly important question for solid breeder blankets. If the reactor were to operate for extended periods of time (days to weeks) and tritium was not released from the blanket (due, for example to lower temperatures in the solid breeder material), then low power operation would entail serious consequences such as the need for substantial storage of reserve tritium. Therefore, blanket designs will be evaluated as to the ability to release tritium during extended operating periods at reduced power levels.

III.2.2.3.5 Ability to Increase Neutron Power Loading

A desirable feature of a particular blanket concept is the ability to operate at wall loadings above the nominal value of 5 MW/m^2 (see Appendix D for further discussion). This item is included here to assess the suitability of the blanket to accommodate improved plasma confinement concepts which may operate at higher power densities. In assessing the possibility of increasing the wall loading for a particular blanket concept (i.e., a particular choice of breeder, coolant, structure, multiplier, and reflector), mechanical design modifications from the reference design at 5 MW/m^2 would be permitted. Examples would include changing the coolant tube spacing, first wall thickness, total blanket/shield thickness and the like. It is assumed that the surface heat flux is proportional to the total wall loading. The value of the index for this item is given by

$$I_i = \frac{P_{NW} - 5}{5} \begin{cases} I_i = 0 & P_{NW} \leq 5 \text{ MW/m}^2 \\ I_i = 1 & P_{NW} \geq 10 \text{ MW/m}^2 \end{cases} \qquad \text{[III.2-10]}$$

where P_{NW} is the average neutron wall loading in MW/m^2.

Implicit in the consideration of the advantages of operating at high wall loadings (with the obvious impact of higher power density and possibly smaller reactors) is the ability to obtain longer lifetimes in terms of fluence. While there may be some merit to operations at higher wall loadings with cor-

responding shorter lifetimes (i.e., the same fluence), it is most likely that the benefits of operating at higher wall loadings will require blanket concepts which can obtain higher fluence lifetimes. Thus we will require a minimum lifetime of 2 years or a fluence of up to 20 MW-yr/m^2 for a wall loading of 10 MW/m^2.

III.2.2.3.6 Higher Surface Heat Flux with High Erosion

For the tokamaks, the surface heat flux and erosion of the first wall might be considerably higher than those adopted in the design guidelines. For the case of the mirrors, such a situation is highly unlikely. More work is required to devlop this index. One suggestion is as follows, for the case of the tokamaks, the value of the index is given by

$$I_i = \frac{q - 0.5}{1.5} + \frac{t - 2}{16}$$

$$I_i = 0 \text{ at } q \leq 0.5 \text{ and } t \leq 2$$

$$I_i = 1 \text{ at } q \geq 1.25 \text{ and } t \geq 10$$

where q and t are the maximum surface heat flux in MW/m^2 and t is the maximum erosion thickness in mm, respectively, that can be accommodated by the design. The maximum q is evaluated at t = 2 while the maximum t is evaluated at q = 0.5. Note that t is the erosion thickness; therefore, the first wall thickness is the sum of t plus the required end-of-life thickness. (Mirrors would receive $I_i = 1$ for this index.)

III.2.2.3.7 Startup/Shutdown Operations

There are two basic types of startup/shutdown operations: "hot" and "cold" sequences. Hot startup/shutdown operations refer to the required sequences resulting from those conditions in which the blanket remains near nominal operating temperature and the plant is in a stand-by mode. It is unlikely that there would be considerable differences among blankets in this case except for the subsystems that are required to keep the blanket in "hot" conditions. Therefore, hot startup/shutdown is not considered explicity.

On the other hand "cold" startup/shutdown operations, which results from longer shutdowns when the plant is not producing power, do depend on blanket characteristics. It is desirable that the time to bring the blanket from a cold condition to operating conditions, particularly in terms of coolant temperature and pressure, be minimized and that there be no or at least simple additional components of the power conversion system to accomplish such operations. Thus the index for this item is given by the following:

Time Required for Cold Startup	I_i
< 1 day - score 0.6 1 → 3 days - score 0.3 > 3 days - score 0	0 → 0.6

Additional Blanket and Auxillary Subsystems Required	
None - score 0.4 Simple - score 0.2 Complex - score 0	0 → 0.4

III.2.2.3.8 Maintenance and Repair

This category evaluates various features of a blanket concept that impact the ability to maintain and repair the blanket. As with item 2 - Engineering Complexity and Fabrication - this is difficult to quantify. The following features and their scores are used to determine an index for maintenance and repair.

Feature	Maximum Score
• Replacement operations include simple push/pull movements and few disconnects.	0.3
• Simple inspection procedures including vacuum leak checking.	0.2
• Coolant spills result in simple clean-up operations.	0.2
• Blanket can continue to operate with a few coolant tube failures or does not require a large number of tubes.	0.3

III.2.2.4 Research and Development Requirements

As noted in the introduction to this chapter, the research and development requirements are an important consideration in evaluating blanket concepts. There are two important considerations:

- Blankets requiring significant R&D efforts (such as developing a new, advanced structure alloy) will likely require substantial time and funding resources.
- In addition, large R&D requirements imply greater unknowns, and hence less confidence in the performance of the blanket.

If two concepts have similar performance capabilities (in terms of engineering, safety and economic measures) but one requires more R&D efforts, then obviously one would select the concept with minimum R&D needs. However, the more likely situation is that blanket concepts with potentially better performance will require more R&D and thus the selection is not likely to be straightforward. It was therefore decided that R&D requirements would not be a factor in the screening process during first year of the study. However, a methodology to evaluate and compare the R&D requirements will be developed during the second year of the study. This methodology will then be used to estimate a figure of merit that can be used in the blanket comparison and selection process.

REFERENCES FOR CHAPTER III

1. C. C. Baker, et al., "STARFIRE - A Commercial Tokamak Fusion Power Plant Study," Argonne National Laboratory Report, ANL/FPP-80-1 (Sept. 1980).

2. B. G. Logan, et al., "Mirror Advanced Reactor Study, Interim Design Report," Lawrence Livermore National Laboratory Report UCRL-53333 (April 1983).

3. M. Abdou, et al., "A Demonstration Tokamak Power Plant Study (DEMO)," Argonne National Laboratory Report, ANL/FPP/82-1 (Sept. 1982).

4. C. G. Bathke, et al., "Elmo Bumpy Torus Reactor and Power Plant Conceptual Design Study," Los Alamos National Laboratory Report LA-8882-MS (Aug. 1981).

5. K. Evans, et al., "WILDCAT: A Catalized D-D Tokamak Reactor," Argonne National Laboratory Report, ANL/FPP/TM-150 (Nov. 1981).

6. S. C. Schulte, et al., "Fusion Reactor Design Studies - Standard Unit Costs and Cost Scaling Rules," Pacific Northwest Laboratory Report PNL-2987 (Sept. 1979).

7. B. Badger, et al., "UWTOR-M, A Conceptual Modular Stellarator Power Reactor," University of Wisconsin Report UWFDM-550 (Oct. 1982).

8. J. Gordon, TRW, Private Communication, August 1983.

9. M. A. Abdou, "Tritium Breeding in Fusion Reactors," International Conference of Nuclear Data for Science and Technology, Antwerp, Belgium (1982), also ANL/FPP/TM-165, Argonne National Laboratory Report (October 1982).

10. J. Jung, "An assessment of Tritium Breeding Requirement," Argonne National Laboratory Report, ANL/FPP/TM-172 (1983).

10. J. Jung and M. Abdou, "Assessments of Tritium Breeding Requirements and Breeding Potential for the STARFIRE/DEMO Design," Nucl. Tech./Fusion (1983) (to be published).

CHAPTER IV

STRUCTURAL MATERIALS PROPERTIES

TABLE OF CONTENTS

CHAPTER IV - STRUCTURAL MATERIALS PROPERTIES

LIST OF FIGURES FOR CHAPTER IV

LIST OF TABLES FOR CHAPTER IV

IV. STRUCTURAL MATERIALS PROPERTIES

Three classes of alloys are currently considered as leading candidates for the first wall/blanket structure of a commercial fusion reactor, viz., austenitic stainless steels, ferritic (martensitic) steels and vanadium-base alloys. A representative alloy from each class has been selected for analysis in the present study. The materials assessment conducted as part of the study includes: (1) a compilation of available materials properties data, (2) specification of limiting criteria for materials performance, and (3) determination of design allowable parameters. Where data were insufficient for a reliable assessment, best estimates based on extrapolation of available information were used to provide a consistent basis for evaluation of various designs. Established design rules and codes, e.g., ASME Pressure Vessel Code, were applied where possible. This section provides a review of the critical thermophysical and mechanical properties of three reference alloys and the effects of the radiation environment on the properties. The corrosion/compatibility assessment of these alloys in various chemical environments is presented in Chapter VI.

IV.1 Austenitic Stainless Steel

Austenitic stainless steels have been used extensively in fission reactor applications and therefore, possess the most developed data base for nuclear applications. For this reason the austenitic steels are generally regarded as a reference to which other candidate alloys are compared. In addition to the substantial data base for both irradiated and unirradiated material, the austenitic steels are readily fabricated and welded. Primary limitations relate to critical physical properties, which result in relatively high thermal stresses. As discussed in Chapter VI, corrosion in the liquid metal breeders is also a concern. The primary candidate alloy (PCA), which has been developed in the U.S. alloy development program, is selected as the reference austenitic steel. This alloy is similar to Type 316 but has a somewhat higher nickel concentration and lower Cr and contains a small amount of titanium. This chemistry modification derived from several years of development has provided improved resistance to radiation swelling. To further enhance the swelling resistance of this alloy and to increase its elevated temperature strength, this material will be used in the nominal 20-25% cold-worked condition, with aging treatments to control precipitate distribution.

IV.1.1 Physical Properties

The reference physical properties for PCA are given in this section. In most cases the data are assumed to be the same as for Type 316 stianless steel. The temperature independent or temperature insensitive properties, viz., melting temperature, density and Poisson's ratio are given in Table IV.1-1.[1] The specific heat[2], electrical resistivity[3], thermal conductivity[4], thermal expansion coefficient[5] and the modulus of elasticity[6] are plotted as a function of temperature in Figs. IV.-1 through IV-5. The thermal stress factor, which provides a figure of merit for accommodating thermal stresses, based on the physical properties at 400°C is listed in Table IV-1. A lower value of the thermal stress factor indicates lower thermal stresses for a comparable thermal gradient or heat flux.

TABLE IV-1. SELECTED PHYSICAL PROPERTIES OF THREE REFERENCE ALLOYS

	PCA	HT-9	VCrTi
Melting Temperature, °C	1400	1420	1890
Density, g/cm^3	8.0	7.8	6.1
Poisson's Ratio	0.27	0.27	0.36
Thermal Stress Factor $\frac{\alpha E}{k(1-\nu)}$, MPa • M/W	0.22[a]	0.11[a]	0.055[b]

[a] At 400°C.

[b] At 500°C.

IV.1.2 Baseline Mechanical Properties

The unirradiated tensile properties of cold-worked PCA are presented in Figs. IV-6 through IV-9. The curves are based on actual tests of PCA and were obtained from References 7. Examination of the ultimate and yield strength curves shows that at low temperatures (500°C) the strength is slightly below that of 20% cold worked stainless steel as reported in the open literature. However, above this temperature the strength of PCA is above that of 316 stainless steel. The strength differences may be due to the titanium

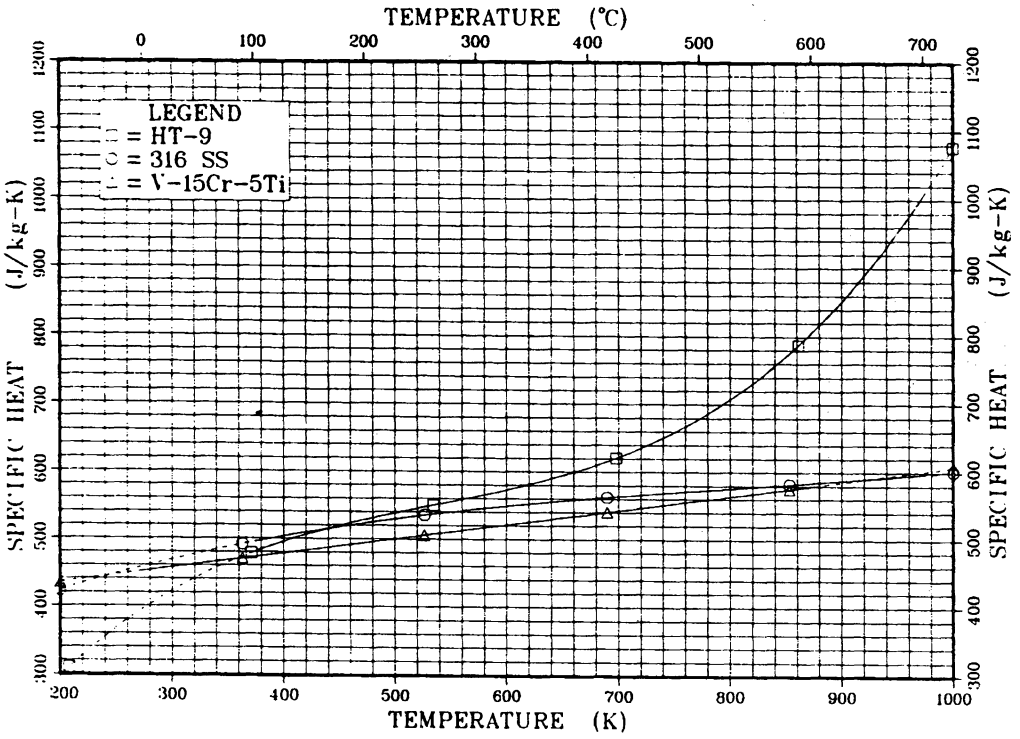

Figure IV-1. Specific heat of several metals.

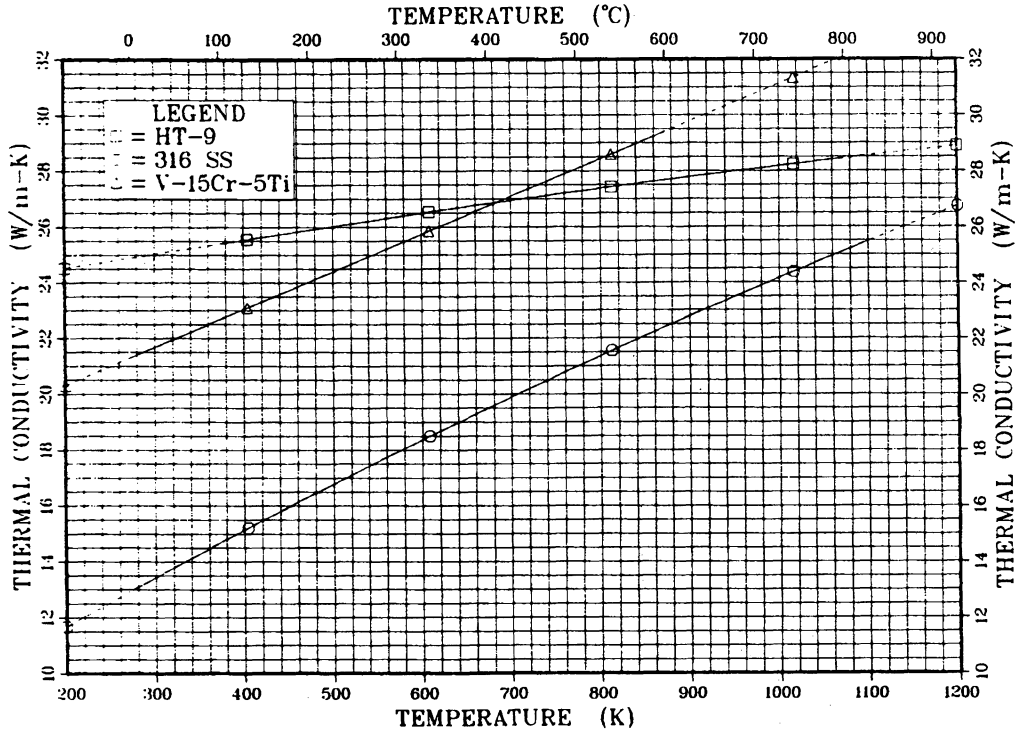

Figure IV-2. Thermal conductivity of several metals.

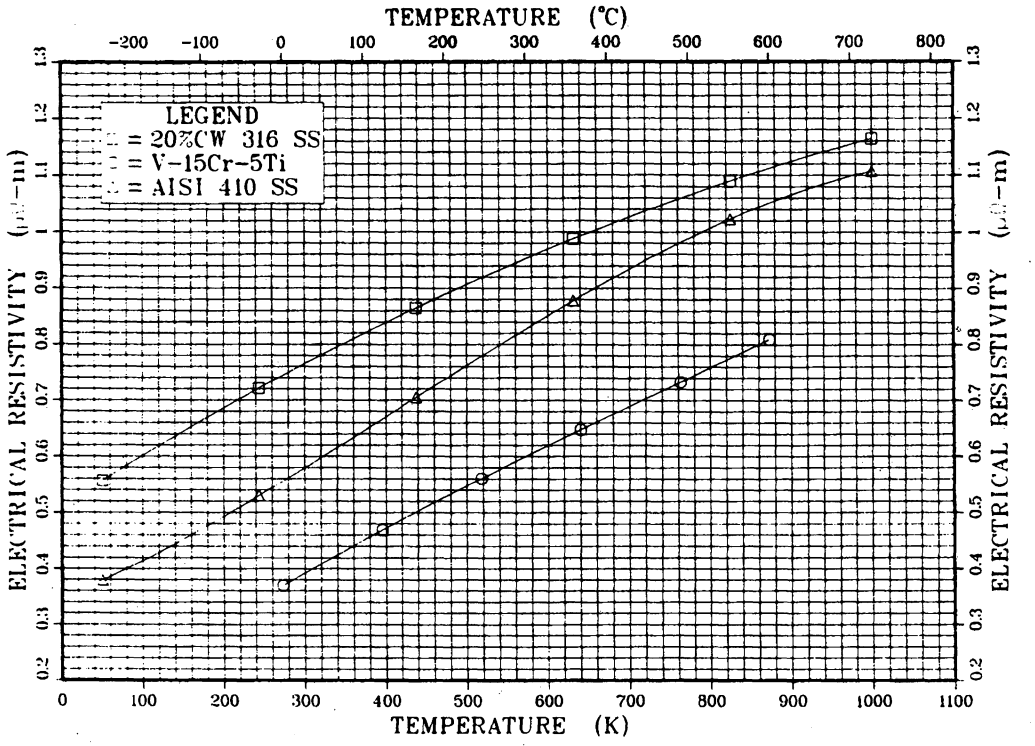

Figure IV-3. Electrical resistivity of several metals.

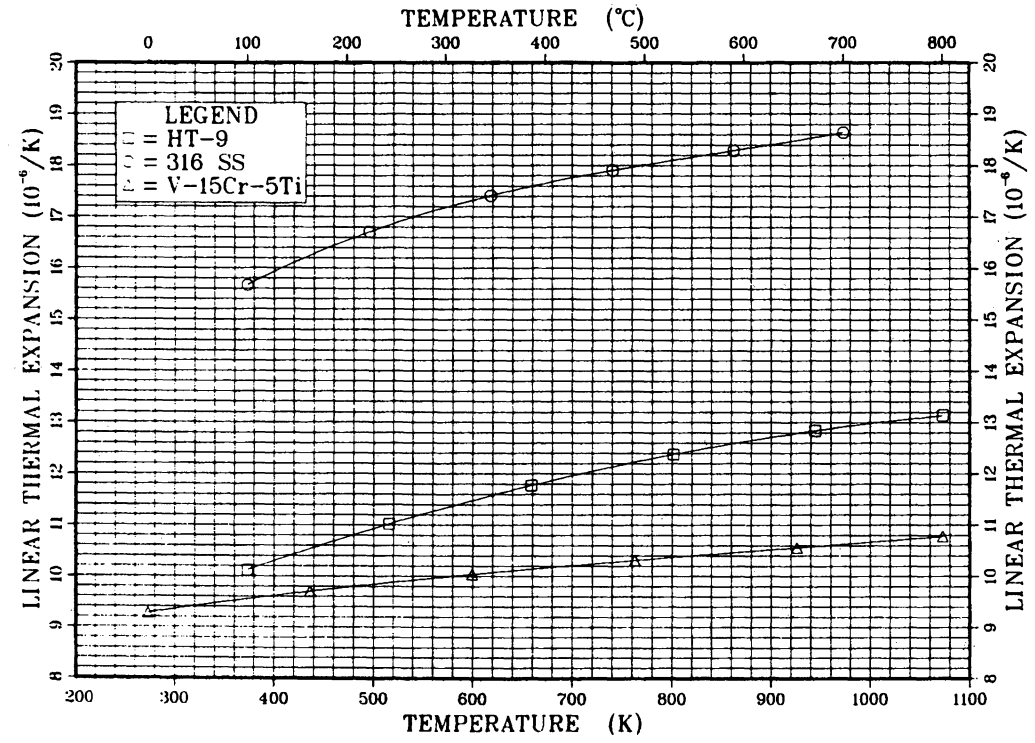

Figure IV-4. Mean CTE of several metals.

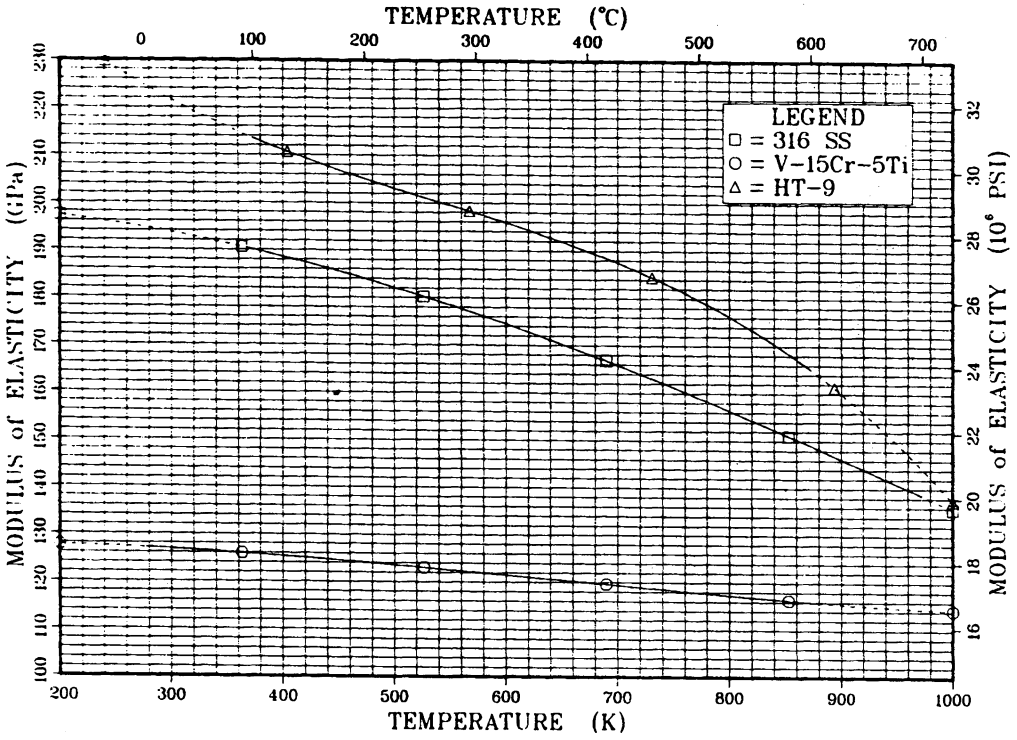

Figure IV-5. Modulus of elasticity of several metals.

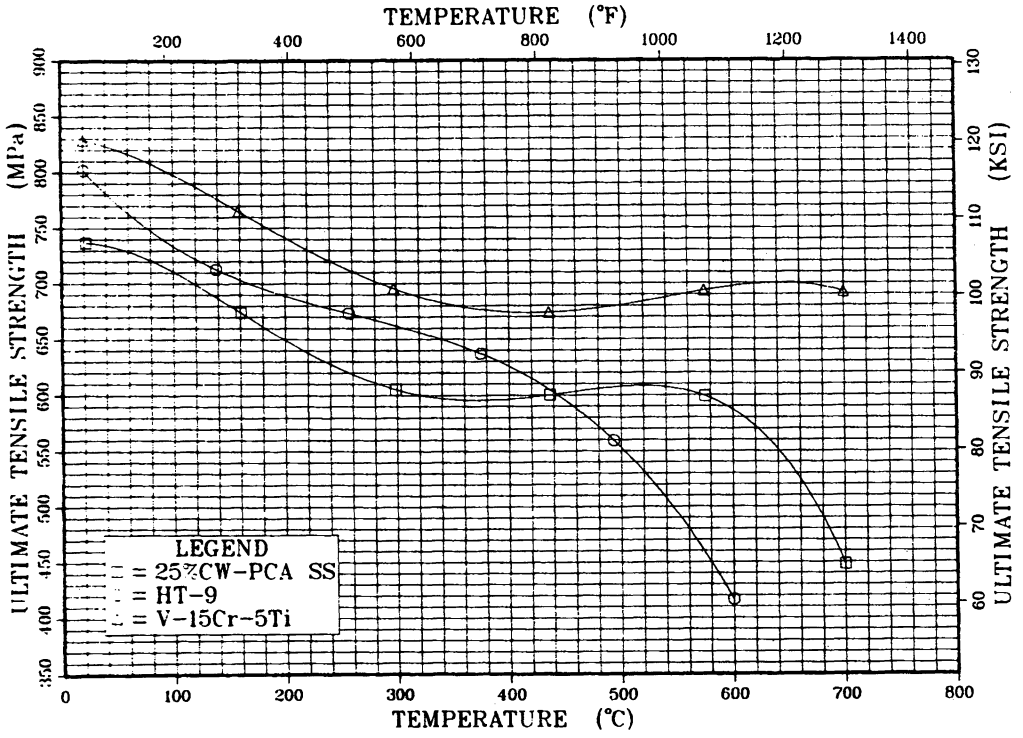

Figure IV-6. Average ultimate tensile strength of several metals.

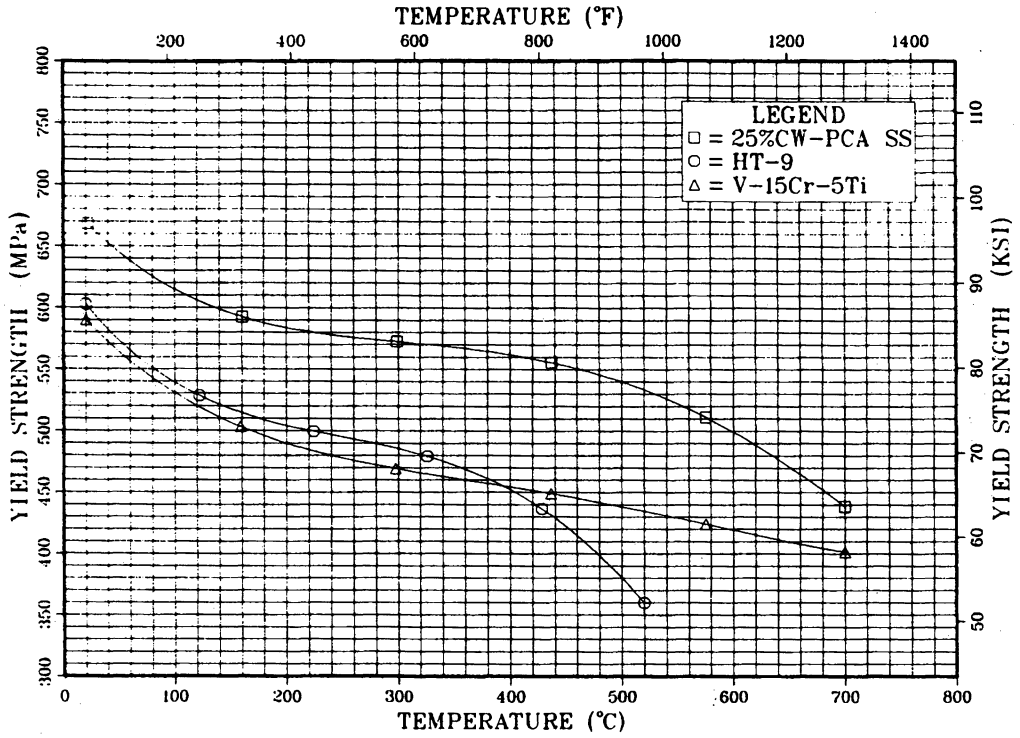

Figure IV-7. Average yield strength of several metals.

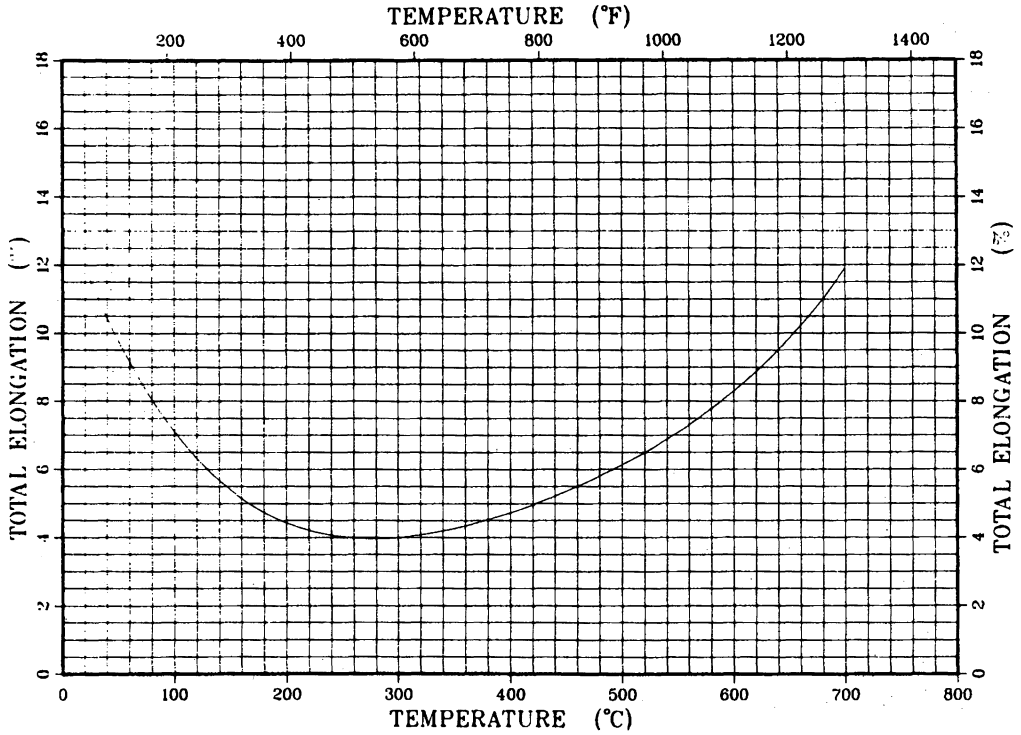

Figure IV-8. Total elongation of 25% CW-PCA SS.

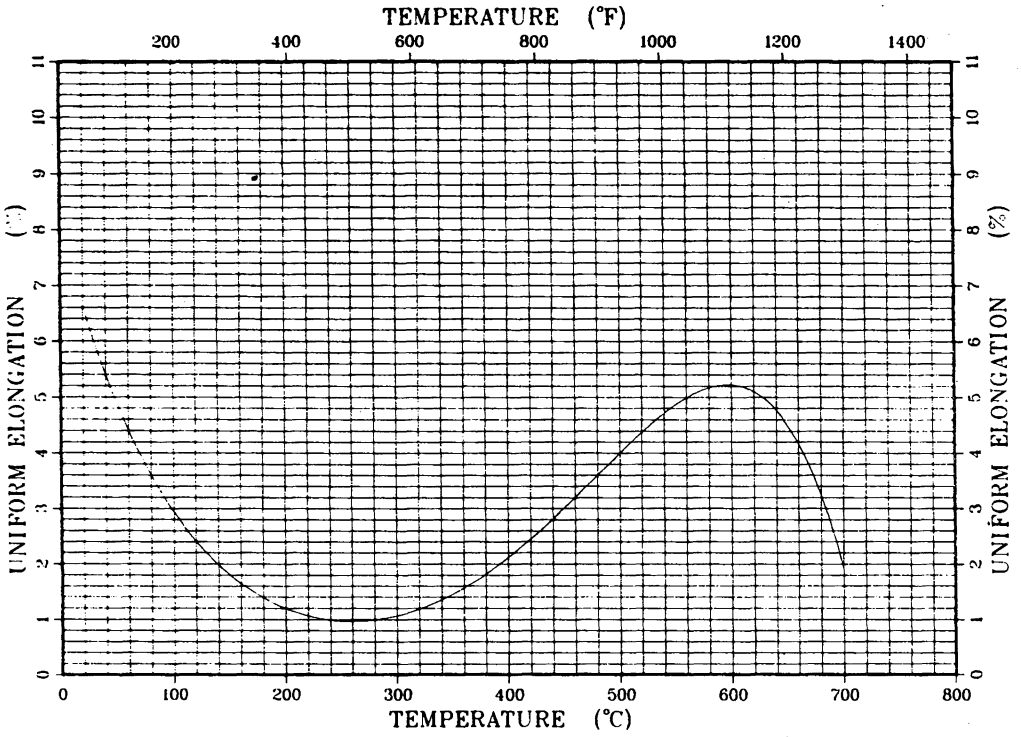

Figure IV-9. Uniform elongation of 25% CW-PCA SS.

additions or may be a result of differences in test conditions. The cold-worked austenitic steel provides an advantage of ~ 50% in ultimate strength and over 100% in yield strength compared to annealed material at temperatures of interest. The uniform and total elongation of PCA is similar to that found for cold-worked Type 316 stainless steel. In the case of PCA, there is a region of low elongation around 250-300°C. Examination of the data indicates that this trend is probably characteristic of the austenitic stainless steels and is not unique to PCA. However, it does point out that care needs to be exercised when designing for maximum loads in this temperature region.

IV.1.3 Radiation Effects

The effects of radiation on the projected performance characteristics of PCA are based partially on data for Type 316 stainless steel. Data for swelling and effects on mechanical properties are presented.

IV.1.3.1 Swelling

The swelling of PCA is modeled on the assumption that it will behave similar to Type 316 stainless steels. The high fluence data have been obtained in fast breeder reactor irradiations, primarily EBR-II, in which the helium generation rates are low. Extensive data produced by EBR-II irradiations are summarized in Fig. IV-10.[8] Effects of helium are based primarily on lower fluence, mixed spectrum reactor (HFIR) irradiations. The swelling response of PCA assumed for the present study is approximated by a bilinear swelling curve as shown in Fig. IV.-11. Based on available information, we have extrapolated the data to predict an incubation period of 150 dpa for irradiation temperatures of $\leq$ 400°C and 100 dpa for irradiation temperatures in the range 450 - 550°C. The initial swelling rate is assumed to be 0.02%/dpa (2% at 100 dpa). Above the incubation fluence limit, breakaway swelling at ~ 0.5%/dpa is predicted. For the present study a swelling limit of 5% is assumed. Because of the high swelling rate above the incubation fluence, the lifetime is quite insensitive to the swelling limit. Therefore, in the present study, a lifetime corresponding to 100 dpa is recommended for PCA at temperatures of 450-550°C.

IV.1.3.2 Radiation Creep

The radiation creep characteristics of PCA have not been extensively

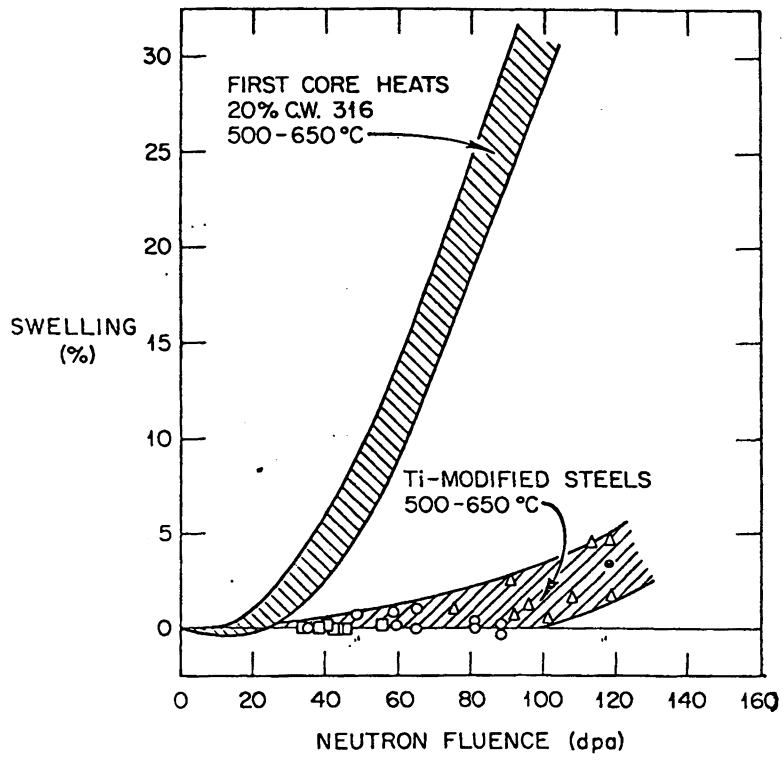

Figure IV-10. Swelling predictions are based in part on high dpa, low He data from EBR-II irradiations.

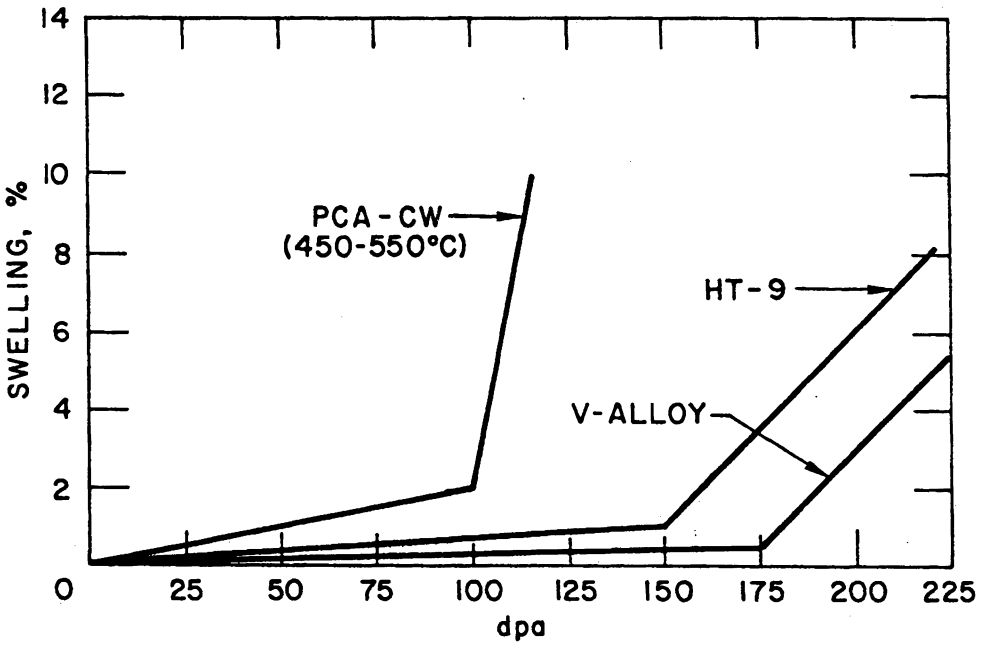

Figure IV-11. Predicted dependence of swelling on dpa for the three primary structural materials.

investigated. A radiation creep equation developed by Mattas,[9] which takes into consideration the lower swelling rates of PCA compared to type 316 stainless steel, is used in the present analysis. Estimates of the effects of radiation creep on the allowable design stresses for PCA are presented in Section IV.4.

IV.1.3.3 Effects on Mechanical Properties

There is very limited information for the effects of irradiation on the mechanical properties of PCA. As a result, extrapolation was made using the results of HFIR irradiations on a specially made heat of 316 stainless steel referred to as the MFE heat.[10] In examining these data, there does not appear to be a strong influence of transmutted helium on either the tensile or yield strength of the MFE heat, and in general, the response of the material is similar to that experienced in previous stainless steel irradiations without helium. Examination of the data shows that for irradiation temperatures $< 400°C$, both the tensile and yield strength increase as a result of matrix hardening up to approximately 25-30 dpa at which point saturation occurs and very little change occurs. Above this temperature, the opposite effect is produced. Using these trends, the irradiated tensile and yield strengths of PCA were developed (Fig. IV.-12, IV.1-13). The same approach was used to develop the uniform elongation curve presented in Fig. IV.-14. The trends shown in this figure are different than previously presented and reflect newer irradiation data on Type 316 and Ti modified 316 stainless steel. This figure shows about the same trend as seen in the tensile curves with saturation occurring at a damage level ~ 30 dpa. It is significant to note that at 575°C the uniform elongation with up to 3000 appm helium is still quite high and substantially above the 0-0.2% previously reported.[11] However, for temperatures below 300°C the uniform elongation falls below 1% into the range of 0.2-0.8%.[12,13] Reasons proposed for the change is that earlier irradiations were performed using material with a different heat treatment.

Most materials exhibit severe loss of ductility attributed to helium embrittlement at temperatures $\geq 0.5\ T_m$. For the present study, a maximum operating temperature of $0.5\ T_m - 50°C$ is recommended to avoid this problem. The 50°C is considered a reasonable margin to allow for both data and operating

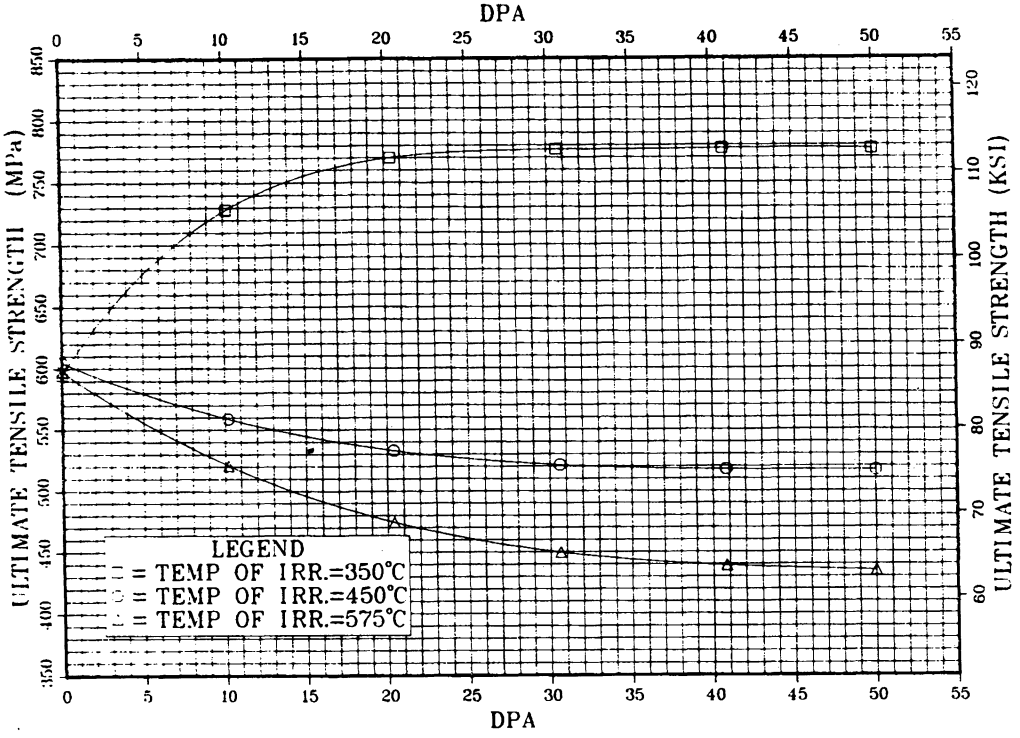

Figure IV-12. Predicted effect of irradiation on UTS of 25% CW-PCA.

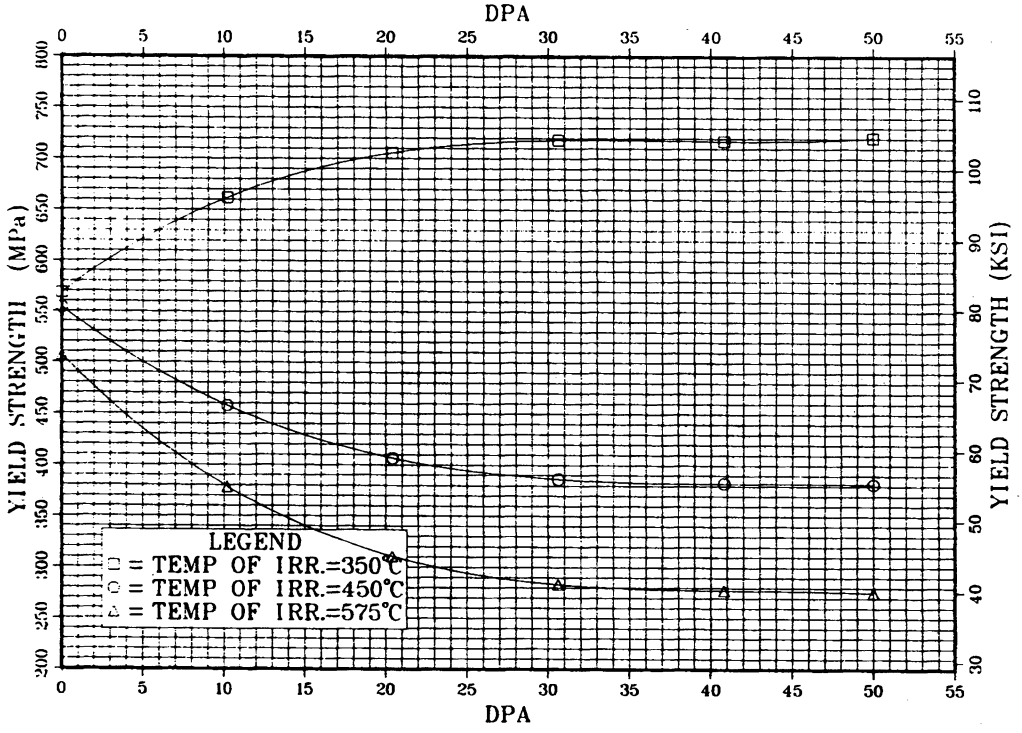

Figure IV-13. Predicted effect of irradiation on yield strength of 25% CW-PCA.

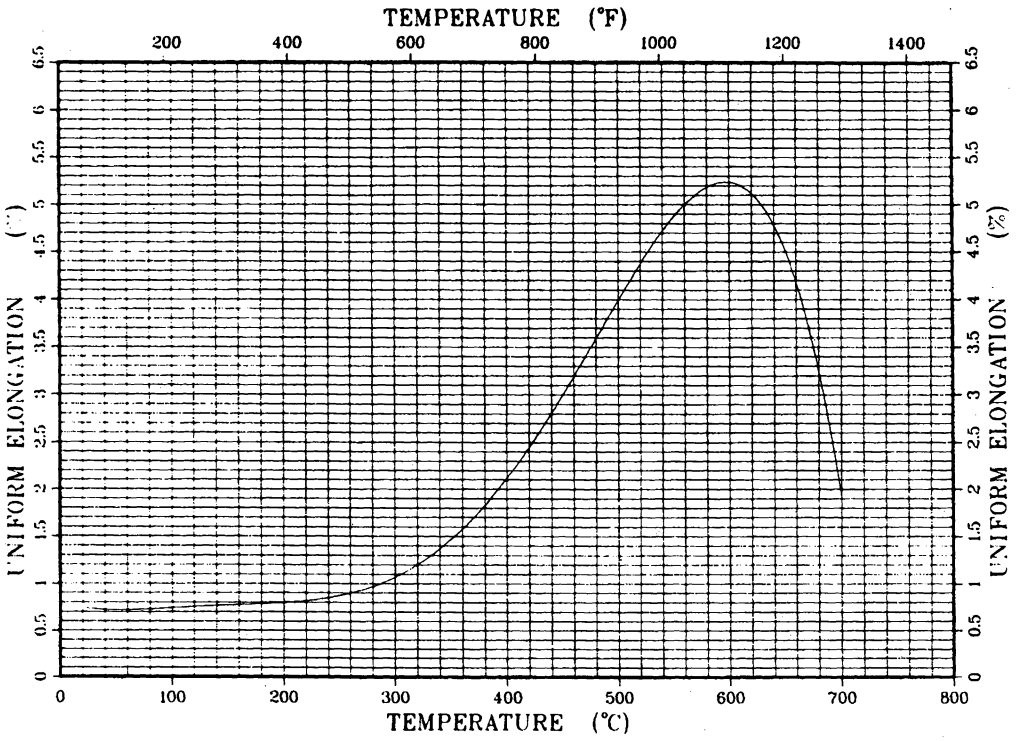

Figure IV-14. Uniform elongation of irradiated PCA (CW).

uncertainties. A maximum operating temperature limit of 550°C is recommended for PCA in the high fluence region.

Since serious problems attributable to increases in the ductile-brittle transition temperature (DBTT) above room temperature are not expected, a minimum operating temperature for this alloy is not specified.

IV.2 Ferritic Steels

Martensitic stainless steels of the 12Cr-1Mo Class, such as Sandvik HT-9, are of considerable interest because of their superior neutron swelling resistance, elevated temperature strength, liquid-metal compatibility and thermal stress resistance. This section briefly reviews HT-9 data which was compiled and used in the designs reported herein. The sections are divided into physical properties, mechanical properties, and radiation effects.

IV.2.1 Physical Properties

A compilation of physical property data was reviewed. Data include HT-9 composition, standard heat treatment, density[14], specific heat[15], thermal[15] and electrical[16] conductivity, Young's modulus[15], thermal expansion[14], and Poisson's ratio[1]. Recommended data for this study are presented in Table IV-1 and Figs. IV-1 through IV-5. In Fig. IV-3 the electrical resistivity of AISI 410 steel (Fe-12Cr) was assumed to approximate the resistivity of HT-9 (Fe-12Cr-1Mo).

IV.2.2 Mechanical Properties

Factors that influence the unirradiated value of the design allowable stresses according to the ASME nuclear pressure vessel code include mechanical strength (UTS and yield), and thermal creep. The code has certain criteria for selecting the allowable limits of stress on a component; the result of which is a factor called S_{mt}. This incorporates the tensile and creep property requirements. The tensile properties, stress rupture, and time to 1% creep strain for several heats of HT-9 are given in Figs. IV.-15 through IV.-17.[17] The average temperature dependent ultimate and yield strength for HT-9 is compared with values for PCA and VCrTi in Figs. IV-6 and IV-7.

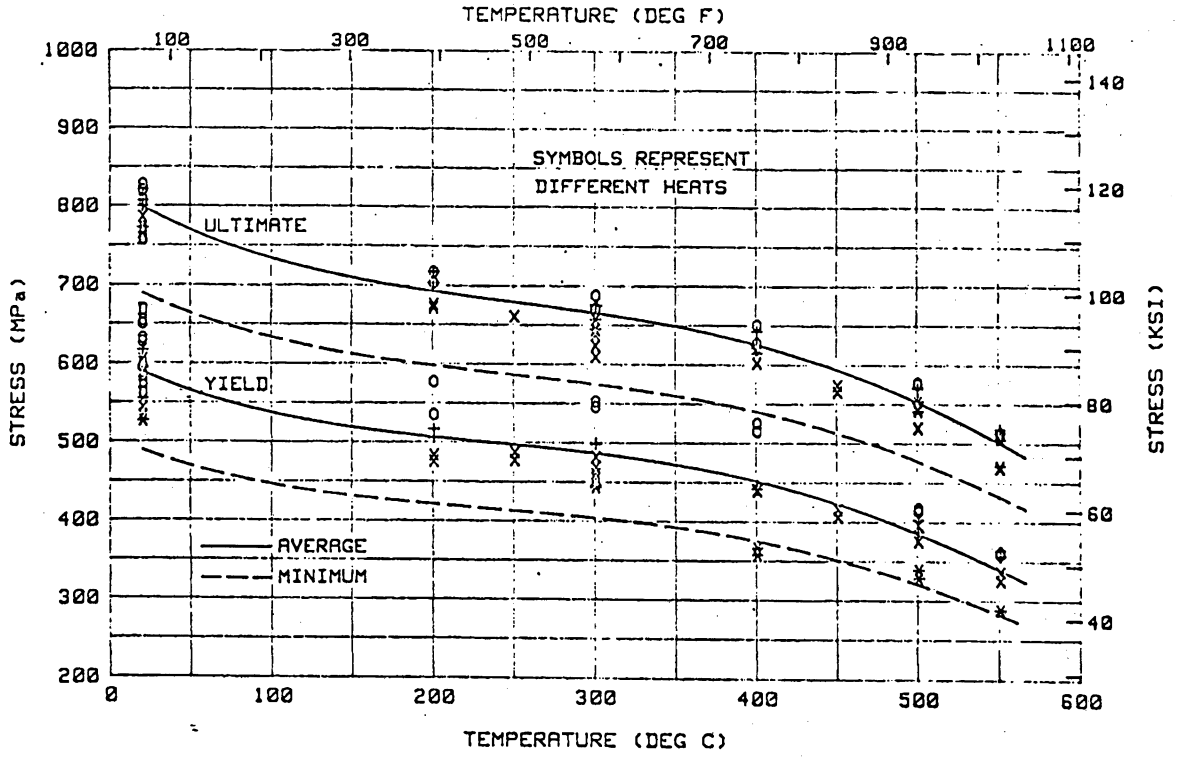

Figure IV-15. HT-9 - Predicted average and minimum tensile ultimate and tensile yield strengths and measured data.

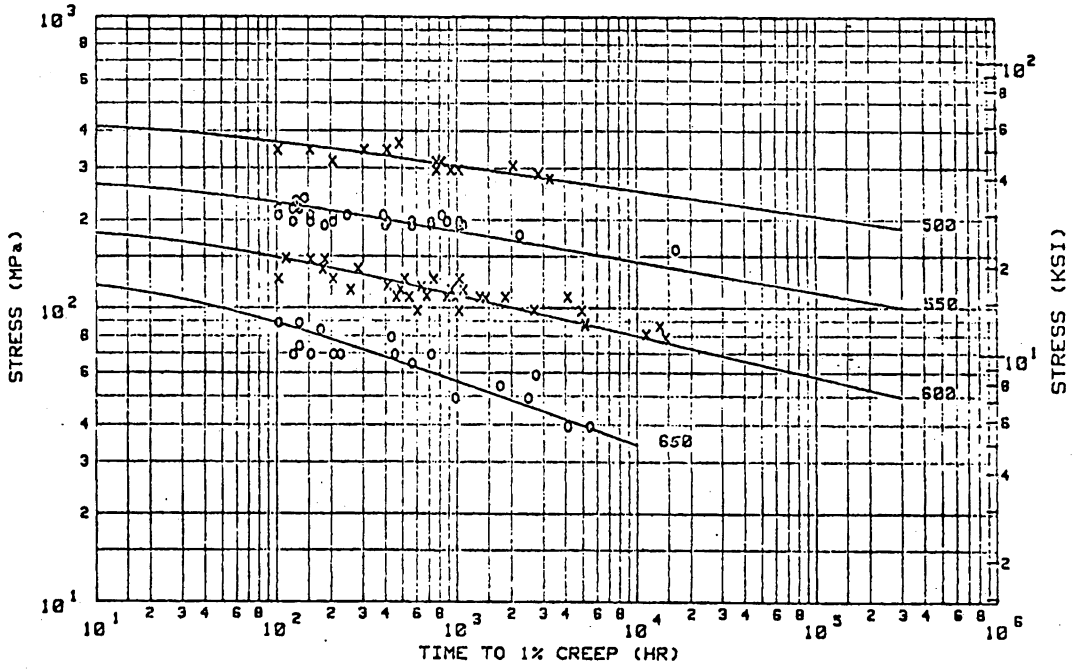

Figure IV-16. Alloy HTS - Predicted average 1% creep curves and measured data.

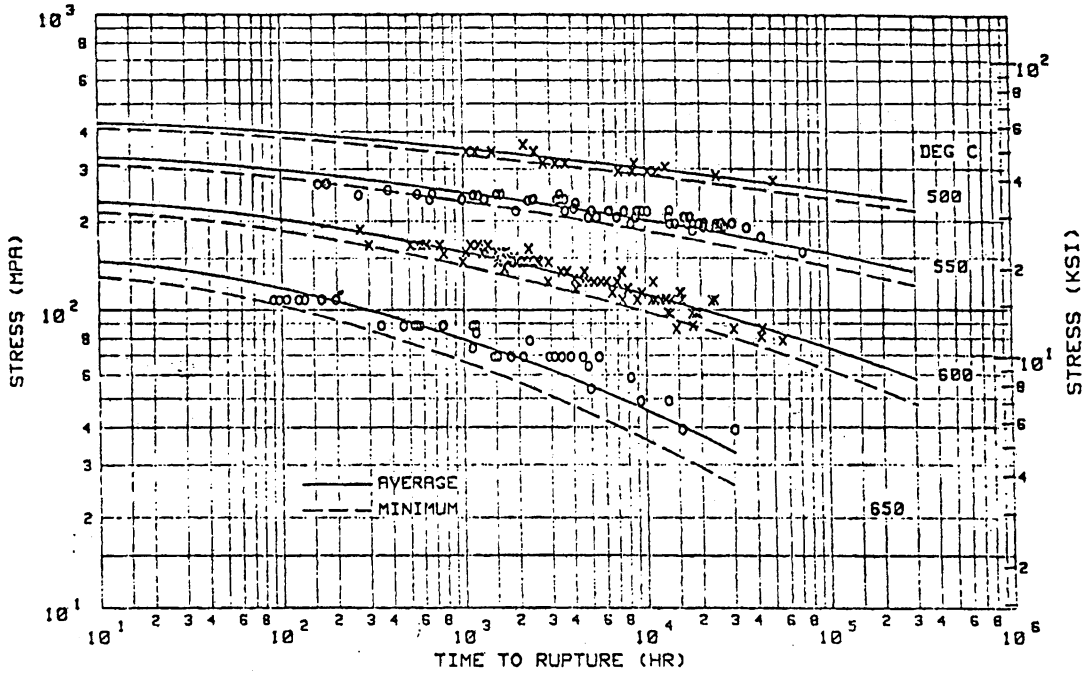

Figure IV-17. HT-9 - Predicted average and minimum creep rupture curves and measured data.

IV.2.3 Radiation Effects

The effects of irradiation on the properties and condition of HT-9 include dimensional changes (swelling and irradiated assisted creep), and embrittlement due to an upward shift in the ductile-brittle transition temperature.

IV.2.3.1 Swelling

Recently, theoretical treatments of the swelling phenomena in ferritic steels show that the swelling of this class will be approximately an order of magnitude less than that for the austenitic class. Although high fluence data do not exist for HT-9, data out to above 100 dpa with low helium contents corroborate this analysis in that the swelling rates were measured to be very small.[18] In Fig. IV.-11, it has been assumed that HT-9 has a bilinear swelling response because some data suggests swelling may increase at higher helium contents, although the theoretical treatments suggest it will not increase in swelling rate until a very high incubation dose. For the recommended swelling limit of 5%, the lifetime for HT-9 corresponds to ~ 190 dpa.

IV.2.3.2 Radiation Creep

The radiation creep characteristics of HT-9 have not been extensively investigated. Based on a comparison with austenitic steels, the body-centered-cubic ferritic steels generally exhibit lower radiation creep rates.[19] Estimates of the radiation creep on the allowable design stress are presented in Section IV.4.

IV.2.3.3 Mechanical Properties

Limited data indicate that the strength of HT-9 increases during irradiation.[20] For purposes of the present design, it is recommended that unirradiated tensile properties be used to obtain allowable design stresses.

The shift in DBTT has been handled by suggestion from LWR data sources on low alloy ferritic steel.[21] It is known that the change in DBTT of low alloy pressure vessel steels saturates at relatively low fluences (~ 0.1 dpa). This is known to be due to the precipitation of a copper-rich strengthening

phase, because as the alloy is depleted in copper, the strengthening mechanism slows thus showing an increase in the DBTT. Since the shift in DBTT in bcc materials probably is due to the hardening that occurs during irradiation, the DBTT stops increasing as the matrix depletes itself of the elements needed in the precipitate. In the alloy HT-9, the irradiation strengthening effect is probably due to a silicon-rich phase, called G-phase, and thus the change in DBTT of HT-9 may diminish at high fluences. Data on HT-9 at 13 dpa irradiated at 390°C show a DBTT of ~ 150°C, which may not increase further if HT-9 behaves similarly to the low alloy pressure vessel steels mentioned above, and which is well below the lowest proposed operating temperature.[22] A critical question remains as to whether a greater shift in the DBTT occurs for HT-9 at lower irradiation temperatures as is the case for some pressure vessel steels. It has been assumed for this study that the DBTT stays below the coolant temperature. Other factors such as afterheat to maintain a temperature above the DBTT even after shutdown, novel thermomechanical treatments, and alloy composition modifications may further ensure that the structure never operates on the lower shelf.

IV.3 Vanadium Alloys

Vanadium-base alloys offer the potential of significant advantage over other candidate alloys as a fusion reactor structural material. High fluence irradiations under LMFBR conditions and high damage level ion irradiations have demonstrated an inherent resistance of certain vanadium alloys to void swelling and ductility loss in comparison to most other candidate alloys. Of particular importance in projecting the potential radiation damage resistance of vanadium alloys to fusion reactor conditions is the apparent insensitivity to moderate compositional and microstructural variations. The relatively high thermal conductivity and low thermal expansion coefficient, which result in lower thermal stresses for a given heat flux compared to most other candidate alloys, should enhance the wall load and lifetime limitations. Since the mechanical strength of vanadium alloys is retained at relatively high temperatures, higher operating temperatures are projected for vanadium alloys than for austenitic or ferritic steels. Vanadium alloys produce the least impact on tritium breeding of the primary candidate alloys and selected vanadium alloys offer the potential for low long term (> 30 y) activation.

Major concerns regarding the use of vanadium-base alloys relate primarily to their reactivity with nonmetallic elements such as oxygen and nitrogen; for example, as impurities in liquid metal systems, during accidental exposure to air at high temperature, and contamination during welding or fabrication. A second problem arises from the relatively limited data base for this alloy system.

The V-15Cr-5Ti alloy exhibits many favorable characteristics for the fusion reactor application, and therefore, is used as a reference material in the present study. Further investigations may provide more optimized alloys with improved performance characteristics. This section presents a summary of the physical properties, mechanical properties and radiation effects data for the V-15Cr-5Ti alloy. For cases where insufficient data exist for reliable evaluation, projections based on available information are presented for use in this study. Further effort will be required to verify and more reliably predict the alloy performance for conditions of interest. Data for corrosion/compatibility of vanadium alloys in liquid metal, water, and gaseous systems are presented in Chapter VI.

IV.3.1 Thermophysical Properties

The temperature-dependent thermophysical properties of V-15Cr-5Ti are given in Figs. IV-1 thru IV-5. The specific heat values are for vanadium[23], thermal conductivity and thermal expansion[24] and the elastic modulus values are those of a similar alloy (V-15Ti-7.5Cr)[25] The melting temperature of the alloy is estimated to be 2150°K, which is slightly below that of pure vanadium. The density of V-15Cr-5Ti is 6.16 g/cm^3 and Poisson's ratio is 0.36[25]. Electrical resistivity is from Ref. 26.

IV.3.2 Mechanical Properties - V-15Cr-5Ti Alloy

The purpose of this section is to review and summarize the mechanical properties of the V-15Cr-5Ti alloy in the nonirradiated condition. Property data determined most recently for this alloy on OFE-sponsored research programs are emphasized. Data for the tensile behavior (0.2% yield strength, ultimate strength, and tensile ductility) and thermal creep behavior (stress for 1% strain in 1000 h) are presented.

IV.3.2.1 Tensile Properties

The tensile properties, measured on 0.76 mm thick sheet specimens prepared from recrystallized material, are summarized in Table IV-2. Details of the testing conditions and material chemistry can be found in Ref. 27. The strength data are plotted as a function of test temperature in Fig. IV-18. Observe from Table IV-2 the consistently uniform values of tensile ductility over the 25-750° temperature range. The slight increase in strength, particularly the ultimate strength, in the 550-750°C temperature range is due to dynamic strain aging and is regularly observed in vanadium alloys in the 0.35-0.45 T_m range.

IV.3.2.2 Thermal Creep Behavior

The creep strength of V-15Cr-5Ti sheet specimens, expressed as the stress to produce 1% strain in 1000 h, is summarized in Table IV-3.[28] These data have been extrapolated or interpolated from creep tests performed in ultra-high vacuum (< 10^{-8} torr) creep test stands on the same heat of material (also on 0.76 mm thick sheet) for which tensile data were given in Sec. IV.3.2.1.

TABLE IV-2. TENSILE PROPERTIES OF V-15Cr-5Ti SHEET

Temperature (°C)	Strength (MPa)		Elongation (%)	
	0.2% YS	UTS	Uniform	Total
25	490	690	23	28
450	340	540	13	17
500	320	530	14	17
550	330	550	15	19
600	305	555	13	16
650	310	550	14	17
700	310	590	16	19
750	305	560	12	16

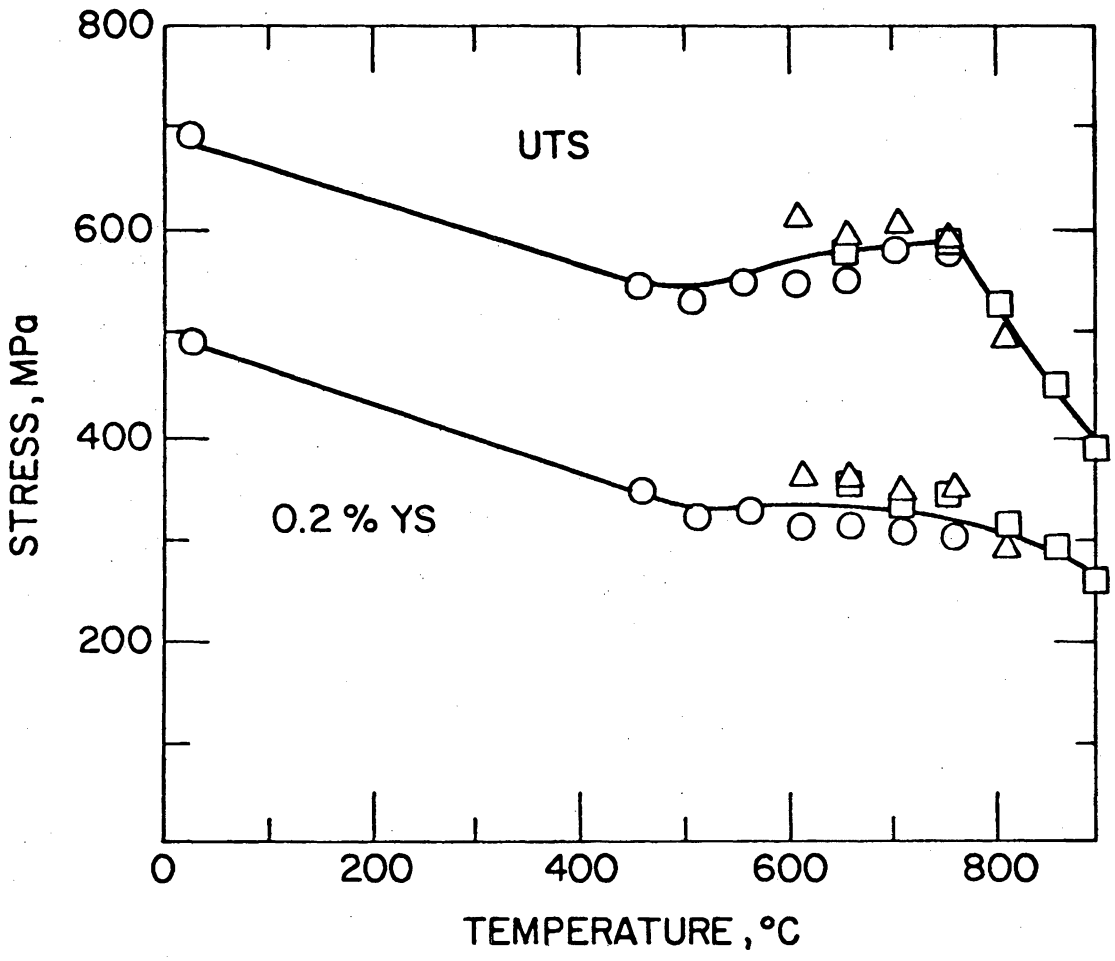

Figure IV-18. Tensile properties of V-15Cr-5Ti.

TABLE IV-3. CREEP STRENGTH OF V-15Cr-5Ti SHEET

Temperature (°C)	Stress for 1% Thermal Creep in 1000 h (MPa)
25 - 550	>> 400
600	> 400
650	> 400
700	380
750	330
800	~ 270

These creep data[28] are plotted in terms of rupture properties, along with data for a V-13Cr-3Ti alloy,[29] on Fig. IV-19. The creep strength of these two alloys appears to be comparable for the 650-750°C temperature range. Rupture strains for the specimens tested at 650-800°C and reported in Refs. 28 and 29 were in the 13-33% range.

IV.3.2.3 Discussion of Mechanical Properties of V-15Cr-5Ti

In dealing with alloys based on metals of Group V [V, Nb, Ta] it is important to consider the possibility of an unacceptably high ductile-brittle-transition-temperature (DBTT) and the consequences of nonmetallic contamination. For the data presented in Table IV-2 note the very high uniform and total elongations (23 and 28%, respectively). While not definitive in establishing the DBTT, these values and the 100% ductile shear failure mode reported in Ref. for these specimens suggests the nonirradiated DBTT is well below room temperature. In addition, intentional increases of up to 1200 wppm oxygen to these specimens did not induce brittle (cleavage) behavior at room temperature. These results, albeit very limited and qualitative in nature, do not indicate a problem for the V-15Cr-5Ti alloy over the temperature range of interest to this study.

As a final point of discussion it is worthwhile to consider the possibility that the mechanical properties of V-15Cr-5Ti might be enhanced by strain hardening. Strain hardening is known to be a potent means of increasing the strength of metal alloys, including the body-centered-cubic (BCC) refractory metal alloys,[30,31] although the levels of strength increase which can be

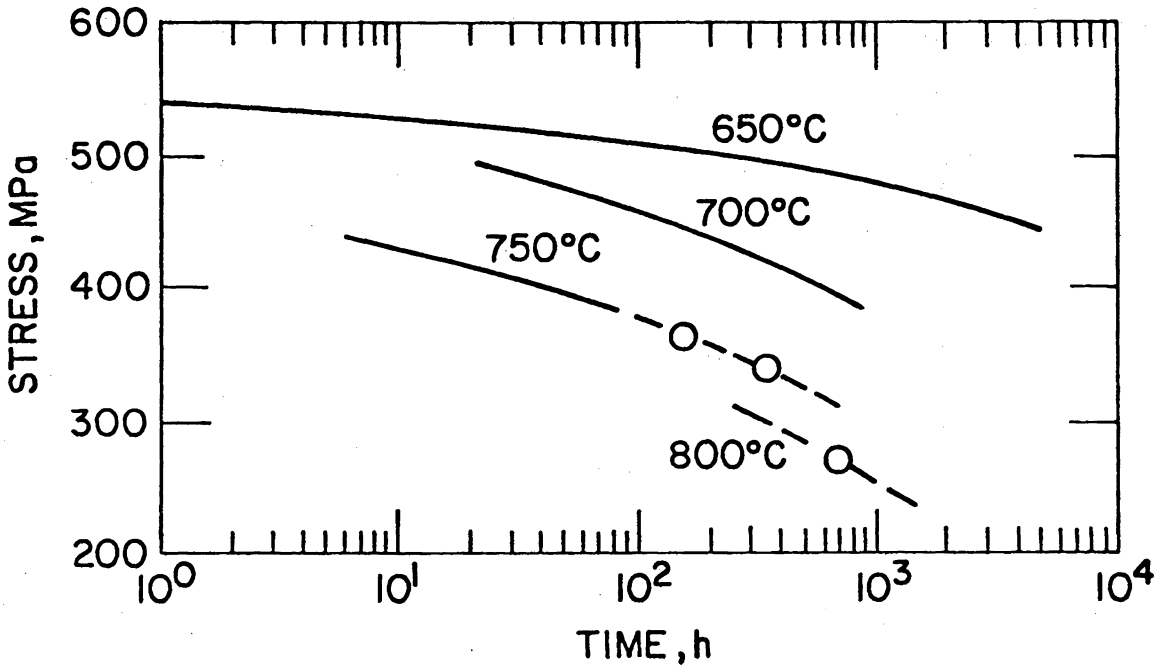

Figure IV-19. Creep-rupture behavior of V-3Ti-13Cr.

realized are comparatively less than those attainable in face-centered-cubic metal alloys such as stainless steels or aluminum alloys.

Strain hardening is regularly used to advantage with the Group VI (Mo, W) BCC alloys where an additional advantage is gained by the lowering of the DBTT. In reviewing the elevated temperature creep data for the refractory metals, however, Begley, et al.[32] found that, for temperatures above about 0.4 T_m, V, Nb and Ta-base alloys exhibited inferior time-dependent strength in the strain hardened condition compared to the fully recrystallized, fine grain microstructural condition. This partially explains why essentially all long-time mechanical property testing is carried out on fully recrystallized V, Nb or Ta alloys. This practice has been biased in the past by the fact that the applications of interest have usually been at quite high (to $\gtrsim$ 0.45 T_m) temperatures in space power conversion systems.

The reasons that V, Nb and Ta alloys are relatively less able to maintain high levels of strain hardening at elevated temperatures, compared to Mo or W alloys, are related to their lower elastic and shear moduli and the higher self-diffusivities of the former at equivalent fractions of their melting temperatures. Thus, even Ta with a 3269 K melting temperature is unable to sustain the same level of strain hardening which is achievable with Mo which has a 2883 K melting temperature. Strain hardening is achieved by increasing the microscopic flow stress which is proportional to the square roots of the dislocation density. Hence, the degree of strengthening which can be realized depends strongly on the shear modulus (G). Moreover, since atom movements participate in the recovery and recrystallization processes which negate the strain hardening effect, (self and substitutional element) diffusion are of obvious critical importance.

For the current study, with somewhat lower temperatures than are generally considered for vanadium-base alloys, it is useful to reexamine this situation. Data summarized by Tietz and Wilson[33] indicate that recovery in moderately strain hardened Group V metal alloys begins at about 0.32-0.34 T_m and continues until recrystallization dominates at about 0.38-0.42 T_m upward. For vanadium-base alloys these data suggest useful levels of strain hardening could be maintained to at least 450°C (0.33 T_m) and possibly to temperatures as high as 550°C (0.38 T_m). An important factor that would affect the realization of this strengthening increment would be the level of strain intro-

duced. Thus, by introducing perhaps 30-50% strain at cold-to-warm deformation conditions, and following this by a thermal anneal at sub-recovery temperatures it should be possible to induce polygonization (i.e., subgrain formation) of the dislocation substructure which would then, by virtue of the lower residual stored energy, resist further recovery and recrystallization better than a heavily cold-worked structure.

In this way it seems highly likely that a minimum increase of 20% could be attained over the tensile and creep properties presented in Tables IV-2 and IV-3. Recommended values for the temperature dependent ultimate and yield strength of VCrTi are compared in Figs. IV-6 and IV-7. In view of the radiation environment which will obtain, it is probably prudent to assume this strain hardening increment would be stable only to about 500°C ($\sim$ 0.35-0.36 T_m). However, at that temperature, and probably to 600°C (minimum) additional strengthening will be realized due to the radiation-induced production of matrix-hardening dislocation loops.

IV.3.3 Radiation Effects

The effects of radiation on the projected performance of the V-15Cr-5Ti alloy have been evaluated. In general, the data base for vanadium base alloys is much more limited than for the other two reference alloys. Therefore, this assessment involves significant extrapolations which result in greater uncertainties. Since vanadium alloys were once considered as a backup fuel cladding for fast breeder reactor applications, most of the data were developed in this program. In fact, the reference alloy was originally developed in the fast breeder program. This alloy was found to be highly radiation damage resistant in limited tests; however, it does not necessarily represent an optimized alloy. Because of the limited data, some of the projected performance characteristics recommended for the present study are based on data for similar alloys and for other alloy systems. Recommended values are presented for swelling, and radiation creep. The effects of radiation on the tensile properties are also evaluated. General features of the irradiation performance characteristics are similar to the other alloy systems.

IV.3.3.1 Swelling

The projected swelling response of V-15Cr-5Ti alloy is based on neutron (fast reactor) and ion irradiation data. Vanadium and vanadium alloys exhibit peak swelling at ~ 525°C under fast neutron irradiation. Experiments have shown that titanium concentrations of only a few percent greatly suppress swelling compared to unalloyed vanadium.[34] Similar behavior has been observed under both single and dual ion irradiations. Neutron irradiation to ~ 20 dpa for V-15Cr-5Ti and ~ 35 dpa for V-20 Ti indicated no tendency for void formation or swelling. Both single and dual (He/dpa of 3 to 50) ion irradiations of V-15Cr-5Ti to 60 dpa produced essentially no swelling for all conditions tested.[35,36] Although these data are limited, comparison with swelling data under similar conditions for either PCA or HT-9 indicate lower swelling for the vanadium alloy. Effects of helium are also projected to be less for VCrTi since the helium generation rate is much less than for PCA or HT-9. Based on this limited data and the comparison with irradiation data for the other alloys, the projected bilinear swelling curve for VCrTi is given in Fig. IV-11.

IV.3.3.2 Radiation Creep

The radiation creep characteristics of vanadium alloys have not been determined experimentally. For purposes of the present study the creep characteristics of VCrTi are assumed to be similar to those for HT-9. The temperature dependence has been modified by the ratio of the absolute melting temperatures of the two alloys.

IV.3.3.3 Effects on Mechanical Properties

Data on the effects of irradiation on vanadium alloys are even more limited than the swelling. The V-20Ti alloy irradiated to 36 dpa at temperatures of 500 - 750°C exhibited some hardening with little effect on the elongation. For purposes of the present study it is assumed that V-15Cr-5Ti will be strengthened at temperatures below ~ 650°C. Therefore, the unirradiated ultimate, yield, and creep strength are used to obtain the design allowable stresses.

Existing data have not indicated that the DBTT of vanadium alloys are increased above room temperature by irradiation. Since this effect is typi-

cally observed to saturate at relatively low fluences, it is assumed for the present study that this constraint is not critical for the VCrTi alloy.

As is the case for PCA and HT-9, a maximum design temperature limit of 750°C is recommended for the present study. This limit is based on helium embrittlement which is commonly observed in metals at temperatures > 0.5 T_m. A margin of ~ 50°C results in the allowable limit of 750°C.

IV.4 Allowable Design Stresses

The allowable stresses for three candidate structural materials (PCA, V-15Cr-5Ti and HT-9) for fusion application have been determined for both irradiated and unirradiated conditions. Although the ASME Boiler and Pressure Code, Section III has been used as a guidance in obtaining these stress limits, it should be kept in mind that none of these candidate materials is currently approved by the code. The ASME Code normally allows only annealed materials because many of the code analysis techniques rely heavily on the sustained ductility of the material. Use of these code rules in a radiation environment where ductility in reduced drastically requires extreme caution on the part of the designers.

A recurring problem in determining the allowable stresses is the lack of a sufficient data base. In some cases we do not have any data at all; in the majority of cases the data base is not extensive enough to allow the determination of valid minimum properties. In such cases extrapolation of whatever data are available and empirical methods are used to establish a required property when the necessary data for determining the property is lacking.

The time dependent (unirradiated) primary stress limit S_{mt} for any material is determined by the lesser of S_m and S_t defined as follows:

S_m = Least of - 1/3 S_u at R.T.
- 1.1/3 S_u at T
- 2/3 S_y (0.9 S_y for austenitic SS at T)
- 2/3 S_y at R.T.

where

S_u = minimum ultimate tensile strength

S_y = minimum yield strength

S_t = Least of - 2/3 minimum stress to cause rupture in time t
- 80% minimum stress to beginning of tertiary creep in time t
- minimum stress to cause 1% creep strain in time t

The code allows a higher fraction of the yield strength to be used in the case of annealed austenitic stainless steels to take advantage of their large strain hardening capability. However, it is questionable whether such advantage should be taken for 25% cold worked materials. In the present exercise the S_m values are determined by S_u in all cases and not by S_y and so the question becomes moot.

Although it is recognized that material properties vary in a continuous manner with neutron fluence, for simplicity 10 dpa is chosen arbitrarily as the demarkation point between irradiated and unirradiated properties. The S_m value for the irradiated material is determined from the same formalism as for the unirradiated case with the post-irradiated properties replacing the unirradiated properties, and taking the minimum of the two values of S_m. In determining the S_t value for the irradiated case it is recognized that radiation-induced creep at low stresses is nondamaging. Thus, S_t for the irradiated material is determined from the minimum of the S_t for the unirradiated material and the minimum stress to cause a radiation-induced plus thermal creep strain of 5% in a given time and fluence. The number 5% has been chosen arbitrarily to limit excessive deformation in the structure. More detailed analysis of fusion reactor structures in the future will indicate whether such a limit is reasonable or not.

Computed values of S_m and S_{mt} for PCA (25% CW), V-15Cr-5Ti (SH) and HT-9 (N&T) are included in Tables IV-4, IV-5, and IV-6.

TABLE IV-4. ALLOWABLE STRESSES FOR PCA (25% CW)

Temperature (°C)	S_m (MPA)	Unirradiated (< 10 DPA) S_{mt}[a] (MPA)				Irradiated (> 10 DPA)		
		10^4 h	2×10^4 h	3×10^4 h	5×10^4	S_m (MPA)	S_{mt}[b] (MPA) 75 DPA	(MPA) 100 DPA
100	225	225	225	225	225	225	190	155
200	208	208	208	208	208	208	190	155
300	205	205	205	205	205	205	190	155
400	205	205	205	205	205	205	190	155
500	205	205	205	205	205	190	185	150
550	195	195	195	190	175	175	150	130

[a]For $t \leq 2.8 \times 10^4$ h, $S_{mt} = S_m$ (unirradiated).

[b]For DPA $\leq$ 70, $S_{mt} = S_m$ (irradiated) based on a maximum strain limit of 5%.

TABLE IV-5. STRESS ALLOWABLES FOR V-15Cr-5Ti (STRAIN HARDENED)

Temperature (°C)	Unirradiated (< 10 dpa)					Irradiated (> 10 dpa)				
	S_m(a) (MPA)	S_{mt} (MPA)				S_m(a) (MPA)	S_{mt} (MPA)			
		10^4 h	2×10^4 h	3×10^4 h	5×10^4 h		100 dpa	150 dpa	200 dpa	250 dpa
20	275	275	275	275	275	275	165	125	105	90
200	250	250	250	250	250	250	165	125	105	90
300	240	240	240	240	240	240	165	125	105	90
400	230	230	230	230	230	230	165	125	105	90
500	220	220	220	220	220	220	165	125	105	90
600	235	235	235	235	235	235	165	125	105	90
650	235	235	235	235	235	235	165	125	105	90
700	235	230	190	175	155	235	165	125	105	90
750	230	160	125	115	85	230	155	115	95	80

[a]Since these S_m values are based on average rather than equal minimum values of S_u from a single heat of material they are equal to 1/3 S_u and not 1.1/3 S_u.

TABLE IV-6. ALLOWABLE STRESSES FOR HT-9 (NORMALIZED AND TEMPERED)

Temperature (°C)	Unirradiated					Irradiated				
	S_m (MPA)	S_{mt} (MPA)				S_m (MPA)	S_{mt} (MPA)			
		10^4 h	3×10^4 h	10×10^4 h	30×10^4 h		50 dpa	75 dpa	100 dpa	150 dpa
20	250	250	250	250	250	250	235	198	163	125
200	220	220	220	220	220	220	220	198	163	125
300	210	210	210	210	210	210	210	198	163	125
400	200	200	200	200	200	200	200	198	163	125
500	175	160	150	140	125	175	175	175	163	125
550	160	110	90	80	75	160	160	160	150	115
600	140	60	50	40	30	140	105	80	70	50

REFERENCES FOR CHAPTER IV

1. D. L. Smith, et al., "Fusion Reactor Blanket/Shield Design Study," ANL/FPP/79-1, Argonne National Laboratory, pp. 4-8 (1979).

2. Anon, Areospace Structural Metals Handbook, Ferrous Alloys - Type 316 and 317, Metal and Ceramics Information Center, Battelles Columbus Laboratories, p. 1307-5 (1974).

3. J. W. Davis, editor, Material Handbook for Fusion Energy Systems, U.S. Department of Energy, p. AB02-3201 (1982).

4. T. K. Chu and C. Y. Ho, "Thermal Conductivity and Electrical Resistivity of Eight Selected AISI Steels," Thermal Conductivity, 18 pp. 79-104 (1978).

5. C. F. Lucks and H. W. Deem, Thermal Properties of 13 Metals, ASTM STP-227 (1958) and D. E. Furman, "Thermal Expansion Characteristics of Stainless Steels between 300 and 1000 F, Journal of Metals 188 (1950).

6. F. Garofalo, "Temperature Dependence of the Elastic Moduli of Several Stainless Steels," Proceedings BSTM, 60, pp. 738-749 (1960).

7. D. N. Braski and P. J. Maziasz, "The Tensile Properties of Unirradiated Path A - PCA," Alloy Development for Irradiation Performance - Semiannual Progress Report, DOE/ER-0045/9, pp. 63-70 (February 1983) and DOE/ER-0045/10, pp. 49-52 (to be published).

8. P. J. Maziasz and D. N. Braski, "Swelling of Path A - PCA Irradiated to 10 dpa in HFIR," Alloy Development for Irradiation Performance - Semiannual Progress Report, DOE/ER 0045/8, pp. 98-117 (September 1982).

9. Personal Communication, R. F. Mattas and D. L. Smith, January 1983.

10. R. L. Kluck and M. L. Grossbeck, Tensile Properties and Swelling of 20% Cold Worked Type 316 Stainless Steel Irradiated in HFIR, Alloy Development for Irradiation Performance - Quarterly Progress Report DOE/ER-0045/6, pp. 58-69 (July 1981) and Semiannual Progress Report DOE/ER-0045/9, pp. 71-77 (February 1983).

11. E. E. Bloom and F. W. Wiffen, "The Effects of Large Concentrations of Helium on the Mechanical Properties of Neutron Irradiated Stainless Steel," Journal of Nuclear Materials, 58, pp. 171-184 (1975).

12. R. L. Kluck and M. L. Grossbeck, "Tensile Properties and Swelling of 20% Cold Worked Type 316 Stainless Steel Irradiated in HFIR," Alloy Development for Irradiation Performance, Semiannual Progress Report DOE/ER-0045/10, pp. 60-66 (to be published).

13. R. L. Kluck and M. L. Grossbeck, "Tensile Properties of U.S.S.R. Austenitic Stainless Steel After Low Temperature High Flux Reactor Irradiation," Alloy Development for Irradiation Performance - Semiannual Progress Report, DOE/ER-0045/8, pp. 266-275 (September 1982).

14. J. W. Davis, editor, Materials Handbook for Fusion Energy Systems (1983) density page AA01-3304, thermal expansion AA01-3114.

15. Personal Communication J. W. Davis - proposed datasheet for Materials Handbook for Fusion Energy Systems.

16. T. K. Chu and C. Y. Ho, op. cit.

17. J. E. Chafey and J. B. Wattier, "Estimation of Allowable Design Stress Values for 12Cr-1Mo-0.3V Steel," General Atomic Company Report GA-A14610.

18. J. L. Straalsand and D. S. Gelles, "Assessment of the Performance Potential of the Martensitic Alloy HT-9 for Liquid Metal Fast Breeder Reactor Applications," presented at Topical Conference on Ferritic Alloys for Use in Nuclear Energy Technologies, Snowbird, Utah, June 19-23, 1983.

19. R. J. Puigh and G. L. Wire, "In-Reactor Creep Behavior of Selected Ferritic Alloys," presented at Topical Conference on Ferritic Alloys in Nuclear Energy Technologies, Snowbird, Utah, June 19-23, 1983.

20. T. Lauritzan, et al., Effects of Irradiation on the Mechanical Properties of Ferritic Alloys HT-9 and 2.25 Cr-1Mo," presented at Topical Conference on Ferritic Alloys in Nuclear Energy Technologies, Snowbird, Utah, June 19-23, 1983.

21. T. V. Marston, "Use of Ferritic Steels in Light Water Reactor Plants," presented at Topical Conference on Ferritic Alloys in Nuclear Energy Technologies, Snowbird, Utah, June 19-23, 1983.

22. W. L. Hu and D. S. Gelles, "Miniature Charpy Impact Test Results for the Irradiated Ferritic Alloys HT-9 and Modified 9Cr-1Mo," presented at Topical Conference on Ferritic Alloys in Nuclear Energy Technologies, Snowbird, Utah, June 19-23, 1983.

23. Y. S. Tauloukian, editor, Thermophysical Properties of High Temperature Solid Materials, The MacMillan Company, New York (1967).

24. F. L. Yaggee, et al., "Thermal Expansivities, Thermal Conductivities, and Densities of Vanadium, Titanium, Chromium, and Some Vanadium Base Alloys," Journal of the Less-Common Metals, 19, pp. 39-51 (1969).

25. R. E. Gold, et al., "Technical Assessment of Vanadium Base Alloys for Fusion Reactor Applications, Westinghouse Electric Corporation Report COO-4540-1, Vol. 2 (April 1978).

26. B. A. Loomis and D. L. Smith, "Evaluation and Development of Vanadium Base Alloys for Fusion Reactor Applications," Alloy Development for Irradiation Performance - Semiannual Progress Report DOE/ER-0045/10, pp. 87-90 (to be published).

27. Tensile curves developed using data obtained from following four references. The curves were increased by 20% to allow for strength enhancement as a result of strain hardening.

a) R. F. Mattas, et al., "Elevated Temperature Tensile Properties of V-15Cr-5Ti Containing Helium Induced by Ion Bombardment and Tritium Decoy," Proceeding of the 2nd Topical Meeting on the Technology of Controlled Nuclear Fusion, CONF-760935-P1, Volume 1, p. 199 (1977).

b) A. T. Santhanan, et al., Journal of Nuclear Materials, 18, p. 302 (1973).

c) R. E. Gold, op. cit.

d) R. E. Gold and R. L. Ammon, "Mechanical Property Evaluations of Patch C Vanadium Scoping Alloys," Alloy Development for Irradiation Performance - Quarterly Progress Report DOE/ER-0045/6, pp. 96-105 (July 1981).

28. The creep data was extracted from the following sources:

a) R. E. Gold and R. Bajaj, "Mechanical Property Evaluation of Path C Vanadium Scoping Alloys," Alloy Development for Irradiation Performance - Semiannual Progress Report DOE/ER-0045/9, pp. 122-141 (February 1983).

b) R. Bajaj and R. E. Gold, "Mechanical Property Evaluations of Path C Vanadium Scoping Alloys," Alloy Development for Irradiation Performance - Semiannual Progress Report DOE/ER-0045/10, pp. 74-80 (to be published).

29. M. Schirra, "Creep and Creep-Rupture Behavior of Vanadium Based Alloys," United States - Euratom Fast Reactor Exchange Program, EURFNR-1449 (1977).

30. T. E. Tietz and J. W. Wilson, "Behavior and Properties of Refractory Metals," Stanford University Press, Stanford, CA (1965).

31. B. A. Wilcox, "Basic Strengthening Mechanisms in Refractory Metals," Refractory Metals Alloys, Tetallurgy and Technology, I. Machlin, et al., editors, Plenum Press, NY, pp. 1-40 (1968).

32. R. T. Begley, D. L. Harrod and R. E. Gold," High Temperature Creep and Fracture Behavior of the Refractory Metals," Refractory Metal Alloys, Metallurgy and Technology, J. Machlin, et al., editors, Plenum Press, NY, pp. 41-84 (1968).

33. T. E. Tietz and J. W. Wilson, Behavior and Properties of Refractory Metals, Stanford University Press, pp. 331-374 (1965).

34. R. Carlander, et al., "Effects of Radiation on Substructure and Mechanical Properties of Metals and Alloys," American Society for Testing and Material publication ASTM-STP529, p. 399 (1973).

35. A. T. Santhanam, et al., Defects and Defect Clusters in B.C.C. Metals and Their Alloys, Nuclear Metallurgy, 18, p. 302 (1973).

36. B. A. Loomis and G. Ayrault, "Cavity Formation in Single- and Dual-Ion Irradiated V-15Cr-5Ti Alloy," Damage Analysis and Fundamental Studies - Quarterly Progress Report DOE/ER-0046/12, pp. 194-205 (February 1983).

TABLE OF CONTENTS

CHAPTER V - SPECIAL MATERIALS

LIST OF FIGURES FOR CHAPTER V

LIST OF TABLES FOR CHAPTER V

V. SPECIAL MATERIALS

Three areas, tritium breeding materials, neutron multipliers and electrical insulators (coatings) were addressed by the Special Materials Task during the first year of the Blanket Comparison and Selection Study. In the area of tritium breeding materials, the effort has primarily been focussed on the collection, compilation and limited assessment of properties for liquid lithium (Li) and liquid lithium-lead (17Li-83Pb). The purpose is to provide a data base on these two materials so that consistent properties values can be used for design within the study. A rather complete set of Li properties is now available, though several properties for 17Li-83Pb are still lacking.

With the possible exceptions of Li_2O and Li_8ZrO_6, neutron multipliers are required to achieve an acceptable tritium breeding performance for virtually all other solid breeders. The definition of blanket research and development (R/D) risk in terms of the tritium breeding ratio (II.3) also adds a strong incentive to use neutron multipliers for Li_2O and Li_8ZrO_6 since they will lower the R/D risk by enhancing tritium breeding. Two neutron multipliers, beryllium (Be) and lead (Pb), are considered for the solid breeder blanket designs in this study. Beryllium is the reference neutron multiplier for the STARFIRE blanket.[1] Lead was previously set aside primarily because of its low melting temperature (327°C). If lead were to be used in liquid form, the main concern would be its compatibility with the structural material. This chapter gives selected properties for Be and Pb based on previous reviews.[1,2] Irradiation effects in beryllium are discussed with emphasis on methods to accommodate the swelling caused by helium generation. The resource issue of beryllium is also addressed. Compatibility of liquid lead with structural materials is not covered in this chapter, but can be found in Chapter VI.1.

Electrical insulators are important to liquid metal blankets because they can significantly reduce the magnetohydrodynamic (MHD) pressure-related problems. Preliminary work done to date has been in the identification of potential candidates. More work is planned for next year.

V.1 Tritium Breeding Materials

Liquid Li and liquid 17Li-83Pb are considered as the tritium breeding materials for the liquid-metal blanket designs in this study. In the self-

cooled designs of the liquid metal blankets (VII.1), these two materials also serve as coolants. The following two subsections give the properties information on these two materials.

V.1.1 Li Properties

Recently a set of Li properties has been submitted for incorporation into the Materials Handbook for Fusion Energy Systems.[3] Some of these properties have already been included in the Handbook while others are still undergoing review. The properties given below are taken from the originally submitted set, the ones under review will be indicated. Reference 4 contains discussions of these submitted properties which should be consulted for further information.

Table V.1-1 lists certain general properties of lithium. There are some questions regarding the exact values of the melting and boiling temperatures, and of the heat of fusion, but the differences among the quoted values[4,5] are small.

TABLE V.1-1. GENERAL PROPERTIES OF LITHIUM

Symbol	Li
Atomic Number	3
Atomic Weight	6.941 a.m.u
Isotopes/Abundance	^{6}Li/7.5%, ^{7}Li/92.5%
Crystal Structure	bcc
Cubic Edge Length of Unit	0.351 nm
Molar Volume	13.1 cm^3/gm mole
Melting Point[a]	180.54°C
Boiling Point[a]	1347°C
Heat of Fusion[a]	432.1 kJ/kg
Heat of Vaporization[a]	19595 kJ/kg

[a] These properties are under review.

Figures V.1-1 to V.1-8 show the other submitted lithium properties as a function of temperature. Analytical equations used to generate the curves in these figures are summarized in Table V.1-2. The enthalpies ($\Delta H°$) and free energies ($\Delta G°$) for various lithium reactions at 25°C are given in Table V.1-3.

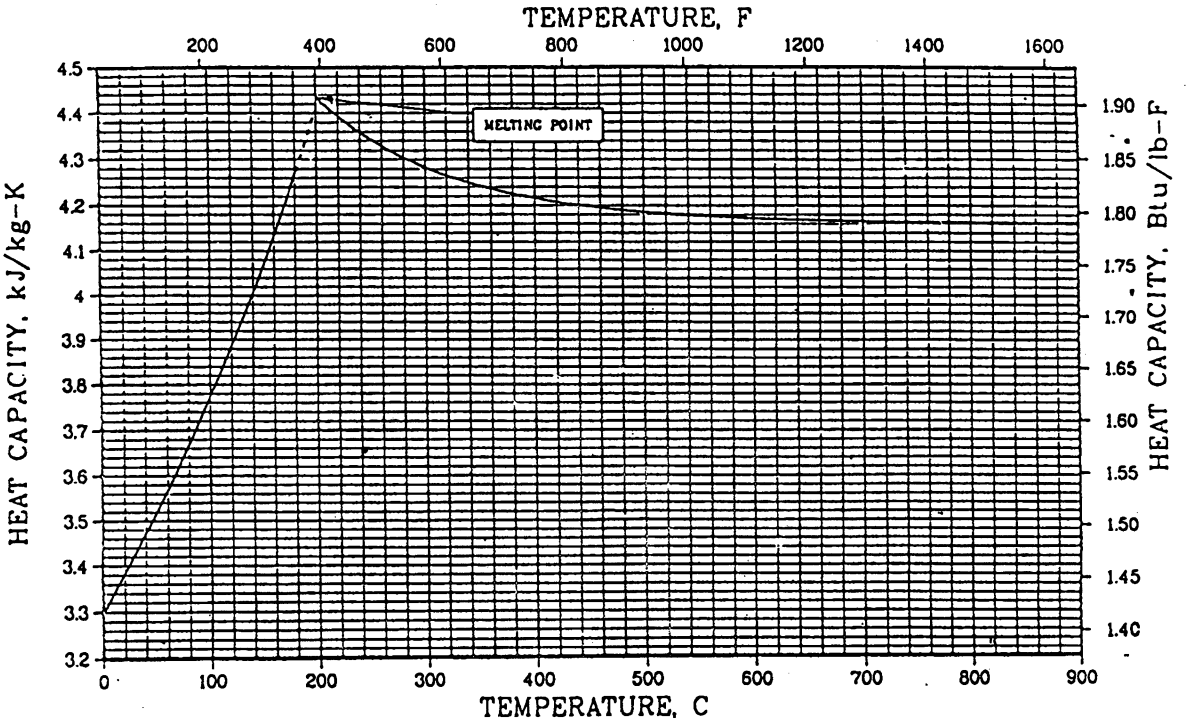

Figure V.1-1. Heat capacity of lithium as a function of temperature (preliminary).

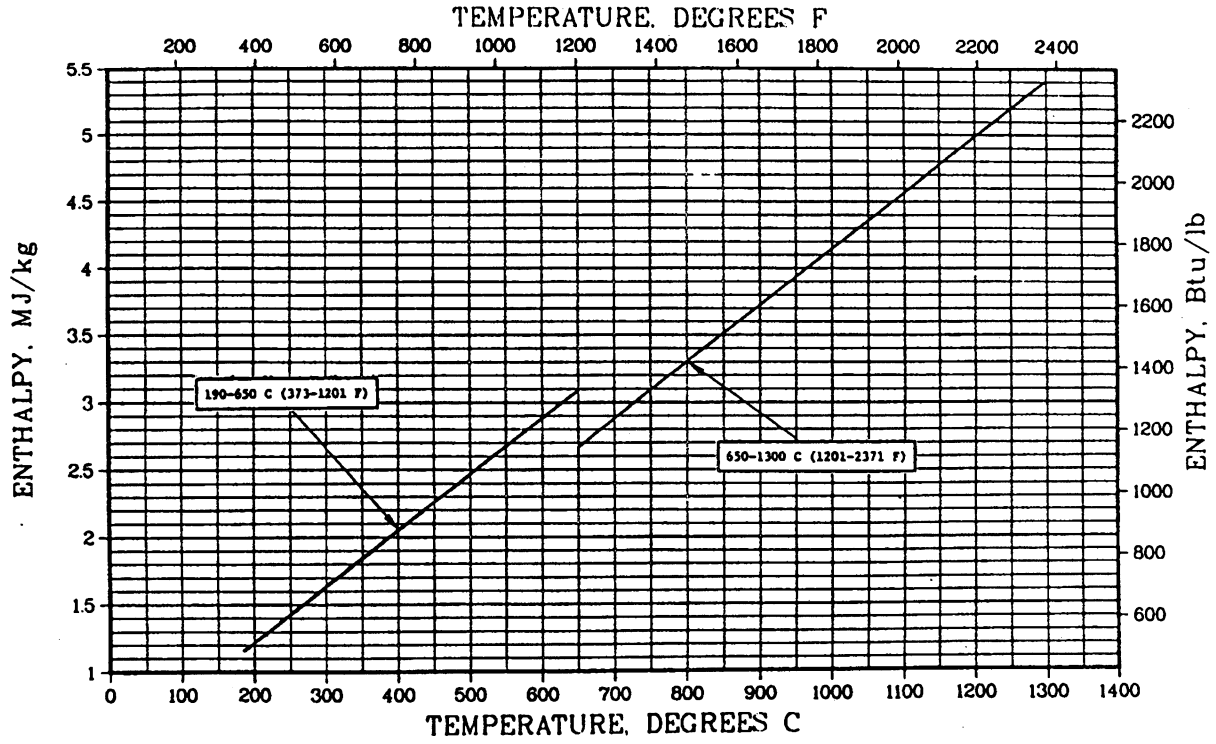

Figure V.1-2. Enthalpy of lithium as a function of temperature.

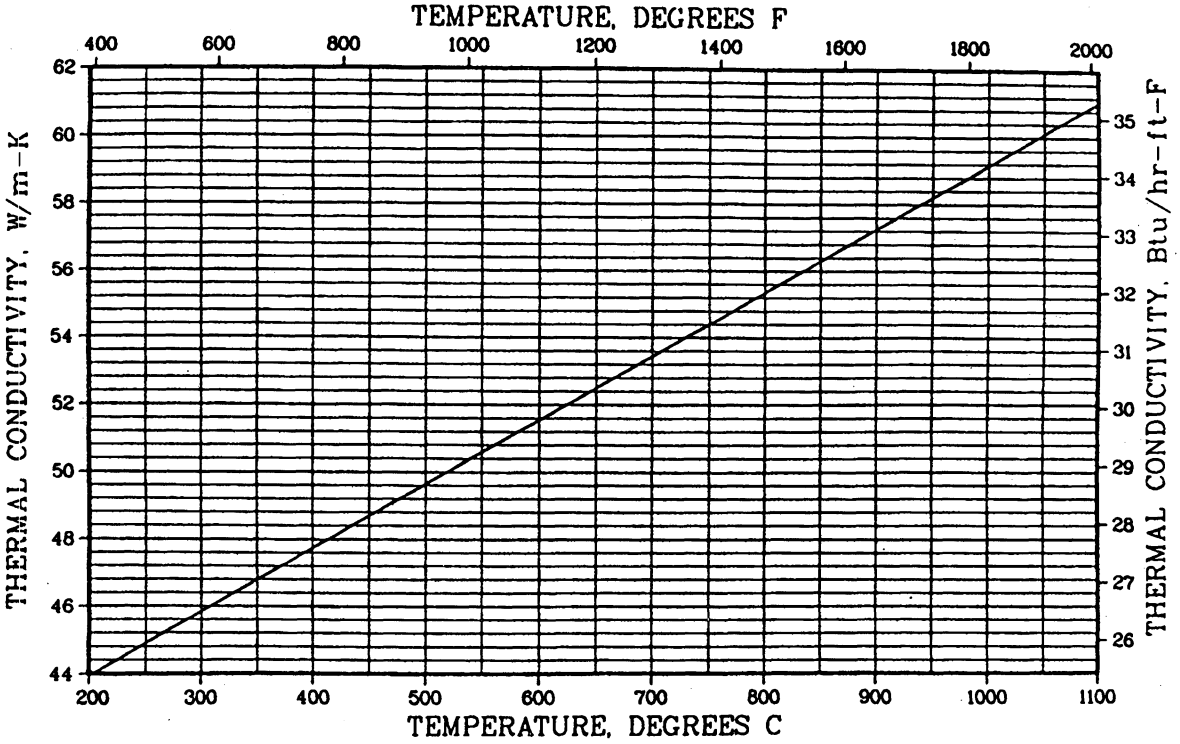

Figure V.1-3. Thermal conductivity of lithium as a function of temperature.

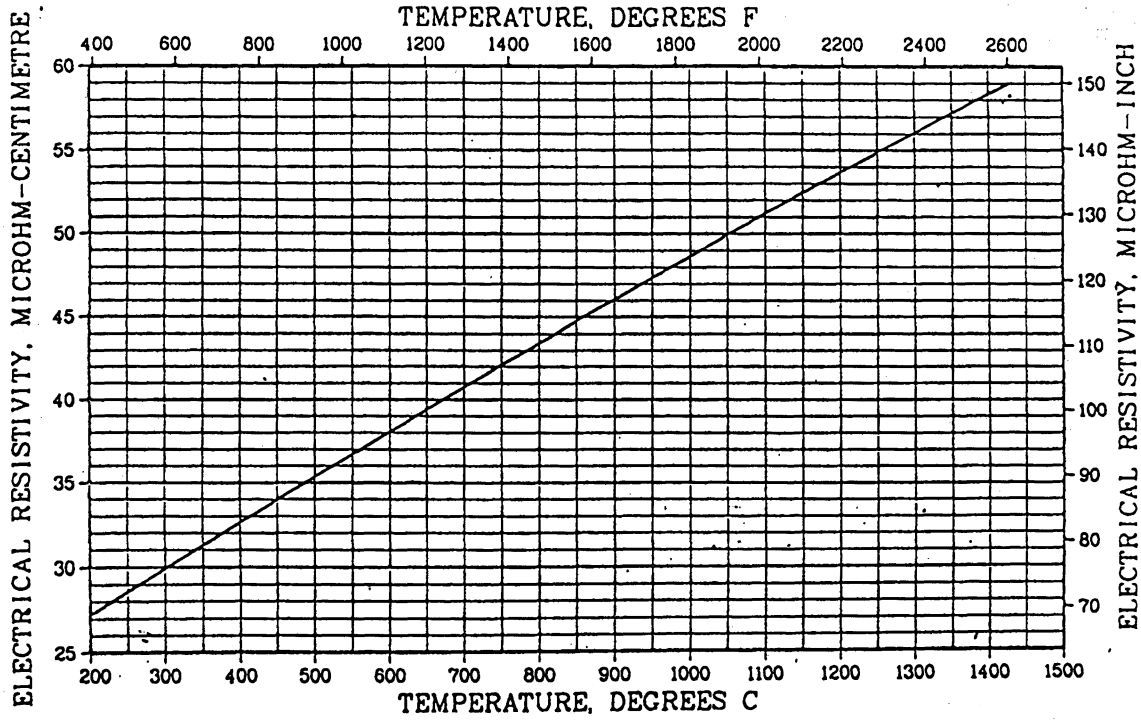

Figure V.1-4. Electrical resistivity of lithium as a function of temperature (preliminary).

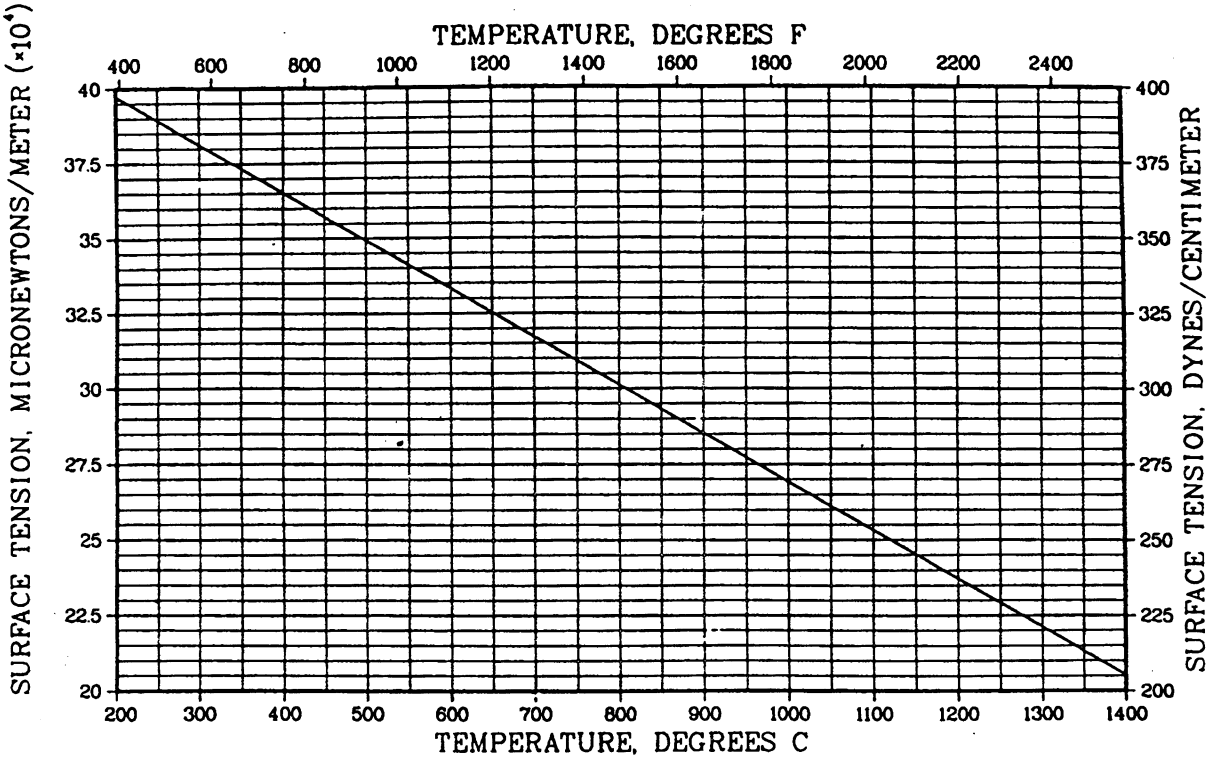

Figure V.1-5. Surface tension of lithium as a function of temperature.

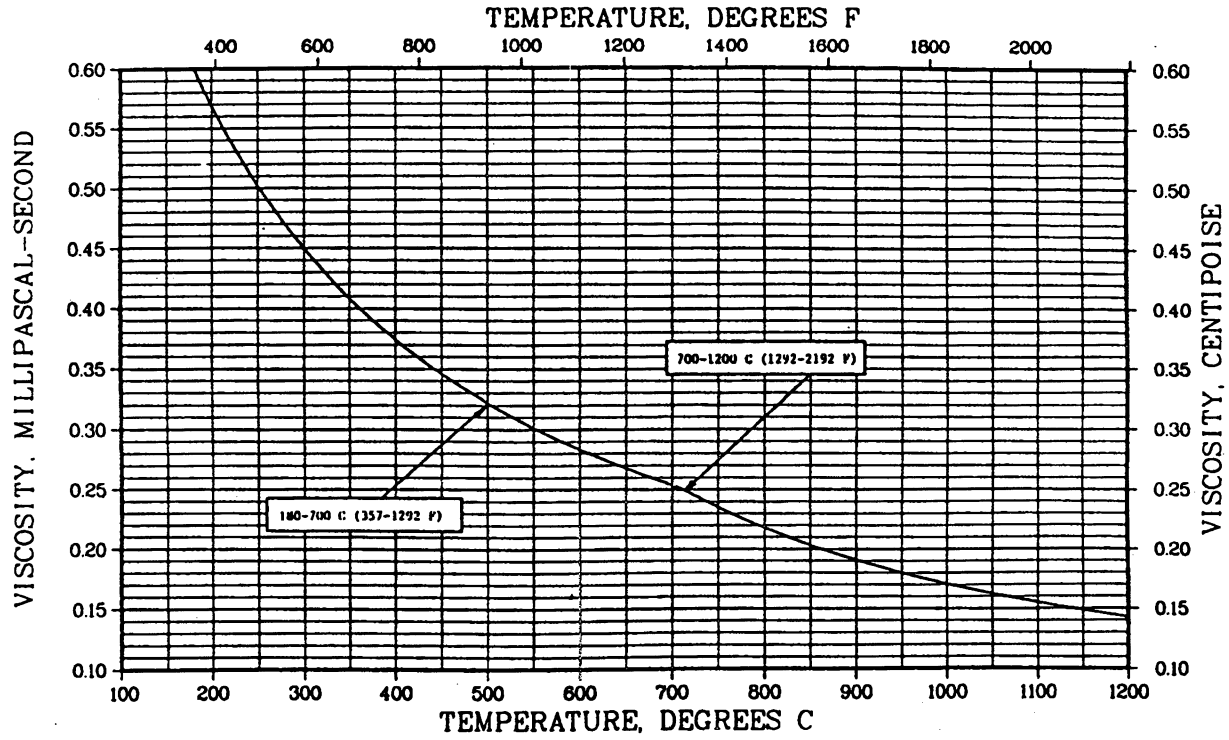

Figure V.1-6. Viscosity of lithium as a function of temperature.

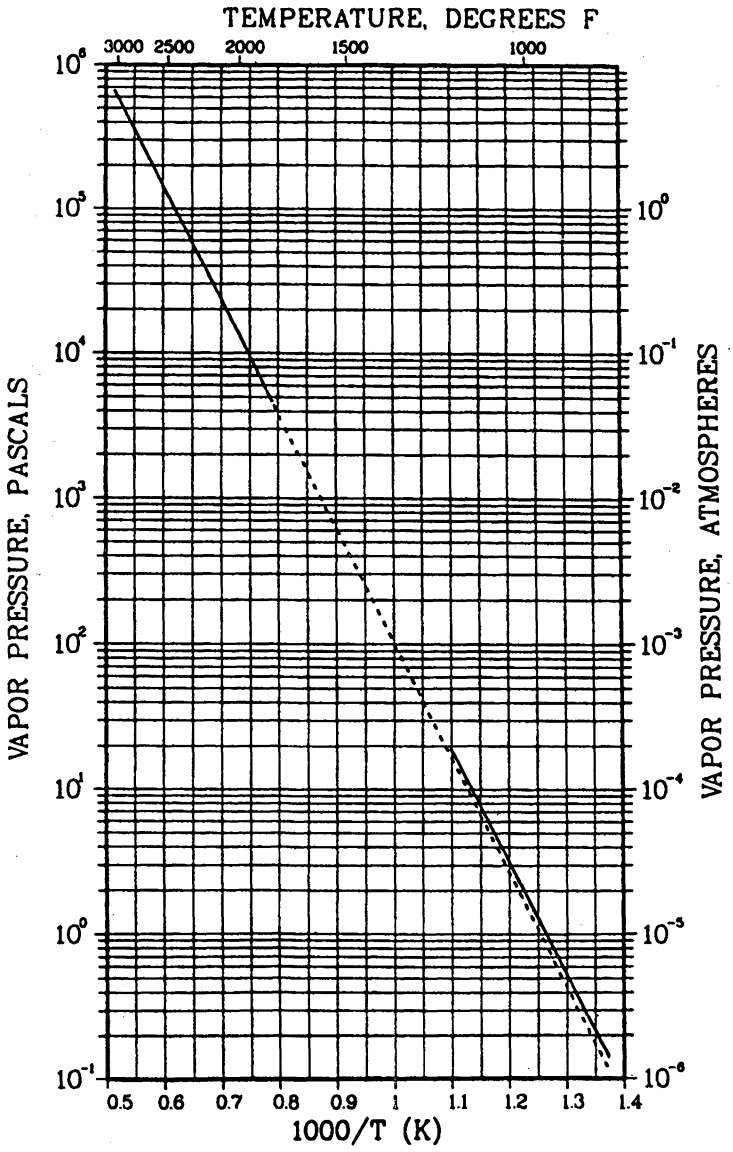

Figure V.1-7. Vapor pressure of lithium as a function of temperature.

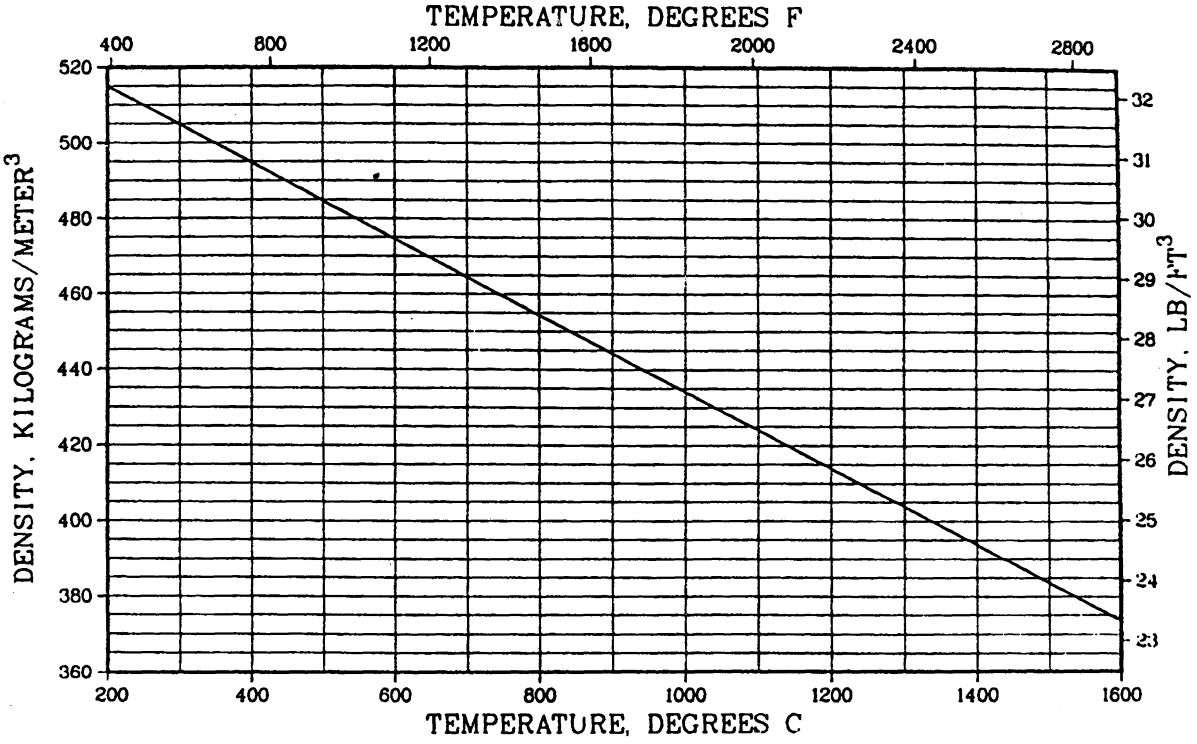

Figure V.1-8. Density of lithium as a function of temperature.

TABLE V.1-2. ANALYTICAL EQUATIONS USED FOR THE VARIOUS LITHIUM PROPERTIES

Property	Equation[b]
Specific Heat[a] C_p, kJ/kg-K	$C_p = 1.0/(0.3034-3.8387 \times 10^{-4}T)$ for $0 < T < 200°C$ $C_p = a_1 a_2^{a_3(T/1000)}$ for $200 < T < 900°C$ $a_1 = 4.1609$ $a_2 = 1.3603$ $a_3 = 3.7757 \times 10^{-4}$
Enthalpy H_T, MJ/kg	$H_T = 1.1321 + Cp\ (T-453.6)$ for $463 < T < 923°K$ $H_T = -2.1248 \times 10^{-2} + 4.1901 \times 10^{-3}\ T$ $-21.658/T$ for $650 < T < 1300°C$
Thermal Conductivity k/W/m-K	$k = 40.1246 + 1.9037 \times 10^{-2}\ (T - 273)$ for $473 < T < 1373°K$
Electrical Resistivity[a] ρ, mΩ-cm	$\rho = 21.934 + 2.598 \times 10^{-2}\ T + 2.581 \times 10^{-6}\ T^2$ $-1.819 \times 10^{-9}\ T^3$ for $200 < T < 1430°C$
Surface Tension σ, dynes/cm	$\sigma = 0.16\ (3550 - T) - 95$ for $473 < T < 1673°K$
Viscosity η, Centipose	$\log_{10} \eta = 1.4936 - 0.7368 \log_{10} T$ $+ 109.95/T$ for $453 < T < 973°K$ $\log_{10} \eta = 726.07/T - 1.338$ for $973 < T < 1473°K$
Vapor Pressure P, Atmospheres	$\log_{10} P = 4.8831 - 7877.9/T$ T in °K
Density d, kg/m^3	$d = 535.2 - 0.101 \times 10^{-4}\ T$ for $200 < T < 1600°C$

[a] These properties are under review.

[b] The temperature unit in each equation should be consistent with the unit given for the associated temperature range.

TABLE V.1-3. ENTHALPIES ($\Delta H°$) AND FREE ENERGIES ($\Delta G°$) FOR VARIOUS LITHIUM REACTIONS AT 25°C

Reaction	$\Delta H°$ (25°C) kJ/mole	$\Delta G°$ (25°C) kJ/mole
$2\ Li(c) + 1/2\ O_2 \rightarrow Li_2O(c)$	-596.85	-560.45
$2\ Li(c) + O_2(g) \rightarrow Li_2O_2(c)$	-635.55	-577.81
$Li(c) + 1/2\ H_2(g) + 1/2\ O_2(g) \rightarrow LiOH(c)$	-487.81	-442.15
$Li(c) + 3/2\ H_2(g) + O_2(g) \rightarrow LiOH \cdot H_2O(c)$	-790.47	-683.82
$Li(c) + H_2O(\ell) \rightarrow LiOH(c) + 1/2\ H_2(g)$	-203.76	-204.97
$Li(c) + H_2O(\ell) \rightarrow LiOH\ (in\ H_2O) + 1/2\ H_2(g)$	-222.35	
$Li(c) + 1/2\ F_2(g) \rightarrow LiF(c)$	-612.12	-584.30
$Li(c) + 1/2\ Cl_2(g) \rightarrow LiCl(c)$	-408.78	-387.02
$Li(c) + 1/2\ I_2(g) \rightarrow LiI(c)$	-271.08	(-260.24)
$3\ Li(c) + 1/2\ N_2(g) \rightarrow Li_3N(c)$	-198.74	-156.06
$Li(c) + 1/2\ H_2(g) \rightarrow LiH(c)$	-90.42	-69.96
$2\ Li(c) + 3/2\ CO_2(g) \rightarrow Li_2CO_3(c) + 1/2\ C(c)$	-621.74	-537.22
$2\ Li(c) + 3\ CO(g) \rightarrow Li_2CO_3(c) + 2\ C(c)$	-880.52	-717.05
$Li(c) + NH_3(g) \rightarrow LiNH_2(c) + 1/2\ H_2(g)$	-135.81	
$2\ Li(c) + 2\ C(c) \rightarrow Li_2C_2(c)$	-59.41	
$2\ Li(c) + Mo(c) + 2\ O_2(g) \rightarrow Li_2MoO_4(c)$	-1528.21	
$Li(c) + Al(c) + 2\ H_2(g) \rightarrow LiAlH_4(c)$	-103.22	
$Li(c) + Sn(c) \rightarrow LiSn(c)$	-70.29	
$Li(c) + Pb(c) \rightarrow LiPb(c)$	-61.09	
$Li(c) + Tl(c) \rightarrow LiTl(c)$	-53.56	
$Li(c) + Hg(c) \rightarrow LiHg(c)$	-87.03	
$3\ Li(c) + 2\ Sb(c) \rightarrow Li_3Sb_2(c)$	-182.00	
$3\ Li(c) + Bi(c) \rightarrow Li_3Bi(c)$	-230.96	
$2\ Li(c) + H_2SO_4(\ell) \rightarrow Li_2SO_4 + H_2(g)$	-623.08	
$Li(c) + CH_3OH(\ell) \rightarrow LiOCH_3\ (in\ CH_3OH) + 1/2\ H_2(g)$	-230.54	
$Li(c) + C_2H_5OH(\ell) \rightarrow LiOC_2H_5\ (in\ C_2H_5OH) + 1/2\ H_2(g)$	-215.89	

V.1.2 17Li-83Pb Properties

There is a general lack of materials properties data of LiPb. Those material properties which have been measured are listed in Table V.1-4. The properties which have not been measured are listed in Table V.1-5. It is the purpose of this section to list and to assess the accuracy of the available data.

Phase Diagram: The phase diagram of LiPb has been well established and is shown in Fig. V.1-9.[6] The melting points of LiPb and 17Li-83Pb were confirmed by different workers.[7,8] The accuracy of the phase diagram and, therefore, the melting temperature of LiPb in various composition appears to be accurate.

Sievert's Constant: There were basically three different measurements on the Sievert's constant of LiPb.[9-11] The results from Veleckis and Wu appear to be in good agreement and are shown in Fig. V.1-10. The results from Ref. (11) were measured at a hydrogen concentration that is judged to be too high.

TABLE V.1-4. MATERIAL PROPERTIES AVAILABLE FOR LiPb

- Phase Diagram
- Sievert's Constant
- Lithium Activity
- Density
- Thermal Expansion Coefficient
- Electrical Conductivity
- Vappor Pressure
- Neutronic Data
- Specific Heat $\leq$ 300°C
- ΔH of Melting

TABLE V.1-5. MATERIAL PROPERTIES NOT AVAILABLE FOR LiPb
(Design Values Based on Pb Properties)

- Thermal Conductivity
- Viscosity
- Specific Heat > 300°C
- Solubility of (Fe, Ni, etc.)
- Diffusivity (T)
- ΔH of Reaction With Water
- ΔH of Reaction With Air

Activity and Partial Pressure: The activity of lithium in the LiPb system has been measured by Knudsen diffusion mass spectrometry at 750 K and reported to continuously decrease from 4.0×10^{-3} to 2×10^{-5} as the lithium composition drops from 61 atom per cent to 5 atom per cent.[12-15] The

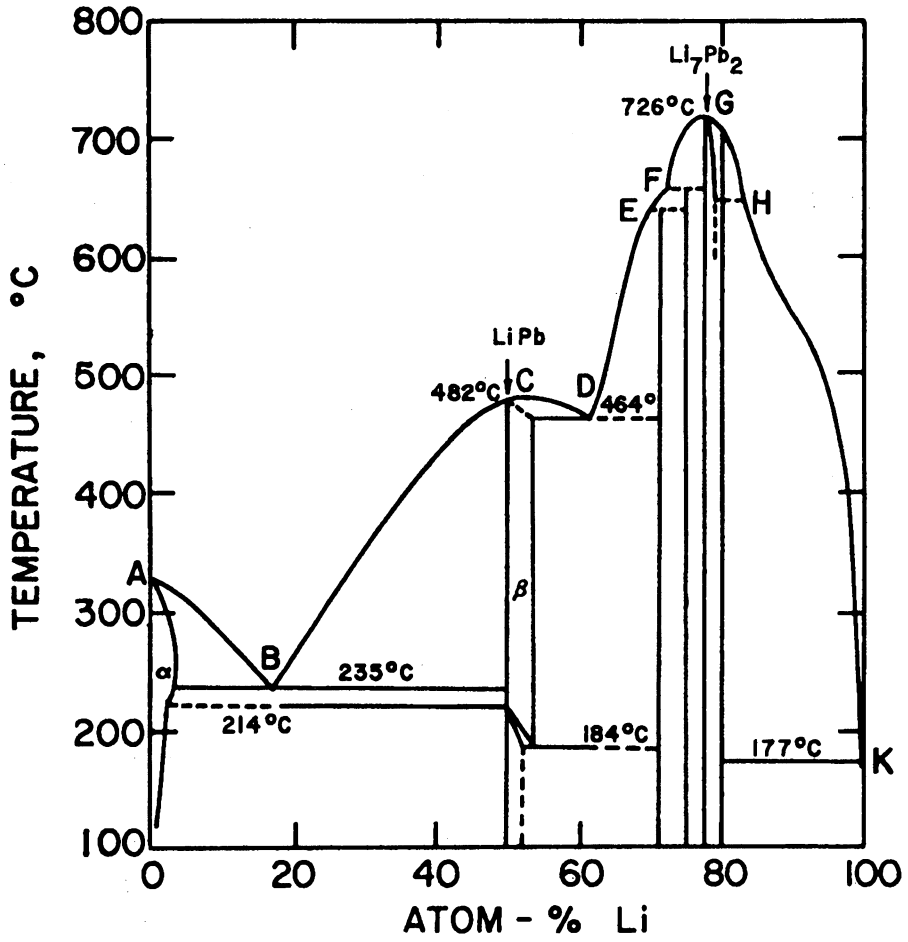

Figure V.1-9. Phase diagram of Li-Pb.

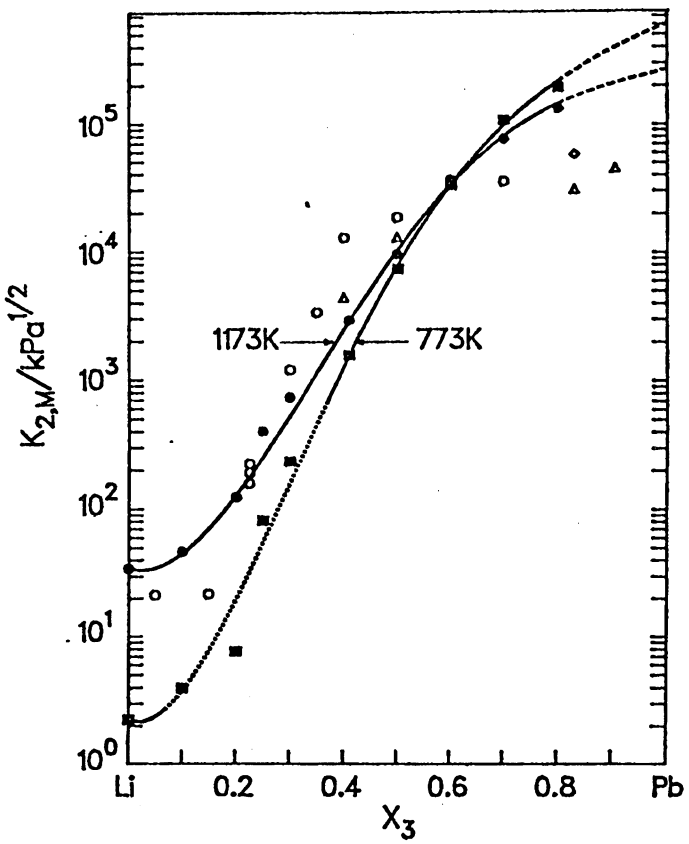

Figure V.1-10. Sieverts' constants for solutions of hydrogen isotopes in liquid Li-Pb alloys.

activity of lithium in 17Li-83Pb can be represented in the following form as a function of temperature,[16] i.e.,

$$\ell n\ a_{Li} = -\ 6960/T + 0.0245\ .$$

Thus, the lithium activity in 17Li-83Pb can be estimated to be about 1×10^{-4} at 750 K. This is an extremely low value, four orders of magnitude lower than that of pure lithium, and it is reasonable to expect that the chemical reactivity of lithium and related safety concerns will be markedly reduced. The chemistry in many respects may be expected to be more similar to that of lead than of lithium. However, the thermodynamic stability of lithium compounds with non-metallic elements (e.g., H, O, N, etc.) is very high and despite the low activity, lithium effects can be significant. The activity of lead can be calculated from the activity of lithium by using the Gibbs-Duhem equation.[13] A typical curve of activity coefficient of LiPb is reproduced from Ref. (14) and shown in Fig. V.1-11. Since $P_n = (rx)P_o = aP_o$ in which

P_n is partial pressure of the material
r is the activity coefficient
x is the mole fraction
a is the activity
P_o is the pressure of the pure material,

the partial pressure of lithium and lead can be calculated from the information of activity. Furthermore, on the lead rich end of the phase diagram, the vapor phase is dominated by lead and, as a first approximation, the vapor pressure of LiPb can be taken the same as that of lead.

Density and Thermal Expansion Coefficient: The density and thermal expansion coefficient of liquid LiPb has been measured[17] and the data are shown in Table V.1-6 and Fig. V.1-12. The results appear to be accurate. The density of solid LiPb has also been reported.[6]

Electrical Conductivity: The electrical conductivity of solid LiPb[6] and the electrical resistivity of liquid LiPb[18] have been reported as shown in Figs. V.1-13 and V.1-14. The data accuracy is uncertain.

Thermodynamic Properties: The specific heat at constant pressure, C_p, enthalpy, and entropy of 17Li-83Pb have been measured[19] and listed in Table V.1-7 as a function of temperature. The latent heat of fusion can be obtained

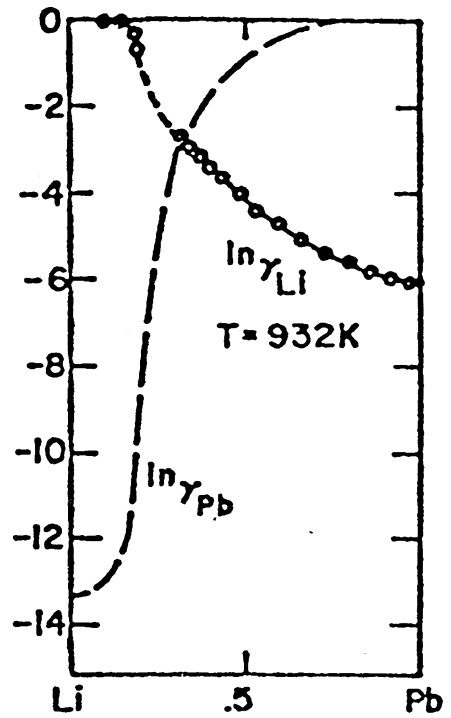

Figure V.1-11. Activity coefficients for Li and Pb.

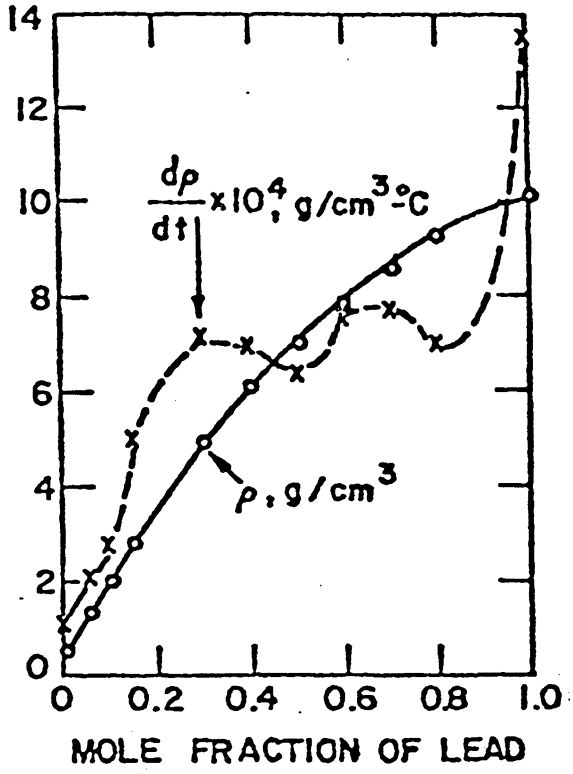

Figure V.1-12. Density and thermal expansion coefficient of LiPb at liquidus temperature.

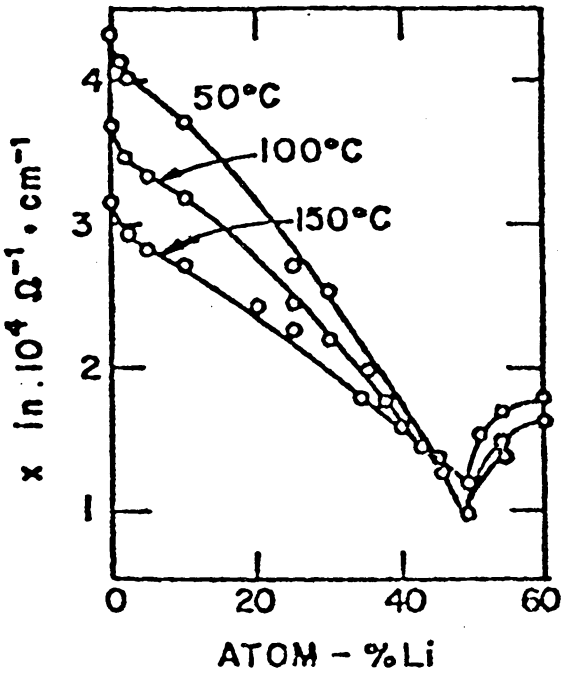

Figure V.1-13. Electrical conductivity of Li/Pb.

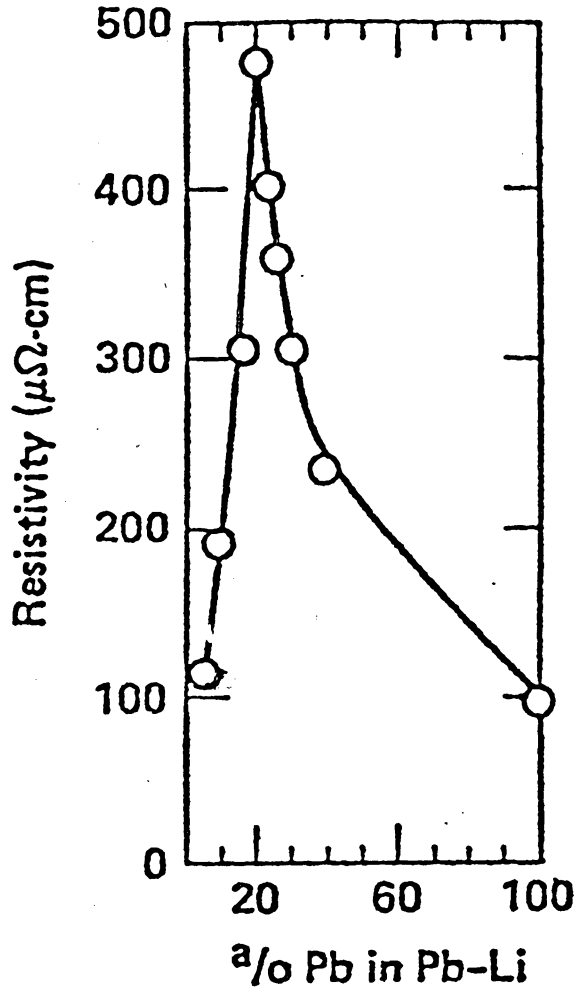

Figure V.1-14. Electrical resistance of Li/Pb at 800°C.

TABLE V.1-6. DENSITY OF LIQUID LITHIUM LEAD ALLOYS

Composition (at % Pb)	Temperature Range (°C)	Liquidus Temperature (°C) (Hansen and Anderko)	Density (g/cm^3) At the Liquidus Temperature	$-d\rho/dT \times 10^4$
0	248-650	180	0.514 ± 0.003	1.1 ± 0.1
1	424-664	180	0.658 ± 0.003	1.1 ± 0.1
2	481-702	340	0.787 ± 0.003	1.4 ± 0.2
3	496-706	420	0.929 ± 0.004	1.4 ± 0.2
5	528-712	480	1.221 ± 0.005	2.1 ± 0.3
7	547-721	515	1.52 ± 0.01	2.1 ± 0.3
10	582-742	550	1.98 ± 0.01	2.8 ± 0.4
15	648-763	620	2.79 ± 0.01	5.1 ± 0.5
17	669-772	640	3.13 ± 0.02	6.6 ± 0.5
30	663-777	642	4.86 ± 0.02	7.2 ± 0.5
40	520-672	470	6.08 ± 0.02	7.0 ± 0.5
50	497-692	482	6.97 ± 0.03	6.4 ± 1
60	465-684	430	7.82 ± 0.03	7.6 ± 1
70	533-644	350	8.65 ± 0.03	7.8 ± 1
80	491-653	260	9.33 ± 0.04	7.0 ± 1
100	363-556	327	10.66 ± 0.06	13.5 ± 2

TABLE V.1-7. THERMODYNAMIC PROPERTIES OF 17Li-83Pb

T(K)	C_p(J/g K)	ΔH (J/g)	ΔS (J/g K)
298.15	0.1372	0.00	0.0000
313.15	0.1396	2.06	0.0072
333.15	0.1432	4.88	0.0160
353.15	0.1473	7.79	0.0244
373.15	0.1519	10.79	0.0326
393.15	0.1569	13.87	0.0407
413.15	0.1625	17.05	0.0486
433.15	0.1685	20.36	0.0564
453.15	0.1750	23.82	0.0642
473.15	0.1820	27.47	0.0719
493.15	0.1895	31.36	0.0796
507.90	0.1953	34.40	0.0843
507.90	0.2504	63.99	0.1426
513.15	0.2438	65.32	0.1455
533.15	0.2172	70.07	0.1542
553.15	0.1886	74.18	0.1616
573.15	0.1580	77.45	0.1677

from these data which is 29.59 J/g. The specific heat is also given in Fig. V.1-15. It appears that the C_p of liquid 17Li-83Pb shows a strong temperature dependence such that extrapolation to the higher temperature is not possible.

In conclusion, the material properties data base of 17Li-83Pb has been built up over the past two years. However, much of the important information is still unavailable. The accuracies of the available data are uncertain.

V.2 Neutron Multipliers

The use of beryllium and lead as neutron multipliers for a solid-breeder blanket has been discussed in the STARFIRE report[1] along with six other candidates. Aside from its neutronic properties, beryllium was chosen as the reference neutron multiplier for STARFIRE because it combines the lowest density with the highest specific heat and thermal conductivity of all the candidate materials. The two main concerns for beryllium are the irradiation swelling caused by helium generation and the resource limitation. Both concerns will be discussed in this section. Lead had previously been set aside primarily because of its low melting point (327°C). If lead were to be used in liquid form, the main concern would be its compatibility with the structural material. Volume expansion/contraction of lead upon melting/freezing, 3.44-3.61%[20] is another aspect that should be taken into design consideration.

Selected properties for beryllium and lead are given in Table V.2-1. More information can be found in references 1, 2, and 20.

V.2.1 Beryllium

Helium gas in beryllium is generated from the (n,2n) and (n,α) reactions. In general, the production of gas alone is not sufficient to cause large magnitude of swelling. The temperature must be high enough to allow both diffusion of the gas and plastic deformation of the material. In this way gas bubbles can nucleate, grow and coalesce into large bubbles either within the grains or along grain boundaries.

Post-irradiation annealing studies[21-24] of beryllium indicated that (1) there is a threshold temperature below which swelling is insignificant, and (2) there is a limit to maximum volume increase (30%) beyond which no further

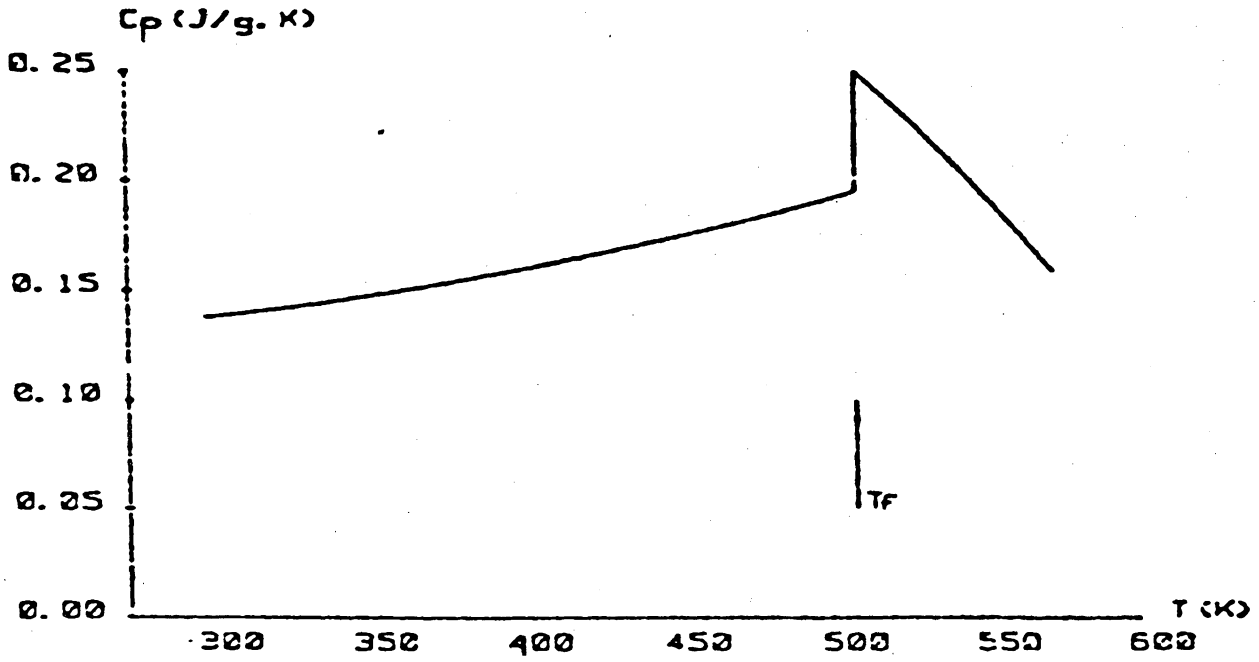

Figure V.1-15. Specific heat at constant pressure C_p of 17Li-83Pb.

TABLE V.2-1. SELECTED PROPERTIES OF BERYLLIUM AND LEAD

Property	Beryllium[a]	Lead[b]
Atomic Number	4	82
Atomic Weight	9.01	207.19
Density, g/cm^3	1.85	11.34
Crystal Structure	hcp	fcc
Melting Temperature, °C	1284	327.3
Boiling Temperature, °C	2970	1740 ± 10
Vapor Pressure, Pa (°C)	10^{-4} (850) 10^{-2} (993) 10^{0} (1192) 10 (1335) (ℓ)	2.6×10^{-2} (600) ℓ 6.6 (800) ℓ
Heat of Fusion (J/g)	1083	23.2
Heat of Vaporization, J/g	24,790	862.5
Heat Capacity, J/g-°C		
500°C	2.25	25°C 0.127
1000°C	2.92	327°C 0.147
1500°C	3.59 (ℓ)	600°C 0.14 (ℓ)
Coefficient of Thermal Expansion, $°C^{-1}$ (10^{-6})		
25-100°C	11.6	20-100°C 29.1
25-500°C	15.9	20-300°C 31.3
25-1000°C	18.4	≳327°C 43 (ℓ)
Thermal Conductivity W/m-k		
50°C	150	50°C 34.1
300°C	125	300°C 30.6
600°C	96	327-600°C 24.7 (ℓ)
Electrical Resistivity, μΩ-cm		
400°C	15	101.4 (ℓ)

[a] Values taken from Reference 2.

[b] Values taken from Reference 20.

swelling occurs. The swelling threshold temperature has been found to depend on the helium gas content in beryllium, decreasing with increasing neutron exposure (Fig. V.2-1). The maximum volume increase of 30% appears to be a geometrical limit at which the majority of the internal bubbles touch and release their gases. Such volume increases were only observed when the annealing temperatures are $\geq$ 1000°C (Fig. V.2-2).

With regard to the methods to accommodate swelling, small grain size and high temperature will generally enhance helium release, thereby reducing the driving force for swelling. It is also known, however, that the gas bubbles on grain edges must become interconnnected to allow venting of the gases. Furthermore, these grain edge tunnels need to remain open against sintering, otherwise the process would repeat itself. Theoretical calculation[25] showed that depending on the ratio of grain boundary and surface energies, there exists a minimum fractional swelling below which no stable system of interconnected tunnels can exist. This minimum swelling has been calculated to be between 5 and 10%. The 5% value was observed experimentally in irradiated UO_2.[26]

The implication from the above discussion is that if one relies on high temperature (> 750°C) for helium release, there will still be swelling even though its magnitude should be less than 30%. The precise value of this minimum swelling for beryllium is not known. One may use 10% as a basis for design calculation.

Another method for swelling accommodation has been recommended in the STARFIRE report.[1] This method uses a beryllium with a 70% theoretical density and interconnected porosity to accommodate swelling. If the added beryllium thickness (due to the low density) does not impose significant penalty on the overall tritium breeding of a fixed-size blanket, the proposed method should be sufficient to solve the swelling problem. An added insurance can be gained when the irradiation temperature is kept below 600°C such that the interconnected porosity will remain open. The 600°C upper temperature limit is lower than the sintering limit (taken to be 0.6 T_m = 661°C) and is partially supported by Beeston's experimental grain growth data on beryllium.[27] The degradation of thermal conductivity of such a porous beryllium should not represent any problem on heat transfer. Using well established formulae[28,29] for the porosity dependence of thermal conductivity, one can

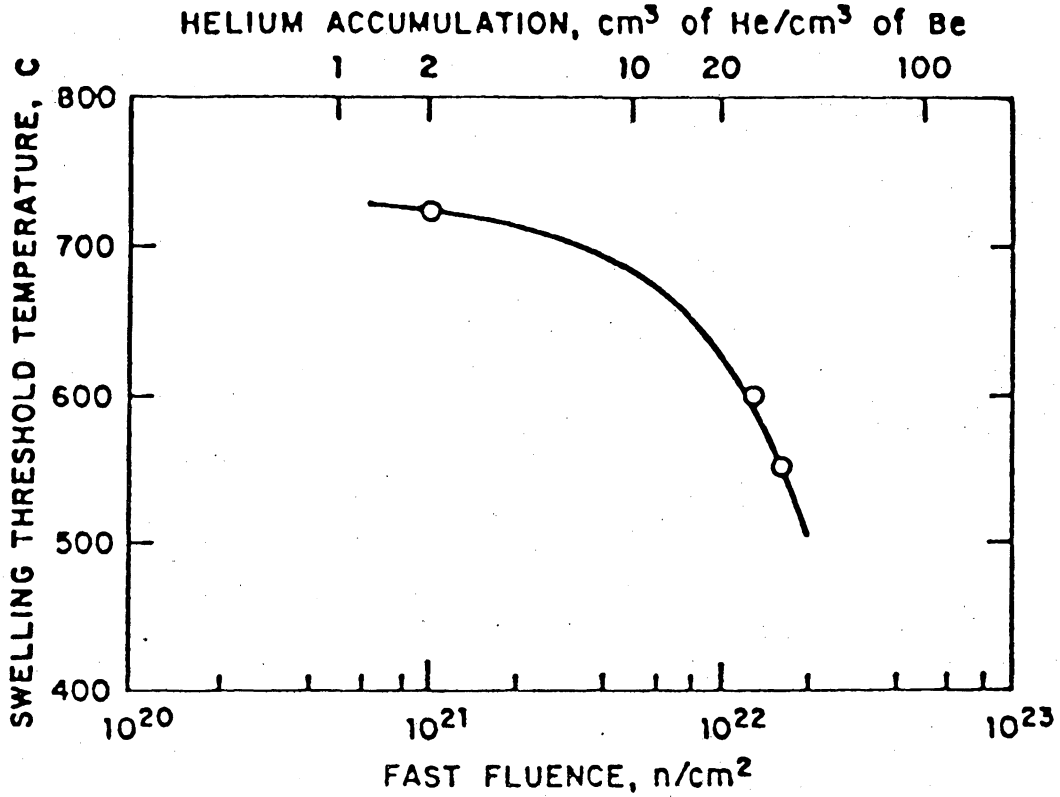

Figure V.2-1. Swelling threshold of beryllium as a function of gas content and fluence (from Reference 2).

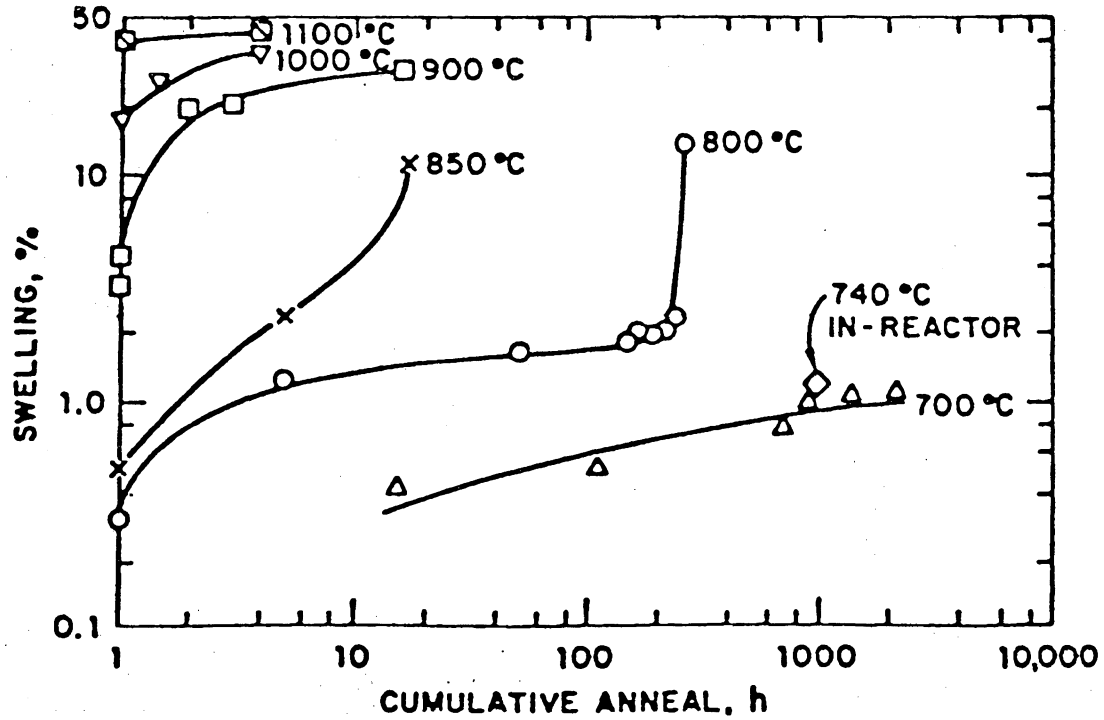

Figure V.2-2. The effect of time and temperature on the swelling of irradiated beryllium (from Reference 2).

estimate the thermal conductivity of a 70%-dense beryllium. The calculated value at 600°C amounts to 44 W/m°C which is still higher than the thermal conductivities of other fusion blanket materials.

In comparing the above two methods for accommodating swelling, the first method has the potential of using a thinner beryllium with high density and high operating temperature (> 750°C). Swelling should be less than 30%, but the exact value is not known at the present time. The second method may be conservative in allowing more porosity and thicker beryllium than there needs to be, but with relatively low irradiation temperature (< 600°C) this method should be sufficient to overcome the swelling problem. Again, if the use of a thinner beryllium is not that crucial, the STARFIRE recommendation should be adopted for the solid breeder blankets in this study.

V.2.2 Beryllium Resource Evaluation

The current and expected usage of beryllium is summarized in Table V.2-2.[30] The principal current use of beryllium is for beryllium-copper alloys in communications, computers, switching, and other electrical and electronic applications. Such usage is expected to dominate the demand through the year 2000. The annual domestic usage that year is projected to continue at about 275 MT/yr, but is quite uncertain (between 100 and 380 MT/yr in the U.S. and roughly twice that level world-wide). Projections indicate that the nuclear and aerospace usage of beryllium will decline while electrical and electronic usage increases.

Through the year 2000, the cumulative usage of beryllium is expected to be quite modest--between 3500 amd 6600 MT in the U.S. and about 1.5 times that level world-wide. These projections do not include any possible use of beryllium in fusion reactors (e.g., an engineering test reactor).

The availability of beryllium is summarized in Table V.2-3 where U.S. Bureau of Mines (U.S.B.M.) and U.S. Geological Survey (U.S.G.S.) estimates are shown.[30,31] These estimates differ primarily in the types of ore bodies which are considered in a given category with the Bureau of Mines data being more conservative in estimating the U.S. reserve and resources and the Geological Survey data being more conservative in the world-wide estimates.

TABLE V.2-2. BERYLLIUM DEMAND

Percent U.S. (1979) Usage

	MT/yr	%
Electrical Uses	102	37
Nuclear Reactors	54	19
Aerospace	50	18
Electronic Components	44	16
Other	24	10
	274	100

Projected (2000) Usage

	MT	
	U.S.	WORLD[a]
Annual	100 - 380	170 - 560
Cumulative	3490 - 6610	5470 - 9330

[a] Includes U.S.

TABLE V.2-3. BERYLLIUM AVAILABILITY DATA

	United States		World[b]	
	Reserves (metric tons)	Resources[a] (metric tons)	Reserves (metric tons)	Resources[a] (metric tons)
U.S. Bureau of Mines	25,000	73,000	380,000	1,105,000
U.S Geological Survey	55,000	282,000	84,000	678,000

[a] Includes Reserves.

[b] Includes U.S.

In our analysis, we have used only the Bureau of Mines estimates as these data are both more recent and more conservative with respect to U.S. resources. The U.S.B.M. defines the domestic resource base as follows:

> "Known domestic resources of beryllium consist primarily of bertrandite located at Spor Mountain and Gold Hill, Utah, and the Seward Peninsula, Alaska, and of beryl located in the coarse-zoned pegmatites of New England, South Dakota, and Colorado."

In addition to the above resources, sub-economic domestic resources of beryllium occur in fine-grained Spodumene-bearing pegmatites that are being mined for lithium. The U.S.G.S.[31] estimates that about 725,000 MT of beryl are available in such deposits in North and South Carolina alone. These resources are currently uneconomical because the beryl exists in fine particles (i.e., too small to hand sort) and at low concentration (~ 0.5% beryl or 0.025% beryllium). Due to these characteristics, recovery of the contained beryl is considered to be impractical, even in conjunction with floatation of the other minerals.[31]

The bertrandite ($4BeO \cdot 2SiO_2 \cdot H_2O$) which has been mined in Utah since 1969 is found in ~ 7% concentration in the parent ore. The ore is mined, milled, and converted to beryllium hydroxide for later processing into the metal and oxide. Although some beryl ($3BeO \cdot Al_2O_3 \cdot 6SiO_2$) is imported and converted to beryllium hydroxide, the U.S. is projected to be self-sufficient in beryllium by the year 2000.[30] Currently, hand-sorted Brazillian beryl accounts for ~ 40% of the imports. Other sources of imported beryl are mainland China, India, and Argentina. The world resources of beryllium are broken out by country in Table V.2-4. These resources consist entirely of beryl, but firm data are scant and the resource projections are considered to be less certain than the domestic resource projections.[30]

In 1981, the domestic price for beryllium metal was about 310 $/kg.[32] About 425 persons are actively employed in the domestic beryllium mining and primary refining industries.

To investigate the potential usage of beryllium in fusion reactors, we have considered the amount of material which would be consumed in a tokamak of approximately STARFIRE[1] dimensions, wall loading and electrical power output (1200 MWe). The effective thickness of the multiplier was taken to vary between 0.1 cm and 10 cm, depending upon its required usage, with the lower

TABLE V.2-4. WORLD BERYLLIUM RESOURCES[a]
(Metric Tons of Contained Beryllium)

	Reserves	Other	Total
North America			
United States[2]	25	48	73
Canada	--	23	23
Mexico	--	2	2
South America			
Argentina	25	47	72
Brazil	140	256	396
Asia: India	64	119	183
Africa			
Mozambique	6	11	17
Rwanda	11	20	31
Republic of South Africa	15	29	44
Uganda	15	26	41
Zaire	7	14	21
Europe: U.S.S.R.	61	111	172
Oceania: Australia	11	19	30
World Total	380	725	1105

[a] Derived in collaboration with U.S. Geological Survey.

[b] Includes beryllium content of domestic bertrandite resources.

TABLE V.2-5. TYPICAL TOKAMAK BERYLLIUM USAGE WITH NO RECYCLE
(STARFIRE Dimensions and Power, 1.2 GWe)

Thickness	Be in FW/B	Fraction of U.S.B.M. Resources	Be Lifetime	Annual Requirements
0.1 cm	1.5 MT	0.002%	1 yr 4 yr	0.002 %/yr 0.0005 %/yr
1 cm	15 MT	0.02%	1 yr 4 yr	0.02 %/yr 0.005 %/yr
5 cm	75 MT	0.1%	1 yr 4 yr	0.1%/yr 0.025%/yr
10 cm	150 MT	0.2%	1 yr 4 yr	0.2 %/yr 0.05 %/yr

bound corresponding to a low Z coating for the first wall (with no significant neutron multiplication) and the upper bound corresponding to an appropriate thickness for substantial neutron multiplication. As shown in Table V.2-5, the beryllium inventory would then vary between 1.5 and 150 MT or 0.002 and 0.2% of the U.S.B.M. domestic resource estimate.[30]

If we do not recycle the radioactive beryllium,[33] then the annual requirement for beryllium is dependent only upon both the rate of introduction of new electrical plants and its lifetime in existing plants. Assuming a relatively short lifetime (i.e., 1 to 4 years) and a reasonable growth in fusion power generation (e.g., on the order of 10-20%/yr), the annual make-up requirement to replace existing inventories will dominate. As shown in the table, without recycle the make-up requirement per reactor can vary between 0.0005%/yr (0.1 cm thickness and 4 yr lifetime) and 0.2%/yr (10 cm thickness and 1 yr lifetime). Clearly, the lower value is quite tolerable, but the higher value would not be acceptable for more than a few first generation fusion reactors unless a large fraction of the beryllium were to be imported.

To address the resource issue, it is necessary to consider beryllium recycle. With recycle, losses can be limited to the sum of recycle process losses and beryllium burnup losses. Currently, powder metallurgical fabrication process for sintered beryllium metal products result in an approximately 7% recycle process loss rate.[34] Experts believe that, with

sufficient incentive, this loss rate could be reduced to about 1%.[35] For powdered beryllium, a 1% loss rate also seems to be reasonable.

The beryllium burnup losses will be small, but will compete with the recycle losses when recycle is very efficient. The details of beryllium burnup are somewhat design dependent; varying with the blanket geometry and composition. Nevertheless, a representative idea of beryllium burnup and its spatial profile can be deduced from existing studies of beryllium multipliers.

For instance, the beryllium helium production rate as a function of position for the thick multiplier blanket considered in Reference 33, is shown in Fig. V.2-3. For a 1 MW/m^2 neutron wall loading, the helium production rate of Reference 33 (in appm per full power year) is given by:

$$He(x) = 3750 \exp(-0.0841\ x)$$

where, in slab geometry, x is the distance from the first wall.

The beryllium burnup is roughly half the helium production rate (neglecting any beryllium n,α reactions), and we can express the average percentage of beryllium burned in a reactor per calendar year as:

$$B\ (\%/yr) = \frac{\Gamma\ C_f}{10{,}000\ X_1} \int_o^{x_1} \frac{He(x)}{2}\, dx = \frac{2.2\ \Gamma\ C_f}{x_1} \left[1-e^{-.084x_1}\right]$$

where Γ is the neutron wall loading (MW/m^2), C_f is the average plant capacity factor, and x_1(cm) is the beryllium plate thickness in analogy to Fig. V.2-3 (i.e., explicitly including other materials in the blanket rather than at 100% volume fraction). If we simulate STARFIRE for Γ = 3.6 MW/m^2, C_f = 75%, and x in the range shown in Table V.2-5, the resulting beryllium burnup is estimated to be as indicated in Table V.2-6.

The total mass of beryllium required to support a given reactor economy is then:

$$M = NI\left[\left(1 + \frac{\tau}{\ell}\right) + T\left(\frac{\varepsilon}{\ell} + \frac{B}{100}\right)\right]$$

where N (GWe) is the size of the reactor economy, I (MT/GWe) is the in-core beryllium inventory, τ (yr) is the beryllium fabrication time (to express the ex-core inventory), ℓ (yr) is the beryllium lifetime, T (yr) is the duration

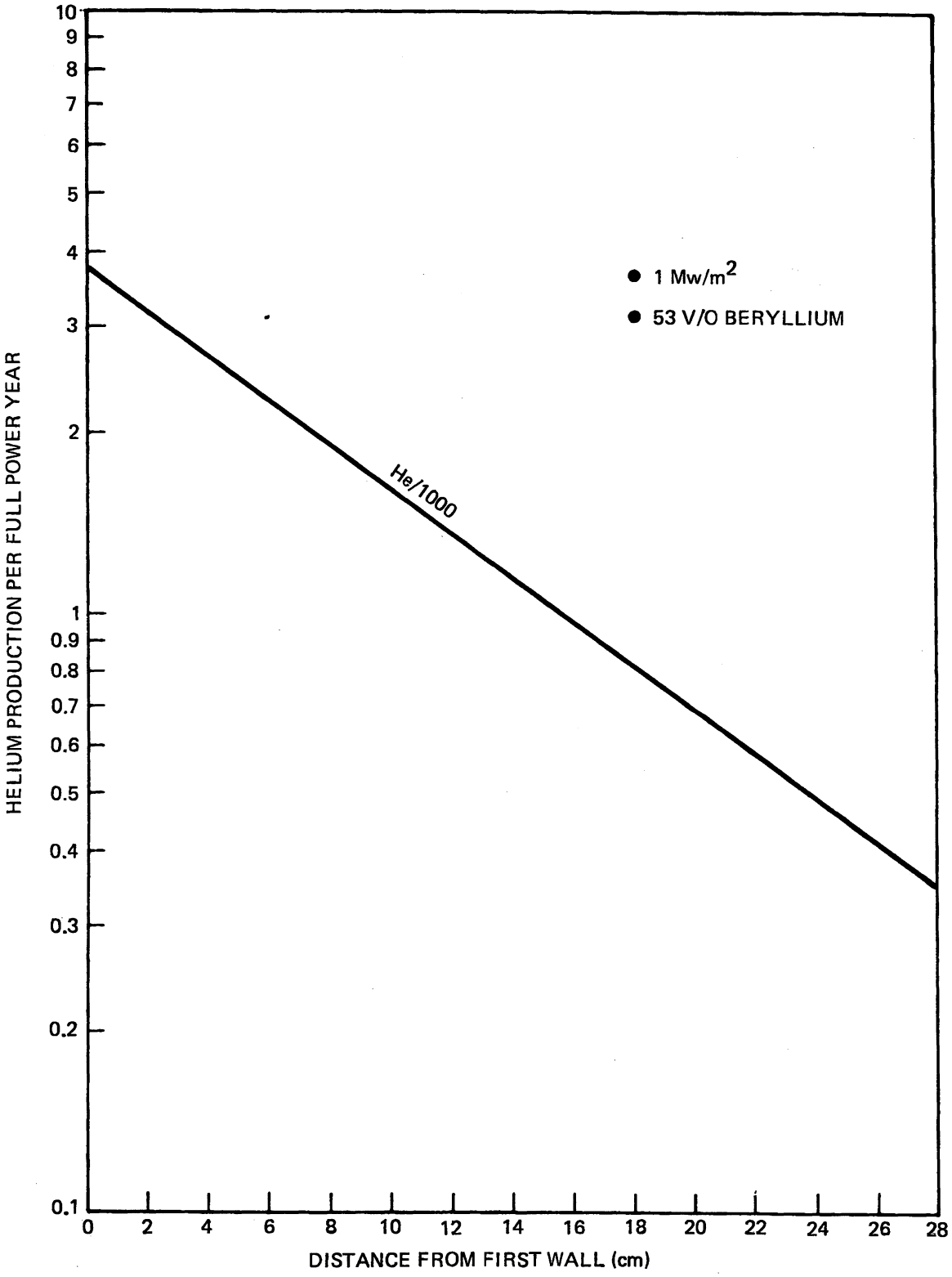

Figure V.2-3. Typical beryllium burnup profile.

of the reactor economy, ε is the recycle loss rate, and B (%/yr) is the beryllium burn-up rate (as defined above). For the purpose of this discussion we will take τ = 1 yr in analogy with typical LWR fuel fabrication times.

TABLE V.2-6. TYPICAL BERYLLIUM BURN-UP IN TOKAMAKS (STARFIRE dimensions in power)

Solid Thickness	Effective Thickness[a]	Annual Burn-up	As Fraction of U.S.B.M. Resources
0.1 cm	0.19 cm	7.4 Kg/yr	0.000010%/yr
1 cm	1.9 cm	69 Kg/yr	0.000094%/yr
5 cm	9.4 cm	306 Kg/yr	0.00042%/yr
10 cm	18.9 cm	506 Kg/yr	0.00069%/yr

[a]At 53% v/o (to correspond with Fig. V.2-3).

Before developing results which include recycle, it is of interest to propose the resource life definitions. The following definitions are proposed:

- short term service - 60 GW_e x 30 years (first generation)
- intermediate term service - 50 GW_e x 60 years (second generation)
- long term service - 1000 GW_e x 200 years.

The short term service requirement is a direct analogy to the first generation of light water fission reactors currently operating in the U.S. The intermediate term service requirement is a crude estimate of the average potential for fusion reactors within the first century after commercial introduction and is expected to satisfy the first and second generations of fusion reactors. The long term service requirement would satisfy a fusion-electric economy which is considerably larger than the current U.S. electrical demand (but is similar to the demand projected for the year 2000) for a period roughly equivalent to that of the industrial revolution (i.e., the past 200 years). This period is considered to be long enough to develop fusion blankets with sufficient excess breeding without the use of beryllium and/or to implement

fusion fuel cycles which relax breeding (e.g., semi-catalized D-D fuel cycles).

Improved results which consider initial inventory and make-up requirements (with and without recycle) and assume that 50% of the U.S.B.M. domestic resource estimate could be utilized for U.S. fusion applications are shown in Table V.2-7.

TABLE V.2-7. RESULTS OF THE BERYLLIUM RESOURCE ASSESSMENT
[U.S. Electrical Capacity (GW_e)]

Thickness (cm)	Fusion Economy Duration (yr)	No Recycle	Recycle Loss		
			7%	1%	0%
10	30	33	155	205	215
	60	18	115	180	200
	200	5.6	54	120	150
5	30	66	310	405	425
	60	35	230	355	390
	200	11	105	225	280
1	30	330	1,550	2,000	2,100
	60	175	1,130	1,740	1,190
	200	56	515	1,090	1,350
0.1	30	930	8,350	17,200	20,900
	60	475	5,080	13,600	18,900
	200	145	1,800	6,900	13,100

These results indicate that, for extended service, efficient recycle is required and that the recycle process losses must decrease as the thickness increases. The improvement in supported U.S. electrical capacity which results from a 0% recycle loss rate is only minimal compared with 1% losses.

Using the above analysis, which considers only the domestic beryllium resource, we reach the following conclusions:

- Thin Be coatings (< 0.1 cm) are acceptable for intermediate term service without recycle. With 7% recycle losses they are acceptable for long term service.

- Thicker coatings (~ 1 cm) are more than acceptable for short term service without recycle, but require recycle for intermediate term service and efficient recycle for long term service.

- Thin multipliers (~ 5 cm) are acceptable for short term service without recycle. They can nearly qualify for intermediate term service with very efficient recycle (<1% loss/recycle).

- Thick multipliers (~ 10 cm) are unacceptable for short term service without recycle. Very efficient recycle (< 1% loss/recycle) is not sufficient for intermediate term service. Thick multipliers do not appear to offer potential for long term service.

Nevertheless, it must be recognized that the above analysis is conservative in that imported beryllium is not considered in the reactor support calculations. Clearly, some level of imported beryllium is relevant, but economic and political conditions during the latter half of the next century remain unclear. As a first guess, we might assume that the U.S., with about 5% of the world population, might use about 15% of the world beryllium resource, or about 166,000 MT (according to the U.S.B.M. estimate). If again, half of this quantity were available for fusion applications, the resulting 83,000 MT resource would increase the resource lives by 2.3 fold.

Considering some continuing U.S. usage of the worled beryllium resource, the results for beryllium multipliers would change. Specifically, thick multipliers (~ 10 cm) would become acceptable for short term service without recycle and would become nearly acceptable for intermediate term service with 1% recycle losses. Similarly, thin multipliers (~ 5 cm) would become acceptable for intermediate term service with 7% recycle losses. Under the above assumptions, thick multipliers would not be acceptable for long term service, but could become acceptable with 1% recycle losses if about 300,000 MT (~ 27% of the U.S.B.M. worled resource estimate) were made available for consumption in U.S. fusion reactors. A similar requirement for the thinner (~ 5 cm) multipliers would be 160,000 MT (~ 14% of the U.S.B.M. world resource).

Based upon these observations, it appears reasonable to consider beryllium multipliers for the first and second generations of fusion reactor

service, but close attention to beryllium recycle losses will be required. Since beryllium will activate in the fusion environment (primarily due to impurities), a remote refabrication technology will be required.[33,34] Without very sufficient recycle, thick beryllium multipliers should only be considered for use in the first generation of fusion reactors.

V.3 Electric Insulator Coatings

Magnetohydrodynamic (MHD) pressure losses are an important consideration in the design of liquid metal cooled blankets. Both MHD experiment and theory indicate that the pressure losses would be significantly reduced if high electrical resistance structural walls were used in the design. Two possible methods of achieving this benefit have been considered. The first utilizes a thin insulator film on the surface of the conducting wall. Compatibility of the insulator with the liquid metal is a major concern. The second consists of a laminated structure with a thin metallic layer over an insulator layer on the wall. In this case the insulator is protected from the corrosive effects of the liquid metal coolant. However, the corrosion and mechanical integrity of the thin metal clad become more critical. In both cases radiation effects are critical, particularly for the insulator.

A preliminary attempt has been made to identify possible candidate insulator materials for this application. Both oxides and nitrides have been considered. Selected nitrides, e.g., TiN, ZrN, and AlN, are predicted to be thermodynamically stable in liquid lithium and Li-Pb alloy. However, the electrical resistivities of nitrides as a class are probably not sufficiently high to provide significant benefits.

Selected oxides may be acceptable for this application. Yttrium oxide (Y_2O_3) is currently being evaluated as a potential candidate. Alternate oxides that are possible candidates include scandium oxide (Sc_2O_3) and calcium oxide (CaO). Much more effort is required to fully evaluate these and any other potential candidates. The following paragraph summarizes some of the first-order considerations regarding the use of Y_2O_3 for this purpose.

Yttrium oxide is one of the few oxides that are stable in low-oxygen lithium. Yttrium has been used as a getter for nonmetallic elements in experimental lithium loops.[36] Exposure of yttrium to relatively high purity lithium (400-600°C) results in a uniform adherent oxide film.[36] Preliminary

measurements indicate that this film is highly resistive (ρ of the order of 10^8-10^9 Ω-cm).[37] Also based on limited data,[38] Y_2O_3 appears to be among the most radiation damage resistant oxides that have been tested. In order to be effective for the proposed application it is generally conceded that a self-healing coating is required. Microcracks formed during thermal cycling, e.g., startup/shutdown, could severely degrade the effectiveness of the coating unless it would reform during operation. Typical oxygen concentrations in lithium are probably adequate for this purpose. An important concern regarding the use of yttrium is its high affinity for hydrogen (tritium). A minimal amount of yttrium should be used. Incorporating yttrium into a thin surface region of the structural alloy may be sufficient to provide the desired insulating properties.

Obviously a more detailed evaluation, both analytical and experimental, is necessary to provide an adequate assessment of yttrium oxide, or any other candidate material, as a coating for reducing MHD effects. For the current study it is recommended that the benefits to a design with a 10-50 μm coating of Y_2O_3 (estimated resistivity = 10^8 Ω-cm) be evaluated. If significant reductions in MHD pressure losses are predicted, further feasibility studies should be initiated.

REFERENCES FOR CHAPTER V

1. C. C. Baker, et al., STARFIRE - A Commercial Tokamak Fusion Power Plant Study, Argonne National Laboratory Report, ANL/FPP-80-1, Sept., 1980.

2. M. A. Abdou, et al., U.S. Contribution to INTOR Study, Chapter VII Impurity Control and First Wall Engineering, FED-INTOR/ICFW/82-17.

3. Materials Handbook for Fusion Energy Systems, Department of Energy Report, DOE/TIC-10122, April, 1980.

4. D. W. Jeppson, et al., Lithium Literature Review: Lithium's Properties and Interactions, Hanford Engineering Development Laboratory Report, HEDL-TME-78-15, UC-20, April, 1978.

5. Letter, D. L. Smith (ANL) to J. W. Davis (MDAC), February 8, 1983.

6. G. Grube and H. Klaiber, Z. Electrochem 40, 745 (1934).

7. N. A. Frigerio and L. L. LaVoy, "The Preparation and Properties of LiPb, A Novel Material for Shields and Collinators," Nuclear Technology, 10, p. 322, March 1971.

8. V. Coen, Ispra, Italy, private communication.

9. E. Veleckis, ANL, private communication.

10. C. H. Wu and A. J. Blair, "A Study of the Interaction of Tritium with Liquid $Li_{17}Pb_{83}$," Proceedings of the 12th Symposium on the Fusion Technology, Julich, Germany, Sept. 1982.

11. G. Pieriui, et al., "Tritium Recovery from $Li_{17}Pb_{83}$," Proceedings of the 12th Symposium on the Fusion Technology, Julich, Germany, Sept. 1982.

12. H. Ihle, A. Neubert and C. H. Wu, "The Activity of Lithium, and the Solubility of Deuterium, in Liquid-Lead Alloys," EURATOM Conf., 9th Symp. on Fusion Technology, Sept., 1978, Ispra, Italy.

13. M. L. Saboungi, J. Marr and M. Blander, "Thermodynamic Properties of a Quasi-Ionic Alloy from Electromotive Force Measurements - The Li-Pb System," J. Chem. Phys. 68 (1978), 1375-1384.

14. A. I. Demidov, A. G. Morachevskii and L. N. Gerasimenko, "Thermodynamic Properties of Liquid Lithium-Lead Alloys," Sov. Electrochem. 9 (1973), 813-814.

15. S. P. Yatsenko and E. A. Saltykova, "Thermodynamic Properties of Liquid Lithium-Lead Alloys," Russ. J. Phys. Chem. 50 (1976), 1278.

16. M. Ortman, University of Wisconsin, private communication.

17. H. Ruppersburg and W. Speicher, Z. Naturforsch A 31A, 47 (1976).

18. V. T. Nguyen and J. E. Enderby, "The Electronic Structure of Lithium-Based Liquid Semiconducting Alloys," Philosophical Magazine 35, 4, 1013-1019 (1977).

19. F. Reiter, et al., "Thermodynamic Properties of $Li_{17}Pb_{83}$," Proceedings of the 12th Symposium on Fusion Technology, Julich, Germny, Sept. 1982.

20. W. Hofmann, Lead and Lead Alloys, Properties and Technology, Springer-Verlag Berlin, 1970, p. 12.

21. J. B. Rich, et al., "The Effects of Heating Neutron Irradiated Beryllium," J. of Nucl. Mater. 1 (1959) 96-105.

22. C. E. Ells and E. C. W. Perryman, "Effects of Neutron-Induced Gas Formation on Beryllium," ibid, 73-84.

23. J. R. Weir, "The Effect of High-temperature Reactor Irradiation on Some Physical and Mechanical Properties of Beryllium," Proc. of Inter. Conf. on the Metallurgy of Beryllium, Institute of Metals, London, Oct. 16-18, 1961, pp. 362-371.

24. J. B. Rich, et al., "The Mechanical Properties of Some Highly Irradiated Beryllium," J. of Nucl. Mater. 4, No. 3 (1961) 287-294.

25. M. O. Tucker and R. J. White, "The Geometry of Interlinked Grain Edge Porosity," Res. Mechanical (1980) 21-30.

26. J. A. Turnbull and M. O. Tucker, "Swelling in UO_2 Under Conditions of Gas Release," Phil. Mag. Vol. 30, 1974, pp. 47-63.

27. J. M. Beeston, "Gas Release and Compression Properties in Beryllium Irradiated at 600 and 750 C," in Effects of Irrad. on Structural Metals, ASTM STP 426, 1967, pp. 135-148.

28. A. L. Loeb, "Thermal Conductivity: VIII, A Theory of Thermal Conductivity of Porous Materials," J. Am. Ceram. Sec. 37 (1954) 96.

29. G. P. Marino, "The Porosity Correction Factor for the Thermal Conductivity of Ceramic Fuels," J. of Nucl. Mater. 38 (1971) 178-190.

30. D. Petkof, "Beryllium," Mineral Facts and Problems, U.S. Bureau of Mines Bulletin 650 (1980).

31. W. R. Griffitts, "Beryllium," U.S. Geological Survey Prof. Paper 820 (1973).

32. B. Petkof, "Beryllium," U.S.B.M. Mineral Commodity Summaries (1982).

33. J. D. Lee, et al., "Feasibility Study of a Fission-Suppressed Tandem Mirror Hybrid Reactor," Lawrence Livermore National Laborataory, UCID-19327 (1982).

34. D. H. Berwald, et al., "Fission Suppressed Hybrid Reactor - The Fusion Breeder," Lawrence Livermore National Laboratory, UCID-19638.

35. F. Fulton (Lawrence Livermore National Laboratory) to D. Berwald (TRW), personal communication, January, 1983.

36. D. L. Smith, et al., "Investigation of Nonmetallic Element Interactions in Vanadium-Alloy/Lithium System," 2nd Inter. Conf. Liquid Metals in Energy Production, Richland, WA, April, 1980, p. 2-72.

37. D. L. Smith, personal communication.

38. F. W. Clinard, Jr., "Ceramics for Applications in Fusion Systems," Proc. of 1st Topical Meeting on Fusion Reactor Materials, Miami Beach, Florida, January 29-31, 1979, pp. 393-404.

TABLE OF CONTENTS

CHAPTER VI - CORROSION OF STRUCTURAL ALLOYS

LIST OF FIGURES FOR CHAPTER VI

LIST OF TABLES FOR CHAPTER VI

VI. CORROSION OF STRUCTURAL ALLOYS

Critical aspects of liquid metal, gaseous and water corrosion/compatibility for the three candidate structural materials have been evaluated as part of the present study. The following assessments and analyses have been conducted.

- Liquid Metal Corrosion/Compatibility (Li and Li-Pb)
  - Assessment of Data Base
  - Development of Mass Transfer Model

- Gaseous Corrosion/Compatibility Vanadium
  - Helium With Impurities
  - Air or Oxygen Characteristic of Accident Conditions
  - Hydrogen Plasma Environment

- Water (200 - 350°C)
  - Vanadium Alloys
  - Cold-Worked Austenitic Steel

VI.1 Liquid Metal Corrosion/Compatibility

VI.1.1 Corrosion/Compatibility Data Base

Compatibility considerations with liquid metals have a major influence on the material selection and operating limitations of the structural materials for liquid metal fusion reactor blankets. The two major compatibility concerns arising from the use of liquid metals, such as lithium or Pb-17Li, are (a) corrosion, and (b) degradation of mechanical strength of the containment material. The corrosion and mass transfer of structural material can be deleterious in any application of circulating liquid metals. Corrosion in the form of uniform or selective dissolutive, intergranular penetration, and interstitial-element transfer to and from the liquid metal can result in (a) significant wall thinning/wastage and (b) deposition of corrosion products that may cause severe flow restrictions and excessive accumulation of radioactive material in unshielded regions. The former consequence results in a loss of mechanical integrity and the latter phenomenon would increase pumping

power requirements, decrease the energy conversion efficiency, and complicate system maintenance. The corrosion and mass transfer problem varies for different combinations of containment material and liquid metals and depends on many variables. These include the liquid metal and its purity (i.e., concentration of N, O, C, etc. in the liquid metal); composition and microstructure of the containment material; temperature; exposure time; and system parameters such as flow velocity (including MHD effects), ΔT (difference in temperature across the circulating system), surface area and temperature profile of the system, and material combination (i.e., bimetallic or monometallic system).

Deterioration of the mechanical properties of structural materials can result from the influence of the environment itself and the effects of microstructural and compositional changes that occur in the material during long-term high-temperature exposure to the liquid metal environment. Liquid metals can influence the surface-active properties of the material through liquid metal embrittlement (LME), oxidation, nitridation, or carburization-decarburization phenomena, all of which can alter the near-surface deformation behavior and thus affect mechanical properties such as fatigue crack propagation, creep ductility, etc. The long-term exposure of the material to a liquid metal environment can change bulk properties, primarily through compositional and microstructural modifications caused by selective corrosion, interstitial-element transfer, and thermal aging. The environmental interactions and the nature and extent of the changes in the material depend on liquid metal chemistry, temperature, time, and material composition and microstructure.

VI.1.1.1 Corrosion Data Base

Experimental data on the corrosion behavior of several austenitic and ferritic steels in liquid lithium and Pb-17Li environments have been obtained in static liquid-metal pots or capsules as well as in circulating systems such as thermal convection loops (TCLs) and forced-circulation loops (FCLs).[1-23] The experimental conditions for the corrosion data in liquid lithium and Pb-17Li are summarized in Tables VI.1-1 and VI.1-2, respectively. Relatively little data are available on corrosion in Pb-17Li environment. Recent experiments with static and circulating Pb-17Li indicate that the dissolution rates are substantially greater than those in lithium. In both environments, austenitic stainless steels, e.g., types 316 and 304 stainless steel and primary

TABLE VI.1-1. SUMMARY OF SYSTEM AND MATERIAL CONDITIONS FOR CORROSION DATA IN LIQUID LITHIUM

		System Conditions							Material Conditions			
Lab.[a]	Ref.	Type[b]	Material	Velocity m/s	Impurity	Temp. °C	ΔT °C	Max. Time h	Material[c]	TMT[d]	Stress	Results[e]
ORNL	1-3	Capsule	316 SS, HT-9, 9 Cr, 2 1/4 Cr	-	O, N < 175 ppm Li_3N Addition	400-700	-	10,000	Same	2 1/4 Cr	-	W,P
ORNL	4-9	TCL	316 SS, HT-9	0.03	O, N < 175 ppm	500-650	150	16,000	PCA, 316 SS, LRO, HT-9, 9 Cr	PCA	-	W/L/ M, P
ORNL	10	TCL	Alloy 800	0.03	O, N < 175 ppm	500	175	3,000	Path B, Alloy 800	-	-	W, M
UW	11	FCL	316 SS	0.45-1.36	N = 50-120 ppm O = 275 ppm	440,490	110-195	4,000	Same	-	-	W/L
SU	12	FCL	304 SS	0.16-0.85	-	421-612	10-212	100	Same	-	-	W
ANL	13,14	FCL	304 SS	~0.03	N = 50-250 ppm	427-482	70	5,000	316 SS, 304 L, PCA HT-9, 9 Cr	316 CW	Yes	W, P
WARD	15	FCL	Austenitic	1.82	-	538	150	1,000	316 SS, 304 SS, 9 Cr	-	-	W/L
JAERI	16	TCL	-	0.03	-	600	100	2,500	316 SS	-	-	W
CSM	17,18	Pot	Armco Iron	-	N > 3000 ppm	565-592	-	135	Same	-	Yes	P
CSM	19	Pot	304 L	-	N > 1.2%	800	-	35	Same	-	-	P
ISPRA	20	Capsule	γ-Mn Steel	-	N = 20 ppm	600	-	6,000	Same	-	-	P

[a] ORNL - Oak Ridge National Laboratory
UW - University of Wisconsin
SU - Syracuse University
ANL - Argonne National Laboratory
WARD - Westinghouse Advanced Reactor Division
JAERI - Japan Atomic Energy Research Institute
CSM - Colorado School of Mines
ISPRA - Commission of European Communities, Joint Research Centre

[b] TCL - Thermal Convection Loop
FCL - Forced Circulation Loop with Cold Trap Purification System

[c] Materials other than the lithium system construction material are listed.

[d] Materials tested in various thermo-mechanical conditions are listed.

[e] W = weight loss in $mg/m^2.h$.
W/L = weight change as a function of loop position.
P = depth of corrosive penetration.
M = mass transfer/deposition.

TABLE VI.1-2. SUMMARY OF SYSTEM AND MATERIAL CONDITIONS FOR CORROSION DATA IN LIQUID LEAD - 19 at.% LITHIUM

		System Conditions						Material Conditions		
Lab.[a]	Ref.	Type[b]	Material	Velocity	Temp.	ΔT	Max. Time	Material	TMT[c]	Results[d]
ORNL	21	Capsule	316 SS, HT-9	-	300-700	-	5,000	316 SS, HT-9	-	W, P
ORNL	-	TCL	316 SS	0.03	500	150	500	316 SS, HT-9	-	W, P
ANL	14	FCL	Carbon Steel/304 SS	0.03	427,454	150	3,500	316 SS, PCA, HT-9 9Cr	PCA 316 SS	W, P
CSM	23	Pot	2 1/4 Cr	-	300-600	-	135	2 1/4 Cr	-	P
ISPRA	23	Pot	Armco Iron	-	400-600	-	6,000	316 L	-	P
		Capsule	304 L	-	400	-	1,000	316 L	-	P

[a] ORNL - Oak Ridge National Laboratory
ANL - Argonne National Laboratory
CSM - Colorado School of Mines
ISPRA - Commission of European Communities, Joint Research

[b] TCL - Thermal Convection Loop
FCL - Forced Circulation Loop

[c] Materials tested in various thermo-mechanical treatment are listed.

[d] W - Weight change in $mg/m^2.h$
P - depth of corrosive penetration

candidate alloy (PCA) develop a ferrite layer due to preferrential depletion of nickel and to a lesser extent chromium from the surface, whereas, the ferritic steels, e.g., HT-9 alloy and Fe-9Cr-1Mo steel, show little or no surface degradation. Intergranular penetration of both ferritic and austenitic steels has been observed in lithium containing high (> 1000 ppm) concentrations of nitrogen.

For most studies, the corrosion behavior has been evaluated in terms of weight loss per unit surface area and/or as depth of internal corrosive penetration. However, the rate of weight loss is expressed either as the average value for the entire time of exposure or as the steady state value attained after the initial transient period of high dissolution rates. For austenitic stainless steels, the difference between the average and steady-state dissolution rates can be significant, particularly for long exposure times. Furthermore, the system parameters, such as flow velocity, ΔT, surface area of the liquid metal system, and liquid metal purity, vary significantly for the various investigations. The existing experimental data are insufficient to accurately establish the influence of the different material and system parameters on the corrosion behavior of structural materials. It is possible, however, to qualitatively assess the corrosion behavior of various alloys and determine the preliminary operating temperature limits for circulating and static liquid-metal systems.

VI.1.1.1.1 Lithium System

Corrosion tests in static lithium systems have been used in identifying and characterizing the various reactions between lithium and containment materials and to study the influence of lithium purity, stress, and material variables on these interactions. For most studies, the corrosion behavior in static lithium has been evaluated in terms of the depth of internal corrosive penetration. The dissolution and mass transfer behavior has been investigated from data in circulating lithium systems. The significant results from corrosion tests in lithium are summarized as follows:

(a) The dissolution rates for austenitic stainless steels reach steady-state values after an initial period of 1500-3000 h characterized by higher, rapidly changing rates. The weight loss, W (mg/m^2), may also be expressed by a power-law relationship with time, t, given by $W = kt^n$.

For the data in TCL and FCL systems, the average value of the time exponent is 0.7.

(b) The weight loss for ferritic HT-9 alloy and Fe-9Cr-9Mo steel in circulating lithium systems follows a linear relationship with time.

(c) The dissolution rates of austenitic stainless steels in FCL are a factor of 5 to 20 greater than in TCL. All FCL systems used for corrosion studies are equipped with a cold trap purification loop. The greater dissolution rates in FCL may be attributed to greater mass transfer/deposition behavior because of the cold trap/purification loop. The dissolution rates for ferritic steels are comparable in TCL and FCL.

(d) After exposure to flowing lithium, the austenitic stainless steel develop a very porous ferrite layer due to preferential depletion of nickel and to a lesser extent chromium from the material. Data indicate that the thickness of the ferrite layer may increase linearly with time. Figure VI.1-1 shows the thickness of the ferrite layer for type 316 stainless steel in TCL and FCL systems. The results yield a growth rate of ~ 100 μm/y at 482°C in FCL and 55 μm/y at 570°C in TCL. Furthermore, the ferrite layer on austenitic stainless steel is very weak and may spall off under thermal transients or cyclic straining.

(e) The ferritic steel show little or no internal corrosive attack in low-nitrogen flowing lithium. The near-surface region shows slight depletion of chromium.

(f) Weight loss for 20% cold-worked type 316 stainless steel is a factor of ~ 2 greater than that for annealed steel.

(g) Dissolution rates of austenitic steels increase with an increase in the nickel content. Weight loss for cold-worked PCA is a factor of ~ 1.5 greater than that for cold-worked type 316 SS.

(h) For FCL systems, the dissolution rates for ferritic steels are an order of magnitude lower than the steady-state dissolution rates for annealed

type 316 stainless steel. However, dissolution rates for ferritic HT-9 alloy and type 316 stainless steel are comparable in TCL system. Additional long-term data are needed to establish the effects of material composition on corrosion.

(i) Weight loss for types 304 and 316 stainless steel in flowing lithium are comparable, although the data from different FCL systems show significant scatter.

(j) FCL data indicate that the dissolution rates in flowing lithium increase with an increase in flow velocity or an increase in ΔT in the system. However, the data are insufficient to obtain accurate correlations.

(k) Limited data in FCL show that the weight loss for both ferritic and austenitic steels in lithium containing 50 ppm nitrogen is a factor of 2 to 5 lower than in lithium with 200 ppm nitrogen. Similar changes in nitrogen content in TCL show no effect on corrosion. Additional data are required to establish the effects of lithium purity on corrosion and mass transfer in flowing lithium systems.

(l) The variation in dissolution rates with temperature have been investigated for type 316 SS in TCL systems at 500, 550, and 600°C. An Arrhenius plot of dissolution rate data yield an activation energy of 38 kcal/mole. The data from FCL systems show considerable scatter and yield values of activation energy between 11 and 30 kcal/mole. However, such analyses are based on data obtained for < 100 h exposure time or < 50°C difference in exposure temperature. Long-term data in FCL systems under controlled liquid metal and system conditions, at temperatures between 350 and 500°C are needed to determine the variation in dissolution rates with temperature.

Because of the many variables, viz., lithium purity, temperature, ΔT, surface area, etc., it is difficult to compile a definitive data set of measured corrosion rates in flowing lithium. An activation energy of 38 kcal/mole measured for TCL systems is comparable to the value of 36 kcal/mole observed for type 316 stainless steel and Alloy 800 in large flowing sodium

systems. When exposed to high temperature sodium, Alloy 800 develops a porous ferrite layer similar to that observed for type 316 stainless steel in flowing lithium. Figure VI.1-2 shows an Arrhenius plot of dissolution rate data for various ferritic and austenitic steels in flowing lithium. The data in lithium were normalized for velocity effects using the relationship for corrosion of stainless steel in sodium. In sodium, the corrosion rate, R, is expressed as

$$R \alpha (2.97 + 2.71\ V) \qquad [VI.1\text{-}1]$$

where V is the velocity in m/s. The data for FCL systems fall within a wide scatter band. The Arrhenius temperature dependence for the dissolution rate of type 316 SS in TCL and FCL systems was assumed to be the same as that observed in sodium. The results show that the dissolution rates for type 316 SS in FCLs are an order of magnitude greater than in TCL systems. Dissolution rates for HT-9 alloy in TCL and FCL are identical and similar to those for type 316 SS in TCLs.

VI.1.1.1.2 Pb-17Li System

Relatively little data are available for corrosion and mass transfer behavior of structural materials in Pb-17Li. The significant results from corrosion tests in static capsules and FCL system are as follows:

(a) The weight loss for ferritic HT-9 alloy and Fe-9Cr-1Mo steel in flowing Pb-Li at 454 and 427°C and exposure times up to 3,300 h, follow a parabolic relationship with time.

(b) The weight loss for both ferritic and austenitic steels in static Pb-Li capsules is significantly lower than that in flowing Pb-Li and reaches a constant value after a short period of 1000 to 3000 h.

(c) The weight loss for ferritic HT-9 alloy and Fe-9Cr-1Mo steel in flowing Pb-Li are a factor of 5 to 10 lower than type 316 SS and shows a linear relationship with time.

(d) Dissolution rates of cold-worked type 316 SS are a factor of 1.5 greater than those for the annealed steel.

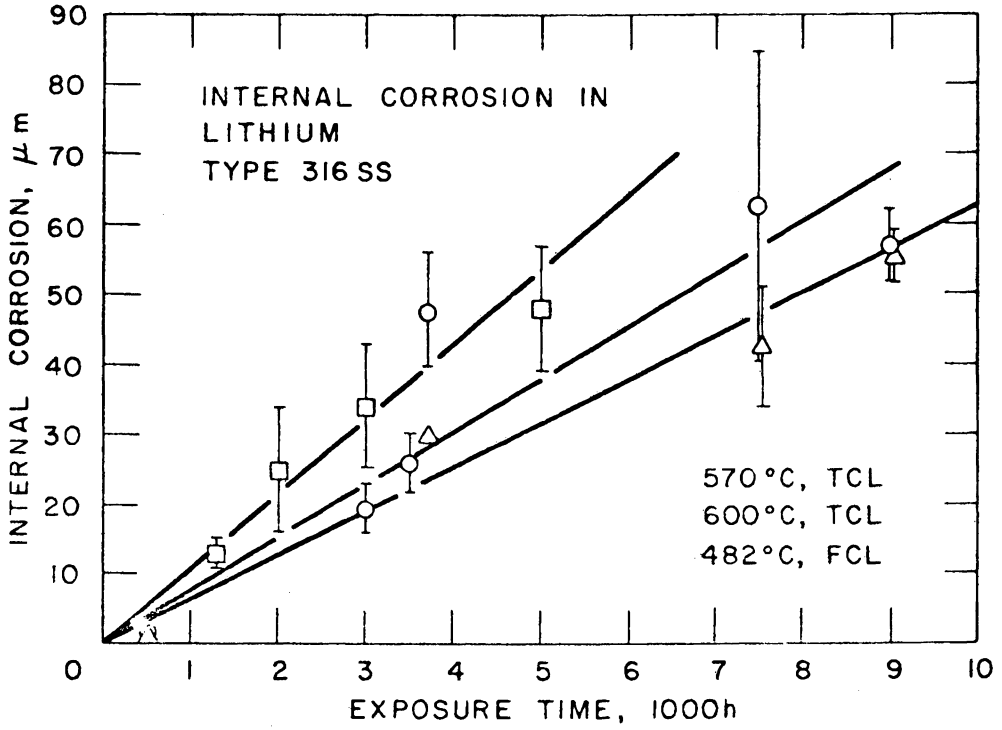

Figure VI.1-1. Depth of internal corrosion of type 316 stainless steel exposed to flowing lithium.

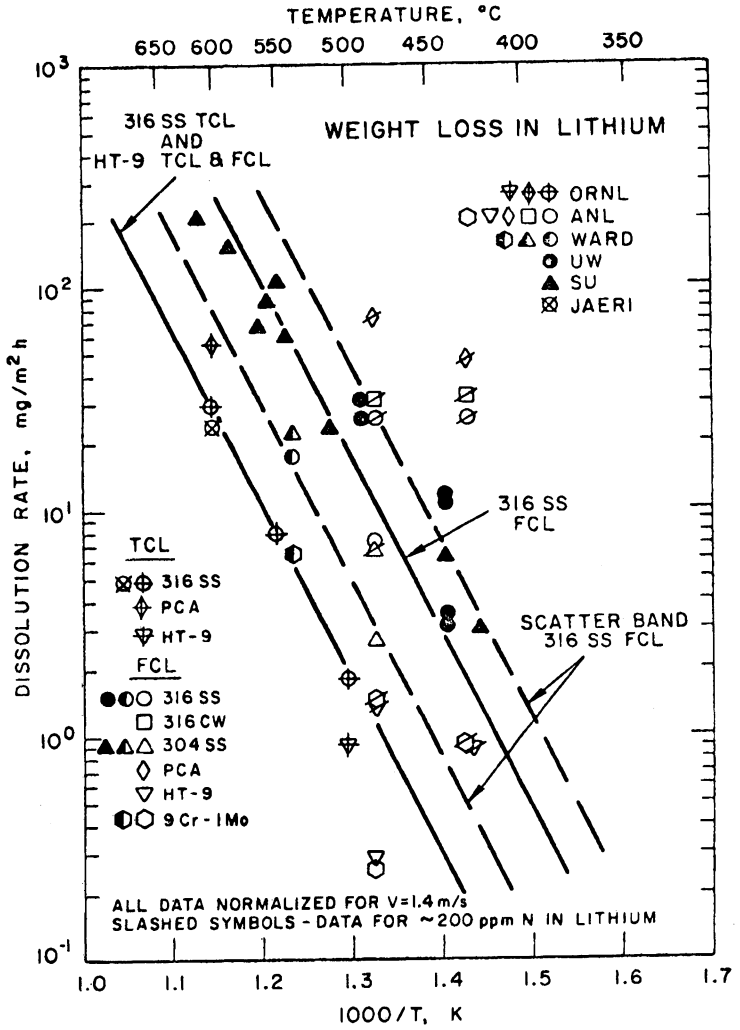

Figure VI.1-2. Arrhenius plot of corrosion rate data for types 304 and 316 stainless steel, PCA alloy, HT-9 alloy and Fe-9Cr-1Mo steel exposed to flowing lithium.

(e) After exposure to flowing Pb-Li the austenitic steels develop a very porous and weak ferrite layer which spalls off easily. The ferritic HT-9 alloy and Fe-9-Cr-1Mo steel show little or no internal corrosion. Limited data show significant weight loss for PCA alloy after relatively short exposure times. The entire ferrite layer spalls off during cleaning of the specimens.

(f) Figure VI.1-3 shows an Arrhenius plot of the dissolution rate data for annealed and cold-worked type 316 SS, HT-9 alloy, and Fe-9Cr-1Mo steel in flowing Pb-17Li. The data are normalized for velocity effects using Eq. VI.1-1. The temperature dependence is identical to that observed for lithium TCLs or for sodium systems.

VI.1.1.1.3 Criteria and Corrosion Limits

The corrosion and mass transfer behavior of structural material depend on the particular liquid-metal blanket design. For example, a liquid metal system used solely for tritium breeding could be isothermal and have very low flow velocities, but the use of liquid metals as a coolant requires large ΔT and high flow velocities. Ideally, the corrosion limits for an isothermal semistagnant blanket system should be determined from the static lithium data and the FCL data should be used to establish the limits for coolant system. However, even the semistagnant tritium breeding blanket systems will have some ΔT and thus mass transfer, particularly during off normal operating conditions. Some blanket systems are designed for use as a coolant during loss of flow accidents. Consequently, the design limits for the static or semistagnant blanket systems are determined from the TCL data.

The basis for a temperature limit from corrosion considerations can be from radioactive mass transport, wall thinning/wastage, or mass transfer and deposition. Based primarily on sodium-cooled fact breeder reactor experience, corrosion rate limits for hands-on maintenance of intermediate heat exchangers (IHX) are estimated to be ~ 0.5 μm/y. Although these values are based on austenitic steel systems, the same values are recommended as limits for other structural materials in the present study. The temperature limit for radioactive mass transport based on a corrosion rate of 0.5 μm/y is too restrictive for acceptable performance of most blanket systems considered. Therefore,

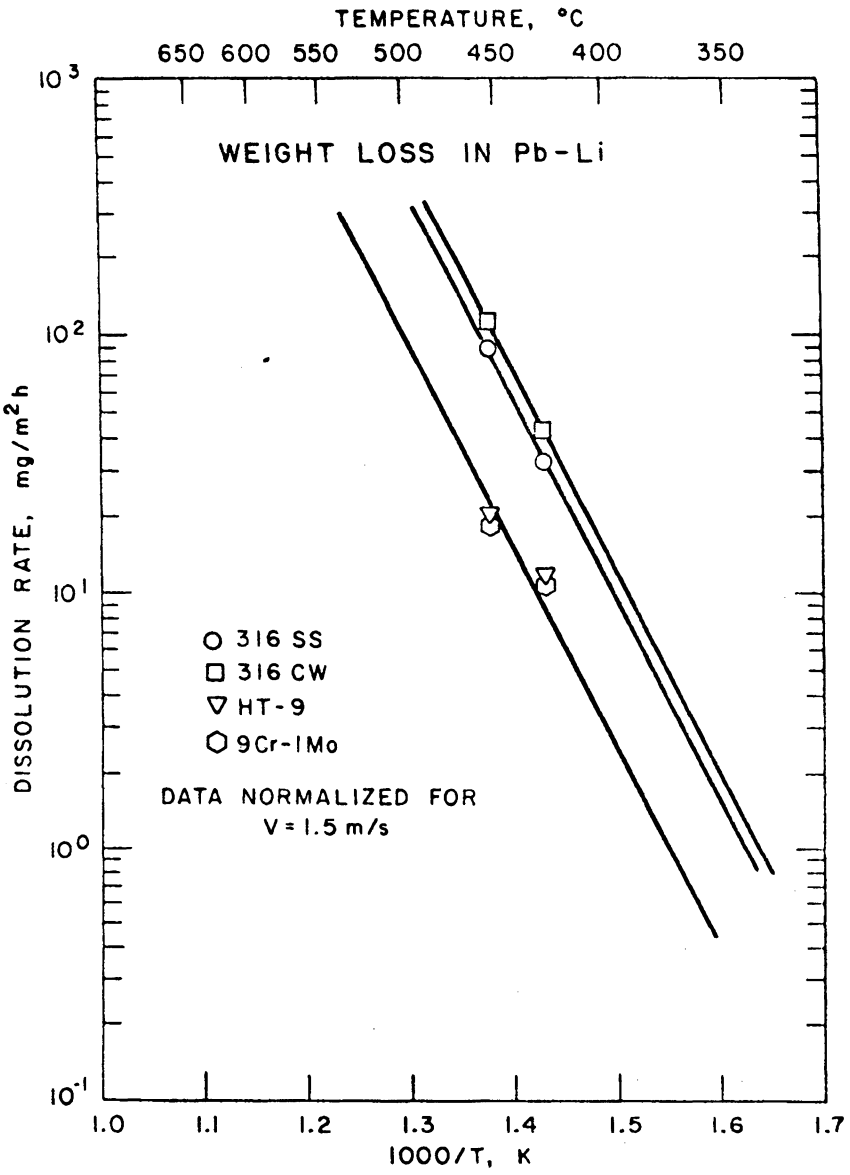

Figure VI.1-3. Arrhenius plot of corrosion rate data for austenitic type 316 stainless steel and ferritic HT-9 alloy and Fe-9Cr-1Mo steel in flowing Pb-17Li.

remote maintenance of the IHX (or steam generators if no IHX is used) will probably be required.

The allowance for wall thinning/wastage from corrosion of breeder reactor cladding is generally established as 10% of the wall thickness. A similar value is recommended for the present blanket study. This criterion is not likely to be restrictive for section thicknesses > 1 mm during a service life of 2 to 3 years.

Mass transfer and deposition is likely to be the most restrictive criterion for corrosion under most conditions of interest. Based primarily on experience from operation of liquid sodium systems, a reference corrosion limit of 5 μm/y is recommended. Plugging flow perturbations, and effects on pumps and values are frequently encountered when corrosion rates significantly exceed this limit. One must also consider enhanced corrosion caused by local "hot spot" conditions and high velocity or turbulent regions. The benefits of using an optimistic limit of 20 μm/y is evaluated for comparison.

Figures VI.1-4 and VI.1-5 show the Arrheneus temperature dependence of the corrosion rates for PCA alloy and HT-9 in lithium and Pb-17Li environments. The curves for PCA alloy were obtained from the type 316 stainless steel data in FCLs and applying a factor 3 increase (i.e., a factor of 2 increase for cold-worked 316 SS and a factor of 1.5 increase for PCA alloy) in dissolution rates. The curve for the static lithium system was obtained from the TCL data. The operating temperature limits for static and circulating (at three different velocities) liquid metal systems are listed in Table VI.1-3. The temperatures within brackets are based on an optimistic value of allowable corrosion rate, i.e., 4 x 5 = 20 μm/y. The results show that the use of austenitic stainless steels with Pb-17 Li environment may not be practical.

VI.1.1.2 Mechanical Property Degradation

Environmental effects on the mechanical properties of materials can be divided into two classes: the influence of the environment itself and the effects of microstructural and compositional changes that occur in the material during long-term high-temperature exposure to the environment. The influence of the environment itself on mechanical behavior of materials is evaluated by conducting mechanical tests in the liquid-metal environment of controlled purity and comparing the results with data obtained in other envi-

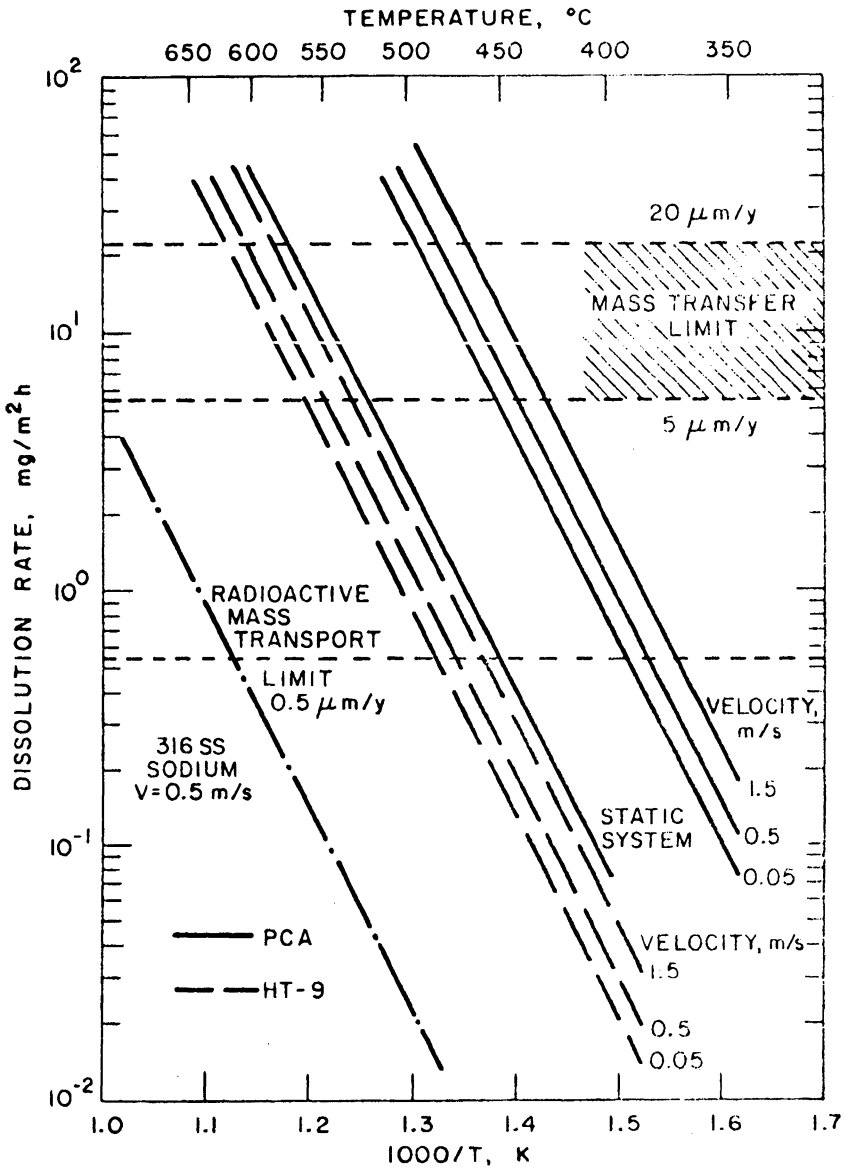

Figure VI.1-4. Effect of temperature on the corrosion rate of PCA and HT-9 alloy in flowing lithium.

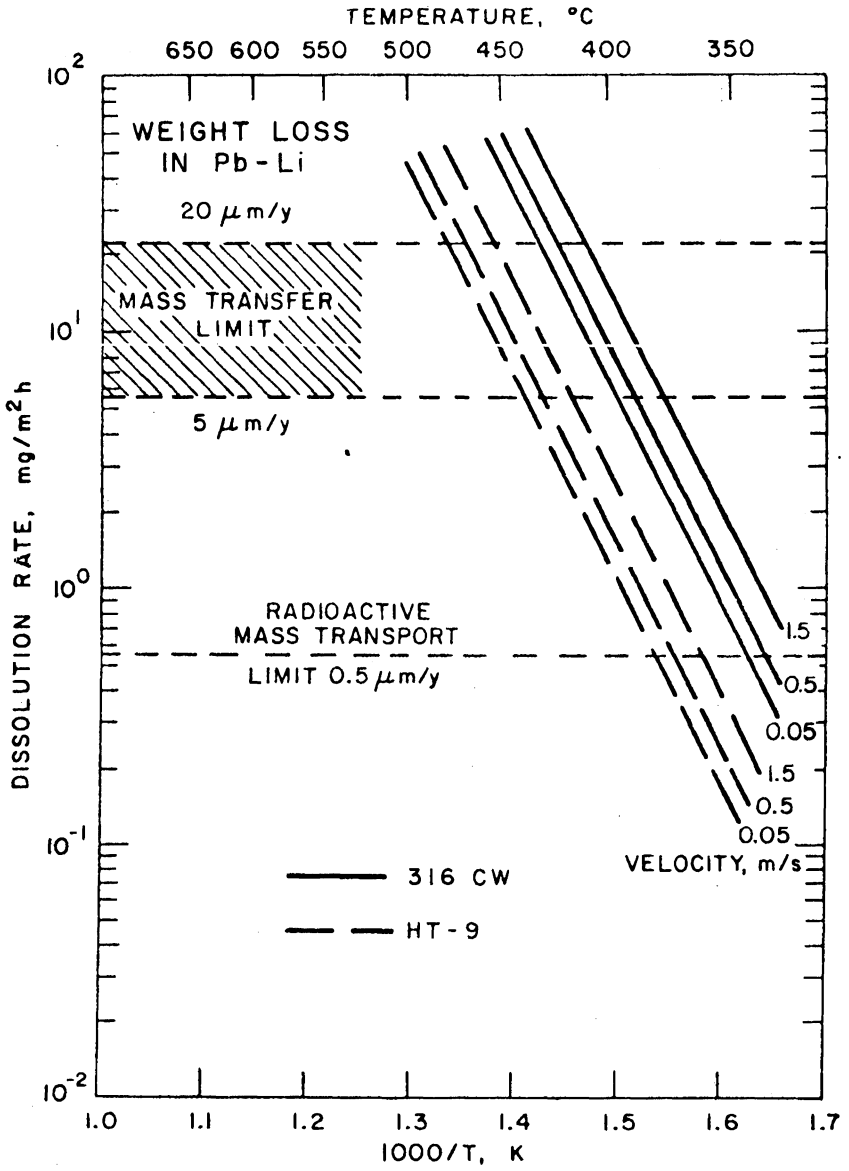

Figure VI.1-5. Effect of temperature on the corrosion rate of 20% cold worked type 316 stainless steel and HT-9 alloy in flowing Pb-17Li.

TABLE VI.1-3. PRELIMINARY DESIGN TEMPERATURE LIMITS (°C)[a]

System	Flow Velocity m/s	Austenitic Steel (PCA)[b]	Ferritic Steel (HT-9)	Vanadium Alloy[c] (V-15Cr-5Ti)
Lithium				
Circulating	1.5	430 (470)	535	750
	0.5	445 (480)	550	
	0.05	455 (495)	565	
Static	-	525 (575)	565	750
Pb-17Li				
Circulating	1.5	375 (410)	415 (450)	> 650
	0.5	385 (420)	425 (465)	
	0.05	395 (430)	435 (475)	
Static	-	395 (430)	435 (475)	> 650

[a] Limits based on a uniform dissolution rate of 5 μm/y (or ~ 5.5 mg/m^2.h). The values within brackets correspond to a rate of 20 μm/y.

[b] Temperature limits for Pb-17Li system are for 20% cold worked type 316 SS.

[c] Nonmetallic element transfer are expected to dominate corrosion limits.

ronments, such as air, vacuum, or inert gas. The long-term effects of environment, i.e., interstitial- or substitutional-element transfer and thermal aging, on the mechanical properties are determined by conducting tests on material that is either pre-exposed to the liquid-metal environment or thermally aged in an inert environment. Preexposure of the material is carried out in liquid metals of known purity, namely service conditions anticipated in real systems.

The tensile, creep, fatigue, and crack-growth properties of various austenitic and ferritic steels have been investigated in liquid lithium environment. Most of the data have been obtained by conducting tensile or creep tests in static lithium pots or on tube specimens filled with lithium. However, the purity of the lithium is not specified for all the tests. Corrosion phenomena, such as intergranular penetration or preferential leaching of substitutional elements, are likely to have a profound effect on mechanical properties. Studies on the corrosion behavior of materials in liquid lithium indicate that the nature and kinetics of corrosive attack, strongly depends on the impurity content in the environment. For example, it is well known that an increase in the concentration of nitrogen in lithium increases the corrosion rates and causes intergranular penetration of most materials. Consequently, mechanical property data obtained in liquid metal of unknown purity may be biased by the effects of the corrosive interactions and not representative of the anticipated service conditions.

Relatively little or no information is available on the influence of liquid Pb-17Li on the mechanical properties of materials. The influence of applied stress on the corrosion behavior and the effects of preexposure on tensile properties of materials have been investigated in Pb-17Li. However, the current assessment of the environmental effects in Pb-17Li are based on mechanical property data obtained in liquid lead, bismuth, or lead-bismuth environments.

The significant results from these studies can be summarized as follows:

(a) Tensile and creep strength of austenitic stainless steels is not significantly affected by both static or flowing lithium. The

influence on tensile ductility depends on strain rate, e.g., elongation is slightly reduced at slow strain rates ($\sim 4 \times 10^{-5} s^{-1}$).

(b) The tensile strength and, most particularly, ductility of Armco iron in static lithium are considerably lower than in vacuum. The reduction in tensile properties occurs in the temperature range of 200 to 500°C and is more pronounced at slow strain rates. At the critical temperatures the material fails by a brittle fracture mode and the elongation is ~ 5%.

(c) The creep-rupture strength of Armco iron is also reduced in lithium at temperatures < 500°C.

(d) Addition of hydrogen (up to ~ 40 ppm) in lithium has little or no effect on the tensile properties of austenitic stainless steels. Influence of other impurities (e.g., N, O, or C) in lithium is not established.

(e) Preexposure of austenitic and ferritic steels to flowing lithium reduces the tensile strength owing to the formation of a weak ferrite layer in austenitic steels or decarburization of the ferritic steels (particularly low-alloy ferritic steels).

(f) Nitrogen content in lithium plays an important role in controlling the fatigue properties of materials. Low-cycle fatigue life of austenitic and ferritic steels in low-nitrogen flowing lithium (i.e., < 100 ppm) is superior to that in air. Limited data also indicate that fatigue life is independent of strain rate in low-nitrogen lithium. However, fatigue life is significantly reduced in flowing lithium containing > 1000 ppm nitrogen due to intergranular attack of the material. The reduction in life is greater at slow strain rates.

(g) Preexposure of medium chromium ferritic steels (e.g., HT-9 alloy) to low-nitrogen lithium has no effect on fatigue life, whereas preexposure of austenitic stainless steel to lithium reduces fatigue life because of the formation of the ferrite layer.

(h) Fatigue crack propagation rates (da/dN) for type 304 stainless steel and Fe-2¼Cr-1Mo ferritic steel are greater in static lithium than in argon. The growth rates depend on temperature and test frequency. For austenitic type 304 SS, the growth rates increase with a decrease in frequency, whereas the crack growth rates show a minima at intermediate frequencies for the Fe-2¼Cr-Mo steel. The increase in growth rates is attributed to corrosive interactions at low frequencies and due to strain-rate-induced liquid-metal-embrittlement at high frequencies.

(i) Data are not available on the mechanical behavior of materials in liquid Pb-17Li environment. Severe loss in ductility and reduction in fatigue strength have been observed for austenitic and ferritic steels wetted with liquid Pb, Bi, or Pb-Bi.

These results indicate that a low-nitrogen lithium environment itself has no deleterious effects on the mechanical properties of austenitic stainless steels. In a lithium environment of controlled purity, the tensile and creep properties are similar and the fatigue properties are superior to that in air. Limited data indicate that exposure of austenitic stainless steels to flowing lithium can reduce mechanical strength due to the formation of the ferrite layer (i.e., a reduction in the load bearing area of the material). Long-term corrosion data in flowing lithium of controlled purity are required to determine the growth rates of the ferrite layer as a function of time and temperature, and to establish an allowance for wall thinning/wastage over the service life of the component. Data are also needed on the creep-fatigue behavior of austenitic stainless steels.

The results also indicate that embrittlement of ferritic steels, particularly low-alloy steels, may occur in lithium at temperatures between 200 and 400°C. However, data are insufficient for a reliable assessment of the environmental effects on the mechanical properties of ferritic steels. For example, the low-cycle fatigue data on HT-9 alloy show that the fatigue life in low-nitrogen lithium is independent of strain rate and is superior to that in air. Fatigue crack propagation studies on Fe-2¼Cr-1Mo steel indicate that at temperatures < 500°C the crack growth rates in lithium increase with an increase in test frequencies. Also, the crack growth rates in lithium are

greater than that in argon. Additional data are needed to evaluate the possible embrittlement of ferritic steels in lithium. Limited data indicate that preexposure of ferritic steels to lithium has no effect on fatigue strength, while the tensile strength is reduced due to decarburization of the steel.

No data are available to evaluate the influence of Pb-17Li environment on mechanical properties. The current assessment of environmental effects is based on data for Pb or Bi. The results indicate that Pb-17Li may significantly affect mechanical properties of materials.

VI.1.2 Mass Transfer Model

A computer model has been developed to predict dissolution and deposition rates in a liquid metal primary coolant loop of a fusion reactor. The model is general in that it can be applied to any liquid metal coolant loop as long as one provides the proper geometrical design parameters (i.e., tube diameters, surface areas, etc.). To date, we have applied the computer model to the MARS design which has 83Pb-17Li coolant and HT-9 structure. Also the considerations and methods used in this model have been used to evaluate potential mass transfer concerns in other blanket designs.

The parameters which can be included in the model are the following:

- Coolant (Li or 83Pb-17Li)
- Local Wall Temperature
- Total Temperature Difference (ΔT) in the Loop
- Coolant Velocity
- Geometry of Flow (e.g., in a Tube or Across a Tube Bundle as is the Case for a Shell and Tube Heat Exchanger)

VI.1.2.1 Description of the Mass Transfer Model

The transport model is based to some extent on the work of Cooper and Taylor[24] but there are major differences which will be described shortly. The fundamental assumption incorporated by Cooper and Taylor in their model is that mass transport rates are determined by the rate of material diffusion through a liquid metal boundary layer at the metal/liquid metal interface. If this is the case, then the Chilton-Colburn analogy can be invoked and engineering heat transfer correlations can be used to predict mass transfer coef-

ficients. The use of heat transfer correlations to predict mass transfer coefficients has been verified experimentally.[25]

A major difference between the model developed by Cooper and Taylor and the one described herein is that Cooper and Taylor had access to experimentally determined corrosion product release rates and hence they only needed to model the deposition rates. Because experimental data for fusion reactor systems do not exist at the present time, it was necessary for the present work to model the corrosion rate also.

Another important difference between the model developed here and Cooper and Taylor's work concerns the transport rate to a wall during the deposition process. Cooper and Taylor assumed that the flux to the wall occurred at the maximum possible rate, that is, it was assumed that the interfacial concentration was zero. However, to account for the fact that not all material carried to the wall was deposited there, they incorporated sticking coefficients into their model. The model developed here, assumes that the equilibrium concentration is maintained at the interface. Therefore, the driving force for mass transfer is not solely based on the bulk concentration of the transported species but is reduced according to its equilibrium solubility at the interface. This approach is an alternative to the use of sticking coefficients, and has more basis for justification from a theoretical standpoint.

Two mechanisms of corrosion product release were considered. The first mechanism assumes that transport of species through a liquid metal boundary layer controls the dissolution rate. For this case, it is assumed that the equilibrium solubility of the species of interest is maintained at the liquid metal/metal interface. For the corrosion product transport computer model, this mechanism is applied to iron dissolution and deposition and also to the deposition of Cr, and Ni, but not to the dissolution of Cr and Ni. Experimental evidence is available which supports this mechanism in liquid lithium[4,26] and liquid sodium systems.[27]

The other mechanism for corrosion product release assumes that the release rate is controlled by diffusion of alloying constituents through the solid metal. In the corrosion product transport model, this mechanism is used to give release rates of Ni and Cr. A difficulty in applying a strict solid diffusion mechanism arises for stainless steel in Li or 83Pb-17Li systems.

For these situations a porous ferrite layer develops at the interface as nickel and chromium are preferentially released from the matrix.[4,28] For stainless steel in lithium the width of this ferrite layer reportedly reached a steady value of ~ 60 μm after which iron dissolution appears to control the release rates of Ni and Cr.[29] More recent data indicate that the ferrite layer continues to grow under certain conditions.

The mathematical equations incorporated into the computer model are shown in Table VI.1-4 with symbol explanations shown in Table VI.1-5. Basically, the model splits the reactor tubes, transfer lines and heat exchanger into isothermal segments. A differential mass balance is performed on the liquid metal coolant and on each segment as the coolant passes through the loop.

For liquid boundary layer control of corrosion product release and deposition, mass transfer coefficients are calculated from mass transfer correlations which are typically of the following form,

$$Nu_m = C\ Re^{\alpha} Sc^{\beta} \qquad [VI.1-2]$$

where Nu_m, Re, and Sc are the Nusselt number for mass transfer, the Reynolds number, and the Schmidt number, respectively. C is a constant which is determined experimentally and α and β are powers which are also determined from experiment. The Reynolds number and Schmidt number are given by the following expressions,

$$Re = \frac{Vd}{\nu} \qquad [VI.1-3]$$

$$Sc = \frac{\nu}{D} \qquad [VI.1-4]$$

where V is the bulk velocity of the fluid into which mass transfer is occurring, d is the diameter or characteristic length of the object from or to which mass transfer is taking place, ν is the kinematic viscosity of the fluid, and D is the diffusion coefficient of the transported species.

After the Reynolds and Schmidt numbers are determined, the Nusselt number is calculated and from this, the mass transfer coefficient is determined by means of the following equation.

TABLE VI.1-4. MATHEMATICAL EQUATIONS USED IN COMPUTER MODEL

Mechanism 1 Liquid Boundary Layer Control

Differential Mass Balance on a Coolant Loop Segment

$$\frac{dX}{dy} + \frac{k\rho AS}{m} \left[X - X_w\right] + \frac{\lambda\rho a}{\dot{m}} X = 0 \qquad (a)$$

Solution

$$X = \frac{1}{\alpha} \left[K - \left(K - \alpha X_o\right) \exp\ (-\alpha y)\right] \qquad (b)$$

where

$$\alpha = \frac{k\rho AS}{\dot{m}} + \frac{\lambda\rho A}{\dot{m}} \qquad (c)$$

$$K = \frac{k\rho AS}{\dot{m}} X_w \qquad (d)$$

Mechanism 2 Solid Diffusion Control

Differential Mass Balance on a Coolant Loop Segment

$$\frac{dX}{dy} - \frac{DA}{\dot{m}} \frac{dc}{dz} + \frac{\lambda\rho a}{\dot{m}} X = 0 \qquad (e)$$

Solution

$$X = \frac{b}{h} - \left(\frac{b - hX_o}{h}\right) \exp\ \left(-h(y - y_o)\right) \qquad (f)$$

if $h = 0$

$$X = X_o + b(y - y_o) \qquad (g)$$

where

$$h = \frac{\lambda\rho a}{\dot{m}} \qquad (h)$$

$$b = \frac{DA}{\dot{m}} \frac{dc}{dz} \qquad (i)$$

TABLE VI.1-5. LEGEND FOR SYMBOLS SHOWN IN TABLE VI.1-4

A	=	Specific Area (cm^2/cm)
a	=	Cross Sectional Area for Flow (cm^2)
D	=	Diffusion Coefficient in Solid (cm^2/s)
$\frac{dc}{dz}$	=	Concentration Gradient in Solid
k	=	Mass Transfer Coefficient (cm/sec)
$\dot{m}$	=	Mass Flowrate (g/sec)
S	=	Sticking Coefficient (Dimensionless)
X	=	Weight Fraction of Element in Bulk Fluid
X_w	=	Equilibrium Weight Fraction of Element at Wall
y	=	Distance Along Segment (cm)
λ	=	Decay Constant (sec^{-1})
ρ	=	Density of Fluid (g/cm^3)

$$k = \frac{Nu_m D}{d} \qquad [VI.1\text{-}5]$$

As previously mentioned for nickel and chromium dissolution, the release rate is controlled initially by the rate of diffusion of these elements through the solid. Since pores develop in the surface region as the nickel and chromium are leached out, the diffusion path length and diffusion profiles are not the same as those which would be calculated from a one dimensional non-steady state diffusion model. An assumption was made that the flux of nickel and chromium could be regarded as constant with time and that the diffusion path length is half the distance between voids. Three reasons justify this assumption: (1) the formation of pores decreases the path length for diffusion, (2) the liquid metal/metal surface area increases as pores are formed, and (3) as the pores are opened, relatively undepleted chromium and nickel rich regions become exposed. Calculations indicate that this simple picture of diffusion predicts a penetration rate which is about the same as what is observed experimentally.

VI.1.2.2 Results

The computer transport model has been applied to a version of the MARS blanket and heat transport system. In addition, various coolants besides 83Pb-17Li have been modeled, and some of the mathematical and transport considerations incorporated in the model have been used to analyze other fusion reactor designs. Figure VI.1-6 shows the MARS design which was used in the computer model, and Table VI.1-6 lists velocities and temperatures at various locations in the primary coolant loop. Not shown in Table VI.1-6 are the transfer lines which pass between the reactor and heat exchanger. These transfer lines are 25 m long and have a diameter of 50 cm.

Some of the results of the model are presented in Fig. VI.1-7 which shows the mass transfer coefficients in the reactor tubes and heat exchanger as a function of temperature. Also shown are mass transfer coefficients from various other designs: two "static" pod designs, an example of which is shown in Fig. VI.1-7, and the ANL reference tokamak design. As can be seen, the mass transfer coefficients in the heat exchanger are an order of magnitude higher than the mass transfer coefficients in the reactor tubes. This is reasonable

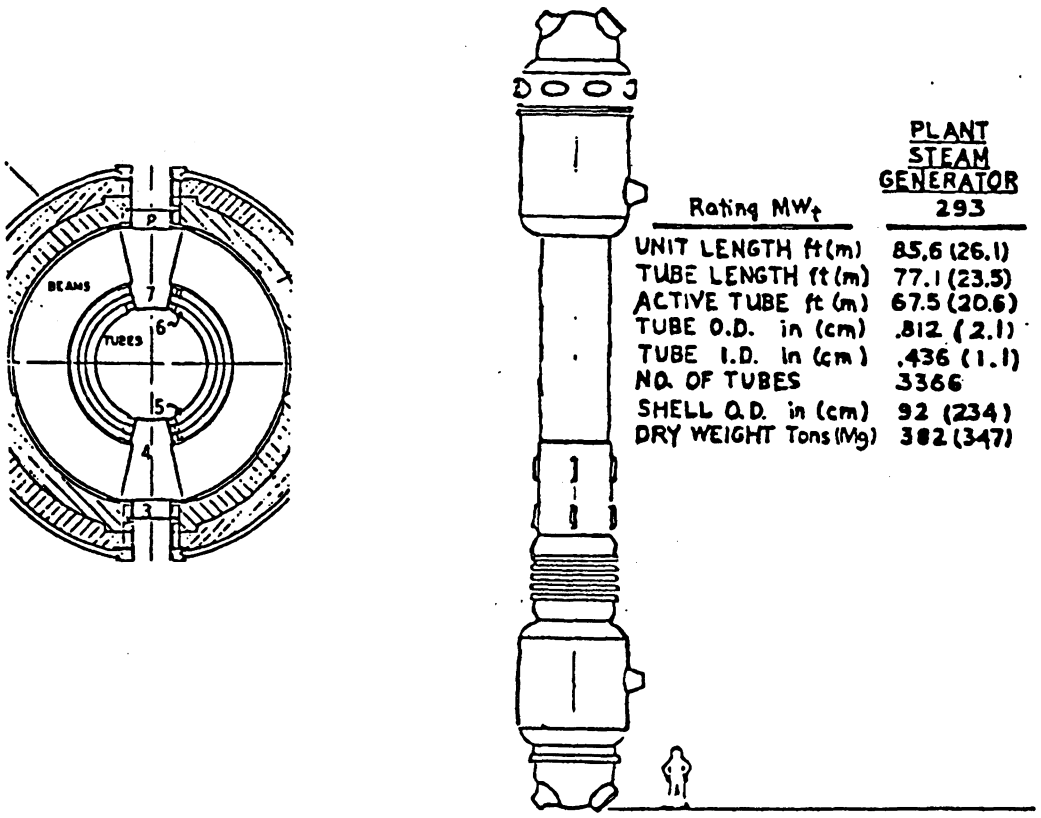

Figure VI.1-6. Diagram of MARS heat transport system.

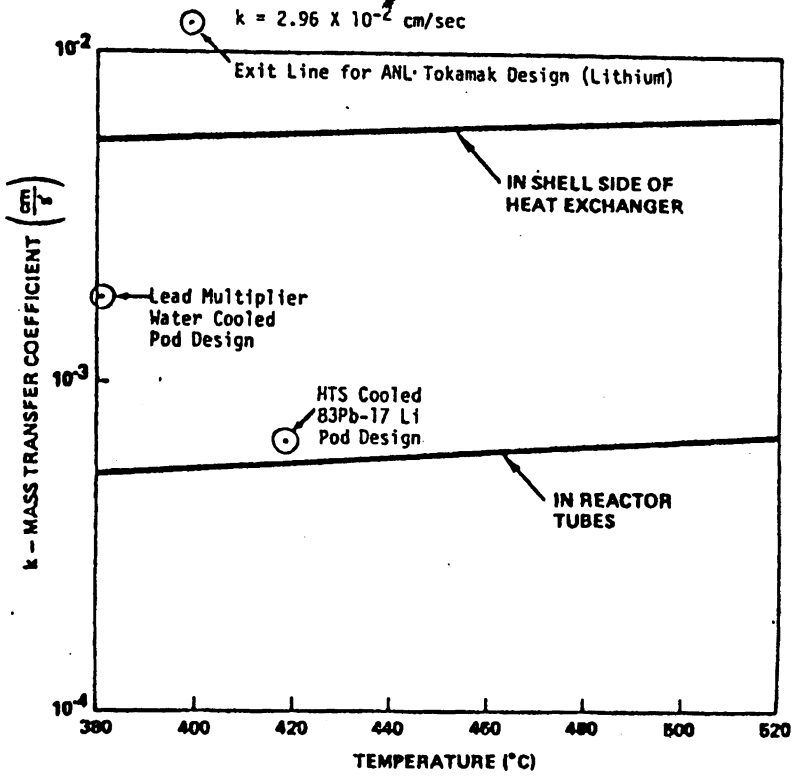

Figure VI.1-7. Mass transfer coefficients for iron in 83Pb-17Li (MARS design, MHD effects not included).

TABLE VI.1-6. TEMPERATURES, DIMENSIONS AND COOLANT FLOW VELOCITIES FOR THE MARS REACTOR DESIGN (83Pb-17Li Coolant)

Coolant Temperature at Reactor Inlet	380°C
Coolant Temperature at Reactor Outlet	520°C
Diameter of Reactor Inlet and Outlet Feed Pipes	50 cm
Velocity of Coolant in Inlet and Outlet Pipes	50 cm/sec
Linear Velocity of Coolant in Heat Exchanger	23 cm/sec
Velocity of Coolant in Reactor Tubes	16 cm/sec
Number of Reactor Tubes per Inlet Feed Pipe	100
Number of Reactor Modules Feeding One Heat Exchanger	6

since the flow in the heat exchanger is perpendicular to the tube bundles whereas in the reactor tubes, the flow is parallel to the tube walls. Also of interest, is the magnitude of the mass transfer coefficients for the two "static" pod designs. For these situations, temperature differences within the pods give rise to fluid thermal convection velocities which, in the absence of a magnetic field, are between 2 and 4 cm/s. In the presence of a magnetic field as strong as what is expected for fusion devices, the thermal convection process is expected to be suppressed.[30] For the ANL reference tokamak design, which is a lithium forced convection loop, a high mass transport coefficient is obtained. This is caused by the high velocity of the exit stream. One design trade-off here might be to allow for a higher exit temperature and then slow down the flow velocity. The higher temperature would increase the equilibrium interfacial concentration, but the reduction in mass transfer coefficient may more than offset this effect on the total mass flux.

Figure VI.1-8 shows the rate of iron deposition or recession in various parts of the MARS reactor's primary coolant loop for 83Pb-17Li. A similar case for lithium as the coolant is shown in Fig. VI.1-9. The rate is given in mils per year (mpy) and the segment numbers, except for the isothermal transfer lines, correspond to specific temperatures. Segment 1 of both the reactor and heat exchanger is at 380°C, and segment 2 of both is at 400°C and so on up to segment 8 which is at 520°C. Two important features are immediately apparent from this figure. One is that the rate of recession or deposition is an order of magnitude higher in the heat exchanger than it is in the reactor tubes or transfer lines and therefore the bulk of mass transfer takes place within just the heat exchanger. The second important characteristic is that deposition can occur in the reactor tubes at the lower temperatures. This indicates that the heat exchanger is not perfectly efficient in removing all dissolved iron in a single pass.

This inefficiency in removal is undoubtedly helpful in that if all iron were removed in the cold sections during one complete pass, then the driving force for mass transfer in the hotter sections becomes greater because of the reduced bulk concentration of iron. The ultimate outcome of this situation would be more mass being transferred from the hot zones to the cold zones, and the problems associated with mass transfer (i.e., potential plugging, wall thinning, and radioactive mass transport) would be correspondingly greater.

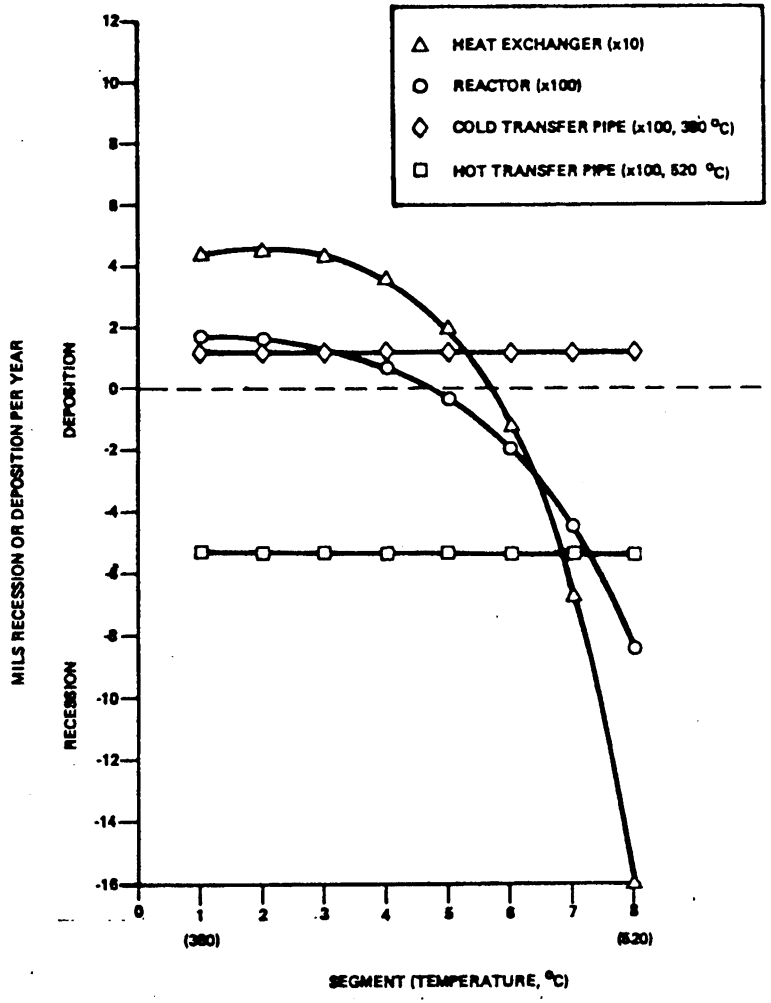

Figure VI.1-8. Transport of iron in MARS reactor with 83Pb-17Li coolant (T_{min} = 380°C, T_{max} = 520°C).

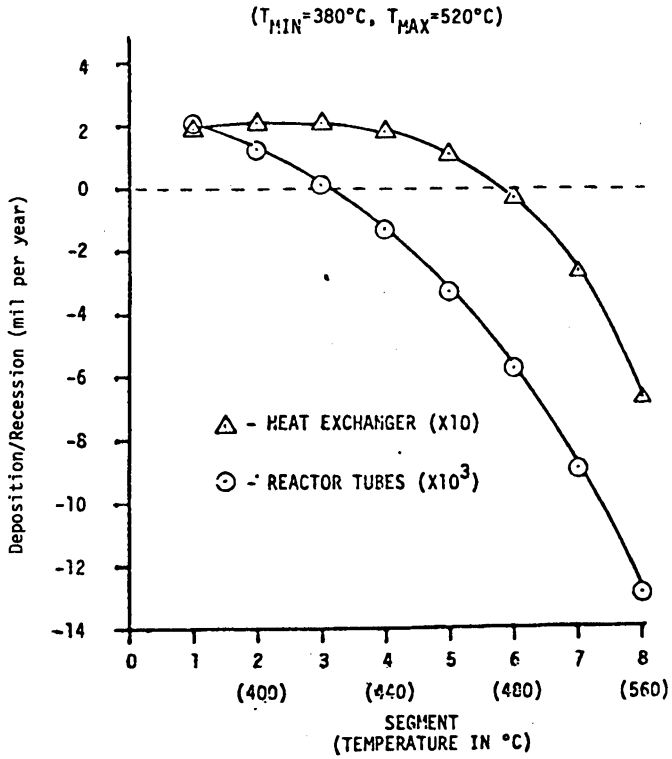

Figure VI.1-9. Transport of iron in MARS reactor with lithium coolant.

The steady state concentration of iron in the various parts of the coolant loop is shown in Fig. VI.1-10. Also shown is the equilibrium concentration of iron as a function of temperature. The computer model shows the concentration of dissolved iron to be fairly uniform throughout the loop. It also shows that the concentrations in the cold and hot sections of the reactor and heat exchanger are respectively above and below the equilibrium concentration.. This indicates that the driving force for mass transfer is about the same for segments of the heat exchanger and reactor which are at the same temperature and that therefore the differences in mass recession or deposition are primarily a reflection of the mass transfer coefficients which in turn is very geometry dependent.

The chromium profile in the primary coolant loop after 1 month of operation is shown in Fig. VI.1-11. The profile shows that deposition occurs only at the lowest system temperature (380°C) and that for the rest of the loop, the penetration rate is uniform. It appears that the deposition efficiency is high enough at the lowest temperature to insure that a less than equilibrium concentration is maintained in the rest of the loop.

Figure VI.1-12 shows the rate of nickel buildup in 83Pb-17Li coolant up until about 1 month after start-up. Because of the higher solubility of nickel in the coolant when compared with iron and chromium solubility, for the current assumptions the attainment of the equilibrium solubility in the bulk takes a longer period of time and therefore the model predicts that nickel deposition will occur after iron and chromium have started to deposit. For austenitic steels, preferential leaching of nickel is generally observed during early stages.

The results of the computer model have been compared with the results of reported experimental findings, and a number of similarities are apparent. Perhaps the most important computer model result is that the reactor tubes will be free of problems associated with recession and deposition whereas these effects will be fairly large in the heat exchanger. This correlates well with experience that shows coolant loop failure because of localized deposition in the heat exchanger, leading to plugging, to be a more serious problem than wall thinning due to dissolution in the hot sections of the loop.[6] Another similarity between the model results and experiment is that the concentration of corrosion product in the bulk coolant does not vary much

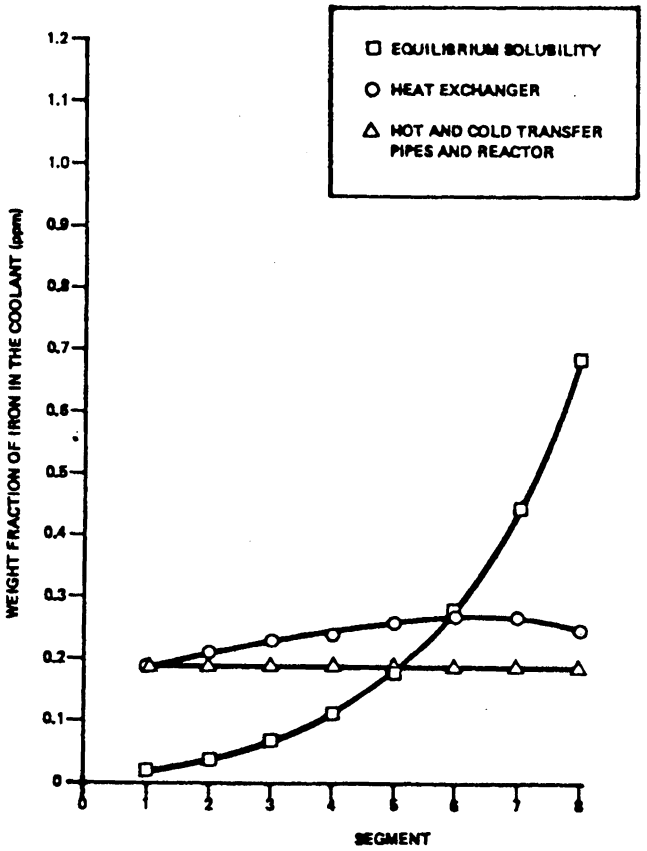

Figure VI.1-10. Distribution of iron in 83Pb-17Li coolant (MARS design T_{max} = 520°C, T_{min} = 380°C).

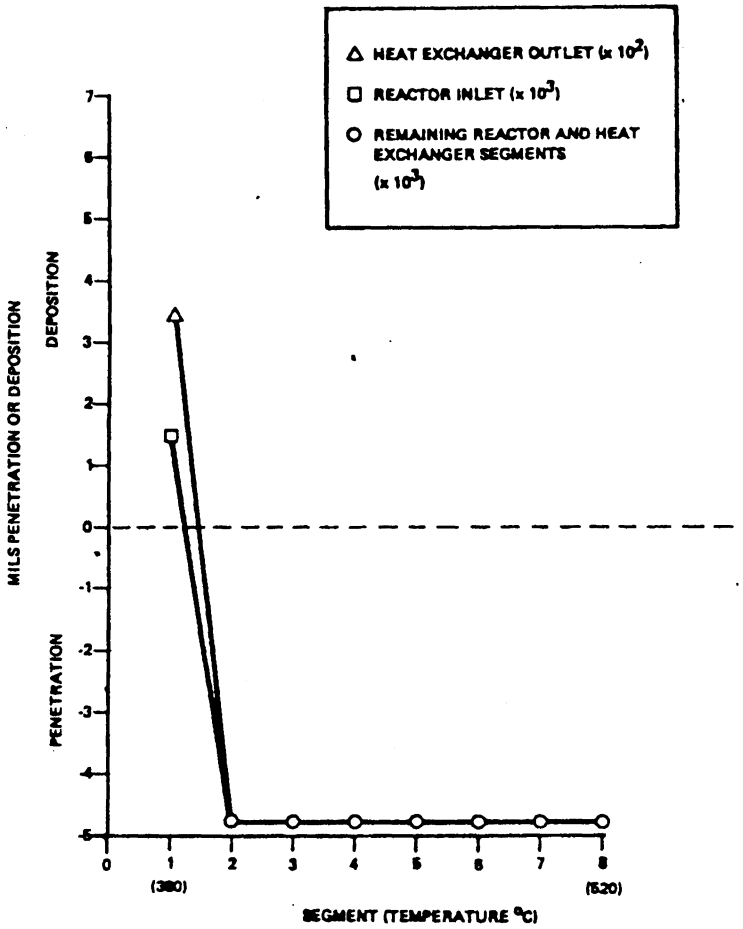

Figure VI.1-11. Chromium profile in the MARS reactor after one month of operation (83Pb17Li coolant).

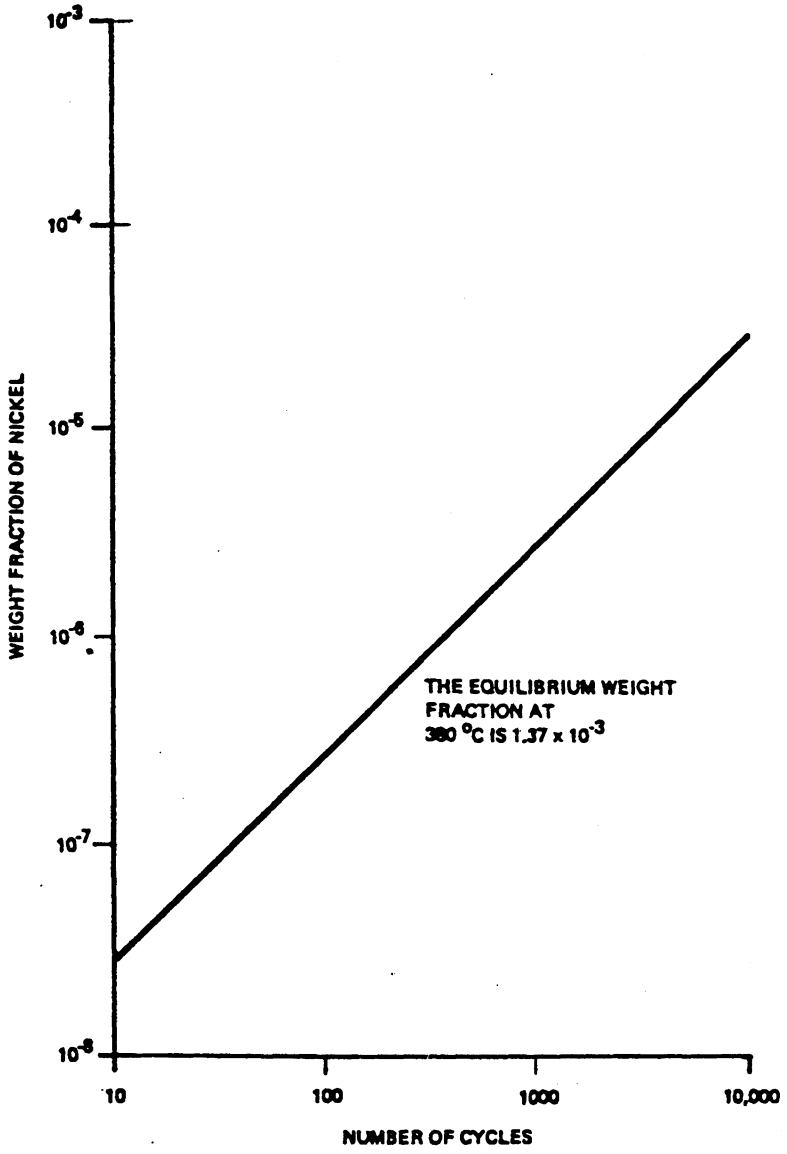

Figure VI.1-12. Dissolved weight fraction of nickel at reactor tube entrance (380°C).

between different locations in the coolant loop.[29] This concentration, as is illustrated in Fig. VI.1-10 is sometimes above the equilibrium saturation concentration and sometimes below the equilibrium saturation concentration depending on position in the loop. When the bulk concentration is above the equilibrium saturation value, there is a possibility that homogeneous nucleation and growth of particulates may occur. Particulates have been observed in sodium systems.

One of the limitations of the model at the present time with regard to material transport is that the transport of one metallic constituent is considered independent of the transport of other dissolved constituents. There is evidence in the literature to indicate that the bulk activity of a dissolved metal may be reduced by the formation of stable complexes with other dissolved species. This is one problem which should be investigated in the future. Another limitation is that changes in flow characteristics (e.g., velocity, turbulence), which occur at bends or as deposition leads to flow restriction, are not included in the computer model. The main effect here would be a change in the mass transfer coefficient which increases with velocity. Intuitively one would expect that deposition is a self enhancing process, as the flow is restricted, the tendency for deposition becomes greater. The inclusion of this process into the model would not be difficult and should be done in the future.

Future work should look at the inclusion of a cold trap into the coolant loop circuit. There are two potential advantages to the use of a cold trap. One is that deposition of iron, nickel, and chromium may be localized into a unit which can be easily changed out. The other potential advantage is that radioactive material deposition may also be localized allowing more access for maintenance in other sections of the loop. A potential disadvantage of a cold trap is that if bulk concentrations of soluble species are reduced, then the driving potential for dissolution in the hot zones of the reactor becomes greater.

Two other areas should also be included in future work. One is the transport of radioactive materials. The difficulty here is that since it has been found that the majority of mass transport takes place within the heat exchanger itself, radioactive material transport from the reactor must be separately taken into account. The other area for future work involves the

design tradeoffs which could be made with regard to coolant flow velocity, geometry of flow, and temperature limits. One suggestion along these lines was previously discussed, i.e., reducing the mass transfer coefficient in the exit line of the ANL Tokamak reference design by reducing the flow velocity, and letting the exit stream temperature rise. The model can investigate these tradeoffs in detail and provide feedback to designers as to some of the likely consequences of design changes on dissolution and deposition rates.

In conclusion, of the various problems associated with mass transport in a coolant trap, the corrosion product transport model indicates that wall thinning of coolant containment structure in the reactor is of small concern while recession and deposition within the heat exchanger is of great concern. The primary reason for this is the difference in mass transfer coefficients due to differences in flow geometry. An implication of this conclusion is that thermal or forced convection test loops which consist of only single tube flow in the hot and cold sections, may be missing a large mass transport effect which can only be seen when actual flow geometrics are considered.

VI.1.3 Corrosion Product Clean-up

The corrosion of the blanket has three impacts on the operation of the primary loop.

1. Thinning of the blanket structure.
2. Radioactive mass transfer to the primary heat exchanger.
3. Blockage of the primary loop.

For 17Li-83Pb in contact of HT-9, the corrosion rate at 500°C is ~ 22 mg/m^2-h which corresponds to 20 μm/y. Therefore, the thinning of the blanket structure is not a critical problem considering that the blanket life is only 2 to 3 years. The radioactive material transport can be a problem. This causes a high radiation dose around the piping and primary steam generator. A recent calculation shows that the dose rate around the steam generator of MARS,[31] as shown on Fig. VI.1-13. The dose rate is very high and will probably preclude hand on maintenance. However, remote maintenance of the steam generator is state-of-the-art which, undoubtly will increase the cost of

maintenance, is not a feasibility problem. Therefore, it appears that the blockage of the primary loop is the most potentially critical problem.

For MARS reactor design, 17Li-83Pb enters the blanket at 350°C and exits at 500°C.[32] The total corrosion product is estimated to be 620 kg/y. While this is a very large number, it is small comparing to the size of the steam generator. However, corrosion product deposition is very selective, i.e., it will deposit where the boundary layer is disruptive such as near a valve. Therefore, local blockage is possible and is not acceptable. Deposition of the corrosion product will occur if only the coolant, while releasing its thermal energy in the heat exchanger, becomes supersaturated. If the primary coolant is kept below supersaturation in the primary loop, there will be no corrosion product deposition problem. A corrosion product clean-up scheme is developed based on this principle. A cold trap is used to clean-up the primary coolant and the corrosion product will be deposited here instead of the main loop.

The corrosion product clean-up system is shown schematically on Fig. VI.1-14. For the ideal case, the concentration of the corrosion product in the main loop remains in between C_s and $C_s - \Delta C$, in which C_s is the saturate concentration at the lowest temperature and ΔC is the concentration increase per pass. Since the clean-up system must remove the ΔC for every pass, the side stream flow rate to the clean-up system is given by:

$$M_s = Mn \frac{\Delta C}{(C_s - C_{ct})\,\varepsilon}$$

in which

M_s is clean-up flow rate
Mn is the main flow rate
C_{ct} is the saturate concentration at the cold trap temperature
ε is the cold trap efficiency

The operating parameters of the clean-up system are listed on Table VI.1-7. A side stream of 6% of the main coolant stream will be by-passed to the cold trap. A regenerative heat exchanger and a cooler will cool the side stream to

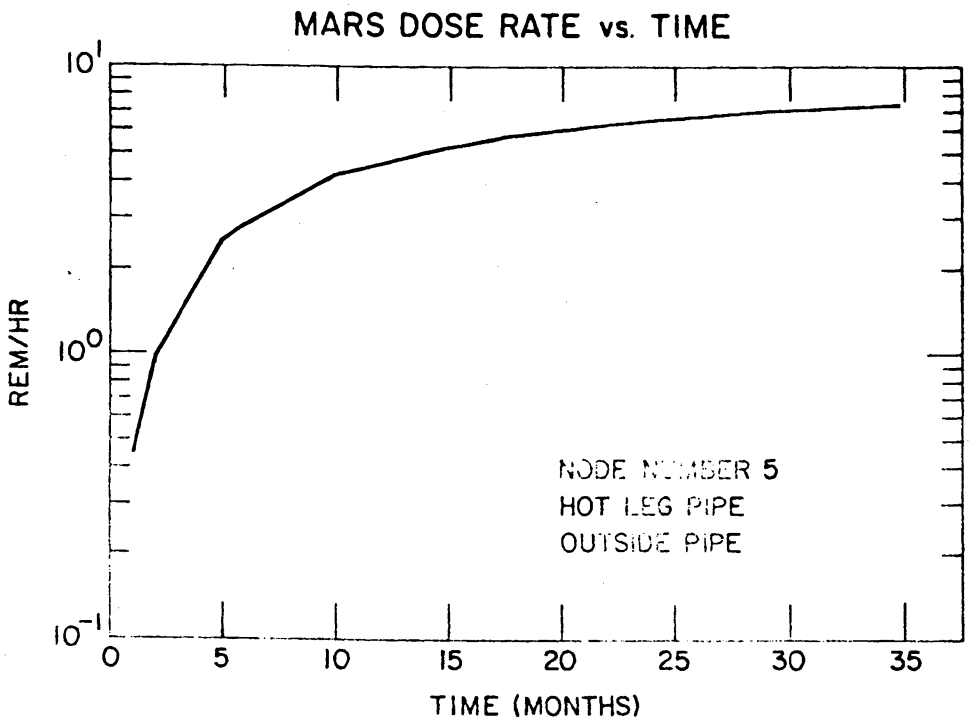

Figure VI.1-13. Contact dose rate for the MARS hot leg pipe, Li-Pb removed from pipe.

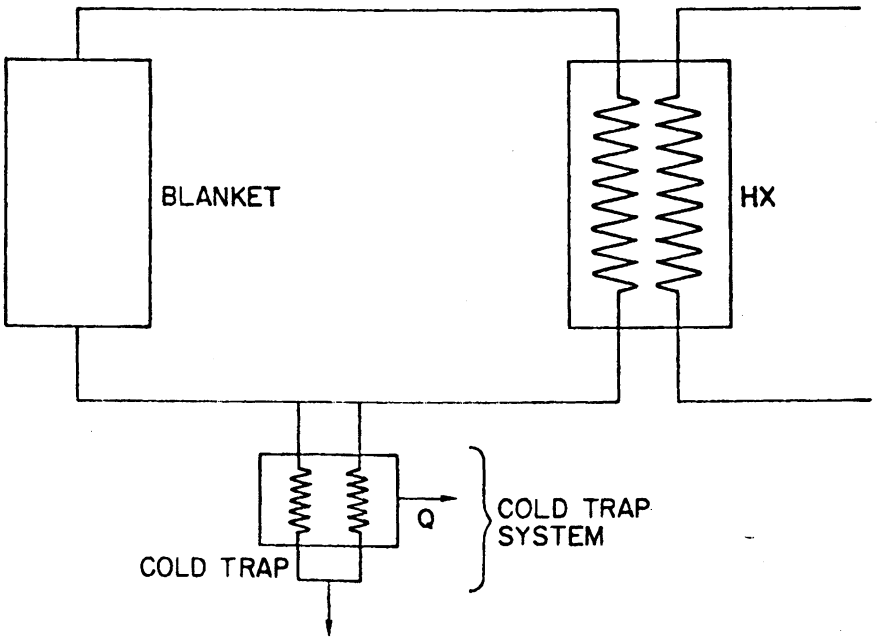

Figure VI.1-14. Cold trap of corrosion product.

TABLE VI.1-7. COLD TRAP CONDITION

Coolant Flow Rate	10^8 g/s
Saturation Concentration at 350°C (Fe in Pb)	6×10^{-9} g/g
Corrosion Rate	2×20^{-2} g/s (613 kg/y)
ΔC/Pass	2×20^{-10} g/g
Fraction of Flow to Cold Trap	6.7% (50% efficiency)
Cold Trap Concentration	1.3×10^{-9} g/g
Cold Trap Temperature	310°C
Economizer Area	20 m^2

310°C. Due to the supersaturation, the corrosion product will either be deposited on the surface of the heat exchanger or becomes particulate and suspended in LiPb. The particulates can be removed by a filter system. The surface area of the regenerative heat exchanger is only 20 m^2 and is cheap to replace. The heat rejected in the cooler is 9 MW. By this scheme, it is expected that the deposition will occur only in the cold trap system, which has to be replaced periodically. No deposition is expected to occur in the main loop because the coolant is designed to be undersaturated in the main coolant loop.

The corrosion clean-up system described here appears to be workable on theory. However, experimental verification of the concept is needed. This concept may provide a possible way to alleviate the problem associated with corrosion product transport problem. Therefore, the maximum allowable corrosion rate and, consequently, the highest blanket operation temperature is design dependent. The corrosion temperature limit will be more precisely determined after the design is finalized.

VI.2 Gas/Water Corrosion

An important consideration regarding the use of vanadium base alloys for blanket structural applications relates to chemical reactivity with possible gaseous and water environments. The purpose of this phase of the study is to better quantify conditions where vanadium alloys may be used. Environments considered include helium with impurities, air or oxygen environments, the hydrogen plasma, and pressurized water coolant. Stress corrosion aspects related to the use of austenitic steel in pressurized water are also reviewed.

VI.2.1 Gaseous Corrosion

VI.2.1.1 Hydrogen Effects

VI.2.1.1.1 Solubility Relations

The application of vanadium and/or vanadium alloys to the blanket of a fusion reactor is predicated on the requirement that the material has a low solubility for hydrogen isotopes since a large tritium inventory in the blanket is unacceptable. Figure VI.2-1 illustrates pressure-concentration-temperature isotherms for the vanadium-hydrogen system[33] for the expected range of blanket operating temperatures. Isotherms for the vanadium-tritium system should be nearly identical to those shown here. Typical tritium pressures in the blanket are not expected to exceed 1 Pa (i.e., 10^{-2} torr). Figure VI.2-1 indicates that tritium solubility should not exceed 50 wppm during reactor operation. For typical projected reactor sizes this does not constitute unacceptably high tritium inventory in a vanadium blanket structure. The effects of alloying with Cr and Ti appear to have only a slight effect on this conclusion.[34]

VI.2.1.1.2 Mechanical Properties

Hydrogen embrittlement of vanadium has been documented below room temperature;[35] however, at the low concentrations of hydrogen expected in vanadium, the effects of hydrogen on tensile, fatigue and DBTT appear to pose no serious problems for vanadium or its alloys.[35]

VI.2.1.1.3 Effect of Oxide Film Formation on H-Uptake

During blanket cooldown procedures or during off-nominal operations (i.e., fault condition), in which the solubility of hydrogen in the metal increases significantly with decreasing temperature, it is likely that a protective oxide film will form at temperatures less than 300°C on the surface of the metal due to oxidation by impurities in the coolant gas stream. The formation of this oxide layer will be discussed in more detail in Section VI.2.1.2. The oxide layer will function as a barrier to limit the introduction of hydrogen isotopes into the metal from the coolant at lower temperatures.[36] Thus, it is not expected that hydrogen embrittlement and/or tritium inventory in vanadium or its alloys will pose any serious obstacles to its use over the range of pressures and temperatures expected in the blanket, including cooldown conditions.

VI.2.1.2 Oxygen Effects

VI.2.1.2.1 Helium Cooled Solid Breeder Blanket

VI.2.1.2.1.1 Unalloyed Vanadium

Vanadium has a strong affinity for oxygen as shown in Fig. VI.2-2 which is the pressure-concentrating-temperature diagram for the vanadium-oxygen system.[37] Figure VI.2-2 indicates that the equilibrium pressure of oxygen over vanadium to prevent room temperature embrittlement of the metal must be less than 10^{-42} atm. Room temperature embrittlement occurs at oxygen contents exceeding 2000-3000 wppm.[35] Since oxygen pressures this low are not achievable in any gas-handling system the time necessary for the eventual degradation of the metal will be determined by the rate of oxygen attack from the oxygen impurities in the helium coolant and the subsequent oxygen embrittlement of the metal.

To describe the rate of oxygen contamination of vanadium a model for oxygen absorption from the gas phase was constructed in which the oxygen (in the form of O_2 or H_2O) absorbed by the bare, oxygen-free surface was allowed to diffuse into the bulk metal. At any given temperature and gas pressure the net oxygen concentration on the surface will build up in time to the point at which an oxide phase will nucleate on the surface. It was assumed that this

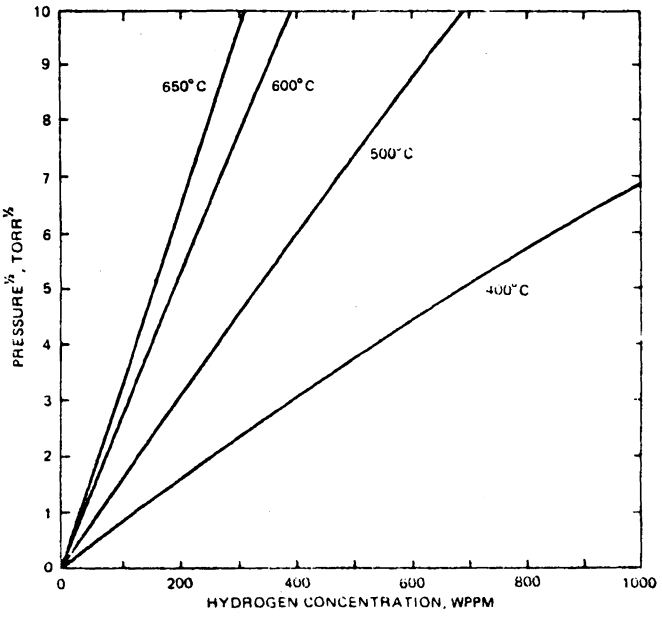

Figure VI.2-1. Pressure-concentration-temperature isotherms for the V-H system.

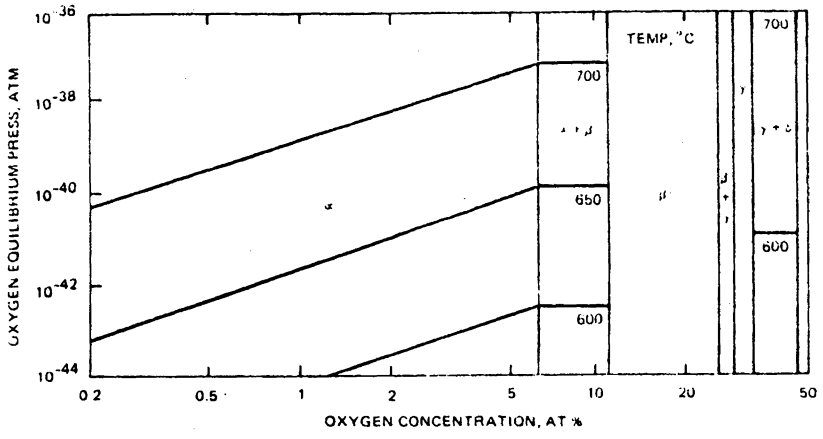

Figure VI.2-2. Pressure-concentration isotherms in the V-O system.

would occur at the point of terminal solid solubility of oxygen in vanadium (TSO) as described in the equilibrium diagram[38] shown in Fig. VI.2-3. At this point the surface of the metal will become saturated in oxygen and will remain in local equilibrium with the interface oxide for all subsequent times. This model is illustrated in Fig. VI.2-4.

To determine the oxygen distribution in the metal as a function of temperature, time, wall thickness, and impurity level of oxygen or water vapor in He, the diffusion equation was solved for known fluxes of oxygen (in the form of O_2 and H_2O) absorbed at the oxide-free surface. These fluxes were determined from experimental measurements of the absorption of oxygen, water vapor, and oxygen in He on vanadium surfaces at temperatures greater than 600°C. It was assumed that the experimentally measured rates of absorption could be extrapolated to the temperatures encountered during blanket operation.

From the kinetic theory of gases the rate of oxygen impingement on a surface is given by

$$F_o = 3.513 \times 10^{22} \, p_{o_2} / (MT)^{1/2} \qquad [VI.2\text{-}1]$$

where

F_o = flux of oxygen (molecules/cm^2-s)
p_{O_2} = oxygen pressure (torr),
M = molecular weight of oxygen, and
T = temperature (K).

From experiments at 600-800°C the molecular sticking coefficient for oxygen on vanadium, S,[40] was measured to be 0.185. Thus

$$F = SF_o = 6.5 \times 10^{21} P/(MT)^{1/2} \qquad [VI.2\text{-}2]$$

where

F = absorption rate of oxygen in vanadium.

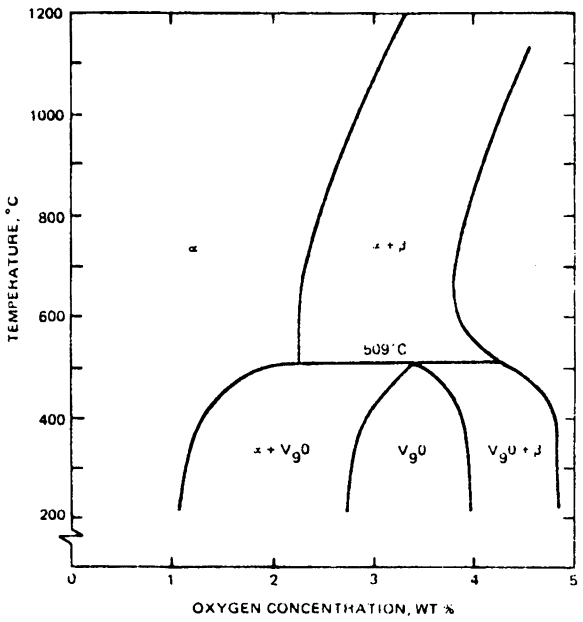

Figure VI.2-3. Solubility limits of oxygen in vanadium.

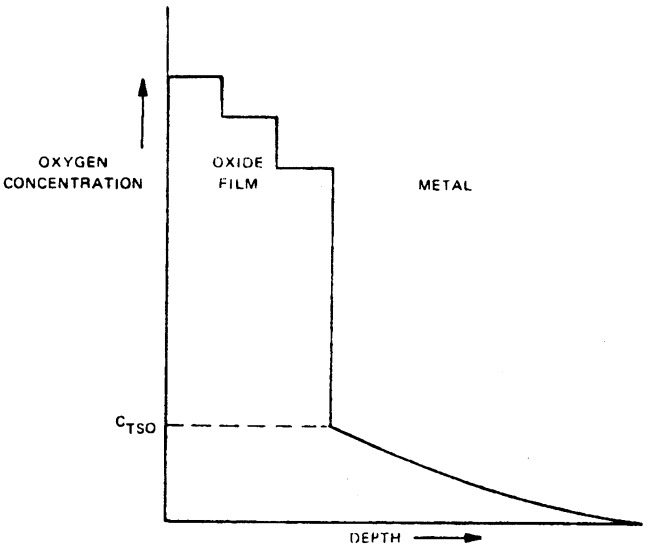

Figure VI.2-4. Model for oxide film formation and oxygen diffusion in vanadium for times greater than that needed to nucleate oxide showing local equilibrium between oxide and metal interface.

For water vapor attack on vanadium the experimentally measured rate of oxygen pick-up was shown to be[40]

$$V_o = 6.25 \times 10^{17} \exp(-4400/RT) P_{H_2O} \qquad [VI.2-3]$$

where

V_o = flux of water vapor molecules (molecules/cm^2-s)
P_{H_2O} = water vapor pressure (torr), and
R = gas constant.

Figure VI.2-5 describes the temperature dependence of the ratio of the reactivity of vanadium surfaces (gmO/cm^2-s) with oxygen and water vapor and clearly indicates that water vapor is a significantly less reactive species over the temperature range of interest to blanket application.

The effect of helium pressure on the reactivity of oxygen on vanadium surfaces is given by[41]

$$F_o = 3.75 \times 10^{22} \exp(4030/RT) p_{o_2} / P_{He}^{2/3} \qquad [VI.2-4]$$

where

F_o = oxygen pressure (torr), and
P_{He} = helium pressure (torr).

Using the definition

$$X_o = \frac{P_{o_2}}{P_{o_2} + P_{He}} \qquad [VI.2-5]$$

where X_o = volume fraction of oxygen in He, and assuming that the effect of high pressures of helium on the reactivity of water vapor is analogous to oxygen, an expression for the reactivity of water vapor in pressurized helium is derived as

$$F_{H_2O} = 1.613 \times 10^{16} X_o \exp(-370/RT)(T)^{1/2} P_{He}^{1/3} \qquad [VI.2-6]$$

Assuming an oxide-free surface and using this flux of water vapor we solve the diffusion equation for the diffusion of oxygen in a plate of thickness 2L, with the boundary conditions: F_{H_2O} = constant at x=L and no loss of oxygen atoms at x=0. We obtain[42]

$$C(x,t) = \frac{F_{H_2O}\,t}{L} + \frac{F_{H_2O}\,L}{D}\left[\frac{3x^2 - L^2}{6L^2} - \frac{2}{\pi^2}\sum_{n=1}^{\infty}\frac{(-1)^n}{n^2}\exp(-D\pi^2n^2t/L)\cos\frac{n\pi x}{L}\right] \qquad [VI.2\text{-}7]$$

where

$C_o(x,t)$ = concentration of oxygen,
D = diffusion coefficient for oxygen in V (cm^2/s),
t = time (s),
x = distance from blanket centerline (cm), and
2L = thickness of plate (cm).

To estimate the time to reach the TSO a least squares polynominal fit of the TSO line in Fig. VI.2-3 was performed using

$$C_o = a_0 + a_1 T + a_2 T^2 + \ldots \qquad [VI.2\text{-}8]$$

where

C_o = TSO (T)
T = Temperature (°C), and
a_0, a_1, a_2, ... = coefficients of least squares fit.

Setting $C_o(x,t) = C_o$ and solving for t in Eq. [VI.2-8], a plot of t vs. X (for a plate thickness of 2 mm) is shown in Fig. VI.2-6. Figure VI.2-6 indicates that for operation at 350°C water vapor concentrations must be maintained below 0.1 vppm to avoid oxide film formation in 10^4 h while a concentration of 1 ppm at 600°C would be needed to nucleate the oxide in the same time. For water vapor concentrations of 100-200 vppm expected from steam generator leakage an oxide film would form almost immediately at all temperatures of interest.

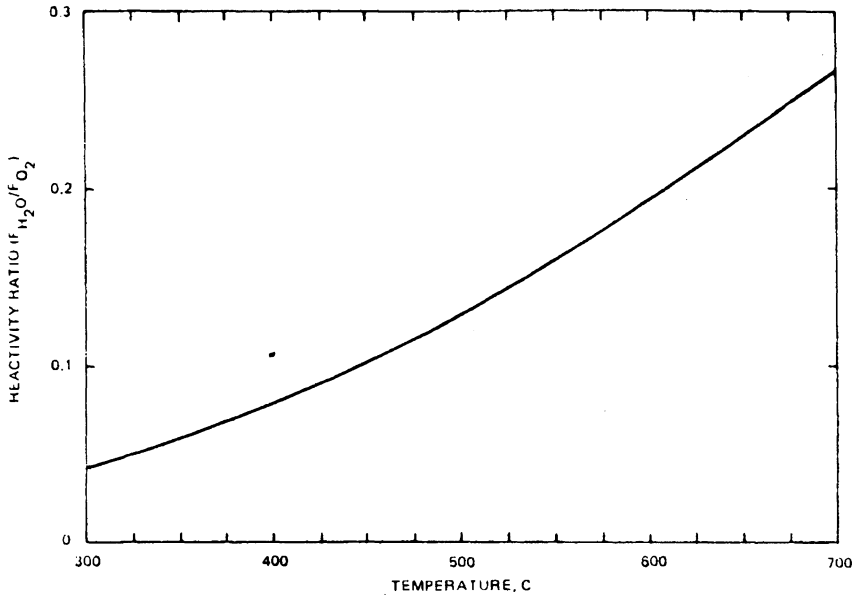

Figure VI.2-5. Effect of temperature on ratio of rate of oxygen pickup in V with water vapor and oxygen.

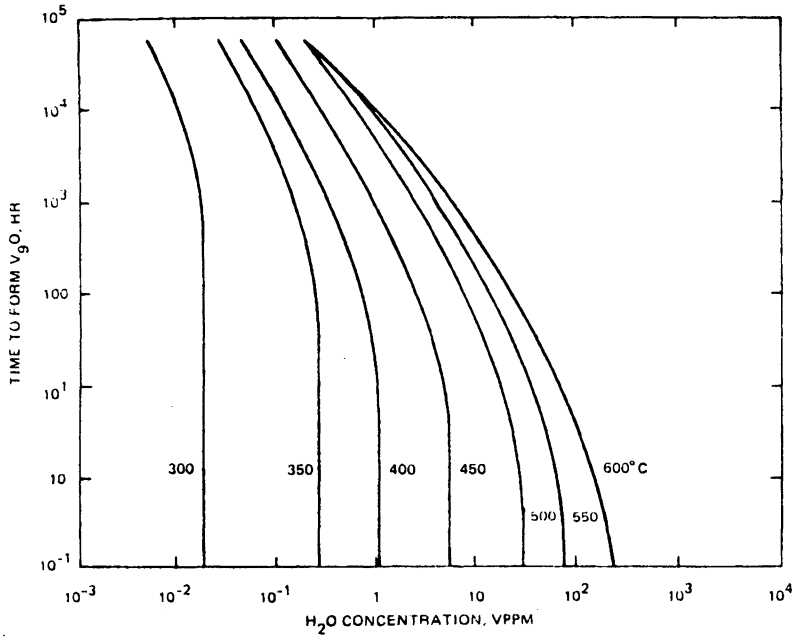

Figure VI.2-6. Effect of water vapor concentration in 50 atm helium on time to form oxide film (V_9O) on 2 mm vanadium wall at various temperatures.

Figure VI.2-7 illustrates the effect of 0.1, 0.2 and 0.5 vppm H_2O on the depth distribution of oxygen in a 2 mm thick vanadium wall in 10^4 h at 500°C and 600°C. At 500°C the water vapor content must be kept below 0.1 vppm to prevent excessive contamination. At 600°C the oxygen concentration profile is nearly uniform and the level of oxygen at 0.1 vppm is marginal for embrittlement.

For water vapor levels of 100-200 vppm a new model is needed which includes an oxide surface. Since appropriate oxide growth constants are not available, the rate of oxide growth is assumed to be negligible compared to significant oxygen penetration into the metal. The solution of the diffusion equation for the diffusion of oxygen in a plate of thickness 2L with the oxygen concentration at the oxide-metal interfaces fixed by local equilibrium at the TSO (see Fig. VI.2-4) is[42]

$$C_o(x,t) = C_o\left[1 - \frac{4}{\pi}\sum_{n=1}^{\infty}\frac{(-1)^n}{(2n+1)}\exp\left[-(2n+1)^2\pi Dt/L^2\right]\cos\frac{(2n+1)\pi x}{2L}\right] \qquad [VI.2\text{-}9]$$

Solutions are illustrated in Fig. VI.2-9. For water vapor levels of 100-200 vppm substantial embrittlement of the vanadium is to be expected in 10^4 h, at temperatures 400°C-600°C.

VI.2.1.2.1.2 Alloy Effects

In the case of the V-15Cr-5Ti alloy the mechanism for oxygen attack may be entirely different than that of the unalloyed metal. The presence of the titanium can lead to internal oxidation. The presence of chromium in the alloy would change the TSO and would alter the oxygen distribution significantly. Further uncertainties are indicated by the lack of experimental data on gaseous oxidation mechanisms of V-15Cr-5Ti in either H_2O or O_2 and the effect of oxygen content on the DBTT and/or tensile and fatigue properties.

Figure VI.2-8 illustrates the internal oxidation model assumed for oxidation of the alloy. In this model an oxide film is present on the surface at t=0 and is in local equilibrium with the alloy at x=0 such that the interface concentration remains constant for all $t > 0$. After time t an internal oxidation zone of depth x_o has developed in which all the titanium in solution has precipitated as TiO_2. At the end of this zone, the oxygen concentration is fixed at zero. An approximate solution to this problem is given by

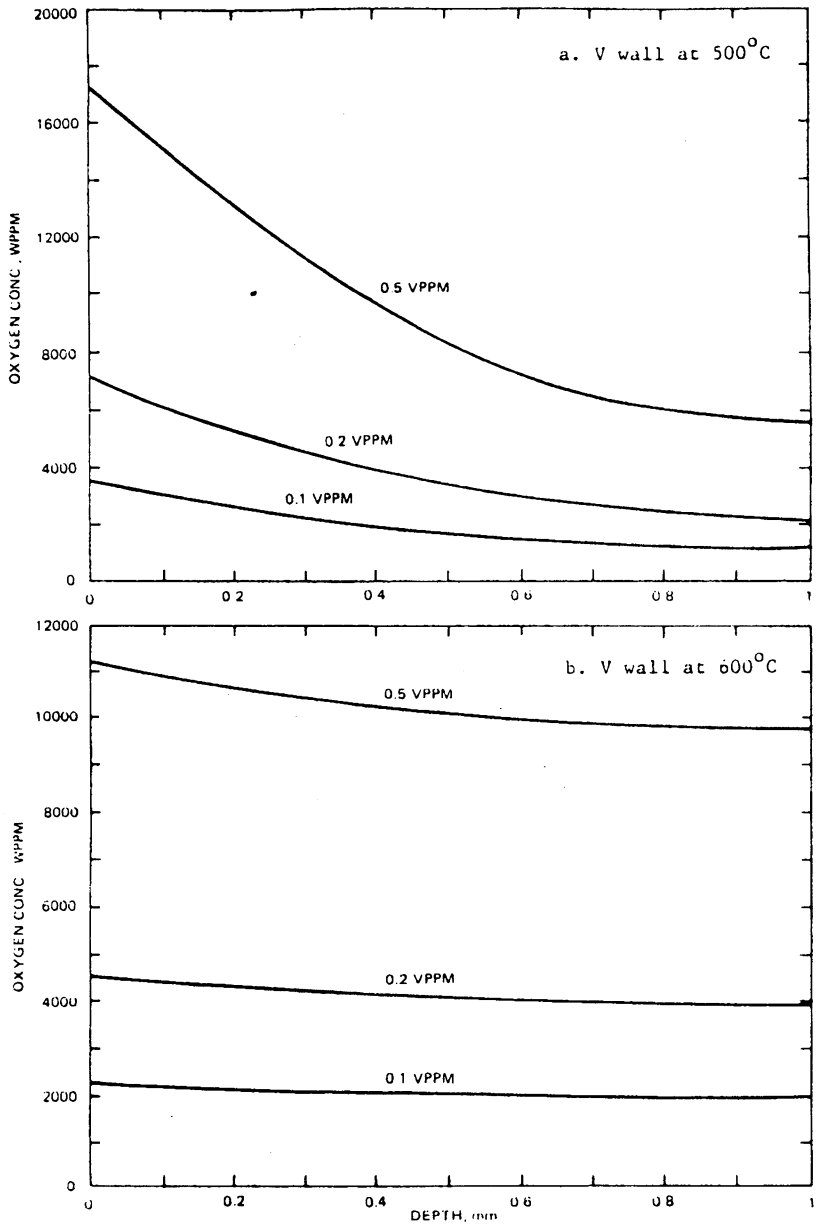

Figure VI.2-7. Effect of water vapor content on 50 atm He on depth penetration of oxygen in 2 mm wall at 500°C and 600°C in 10^4 h.

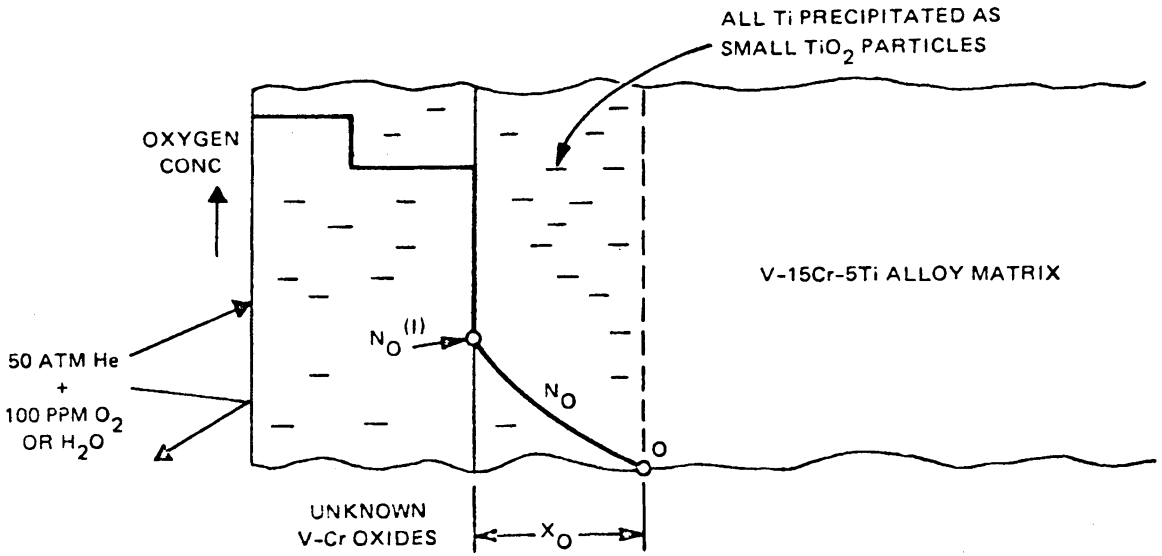

- $N_O = N_O^{(I)}$ = TERMINAL SOLUBILITY IN V-Cr MATRIX AT OXIDE INTERFACE
- $N_O = 0$ AT $X \geq X_O$
- $N_{TI} = .05$ AT $t = 0$
- $N_{TI} = 0$ FOR $X \leq X_O, t > 0$
- SURFACE OXIDE DOES NOT GROW

Figure VI.2-8. Internal oxidation model for V-15Cr-5Ti.

$$N_o = N_o^{(I)} \left[1 - \frac{\text{erf}\left(x/2(Dt)\right)^{1/2}}{\text{erf } \gamma}\right] \qquad \text{[VI.2-10]}$$

where

$$\gamma \simeq \frac{1}{2} \left(\frac{N_o^{(I)}}{N_{Ti}}\right)^{1/2}$$

where

$N_o^{(I)}$ = TSO of V-15Cr alloy and

N_{Ti} = mol fraction titanium in solution.

It is assumed that the oxygen diffusivity in the V-Cr solid solution is comparable to that of pure vanadium.

Figure VI.2-9a illustrates the oxygen distribution in the alloy after 10^4 h at 400°C. The TSO assumed here is equal to that of unalloyed vanadium at 400°C. For comparison, the equivalent oxygen distribution in pure vanadium is also shown. Figure VI.2-9a indicates that the effect of internal oxidation is to lower significantly the oxygen penetration into the alloy relative to the pure metal. Figure VI.2-9b illustrates the same conditions at 600°C. The alloy has significant oxygen penetration up to 2 mm depths while the unalloyed material is almost completely saturated in oxygen. In the absence of TSO data on the alloy it is not possible to decide on the reality of the calculated oxygen distributions; however, lowered TSO in the alloy would also lower the oxygen distribution in solution and alter the assessment for the applicability of V-15Cr-5Ti up to 600°C.

VI.2.1.2.2 Helium-Cooled Liquid Lithium Breeder Blanket

VI.2.1.2.2.1 Model for Oxygen Attack on Unalloyed Vanadium

One of the helium-cooled designs of current interest involves the use of a liquid lithium breeder in which the liquid Li is inlet at 300°C and outlet at 550°C and which is contained in thin walled (1/4 mm) vanadium tubes which are cooled by a 50 atm helium coolant. Since lithium is known to remove oxygen from vanadium, the oxygen concentration at the liquid Li/vanadium interface was set at zero for all $t > 0$. On the helium-cooled side, water

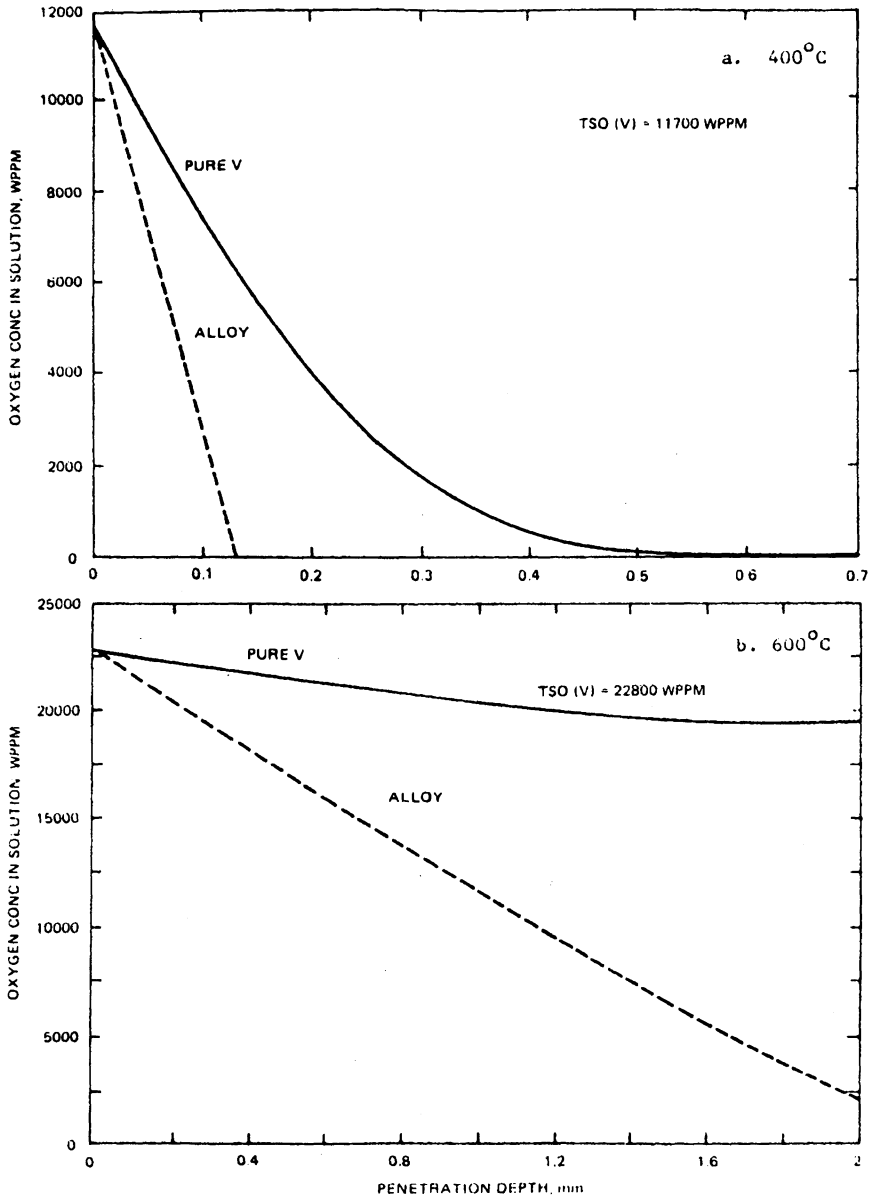

Figure VI.2-9. Oxygen penetration in V-15Cr-5Ti and V at 400°C and 600°C, in 10^4 h for 4 mm wall assuming same terminal solubility of oxygen (TSO) in alloy matrix.

vapor impurities were assumed to provide the source of oxygen. The solution of the diffusion equation with these boundary conditions:[10] $C_o(x,t) = 0$ at $t = 0$, $0 \leq x \leq L$, constant flux F_{h_2O} at x=L, and C=0 at x=0 for all $t > 0$, is given by

$$C(x,t) = \frac{F_{H_2O}x}{D} - \frac{8F_{H_2O}L}{\pi^2 D} \sum_{n=0}^{\infty} \frac{(-1)^n}{(2n+1)^2} \exp\left[-D(2n+1)^2\pi^2 t/4L^2\right] \sin(2n+1)\pi x/2L$$

[VI.2-11]

Figure VI.2-10 illustrates the time required to form the V_9O oxide on the surface as a function of water vapor impurity level and temperature. Figure VI.2-10 indicates that for operation below 350°C an oxide layer would form in less than 10^4 h unless the impurity level were below 0.1 vppm H_2O. Figure VI.2-11a illustrates the effect of H_2O impurity level in the He on the oxygen gradient after 10^4 h at 350°C. High levels of oxygen contamination are observed for H_2O contents above 0.01 vppm. Thus, this design would impose severe constraints on the He cleanup system. Figure VI.2-11b illustrates the same conditions for operation at temperatures of 550°C. In this case the water vapor impurity content may be relaxed to about 0.6 vppm before severe embrittlement would occur. Thus, the lower temperature operational requirement places more severe constraints upon the gas cleanup system than the higher temperature operation. Since the liquid breeder must operate over this range of temperatures, it does not appear that this design is practical unless significant advances in gas cleanup were achieved.

VI.2.1.2.3 Helium-Cooled First Wall System

The same considerations that were used to evaluate vanadium for the blanket application apply to the first wall. In this instance, a 4 mm thick first wall was considered, and it was assumed that oxygen contribution from the plasma side of the wall was negligible compared to the oxygen contamination on the helium side of the wall. This assumption is probably justified if the oxygen content in the plasma is about 1 ppm and the hydrogen flux to the wall is less than 10^{14} ions/cm^2-s.

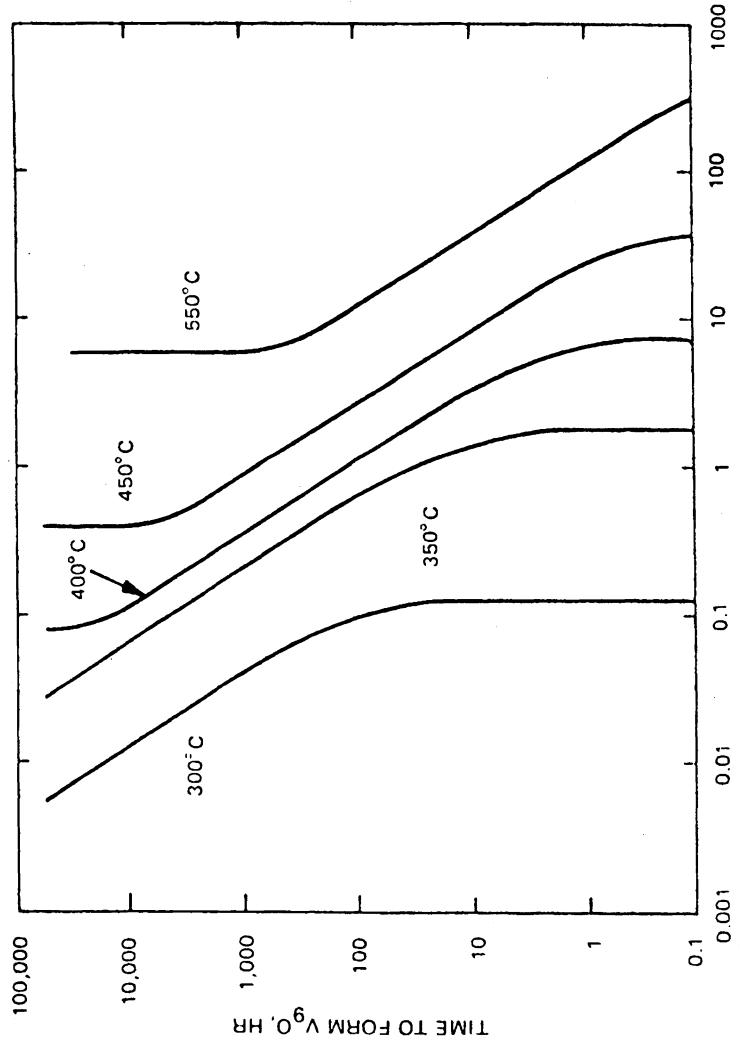

Figure VI.2-10. Effect of water vapor level in 50 atm He on time to form oxide film (V_9O) on 1/4 mm V wall at various temperatures.

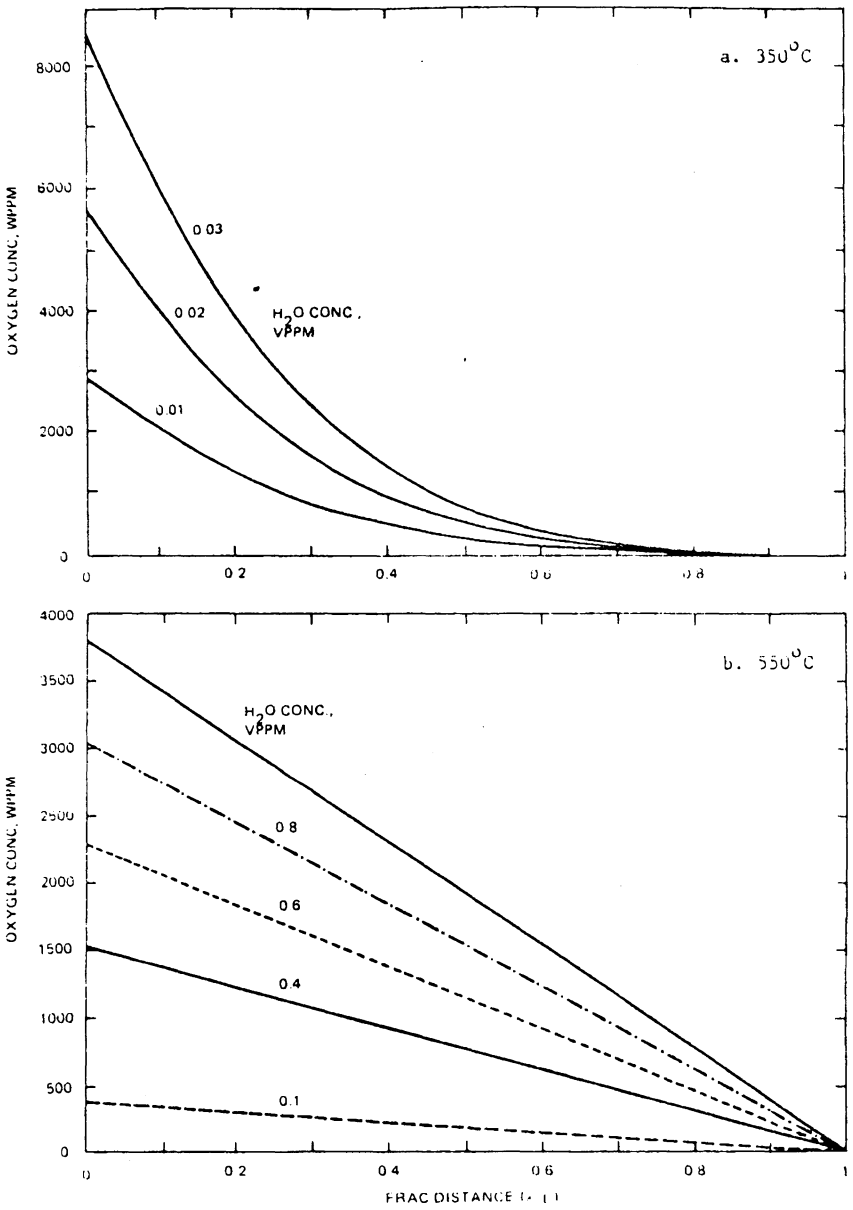

Figure VI.2-11. Effect of water vapor impurity level in He on oxygen penetration in 1/4 mm V wall in contact with liquid lithium breeder at 350°C and 550°C in 10^4 h.

Figure VI.2-12a illustrates the oxygen profile in a 4 mm vanadium wall at 500°C after 10^4 h. For these conditions a water vapor content below 0.2 vppm will be needed to prevent significant wall contamination. Such levels have been achieved in the Ft. St. Vrain reactor; however, it is not clear that such levels would be achievable for a He cooled first wall in a fusion reactor. Figure VI.2-12b indicates the oxygen profile in the V-15Cr-5Ti alloy assuming various values of TSO in the alloy with the internal oxidation model. For a TSO below 9000 wppm acceptable alloy performance is achieved at 500°C.

VI.2.1.3 Recommendations for Future Work

The analyses of gaseous alloy oxidation revealed a number of uncertainties that preclude a detailed theoretical analyses of alloy performance. For example, the contribution of internal oxide precipitates and oxygen in solution to alloy embrittlement is not known. Furthermore, little is known about the effects of temperature, pressure and gas species on the mechanism of oxidation of the alloy. Experimental measurements have not been made on the effect of temperature and/or alloy content on the TSO.

A series of oxidation experiments have been started at Grumman Aerospace Corporation with internal funding, on both unalloyed vanadium and V-15Cr-5Ti in pure flowing oxygen (1 atm) in the temperature range 400-650°C. Preliminary results are shown in Figs. VI.2-13 and VI.2-14, and indicate a substantial reduction in O-pickup of the alloy over pure V.

VI.2.1.4 Summary

The work on vanadium and the V-15Cr-5Ti alloy may be summarized as follows.

VI.2.1.4.1 Vanadium (Unalloyed)

VI.2.1.4.1.1 Effects of Hydrogen and Oxygen on Properties

- At operating temperatures and pressures of blanket tritium inventory is acceptable - 7 wppm at 650°C and 40 wppm at 400°C.

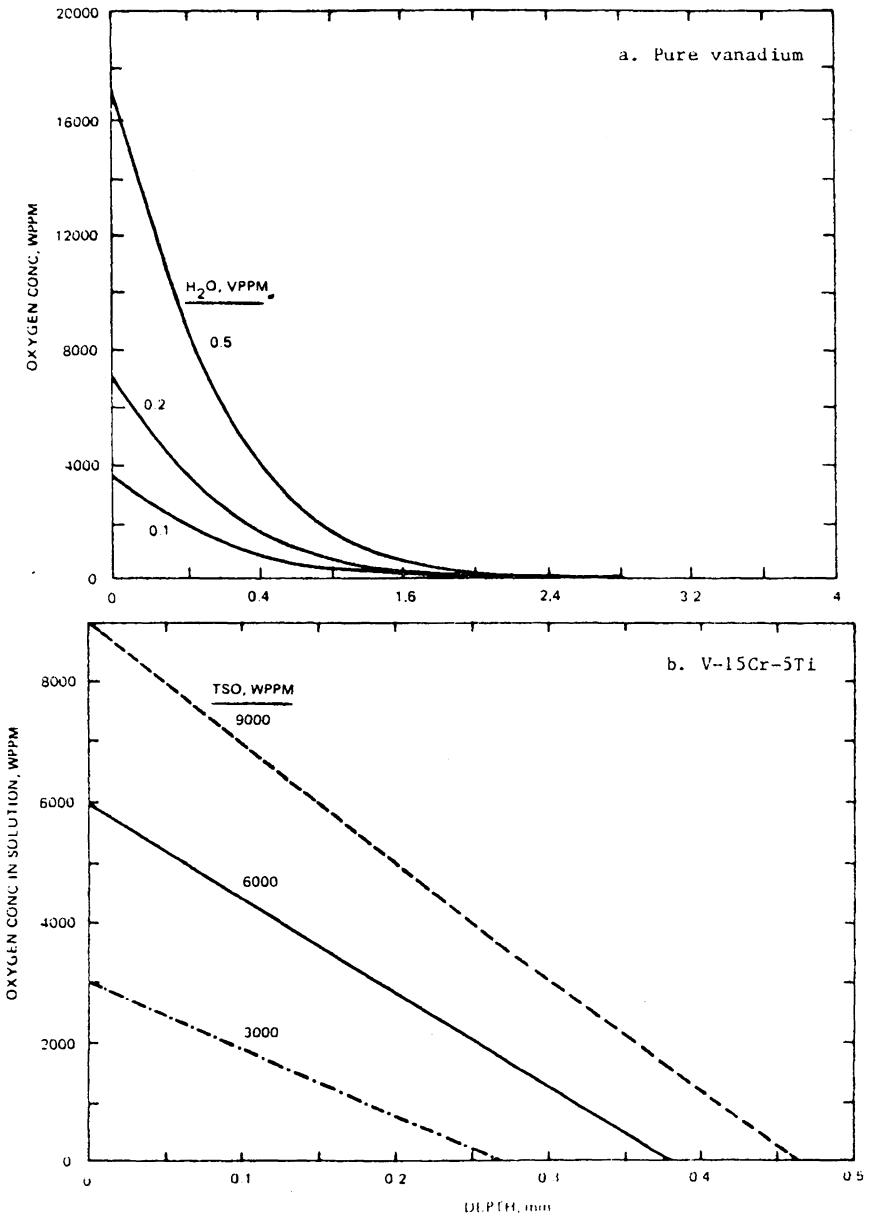

Figure VI.2-12. Effect of water vapor impurity level in He on the oxygen penetration in 4 mm V first wall at 500°C and 10^4 h.

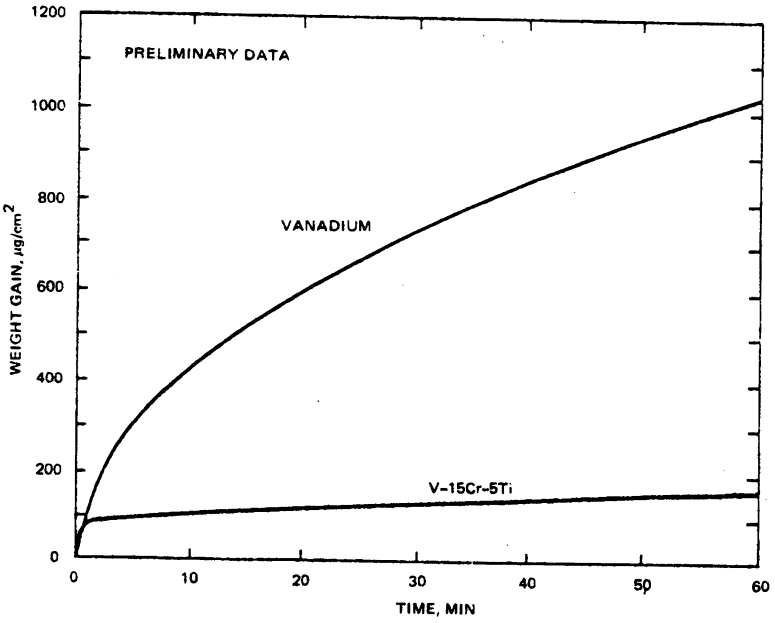

Figure VI.2-13. Weight gain on vanadium and V-15Cr-5Ti at 600°C in flowing oxygen.

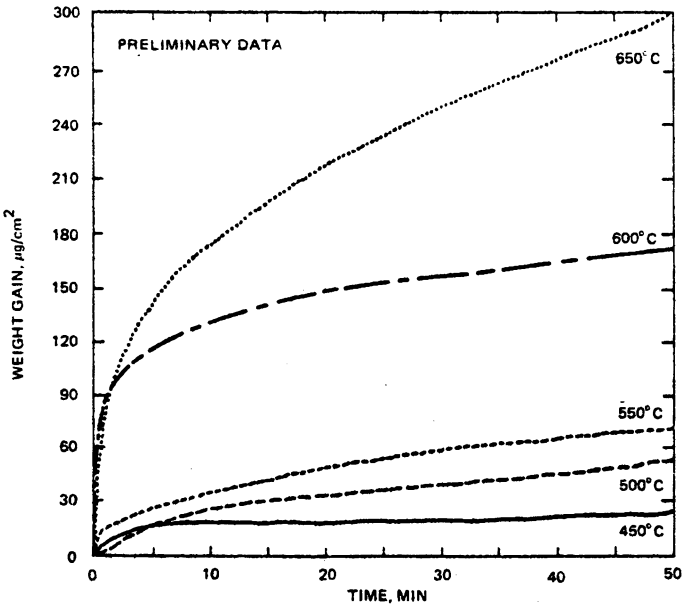

Figure VI.2-14. Effect of temperature on weight gain of V-15Cr-5Ti in flowing oxygen.

- Dissolved hydrogen isotopes do not seriously affect mechanical properties at operating blanket temperatures.

- For a fault condition leading to rapid reactor cooldown oxygen in the form of O_2 and H_2O will quickly form a protective oxide skin thus preventing excessive hydrogen uptake.

- Oxygen embrittlement due to the diffusion of oxygen into the bulk metal poses the most serious obstacle to the use of vanadium.

VI.2.1.4.1.2 50 atm Helium Coolant with Solid Breeder

- For operating temperatures below 400°C vanadium can be safely used for 10^4 h for any impurity level and species of oxygen.

- For operating temperatures between 400°C and 600°C the impurity level of water vapor in the helium must be maintained below 0.1 vppm to insure safe operation in 10^4 h for wall thickness = 2 mm.

- Embrittlement is due both to the high oxygen diffusivity and to the high oxygen terminal solubility (TSO) above 400°C.

VI.2.1.4.1.3 50 atm He Coolant with Liquid Lithium Breeder

- For one face of 0.25 mm vanadium wall in contact with liquid lithium and the other face cooled by helium and operating between 350-550°C, water vapor impurity levels must be maintained below 0.01 vppm for safe operation in 10^4 h.

- For operation above 500°C, impurity levels may be relaxed to 1 vppm H_2O.

VI.2.1.4.1.4 50 atm He Coolant on Vanadium First Wall

- Oxygen fluxes to the wall on the plasma side are expected to be too low to provide a source of wall contamination.

- For operating temperature of 500°C water vapor impurity in He must be maintained below 0.3 vppm to insure safe operation in 10^4 h for wall thickness = 4 mm.

VI.2.1.4.2 V-15Cr-5Ti Alloy

VI.2.1.4.2.1 General Considerations of Hydrogen and Oxygen in Alloy

- Alloying would have minimal impact on tritium inventory at operating temperatures.

- Alloying has an advantage in reducing oxygen transport due to internal oxidation. Oxygen solubility in equilibrium with interface oxide (TSO) could be lower than for vanadium.

- For internal oxidation model, TSO and oxygen diffusion in alloy matrix (V-Cr-O) are critical to oxygen transport.

- Criteria for embrittlement are uncertain. The oxygen content of matrix and formation of internal oxides must be considered.

- Growth of surface oxide does not appear critical to mechanical property degradation.

VI.2.1.4.2.2 Solid Breeder Blanket/First Wall Material in 50 atm Helium with 100 vppm Oxygen

- For blanket operating at 600°C, TSO must be less than or equal to the maximum oxygen concentration for embrittlement.

- For a first wall of 4 mm thickness operating at 500°C or below this requirement may be relaxed by a factor of 3.

VI.2.2 Water Corrosion

Critical aspects related to the corrosion of vanadium alloys and austenitic steels in pressurized water are assessed.

VI.2.2.1 Vanadium-base Alloys

The corrosion/compatibility of vanadium alloys in water is a critical issue regarding the viability of a vanadium alloy structure in a water-cooled blanket. Most previous design studies have not considered this combination because of the relatively high oxidation potential of vanadium. However, on closer examination, one concludes that the kinetics of the oxidation reaction may be acceptably low at the relatively low temperatures of interest for water-cooled systems; similar to the case for zircaloy. It was also considered possible that the 15% chronium in the V-15Cr-5Ti alloy might serve a similar role as in the case of stainless steel, i.e., the formation of a continuous adherent protective oxide film. The existing data base on the corrosion of vanadium alloys in pressurized water is very limited; however, as indicated below, the data are quite encouraging. At this time the possible use of vanadium alloys in water-cooled systems cannot be ruled out, although additional data are required to provide a definitive answer.

Vanadium has an inherently high resistance to corrosive oxidation by water due to the formation of a continuous thin oxide film. At temperatures below the boiling point of water, the metal and a number of its alloys have shown good corrosion resistance in a number of solutions, notably sodium chloride and tap water. Its aqueous corrosion resistance is reported to be improved by alloying with niobium, tantalum, or titanium. It is reported to "passivate" in alkaline solutions upon anodic polarization, perhaps indicating optimum corrosion resistance in an oxidizing alkaline aqueous environment. It has been shown to crack under stress in strong solutions of hydrochloric acid or sulfuric acid, but not in other acids and not in alkalies. Three recent studies have been conducted to provide additional scoping data on the corrosion of vanadium alloys in water.

W. Reuther exposed several vanadium alloys (V, V-15Cr, V-20Ti and V-15Cr-5Ti) to 98°C distilled water for 100 h. Negligible corrosion was observed in these tests. A second test was conducted with electropolished V-15Cr and V-15Cr-5Ti at 250°C in a refreshed autoclave. The oxygen concentration in the water was maintained at 0.04 ppm. Corrosion rates in terms of weight gain for the two alloys following an 85 h exposure (temperature exceed 250°C for a short time during the test) are summarized in Table 1. No change in appearance of the specimens was observed after test. Although the V-15Cr alloy is

the more corrosion resistant of the two alloys, both alloys exhibited excellent corrosion resistance to 250°C deoxygenated water. For comparisons, the corrosion rate for stainless steel is ~ 0.06 g/m^2 in high purity H_2O under similar conditions.

TABLE VI.2-1. CORROSION RATES OF VANADIUM ALLOYS IN PRESSURIZED WATER

Alloy	Weight Change, g/m^2	
	85 h @ 250°C[a]	100 h @ 300°C[b]
V-15Cr-5Ti + 0.23 - 0.5[c,d]	+ 0.23 + 0.8[c]	+ 1.7
V-15Cr + 0.009	+ 0.007	
V-20Ti + 1.8[c] + 0.2[c,d]		+ 1.6

[a]Reuther and Smith.
[b]Tortorelli and DeVan.
[c]Hydrogen overpressure of 83 KPa.
[d]Cold-worked material.

A third scoping test has been conducted to evaluate the effect of a hydrogen overpressure on the corrosion of vanadium alloys in pressurized water. Tests were conducted on V-20Ti, V-15Cr-5Ti and Vanstar-7 for 100 h in 300°C deionized water. Results of tests conducted with and without a hydrogen overpressure of 83 KPa are summarized in Table 1. Very little effect of the hydrogen addition on the corrosion rate was observed. All specimens picked up a small amount of hydrogen after test. The cold-worked V-15Cr-5Ti alloy indicated a small weight loss.

Based on these very limited data, selected vanadium-base alloys may be acceptable for use in pressurized water (~ 320°C) systems. The chromium content (~ 15%) appears to be beneficial for maintaining a protective oxide film. The corrosion rates observed are the same order of magnitude as generally observed for the ferritic steels. Obviously longer term tests are required to confirm these scoping results. Also, the potential for hydrogen embrittlement

and stress corrosion effects must be investigated. For purposes of the current study it is recommended that the V-15Cr-5Ti alloy be considered acceptable for use in pressurized water at temperatures 350°C. Steady state corrosion rates are predicted to be less than 1 mg/m^2 h.

VI.2.2.2 Austenitic Stainless Steel (PCA)

Austenitic stainless steels, in general, have good corrosion resistance to degassed high-temperature water. The corrosion resistance is attributed primarily to the formation of an adherent protective spinel film of the type M_3O_4. The corrosion rate under well controlled conditions is about 0.5 mg/m^2-h or about 0.75 μm/y.

The major concerns regarding compatibility of stainless steel and water relate to effects of water purity, stress, and steel microstructure. Sensitization, i.e., precipitation of chromium carbides at grain boundaries that occurs after certain heat treatments, appears to have little effect on the corrosion rate of stainless steels in pressurized water with a pH of 7 to 11. However, intergranular attack has been observed in both Types 304 and 316 stainless steel exposed to water with a pH of 3.5. Stress corrosion cracking can occur in stainless steel structural components particularly under heat transfer conditions where steam blanketing can occur or at liquid-vapor interfaces which provide alternate wetting and drying. The principal problems in this area relate to boiling water reactor or steam generator applications where chlorides or free caustic in water become sufficiently concentrated to produce cracking. If there is a concentrating mechanism present, chloride and caustic concentrations of the order of ppm in the bulk water can cause cracking. It is generally agreed that some oxygen is required to cause chloride cracking whereas none is required for caustic cracking.

Hydrogen additions to water reduce the tendency for corrosion cracking. The most susceptible areas are welds and the heat affected zones where microstructural effects in the heat-affected zones can be minimized by either reducing the carbon content or adding stabilizers such as titanium, niobium, or tantalum to the stainless steel. The cold worked materials are generally regarded as more susceptible to stress-corrosion effects than solution-annealed material.

Since the blanket application is quite severe in that it includes (1) high thermal stresses, (2) radiation that can cause hydrolysis of the water and microstructural changes and embrittlement of the steel, and (3) cold-worked material; stress corrosion effects could severely compromise the use of austenitic steels in fusion reactor blankets. Further analyses should be conducted to evaluate the effects of tritium control requirements on the water chemistry, since careful control of water chemistry is necessary to minimize stress corrosion effects. For the current study it will be assumed that austenitic steel (PCA) can be used in a pressurized water-cooled system. However, if water-cooled stainless steel blanket concepts appear attractive, further investigations of stress corrosion effects in cold-worked material should be conducted to assure satisfactory operation.

REFERENCES FOR CHAPTER VI

1. P. F. Tortorelli, J. H. DeVan, and J. E. Selle, "Effects of Nitrogen and Nitrogen Getters in Lithium on the Corrosion of Type 316 Stainless Steel," preprint 115, NACE Corrosion/79, March 1979.

2. P. F. Tortorelli and J. H. DeVan, ADIP Quarterly Progress Report, Sept. 30, 1979, U.S. Department of Energy Report DOE/ET-0058/7, pp. 162-169.

3. P. F. Tortorelli, J. H. DeVan, and R. M. Yonco, "Compatibility of Fe-Cr-Mo Alloys with Static Lithium," accepted for publication in Journal of Materials for Energy Systems.

4. P. F. Tortorelli and J. H. DeVan, J. Nucl. Mater. 85 & 86 (1979) 289-293.

5. P. F. Tortorelli, J. H. DeVan, and J. E. Selle, Proc. Second Int. Conf. Liquid Metal Technology in Energy Production, U.S. Department of Energy Report CONF-800401-P2 (1980), pp. 13-44-13-54.

6. P. F. Tortorelli and J. H. DeVan, "Mass Transfer Deposits in Lithium - Type 316 Stainless Steel Thermal Convection Loops," Proc. Second Int. Conf. Liquid Metal Technology in Energy Production, U.S. Department of Energy Report CONF-800401-P2 (1980) pp. 13-55 - 13-63.

7. P. F. Tortorelli and J. H. DeVan, ADIP Semiannual Prog. Rep. March 31, 1982, DOE/ER-0045/8, U.S. Department of Energy, Office of Fusion Energy, pp. 482-490.

8. P. F. Tortorelli and J. H. DeVan, ADIP Semiannual Prog. Rep. March 31, 1983, U.S. Department of Energy, Office of Fusion Energy.

9. P. F. Tortorelli and J. H. DeVan, "Corrosion of an Fe-12Cr-1Mo VM Steel in Thermally-Convective Lithium," presented at Topical Conf. on Ferritic Alloys for use in Nuclear Energy Technologies, Snowbird, June 19-23, 1983.

10. P. F. Tortorelli and J. H. DeVan, "Effect of Nickel Concentration on the Mass Transfer of Fe-Ni-Cr Alloys in Lithium," J. Nucl. Mater. 103 & 104 (1981), pp. 633-638.

11. D. G. Bauer, W. E. Stewart, I. N. Sviatoslavsky, and D. K. Sze, Proc. Second Int. Conf. Liquid Metal Technology in Energy Production, U.S. Department of Energy Report CONF-800401-P2 (1980), pp. 13-73-13-81.

12. W. N. Gill, R. P. Vanek, R. V. Jelinek, and C. S. Grove, Jr., AIChE J. 6 (1960) 139-144.

13. O. K. Chopra and D. L. Smith, ADIP Semiannual Prog. Rep. September 30, 1982, DOE/ER-0045/9, U.S. Department of Energy, Office of Fusion Energy, pp. 309-309.

14. O. K. Chopra and D. L. Smith, ADIP Semiannual Prog. Rep. March 30, 1983.

15. G. A. Whitlow, W. L. Wilson, W. E. Ray and M. G. Down, J. Nucl. Mater. 85 & 86 (1979) 283-87.

16. I. Nihei, I. Sumiya, Y. Fukaya, and Y. Yamazaki, Japanese Atomic Energy Research Institute Report JAERI-M 5683 (1974).

17. W. Jordan, W. L. Bradley, and D. L. Olson, Nucl. Technol. 29 (1976) 209-214.

18. T. A. Whipple, D. L. Olsonl, W. L. Bradley, and D. K. Matlock, Nucl. Technol. 39 (1978) 75-82.

19. D. L. Olson, G. N. Reser, and D. K. Matlock, Corrosion (Houston) 36 (1980) 140-144.

20. E. Ruedl, V. Coen, T Sasaki, and H. Kalbe, J Nucl. Mater. 110 (1982) pp. 28-36.

21. P. F. Tortorelli and J. H. DeVan, J. Materials for Energy Systems 4 (2) (1982), pp. 78-83.

22. B. D. Wilkinson, G. R. Edwards, and N. J. Hoffman, J. Nucl. Mater. 103 & 104 (1981) pp. 669-674.

23. V. Coen, P. Fenici, H. Kolbe, and T. Sasaki, J. Nucl. Mater 110 (1982) pp. 108-114.

24. M. H. Cooper and G. R. Taylor, "A Transport Model for Radioactive Corrosion Product Deposition in an LMFBR," Nucl. Engr. and Des. 32, (1975), 246-251.

25. M. H. Cooper, and G. R. Taylor, "Radiochemical Measurements of Mass Transfer Coefficients in Forced-Convection Sodium," Trans. Amer. Nucl. Soc. 13, Nov. (1970), 579.

26. P. F. Tortorelli and O. K. Chopra, "Corrosion and Compatibility Considerations of Liquid Metals for Fusion Reactor Applications," J. Nucl. Mater. 103 & 104, (1981), 621-632.

27. W. F. Brehm, P. L. Koehmstedt, E. A. Kovacevich and D. W. Shannon, "Radioactive Material Transport in Flowing Sodium System," in Corrosion by Liquid Metals ed by Draley, J. E. and Weeks, J. R., Plenum Press, NY (1970), 97-113.

28. A. B. Fisher, "Atomic Diffusion in Alloys Exposed to Liquid Sodium," J. Nucl. Matr., 62, (9176), 247-256.

29. J. H. DeVan, "Compatibility of Structural Materials with Fusion Reactor Coolant and Breeder Fluids," J. Nucl. Mater. 85 & 86, (1979), 249-256.

30. D. D. Papailiou and P. S. Likoudis, "Magneto Fluid-Mechanic Laminar Natural Convection - An Experiment," Int. J. Heat Mass Transfer, 11, (1968), 1385-1391.

31. B. G. Logan, et al., "Mirror Advanced Reactor Study - Interim Design Report," UCRL-53333 (April 1983).

32. A. Klein, University of Wisconsin, Private Communication.

33. E. Veleckis and R. K. Edwards, J. Phys. Chem., 73, 683 (1969).

34. J. F. Lynch, J. J. Reilly, and F. Millot, J. Phys. Chem. Solids, 39, 883 (1978).

35. R. Gold, D. Harrod, R. Ammon, R. Buckman, and R. Svedberg, "Technical Assessment of Vanadium-Base Alloys for Fusion Reactor Applications," Vol. 2, Westinghouse Electric Corporation, COO-4540-1 (1978).

36. D. Chandra, T. S. Elleman, K. Verghese, J. Nuc. Mat., 59, 263 (1976).

37. E. Fromm and R. Kirchheim, J. Less Common Metals, 26, 403 (1972).

38. J. L. Henry, S. A. O'Hare, R. A. McCune, and M. P. Krug, J. Less Common Metals, 21, 115 (1979).

39. R. C. Svedberg, J. Vac. Sci. Techn. 8, 41 (1971).

40. H. Jehn and G. Horz, Z. Metallkde, 67, 417 (1976).

41. H. K. Kohl, J. Nuc. Mat. 41, 231 (1971).

42. H. Carslaw and J. Jaeger, "Conduction of Heat in Solids," Oxford Press (1959).

TABLE OF CONTENTS

CHAPTER VII - LIQUID METAL BLANKET DESIGNS

LIST OF FIGURES FOR CHAPTER VII

LIST OF TABLES FOR CHAPTER VII

VII. LIQUID METAL BLANKET DESIGNS

The viability of blanket concepts based on the use of liquid metals, either lithium or 17Li-83Pb, as the tritium breeding material have been evaluated in the present study. The blanket concepts considered for both tokamak and mirror reactors represent two classes: (1) self-cooled systems in which the liquid metal serves as both breeder and coolant, and (2) separately-cooled liquid metal blanket concepts. The six concepts evaluated include:

- Self-cooled Systems (Breeder/Coolant)
  - Lithium/Lithium
  - 17Li-83Pb/17Li-83Pb

- Separately-Cooled Systems (Breeder/Coolant)
  - 17Li-83Pb/Sodium
  - 17Li-83Pb/Water
  - Lithium/Helium
  - 17Li-83Pb/Helium

In addition, for tokamak reactors, a preliminary evaluation of a non-breeding inboard blanket with a self-cooled outboard blanket has been conducted. Results of the liquid metal blanket study are presented in Chapter VII.

VII.1. Self-Cooled Blanket Concepts

The key feature of the self-cooled blanket concepts relate to the use of the same liquid metal as both tritium breeder and coolant. This factor greatly simplifies both materials and design considerations since the blanket requires only a structure and a breeder-coolant. Coolant-breeder compatibility/reactivity is not a factor and structure compatibility considerations are less restrictive. Heat transfer requirements are also reduced because most of the nuclear heating is deposited directly in the breeder-coolant. Lithium and Li-Pb both provide relatively high tritium breeding capability and tritium recovery with relatively low tritium inventory is feasible. The liquid metals have good heat transfer characteristics with high thermal conductivities and heat capacities, which are beneficial for normal and transient operation.

VII.1.1 Mechanical Design

VII.1.1.1 Introduction

Mechanical design is an integral part of the overall considerations and analyses of the self-cooled liquid-metal blanket. It is in one respect, dictated by the consideration of system maintainability, reliability, and fabrication. It is also strongly dependent on the various constraints imposed from neutronic, thermal hydraulic, MHD, structural and material considerations. Mechanical design evolves and will continue to evolve as more information (experimental and analytical) becomes available and as the understanding of various physical phenomena improves. The various concepts described here are based on current understanding and requirements for the blanket.

The most important design requirements and considerations are from neutronics, thermal-hydraulics, MHD, and structural analysis. This is particularly true in the inboard region in view of the limited space and access, and as a result of the relatively high magnetic flux density. Thus, the design is driven to a large extent by the consideration of the requirements for the inboard blanket. The allowable inboard blanket thickness (in the radial direction) is severely limited by economic considerations. The minimum blanket thickness and material composition is constrained by neutronic considerations, viz., tritium breeding requirements and energy absorption. Thermal-hydraulics determines the minimum average velocity required to provide enough cooling of the first wall (interface temperature requirement) and to provide high enough exit temperature for power generation. MHD analysis determines the total pressure drop (based on the average velocity determined by the overall ΔT requirement) through the blanket. Structural analysis receives input from thermal and MHD analyses, and determines whether the primary and the secondary stress requirements are satisfied. The various candidate design options were developed in an iterative manner using the results of neutronics, thermal-hydraulics, MHD, and structural analyses performed as needed. As a result of the limited resources and schedule, it is not possible to perform detailed analyses for all the design options described here and sometimes qualitative arguments are used in comparing different design options in order to select a reference design.

VII.1.1.2 Concept Development

In the present study, self-cooled liquid metal blanket designs have been driven primarily by magnetohydrodynamic (MHD) considerations. This involves:

- Incorporation of manifolds into blanket modules to minimize flow velocities perpendicular to the primary magnetic field (Tokamak-Toroidal field; Mirror-Axial field).
- Some method of flow enhancement is required to provide adequate cooling for the first wall of a tokamak.

Generic blanket concepts considered include:

- Poloidal flow manifold/module
  - Large Straight Channels
  - Induced Helical Flow
- Poloidal Flow Manifold/Module with Toroidal/Axial Flow First Wall
- Poloidal Flow Manifold/Module with Radial Flow First Wall

The following sections summarize the critical aspects of these generic concepts and others with minor modifications. The poloidal flow manifold/module with a toroidal/axial flow first wall is selected as a reference for the comparison study.

VII.1.1.2.1 Poloidal Flow

A schematic of the poloidal-flow blanket is shown in Fig. VII.1-1. The poloidal-flow blanket is geometrically the simplest among all the design options considered. It is composed of simple ducts with liquid-metal flowing in the poloidal direction in and out of the blankets (inboard and outboard). However, it can be shown (see Section VII.1.3) that the average velocity required to maintain the maximum interface temperature at an acceptable level is too high from either thermal efficiency (which depends on the overall ΔT rise through the blanket for fixed inlet temperature) point of view or from MHD pressure drop (which determines the maximum primary stress level) point of view. This is the consequence of relatively poor heat transfer (assuming slug flow with thermal conduction only) from the first wall to the bulk of the fluid. Thus, within the validity of the assumptions made in the heat transfer analysis, the poloidal-flow blanket does not look attractive. However, it must be pointed out that deviations from the assumptions (such as slug flow

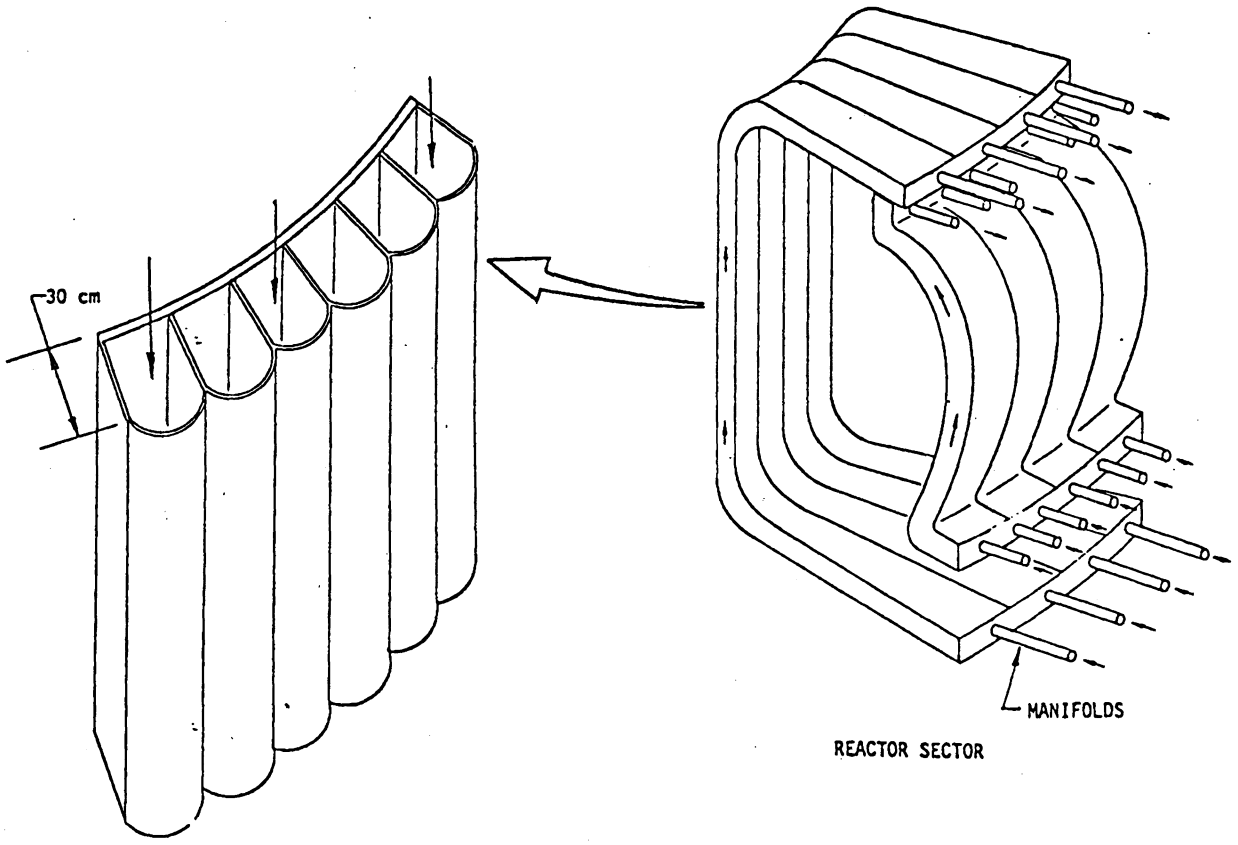

Figure VII.1-1. Schematic of simple poloidal-flow blanket.

and no natural convection) described in Section VII.1.3 are not only possible but also probable. The impact of these factors on the design cannot become clear until the fluid-dynamic and heat transfer aspects of liquid-metal flow in a transverse magnetic field are better understood. In the mean time, various design solutions are sought to help resolve the first wall cooling problem. The possibility of magnetically-induced circulation to enhance cooling of the first wall will be evaluated later when a better understanding of MHD effects is provided.

VII.1.1.2.2 Helical Flow

As described previously, the simple poloidal-flow blanket does not look attractive as a result of relatively poor heat transfer performance if fully developed flow (no mixing of any kind) is assumed. Thus, the temperature near the first wall is rather high while that of the bulk fluid is relatively low (see also Fig. VII.1-13). The helical-flow blanket shown in Fig. VII.1-2 is intended to help reduce the interface temperature by mechanically bringing in the colder fluid away from the first wall to the first wall. This is done mechanically by placing turning vanes inside the ducts as shown in Fig. VII.1-2. This design provides an effective way of using the bulk fluid to cool the first wall. Placing mechanical vanes inside the duct could introduce an additional pressure drop thorugh the blanket. It is very difficult to estimate the magnitude of this pressure drop at present. However, it should be pointed out that all the design options considered will introduce some additional pressure drop over that of the simple poloidal-flow blanket. The key to the problem would be to provide enough cooling for the first wall while minimizing this additional pressure drop. The helical-flow blanket is a viable concept if this additional Δp is not excessive. This design provides a possible alternate to the reference design.

VII.1.1.2.3 Radial/Poloidal Flow

Figure VII.1-3 shows the 3-dimensional sketch of the radial/poloidal flow blanket. It has several poloidal-flow manifolds which supplies many radial-flow modules exposed to the plasma. Baffles are placed inside the radial modules as shown in Fig. VII.1-3. Heat transfer calculations indicate that best results could be achieved by connecting the flow path of the two adjacent

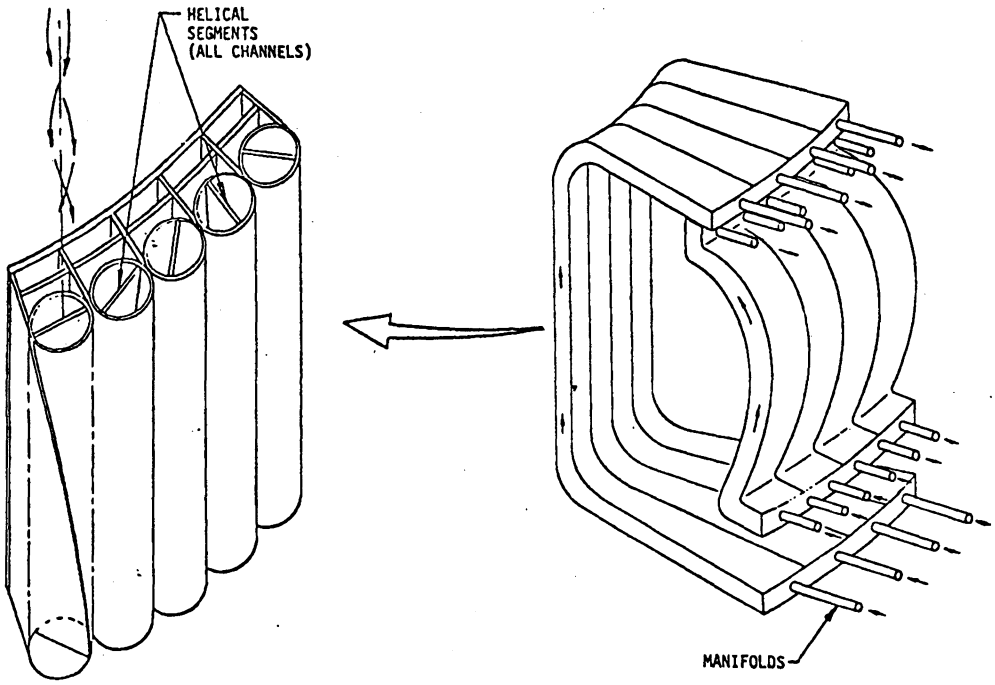

Figure VII.1-2. Schematic of helical-flow blanket.

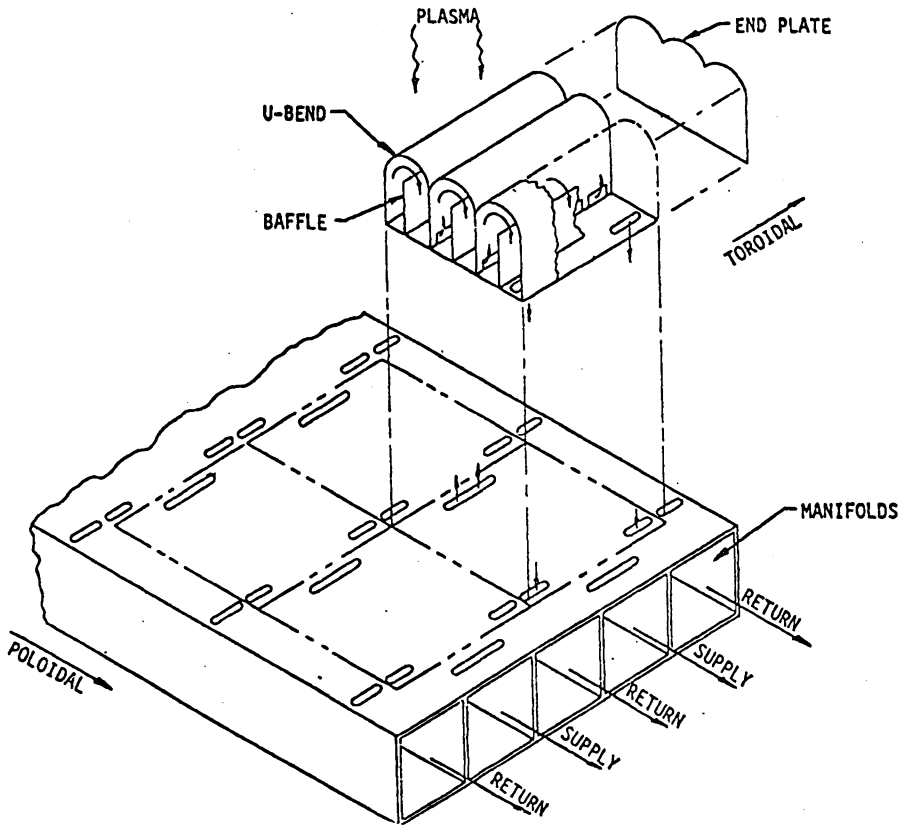

Figure VII.1-3. Schematic of radial/poloidal flow blanket.

radial modules. By forcing the entire coolant flow through the radial modules, efficient cooling of the first wall could be accomplished. Many of the features of this design are similar to that of the toroidal/poloial flow blanket. The major difference is that the radial modules requires considerable space in the radial direction which leaves relatively smaller space for the poloidal manifold compared to the toroidal/poloidal flow blanket (particularly in the inboard region where the space is limited). This would result in relatively higher velocity in the poloidal manifold and thus a larger pressure drop for the radial/poloidal flow blanket compared to the toroidal/poloidal flow blanket. If an electrical insulator is found to be stable in the fusion reactor blanket environment, this design may become attractive since the poloidal manifold is protected by the radial modules against the strong radiation and surface heat flux near the first wall, and since the insulator could be placed (coated) on all sides of the poloidal manifold.

VII.1.1.2.4 Toroidal/Poloidal Flow

Figure VII.1-4 shows the schematic of the toroidal/poloidal flow blanket. It is composed of slightly slanted poloidal manifolds and relatively small toroidal channels. Each manifold supplies a number of toroidal channels. The toroidal channels are exposed to both the surface heat flux and the relatively high nuclear heating rate while the poloidal manifold is heated mainly by nuclear heating. The poloidal manifold is protected by the toroidal channels both thermally from the surface heat flux and structurally from radiation damage. The mean velocity in the poloidal manifold can be kept at relatiely low values which will reduce the MHD pressure drop through the manifold. Since the pressure drop through the manifold is the single largest pressure drop of the entire blanket, its reduction will reduce significantly the overall pressure drop of the blanket. A second advantage of the toroidal/poloidal flow blanket is that the walls of the poloidal manifold can take higher stress (primary and thermal) levels than the first wall since the former is not exposed to the surface heat flux and receives less radiation dosage than the latter. The first wall is cooled by the coolant flowing through the small toroidal channels which are parallel to the toroidal magnetic field. The flow in the toroidal channels is perpendicular to the poloidal field which is much smaller than the toroidal field. Thus, the velocity in the toroidal channels can be increased considerably over that in

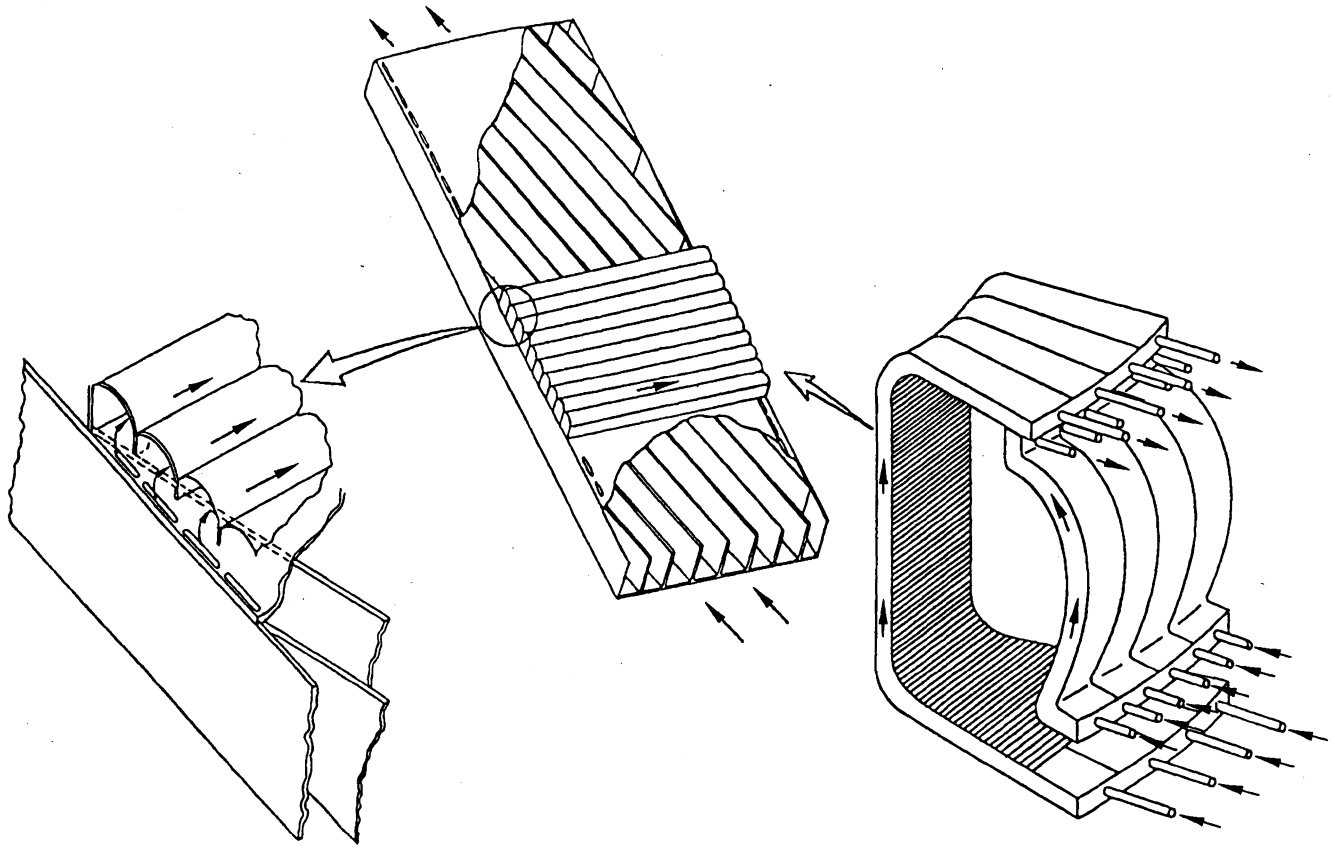

Figure VII.1-4. Liquid metal flow concept (poloidal/toroidal flow).

the poloidal manifold without increasing significantly the overall pressure drop through the blanket. It is this relatively high velocity in the toroidal channels (compared to the velocity in the manifold) and the relatively short length of the toroidal channels (compared to the full length of the manifold in the poloidal direction) that could reduce the maximum interface temperature to an acceptable level provided that the flow is evenly distributed in the toroidal channels. There is, of course, some additional pressure drops associated with the bends. However, as mentioned previously, any mechanical design aimed to provide more cooling near the first wall is likely to introduce more pressure drops compared to the simple poloidal-flow blanket. The important concept is to provide adequate and efficient cooling of the first wall region while minimizing these additional pressure drops.

The toroidal/poloidal flow blanket was selected as the reference design. More detailed descriptions and analyses can be found in the following sections.

VII.1.1.2.5 Other Concepts

There are a number of design concepts being proposed in addition to those already described. All of these designs are intended to provide more cooling near the first wall and thus reduce the maximum temperature in the blanket. It is impossible to perform analyses for all these concepts and compare the advantages and disadvantages. Some of these designs will be described briefly for future references and considerations.

Figure VII.1-5 shows the concept of dual-channel poloidal-flow blanket. Since the velocity in the smaller channel is higher than that in the larger channel, the pressure drop will be different for these two channels. An additional booster pump will be required for the high velocity channel.

Figure VII.1-6 shows another variation of the dual-channel poloidal-flow blanket. A cut at the mid-section of the blanket is provided which reduces the heated length of the first wall by a factor of two for both the upper and the lower halves of the blanket. A separate pump for the high and low velocity channels is not needed. However, higher MHD pumping power is required for the entire coolant flow.

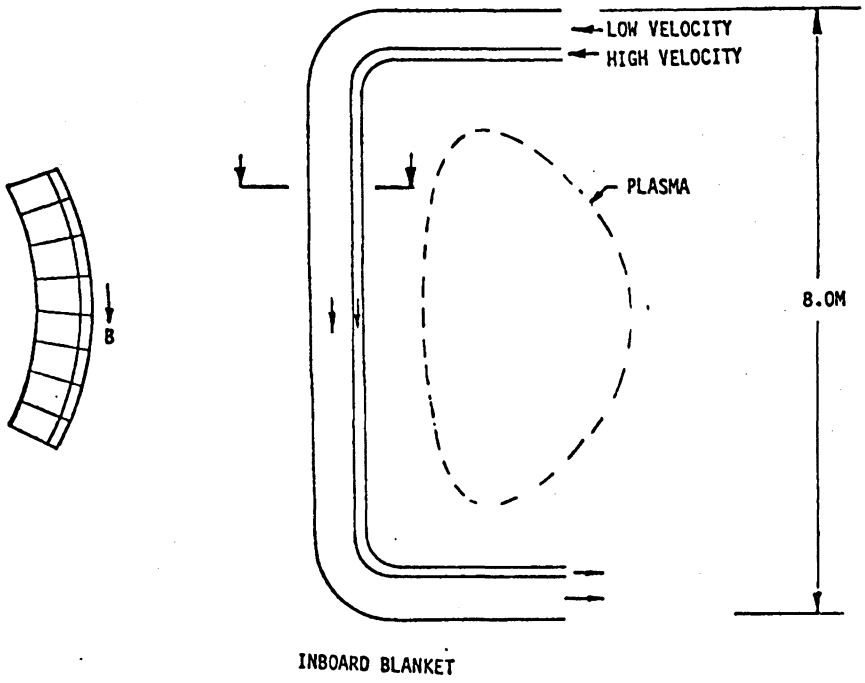

Figure VII.1-5. Dual-channel poloidal flow.

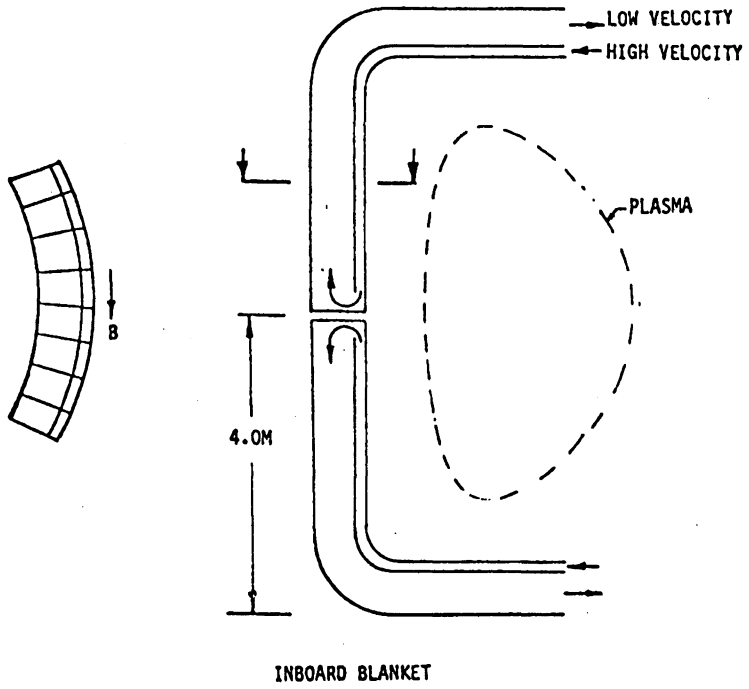

Figure VII.1-6. Dual-channel poloidal flow.

Figure VII.1-7 shows the schematic of the poloidal-flow blanket with internal baffles. The idea is to control the amount of flow near the first wall by varying the number of baffles, the size of the baffles, and the number and size of the restrictions in the baffles. By forcing enough flow towards the first wall, the maximum temperature could be reduced. However, additional pressure drops caused by these baffles are difficult to estimate.

VII.1.1.3 Reference Design

The reference design is the toroidal-poloidal flow blanket described in Sec. VII.1.1.2 and shown in Fig. VII.1-4. Figure VII.1-8 shows the cross-sectional view of the toroidal/poloidal flow blanket. The blanket can be divided into three regions in the radial direction, i.e., the toroidal channels, the poloidal manifolds, and the reflector. Neutronic considerations require that the reflector be composed of a substantial fraction of structural material (PCA) (Although other materials may eventually prove beneficial, in the initial phases of this study, the reflector consists only of structure and coolant). The arrangement shown in Fig. VII.1-8 will satisfy the neutronic requirement. The partitions shown in Fig. VII.1-8 are not necessarily partitions for coolant flow. These partitions can be perforated plates and thus the coolants between the manifold and the reflector regions can be connected. Therefore, pressure drops are the same in the manifold and the reflector region. In the thermal-hyraulic and MHD analyses, no distinction was made between the manifold and the reflector. The full cross section for coolant flow is utilized for heat removal. At the back of the blanket, a 4 cm thick structure is provided for additional high-temperature shielding. In this region, the nuclear heating rate is relatively low and the temperature of the reflector material, which is the same as the structural material, can be maintained at the acceptable level by the coolant flow.

In the current design, the outboard blanket is geometrically similar to the inboard blanket. The only difference is that the overall blanket thickness in the radial direction is 84 cm for the outboard blanket (including top and bottom), while it is 64 cm for the inboard blanket (including high temperature shield). The constraints are more restrictive in the inboard region than the outboard region as a result of limited space, higher magnetic field, and longer heated length in the inboard blanket. Detailed neutronic, thermal-

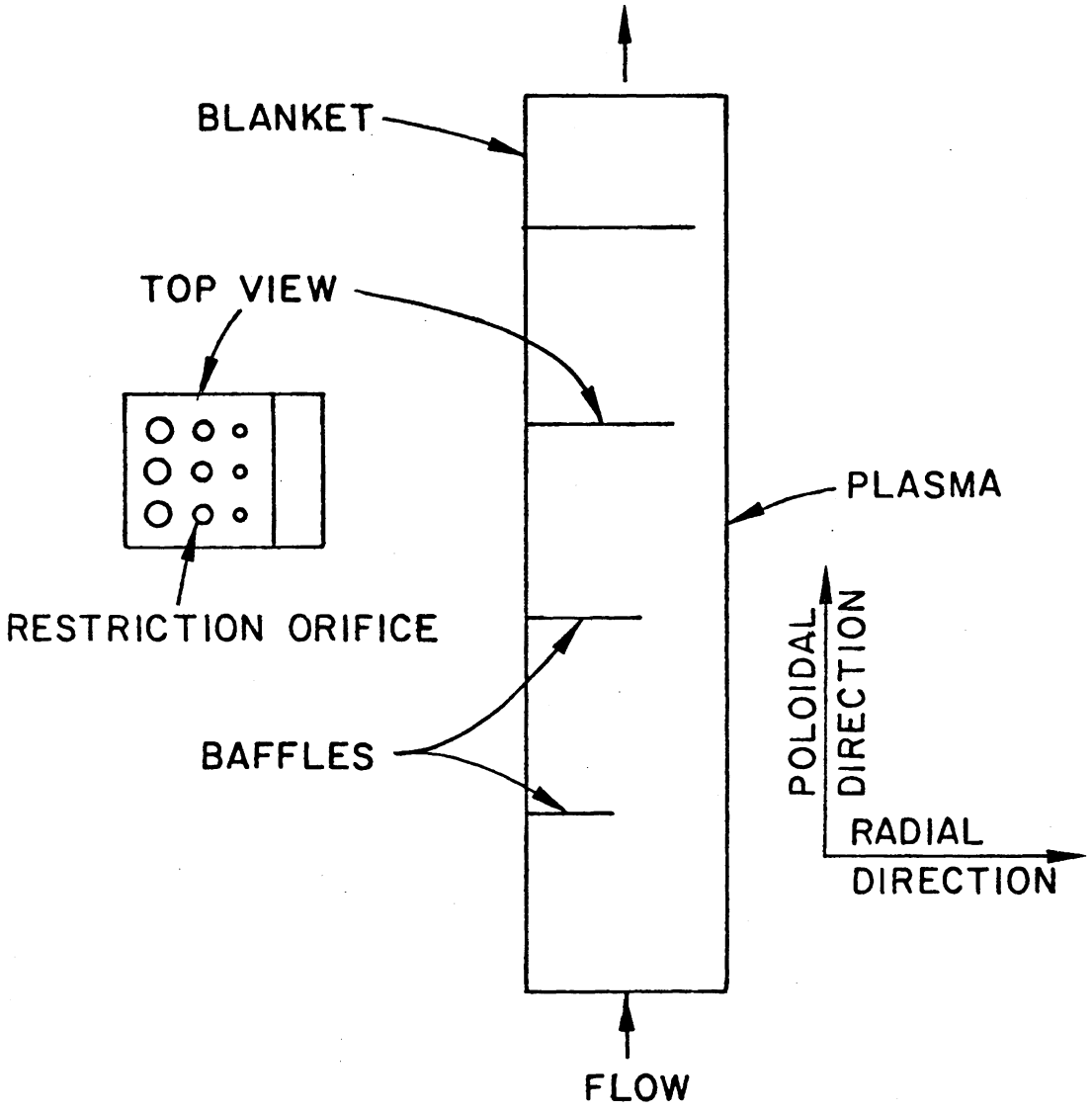

Figure VII.1-7. Poloidal flow blanket with internal baffles.

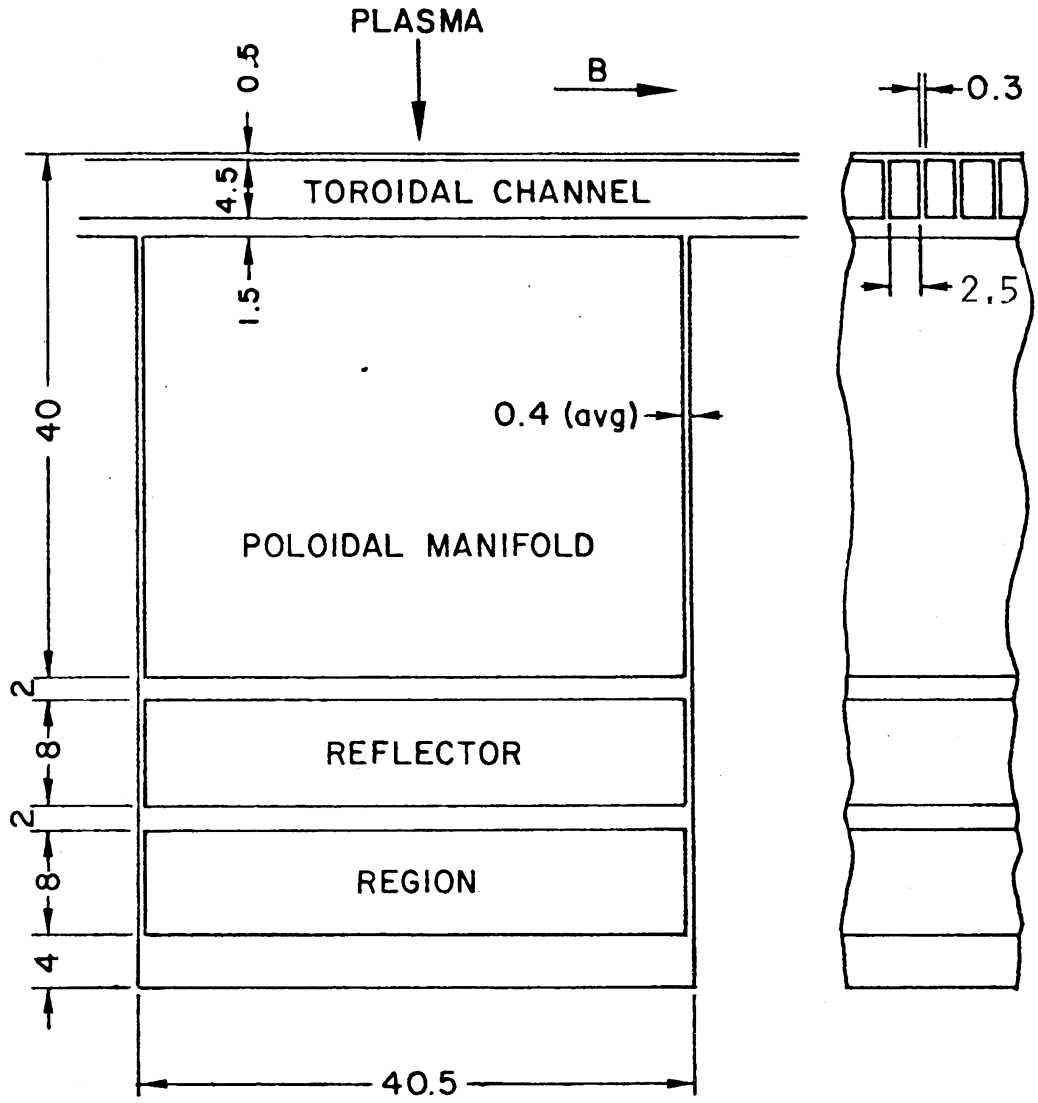

Figure VII.1-8. Cross-sectional view and dimensions of the toroidal/poloidal blanket.

hydraulic, MHD, and structural analyses of this reference design are described in the following sections.

VII.1.1.4 Blanket Sector and Structural Support

There are a total of 10 blanket sectors for the current design of a tokamak fusion power reactor. Figure VII.1-9 shows the preliminary design of such a blanket sector. The blanket sector includes the inboard and outboard blankets, the limiter, the shield, and the supply and return manifolds for the blankets. The entire blanket sector can be removed as a whole for maintenance.

Structural support for the inboard and the outboard blankets needs further study. The way the blankets are supported mechanically influences the response of the structure during normal and off-normal operations. The current design provides for primary support from the top of the blanket sector in order to minimize compressive buckling stresses on the modules

VII.1.2 MHD Analysis

VII.1.2.1 Introduction

Magnetohydrodynamic effects are of paramount importance in self-cooled liquid-metal blankets. This is because the interaction between the high magnetic fields and flowing liquid metals results in large body forces exerted on the liquid metal. To overcome these MHD body forces large pumping pressures must be applied on the liquid metal coolant. Such large pumping pressures not only require large parasitic pumping power but, more importantly, may make containment of the coolant impossible. This is because an increase of the conduit wall thickness, in an effort to reduce the material stresses, results in further MHD pressure drop increases. As a matter of coincidence, the operational and geometrical constraints of the inboard blanket are such that MHD considerations become the primary driving force in the design process. If the MHD pressure drop is not minimized by appropriate design features, self-cooled liquid-metal inboard blankets will not be just unattractive, they will be impossible.

The reference design evolved as the result of the effort to minimize MHD pressure drops while satisfying, at the same time, the heat removal and first

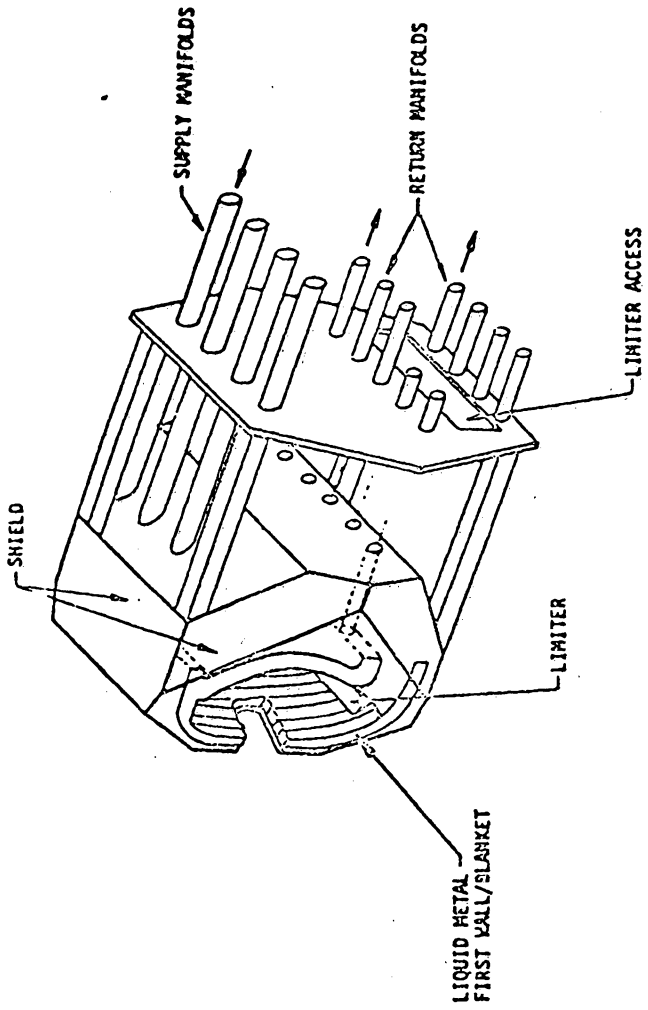

Figure VII.1-9. Preliminary design of a self-cooled, liquid metal blanket sector.

wall cooling requirements. As a matter of fact, the rather large coolant velocities required to cool the first wall, in the absence of turbulent mixing, dictated the placement of the first wall coolant channels in the toroidal direction, so that the high coolant velocities be parallel to the large toroidal magnetic field.

VII.1.2.2 MHD Non-Dimensional Parameters

The study of magnetohydrodynamics involves the simultaneous solution of the Navier-Stokes equations for fluid motion (including a ponderomotive force term) and Maxwell's equations. This formidable task is made possible by considering various regimes over which the equations are greatly simplified. These reqimes are characterized by the following non-dimensional numbers.

Magnetic Reynolds number	$Re_m = B_{ind}/B$	[VII.1-1]
Hartmann number	$M = aB\sqrt{\sigma}/\mu$	[VII.1-2]
Interaction Parameter	$N = aB^2\sigma/V\rho$	[VII.1-3]
Conductivity Ratio	$\phi = \sigma_w t_w/\sigma a$	[VII.1-4]

where B = magnetic field strength, a = pipe radius or channel half width in the direction parallel to B, σ = conductivity of liquid, μ = viscosity of liquid, σ_w and t_w = conductivity and thickness of pipe wall or of wall normal to B, V = liquid velocity, B_{ind} = induced magnetic field strength.

For the reference design these non-dimensional numbers are of the following order of magnitude.

$$R_{e_m} \sim 0(10^{-3}),\ M \sim 0(10^4),\ N \sim 0(10^4),\ \Phi \sim 0(10^{-2} - 10^{-3})$$

The smallness of the magnetic Reynolds number makes it possible to neglect the induced magnetic field and set the total magnetic field equal to the applied one.

As a result of the large value of M, the fluid flow and current density are uniform throughout most of the flow cross section, with variations confined in thin layers near the walls.

The large value of N makes inertial effects negligible; turbulence is also suppressed everywhere, with the possible exception of fluctuations that may exist in thin shear layers under some special circumstances.

Finally, the condition $\Phi << 1$ combined with $M\,\Phi >> 1$ defines the "thin wall" regime, in which the induced currents and, thus, the pressure drops are controlled by the wall resistance.

VII.1.2.3 Rectangular or Circular Duct in a Uniform or Slow Varying Transverse Magnetic Field

Fully developed flow in circular or rectangular ducts has been, since the mid-thirties, the subject of several investigations both analytical and experimental. The analyses available cover the whole range of M (the interaction parameter, N, is irrelevant for a fully developed flow, since there are, by definition, no inertial effects). The analyses pertinent to the fusion reactor are those for high M and $\phi << 1$. References (1) through (7) are some of the publications where details of the analyses or experimental verification of the anaytical results can be found. It can be stated, with considerable certainty, that fully developed MHD flow is well understood and that existing analyses, validated through experiments up to $M \sim O(10^3)$, are expected to be valid for $M \sim O(10^4)$ and higher.

At high Hartmann numbers, the MHD pressure gradient in thin-wall circular pipes is given by[1]:

$$\frac{dp}{dx} = \sigma \overline{V} B^2 \frac{\Phi}{1 + \Phi} \qquad \text{[VII.1-5]}$$

where the various terms have been defined in the previous section ($\overline{V}$ is the average fluid velocity).

The pressure gradient is rectangular ducts with unequal wall thickness and wall conductivities, as will be the case for the reference design, is[8]:

$$\frac{dp}{dx} = V_{core} B^2 \frac{\sigma_1 t_1}{a} = \sigma \frac{Q_{core}}{4a^2\beta} B^2 \Phi_1 \qquad \text{[VII.1-6]}$$

where Q_{core} is the mass flow rate in the uniform velocity core of the flow, and β is the duct aspect ratio (see Fig. VII.1-10).

The velocity and current density are uniform throughout most of the cross section, except for very thin layers of thickness of $O(1/M)$ for the layers adjacent to the walls normal to B and of $O(1/\sqrt{M})$ for the sidewalls parallel to B. The velocities in the side layers are large; of the order of $V_{core} \cdot \sqrt{M}$. The mass flow rates associated with the side layers are

$$Q_2 = \frac{\sigma_1 t_1}{6\ \sigma_2 t_2\ \beta}\, Q_{core} \quad \text{and} \quad Q_3 = \frac{\sigma_1 t_1}{6\ \sigma_3 t_3\ \beta}\, Q_{core} \qquad \text{[VII.1-7]}$$

for the layers near the sidewalls of thickness t_2 and t_3 respectively.

Therefore,

$$\frac{dp}{dx} = \sigma \frac{B^2 \phi_1}{4a^2 \beta} \frac{Q_{total}}{1 + \frac{\sigma_1 t_1}{6\ \sigma_2 t_2 \beta} + \frac{\sigma_1 t_1}{6\ \sigma_3 t_3 \beta}} \qquad \text{[VII.1-8]}$$

For the reference design, t_2 and t_3 are much larger than t_1. As a result, the two terms in the denominator are much smaller than one and can be neglected. The equation is then reduced to

$$\frac{dp}{dx} = \sigma \frac{B^2 \Phi_1}{4a^2 \beta}\, Q_{total} \qquad \text{[VII.1-9]}$$

It is evident from these results that the thick sidewalls do not have any effect on the pressure drop. Also, although the velocities at the sidewall layers are high, the mass flow rates associated with the sidewalls are small. Thus, the effect of these layers on mass transfer, and, thus, on corrosion will be small. The pressure drop is proportional to the conductivity and thickness of the walls normal to B. Therefore, a decrease in wall thickness is translated to a proportional decrease in pressure drop. However, because the hoop stress is inversely proportional to the wall thickness, this decrease in pressure is not accompanied by a decrease in hoop stress. It should be noted that, when two conduits share a common wall normal to B, the appropriate wall thickness that enters in the aforementioned formulae is equal to one half of the physical wall thickness dimension.

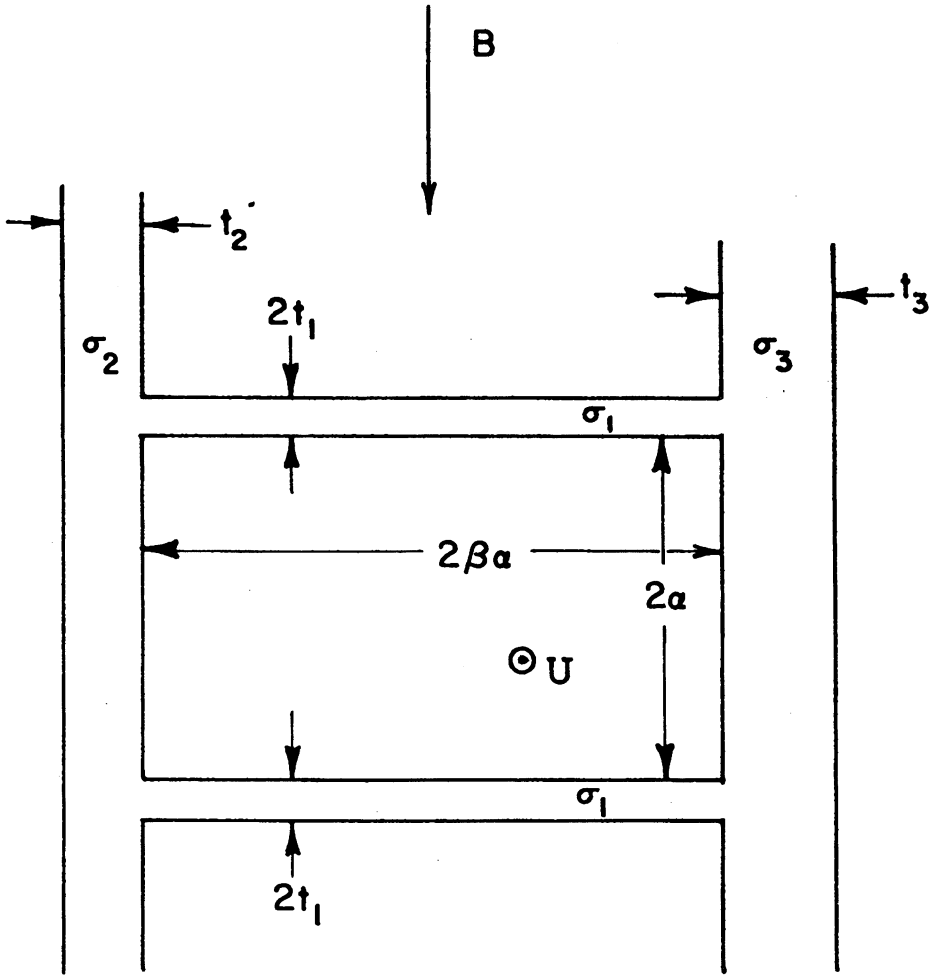

VII.1-10. Rectangular conduit in a transverse magnetic field.

The pressure drop for insulated walls is smaller by a factor of $M\Phi$ ($\sim 0(10^2)$ for the reference design) from that for thin walls. Therefore, if the walls could be made from insulating material an improvement of two orders of magnitude in pressure drop and material stresses could be made. Whereas insulating walls do not appear, at present, feasible, thin insulating coatings could be of substantial benefit. Analyses, similar to the ones that led to the above results, are being carried out to quantify the improvement in pressure drop in terms of the insulating layer resistivity and thickness.

For those cases where the magnetic field, the wall thickness, the channel dimensions and geometry, a and β, change gradually in the flow direction, the equation for dp/dx is still valid locally and it can be integrated to yield the overall pressure drop. Obviously, the more gradual the aforementioned variations, the more reliable the calculation of the overall pressure drop. Unfortunately, at present, accurate criteria for establishing whether a variation is sufficiently gradual do not exist, especially for non-circular conduits. Nevertheless, it is the consensus of the MHD community[9] that, although deviations from the fully developed character of the flow can have a strong effect on velocity profiles, the effects on pressure drop are expected to be moderate.

VII.1.2.4 Three Dimensional Effects in MHD Duct Flow

Three dimensional perturbations result from changing B field (direction or magnitude), changing cross sectional area dimensions, changing wall thickness, bends, manifolds, etc. Such variations set up axial electric field gradients which, in turn, set up circulating currents within the liquid. These currents interact with the magnetic field and result in pressure drop over and above that predicted by fully developed flow theory.

Analyses that have been carried out to date predict stagnant regions at the center of the conduit with most of the flow rate carried in layers adjacent to the walls. Also, theory predicts significantly different behavior for rectangular and for circular conduits, with the rectangular ones being more prone to the adverse three dimensional effects.

Unlike the case for a straight duct normal to a uniform magnetic field, analysis of three dimensional effects is highly case specific, involved, and, for some cases, not amenable to solution with currently available analytical

tools. Nevertheless, fair estimates of the pressure drop associated with a number of three dimensional effects exist, and are supported by limited experimental data[10] albeit at much lower values of M and N than those prevailing in the blanket.

It was assumed in the analysis of the MHD pressure drop in the fusion blanket that the variation of magnetic field strength is sufficiently gradual, so that the associated three dimensional effects are minimal. The other remaining three dimensional effects are associated with the abrupt change of the magnetic field at the inlet and outlet regions, the effects associated with abrupt changes in wall thickness and those associated with conduit bends, either on a plane normal to B or, as is the case of the reference design manifolds, from a direction normal to B to a direction parallel to B.

The pressure drop associated with abrupt changes in B (or equivalently with abrupt changes in wall thickness or cross-sectional areas), has been analyzed for thin wall circular ducts[11]. This pressure drop is found to be equal to

$$\Delta p = C\ \sigma V a B^2 \sqrt{\Phi} \qquad \text{[VII.1-10]}$$

with the coefficient C depending on the magnitude of the discontinuity. The peak value of C was computed to be 0.16. A conservative value of 0.2 is adopted in the analysis of the blanket. The pressure drop for a bend in a plane normal to B can also be estimated by the same equation.

The pressure drop for a bend from a direction normal to B to one parallel to B can be computed from the following formula.

$$\Delta p = 0.5\ \sigma V a B^2 N^{-1/3} = 0.5\ V^{4/3} B^{4/3} \sigma^{2/3} \rho^{1/3} a^{2/3} \qquad \text{[VII.1-11]}$$

Such a correlation is based on theoretical considerations (Ref 39) and the coefficient of 0.5 has been established through experimental work at $\Phi = 0.155$ and $N < 90$. If the theoretical foundation of the above correlation is valid, the formula is applicable to values of N prevailing in the fusion reactor (10^4). The coefficient of 0.5 refers to the value of Φ of 0.155. Although the scaling of the numerical coefficient with Φ has not been established, it will undoubtedly decrease with decreasing Φ. Therefore, for

the fusion reactor, with its lower value for Φ the pressure drop will be smaller than that given by the above formula. Nevertheless, the conservative value of 0.5 has been adopted in the analysis.

VII.1.2.5 Poloidal Flow Design

The poloidal flow design, shown in Fig. VII.1-1 was the first design considered because of its attractive simplicity. The pressure drop was calculated by the method outlined in VII.1.2.7. The sizes of the conduits were chosen so that the outer envelope of the inboard blanket would be identical to the reference design. Since there are no toroidal channels the poloidal conduits can be made larger. However, the curvature of the conduit wall facing the plasma, causes a decrease in effective cross sectional area, thus leading to increased velocity and increased pressure drop. Of course, the poloidal design does not suffer from pressure drops associated with manifolding, nor does it suffer the pressure drop in the toroidal channels due to the small poloidal field. The calculation of the pressure drop yields an overall pressure drop of 2.6 MPa. However, the velocities that were used in this calculation were those needed to remove the heat deposited in the blanket with the prescribed mixed-mean temperature rise of 150°C. When the velocities were increased to reduce the first wall temperature to acceptable levels the pressure drop became prohibitively high.

VII.1.2.6 Helical Flow Design

The helical flow design was developed in an effort to cool the first wall without increasing the average velocity and, thus, the pressure drop. As a result of its complex cross section, the helical design could not be analyzed vigorously. Nevertheless, an effort was made to provide estimates of the pressure drop. It was argued that when the turning vane is parallel to B the local pressure gradient is not affected by its presence, whereas, when the vane is normal to B, the local pressure gradient is doubled ("a" is halved). It was then assumed that, since the vane is turning continuously, the overall pressure drop will be increased by 1.5 (the average between 1.0 and 2.0). Under these assumptions, it was found that the overall pressure drop was 3.5 MPa. This pressure drop resulted in a hoop stress equal to the limiting value of 190 MPa. Given the large uncertainty of the assumptions that had to be

made to arrive at this value, and the absence of any margin for error, this design was rated conditionally acceptable and the reference design was developed.

VII.1.2.7 Poloidal-Toroidal Flow Reference Design

The design of both the inboard and outboard blankets involves poloidal manifolds and toroidal first wall channels. A three dimensional view of the flow channel arrangement is shown in Fig. VII.1-4. The layout of the blankets is shown to scale in Fig. VI.1-11. Coolant enters the magnetic field at a radial location of 12.2 m (point 1, not shown in Fig. VI.1-11) through a conduit of uniform cross sectional area of 0.43 m × 0.7 m. The effective cross sectional area changes at the point 2 to 0.43 × 0.66 m because of the presence of two 2" thick reflector plates placed near the outer wall of the conduit. Starting at point 3 the channels become inclined by 18° and their manifold cross sectional area for flow becomes 0.405 m × 0.6 m. As a result of this inclination, the poloidal manifolds terminate at the end walls of the sector and the flow is forced through appropriately designed openings to the toroidal channels. The toroidal channels run the entire width of the sector and communicate through similar openings with another poloidal manifold which takes the coolant out of the reactor. Geometric considerations dictate that there be seven manifolds/sector for the inboard blanket and forty-nine toroidal channels/manifold. The manifold cross section changes again at point 4 to 0.405 m × 0.5 m and remains constant thereafter until it reaches point 6 where it becomes again 0.405 m × 0.6 m. Beyond point 8 the cross sectional area remains constant at 0.43 m × 0.7 m. For the purposes of MHD analysis, only the wall thickness normal to the magnetic field is of consequence. This wall thickness is 8 mm from point 1 to point 3, 6 mm from point 3 to point 4, changes linearly from 6mm to 2 mm from point 4 to point 6, and remains constant at 2 mm until the exit from the magnetic field at point 9 (not shown in the figure). Figure VII.1-8 shows the details and dimensions of the cross sectional area of the poloidal manifolds and the toroidal channels. A development of the inboard blanket from point 3 to point 8 is shown in Fig. VII.1-12. In this development, and in the subsequent calculations, the expansion resulting from increased radius between points 4 and 3 and 6 and 8 is not taken into account. Such an expansion results in increased duct sizes and therefore decreased pressure drops. No credit for these decreases is

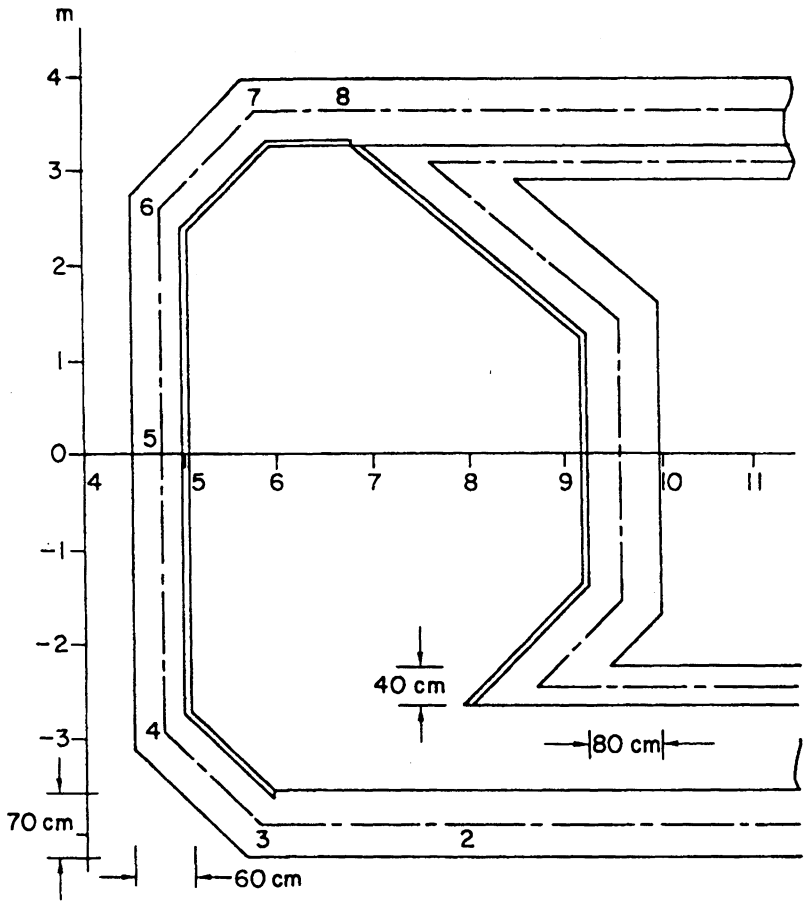

Figure VII.1.11. Poloidal view of blanket.

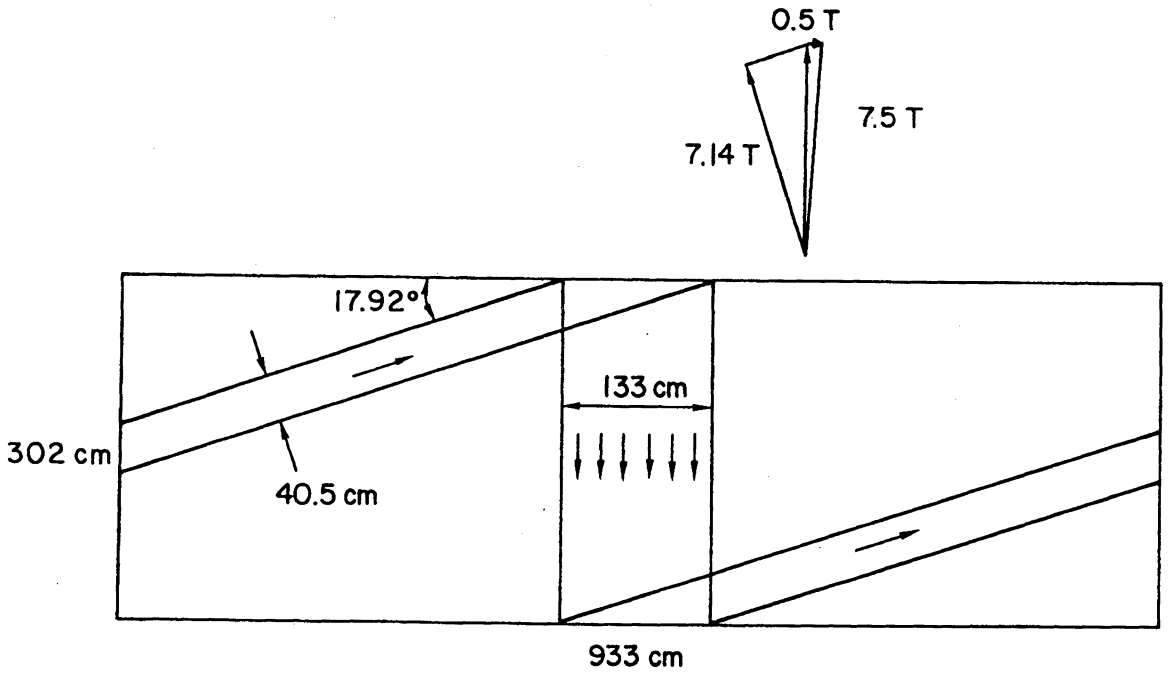

Figure VII.1.12. Diagram showing flow path of reference blanket concept.

taken because the non-uniformities in magnetic field and cross sectional area will introduce small increases in pressure drop.

To compute the pressure distribution along the flow path, the average velocity distribution must be known. The velocity, of course, depends on the cross sectional areas and the mass flow rate of the coolant which, in turn, depends on the energy deposition rate in the blanket and the specified mixed mean temperature rise.

In the following, the calculations for the pressure distribution in the inboard blanket are outlined. The analysis for the outboard blanket is identical.

The heat deposition in the inboard blanket is computed in MW's as

$$\dot{Q} = A(m^2) \times [5 \times 1.2 \times 0.9 + 0.5] \qquad \text{[VII.1-12]}$$

In the formula, A is the area of the surface facing the plasma, 5 represents the neutron wall loading, the factors 1.2 and 0.9 account for the energy multiplication and energy losses respectively, and 0.5 is the surface heat flux. For the inboard blanket the surface area is 36.6 m^2/sector. This results in an energy deposition rate of 191 MW/sector (27.3 MW/manifold); it was assumed that, because of the presence of the limiter, the energy deposition rate for the portion of the blanket between points 2 and 3 was half that given by the above formula.

As a result of this energy deposition rate and the specified mixed mean temperature rise of 150°C, the mass flow rate/manifold is 42.3 kg/s. The average coolant velocities in the poloidal manifolds are then as follows:

1-2	0.28 m/s
2-3	0.30 m/s
3-4	0.35 m/s
4-6	0.42 m/s
6-8	0.35 m/s
8-9	0.28 m/s

The velocity in the toroidal channels is 1.60 m/s.

The coolant flows through a series of interconnected channel segments of uniform cross section most of which are at right angles to the toroidal magnetic field.

The pressure gradient for a uniform channel segment in a uniform transverse magnetic field is given, as explained earlier, by:

$$\frac{dp}{dz} = \sigma V B^2 \frac{\Phi}{1 + \Phi} \qquad \text{[VII.1-13]}$$

where

V is the average velocity in the channel
σ is the coolant electrical conductivity
B is the magnetic field strength
Φ is the wall conductivity ratio

where

$$\Phi = \frac{\sigma_w t_w}{\sigma a}$$

σ_w is the wall electrical conductivity
t_w is the wall thickness (wall normal to the B field)
a is the half-channel width in the direction of B

(In the proposed design the channels have common walls; in this case t_w is one-half of the common wall thickness.)

If it is assumed that the magnetic field variations are small enough, equation [VII.1-13] can be integrated to give the pressure drop for those cases where the field is not uniform (horizontal segments of the manifolds). For a field variation given by B = 36/R the result is:

$$\Delta p = \sigma V \, 36^2 \left(\frac{1}{R_1} - \frac{1}{R_2}\right) \frac{\Phi}{1 + \Phi} \qquad \text{[VII.1-14]}$$

The pressure drop associated with strong variations of the magnetic field at the inlet and outlet is given by:

$$\Delta p = 0.2\ \sigma V B^2 a\ \sqrt{\phi} \qquad \text{[VII.1-15]}$$

The pressure drops associated with the bends in planes normal to B were estimated to be small, as were the pressure drops associated with the modest changes of wall thickness and cross-sectional area. To account for these small corrections, segments of the channels that were in diminishing magnetic fields were treated as if they were in their entirety in the maximum toroidal field.

Pressure drop associated with a bend from a channel transverse to B to one parallel to B is given by:

$$\Delta p = 0.5\ \sigma V B^2 a N^{-1/3}$$

$$= 0.5\ V^{4/3} B^{4/3} \sigma^{2/3} \rho^{1/3} a^{2/3} \qquad \text{[VII.1-16]}$$

where N is the interaction parameter = $\frac{\sigma a B^2}{\rho V}$, ρ is the coolant density, and "a" and V are the channel half width and coolant velocity associated with the channel normal to B.

When these formulas are applied to the inboard blanket they yield the following results:

Δp_{inlet}	= 0.03 MPa
Δp_{1-2}	= 0.35 MPa
Δp_{2-3}	= 0.36 MPa
Δp_{3-4}	= 0.36 MPa
Δp_{4-6}	= 1.22 MPa
Δp_{6-7}	= 0.12 MPa
Δp_{7-8}	= 0.05 MPa
Δp_{8-9}	= 0.12 MPa
Δp_{exit}	= 0.01 MPa
Δp_{bends}	= 0.26 MPa
poloidal → toroidal	
$\Delta p_{toroidal}$	= 0.15 MPa
Total Pressure Drop	= 3.03 MPa

If the outlet pressure is to be maintained at 0.2 MPa then the inlet pressure, accounting for the hydrostatic pressure should be 3.28 MPa.

The pressure distributions are therefore:

P_{inlet} = 3.28 MPa
P_1 = 3.25 MPa
P_2 = 2.90 MPa
P_3 = 2.54 MPa
P_4 = 2.18 MPa
P_6 = 0.92 MPa
P_7 = 0.79 MPa
P_8 = 0.73 MPa
P_8 = 0.32 MPa
P_9 = 0.20 MPa

In the above pressure distribution it was assumed that the poloidal to toroidal bend was made at point 8, since this distribution will stress the thin walls of the blanket the most. The two values for P_8 correspond to positions upstream and downstream of the toroidal channels.

Similar calculations performed for the outboard blanket have yielded a total drop of 1.7 MPa.

It should be stressed that the possibilities to optimize the design so that the MHD pressure drop is minimized have not been exhausted. Based on available information on MHD pressure drop calculations, it can be stated that, as more analysis and data become available, the pressure drop estimates should not change drastically.

VII.1.2.8 MHD Pressure Drop for Different Structural Materials

The preceeding calculations are based on lithium coolant and S/S structure. If vanadium is used in place of S/S the allowable temperature rise can be increased to 200°C. As a result, all the velocities will decrease by a factor of 0.75. However, the higher electrical conductivity of vanadium of 1.43×10^6 S/m, compared to 1.0×10^6 S/m for S/S, will cause the ϕ's to increase by a factor of 1.43.

The final result of this decrease in velocity and increase in conductivity ratio is that, for a vanadium blanket with $\Delta T = 200$ K temperature rise, the pressure drop will be 3.14 MPa for the inboard blanket and 1.71 MPa for the outboard.

VII.1.2.9 MHD Pressure Drop for Different Coolants

Although the MHD pressure drop appears to depend on the conductivity of the liquid, σ, the fact that Φ is inversely proportional to σ makes the fully developed flow pressure drop independent of σ. The pressure drop due to three-dimensional effects still depends on the conductivity of the liquid, but these pressure drops are only a small fraction of the overall pressure drop. As a result, changing coolant will effect the pressure drop mainly through a change in required coolant velocity.

For a given geometry, energy deposition rate, and mixed mean temperature rise, the coolant velocity is inversely proportional to the product $\rho \cdot C_p$. Although the density of LiPb is much larger than that of Li, its specific heat is much lower. In fact, the product of ρC_p for lithium and lithium/lead is almost identical. For this reason, the velocity distribution for LiPb will be identical to that for Li, as will the pressure drops for the fully developed or quasi-fully developed flow regions. The inlet and outlet pressure drops for the LiPb will be smaller by a factor of $\sqrt{\sigma_{Li}/\sigma_{LiPb}} \simeq 2$ from those for Li. The pressure drop for a bend from a conduit transverse to B to one parallel to B, will be the same for Li and LiPb because $(\sigma_{LiPb}/\sigma_L)^{2/3}(\rho_{LiPb}/\rho_{Li})^{1/3}$ is equal to one. Finally, the hydrostatic pressure for LiPb will be much larger than that for Li (0.72 MPa compared to 0.04 MPa). Therefore, if the coolant inlet is at the lower level, the inlet pressure will be 3.94 MPa. For the coolant entering from above the inlet pressure would be 3.22 MPa.

VII.1.3 Thermal Hydraulics Analysis

VII.1.3.1 Introduction

Thermal-hydraulics is an integral part of the design and analysis of liquid-metal blankets for fusion power reactors. It is directly coupled to the MHD analysis through the momentum equations. It receives input from the

neutronic analysis and provides input to the stress analysis. The objective of the thermal-hydraulic analysis is to determine whether adequate cooling is provided for both the first wall and the blanket under certain constraints such as geometry, surface heat flux, maximum interface temperature, thermal efficiency, etc.

The geometry considered is that of the reference design, i.e., poloidal/toroidal flow shown in Fig. VII.1-4. The structural material is austenitic steel (PCA) and the breeder/coolant is liquid lithium. Lithium lead (17Li-83Pb) is not considered to be compatible with stainless steel since the maximum interface temperatures is limited to 370°C as compared to ~ 420°C for lithium. This temperature limit plus the fact that the melting point for 17Li-83Pb is approximately 50°C higher than lithium make the ΔT window extremely narrow for 17Li-83Pb. Thus, 17Li-83Pb/PCA combination will not be considered here. Later when vanadium alloy is used as structural material, both lithium and lithium-lead will be evaluated as the breeder/coolant.

Neutron wall loading is fixed at 5 MW/m^2 and the surface heat flux employed is 0.5 MW/m^2. Parametric calculations were performed by varying the parameters such as the blanket thickness, the dimension of the first wall channels, the overall mean ΔT rise through the blanket, etc. In Sec. VII.1.3.2, the methods of analysis and major assumptions are described. The results of the parametric analysis and the reference design are presented in Sec. VII.1.3.3.

VII.1.3.2 Analyses and Assumptions

VII.1.3.2.1 First Wall

One side of the first wall is exposed to the plasma surface heat flux and the other side is cooled by the liquid-metal coolant. There is also bulk nuclear heating in the first wall itself. If the first wall is relatively thin and the temperature gradient in the radial direction is large compared to that in the other direction, then the steady state, one-dimensional, temperature distribution in the first wall is given by

$$T - T_o = q(t_1-x)/k + Q(t_1^2-x^2)/2k \qquad [VII.1-17]$$

where T_o is the coolant temperature at the structure/coolant interface, q is the surface heat flux, Q is the volumetric nuclear heat rate, t_1 is the thickness of the first wall in the radial direction, k is the thermal conductivity of the first wall material, and x is the radial distance measured from the plasma side. Maximum temperature always occurs on the plasma side (x = 0) and is

$$T_{max} = qt_1/k + Qt_1^2/2k + T_o \qquad [VII.1-18]$$

For a relatively thin first wall, the surface heat flux is usually the controlling factor under a typical fusion power reactor environment.

VII.1.3.2.2 Poloidal-Flow Blanket

Understanding the poloidal-flow blanket is a prerequisite for the understanding of the toroidal/poloidal-flow blanket. Furthermore, the results obtained for the poloidal-flow blanket will be used to estimate the maximum temperature in the toroidal/poloidal-flow blanket. This is why the analysis and the results of the poloidal-flow blanket are described here in detail. Poloidal-flow blanket is geometrically simple and consists of a vertical, straight duct with constant cross-sectional area. For heat transfer calculations, it will be assumed that the duct is rectangular. The following assumptions are made:

1. The flow is laminar and the velocity fluctuations carried from upstream (in the absence of a magnetic field) is completely suppressed in the blanket by the magnetic field.

2. Natural circulation induced by temperature gradient is completely suppressed by the magnetic field.

3. Variations in the toroidal direction are negligible and the flow and temperature fields are two-dimensional.

4. The boundary layers in the duct is extremely thin (due to high Hartmann's number ~ 10^5) and the velocity is essentially uniform over the entire cross section of the duct (slug flow).

Variations from the assumptions may affect the temperature profile significantly and should be investigated further in the future.

To calculate the temperature distribution in the poloidal-flow blanket, the computer code COMMIX is used.[12] COMMIX is a general-purpose, three-dimensional, transient, thermal-hydraulic code. COMMIX capability does not include the effect of magnetic field on the flow and temperature distribution. However, assumptions 1, 2, and 4 essentially include the influence of the magnetic field as a first approximation. The two-dimensional flow and temperature field in the blanket is divided into a number of computational cells. The first wall-coolant interface is subjected to a heat flux equal to the surface heat flux while no heat transfer occurs at the back of the blanket (insulated). Liquid-metal coolant comes in from the bottom and leaves the blanket at the top. Uniform mesh size is used in the vertical (y) direction while variable mesh is used in the radial (x) direction in anticipation of relatively large temperature gradient near the first wall. To accommodate assumption 2, one can either set the gravitational acceleration equal to zero or set the density equal to a constant. The difference turned out to be small over the temperature range covered in the present study. To accommodate assumption 4, slip boundary condition is used in the computation.

Typical temperature distributions across the blanket thickness at various axial (vertical) locations are shown in Fig. VII.1-13. Also shown in Fig. VII.1-13 is the variation of the nuclear heating rate (in the inboard blanket) with blanket thickness provided by neutronic calculations. It can be seen that there is a thermal boundary layer near the first wall where the temperature rises sharply due primarily to the effect of the surface heat flux. Away from the thermal boundary layer, the temperature gradient is relatively small. The maximum temperature always occurs at the first wall/coolant interface, and it increases with axial distance. For PCA/Li combination, the structure/coolant interface temperature is limited to 400°C. This temperature limit could be satisfied by increasing the average velocity over that shown in Fig. VII.1-13, and thus decreasing the maximum interface temperature. However, there are two other constraints which prevent one from doing so. The first constraint is that the mean ΔT rise through the blanket has to be maintained at a certain level from a thermal efficiency point of view. Mean ΔT rise through the blanket is inversely proportional to the average velocity.

Therefore, increasing the average velocity could decrease the mean blanket outlet temperature and make the design unattractive from an efficiency point of view. The second constraint is the MHD pressure drop which is directly proportional to the average velocity. A large pressure drop could cause a structural problem. The problem is particularly serious in the inboard region where the magnetic flux density is high ($\Delta p \alpha B^2$). Figure VII.1-14 shows the variation of maximum (interface) temperature with surface heat flux for various average velocities. These results were obtained for lithium at an axial distance of approximately 8 meters. It can be observed that in order to maintain the maximum interface temperature at 400°C for a surface heat flux of 0.5 MW/m^2, the average velocity has to be at least 5 m/s. Such a velocity would give a mean ΔT of ~ 7°C (for a blanket thickness of 0.65 m) and a ΔP of ~ 56 MPa (B_T = 7.5 T, wall thickness = 5 mm, blanket depth = 0.4 m) in the inboard region. This mean ΔT is one order of magnitude lower and the Δp is one order of magnitude higher than that considered to be acceptable and attractive. For vanadium alloy and lithium coolant, the interface and structural temperature limits are ~ 750°C. If a ΔT of 100-150°C is reserved for the temperature rise in the first wall, then the maximum interface-temperature limit is 600-650°C. Results in Fig. VII.1-14 show that the average velocity is approximately 0.75 m/s at a surface heat flux of 0.5 MW/m^2. This velocity is one order of magnitude smaller than the velocity of the case with an interface temperature limit of 400°C. However even with V = 0.75 m/s, the pressure drop is still rather large (Δp ~ 12 MPa) and the design does not look very attractive. These results demonstrate that the coolant is not removing the heat in the blanket and the first wall in a very efficient manner. The maximum interface temperature is too high and the mean temperature rise through the blanket is too low. The sharp temperature rise in the thermal boundary layer near the first wall is the result of relatively poor heat transfer, which is by molecular conduction only, and the result of relatively long fluid residence time (vertical length of the blanket divided by the average velocity) in the blanket. This critical, thermal-hydrualic problem can be alleviated by other design solutions. The various mechanical design configurations described in Sec. VII.1.1 are just a few of the many possible ways to reduce the maximum interface temperature while attempting to minimize the impact on other areas such as structural and MHD effects. Since the time and effort of this project does not allow each design to be analyzed in detail, a reference

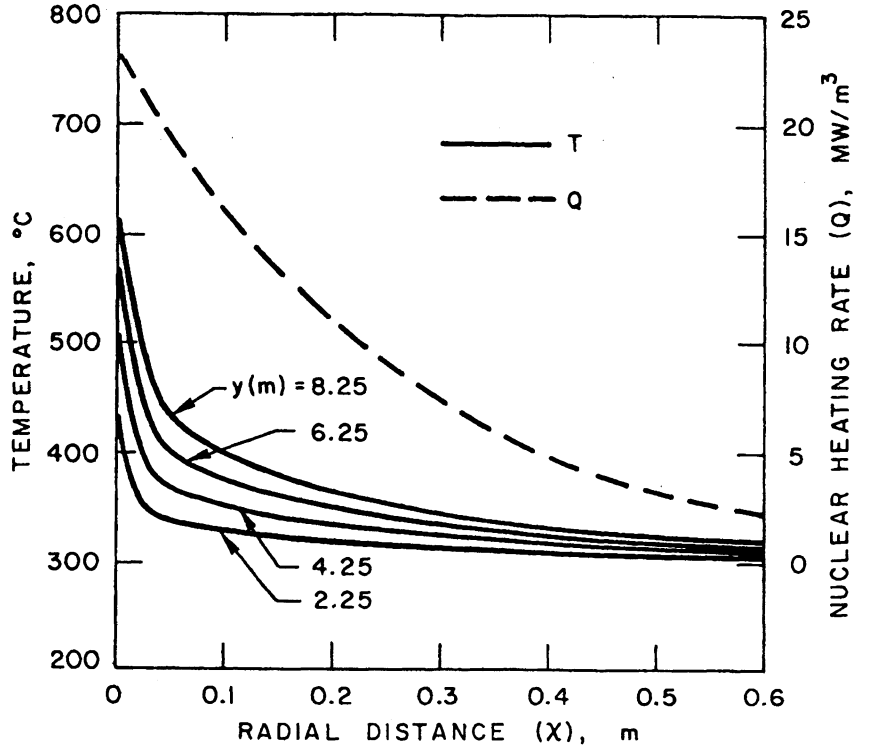

Figure VII.1-13. Radial temperature and nuclear heat rate distributions at various vertical locations in the inboard region of a poloidal flow blanket.

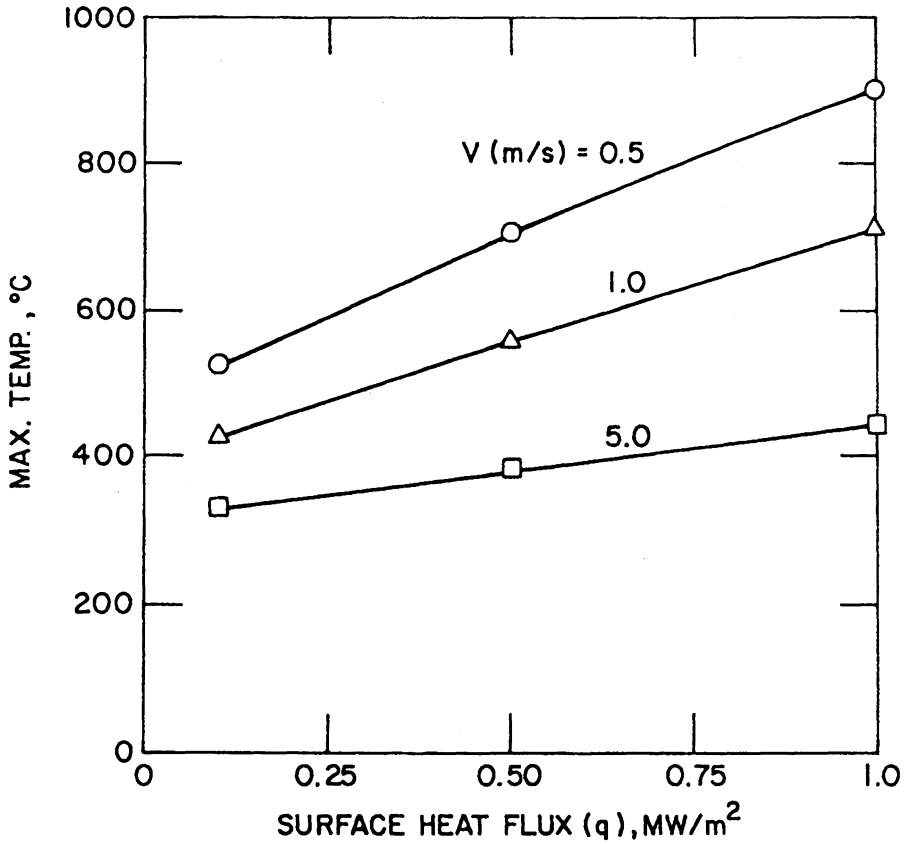

Figure VII.1-14. Maximum coolant temperature versus surface heat flux at a vertical height of 7.75 m of a poloidal flow blanket for various average coolant velocities.

design is selected for comparison purposes. The analysis of this reference design (toroidal/poloidal flow blanket) will be described next.

VII.1.3.2.3 Toroidal/Poloidal Flow Blanket

The toroidal/poloidal flow blanket is composed of mainly poloidal manifolds and toroidal first wall channels as shown in Fig. VII.1-4. The toroidal channels are adjacent to the first wall and thus are exposed to the surface heat flux in addition to volumetric nuclear heating. The poloidal manifolds receives a certain amount of heat from the first wall by conduction through the common walls in addition to volumetric nuclear heating. It is important to keep the velocity in the manifld as low as possible since a large portion of total pressure drop occurs here as a result of a strong toroidal magnetic field. It is possible to do so because the nuclear heating rate decreases rapidly away from the first wall. The heat conducted from the first wall channels to the manifolds should be minimized so that the maximum temperature in the manifold can be maintained relatively low at such low velocities. One way to do this is to keep the width of the first wall channel approximately equal to or greater than the thickness of the thermal boundary layer shown in Fig. VII.1-13. The temperature gradients on either side of the common wall between the manifold and the first wall channels will be relatively small. Thus, to a first approximation, heat transfer by conduction between the first wall channels and the manifold can be neglected.

The temperature distributions in the first wall channel can be calculated in the same manner as that described in Section VII.1.3.2.2. The vertical coordinate (y) is now replaced by the horizontal coordinate in the toroidal direction (z). The assumptions described in Section VII.1.3.2.2 are again employed here. It is further assumed that the flow from the manifold is evenly distributed among the first wall channels and that the transition from manifold to first wall channels (or vise versa) does not invalidate assumptions 1 to 4 described in Section VII.1.3.2.2.

The temperature distribution in the manifold is expected to be relatively flat and is assumed to be uniform in the radial direction before the flow turns into the first wall channels. The temperature rise in the slanted manifold can be estimated in the following manner. The volumetric heat distribution shown in Fig. VII.1-13 can be expressed approximately by the following equation:

where q is expressed in MW/m^2. In deriving Eq. [VII.1-22] z was set equal to ℓ in Eq. [VII.1-21]. Thus, Eq. [VII.1-22] gives the fractional ΔT through the manifold as a function of blanket width (b), first wall channel dimension (b_1), and surface heat flux (q).

VII.1.3.3 Results

VII.1.3.3.1 Parametric Studies

Figure VII.1-15 shows the variation of the maximum structural temperature with first wall thickness for various structure/coolant interface temperatures with q = 0.5 MW/m^2. In Fig. VII.1-15 the structural material is PCA (Q = 49.2 MW/m^3, k = 20 W/m-k), and the coolant is lithium. It can be observed that the maximum structural temperature increases monotonically with wall thickness and with interface temperature (T_o). If the interface temperature is 400°C (maximum limit for PCA/Li combination) and the maximum structural limit is 550°C, Fig. VII.1-15 indicates that the wall thickness should not be greater than 5 mm. Fig. VII.1-16 shows a similar result for vanadium alloy (Q = 20 MW/m^3, k = 28 W/m-k). If the interface temperature is 500°C and the structural temperature limit is 750°C, Fig. VII.1-16 indicates that the first wall thickness can be over 11 mm without exceeding the temperature limit. The results for q = 1 MW/m^2 are shown in Figs. VII.1-17 and VII.1-18.

To show the results for the first wall channels and the manifold, it is helpful to refer to the nomenclature shown in Fig. VII.1-19. As shown in Fig. VII.1-19, there are a large number of geometrical parameters, and it is not feasible at this time to perform parametric analysis of all these parameters. Only the important parameters such as total blanket thickness (2b), total ΔT rise through the blanket, and surface heat flux (q) will be varied. Emphasis will be placed on the inboard region where the constraints are more restrictive than the outboard region.

Figure VII.1-20 shows the variation of mean velocity in the manifold and the first wall channel with overall blanket thickness (2b) for two different mean ΔT rise through the blanket. The surface heat flux is 0.5 MW/m^2 and the rest of the geometrical parameters are fixed. It can be observed that the velocity in the manifold decreases with blanket thickness while the velocity in the first wall channel increases with blanket thickness. When the blanket

$$Q = Q_o \, e^{-4x} \qquad \text{[VII.1-19]}$$

where Q_o is the nuclear heating rate at the first wall/fluid interface ($Q_o \cong 24$ MW/m^3 for the inboard blanket and $Q_o = 26$ MW/m^3 for the outboard blanket), and x is the radial distance measured from this interface. It will be assumed that Eq. [VII.1-19] applies to the toroidal/poloidal flow blanket. Steady-state energy balance for the manifold gives

$$\dot{m} \, C_p \, \Delta T_m = 2az \int_{b_1}^{2b} Q \, dx \qquad \text{[VII.1-20]}$$

where $\dot{m}$ is the mass flow rate through a blanket section, C_p is the specific heat of the fluid, ΔT_m is the mixed mean temperature rise in the manifold, z is the coordinate in the poloidal (vertical) direction, 2a is the blanket width in the toroidal direction, 2b is the blanket thickness in the radial direction, and b_1 is the thickness of the first wall channel (including wall thicknesses) in the radial dirction. The total mean ΔT_t, including the first wall channels, rise through the blanket is

$$\dot{m} \, C_p \, \Delta T_t = 2a\ell \left(q + \int_o^{2b} Q dx\right) \qquad \text{[VII.1-21]}$$

where ℓ is the total length of the blanket in the poloidal direction exposed to the surface heat flux q. Dividing Eq. [VII.1-20] by Eq. [VII.1-21] and utilizing Eq. [VII.1-19],

$$\frac{\Delta T_m}{\Delta T_t} = \frac{\left(e^{-4b_1} - e^{-8b}\right)}{q + \left(1 - e^{-8b}\right)} \qquad \text{[VII.1-22]}$$

where q is expressed in MW/m^2. In deriving Eq. [VII.1-22] z was set equal to ℓ in Eq. [VII.1-21]. Thus, Eq. [VII.1-22] gives the fractional ΔT through the manifold as a function of blanket width (b), first wall channel dimension (b_1), and surface heat flux (q).

VII.1.3.3 Results

VII.1.3.3.1 Parametric Studies

Figure VII.1-15 shows the variation of the maximum structural temperature with first wall thickness for various structure/coolant interface temperatures with q = 0.5 MW/m^2. In Fig. VII.1-15 the structural material is PCA (Q = 49.2 MW/m^3, k = 20 W/m-k), and the coolant is lithium. It can be observed that the maximum structural temperature increases monotonically with wall thickness and with interface temperature (T_o). If the interface temperature is 400°C (maximum limit for PCA/Li combination) and the maximum structural limit is 550°C, Fig. VII.1-15 indicates that the wall thickness should not be greater than 5 mm. Fig. VII.1-16 shows a similar result for vanadium alloy (Q = 20 MW/m^3, k = 28 W/m-k). If the interface temperature is 500°C and the structural temperature limit is 750°C, Fig. VII.1-16 indicates that the first wall thickness can be over 11 mm without exceeding the temperature limit. The results for q = 1 MW/m^2 are shown in Figs. VII.1-17 and VII.1-18.

To show the results for the first wall channels and the manifold, it is helpful to refer to the nomenclature shown in Fig. VII.1-19. As shown in Fig. VII.1-19, there are a large number of geometrical parameters, and it is not feasible at this time to perform parametric analysis of all these parameters. Only the important parameters such as total blanket thickness (2b), total ΔT rise through the blanket, and surface heat flux (q) will be varied. Emphasis will be placed on the inboard region where the constraints are more restrictive than the outboard region.

Figure VII.1-20 shows the variation of mean velocity in the manifold and the first wall channel with overall blanket thickness (2b) for two different mean ΔT rise through the blanket. The surface heat flux is 0.5 MW/m^2 and the rest of the geometrical parameters are fixed. It can be observed that the velocity in the manifold decreases with blanket thickness while the velocity in the first wall channel increases with blanket thickness. When the blanket

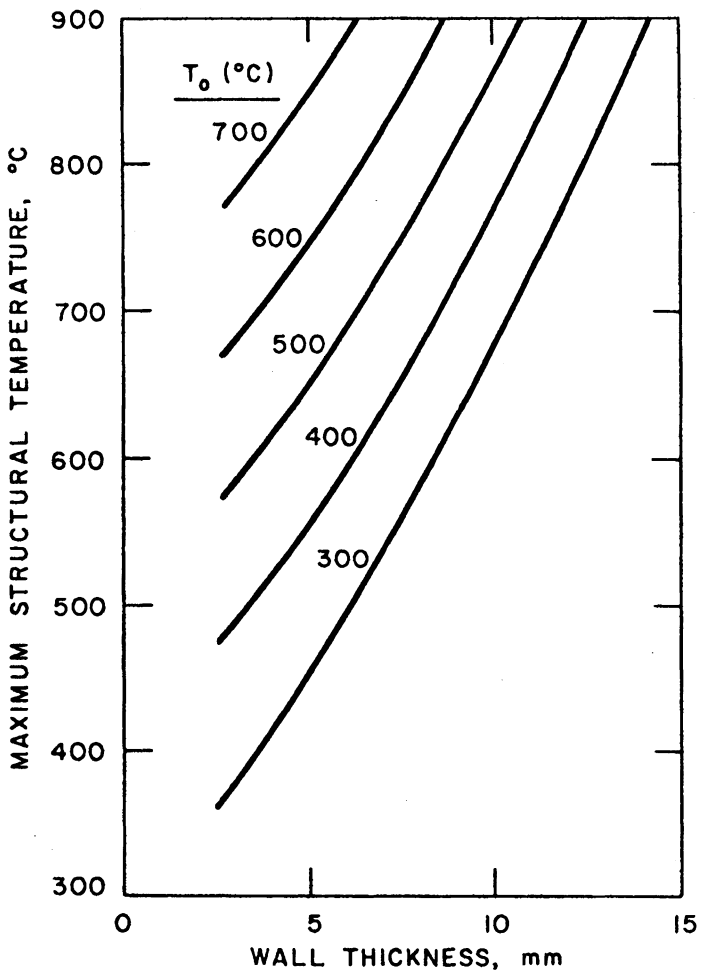

Figure VII.1-15. Maximum structural (PCA) temperature versus first wall thickness for various interface temperatures with q = 0.5 MW/m^2.

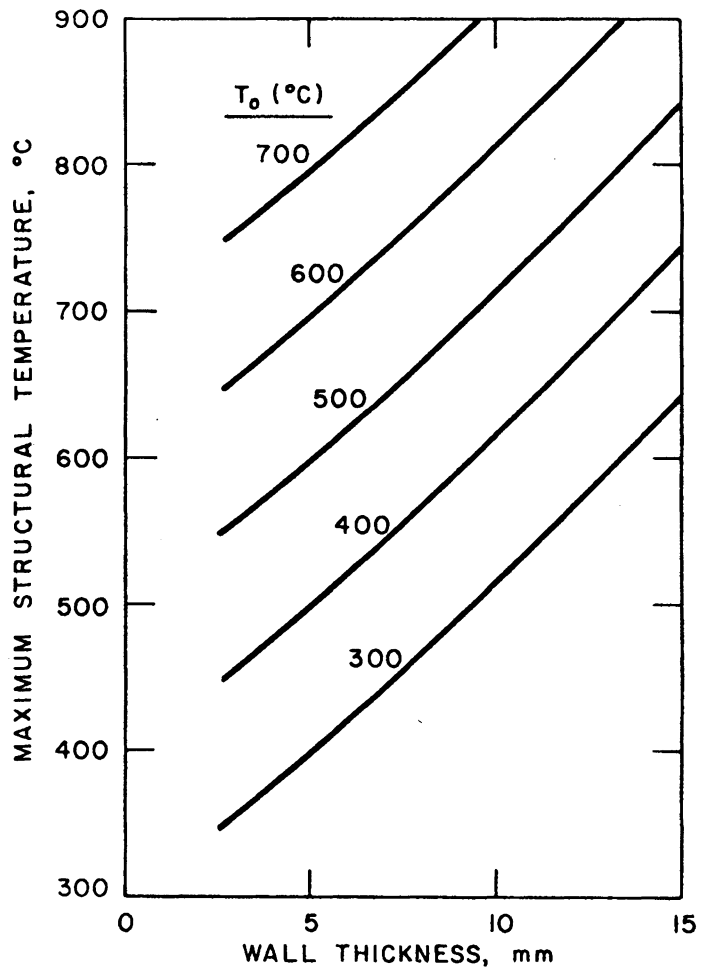

Figure VII.1-16. Maximum structural (vanadium) temperature versus first wall thickness for various interface temperatures with q = 0.5 MW/m^2.

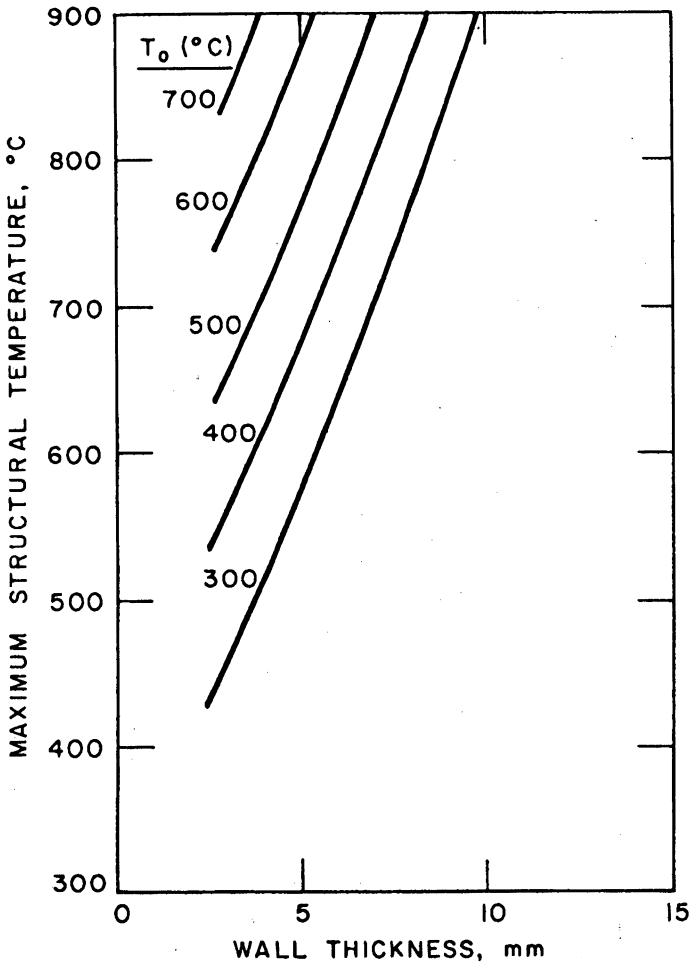

Figure VII.1-17. Maximum PCA structural temperature versus first wall thickness for various interface temperatures with $q = 1\ MW/m^2$.

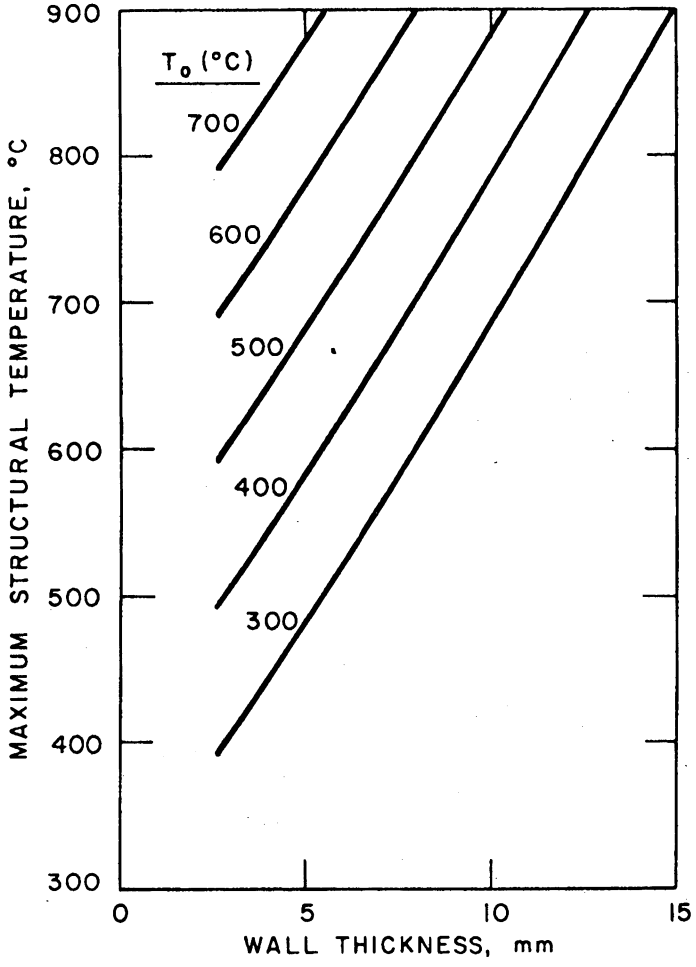

Figure VII.1-18. Maximum vanadium structural temperature versus first wall thickness for various interface temperatures with $q = 1\ MW/m^2$.

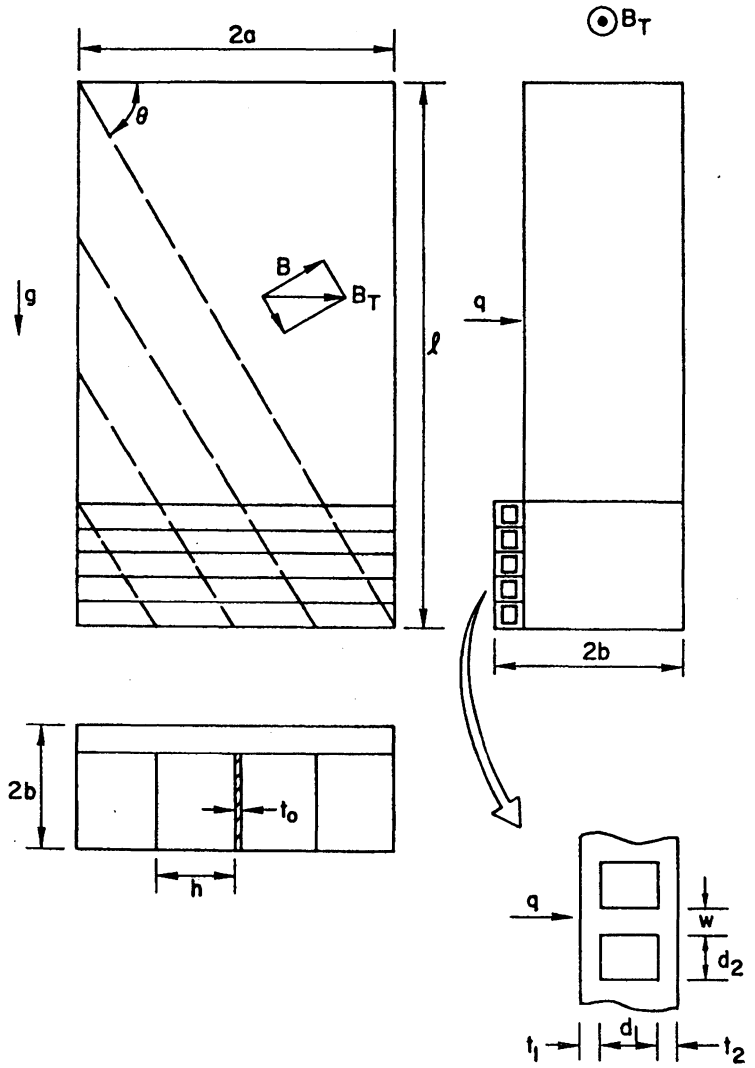

Figure VII.1-19. Definitions of geometrical parameters of the toroidal/poloidal flow blanket.

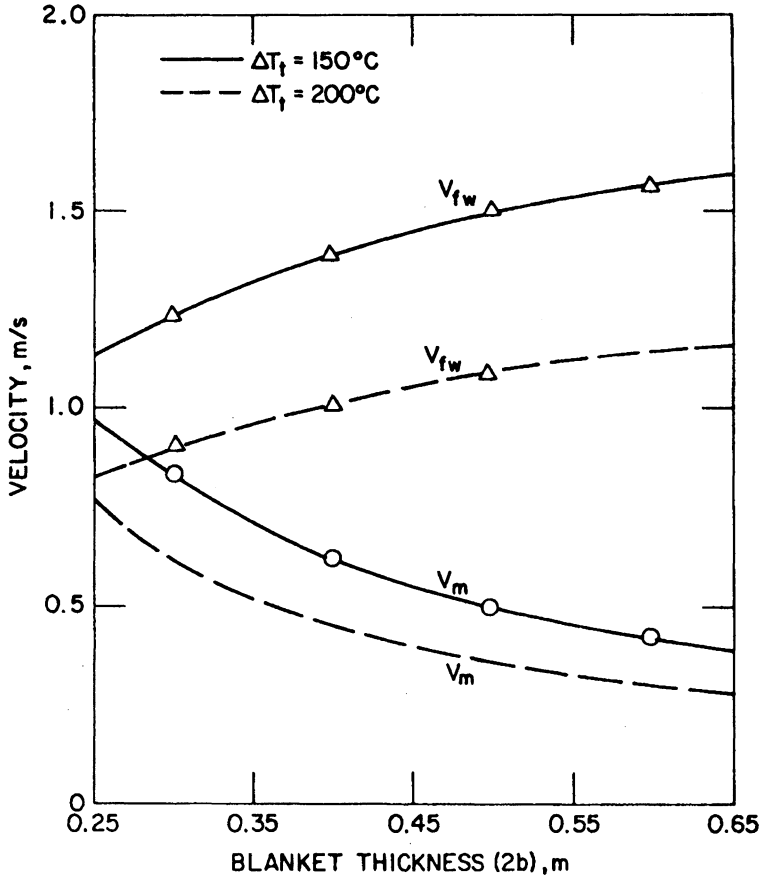

Figure VII.1-20. Variation of the velocities in the manifold and the toroidal channels with blanket thickness for two different ΔT rise through the inboard blanket with q = 0.5 MW/m^2.

thickness (2b) is increased, Eq. [VII.1-21] indicates that the total mass flow (m) is increased for a given total ΔT rise through the blanket. Since all the mass flow must pass through the first wall channels, the velocity in the first wall channel has to increase with blanket thickness. To see how the velocity in the manifold varies with the blanket thickness, Eq. [VII.1-21] can be written in the following form

$$V_m = \frac{\ell \left(q + \int_0^{2b} Q dx\right)}{2b\rho C_p \Delta T_t} \qquad \text{[VII.1-23]}$$

As 2b increases, the value of the integral increases. However, the numerator increases less rapidly than the denominator in Eq. [VII.1-23] and the net result is that V_m decreases with increasing blanket thickness. The increase in total ΔT rise through the blanket helps to reduce the velocities in both the manifold and the first wall channels and, therefore, is desirable from a pressure drop viewpoint. It is also desirable from a pressure drop viewpoint to reduce the manifold velocity since the largest Δp occurs in the manifold as a result of relatively large transverse magnetic field and long fluid path (ℓ).

To estimate the maximum fluid temperature in the blanket, the mean temperature rise in the manifold (it was assumed that the temperature is uniform in the radial direction in the manifold) and the maximum temperature increase in the first wall channel must be determined. Figure VII.1-21 shows the variation of maximum temperature increase in the first wall channel with the velocity in the channel for various values of the blanket depth in the toroidal direction. The curves in Fig. VII.1-21 are obtained from the two-dimensional analysis similar to that shown in Fig. VII.1-13. For a given velocity in the first wall channel (which can be obtained from Fig. VII.1-20 and given blanket depth (for example, 2a = 3m for the inboard blanket of reference design), the variation of maximum temperature increase in the first wall channel with blanket thickness (2b) can be obtained, and the results are shown in Fig. VII.1-22. Also shown in Fig. VII.1-22 are the results of mean ΔT rise through the manifold calculated by using Eq. [VII.1-22]. As shown in Fig. VII.1-22, the mean ΔT rise through the manifold increases with overall blanket thickness as a result of the decrease in manifold velocity with increasing blanket thickness. The maximum temperature rise in the first

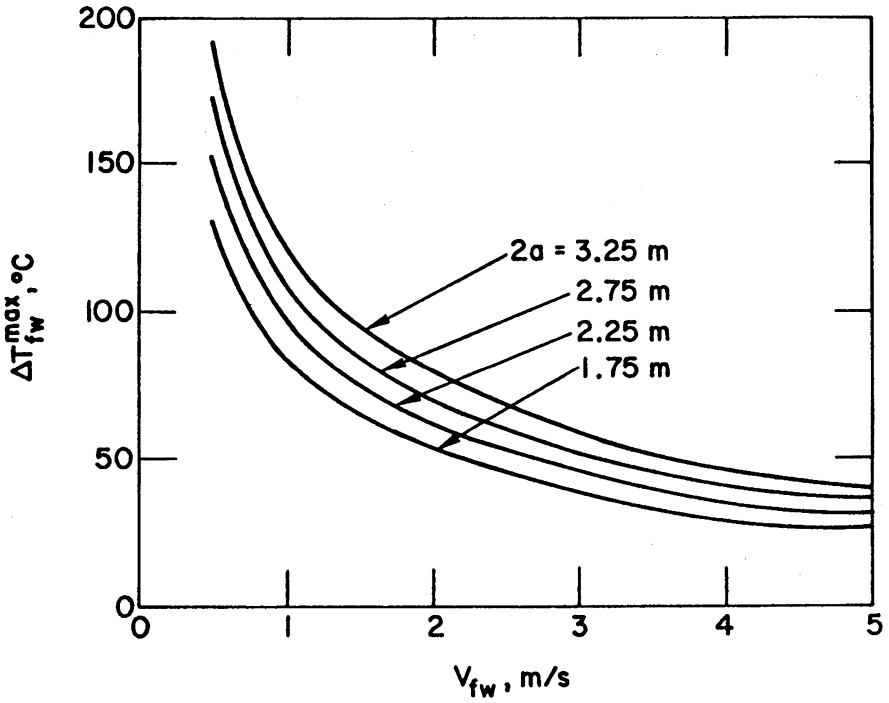

Figure VII.1-21. Variation of maximum temperature rise with velocity in the toroidal channels with q = 0.5 MW/m^2.

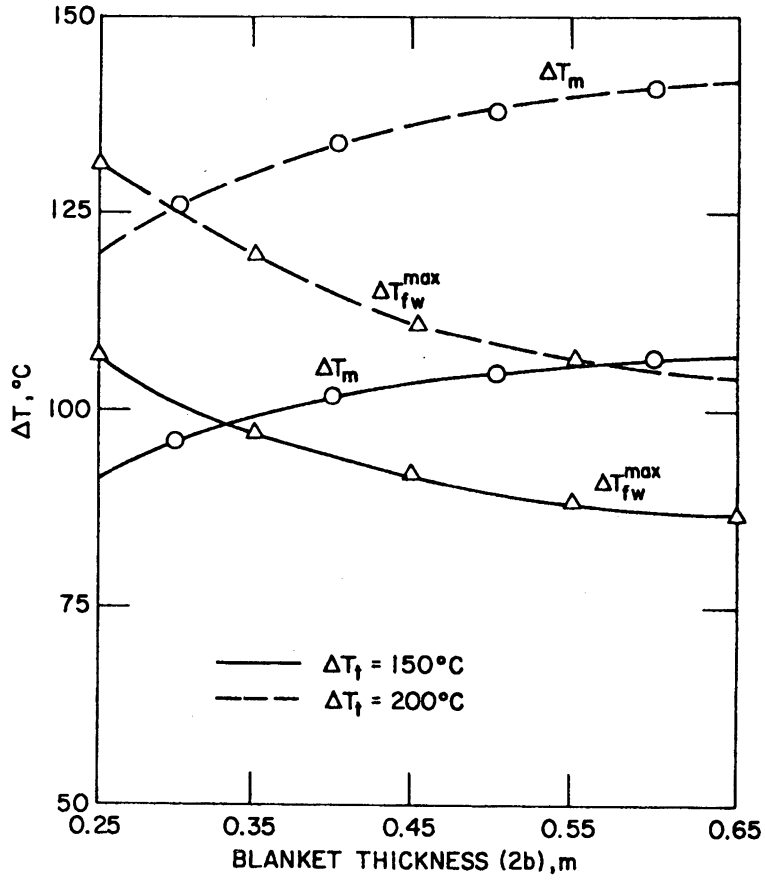

Figure VII.1-22. Variations of maximum temperature rise in the toroidal channels and mean temperature rise in the manifold with blanket thickness for two different ΔT_t and with q = 0.5 MW/m^2.

wall channel decreases with overall blanket thickness as a result of the velocity increase in the first wall channel.

The maximum temperature rise through the entire blanket can then be estimated by adding ΔT_m and ΔT_{fw}^{max}, and the results are shown in Fig. VII.1-23 for various coolant inlet temperature (T_i). The results shown in Fig. VII.1-23 actually apply only to the last manifold (the one that moves all the way up before turning into the last 45 channels near the top of the inboard blanket) and the toroidal channels supplied by this manifold. The maximum temperature is likely to be near the exit of the toroidal channels at the top of the blanket since there is little time for heat transfer to occur and the maximum temperatures in these toroidal channels are not reduced compared to other toroidal channels located at lower levels. Figure VII.1-23 indicates that the maximum coolant temperature is almost independent of the overall blanket thickness. This is the consequence of the result shown in Fig. VII.1-22 where ΔT_m and ΔT_{fw}^{max} varies in the opposite direction as blanket thickness is increased.

Similar results are obtained for the outboard blanket and the detail will not be presented here since the constraints are less restrictive compared to the inboard blanket. It should be noted that the results described applies to both PCA and vanadium alloy since the properties of the structural materials do not affect the coolant heat transfer calculations under steady-state condition.

VII.1.3.3.2 Reference Design

The reference design is the toroidal/poloidal flow blanket with lithium as the breeder/coolant and PCA as the structural material. The surface heat flux (q) is assumed to be 0.5 MW/m^2. Many of the geometrical parameters (such as t_o, t_1, t_2, d_1, d_2, h, and W in Fig. VII.1-19) are determined from stress, MHD, as well as heat transfer considerations. Once these geometrical parameters are chosen for the reference design, the maximum interface (coolant/structure) temperature and the maximum structural temperature can be estimated from the results described in Sec. VII.1.3.3.1. Table VII.1-1 lists the parameters related to thermal hydraulics for the reference design.

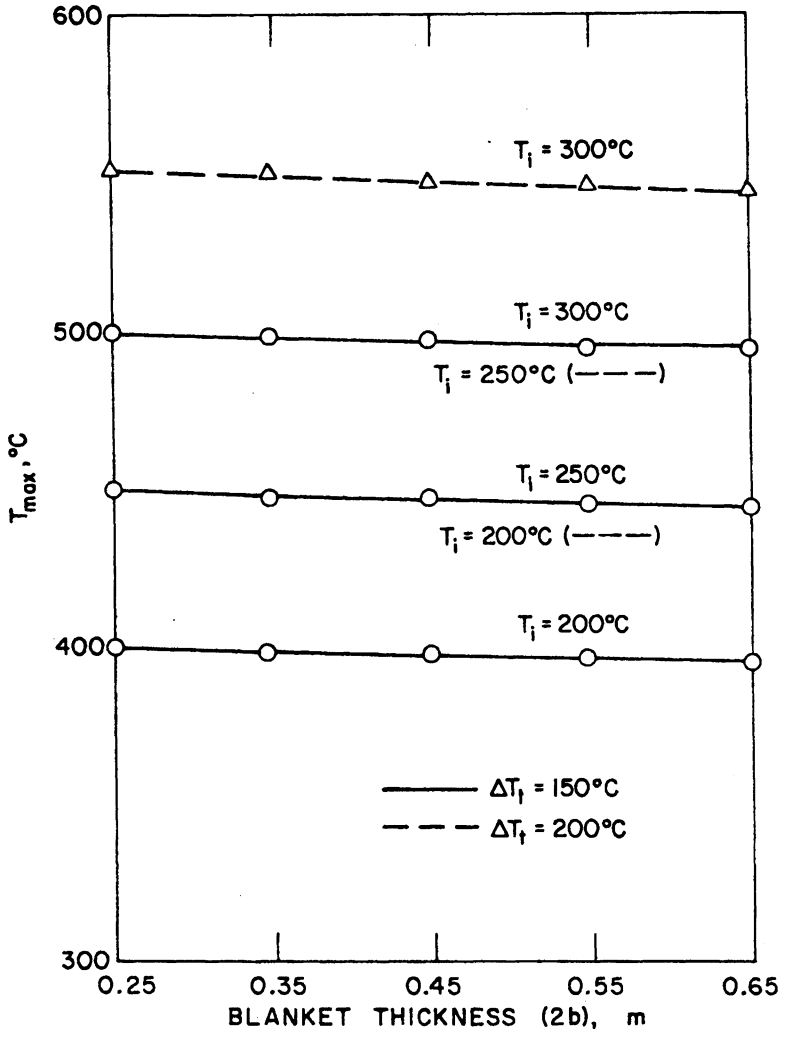

Figure VII.1-23. Variations of maximum temperature with blanket thickness for different inlet temperatures and ΔT_t with $q = 0.5\ MW/m^2$.

TABLE VII.1-1. A LIST OF PARAMETERS FOR THE REFERENCE DESIGN CONDITIONS OF A TOROIDAL/POLOIDAL FLOW BLANKET

Description	Inboard	Outboard
1. Neutron Wall Loading, MW/m^2	5	5
2. Surface Heat Flux, MW/m^2	0.5	0.5
3. Vertical Length of Blanket Exposed to Surface Heat Flux (ℓ), m	9.3	7.0
4. Blanket Thickness (2b), m	0.6	0.8
5. Blanket Depth (2a), m	3.0	5.0
6. Number of Manifold (N)	7 or 8	12
7. Number of Toroidal Channel (n)	332	270
8. Manifold Depth (h), m	0.4	0.4
9. Average Manifold Wall Thickness (T_o), mm	4	5
10. First Wall Thickness (t_1), mm	5	5
11. Wall Thickness Between Toroidal Channel and Manifold (t_2), mm	15	15
12. Toroidal Channel Width (d_1), mm	45	45
13. Toroidal Channel Height (d_2), mm	25	24
14. Wall Thickness of Toroidal Channel in the Poloidal Direction (W), mm	3	2
15. Coolant Inlet Temperature (T_i), °C	225	225
16. Overall Mean Temperature Rise Through the Blanket (ΔT_t), °C	150	150
17. Maximum Interface Temperature (T_o), °C	420	420
18. Maximum Structural Temperature	575	575
19. Average Velocity in Manifold (V_m), m/s	0.42	0.28
20. Average Velocity in Toroidal Channel (V_{fw}), m/s	1.56	2.50

It should be noted that the maximum interface temperature and the maximum structural temperature occur only over a very limited area near the top of the blanket.

It is interesting to find out what kind of temperature distributions exist at different locations of the blanket. With the help of the assumptions and analyses described in Sec. VII.1.3.2, temperature distributions in the first wall and the blanket can be established. Figure VII.1-24 shows the temperature distributions in the radial direction at two locations. The first location is near the top of the blanket ($y \simeq \ell$) and the second location is near the mid-section of the blanket ($y \simeq \ell/2$). Both locations are at the center of the blanket sector, i.e., midway between the entrance and the exit of the toroidal channel. In the manifold, the temperature is assumed to be uniform radially, and the mixed mean temperature depends on the vertical location. In the toroidal channel, the temperature distribution is obtained in a manner similar to that shown in Fig. VII.1-13. The magnitude of the temperature in the toroidal channel also depends on the vertical location of the channel since it determines the inlet temperature to the toroidal channel. The first wall temperature distribution depends on the interface temperature and the wall thickness.

For a relatively thin wall, the first wall temperature is fairly linear. The only unknown temperature distribution is that of the wall between the manifold and the toroidal channels (dashed line in Fig. VII.1-24). In the analysis, it was assumed that there is no heat exchange between the manifold and the toroidal channel. This is, of course, not strictly valid. Figure VII.1-24 indicates that there is some conduction between the two since a temperature difference exists. However, this effect is probably small and it does not affect the maximum temperature which always occurs at the first wall/coolant interface.

VII.1.4 Stress Analysis

The bulk of the stress analysis for the inboard blanket/shield was carried out using linear elasticity theory. The computed stresses were categorized as primary and secondary and various limits (given in Chapter IV) were applied to these stresses following the procedures set forth in ASME Boiler and Pressure Vessels Code, Section III.

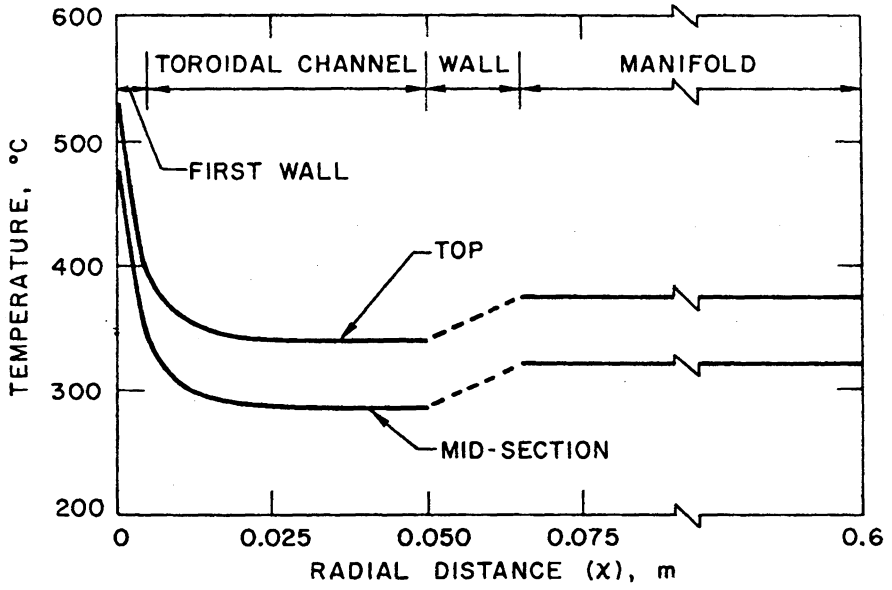

Figure VII.1-24. Radial temperature distribution of the first wall and blanket of a toroidal/poloidal blanket (reference design) with q = 0.5 MW/m^2.

NOMENCLATURE FOR SECTION VII.1.3

$2a$ = Blanket depth in the toroidal direction.

$2b$ = Blanket thickness in the radial direction.

b_1 = Thickness of toroidal channels (including the walls) in the radial direction.

B_T = Magnetic flux density in the toroidal direction.

C_p = Specific heat.

d_1 = Width of the toroidal channel in the radial direction.

d_2 = Height of the toroidal channel in the vertical direction.

g = Gravitational acceleration.

h = Manifold depth in the toroidal direction.

k = Thermal conductivity.

ℓ = Vertical (poloidal) length of blanket exposed to the surface heat flux.

n = Number of toroidal channel.

N = Number of poloidal manifold.

Δp = Pressure drop.

q = Surface heat flux.

Q = Nuclear heating rate.

t_o = Wall thickness of manifold in the toroidal direction.

t_1 = First wall thickness.

t_2 = Thickness of common wall between the toroidal channel and poloidal manifold.

T = Temperature.

T_i = Inlet temperature to the blanket.

T_{max} = Maximum first wall or liquid-metal temperature in the blanket.

T_o = Coolant/First-wall interface temperature.

ΔT_m = Mean temperature rise through the poloidal manifold.

ΔT_{fw}^{max} = Maximum temperature rise through the first wall (toroidal) channels.

ΔT_t = Total mean temperature rise through the blanket (and toroidal channel).

V = Average velocity in the poloidal flow blanket.

V_{fw} = Average velocity in the toroidal channel.

V_m = Average velocity in the poloidal manifold.

W = First wall (toroidal) channel thickness in the vertical (poloidal) direction.

x = Radial (horizontal) coordinate.

y = Poloidal (vertical) coordinate.

z = Toroidal coordinate.

ρ = Density.

The main conclusions drawn from the present analysis are as follows: (1) A critical problem for both the reference design and the poloidal helical flow design is the MHD/stress effects in the manifold dividing sidewalls. A design with the same uniform wall thickness in the inboard vertical and the top and bottom horizontal blankets using either PCA (25% cold worked) or V-15Cr-5Ti (strain hardened) cannot meet the primary stress criterion for any blanket thickness less than 80 cm. However, acceptable designs can be developed by tailoring the sidewall thickness in the inboard and the top and bottom horizontal blankets. (2) As far as the manifold sidewalls are concerned, PCA (at 100 dpa and system ΔT = 150°C) has the same design margin as V-15Cr-5Ti (at 200 dpa and system ΔT = 200°C) because its higher allowable stress and lower electrical conductivity make up for its drawback of being able to sustain a smaller system ΔT than vanadium. Vanadium would be more attractive than PCA if its end-of-life fluence level were reduced to 100 dpa and the system ΔT were increased to 250°C. (3) The maximum first wall thickness of the reference design for a surface heat flux of 50 W/cm^2 is 4.2 mm for PCA and $\geq$ 10 mm for V-15Cr-5Ti. From a thermal stress viewpoint, vanadium is vastly superior to PCA. A vanadium first wall of 5.5 mm thickness can sustain a surface heat flux of at least 100 W/cm^2 and quite possibly greater. To withstand such a high wall loading using PCA, the first wall has to be grooved. The minimum first wall thickness necessary to sustain the coolant pressure is 2.2 mm for PCA and 4.5 mm for V-15Cr-5Ti. (4) The high thermal stress in the first wall can be relaxed by radiation induced creep in a few dpa. The swelling stress in the first wall for PCA is relatively low up to a fluence of 100 dpa.

VII.1.4.1 Primary Stress

Primary stress is any normal or shear stress developed by an imposed loading which is necessary to satisfy the laws of equilibrium between the external load and the internal forces and moments. The various limits to the primary stresses are as follows:

(1) General primary membrane stress intensity, P_m.

$$P_m \leq S_{mt}$$

(2) Primary local membrane stress intensity, P_L, and primary local bending stress intensity, Pb.

$$P_L + P_b \leq 1.5\ S_m \text{ and}$$

$$P_L + \frac{P_b}{1.25} \leq S_t$$

VII.1.4.1.1 Reference Design

The inboard first wall, first wall coolant channels and the back plate (Fig. VII.1-12) were analyzed as a composite anisotropic plate supported radially at regular intervals by the dividing walls of the manifold which are at an angle ϕ ($\approx 15°$) to the vertical direction. A detailed analysis showed that the maximum primary bending stress intensity in the first wall is given by:

$$P_b = \frac{Ez}{D_x - \nu^2 D_y} \frac{p\ell^2}{12} \left[\cos^2\phi + \frac{D'_{x_1y_1}}{D_{x_1}} \sin^2\phi + \frac{D''_{x_1y_1}}{D_{x_1}} \sin 2\phi + \frac{\nu}{1-\nu^2} \frac{D_x - D_y}{D_y} \left(\sin^2\phi + \frac{D'_{x_1y_1}}{D_{x_1}} \cos^2\phi - \frac{D''_{x_1y_1}}{D_{x_1}} \sin 2\phi\right)\right] \qquad [VII.1-24]$$

where

E = Young's modulus.

ν = Poisson's ratio.

z = Distance from the centroidal axis of the composite beam to the plasma side of the first wall.

p = Pressure in the manifold.

ℓ = Distance between manifold dividing walls.

D_x, D_y = Elastic bending stiffnesses of the plate for bending in the toroidal (x) and poloidal (y) direction, respectively.

$D_{x_1}, D'_{x_1y_1}, D''_{x_1y_1}$ = Transformed bending stiffnesses in the x_1, y_1 axes defined by the direction of the manifold dividing walls. $x1$ is at angle of ϕ to x axis.

$$D_{x_1} = D_y + (D_x - D_y) \cos^4 \phi.$$

$$D'_{x_1 y_1} = \nu D_y + (D_x - D_y) \sin^2 \phi \cos^2 \phi.$$

$$D''_{x_1 y_1} = \frac{2}{3} (D_x - D_y) \cos^2 \phi \sin 2\phi.$$

Figure VII.1-25a gives a plot of the primary stress as a function of the first wall thickness and coolant pressure. Since the maximum pressure of the manifold is of the order of 3 MPa, a minimum first wall thickness of 2.2 mm is necessary to satisfy the primary stress criterion using a 25% cold worked PCA (100 dpa) structural material. If strain hardened V-15Cr-5Ti (200 dpa) is used as the structural material, then the minimum thickness necessary is 4.5 mm. Both these minimum thicknesses are controlled by radiation induced creep strain limits and can be further reduced by reducing the design fluence levels.

VII.1.4.1.2 Poloidal Helical Flow Design

The general primary membrane stress intensity in the first wall of the poloidal helical flow design is

$$P_m = \frac{pa}{t} \qquad [VII.1.-25]$$

where

p = Pressure of coolant.
a = Radius of semicircular first wall.
t = Thickness of first wall.

Figure VII.1-25b shows a variation of the general primary membrane stress intensity as a function of the first wall thickness and coolant pressure. Since the coolant pressure in this design may be somewhat higher than in the reference design, a minimum thickness of 3.5 mm of 25% cold worked PCA (at 100 dpa) may be necessary to satisfy the general primary membrane stress intensity criterion if the maximum coolant pressure is 3.5 MPa. If strain hardened V-15Cr-5Ti is used as the structural material, then the minimum thickness required is about 5 mm for a design fluence of 200 dpa. As in the reference

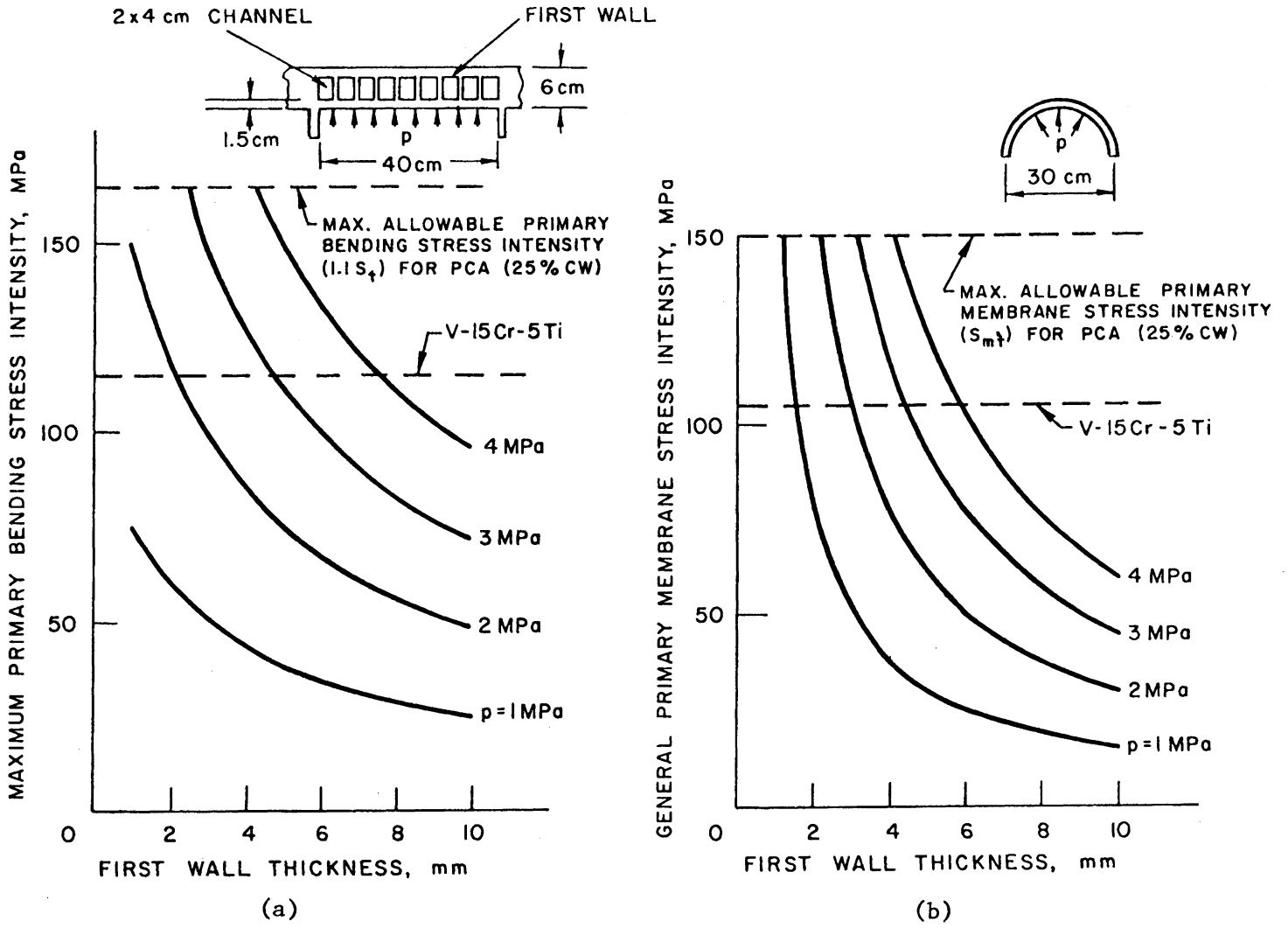

Figure VII.1-25. Maximum primary stresses in the first wall for (a) reference design and (b) poloidal helical flow design.

design these minimum thicknesses can be further reduced by cutting back on the design fluence levels.

VII.1.4.1.3 Blanket Manifold

The dividing side walls of the manifold for either design are subjected to a general primary membrane stress intensity given by:

$$P_m = \frac{pa}{t_w} \qquad \text{[VII.1-26]}$$

where

$2a$ = Width of each manifold.

$2t_w$ = Thickness of the dividing sidewalls.

However, the pressure, temperature, and radiation levels change along the inboard vertical blanket and the top and bottom horizontal blankets. The critical locations for stress have been determined to be at the bottom of the inboard wall, where both the coolant pressure and the fluence are high, and the inlet, where the pressure is the highest but the fluence and temperature are low. Also, since the MHD pressure drop itself is dependent on the manifold geometry, the satisfaction of the primary membrane stress criterion is not as straightforward as it first appears. For example, consider a blanket design with the inboard vertical blanket having a thickness of coolant in the radial direction of 2b with 10 cm additional thickness for structural material (PCA), and the top and bottom horizontal blankets having a thickness of coolant of 50 cm with 20 cm additional thickness for structural material (PCA). Also, assume the width of each manifold section in the toroidal direction to be $2a$ = 40 cm with uniform sidewall thickness of $2t_w$ = 0.5 cm. The total inboard blanket thickness in the radial direction is then given by 2b' (in meters),

$$2b' = 2b + 0.1.$$

There are then two constraints on the design. First, the total temperature rise, ΔT, of the coolant from inlet to outlet is restricted. For this case, it is given by (approximately):

$$\Delta T = \frac{17.7 - 8.6e^{-8b'}}{Vb} \leq \Delta T_{max}$$

which gives a lower bound for the coolant velocity in the manifold of the vertical inboard blanket

$$V \geq \frac{17.7 - 8.6e^{-8b'}}{b\ \Delta T_{max}} \qquad \text{[VII.1-27]}$$

The second constraint comes from the primary membrane stress criterion, evaluated at the inlet. The inlet pressure (ignoring pressure drops at the exit and flow bends) is approximately given by:

$$p = 309.4\ (1 + 4.73b)\ \frac{Vt_w}{a} \qquad \text{[VII.1-28]}$$

If the value of the pressure is put in Eq. [VII.1-26], the expression for the general primary membrane stress intensity reduces to:

$$P_m = 309.4\ (1 + 4.73b)\ V \qquad \text{[VII.1-29]}$$

which shows the curious result that the primary membrane stress intensity cannot be reduced by either decreasing the manifold width, 2a, or increasing the wall thickness, $2t_w$. The primary stress criterion thus gives an upper bound for the coolant velocity

$$V \leq \frac{S_m}{309.4\ (1 + 4.73b)} \qquad \text{[VII.1-30]}$$

Combining Eqs. [VII.1-27] and [VII.1-30],

$$\frac{17.7 - 8.6e^{-8b'}}{b\ \Delta T_{max}} \leq V \leq \frac{S_m}{309.4\ (1 + 4.73b)} \qquad \text{[VII.1-31]}$$

For any design to be acceptable, the above inequality must be satisfied and effectively the only latitude left to the designer is the radial thickness of the inboard blanket. Inequally [VII.4-31] can be rewritten in terms of the inlet pressure by using equation [VII.1-28] to replace the coolant velocity by the inlet pressure.

$$\frac{309.4\ t_w\ (1 + 4.73b)(17.7 - 8.6e^{-8b'})}{ab\ \Delta T_{max}} \leq p \leq \frac{S_m\ t_w}{a} \qquad \text{[VII.1-31a]}$$

where p denotes the inlet pressure.

A plot of the inequality [VII.1-31a] is shown in Fig. VII.1-26a for 25% cold worked PCA. The solid lines in the figure represent the lower bounds and the dashed lines represent the upper bounds of the inlet pressure. Note that for a ΔT_{max} of 150°C there is no acceptable design point up to a blanket thickness of 80 cm using a uniform sidewall thickness. The situation can be improved by reducing the maximum primary stress intensity by redistributing the sidewall thicknesses between the top and bottom horizontal blankets. For example, if the sidewall thicknesses are decreased to 2 mm in the sections above the inboard vertical wall and increased to 8 mm in the sections below, with no change in the inboard wall itself, then inequality [VII.1-31a] can be replaced by:

$$\frac{309.4\ t_w(1 + 4.73b)\ (17.7 - 8.6e^{-8b'})}{a\ b\ \Delta T_{max}} \leq p \leq \frac{1.6\ S_m\ t_w}{a}$$

[VII.1-32]

Note that this redistribution of thickness increases the maximum permissible pressure by 60% (p_{max} = 4.2 MPa) for the same primary membrane stress intensity at the inlet. However, the design pressure can be reduced to coincide with the lower bound by suitably choosing the blanket thickness and the system ΔT within the permissible domain in Fig. VII.1-26b which shows a plot of the permissible range of inlet pressure for a given blanket thickness based on inequality [VII.1-32] for PCA.

In contrast to earlier results, the minimum blanket thickness necessary for a ΔT_{max} = 150°C is now about 50 cm with an inlet pressure of 4.2 MPA. The inlet pressure can be reduced to about 3.5 MPa by increasing the blanket thickness to 65 cm. However, the margin of safety against additional pressure drops due to bends and uncertainties in pressure drop calculation is only 0.7 MPa. The coolant pressure and the primary stress intensity can be further

reduced and the margin of safety increased by tapering the sidewall thickness of the inboard wall and has been discussed in Section VII.1.2.

Unlike in the case of the PCA, if V-15Cr-5Ti is used instead of PCA as the structural material, then the primary stress criterion at the bottom of the inboard wall (hence radiation creep controlled S_{mt}) determines the maximum permissible inlet pressure and inequality [VII.1-32] has to be replaced by:

$$\frac{433.2(1+4.73b)(17.7-8.6e^{-8b'})t_w}{a\ b\ \Delta T_{max}} \leq p \leq \frac{1.6\ S_{mt}\ t_w\ (1+4.73b)}{a(1+2.46b)} \qquad [VII.1-33]$$

The permissible ranges of inlet pressure as functions of the inboard blanket likeness and the system ΔT are shown in Figs. VII.1-26c and VII.1-26d for design fluences of 100 dpa and 150 dpa respectively. As before the solid lines represent lower bounds and the dashed line represent the upper bounds to the coolant inlet pressure. Note that at a design fluence of 100 dpa, the minimum blanket thickness necessary for a ΔT_{max} = 200°C is about 50 cm with an inlet pressure of about 4.5 MPA. This inlet pressure can be reduced to 3.8 MPA by increasing the blanket thickness to 65 cm, thus providing a margin of safety against additional pressure drop due to flow bends, etc. of 0.8 MPA. On the other hand the minimum blanket thickness necessary for a design fluence of 150 dpa in 80 cms (with ΔT = 200°C). In order to retain a blanket thickness of 65 cm the system ΔT has to be increased to 250°C. Assuming that the fluence is attenuated by a factor of two from the front of the first wall to the manifold (a distance ≈ 6 cm), a vanadium blanket cannot be realistically designed to more than 200 dpa unless a larger ΔT than 200°C and an inboard blanket of greater than 65 cm thickness are allowed.

It is interesting to note from a comparison between V-15Cr-5Ti and PCA as structural materials that, although a larger ΔT is permissible for vanadium which makes the lower bound to the inlet pressure lower (see inequality [VII.1-33]), the benefit of a reduced lower bound is more than offset by the higher electrical conductivity which makes the net lower bound curve for V-15Cr-5Ti at ΔT = 200°C slightly higher than that of PCA at ΔT = 150°C. As a result the inlet pressure for the vanadium case will be slightly higher than that for PCA. However, in spite of the lower allowable stress of V-15Cr-5Ti the net upper bound to the inlet pressure is correspondingly higher for V-

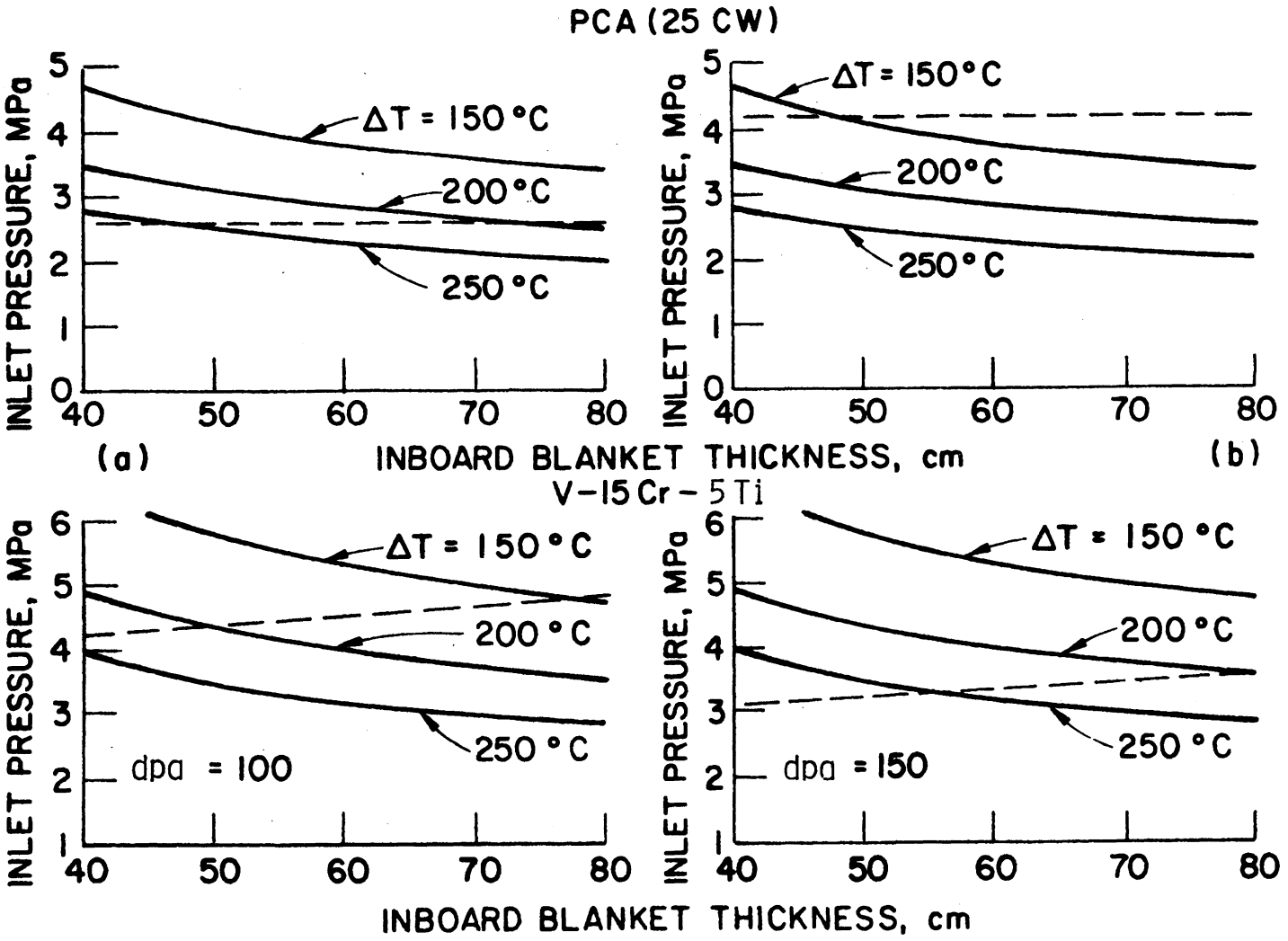

Figure VII.1-26. Allowable range of coolant velocity for (a) PCA using uniform side wall thickness, (b) PCA using variable side wall thickness, (c) V-15Cr-5Ti using variable side wall thickness and $\phi t \leq 100$ dpa, and (d) V-15Cr-5Ti using variable side wall thickness and ϕt = 150 dpa.

15Cr-5Ti than that for PCA. Consequently the margin of safety against higher pressure is about the same for V-15Cr-5Ti than for PCA. Thus from an MHD/stress viewpoint in the manifold, V-15Cr-5Ti (at 200 dpa with $\Delta T = 200°C$) has the same design margin as PCA (at 100 dpa with $\Delta T = 150°C$). Vanadium can be made more attractive than PCA by reducing the inlet pressure by allowing a higher ΔT than 200°C. Also the margin of safety can be improved by increasing its allowable stress by reducing the maximum design fluence. A real solution of this problem will require an alloy with higher S_{mt} (for example, a strain hardened alloy), adequate strength at higher temperature (to allow higher system ΔT), and lower electrical conductivity (to reduce MHD pressure drop) than either material. This is particularly true in view of the fact that the ability of the designer to reduce the primary stress by suitably choosing the manifold geometry is rather limited. More optimized designs may also be required.

Although the net lateral pressure loading on an interior sidewall in the manifold is zero, such is not the case with the end or the last sidewall which has coolant pressure acting only on one side. A 2.5 mm thick plate with a span of 40 cm is not stiff enough to support a lateral pressure of 3 MPa. Solutions to this problem could consist of either reducing the span by putting in additional webs parallel to the back plate in the end manifolds or using stiffening ribs on the laterial surfaces. The former has the advantage of not significantly adding to the MHD pressure drop.

VII.1.4.2 Secondary Stress

Secondary stress is a normal or shear stress developed by the constraint of adjacent material and is normally associated with a deformation controlled quantity such as differential thermal expansion and swelling. The basic characteristic of a secondary stress is that local yielding and minor distortion can limit and/or relieve the stress. For the purposes of the present study, the primary plus secondary stresses have been limited to 3 S_m, i.e.,

$$P_L + \frac{P_b}{1.25} + Q \leq 3\ S_m \qquad \text{[VII.1-34]}$$

where Q is the maximum range of secondary stress.

The adequacy of this criterion has to be determined by future detailed analysis of fusion reactors.

VII.1.4.2.1 Thermal Stress

Thermal stresses in the first wall have been calculated on the assumption that the bulk of the blanket structure is at the temperature of the coolant in the manifold and, being more massive, controls the deformation in the first wall. Thus, the thermal stress in the first wall is caused by both a gradient in temperature across the first wall as well as by any additional temperature gradient between the coolant in the manifold and the metal coolant interface in the first wall channel.

VII.1.4.2.1.1 Reference Design

In the reference design, the thermal stress intensity at any point in the first wall is given by:

$$Q = \frac{E\alpha}{1 - \nu} [T - T_M]$$

where

T = Temperature at any point in the first wall.

T_M = Coolant temperature in manifold directly behind the first wall.

Denoting by ΔT_{FW} the maximum difference in temperature between the metal-coolant interface in the first wall channel and the coolant in the manifold, and noting that the maximum thermal stress occurs at the free surface of the first wall facing the plasma, a conservative estimate for the secondary stress intensity is

$$Q = \frac{E\alpha}{1 - \nu} [\Delta T_{FW} + \frac{q_s}{k} h + \frac{Q_n}{2k} h^2] \qquad [VII.1-35]$$

where

q_s = Surface heat flux.

Q_n = Bulk nuclear heating rate (35 W/cm^3).

k = Thermal conductivity.

h = Thickness of first wall.

Using Eqs. [VII.1-24] and [VII.1-35] in inequality [VII.1-34], it is possible to calculate the maximum permissible thickness of the first wall for any given surface heat flux. The results of such calculations are shown in Fig. VII.1-27a for 25% cold worked PCA for various values of ΔT_{FW}. Assuming that a minimum thickness of 2 mm is required at the end of life and that erosion occurs at the rate of 1 mm/yr, the life of the first wall for a surface heat flux of 50 W/cm^2 is 1.5 yr (assuming a 100% duty factor) for a ΔT_{FW} of 40°C and 2 yr for a ΔT_{FW} of 20°C.

Because of superior thermal properties, a larger surface heat flux can be tolerated if the structural material is changed from PCA to V-15Cr-5Ti (Fig. VII.1-27b). If the first wall coolant temperature is 550°C, the maximum thickness for vanadium is controlled by the maximum allowable structural temperature (750°C) rather than by stress. However, if the first wall coolant temperature is $\leq$ 500°C, then the allowable stress determines the maximum thickness of the first wall. As shown in Fig. VII.1-27b even if it is required to have 3-4 mm thickness at the end of life, sufficient thickness is left as margin for erosion of the first wall for a surface heat flux of 100 W/cm^2. Thus, from a thermal stress and erosion point of view, V-15Cr-5Ti is vastly superior to PCA.

VII.1.4.2.1.2 Alternate Design (Grooved Wall)

An alternate first wall design (using PCA) for reducing the thermal stress (and swelling stress) in the first wall (and consequently permitting a larger thickness to be used as margin against erosion) is to use parallel grooves in both directions. For the purposes of the present study, grooves of 5 mm depth, 2 mm width, and spacing of d are considered with a 1 or 2 mm thick solid back plate. Using a shear log type analysis, the effective thickness of the first wall is given by

$$h_{eff} = \begin{cases} t + \dfrac{d^2}{4\sqrt{3}\,(d + 0.2)} & \text{for } d \leq \sqrt{3} \text{ cm} \\ t + \dfrac{\frac{d}{2} - \frac{\sqrt{3}}{4}}{d + 0.2} & \text{for } d > \sqrt{3} \text{ cm} \end{cases}$$

where t = thickness of the solid back plate.

The first wall is then analyzed for stress with a solid wall thickness of h_{eff} but is analyzed for heat transfer with the full thickness of 0.6 cm. Figure VII.1-27c shows the maximum permissible spacing of grooves as a function of surface heat flux and ΔT_{FW}. In addition, the dashed lines show the maximum allowable groove spacing for a solid back plate thickness of 2 mm. Note that in order to achieve a design capable of withstanding a surface heat flux of 100 W/cm^2, the back plate thickness should be 1 mm, with a groove spacing of about 5 mm. If, however, a 2 mm thick back plate is used, then the maximum allowable surface heat flux is of the order of 70 W/cm^2.

VII.1.4.2.1.3 Poloidal Helical Flow Design

Assuming a cosinusoidal variation of surface heat flux ($q_s = q_o \cos \theta$), the maximum primary plus secondary stress intensity for the poloidal helical flow design is given by

$$P_L + Q = \frac{1 - \frac{\nu}{2}}{1 - \nu} \frac{E\alpha h q_o}{k} + \frac{1 - \frac{\nu}{3}}{2\,(1 - \nu)} \frac{E\alpha h^2 Q_n}{k} - \frac{\nu p a}{h} \qquad \text{[VII.1-36]}$$

Using Eq. [VII.1-36] and inequality [VII.1-34], the maximum permissible first wall thickness can be calculated for a given surface heat flux. However, it can be shown that for coolant temperatures of 400°C for PCA and 550°C for V-15Cr-5Ti, the maximum thickness of the first wall is controlled by the maximum metal temperature criterion (550°C for PCA and 750°C for V-15Cr-5Ti) rather than by stress. Fig. VII.1-28a,b shows the allowable thickness versus surface heat flux plots for PCA and V-15Cr-5Ti, respectively. ($T_{metal} - T_{coolant}$) in these plots refer to the temperature rise between the bulk coolant and the metal-coolant interface. As in the reference design, the superior thermal properties of vanadium allow a considerably thicker wall to be used with vanadium than with PCA. The figures show that a considerable penalty in first wall thickness has to be paid if there is a significant rise in temperature at the interface compared to the bulk of the coolant, indicating that some kind of flow mixing, such as helical flow design, will be necessary to make this design attractive.

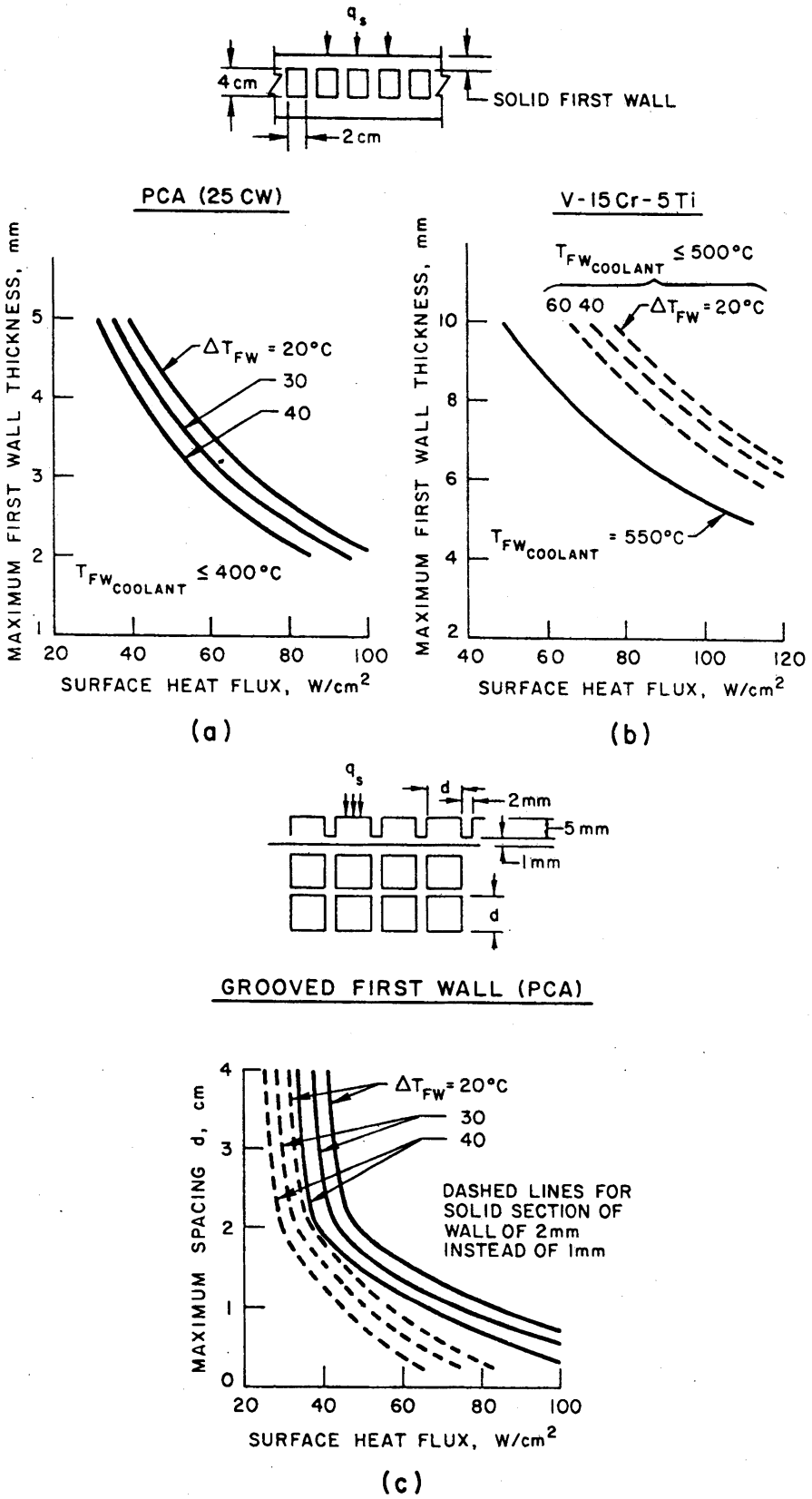

Figure VII.1-27. Allowable maximum first wall thickness for reference design using (a) PCA (25 CW), (b) V-15Cr-5Ti, and (c) allowable spacing of grooves using PCA (25 CW).

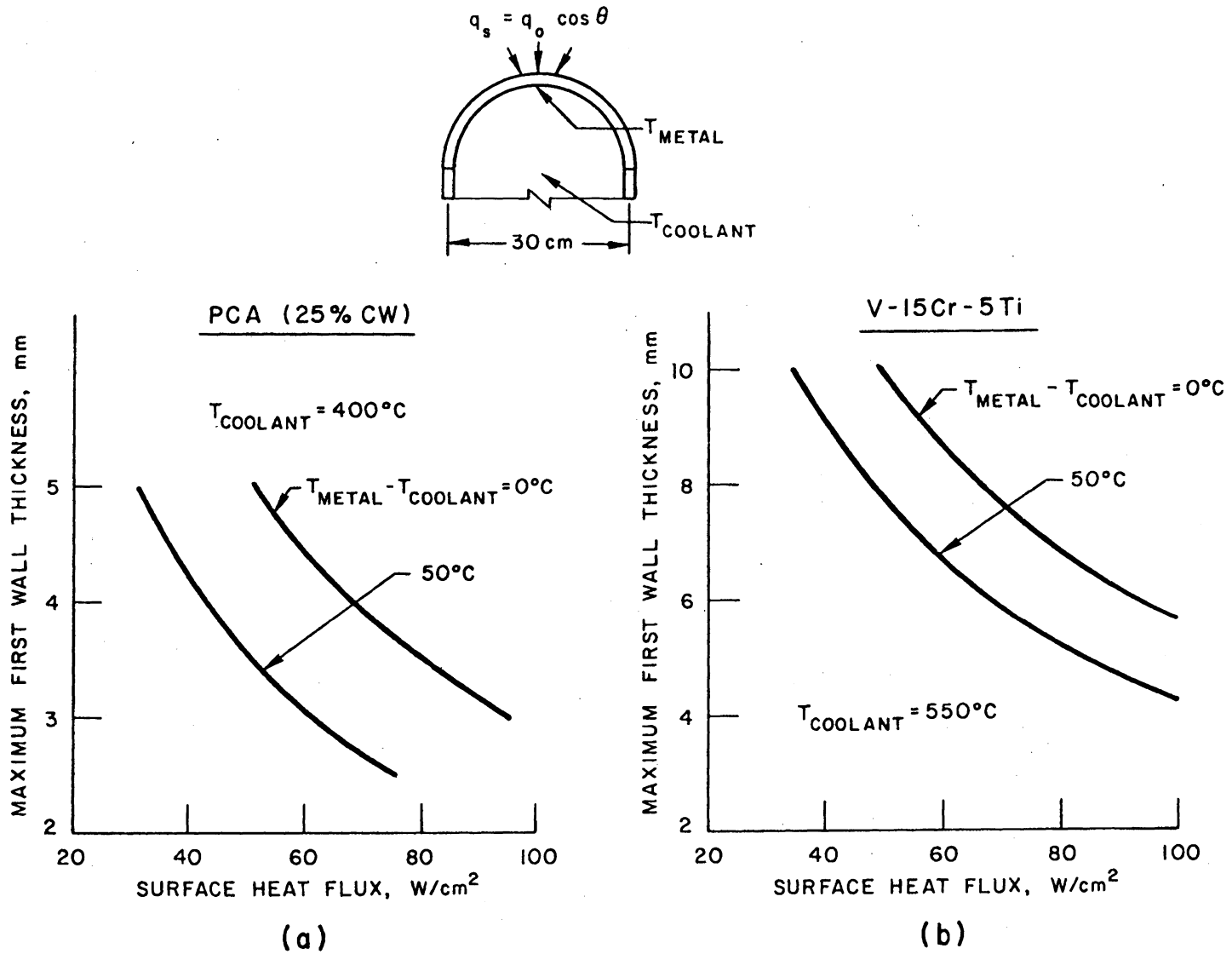

Figure VII.1-28. Maximum allowable thickness of first wall for the poloidal flow design using (a) PCA and (b) V-15Cr-5Ti.

VII.1.4.2.2 Swelling Stress

A detailed study involving the stresses introduced by the complete suppression of swelling strain of the first wall has indicated that unacceptably high elastically computed stresses are generated unless the beneficial effects of radiation induced creep are taken into account. The radiation induced creep relaxes the initial high thermal stresses exponentially with a time constant equal to $\frac{2}{3}\frac{1+\nu}{EA\phi}$ where A is the coefficient for radiation creep rate and ϕ is the neutron flux.

The swelling stress, which is zero initially, builds up with time but reaches an asymplotic value of $-\frac{B}{A}$ where B is the coefficient for the swelling rate. The value of $\frac{B}{A}$ for PCA up to a fluence of 100 dpa (at 550°C) is of the order of 10 MPa. However, beyond 100 dpa, the swelling stress increases rapidly because of runaway swelling. Fig. VII.1-29 shows the variation of the thermal, pressure, and swelling stresses with fluence for the poloidal flow design using PCA as the structural material. Note that the high initial thermal stress is relaxed by radiation induced creep in about 3-4 dpa. It should be remembered that this thermal stress reappears as a tensile stress every time the machine is turned off. The swelling stress builds up in about the same time it takes for the thermal stress to relax out. Thus, it is reasonable not to superimpose the thermal and the swelling stresses for satisfying the primary plus secondary stress criterion.

VII.1.5 Neutronic Analysis

Neutronic analyses were carried out to study the performance of the self-cooled liquid metal blanket concepts. The impact of the breeder materials selection (lithium or 17Li-83Pb), breeding zone thickness, reflector materials selection, reflector composition, and reflector zone thickness were analyzed to determine the main blanket parameters. In the neutronic analyses, the first wall, structural requirement (distribution, and total volume fraction) in the breeding zone, and lithium enrichment were constant during this part of the study.

In the neutronics analyses, three key parameters are considered to compare the different blanket designs; the tritium breeding ratio, the energy deposition in the blanket per fusion neutron, and the energy loss to the shielding systems. The neutronics analyses were performed to examine the

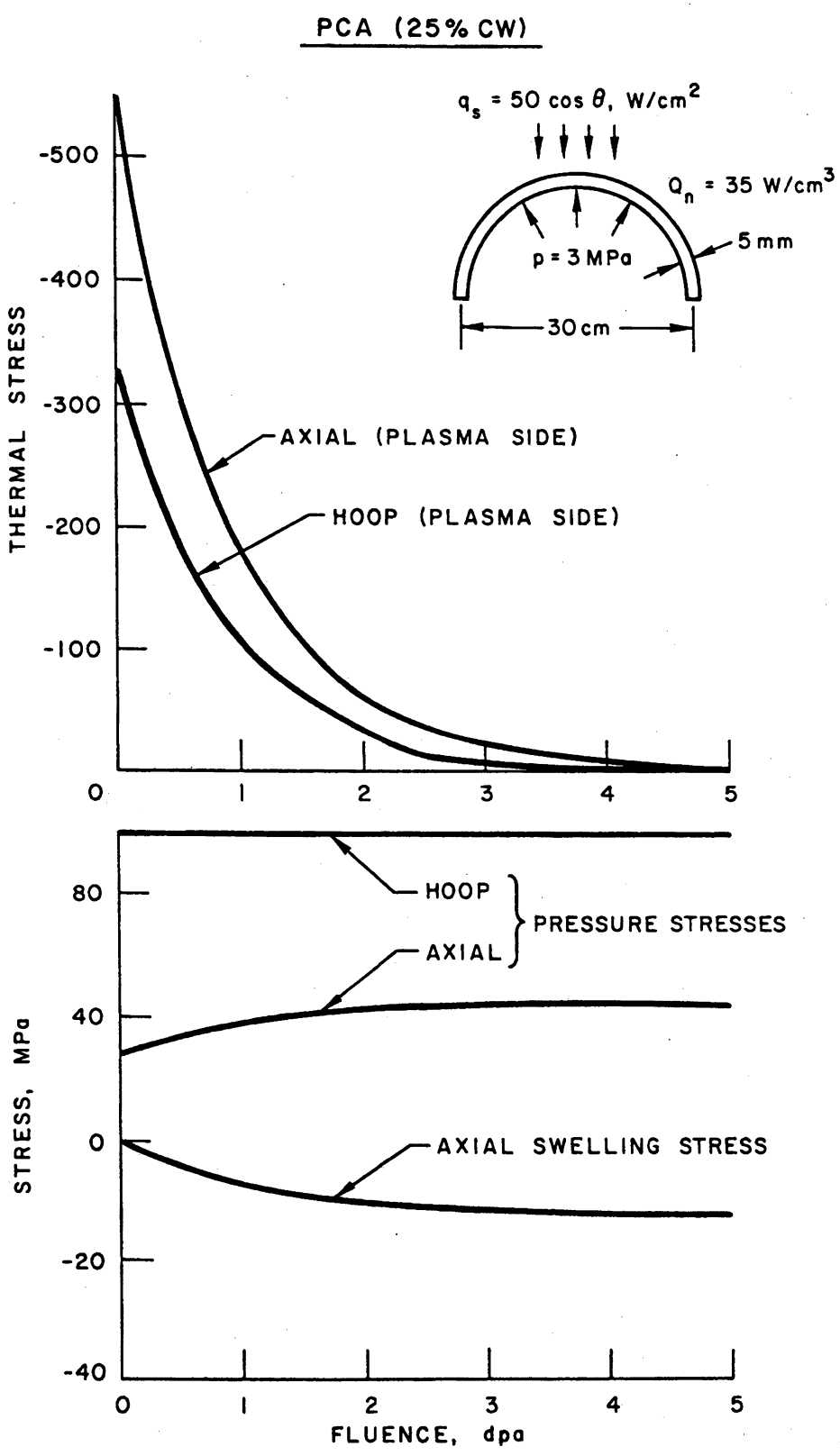

Figure VII.1-29. Variation of thermal, pressure and swelling stresses with fluence for the poloidal flow design using PCA.

tritium breeding potential. The energy deposition in the blanket per fusion neutron is an important parameter that which affects the economics of the reactor in a direct way. The other key parameter is the energy deposition in the shielding system which is recovered at a low temperature and cannot be used for generating electrical power. This energy loss should be limited to ~ 1% of the energy produced per D-T neutron to avoid the degradation of the plant efficiency and building a large cooling system for the shield.

VII.1.5.1 Tritium Breeding Analyses

The tritium breeding analyses were performed for a wide range of blanket parameters. Table VII.1-2 gives the blanket configuration and the volumetric composition for each zone. The first wall thickness is 1 cm with 50% PCA and 50% liquid metal coolant (lithium or 17Li-83Pb). The tritium breeding zone has a variable thickness and constant composition. A 7.5% PCA and 92.5% breeder is the composition used in the neutronic analysis for the tritium breeding zone. The reflector zone has a variable thickness and composition. PCA is the reflector material with liquid metal coolant. A shielding zone is included in the blanket model to get the correct boundary conditions at the outer surface of the reflector zone. Liquid lithium breeder with natural abundance and 17Li-83Pb with 90% ^{6}Li enrichment are the breeder materials for this analysis. The one-dimensional discrete ordinates code ANISN was used to perform the transport calculations with P_3 approximations for the scattering cross section and S_8 angular quadrature set. A 67-coupled group cross section data library (46-neutron and 21-gamma) based on ENDIF/B-IV was employed for these calculations. This data library was obtained from VITAMIN-C and MACKLIB-IV library.

The tritium breeding results are given in Figs. VII.1-30 through VII.1-35. The calculations were done in a parametric way to study and quantify the effect of each blanket parameter. For example, Fig. VII.1-30 gives the tritium breeding ratio (TBR) for the liquid lithium blanket as a function of the combined thicknesses of the first wall and the breeder zone with a 10-cm reflector zone. The steel volume fraction in the reflector was varied from 0.1 to 0.9. Figures VII.1-31 and VII.1-32 show similar results for 20-cm and 30-cm reflector zone thicknesses, respectively. The results in Figs. VII.1-30 through VII.1-32 show that the minimum blanket thickness (first wall, breeder

TABLE VII.1-2. BLANKET PARAMETERS FOR NEUTRONICS ANALYSES

Zone Description	Zone Thickness (cm)	Zone Composition (vol-%)
First wall	1	50% PCA 50% liquid metal (Li[b] or 17Li-83Pb[c])
Tritium breeder	x[a]	7.5% PCA 92.5% breeder (lithium or 17Li-83Pb)
Reflector	y[a]	Z[a]% PCA (100-Z)% liquid metal (lithium or 17Li-83Pb)
Shield	60	90% Fe-1422 steel alloy 10% H_2O

[a]x, y, and z are variables.

[b]Natural lithium.

[c]90% ^{6}Li enrichment.

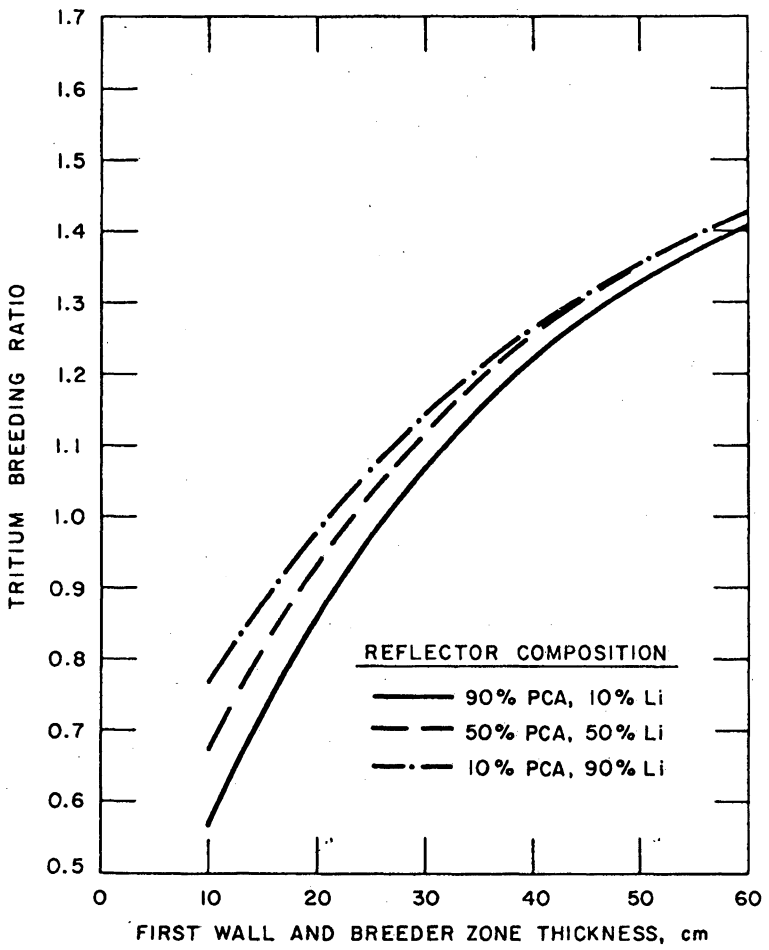

Figure VII.1-30. Tritium breeding ratio as a function of the combined thickness of the first wall and lithium breeding zone with 10 cm reflector zone thickness.

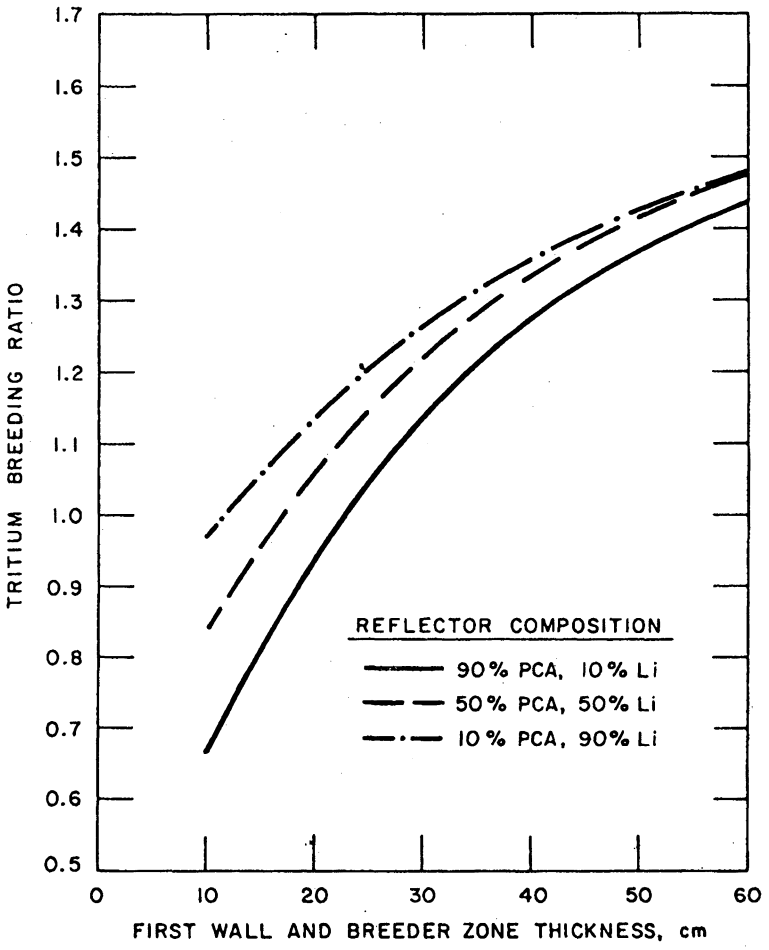

Figure VII.1-31. Tritium breeding ratio as a function of the combined thickness of the first wall and lithium breeding zone with 20 cm reflector zone thickness.

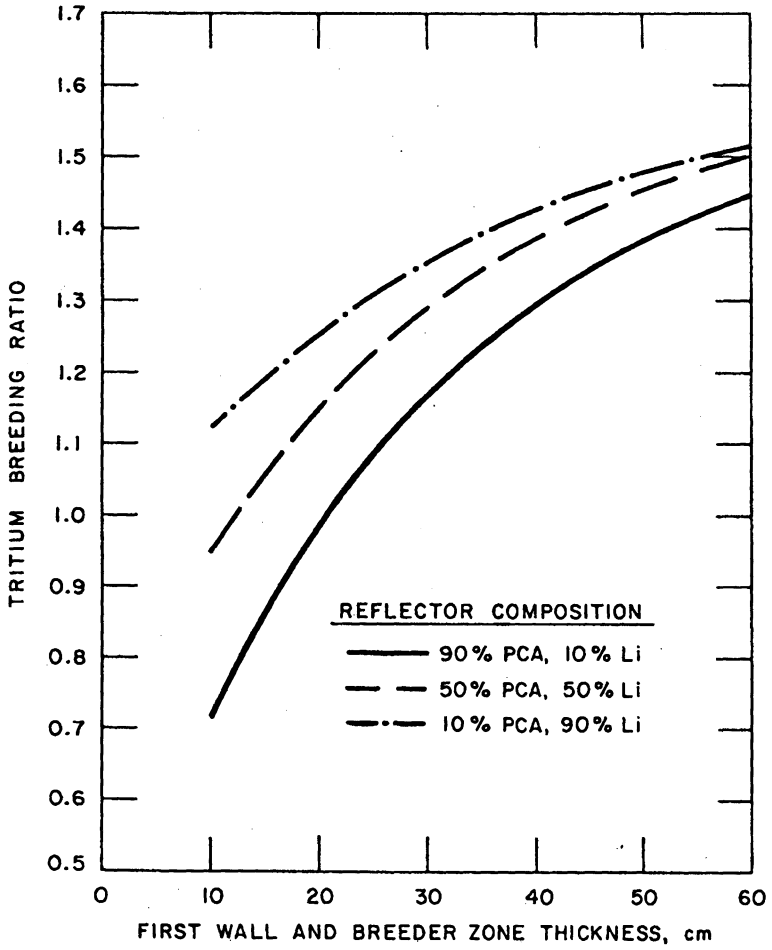

Figure VII.1-32. Tritium breeding ratio as a function of the combined thickness of the first wall and lithium breeding zone with 30 cm reflector zone thickness.

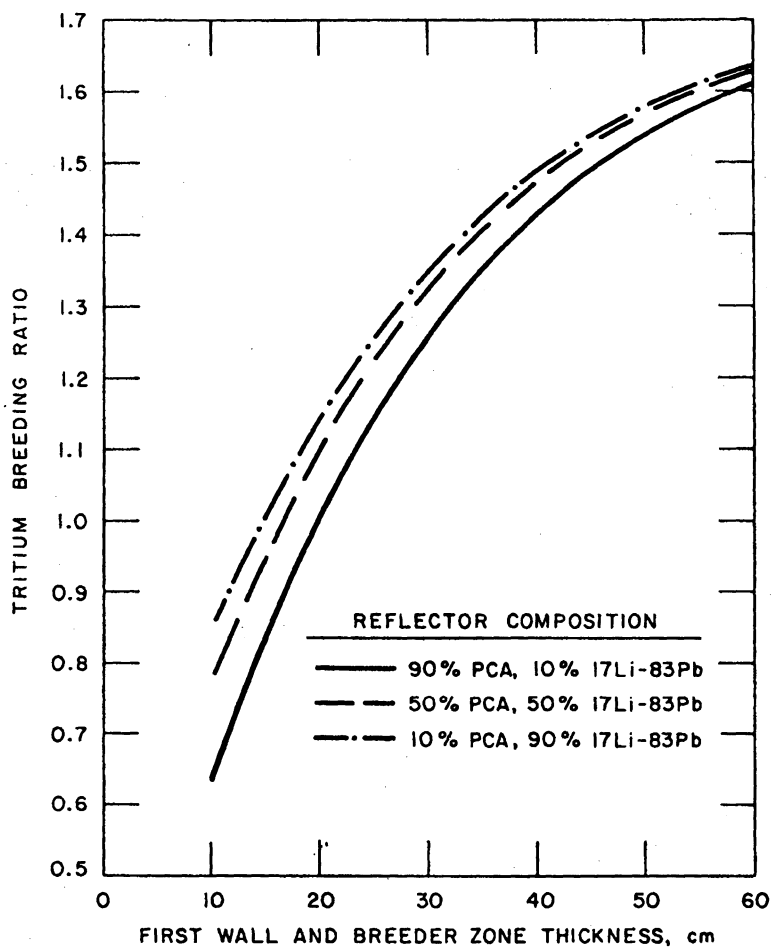

Figure VII.1-33. Tritium breeding ratio as a function of the combined thickness of the first wall and lithium lead breeding zone with 10 cm reflector zone thickness.

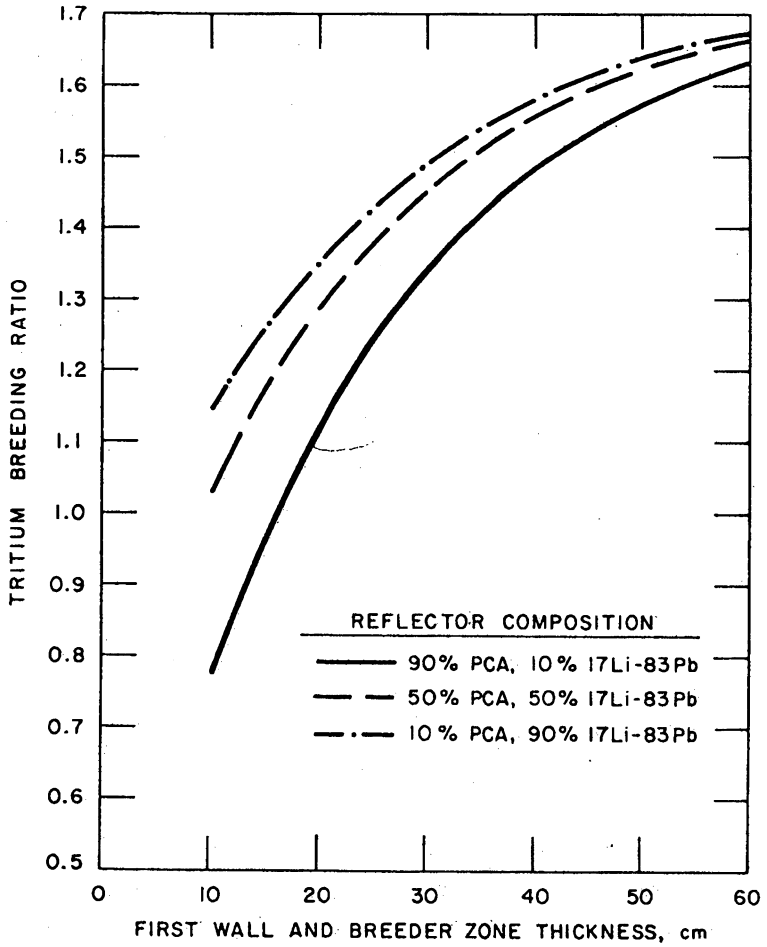

Figure VII.1-34. Tritium breeding ratio as a function of the combined thickness of the first wall and lithium lead breeding zone with 20 cm reflector zone thickness.

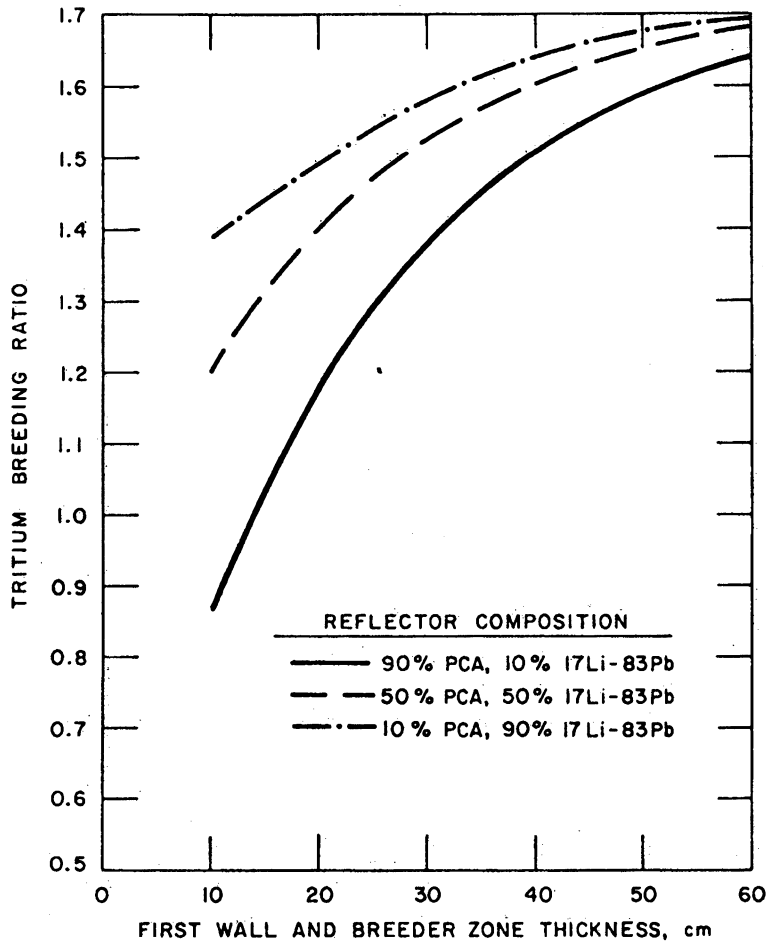

Figure VII.1-35. Tritium breeding ratio as a function of the combined thickness of the first wall and lithium lead breeding zone with 30 cm reflector zone thickness.

zone, and reflector) required to obtain 1.3 TBR is ~55 cm regardless of the reflector thickness. Also, this minimum blanket thickness requires high lithium fraction in the reflector zone as the reflector zone thickness increases. For the 30-cm reflector zone thickness, the minimum blanket thicknesses are 55 and 71 cm for 0.90 and 0.1 lithium volume fraction in the reflector, respectively. The TBR is sensitive to the thickness and composition of the reflector zone. These observations are important for the designs of the inboard blanket for the tokamak reactors where the total thickness of the inboard blanket and shield is constrained. Figure VII.1-32 shows a maximum TBR of 1.51 with a 60-cm blanket thickness. A higher value can be obtained by increasing the blanket thickness, changing the reflector material, or reducing the structure fraction in the blanket. Figures VII.1-30 through VII.1-32 show the effect of breeder reflector zone thickness on the TBR.

Tritium breeding analyses were also performed for the lithium lead (17Li-83Pb) system using the blanket parameters given in Table VII.1-2. Figures VII.1-33 through VII.1-35 show the TBR as a function of the combined thickness of the first wall and breeding zone, reflector composition, and reflector zone thickness. The lead in this system softens the neutron spectrum, which reduces the $^{7}Li(n,n'\alpha)T$ reaction rate to less than 0.02 reaction per D-T neutron. This leads to the consideration of ^{6}Li enrichment to achieve the required TBR. In this analyses a 90% ^{6}Li enrichment is used to assure an adequate amount of ^{6}Li in the blanket. The lithium-lead TBR results show a higher breeding ratio and smaller blanket thickness required for a specific TBR relative to the lithium system. The reflector design (material, thickness, and composition) has larger impact on the TBR as shown in Figs. VII.1-33 through VII.1-35. In this system the ^{6}Li enrichment can be used to control the TBR to the desired value. In fact less tritium breeding results in more energy per fusion neutron which is desirable for power reactors.

The above calculations are based on ENDF/B-IV data which does not account for the recent change in the ^{7}Li cross section. This causes a concern about the actual values of the TBR for the different systems. For the lithium-lead system it does not cause any concern because the ^{7}Li contribution to the TBR is less than 0.0026 (~1%). On the other hand, the TBR of the lithium system is expected to change since the ^{7}Li contribution is ~40% of the TBR. In order to assess this change a set of calculations were performed to quantify this

change. Two blankets were calculated with ENDF/B-IV and -V data. Table VII.1-3 gives the composition and thickness for both blankets. Each blanket was calculated with the continuous energy Monte Carlo code MCNP with ENDF/B-IV and -V data, and the discrete ordinates code ANISN with a 46-neutron group structure based on ENDF/B-IV. The Monte Carlo calculations were performed with 5000 D-T neutrons for each run where satisfactory statistics were obtained. The TBR results show a good agreement between the multigroup-discrete ordinates and the continuous energy-Monte Carlo based on ENDF/B-IV data, the difference between the different results for both blankets within the statistical error of the Monte Carlo calculations. The ENDF/B-V results show a 7.2 and 4.6% drop in the TBR for the blankets with 40 and 60-cm tritium breeding zones, respectively. The ^{7}Li contribution based on ENDF/B-V is 10 to 11% less than the ENDF/B-IV value. However, the impact on the TBR is design dependent. For a thin blanket the neutron spectrum is much harder due to the decrease in the total inelastic cross section of the blanket, which also reduces the $^{6}Li(n,\alpha)t$ reaction rate and increases the neutron leakage from the blanket. For a thick blanket the impact on the $^{6}Li(n,\alpha)t$ reaction rate is small because the blanket has adequate thickness to slow down the D-T neutrons. This means that the use of a correcton factor to adjust the tritium reaction rates based on ENDF/B-IV will give unsatisfactory results.

Table VII.1-4 gives the results for two blankets with different total thicknesses. Two structural materials, PCA and V15Cr5Ti, were used for each blanket. The vanadium blanket gives a better breeding ratio but it has less energy deposition per fusion neutrons as shown in Table VII.1-5.

VII.1.5.2 Blanket Energy Deposition

The primary goal for the blanket design is to produce recoverable heat in suitable conditions for the thermal cycle. From this point of view it is desirable to maximize the recoverable heat deposited in the blanket per fusion neutron and just satisfy the other requirements, such as tritium breeding. Neutronic analyses were performed to study the effect of the design parameters on the blanket energy deposition. Figs. VII.1-36 through VII.1-38 give the energy deposited in the blanket per fusion neutron as a function of the combined thickness of the first wall and lithium breeding zone for different reflector zone thicknesses and compositions. The breeder zone thickness is varied from 10 to 60 cm for 10, 20 and 30 cm reflector zone thickness. For each case

TABLE VII.1-3. BLANKET PARAMETERS FOR THE DISCRETE ORDINATES AND MONTE CARLO CALCULATIONS

Zone Description	Zone Thickness (cm)	Zone Composition (vol-%)
First wall	1	50% PCA 50% natural lithium
Tritium breeder	40/60	7.5% PCA 92.5% natural lithium
Reflector	20	90% PCA 10% natural lithium
Shield	60	90% Fe-1422 10% H_2O

TABLE VII.1-4. TRITIUM BREEDING RATIO RESULTS BASED ON ENDF/B-IV AND ENDF/B-V DATA FILES

Data Base	Transport Method	TBR
	A. 40-cm Tritium Breeding Zone	
ENDF/B-IV	P_3S_8-46 neutron groups - ANISN	1.289
ENDF/B-IV	Monte Carlo-continuous energy MCNP	1.267 ± 0.018
ENDF/B-V	Monte Carlo continuous energy MCNP	1.175 ± 0.018
	B. 60-cm Tritium Breeding Zone	
ENDF/B-IV	P_3S_8-46 neutron group - ANISN	1.432
ENDF/B-IV	Monte Carlo continuous energy MCNP	1.427 ± 0.012
ENDF/B-V	Monte Carlo continuous energy MCNP	1.361 ± 0.012

TABLE VII.1-5. TRITIUM BREEDING AND ENERGY DEPOSITION RESULTS FOR TWO BLANKETS WITH DIFFERENT STRUCTURE MATERIALS

	PCA	V15Cr5Ti
A. 70-cm Blanket (40-cm Breeding Zone, 30-cm Reflector)[a]		
TBR	1.289	1.417
Total energy deposition per D-T neutron	19.42	18.01
Energy deposition in the shield per D-T neutron	0.64	0.78
B. 90-cm Blanket (60-cm Breeding Zone, 30-cm Reflector)[a]		
TBR	1.445	1.565
Total energy deposition per D-T neutron	19.08	17.20
Energy deposition in the shield per D-T neutron	0.31	0.38

[a]10% lithium, 90% reflector material.

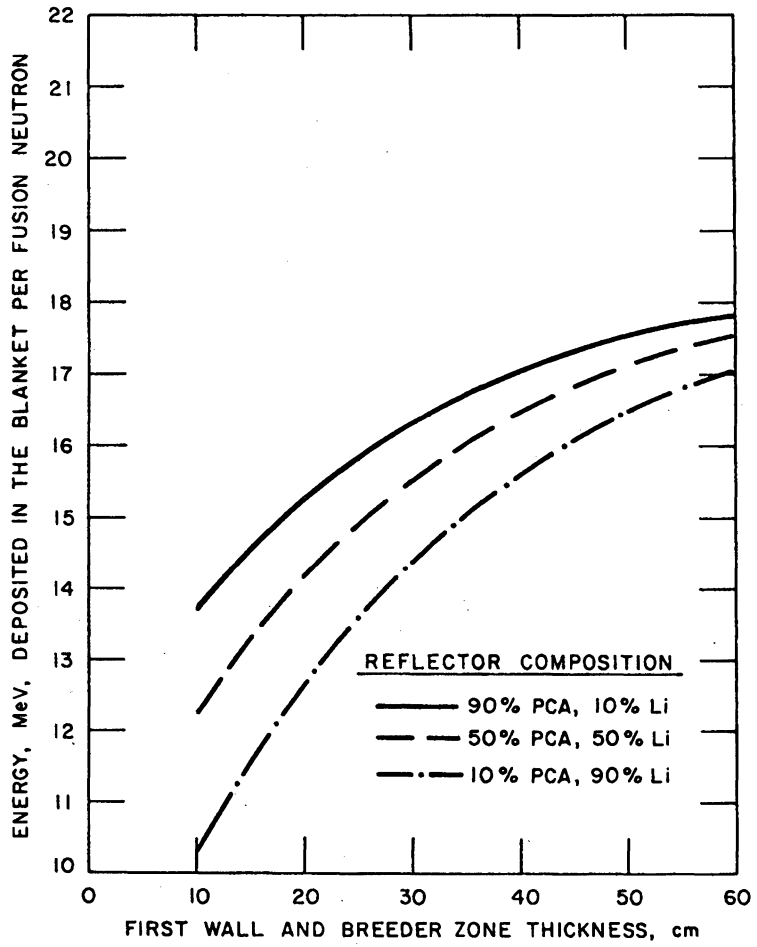

Figure VII.1-36. Energy deposited in the blanket per fusion neutron as a function of the combined thickness of the first wall and lithium breeding zone with 10 cm reflector zone thickness.

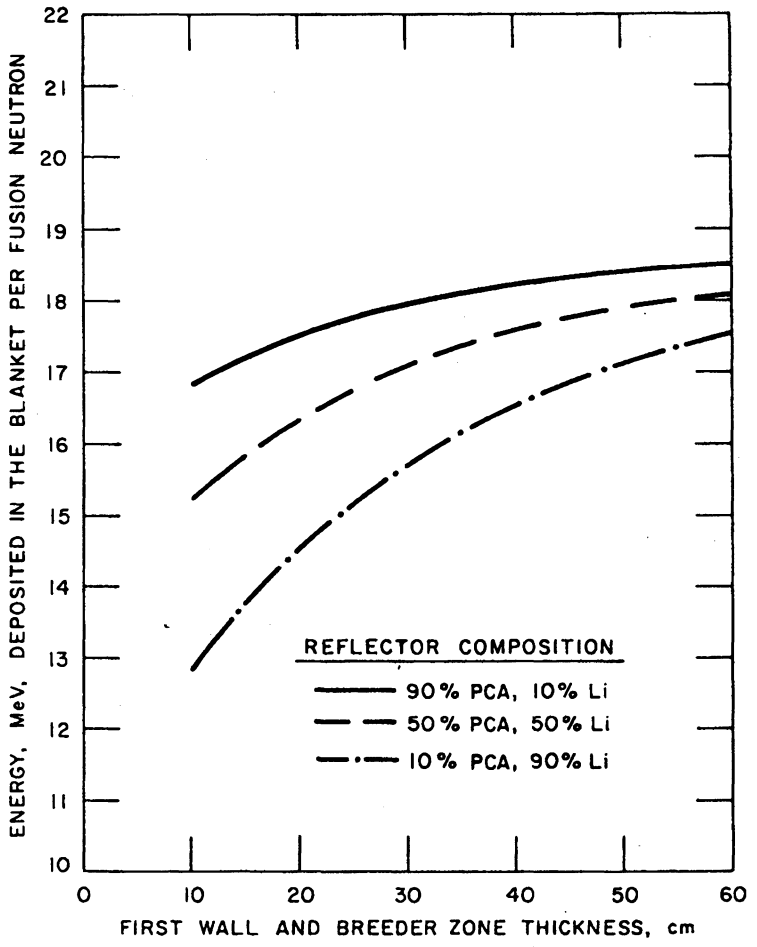

Figure VII.1-37. Energy deposited in the blanket per fusion neutron as a function of the combined thickness of the first wall and lithium breeding zone with 20 cm reflector zone thickness.

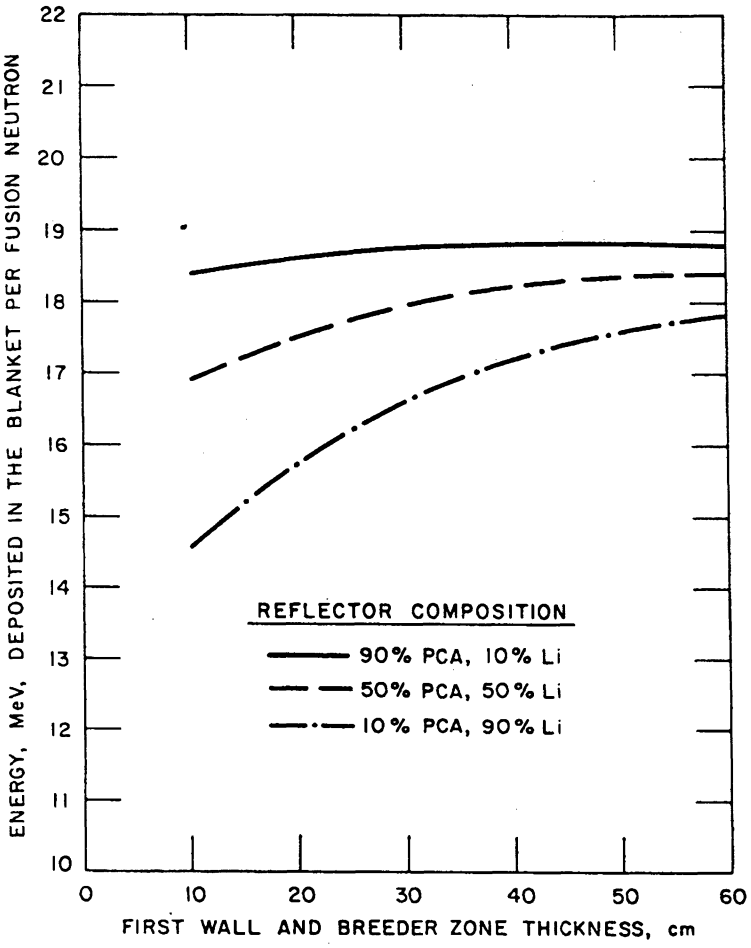

Figure VII.1-38. Energy deposited in the blanket per fusion neutron as a function of the combined thickness of the first wall and lithium breeding zone with 30 cm reflector zone thickness.

the reflector composition is varied from 10 to 90% PCA. Figures VII.1-39 through VII.1-41 give similar results for the lithium-lead system.

The energy deposition in the lithium blanket (first wall, breeding zone, and reflector) shows a strong dependence on the design parameters as shown in Figs. VII.1-36 through VII.1-41. For a thin blanket the energy deposition increase reaches saturation as the blanket gets thicker. As the steel fraction and thickness of the reflector increase, the energy deposition saturation occurs with a smaller breeding zone thickness. Figure VII.1-38 shows that the energy deposition for a 30-cm reflector with a 0.9 steel fraction reaches saturation at a 25-cm breeder zone thickness. This is a very important observation for the blanket design. For this 25-cm breeder zone thickness the TBR is 1.075 which can be increased to 1.45 by increasing the breeder zone to 60 cm without changing the energy deposition. So the blanket can be designed for any breeding ratio without sacrificing the power production, a similar behavior is obtained for the lithium-lead system. However, the saturation values are lower as shown in Figs. VII.1-39 through VII.1-41. The use of vanadium alloy instead of the PCA results in reducing the energy deposition by about 7% relative to the lithium-PCA system, as shown in Table VII.1-5.

VII.1.5.3 Shield Energy Deposition

The energy deposition in the shield system should be minimized since the heat deposited in the shield system is not usable for generating power. In fact, the heat is removed from the shield system at a low temperature of about 60°C. The energy deposited in the shield system, due to the neutron and gamma ray leakage through the reflector, should be limited to about 1% of the total energy produced per fusion neutron to avoid any impact on the system efficiency. It should be also noted that neutrons and gamma rays streaming through the limiter slot, the rf system, and thin gaps between the blanket segments typically contribute ~1% more energy to the shield system. This balance in the energy leakage represents an optimum situation for the blanket and shield design. However, it is difficult to achieve this low leakage level in the inboard section of tokamak reactors. Figures VII.1-42 through VII.1-47 give the fraction of the total energy deposited in the shield as a function of the combined thickness of the first wall and breeder zone thicknesses with different

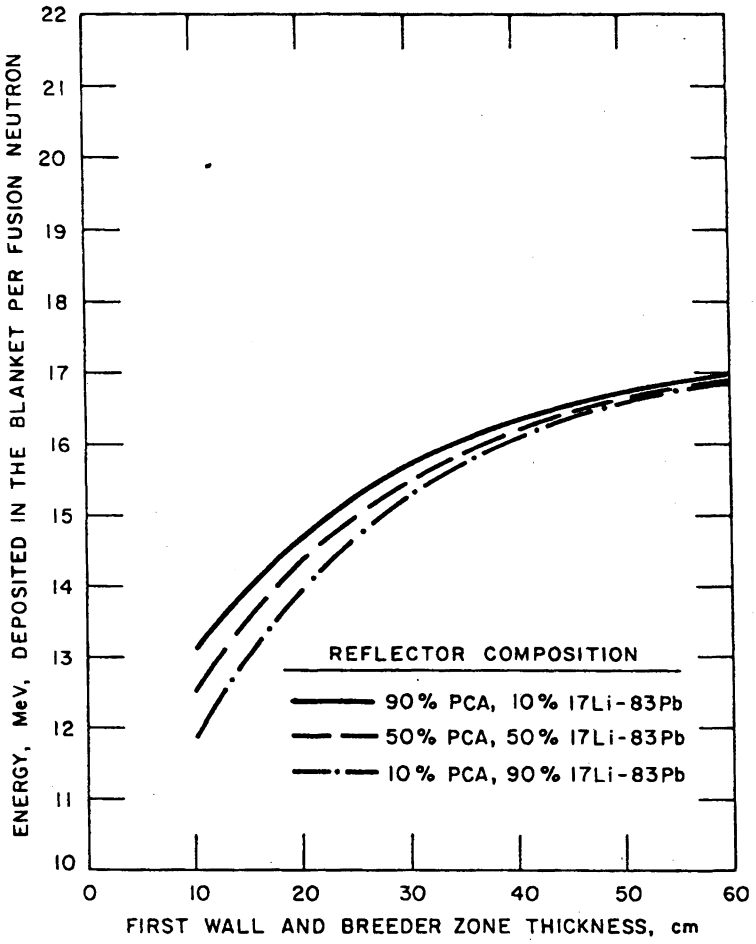

Figure VII.1-39. Energy deposited in the blanket per fusion neutron as a function of the combined thickness of the first wall and lithium lead breeding zone with 10 cm reflector zone thickness.

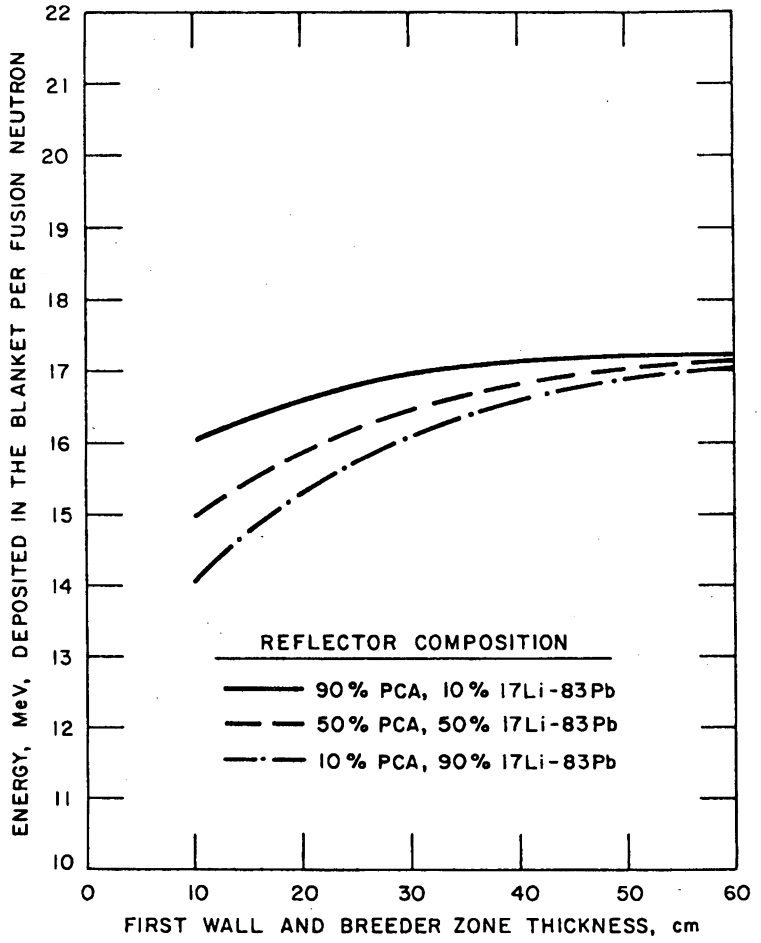

Figure VII.1-40. Energy deposited in the blanket per fusion neutron as a function of the combined thickness of the first wall and lithium lead breeding zone with 20 cm reflector zone thickness.

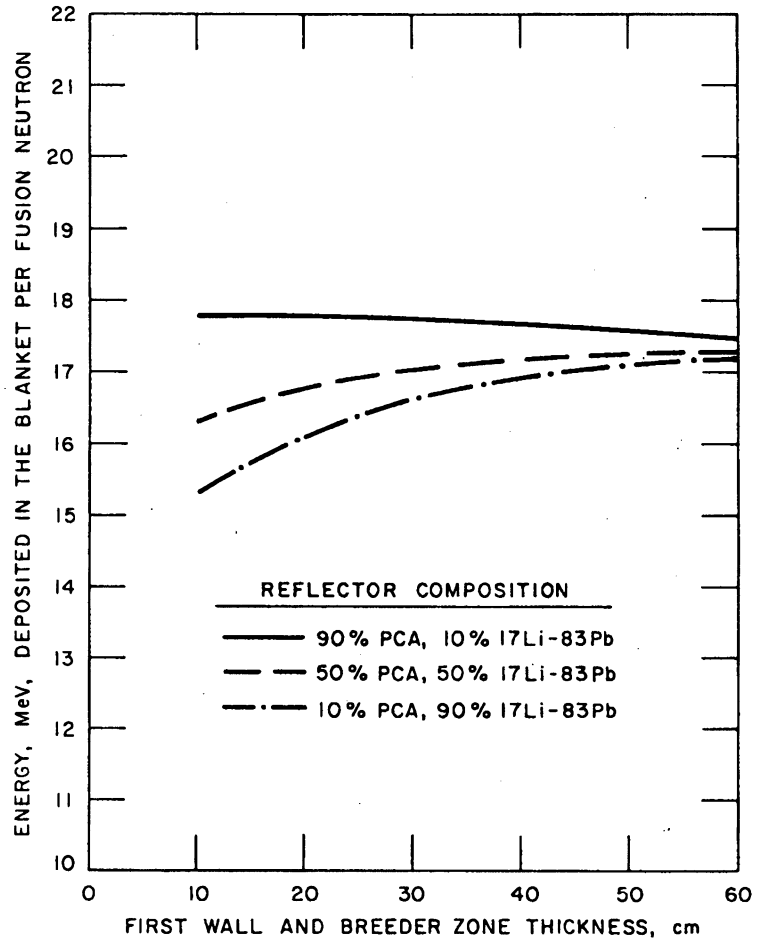

Figure VII.1-41. Energy deposited in the blanket per fusion neutron as a function of the combined thickness of the first wall and lithium lead breeding zone with 30 cm reflector zone thickness.

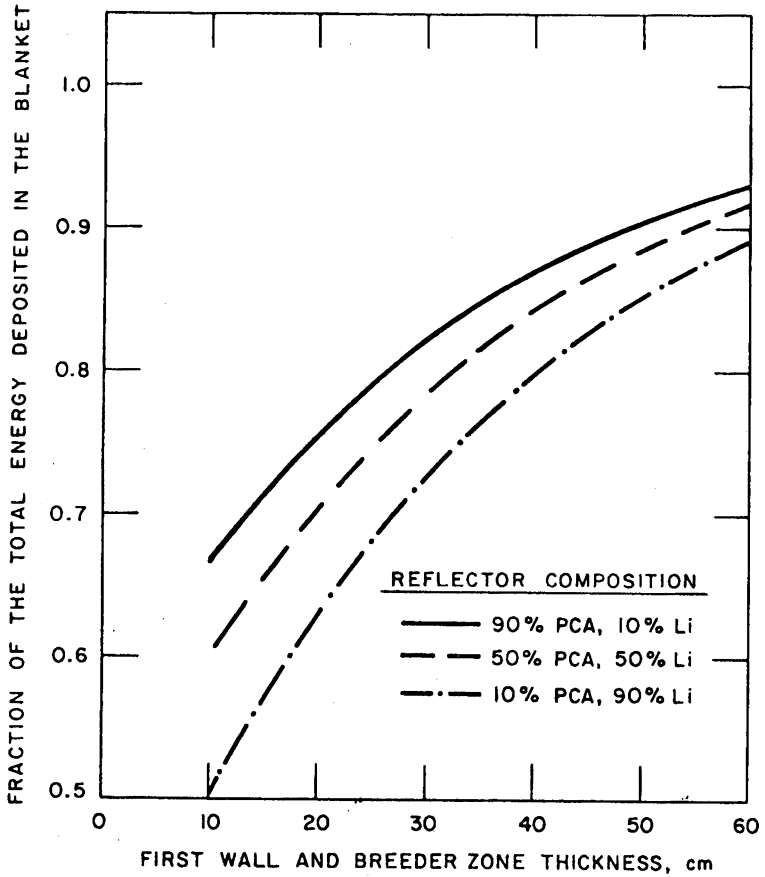

Figure VII.1-42. Fraction of the total energy deposited in the blanket as a function of the combined thickness of the first wall and lithium breeding zone with 10 cm reflector zone thickness.

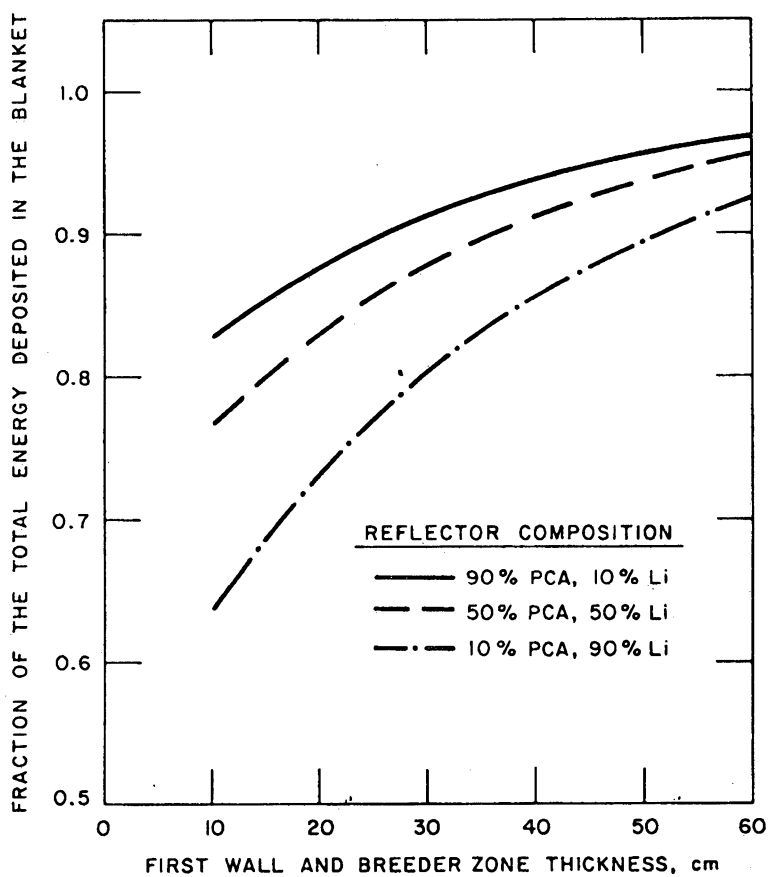

Figure VII.1-43. Fraction of the total energy deposited in the blanket as a function of the combined thickness of the first wall and lithium breeding zone with 20 cm reflector zone thickness.

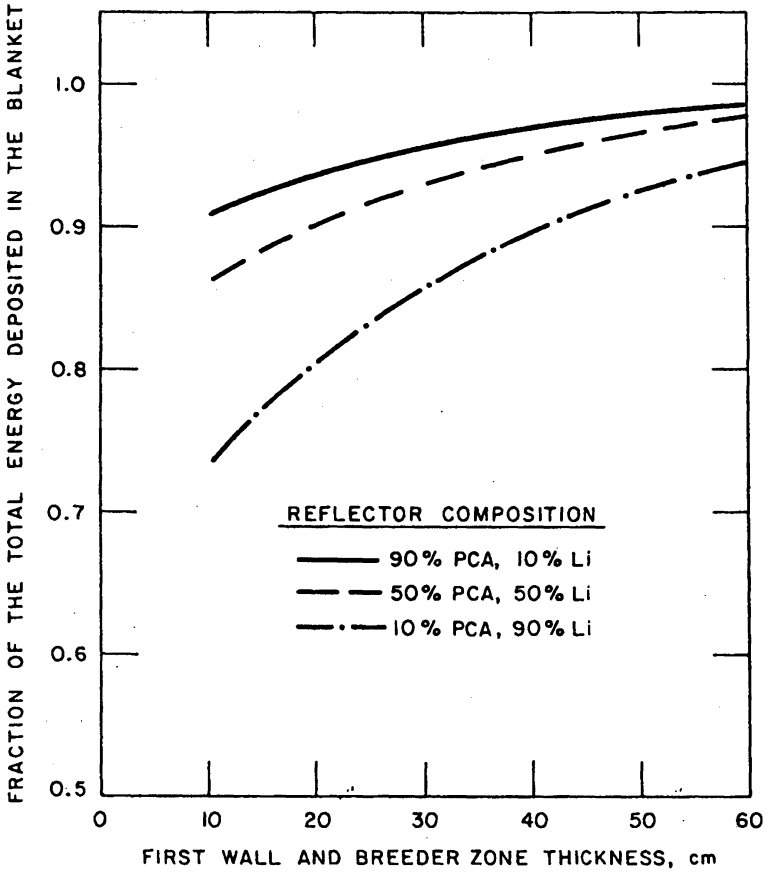

Figure VII.1-44. Fraction of the total energy deposited in the blanket as a function of the combined thickness of the first wall and lithium breeding zone with 30 cm reflector zone thickness.

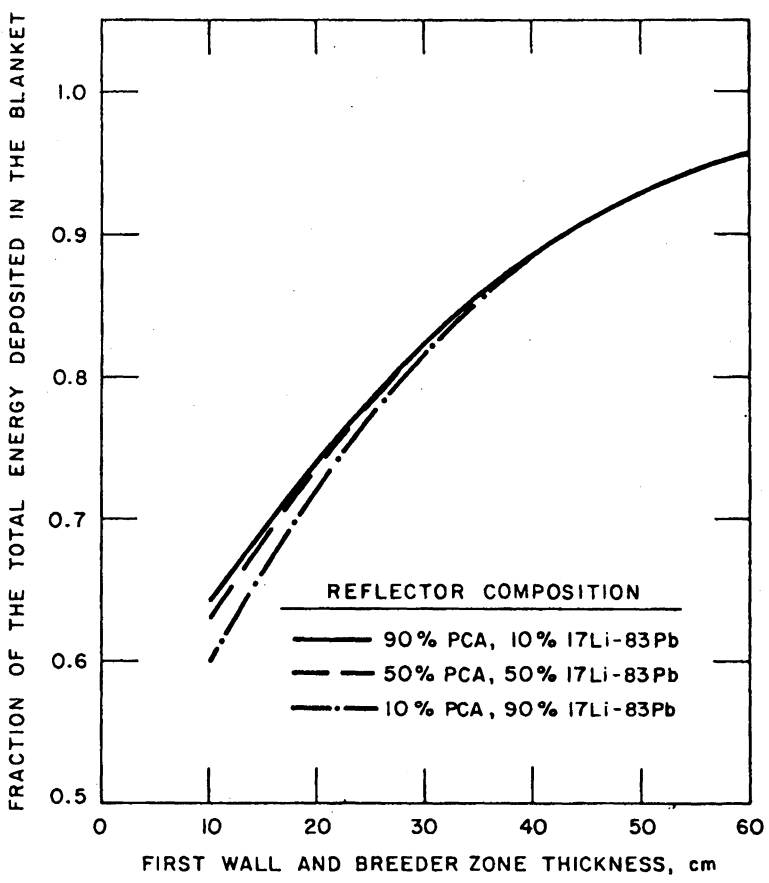

Figure VII.1-45. Fraction of the total energy deposited in the blanket as a function of the combined thickness of the first wall and lithium lead breeding zone with 10 cm reflector zone thickness.

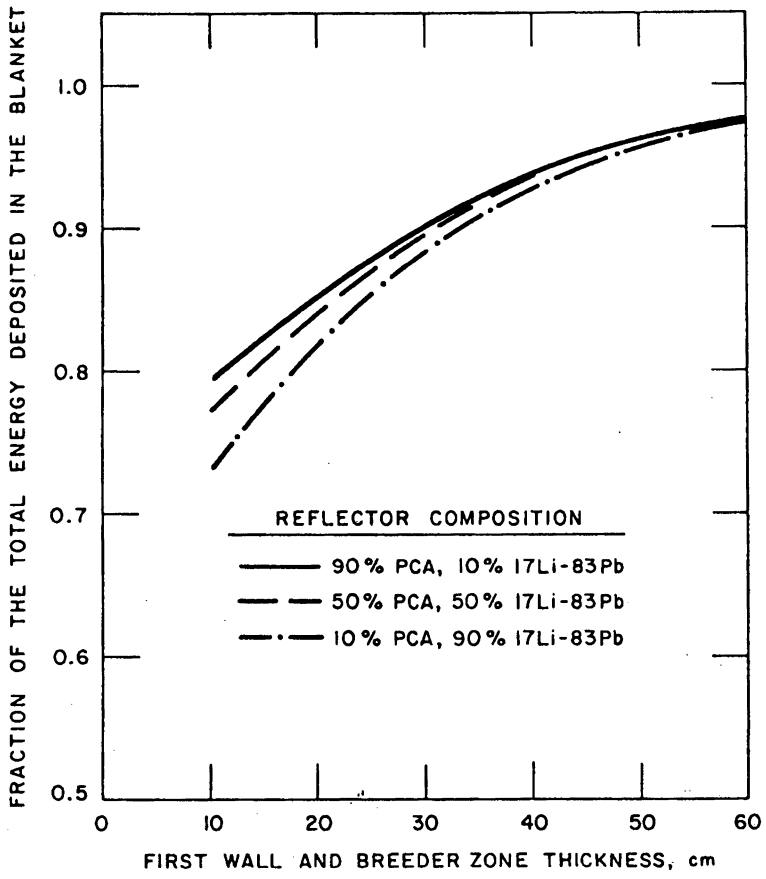

Figure VII.1-46. Fraction of the total energy deposited in the blanket as a function of the combined thickness of the first wall and lithium lead breeding zone with 20 cm reflector zone thickness.

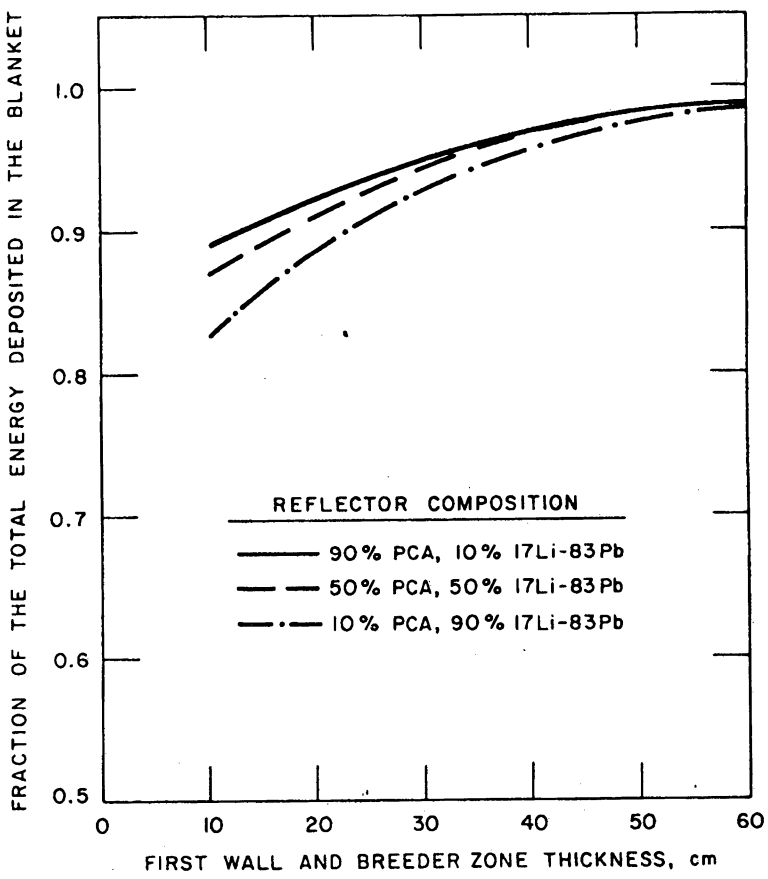

Figure VII.1-47. Fraction of the total energy deposited in the blanket as a function of the combined thickness of the first wall and lithium lead breeding zone with 30 cm reflector zone thickness.

reflector composition and thickness for the two breeder materials under consideration.

For the lithium system, Fig. VII.1-44 shows that the blanket thickness should be about 90 cm to reduce the percentage of the total energy deposited in the shield to 1.6%, assuming a reflector composition of 0.9 PCA and 0.1 lithium. This blanket thickness has a 1.36 TBR based on ENDF/B-V data files. In such cases it is possible to reduce the TBR to a lower value and reduce the blanket thickness by using more PCA volume fraction in the breeding zone. This kind of trade increases the energy produced per D-T neutron. In the inboard section of tokamak reactors this kind of trade between the TBR and the steel fraction in the blanket can not be used since a large lithium fraction in the blanket is required to reduce the lithium average velocity. Also, the inboard blanket thickness is constrained to about 60 cm, which increases the percentage of total energy deposited in the inboard shield to ~ 10%. The inboard region which represents 20% of the first wall surface area, corresponds to deposition of 2% of the total energy in the inboard shield. This situation requires careful trade study for the inboard blanket and provides incentive to reduce the energy in the rest of the shield system.

VII.1.6 Tritium Recovery

In this section, techniques for tritium recovery from liquid metals are reviewed for feasibility, possible problems (e.g., high corrosion rates, high tritium inventory), and potential cost. The emphasis is on the feasibility of tritium recovery and possible problems. Reasonable blanket tritium recovery techniques are identified for both lithium and 17Li-83Pb. The tritium inventory, and hence, the minimum tritium breeding ratio, will depend on which blanket concept is chosen.

Calculations given here are based on a fusion power plant similar to the STARFIRE[13] design. The pertinent parameters include 4000 MW of thermal power, a tritium burnup rate of 0.536 kg/d, a fractional tritium burnup of 0.4, a 7 m major radius for the plasma chamber, 780 m^2 for the first wall area of the blanket, 150 K average temperature rise as the coolant flows through the reactor blanket, and 75% plant availability. The thermal power and the average coolant temperature rise set the coolant flow rate shown in Table VII.1-6 along with an estimate of the mass for each liquid metal and other pertinent

TABLE VII.1-6. LIQUID METAL MASS IN A FUSION REACTOR BLANKET[a]

Liquid Metal	Molecular Weight, kg/kmol	Melting Temp., °C	Coolant Flow Rate, m^3/s	Density, kg/m^3	Mass of Liquid Metal, Mg			Conversion Factor[c]
					Inside Blanket	Outside[b] Blanket	Total	
Li	6.94	179	12.86	490[d]	192	192	384	2.31
17Li-83Pb	173.15[e]	235	15.08	9400[f]	3680	3680	7360	57.7
Na	23.0	98	g	856[h]	0[g]	336	336	7.67

[a]Average temperature of liquid metals is 400°C. Volume of liquid metal in fusion reactor blanket is given in Ref. 14 as 392 m^3. STARFIRE reference design is used.

[b]Assume the same volume is required outside the fusion reactor blanket as is required inside it.

[c]Tritium concentration in liquid metal in appm if given concentration is 1.0 wppm.

[d]See Ref. 15.

[e]Molecular weight was calculated using the atom fraction of the atomic weight of each metal in the lithium-lead alloy.

[f]See Ref. 16.

[g]Because of MHD effects, Na will not be used inside the blanket. However, it could be used in a secondary loop associated with an intermediate heat exchanger (IHX) or with a sodium cold trap.

[h]See Ref. 17.

information. These conditions are referred to below as the STARFIRE reference design.

To look at tritium recovery from liquid metals, consideration is first given to tritium inventory and processing rate. Then the various recovery techniques, gas recovery, solid metal getter, cold trap, molten salt extraction, and tritium permeation, are reviewed. Finally, the methods appropriate to lithium and to 17Li-83Pb are identified.

VII.1.6.1 Tritium Inventory

Tritium recovery techniques should give tritium inventories as low as possible. This gives improved safety, reduced tritium doubling time, and reduced start-up costs for a fusion power reactor.

As a part of the work on tritium inventory, the relation between tritium inventory, effective tritium breeding ratio, and tritium doubling time has been clarified.[18,19] This relation is shown in Fig. VII.1-48 where the recoverable tritium is all the tritium in the fusion power plant less any tritium which can not be recovered and less that tritium which can be given away without jeopardizing reactor operation. The effective tritium breeding ratio is the actual tritium breeding ratio less a correction term for tritium which is permanently lost, e.g., to the environment or trapped in the limiter. For the STARFIRE reference design, this correction term is estimated to be small (0.0012). The main contribution to the correction term is tritium trapped in the limiter wall.[19] Figure VII.1-48 applies to the first fusion power plant making tritium for the second fusion power plant. For this case, the tritium needed to start up the second plant will be very close to the recoverable tritium in the first plant. Thus, the pertinent tritium inventory is the recoverable tritium in the plant. To estimate the recoverable tritium, the fusion power plant has been divided into three parts: fueler system, blanket system, and balance of the plant.

The fueler system consists of the plasma, vacuum pumps, fuel processing units, fueler, and temporary storage. The tritium inventory of the fuel handling components increases as the fractional tritium burnup in the plasma decreases. For the STARFIRE reference design, the fuel system tritium inventory increases from 0.4 to 1.4 to 3.8 to 15.0 to 38 kg as fractional burnup decreases from 0.4 to 0.1 to 0.04 to 0.01 to 0.004, respectively. In addition,

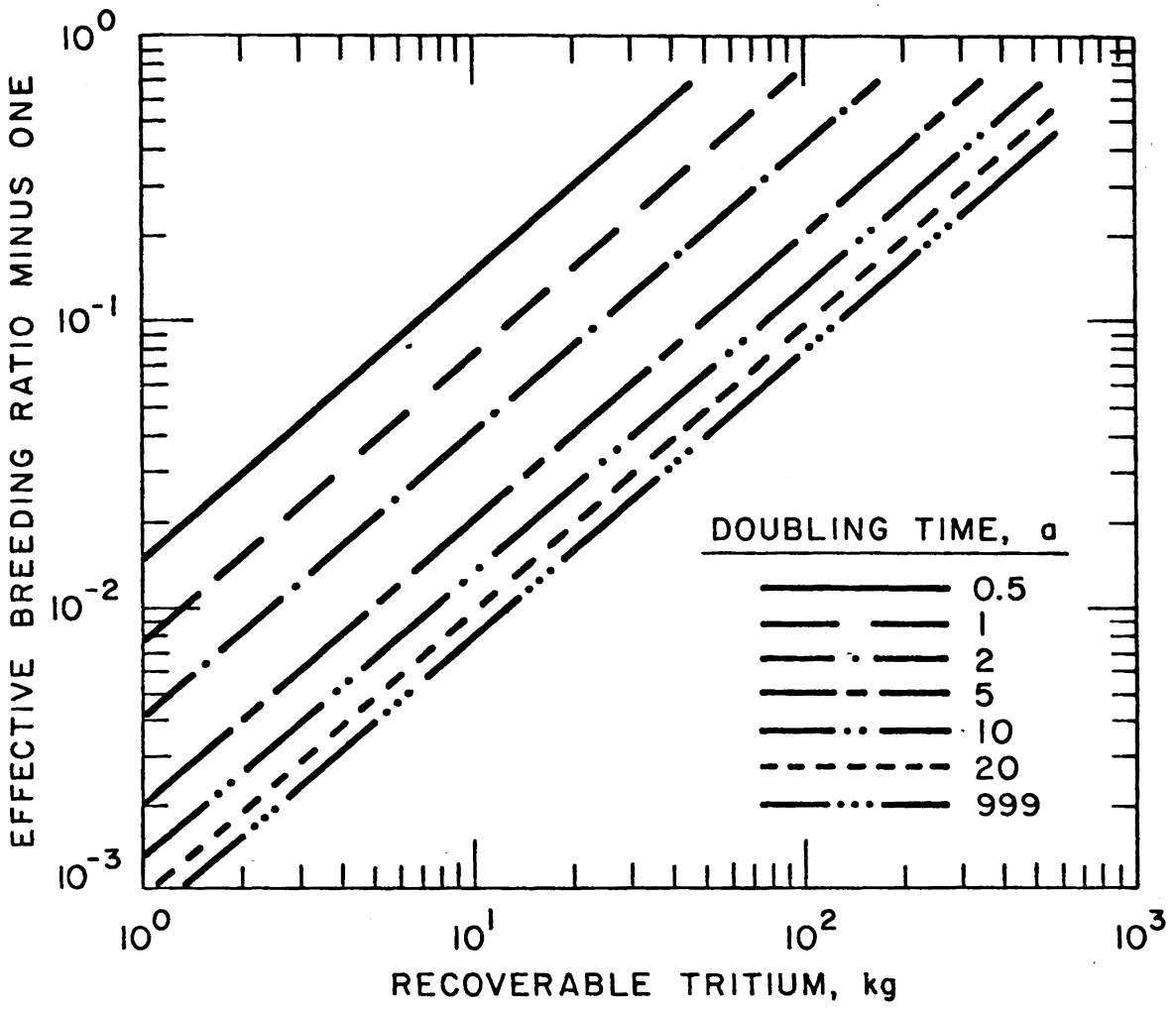

Figure VII.1-48. Relation between the effective tritium breeding ratio, the mass of recoverable tritium, and the tritium doubling time.

if the reactor is to be kept running for one, four, or eight days after the blanket tritium recovery system has been shutdown, further tritium in the amounts of 0.53, 2.1 or 4.3 kg, respectively, is required in temporary storage. This additional tritium is independent of the fractional tritium burnup.

The base case for the fueler system is a fractional burnup of 0.4 and eight days of operation without the blanket tritium recovery system. This gives a tritium inventory of 4.7 kg in the fueler system.

The blanket system consists of the breeder, first wall, and other blanket walls, and will usually have a coolant (this is the breeder in self-cooled liquid metal blankets), intermediate tritium carrier materials (e.g., helium or sodium), a purge gas system, tritium recovery for the purge gas system, a breeder tritium recovery system, and a coolant tritium recovery system. Of these components, the total tritium in the blanket walls other than the first wall and those walls made of vanadium, the intermediate tritium carrier materials, the purge gas, and the purge gas tritium recovery system have only a small amount of tritium so that their combined mass of tritium will be less than 0.1 kg. Figure VII.1-49 shows the amount of tritium in the liquid metal (the breeder) as a function of the tritium concentration in the liquid metal. This concentration depends, in turn, on the tritium recovery method. The tritium in the first wall (PCA at 400°C on the plasma side, 300°C on the coolant side, and 5 mm thick) is estimated to be 2.0 kg based on the results presented by Abdou[20] and assuming a molecular sticking coefficient of 0.5 for the plasma side of the first wall, an oxide barrier of 10x on the coolant side of the first wall, the fraction of the alpha particle heating to the first wall is 0.5, the edge temperature of the plasma is 150 eV, and the first wall particle flux is 8×10^{16} particles (D-T)/($cm^2 \cdot s$). This estimate should decrease if either HT-9 or vanadium is used or if the temperature is higher because, in each case, tritium permeability will be higher. However, tritium trapping factors also need to be accounted for. The amount of tritium in a vanadium wall depends on the pressure of tritium next to the wall and the wall temperature.[21] This relation is given in Fig. VII.1-50. If a wall has a much lower tritium pressure on the other side, the half thickness of the wall should be used in calculating the effective wall volume. For the base case liquid metal blanket design in this report with 17Li-83Pb as the coolant at a tritium pressure of 1.0 Pa and with temperatures ranging from 650°C to 400°C, the effective

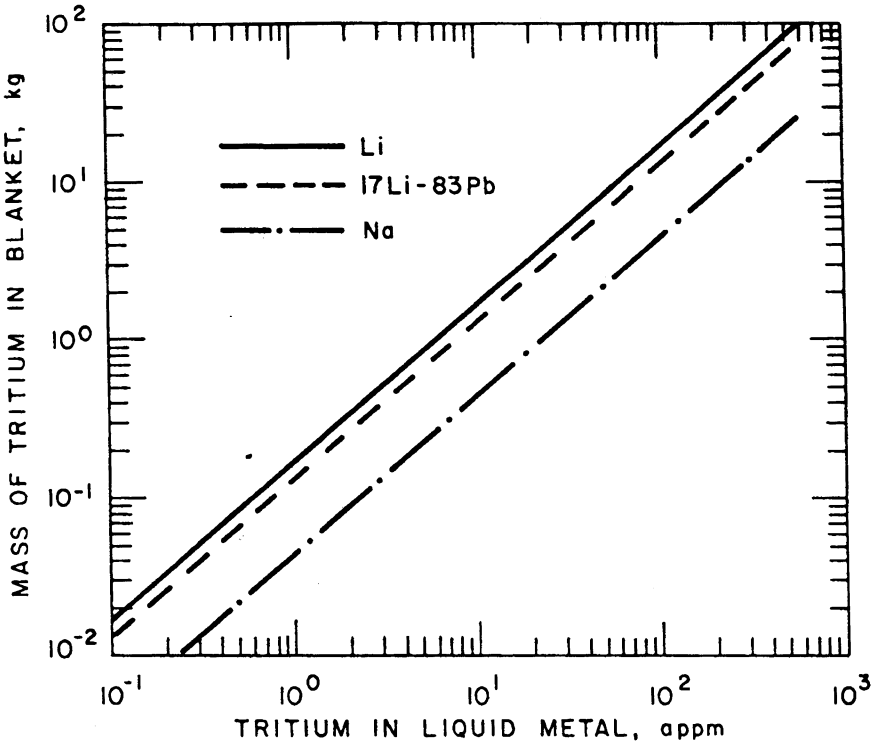

Figure VII.1-49. Effect of tritium concentration on the amount of tritium in the liquid metal for a fusion reactor blanket.

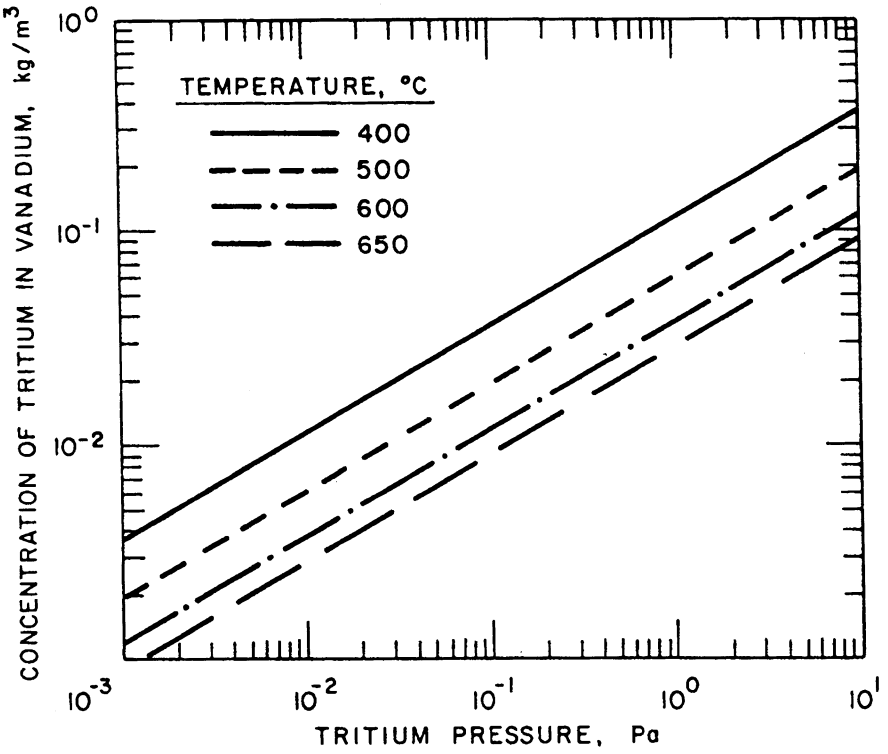

Figure VII.1-50. Effect of temperature and tritium pressure at a vanadium wall on the concentration of tritium in the wall.

vanadium volume (188 m^3) will have a tritium inventory ranging from 5.3 to 21.0 kg, respectively, based on the tritium concentration in vanadium given in Fig. VII.1-50. The tritium inventory for the various tritium recovery systems for the breeder and coolant are discussed below in the section on tritium recovery techniques. Typically, tritium recovery techniques for the coolant and breeder require less than 0.5 kg of tritium inventory. Thus, if vanadium walls are not used, the tritium inventory for the blanket system should be 3 kg or less.

The recoverable tritium inventory in the balance of the plant is estimated to be less than 0.2 kg. This includes the reactor hall, tritium laboratories outside the reactor hall, and the atmospheric tritium recovery system.

The recoverable tritium inventory depends mainly on the number of days of operation desired after the blanket tritium recovery system has been shut down, the fractional burnup of tritium in the reactor, the tritium inventory in the first wall of the reactor, the use of vanadium in the blanket walls, and, in some cases, as will be seen below, the choice of tritium recovery method. Thus, the choice of blanket, blanket design, and blanket tritium recovery system will have an impact on the recoverable tritium inventory in a fusion power plant. As the recoverable tritium inventory goes from 10 to 20 to 40 kg, the minimum tritium breeding ratio goes from 1.019 to 1.038 to 1.077, respectively, for a tritium doubling time of five years or from 1.039 to 1.079 to 1.159, respectively, for a doubling time of two years.

VII.1.6.2 Processing Rate

The processing rate needed if the liquid metal is the coolant, i.e., the fraction of liquid metal which must go to the breeder tritium recovery unit, depends on the amount that the tritium concentration in the liquid metal is reduced in the tritium recovery unit. This relation is shown in Fig. VII.1-51. For the case where the liquid metal is only the breeder, the rate at which the liquid metal must be circulated to the breeder tritium recovery unit is the fraction of liquid metal flow to be processed (Fig. VII.1-51) times the total liquid metal flow (Table VII.1-6).

VII.1.6.3 Recovery Techniques

Recovery techniques for tritium include gas recovery by sparging or vacuum, solid metal getter, cold trap, molten salt extraction, and tritium

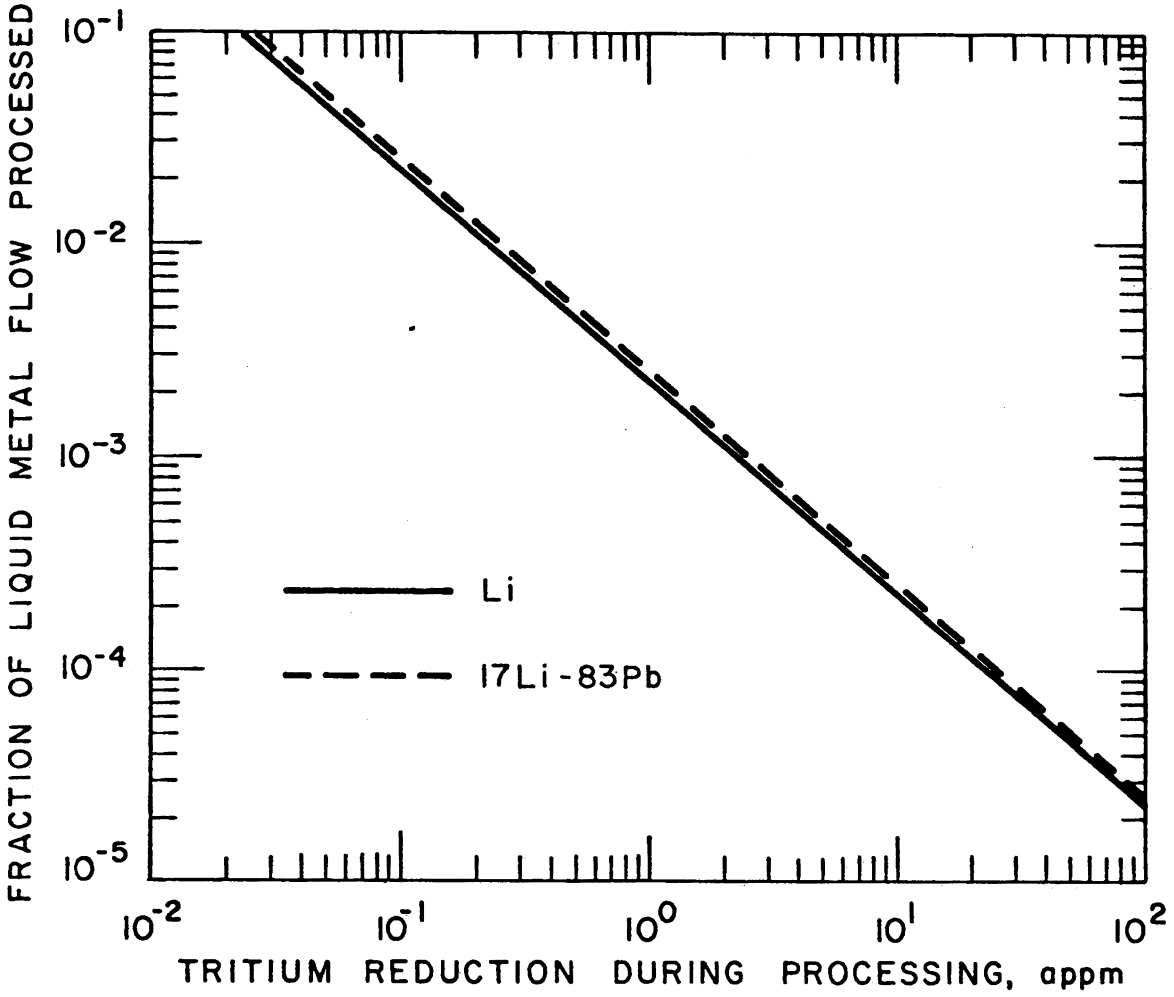

Figure VII.1-51. Effect of tritium concentration reduction during processing on the fraction of the liquid metal flow which must be processed.

permeation. These techniques are used alone or in combination. In particular, resistance to tritium permeation is neglected while other recovery techniques are discussed, then the role of tritium permeation on non-contacting (indirect) tritium recovery schemes is evaluated. An evaluation of tritium recovery for both lithium and 17Li-83Pb is reported here. As discussed elsewhere in this report, the use of sodium as the blanket coolant was not considered because of the high magnetohydrodynamic (MHD) pressures that would be developed by its flow through the fusion reactor blanket.

In the evaluation of various tritium recovery techniques, the tritium concentration in the liquid metal is important. This concentration depends on the metal, the tritium pressure, and the temperature as shown in Fig. VII.1-52. For the same tritium concentration in appm, the tritium pressure over 17Li-83Pb is four orders of magnitude higher than that for sodium. On the same basis, the tritium pressure over lithium is five to eight orders of magnitude lower than that for sodium. Thus, the use of sodium to recover tritium results in tritium inventories which are very low for 17Li-83Pb but very high for lithium.

In general, the 17Li-83Pb system is controlled by the maximum allowable tritium pressure. This pressure is usually taken to be 1.0 Pa (0.065 appm tritium in 17Li-83Pb at 450°C as shown in Fig. VII.1-52) so that the materials of construction are not damaged by the tritium. For these conditions, Fig. VII.1-49 gives a small tritium inventory (0.0085 kg) in the 17Li-83Pb blanket. The processing rates required to maintain the 1.0 Pa tritium pressure may be excessive for some blanket concepts and processing schemes. The lithium system is controlled by the maximum allowable tritium inventory. If this inventory is taken to be 0.5 kg of tritium, then the tritium concentration will be 3 appm which corresponds to a tritium pressure over the lithium of $\sim 10^{-7}$ Pa at 450°C. If the tritium pressure is allowed to increase to 5×10^{-4} Pa at 600°C, the tritium concentration will be 68 appm and the tritium inventory in the lithium corresponds to 12 kg.

VII.1.6.3.1 Gas Recovery

Gas recovery of tritium can be done by either direct or indirect contact of the gas with the liquid metal. For direct contact methods, a vacuum technique is preferred as this minimizes the contamination of the liquid metal by impurities in the gas. The mean free path of gas molecules is ~ 2 cm at 1

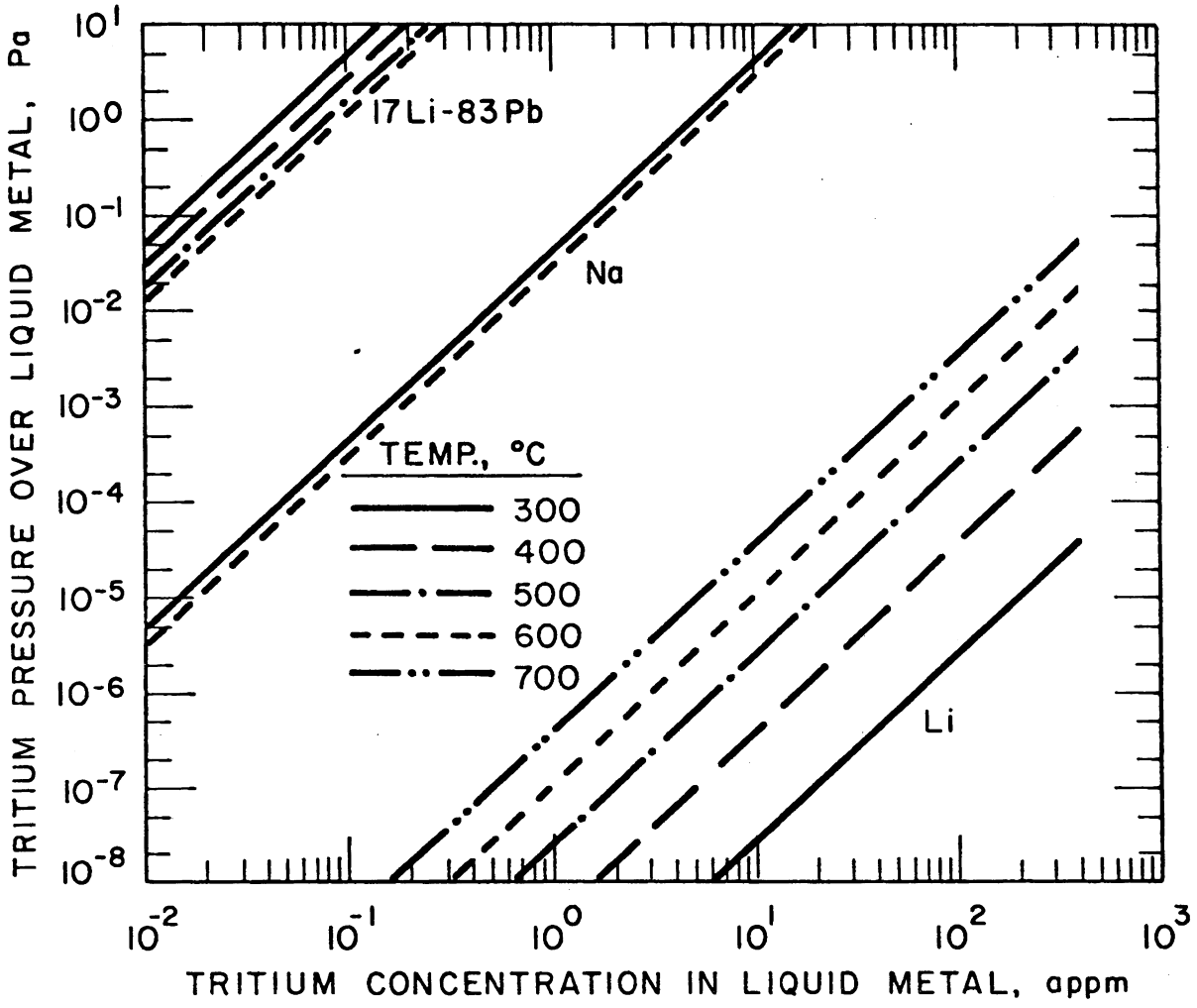

Figure VII.1-52. Effect of tritium concentration in liquid metal on the tritium pressure over the metal. Lithium: Veleckis[22], 17Li-83Pb: Veleckis[23]. Sodium: Maroni[21].

Pa[24] and, as the mean free path is inversely proportional to the pressure, the mean free path of the tritium gas increases as the pressure drops. The transition from viscous flow to molecular flow of the gas occurs when the mean free path exceeds the width of the passages available for gas flow. Thus, vacuum removal may occur in the viscous flow region for 17Li-83Pb systems with large gas passages since the tritium pressure is ~ 1 Pa. Operation in the viscous flow region would appear to be desirable as gas flow rate could be increased by decreasing the exit pressure. Vacuum recovery of tritium from lithium systems will operate in the molecular flow regime since the tritium pressure is $< 10^{-3}$ Pa. To facilitate the vacuum recovery of tritium from lithium an open structure is required so that the tritium can move away from the lithium.

If gas flow methods are employed in a direct contact system with the gas flowing countercurrent to the liquid metal, the gas stream is called a gas sparge. If gas flow methods are utilized in an indirect contact system, the gas stream is called a carrier gas. In either case, the gas flow rate will depend on the tritium pressure and on the total tritium flow through the system. At a tritium pressure of 1.0 Pa and a total tritium flow of 0.536 kg/d, the gas flow rate must be 2.3 m^3/s. This is not an unreasonable gas flow rate. However, at a tritium pressure of 10^{-7} Pa, which is desired for lithium to keep tritium inventory low, the gas flow rate must be 2.3×10^7 m^3/s. This gas flow rate is very high. As a result, compromise lithium systems are considered with tritium pressures up to 5×10^{-4} Pa so that indirect vacuum recovery can be used to recover tritium from lithium.

VII.1.6.3.2 Solid Metal Getter

Solid metal getters can be used to recover tritium from liquid lithium. The use of yttrium as a getter is especially attractive since, below 800°C, its tritium pressure is less than that for lithium for the same tritium concentration in appm.[25] The yttrium temperature should not be too low or tritium diffusion into the yttrium could be slow, requiring more residence time in the bed, and so, a greater tritium inventory. The use of a solid metal getter has been demonstrated in the laboratory using direct contact of lithium with yttrium.[26] In these tests, the lithium was washed off before the tritium was recovered. This tritium recovery procedure raises a concern about the ease of

tritium recovery from yttrium. The wash solution of water or alcohol would bring impurities such as air into the yttrium bed. When air gets to yttrium, it forms compounds with oxygen and nitrogen and the ability to regenerate yttrium is quickly lost.[27,28] In addition, the deactivated yttrium shows spalling and generally loses its mechanical integrity. For all these reasons, it is recommended that tritium be removed from the yttrium bed after draining off the lithium, but without washing off any residual lithium. Vacuum removal would be used to recover the tritium while minimizing introduction of impurities into the yttrium bed. The yttrium would be heated up 300 K to get a more rapid release of the tritium from the yttrium. By this heating, the tritium pressure would increase three orders of magnitude[25] up to 10^{-4} Pa. Work is needed on the design of a yttrium bed that would give effective removal of the tritium from the lithium during normal operation and from the lithium-coated yttrium during vacuum recovery of the tritium.

In practice, the yttrium bed might be at 450°C during normal operation. The tritium concentration in the lithium would be kept to 3 appm so that the tritium pressure would be 10^{-7} Pa. At this tritium pressure, tritium inventory in the lithium would be 0.5 kg but the tritium inventory in any vanadium walls could be neglected. Vanadium walls might be used in the getter beds so that they could be heated to 750°C with lithium present for the vacuum recovery of tritium.

The use of solid metal getters to recover tritium from 17Li-83Pb is easier as this liquid metal has a higher tritium pressure. Direct contact of 17Li-83Pb with yttrium is rejected because of potential impurity problems such as the formation of a yttrium-lead alloy.[29] However, direct contact of 17Li-83Pb with a vacuum or sparge gas could carry the tritium to a metal getter such as yttrium or Zr-Al.[30] This gas recovery system prevents impurity problems caused by direct contact of 17Li-83Pb with yttrium. To prevent the formation of other impurities caused by direct contact with air, the system must be kept air-tight. If vanadium, which is quite permeable to tritium, is used, indirect contact (through the vanadium wall) of 17Li-83Pb with the gas recovery system would prevent gaseous impurities from reacting with the liquid metal, and so, would be the system of choice.

In operation with either lithium of 17Li-83Pb, there would be three solid metal getter (yttrium) beds, one in use, one being heated up under vacuum to

recover the tritium, and one being cooled down for the next cycle. Each bed would have a 24-hour cycle including eight hours when the bed is actually being used to remove tritium from the liquid metal. A 24-hour cycle for the yttrium beds means, at most, a 16-hour holdup of tritium in the beds. This gives the yttrium beds a tritium inventory of 0.4 kg or less.

VII.1.6.3.3 Cold Trap

One method of recovering tritium from liquid metals is the use of a cold trap. The cold trap is a cool section (typically 20 K above the melting point of the liquid metal) of liquid metal loop where metal hydride or tritide forms a solid precipitate which is deposted in a packed bed in this cool region. When the bed becomes full of the tritide, it is taken out of service and regenerated. To regenerate the bed, it is heated up which releases the tritium as a gas.

To evaluate the cold trap potential for a given liquid metal, the solubility of the metal tritide must be known near the melting point of the metal. This tritide solubility, the concentration at which the precipitate forms, is given in Fig. VII.1-53. Data for lithium and sodium are well known. No data are available for 17Li-83Pb so an estimate was made interpolating between the data of Perini, et al[35] at high pressures where a solid hydride precipitate may exist (based on the relatively gradual increase in hydrogen pressure as hydrogen concentration increases) and the data of Chan and Veleckis[23] where the hydride is dissolved in the liquid 17Li-83Pb. This procedure gives an upper and lower bound for the tritide solubility in 17Li-83Pb at 400°C which is shown on Fig. VII.1-53. Based on the data for sodium and lithium, it is expected that tritide solubility will decrease as temperature decreases. This decrease in tritide solubility with temperature would have to be quite steep, like that for sodium, for cold trap operation to work with 17Li-83Pb.

A primary cold trap is a cold trap which is part of a liquid metal loop going through the fusion reactor blanket. Both lithium and 17Li-83Pb loops were considered for a primary cold trap. For a primary lithium cold trap, the tritium inventory would be too high, about 100 kg (see Figs. VII.1-49 and VII.1-53). For a primary 17Li-83Pb cold trap, the tritium inventory would be low (< 0.01 kg) if the cold trap would work. More data are needed on tritide solubility in 17Li-83Pb to determine if a 17Li-83Pb cold trap would work. At

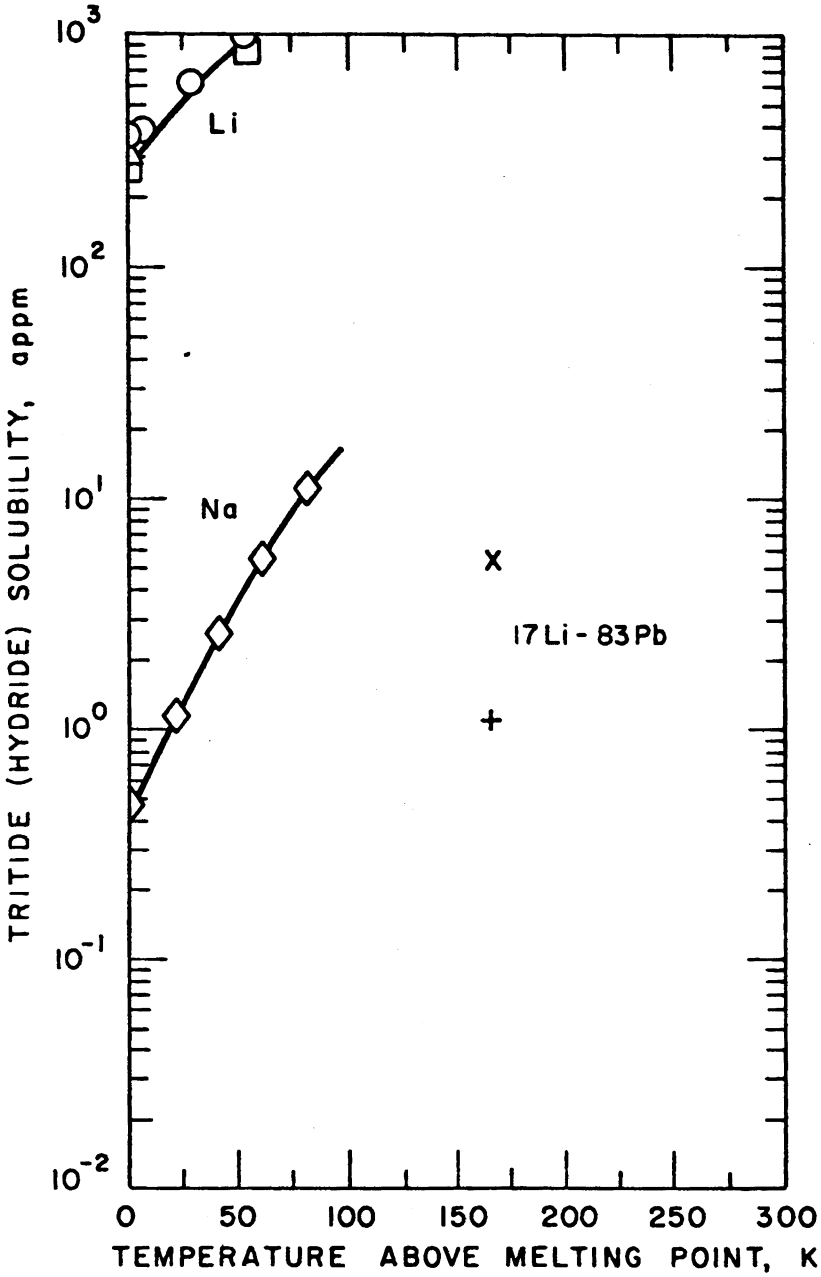

Figure VII.1-53. Effect of temperature above melting point on metal tritide (hydride) solubility in the molten metal. Li: Weston et al.[20] (o), Adams et al[21] (□), Veleckis et al[22] (△). Na: Vissers et al[23] (◇). 17Li-83Pb: high estimate (x), low estimate (+).

20 K above the 17Li-83Pb melting temperature, the tritide solubility should be less than the tritium concentration set by the temperature and allowable tritium pressure in the fusion reactor blanket. If tritium pressure is fixed at 1 Pa, the allowable tritium concentration will increase from 0.05 appm to 0.09 appm as the temperature decreases from 650°C to 350°C.

A secondary cold trap is a cold trap which is part of a secondary liquid metal loop. This secondary loop does not go through the fusion reactor blanket but is indirectly contacted with the primary loop across a solid metal wall which is fairly permeable to tritium. The walls and countercurrent liquid metal flows are designed so the the secondary liquid metal leaving the tritium mass exchanger has almost the same tritium pressure as the primary liquid metal entering the exchanger. Only sodium is considered for the secondary liquid metal loop. This secondary loop could go either to the steam generator, in which case, the tritium mass exchanger would also be the intermediate heat exchanger, or to a side loop.

If a secondary sodium cold trap with a cold trap temperature 20 K above the melting point for sodium were used with a primary lithium loop operating at 700°C, the tritium inventory in the lithium (see Figs. VII.1-49, VII.1-52, and VII.1-53) would be 54 kg. If the cold trap is operated at its limit, i.e., the melting point for sodium, the tritium inventory in the lithium would be 20 kg in agreement with Natesan and Smith.[36] If the lithium temperature in the blanket was reduced, the tritium inventory in the lithium would increase. Thus, the use of a secondary sodium cold trap with a primary lithium loop would be, at best, borderline.

Use of a secondary sodium cold trap with a primary 17Li-83Pb loop would work well without the problem of a high tritium inventory in the 17Li-83Pb. As with all 17Li-83Pb tritium recovery schemes, the fraction of 17Li-83Pb that would have to go to the tritium recovery loop would be high, 6.6% at a blanket temperature of 350°C or 3.2% at 650°C (see Figs. VII.1-51, VII.1-52, and VII.1-53). Other conditions assumed in the 17Li-83Pb loop are that the tritium pressure is 1 Pa and that the cold trap operates at 20 K above the melting point of sodium. If the secondary sodium loop goes to the steam generator, then all the 17Li-83Pb will go to the mass exchanger which is now also the intermediate heat exchanger (IHX). In this case, a small fraction (< 0.001) of the sodium in the secondary loop will be required to go to sodium cold trap.

In practice, there would be three sodium cold traps: one in use, one being heated up under vacuum to recover the tritium as gas, and one being cooled down for the next cycle. Each trap would be on a 24 h cycle including 8 h when the trap is actually being used to capture tritium from the sodium. A 24 h cycle means, at most, a 16 h holdup of tritium in the cold traps. This gives the cold traps a tritium inventory of 0.4 kg or less.

VII.1.6.3.4 Molten Salt Extraction

Molten salt extraction has been demonstrated as a way of recovering tritium from molten lithium.[31,37,38] As the lithum halide salt mixture used in these tests has a melting point of ~ 445°C, process tests were done at 500°C. This high temperature would rule out austenitic stainless steel as a material of constuction although vanadium would still be available. A major concern is the lithium halide salts, which would be present in the lithium in trace amount (~ 500 appm). These salts might enhance the corrosive properties of the liquid lithium just as trace amounts of chloride salts in water enhance the corrosive properties of water with respect to stainless steel. Experimental work is needed to determine whether or not corrosion will be a problem. Tritium recovery by this method is quite good and should allow tritium concentrations of 3 appm or less[31] to be maintained in the molten lithium. This gives a tritium inventory of 0.5 kg in the molten lithium (see Fig. VII.1-49) which would be quite satisfactory.

Since the total residence time of the tritium as it moves through the recovery loop from feed lines, surge tank, molten salt contactor, and molten salt electrolysis to release the tritium as gaseous T_2 would be 20 minutes or less, the tritium inventory in the molten salt extraction recovery loop would be 0.008 kg or less.

No work has been done with the use of molten salts to extract tritium from 17Li-83Pb. The presence of the lead makes this a more complex system and one which might have even more corrosion problems. Also, other methods from recovering tritium from 17Li-83Pb look attractive.

VII.1.6.3.5 Tritium Permeation

If the liquid metal is not brought in direct contact with the tritium recovery material, the tritium must diffuse through a solid metal wall. To

evaluate the rate at which the tritium permeates through the solid metal wall separating the liquid metal from the tritium recovery material, the permeability values in STARFIRE[13] were used. The result, shown in Fig. VII.1-54, gives tritium flux (tritium flow rate per unit area) times wall thickness as a function of temperature, tritium pressure, and wall material. In this figure, the effective tritium pressure p_{eff} is given by $(\sqrt{p_1} - \sqrt{p_2})^2$ where p_1 is the tritium pressure on that side of the solid metal wall which has the higher tritium pressure and p_2 is the tritium pressure on the other side.

For a base case to use with the STARFIRE reference design, the tritium flow rate is taken to be the tritium burn rate (5.36×10^5 mg/d), the wall area (5000 m^2), and the wall thickness (0.0016 m) so that the tritium flux times wall thickness becomes 0.1715 $mg \cdot d^{-1} \cdot m^{-1}$. At 1 Pa tritium partial pressure expected for 17Li-83Pb, vanadium will work above 330°C; ferritic steel will work at 700°C and 1 Pa or at 550°C if tritium pressure is increased to 10 Pa. Austenitic stainless steel will not give sufficient tritium flow rates at the base condition to be useful in any method which recovers tritium using indirect contact, i.e., permeability. Thus, for 17Li-83Pb, the use of vanadium is recommended for those walls through which the tritium generated in the blanket must pass.

At the lower tritium pressures expected for lithium, vanadium will allow tritium to escape at its burn rate if temperatures are in the 600 to 700°C range. At 700°C, the effective tritium pressure in the lithium will be 6×10^{-5} Pa, the tritium concentration in the lithium will be 13 appm, and the tritium mass in the lithium will be 2.2 kg (see Fig. VII.1-49, VII.1-52, and VII.1-54). At 600°C, these values will be 3.7×10^{-4} Pa, 57 appm, and 9.5 kg. Note that this lithium calculation assumes zero tritium pressure on the other side of the wall so that the effective tritium pressure is the actual tritium pressure in the lithium. Thus, at 600°C, if the lithium pressure were 5×10^{-4} Pa and the other side pressure were 1×10^{-5} Pa, the effective pressure would be 3.7×10^{-4} Pa; the concentration, 67 appm; and the tritium mass in the lithium, 12 kg.

While vanadium is the material of choice for any tritium recovery method which requires permeation, this choice imposes a constraint on the system. The system must be such that vanadium is not brought into contact with oxygen.

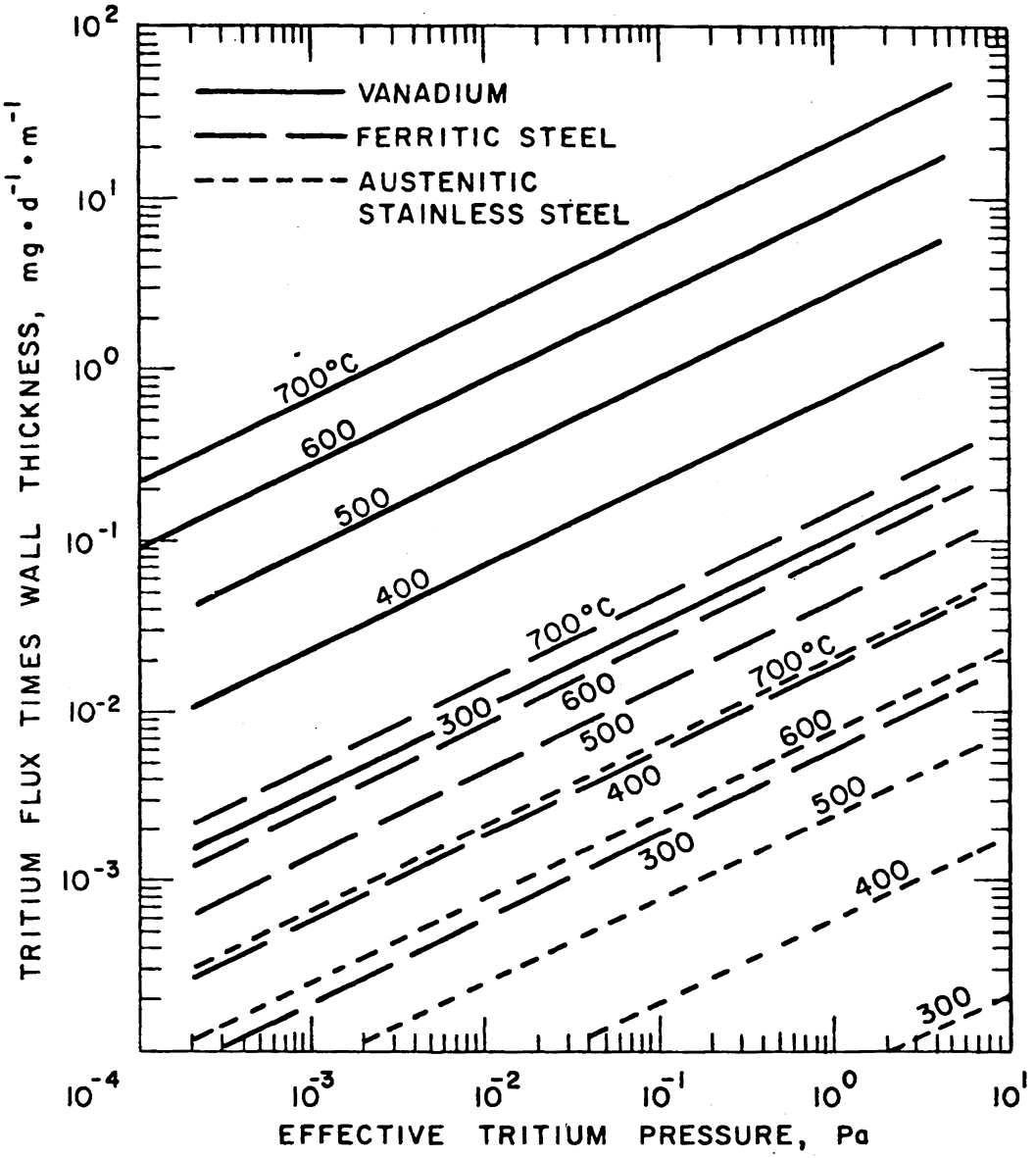

Figure VII.1-54. Effect of temperature, tritium pressure, and structural material on the tritium flux (mass flow rate per unit area) times the wall thickness.

Oxygen forms an oxide barrier on the surface of the vanadium which would greatly reduce its permeability, on the order of 1000x.[39]

VII.1.6.4 Lithium

Four of the methods reviewed above are candidates for the recovery of tritium from liquid lithium: sodium cold trap in a secondary sodium loop, permeation into a vacuum chamber, molten salt extraction, and direct contact with a yttrium getter. The first two methods are not as attractive as the last two methods because of their greater tritium inventories. Because of potential corrosion problems with method three (molten salt extraction), method four (direct contact with a yttrium getter) is recommended.

For the first method, the sodium cold trap in a secondary sodium loop,the tritium inventory would be very high, at least 20 kg in the lithium alone, and this value could go to 54 kg if normal sodium cold trap conditions, i.e., operation at 20 K above the melting point for sodium, are required.

For the second method, tritium permeation through vanadium tubes into a vacuum chamber, a small fraction of the total lithium flow would flow through vanadium tubes at 600°C. Since base vacuum pressures of 10^{-6} Pa are possible, a pressure of 10^{-5} Pa in the vacuum chamber would seem to be reasonable. The vanadium tubes would require sufficient spacing to allow tritium movement from the tubes to the vacuum pump ducts. The tritium concentration in the lithium would be 12 kg. The corresponding tritium pressure in the lithium would be 5 x 10^{-4} Pa so that the concentration of tritium in vanadium would be 8.3 x 10^{-4} kg/m^3. Estimating the total volume of vanadium in the blanket, intermediate heat exchanger, and tritium recovery unit to be on the order of 24 m^3 (1.5 x 10^4 m^2 wall area with a thickness of 1.6 mm), its tritium content would be low, 0.02 kg. Thus, the total recoverable tritium inventory for the fusion power plant with a lithium blanket and a permeation-vacuum recovery system would be 20 kg.

Direct permeation of tritium from the blanket into the plasma vacuum chamber, as suggested below for 17Li-83Pb, is not recommended for lithium as the tritium pressure in the operating reactor plasma chamber is too high, e.g., 0.012 Pa for STARFIRE,[13] to allow tritium permeation from the lithium in the blanket tubes.

The third method, molten salt extraction, has many attractive features and has been demonstrated in the laboratory. The tritium concentration in the lithium would be reduced to 3 appm so that the tritium inventory in the lithium would be only 0.5 kg and the total recoverable tritium in the fusion power plant would be 8 kg. However, the presence of trace amounts of lithium halide salts in the molten lithium could present a corrosion problem. Experimental work is required to determine if corrosion would actually be a problem.

Contact with a yttrium getter, the fourth method, is recommended. The tritium concentration in the lithium would be only 0.5 kg and the total recoverable tritium in the fusion power plant would be 8 kg. A detailed design and subsequent analysis of the yttrium getter bed is required to be sure that tritium can be recovered from the yttrium bed within a reasonable time.

VII.1.6.5 17Li-83Pb

Three methods for recovery of tritium from 17Li-83Pb are considered as candidates. All are indirect contact methods as the use of PCA with 17Li-83Pb has been ruled out and vanadium, which is quite permeable to tritium, has taken the place of PCA. If HT-9 were considered, some of the direct contact methods discussed above would become attractive. The three indirect contact methods are permeation into a vacuum chamber, permeation into a carrier gas going to a solid metal getter, and permeation into a sodium loop with a sodium cold trap. While all three methods are attractive, the last method, tritium permeation into a secondary sodium loop with a cold trap, is recommended. The secondary sodium loop is the most attractive since, for safety reasons, it appears that we will want to have it anyway. The total recoverable tritium inventory in a fusion power plant with a 17Li-83Pb coolant and a secondary sodium loop with a cold trap would be 14 kg. This includes 6 kg of tritium in 200 m^3 of vanadium walls at 650°C with a tritium pressure of 1.0 Pa in the 17Li-83Pb. The tritium concentration in 17Li-83Pb would be 0.086 appm.

If 17Li-83Pb is to be used as the tritium breeder but not as the coolant, an alternative tritium recovery method is available. A schematic of the method is shown in Fig. VII.1-55. The design scheme allows tritium to be recovered directly from the vacuum chamber surrounding the plasma by using vanadium for the outside walls of the long tubes containing the 17Li-83Pb which run the length of the plasma chamber from top to bottom. In the center of each such

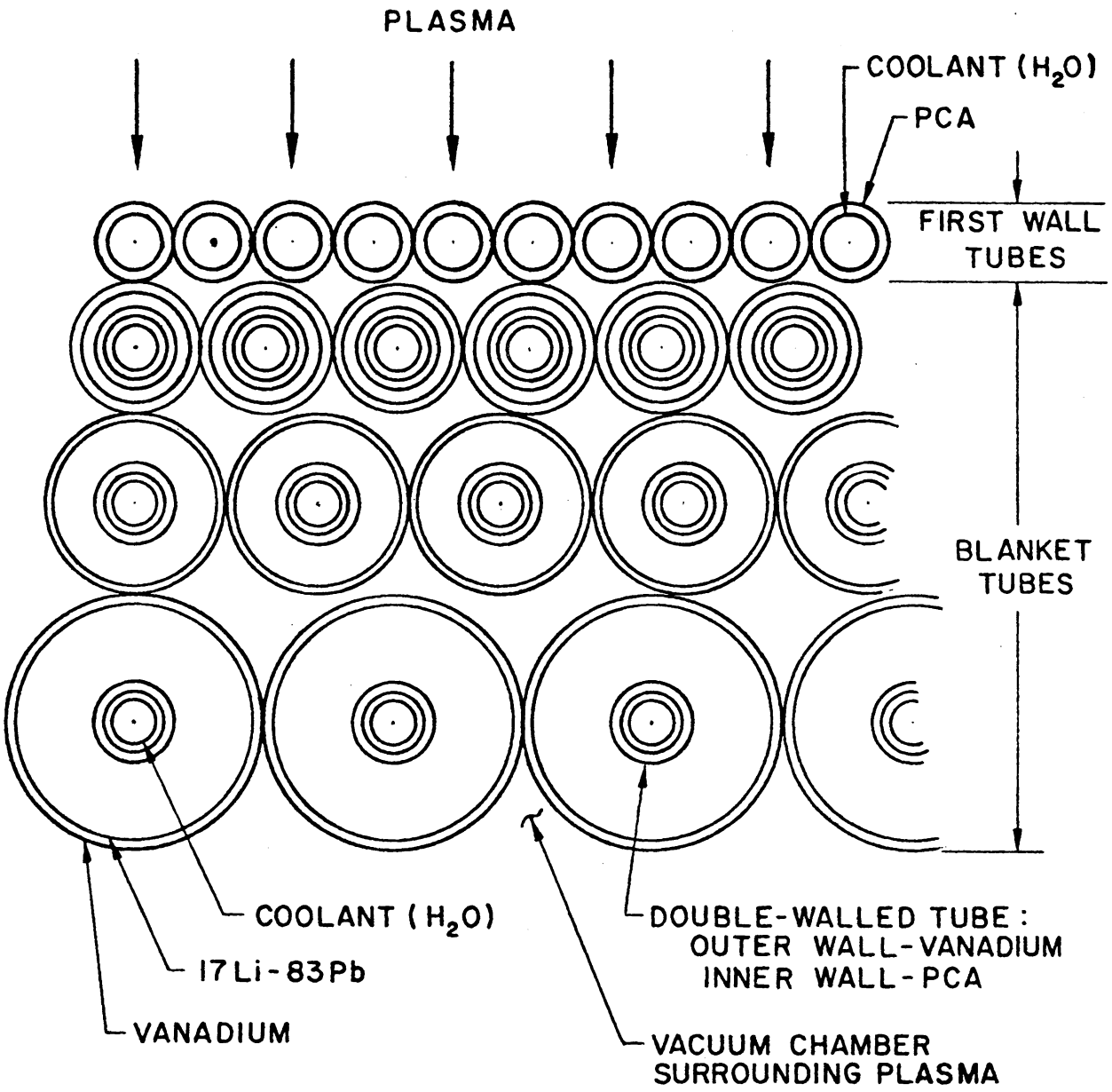

Figure VII.1-55. Schematic of a static 17Li-83Pb blanket with tritium recovery directly into the vacuum chamber surrounding the plasma. Shown in a horizontal cross section of the vertical tubes.

tube containing 17Li-83Pb is a double walled tube (DWT) containing the coolant (either water, as shown in Fig. VII.1-55, or a molten salt). The outer wall of the DWT would be vanadium for compatibility with the 17Li-83Pb (if the coolant were water, the temperature at this wall would be low enough to permit the use of PCA); the inner wall would be PCA for compatibility with the water and to limit the permeation of tritium into the water. The first wall tubes would contain only high pressure water to take the high heat flux at the first wall. For this scheme, the recoverable tritium inventory in the fusion power plant would be 10 kg. This includes 6 kg of tritium in 14 m^3 of vanadium walls at ~ 350°C with a tritium pressure of ~ 1.0 Pa in the 17Li-83Pb. The tritium concentration in the 17Li-83Pb would be 0.05 appm.

REFERENCES FOR SECTION VII.1

1. C. C. Chang and T. S. Lundgren, "Duct Flow in Magnetohydrodynamics," ZAMP, Vol. 12 pp. 100-114 (1961).

2. J. C. R. Hunt and R. J. Holroyd, "Applications of Laboratory and Theoretical MHD Duct Flow Studies in Fusion Reactor Technology," UKAEA Res. Group Report, Culham Laboratory, CLM-R169 (1977).

3. J. C. R. Hunt and R. Hancox, "The Use of Liquid Lithium as Coolant in a Toroidal Fusion Reactor - Part I: Calculation of Pumping Power," UKAEA Res. Group Report, Culham Laboratory, CLM-R115 (1971).

4. M. A. Hoffman and G. A. Carlson, "Calculation Techniques for Estimating the Pressure Losses for Conducting Fluid Flows in Magnetic Fields," Lawrence Radiation Laboratory, UCRL-51010.

5. G. A. Carlson, "Magnetohydrodynamic Pressure Drop of Lithium Flowing in Conducting Wall Pipe in a Transverse Magnetic Field - Theory and Experiment," First Topical Meeting on the Technology of Controlled Nuclear Fusion, San Diego, CA (1974).

6. S. Ihara, K. Tajima and A. Matsushima, "The Flow of Conducting Fluids in Circular Pipes with Finite Conductivity under Uniform Transverse Magnetic Fields," Journal of Applied Mechanics, pp. 29-36 (1967).

7. H. Branover, "Magnetohydrodynamic Flow in Ducts," J. Wiley and Sons (1978).

8. J. S. Walker, Private Communication, University of Illinois, Urbana, IL.

9. Workshop on Liquid Metal MHD in Fusion, Argonne National Laboratory, Argonne, IL (August 1983).

10. R. J. Holroyd, "An Experimental Study of the Effects of Wall Conductivity, Non-Uniform Magnetic Fields, and Variable Area Ducts on Liquid Metal Flows at High Hartmann Numbers - Part 2: Ducts with Conductivity Walls," J. F. M. Vol. 96, Part 2, pp. 355-374 (1980).

11. R. J. Holroyd and J. S. Walker, "A Theoretical Study of the Effects of Wall Conductivity, Non-Uniform Magnetic Fields and Variable Area Ducts on Liquid-Metal Flows of High Hartmann Numbers," J. F. M. Vol. 84, Part 3, pp. 471-495 (1978).

12. W. T. Sha, et al., "COMMIX-1: A Three-Dimensional Transient Single-Phase Component Computer for Thermal-Hydraulic Analysis," ANL-77-96, September, 1978.

13. C. C. Baker, et al., "STARFIRE--A Commercial Tokamak Fusion Power Plant Study," ANL/FPP-80-1 (September 1980).

14. H. Mantz, McDonnell Douglas Astronautics Co., St. Louis, MO, private communication (2-1-83).

15. R. N. Lyon, et al., editor, Liquid Metals Handbook, 2nd Ed. (revised), Atomic Energy Comm. and Dept. of Navy (1954).

16. D.-K. Sze, Univ. of Wisconsin, Madison, WI, private communication (3-9-83).

17. O. J. Foust, editor, Sodium-NaK Engineering Handbook, Vol. 1, Gordon and Breach, NY (1972).

18. M. J. Steindler, et al., Chemical Technology Division, Fuel Cycle Section Quarterly Progress Report, January-March 1983 (in preparation).

19. M. J. Steindler, et al., Chemical Technology Division, Fuel Cycel Section Quarterly Progress Report, April-June 1983 (in preparation).

20. M. A. Abdou, et al., "Chapter VIII-Tritium and Blanket," FED-INTOR/TRIT/82-5 (1982).

21. V. A. Maroni and E. H. VanDeventer, J. Nuclear Matls. 85 & 86, Dec. II, Part A, 257 (1979).

22. E. Veleckis, R. M. Yonco, and V. A. Maroni, "The Current Status of Fusion Reactor Blanket Thermodynamics," ANL-78-109 (1979).

23. Y. C. Chan and E. Veleckis, "A Thermodynamic Investigation of Dilute Solutions of Hydrogen in Liquid Li-Pb Alloys," (To be presented at the Third Topical Meeting on Fusion Reactor Materials, September 19-22, 1983, Albuquerque, NM).

24. S. Glasstone, Textbook of Physical Chemistry, 2nd ed., D. VanNostrand, Princeton, NJ (1946).

25. E. M. Larsen, M. S. Ortman, and K. E. Plute, "Comments on the Hydrogen Solubility Data for Liquid Lead, Lithium and Lithium-Lead Alloys," UWFDM-415 (May 1981).

26. D. L. Smith, R. H. Lee, and R. M. Yonco, "Investigation of Nonmetallic Element Interactions in Vanadium-Alloy/Lithium Systems," 2nd Intern. Conf. on Liquid Metal Technology in Energy Production Proceedings, April 20-24, 1980, Richland, WA, CONF-800401-P1 (August 1980).

27. R. E. Baxbaum, Michigan State Univ., East Lansing, MI, private communication (1983).

28. V. A. Maroni, Argonne National Laboratory, Argonne, IL, private communication (1983).

29. M. A. Abdou, et al., "A Demonstration Tokamak Power Plant Study (DEMO)," ANL/FPP-82-1 (1982).

30. M. F. Singleton and C. M. Griffith, "Evaluation of a Nonevaporable Getter Pump for Tritium Handling in the Tokamak Fusion Test Reactor," UCRL-52584 (1984).

31. J. R. Weston, et al., "Recent Advances in Lithium Processing Technology at the Argonne National Laboratory," Second Intern. Conf. on Liquid Metal Technology, April 20-24, 1980, Richland, WA, CONF-800401-P1 (August, 1980).

32. P. F. Adams, et al., J. of the Less-Common Metals 42, 325 (1975).

33. E. Veleckis, R. M. Yonco, and V. A. Maroni, J. of the Less-Common Metals 55, 85 (1977).

34. D. R. Vissers, et al., Nucl. Technology 21, 235 (1974).

35. G. Pierini, et al., "Tritium Recovery from Liquid $Li_{17}Pb_{83}$," 12th Symposium on Fusion Technology, Julich (FRG), Sept. 13-17, 1982.

36. K. Natesan and D. L. Smith, Nucl. Technology 22, 138-150 (1974).

37. J. R. Weston, et al., "Chemical Processing of Liquid Lithium Fusion Reactor Blankets," Proceedings of the 14th Intersociety Energy Conversion Engineering Conf., Boston, MA, Vol. II, 1572 (1979).

38. W. F. Calaway, Nuclear Technology, 39, 63 (1978).

39. P. A. Finn, Argonne National Laboratory, Argonne, IL, private communication (1983).

VII.2.1 Helium-Cooled Designs

VII.2.1.1 Introduction

The long-range goals of this task are to prioritize the critical issues and evaluate the developmental requirements of liquid metal breeder/helium-cooled blankets. This section presents the selection and design of a prime candidate blanket and its variants which can be used to identify and address the critical issues, and assess the potential advantages of this blanket concept in comparison to alternate breeder/coolant configurations.

The approach adopted for accomplishing the above objectives was as follows:

1. Perform a literature review of liquid breeder, helium-cooled blankets.

2. Evaluate the proposed designs to determine if they satisfied or could be modified to satisfy this project's screening criteria.

3. Perform a preliminary screening of the candidate blankets based on desirable engineering and design characteristics.

4. Select or synthesize a preferred blanket and alternates, if warranted, for further consideration on the basis of the critical issues and this study's selection criteria.

The first three steps described above are presented in more detail in Section VII.2.1.2. The fourth step received the major effort of this study and is presented in Sections VII.2.1.3 through VII.2.1.8.

VII.2.1.2 Blanket Concept Evaluation and Selection

As the first step in arriving at the preferred blanket configuration, a literature review of liquid metal helium-cooled blankets was performed. The conceptual designs were classified based upon the coolant pressure boundary in order to facilitate their comparison. The design classifications are:

- Pressurized modules (lobed submodule)
- Pressurized canister
- Pressurized tubes

The designs found in the literature are listed in Table VII.2-1 and shown in Figs. VII.2-1 through VII.2-3.

TABLE VII.2-1. CLASSIFICATION OF LIQUID BREEDER/HELIUM-COOLED DESIGNS

Pressurized Modules (Lobed Submodule)

GA Synfuel[1] (1982)
GA Demo[2] (1978)
LLNL Tandem Mirror[3] (1977)

Pressurized Canister

Westinghouse Cylindrical Blanket Module[4] (1978)
GA Demo[5] (1976)
Culham Canister[6] (1974)

Pressurized Tube

Tandem Mirror Hybrid Reactor[7] (GA, 1981)
ORNL Demo[8] (1976)

The blanket concepts in Table VII.2-1 were evaluated on their ability to meet the minimum design guidelines of this study. It was determined that all of the concepts could have the potential of meeting the requirements without fundamental changes in the design. The design concepts were then evaluated based upon desirable design characteristics, including:

- Mechanical simplicity
- Minimum required number of joints and connections
- Ability to tolerate selling-induced stresses
- Ease of meeting material temperature limits (maximum structure temperatures, and liquid metal/structure interface temperature limit)
- Pumping power requirements
- First wall thickness/structure fraction
- Number of containment barriers to liquid breeder or tritium release

GA SYNFUEL (1982)

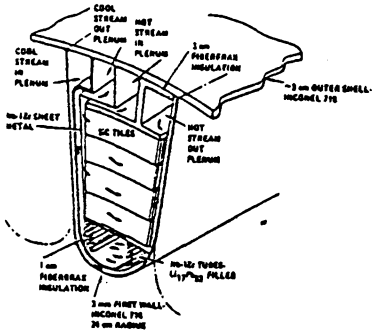

SIMPLE DESIGN
ACCEPTABLE T/H
GOOD NEUTRONICS
THIN FIRST WALL
LOW STRUCTURE FRACTION
HIGHLY SWELLING TOLERANT

GA DEMO (1978)

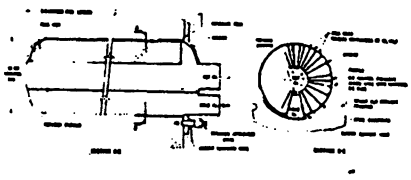

SIMPLE DESIGN
ACCEPTABLE T/H
AVERAGE NEUTRONICS
HIGHER STRUCTURE FRACTION
TWO BARRIERS TO LIQUID BREEDER RELEASE
SWELLING TOLERANT

LLNL TANDEM MIRROR

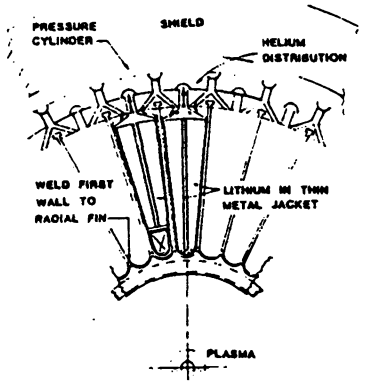

MANY SUBMODULES AND CONNECTIONS TO OBTAIN ACCEPTABLE T/H
HIGH STRUCTURAL FRACTION
TWO BARRIERS TO LIQUID BREEDER RELEASE
SWELLING TOLERANT

Figure VII.2-1. Pressurized module (lobed submodule), liquid breeder, helium-cooled blanket designs.

W CYLINDRICAL MODULE (1978)

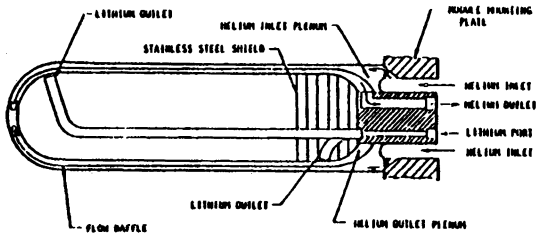

MANY MODULES AND CONNECTIONS
NEEDS T/H MODIFICATIONS
HIGH STRUCTURE FRACTION
TWO BARRIERS TO LIQUID BREEDER RELEASE
SWELLING TOLERANT

GA DEMO (1976)

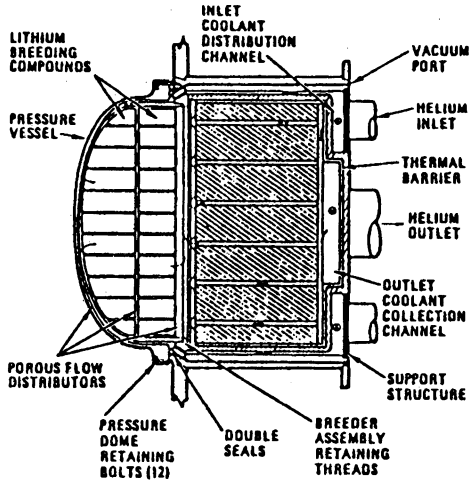

MANY MODULES AND CONNECTIONS
ACCEPTABLE T/H
HIGH STRUCTURE FRACTION
TWO BARRIERS TO LIQUID BREEDER RELEASE
CAN BE MADE SWELLING TOLERANT

Figure VII.2-2. Pressurized canister, liquid breeder, helium-cooled blanket designs.

TANDEM MIRROR HYBRID REACTOR
(GA 1981)

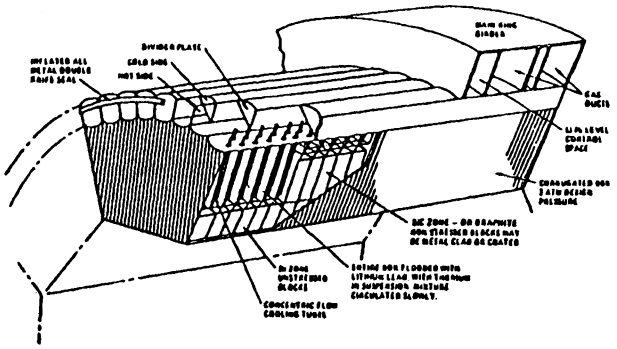

VERY SIMPLE DESIGN
POTENTIALLY HIGH n THERMAL
(HIGH He PRESSURE ACCEPTABLE)
MANY BUT SIMILAR TUBE CONNECTIONS
MAY NEED SEPARATELY COOLED FIRST WALL
(MAY RESULT IN INCREASED FIRST WALL THICKNESS)
GOOD NEUTRONICS
ONE BARRIER TO LIQUID BREEDER RELEASE
SWELLING TOLERANT

ORNL DEMO

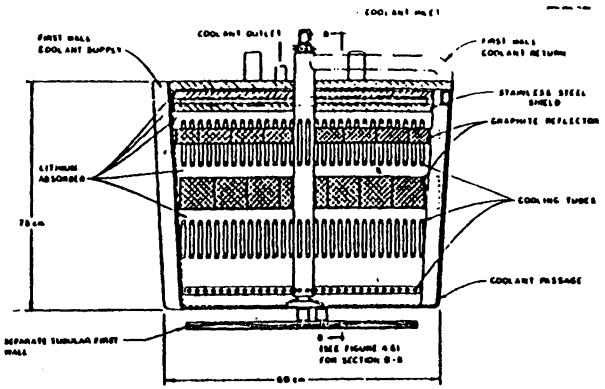

COMPLEX INTERNAL PLENUM DESIGN
SEPARATELY COOLED FIRST WALL
ACCEPTABLE T/H
INCREASED FIRST WALL THICKNESS
ONE BARRIER TO LIQUID BREEDER
RELEASE

Figure VII.2-3. Pressurized tube, liquid breeder, helium-cooled blanket designs.

The results of this evaluation are contained in Figs. VII.2-1 through VII.2-3 and summarized below.

From the perspective of the structural design, the pressurized module designs require the fewest number of submodules [approximately 10^3 for 3000 MW(t)] and are considered of medium complexity relative to the pressurized canister (approximately 10^4 units, higher complexity) and the pressurized tube concept (10^5 tubes, lower complexity). Neutronically, liquid-metal breeder blankets using natural lithium or the 17Li-83Pb eutectic have excellent performance (tritium breeding ratio of 1.2 with M = 1.2). Pressurized tube blankets have slightly lower structural fraction than pressurized modules. The latter offer the potential for an integral, and thus, thinnest first wall design. All the concepts require careful thermal-hydraulics design to accommodate concerns over the compatibility-limited interface temperature of the liquid metal with the structure. Pressurized modules and canisters offer multiple containment of the liquid metal and tritium. The pressurized module was thus chosen for the initial focus of the investigation of critical issues, and the blanket design of Reference 1 was adapted and developed in depth.

VII.2.1.3 Pressurized Module Mechanical Design

The blanket design developed for detailed investigation of critical issues is shown in Fig. VII.2-4. It is a mechanically simple configuration which features a PCA lobed first wall of the bellows type (Section VII.2.1.3), HT-9 tube fuel elements (Section VII.2.1.4) containing either static or very slowly circulating liquid breeder (Li or 17Li-83Pb), and a plate-type PCA reflector/shield region. Helium coolant entering the blanket is directed initially to the first wall region by a flow baffle and subsequently cross-flowed through the breeder tube bank and reflector plates. The characteristic dimensions of the tube and tube pitch are determined from thermal-hydraulics considerations as presented in Section VII.2.1.5. The composition and thicknesses of the breeder and reflector zones are determined from neutronics calculations which are presented in Section VII.2.1.6. Blanket tritium handling is presented in Section VII.2.1.7, and safety considerations in Section VII.2.1.8.

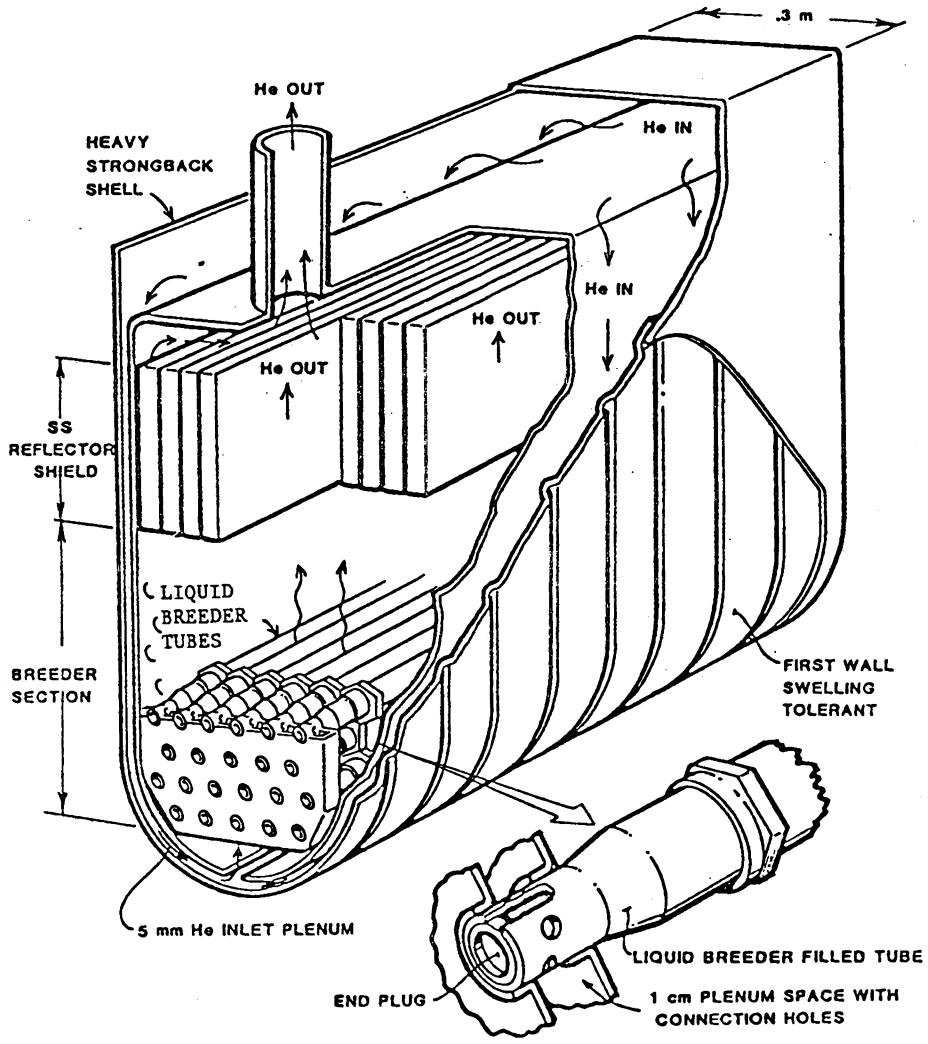

Figure VII.2-4. Helium-cooled/liquid-lithium breeder blanket module.

VII.2.1.3.1 Bellows First Wall Design

The primary mechanical design purpose of the first wall is to provide a boundary between the pressurized coolant and the vacuum of the plasma chamber. At the same time, it has to handle the transmission of thermal power through the wall to the high pressure helium coolant. There are two contributions to the heating of the wall; first, the volumetric power generation due to the neutron and material interaction, and second, a surface heat flux coming from the plasma side. In addition to these effects, the selected structural material has to handle the assumed effects of neutron-induced swelling and other radiation damage under high neutron fluence while being eroded away at a rate of ~ 1 mm/y.

The above task is severe by conventional standards. A service life of two years was selected for the reference design of the liquid metal helium-cooled concepts. Figure VII.2-5 illustrates the first wall which has resulted from our present studies, being an integral part of the blanket. The first wall itself is a semi-cylinder forming a lobe which is tied back to the structural region behind the blanket. The flat sides of the lobes are pressure balanced by adjacent lobes. Thus, the pressure is contained by pure tension in the wall. Thermal effects can be tolerated because of the comparative flexibility of this wall, as discussed below. To render the wall "soft" in the cylinder-axis direction so that it can tolerate disturbances in that direction, the wall is of corrugated (bellows) form. Dimensions of the cross section are delineated in Section 2.1.3.2. The bellows dimensions were decided after some iterations, but have yet to be optimized. Similary, the radius of the lobed semi-cylinder has been set at 15 cm, based upon the trade-offs between first wall thickness and total structure volume fracture and can also be further optimized.

Manufacturing methods for such a wall are worth mentioning. The wall is grooved on both sides by gang milling, this operation being carried out while the wall is a flat plate. The sides of the lobe are then thinned and the wall finally pressed into lobe form with the corrugations in place.

Various aspects of the performance of such a wall in its various functions are set out below. The pressure carrying capability is derived from a simple tension in the wall. Due to the erosion allowance, this tension causes less stress at the beginning of life than at the end. The stress is

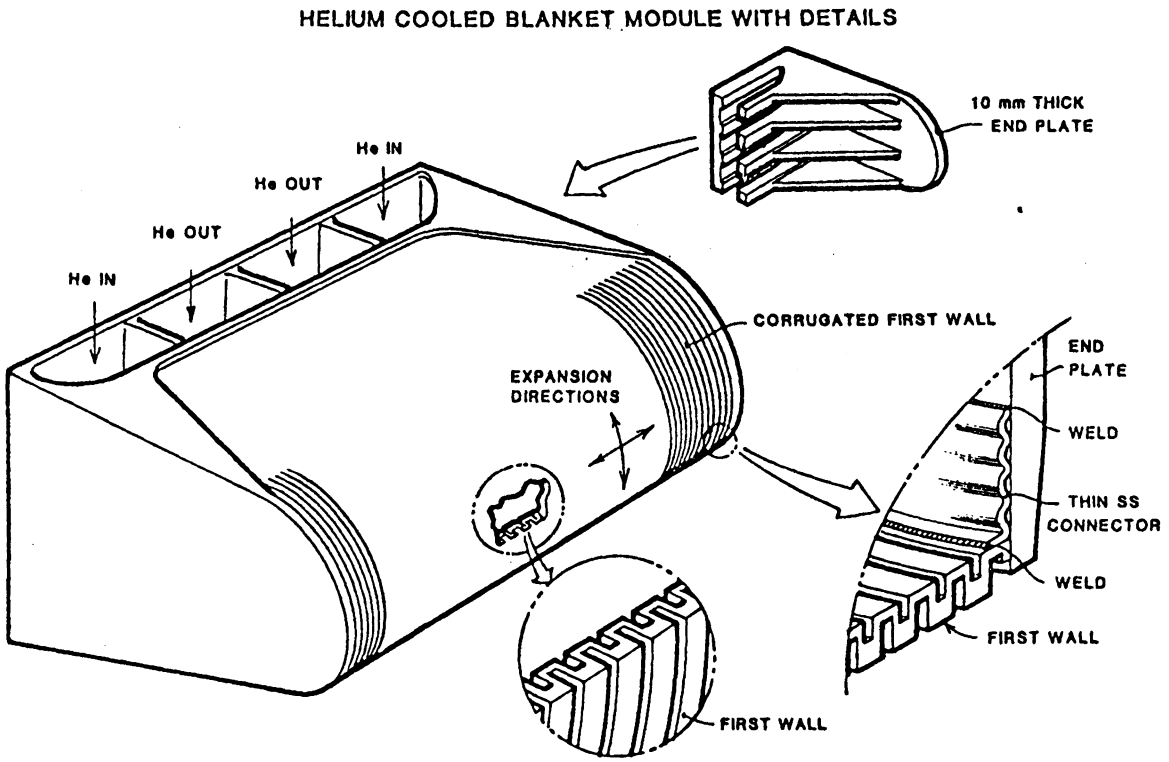

Figure VII.2-5. Blanket module first wall arrangment.

finally around 138 MPa (20,000 psi) and was set on the basis of the creep performance of the material for a two year life. Small pressure stresses exist in the bellows due to the convolutions and these are added into the analysis.

Erosion capability is built in by the corrugation being 2 mm thicker than structurally needed on the plasma side. This material is expected to diminish in thickness progressively during the wall life.

It should be appreciated that thermal changes in dimension only result in stress if constrained. The functional constraints of this wall design do not impose constraints which affect the thermal expansion. The analysis below presents a fairly mature iteration in which, two dimensionally, the hottest material clearly has very low stress levels, as illustrated in the two-dimensional calculation. This manipulation is considered of major importance in this design and probably useable in many other blanket design concepts. Experience indicates that the synthesis and control of stress/thermal patterns for the bellows configuration is entirely feasible even when the section is changing due to erosion. These effects have in the main been investigated two-dimensionally. Due to the physical thickness of the wall caused by the erosion allowance, it has not proven feasible in the other direction to use lobe flexure to accommodate thermal changes in dimensions. The major thermal effect is to tend to cause shortening of the lobe radius, particularly at the point nearest the plasma, and in the simple semi-cylindrical design this gives rise to considerable stresses. However, by changing the lobe shape from a simple radius to some other shape for just a few millimeters at variance from a radius, it may be possible to arrange moments that counter those which the temperature effects generated leading to a working situation where for practical purposes no temperature stresses exist. This can also be interpreted at pre-loading of the first wall. Indeed, if the simple cylindrical wall is left in this temperature/pressure condition long enough, it will creep to this equilibrium condition, however, in doing so it will "use up" some of its creep limit, which, if embrittlement occurs, may be very important.

Irradiation swelling stress in the bellows direction can be fairly easily controlled assuming pessimistically that no creep occurs. It is considered that this should in any case be minimized so as not to deplete the creep

budget (as in the thermal case). Swelling stresses in the lobe direction have not yet been analyzed and are more difficult to handle, although they can in some measure be dealt with as the thermal expansion is.

Some general observations on the proposed design can be made. First, the situation with regard to radiation stimulated dimension change under stress, i.e., radiation creep, it is essential to know whether this is damaging. Present postulates say that it may not be damaging, but that on cessation of the radiation, the material will be hardened. In this state, do hardness and brittleness arrive together? If so, if irradiation is stopped, restarting may call for very low subsequent strains due to low creep secondary capability. These questions need resolutions. What is emerging is that whatever their resolution it appears possible to accommodate the effect satisfactorily in this configuration at a reasonable life.

Further work on the first wall will be most productive if the material design criteria can be changed. However, the present design can further be optimized with present design criteria and, in particular, interaction of the lobe and bellows stress systems needs to be done to produce minimum material contents for a required life.

VII.2.1.3.2 First Wall Thermal-Mechanical Analysis

The bellows first wall concept was proposed as a means of accommodating the temperatures; pressure, thermal, and neutron swelling stresses; and material erosion anticipated for tokamak fusion reactor first walls. The objective of the first wall thermal mechanical analysis was to iteratively manipulate the bellows first wall configuration in such a way as to control the associated temperatures and stresses, keeping both below specified design limits. To accomplish this objective, the two dimensional steady-state temperature distribution at the beginning and end of life was calculated for the bellows first wall using TACO2D, a finite element heat transfer code. The temperature profile calculated by TACO2D was then coupled along with the helium pressure boundary condition into NIKE2D, an implicit, finite deformation, finite element stress code. The neutron swelling effects were not included in the stress analysis; they will be included in future iterations. The results of TACO2D and NIKE2D were graphically displayed using the post-processors POSTACO and THOR, respectively. Both of these codes and their accompanying

post-processors are available on the magnetic fusion energy computer network.

Figure VII.2-6 presents the two dimensional bellows first wall configuration. This basic configuration was analyzed for two conditions: the beginning of life in which the 2 mm sacrificial layer on the plasma side of the wall has not eroded, and at the end of life in which the sacrificial layer has completely eroded. Table VII.2-2 lists the design guidelines used for the analysis. Three surface loading conditions were analyzed. The high surface loading condition is representative of the conditions expected for tokamaks. The lower loading conditions are typical of mirror confinement schemes. Table VII.2-3 summarizes the thermal and structural computer inputs.

TABLE VII.2-2. DESIGN GUIDELINES FOR THE BELLOWS FIRST WALL

Material	PCA stainless steel
Neutron wall loading	5 MW/m^2
Surface wall loading	1 MW/m^2
Maximum sacrificial material temperature	550°C
Maximum structural material temperature	550°C
Maximum stress (primary plus secondary)	390 MPa
Erosion rate	1 mm/y
Blanket lifetime	2 y
Equivalent wall thickness[a]	5 mm

[a]Determined from hoop stress calculations for PCA at the end-of-life.

The principal stresses calculated by NIKE2D for the bellows first wall were computed assuming a hydrostatic pressure on the helium side of the wall coupled with the temperature profile computed by TACO2D. The wall was constrained from moving in the bellows direction along both bellows side interfaces and from moving up and down by a single point located at the wall's center of mass (see Fig. VII.2-6).

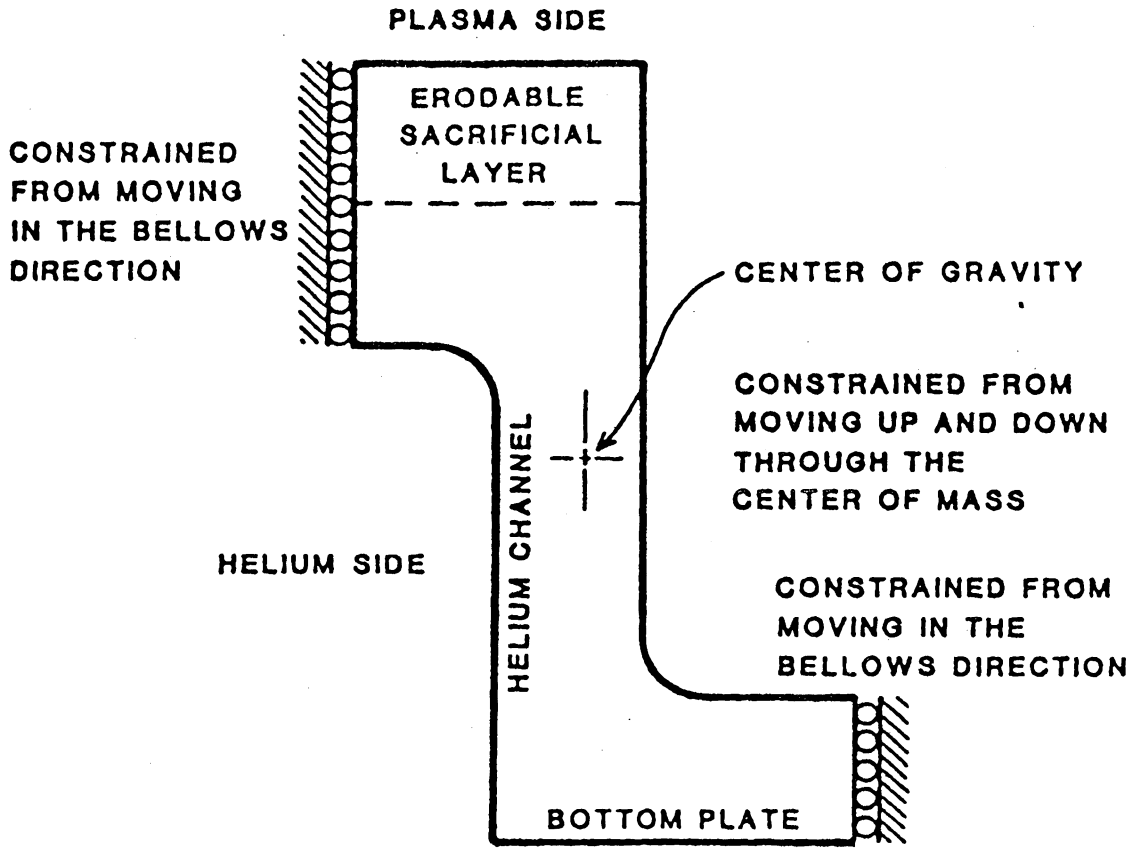

Figure VII.2-6. Two dimensional bellows first wall configuration.

TABLE VII.2-3. THERMAL AND STRUCTURAL COMPUTER INPUTS FOR THE BELLOWS FIRST WALL

	High Surface Loading	Intermediate Surface Loading	Low Surface Loading
Thermal TACO2D Inputs			
Maximum surface heat flux (MW/m^2)[a]	1.0	0.5	0.1
Volumetric neutron heating (MW/m^3)	55.0	55.0	55.0
Beginning of life helium channel convective heat transfer coefficient (W/m^2-K)	8599	8241	8058
End of life helium channel convective heat transfer coefficient (W/m^2-K)	8595	8238	8054
Bottom plate convective heat transfer coefficient (W/m^2-K)[b]	190	190	190
Beginning of life helium coolant temperature (°C)	322	307	300
End of life helium coolant temperature (°C)	319	305	297
Structural NIKE2D Inputs			
Helium side hydrostatic pressure (MPa)	5.0	5.0	5.0

[a]The surface heat flux at each nodal point on the plasma side is equal to the fraction of the total angle seen at that point times the maximum surface heat flux.

[b]The bottom plate convective heat transfer coefficient is smaller than the helium channel convective heat transfer coefficient because heat flowing through the bottom plate must also flow through the end plate that holds the helium.

Figures VII.2-7 and VII.2-8 graphically display the bellows first wall temperature profiles calculated by TACO2D for a maximum surface heat flux of 1.0 MW/m^2 at the beginning and end of life, respectively. Figures VII.2-9 and VII.2-10 present the beginning and end of life principal stresses calculated by NIKE2D. These figures show that with the present bellows first wall design, the design guideline maximum sacrificial and structural material

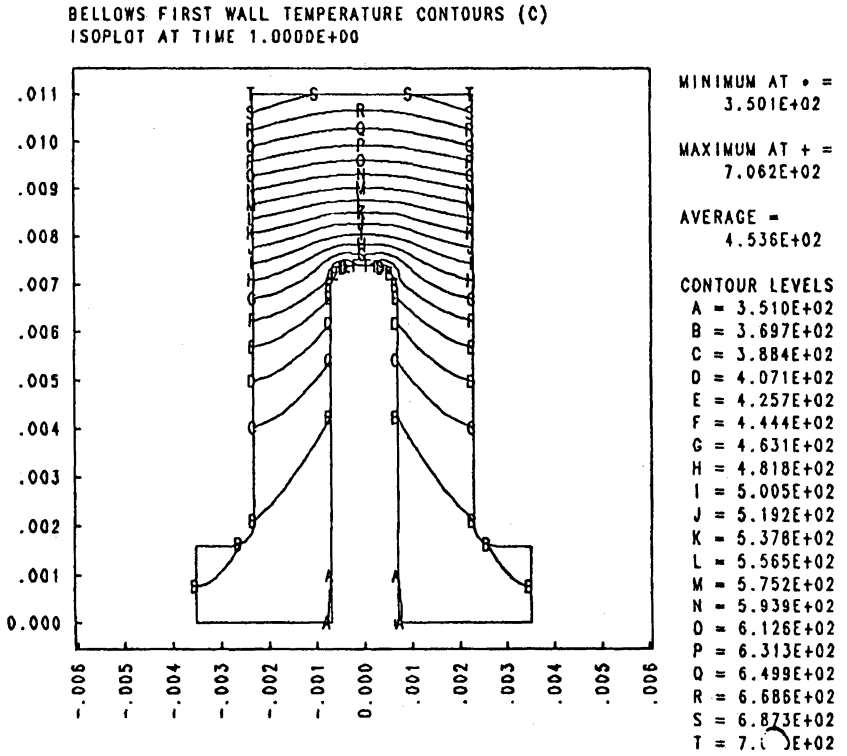

Figure VII.2-7. Beginning of life bellows first wall temperature contours.

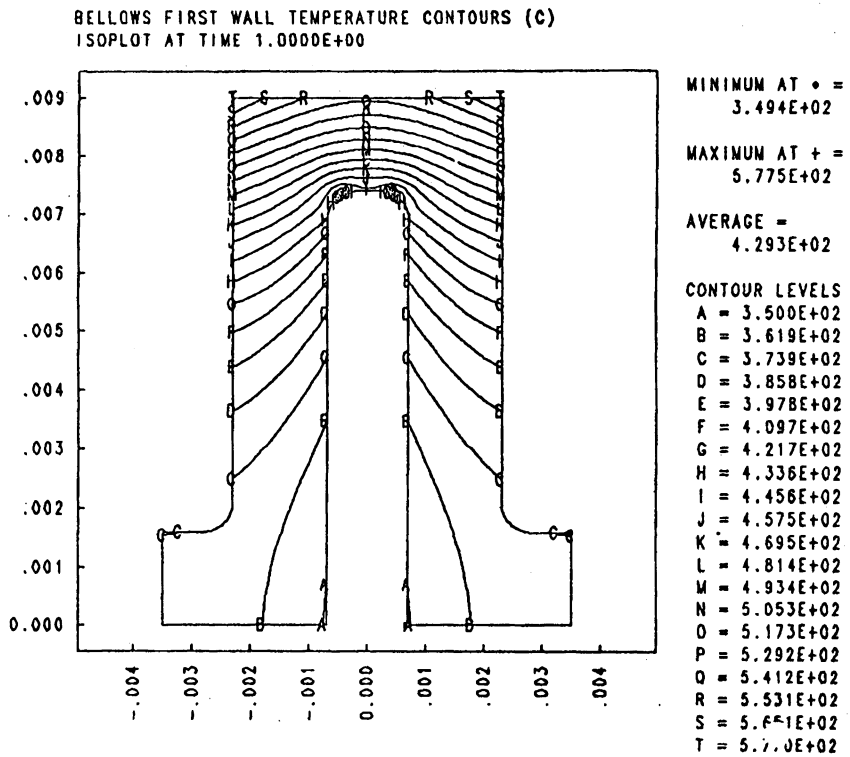

Figure VII.2-8. End of life bellows first wall temperature contours.

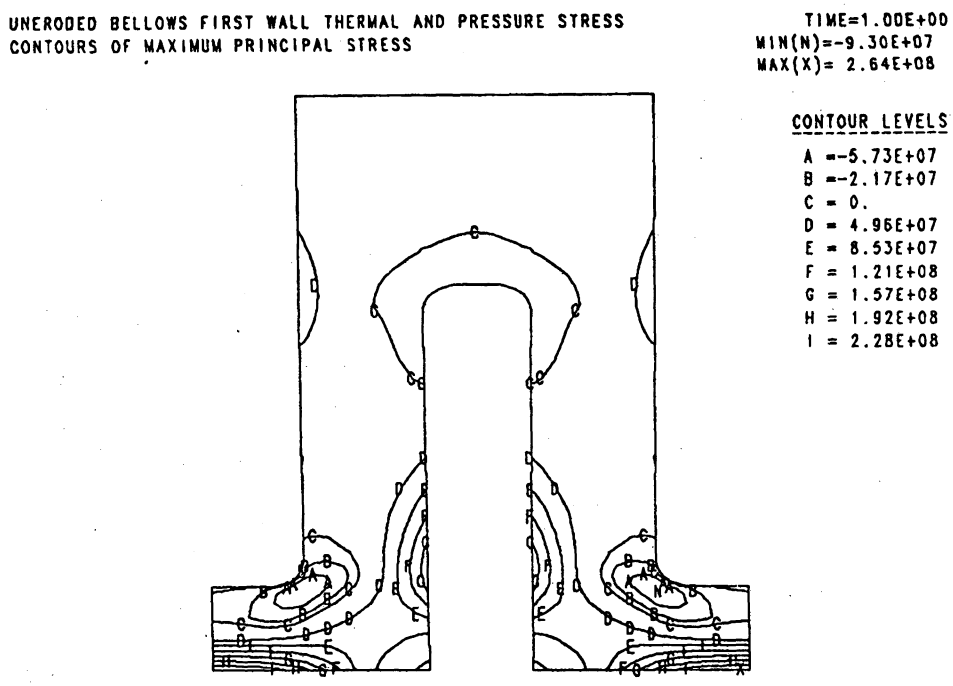

Figure VII.2-9. Beginning of life bellows first wall stress contours (Pa).

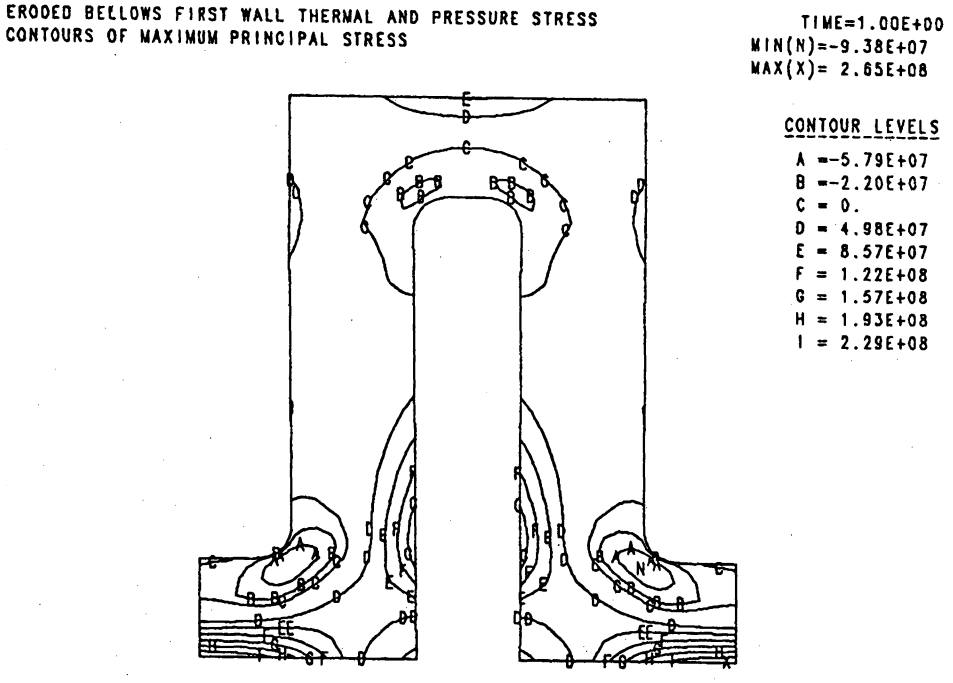

Figure VII.2-10. End of life bellows first wall stress contours (Pa).

temperature (550°C) is exceeded. However, the design guideline maximum stress (390 MPa) is slightly exceeded. It is important to note that the maximum stresses occurs along the bottom plate of the bellows; the hotter portion of the bellows must accommodate only very small stresses. These small stresses increase slightly from the beginning to the end of life owing to the decrease in the stiffness of the bellows when the sacrificial material is eroded. It should be emphasized that although the design guideline temperatures are exceeded for the highest surface heat flux case with the present design, further modifications to the design by varying the bellows geometry are expected to improve the bellows first wall performance.

Figure VII.2-11 shows the effect of decreasing the surface heat flux on the temperature at the center of the top bellow surface and on the maximum tensile stress. As expected, the temperature of the bellows first wall decreases with a lower surface heat flux. The temperature at the beginning of life is higher than at the end of life due to the longer conductance path length. The maximum tensile stress at the end of life is also generally lower, but is about the same at 1.0 MW/m^2 maximum surface heat flux.

These results indicate that the present bellows first wall design meets the thermal and structural design guidelines for maximum surface heat fluxes below 0.5 MW/m^2. Efforts are underway to modify the present design, especially in the lobe direction to further improve the performance of this bellows first wall design.

VII.2.1.3.3 Structural Design Considerations

In view of the difficult function of the first wall, the emphasis in design of this structure is on relief of the first wall from any stress other than pressure containment in its operating environment. This environment is such that the structural function of the lobe has been removed as far as possible from the first wall. The blanket structural tasks are to carry the weight of the blanket contents and those parts of the pressure containment not carried by the first wall. The back of the lobe consists entirely of a structural frame (see Fig. VII.2-12) with gas passages, and the lobe ends, which cantilever from the back to carry the end pressures, relieve the bellows first wall of end load constraints due either to pressure, swelling or thermal effects.

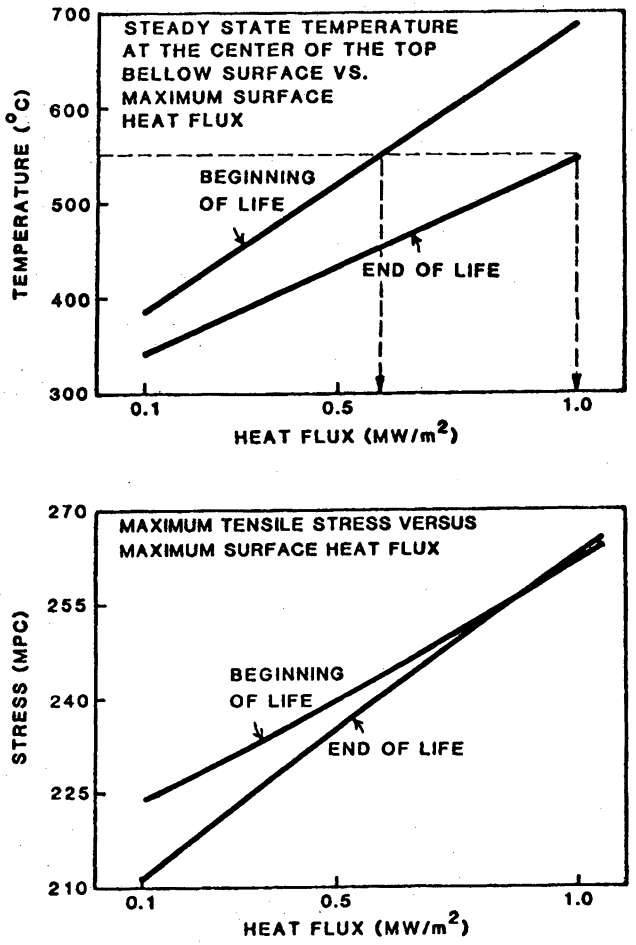

Figure VII.2-11. Effect of surface heat flux of temperature and stress.

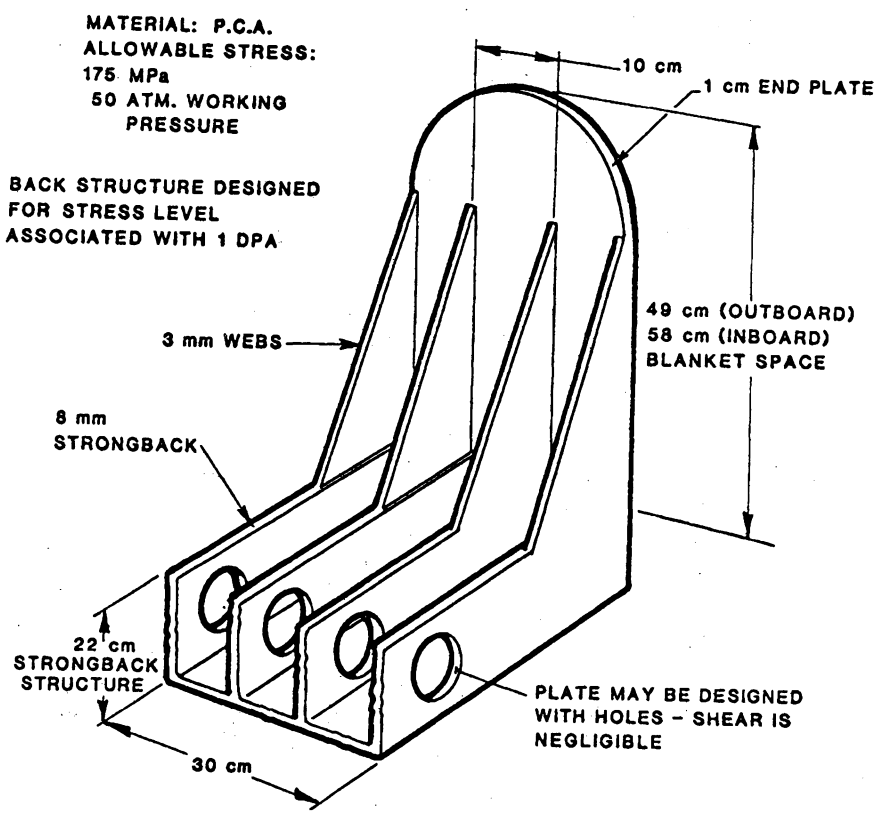

Figure VII.2-12. Lobe structure without first wall.

The reasons for this design are first, relief of the first wall, second, protection of the structure from radiation, and third, the avoidance of structure in front of the blanket which would attenuate the neutron flux. Another advantage comes from this design in that requirements for highly refined designs can be avoided since excess metal merely acts as part of the shield, thus the plenum ducts are capable of being of close-packed rectangular form because comparatively inefficient structural forms, i.e., beams, do not intrude into the blanket function. In addition to the structure shown, the lobes are held against each other and supported by a dee-shaped frame to conform to the tokamak shape and take loads due to the noncircular form, gravity, and earthquake acceleration. This frame can be embedded in the shield and should be considered in detail in the future.

VII.2.1.3.4 Plenum Design

Two plenum designs are shown in Fig. VII.2-13. The thicknesses shown represent the actual dimensions required for flow around the torus cross section. A practical design based upon this layout will have two areas of departure from these idealized dimensions.

Some small differences can be expected in that the idealized gas space is allocated between out and return. Inevitably the detail at any point of the flow from the out to the return line through the blanket must contain space for the distribution across the blanket (i.e., toroidally). A few centimeters will probably cover this.

In addition, the practical details of the structure will involve occupation of some space at the rear of the blanket by structural members with consequent increase of plenum thickness.

The consequence is that the realistic figures for plenum thickness should, when all factors are considered, be increased by about 3 to 5 cm from those shown in the diagram. An optimization is conceivable in which the rear structure penetrates the lithium zone, simultaneously losing mass as it does so, but decreasing the TBR by a small amount. This penetration would allow a thicker blanket to compensate for the TBR loss.

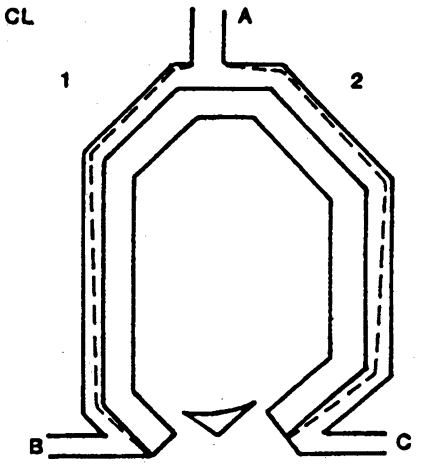

THRU STREAMS

STREAM	LOCATION	THICKNESS cm
1	A	10
1	B	10
2	A	18
2	C	18

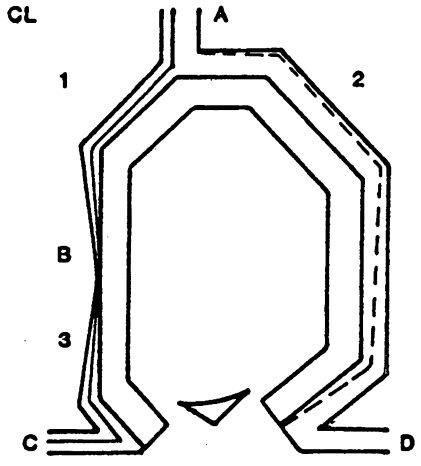

MIXED STREAMS

STREAM	LOCATION	THICKNESS cm
1	A	10
1	B	0
2	A	18
2	D	18
3	B	0
3	C	10

Figure VII.2-13. Coolant-based plenum sizes.

VII.2.1.4 Fuel Element Design

Figures VII.2.14 and VII.2-15 show a lobe with liquid metal breeding elements and details of the breeding elements. In the lithium breeder design, the liquid metal is slowly circulated to recover the tritium. The breeding elements are tubular with the tube axis along the lobes, the tube ends being reduced in diameter to allow reasonable ligature widths in the tube plates at either end of the lobe. These tube plates form a plenum which serves to connect all of the tubes to the slow circulation system. The connection between the tubes and plenum is by holes in the tube wall inside the plenum. The tube ends are plugged. In order to obtain good cooling and to be economic of blanket space, the distance between the tubes is only of the order of two millimeters. This requires that the tube ends be swaged to a reduced diameter. The tube assembly is presently sealed by brazing, although welding would also be possible. Along the tubes at regular intervals are pressed hexagonal parts made from sheet metal, thus where the parts are mounted contact between individual tubes in an assembly is made. This maintains regularity of the matrix and ensures the lobe integrity by supporting the side walls, should a sudden first wall burst cause a short term ΔP between neighboring lobes.

Draining of the liquid metal is expected to be achieved by gas injection with discharge via the assembly low point, since the tube assemblies cannot all easily be connected to give gravitational drainage. In normal operations, freezing of the liquid metal is not featured. The blanket is heated by circulating hot helium prior to filling with liquid metal. The liquid metal is drained before cool-down is allowed. However, in emergencies, freezing, which might cause damage, will only occur slowly, giving time to respond to a blow-down system failure. If in-situ freezing does occur damage may take place, but a scenario for a dangerous accident cannot be imagined from this cause.

Since the tube diameter is comparatively small (few cm diameter), and the tubes are close spaced, a high ΔP between the coolant the liquid metal has little impact, if any, on the structure fraction. The design currently has the breeder metal at 1 atm. This will be the subject of some work later to confirm.

Bowing of the tubes due to swelling will be suppressed by the hexagonal sleeves, but no severe stresses are expected because of this. The breeder

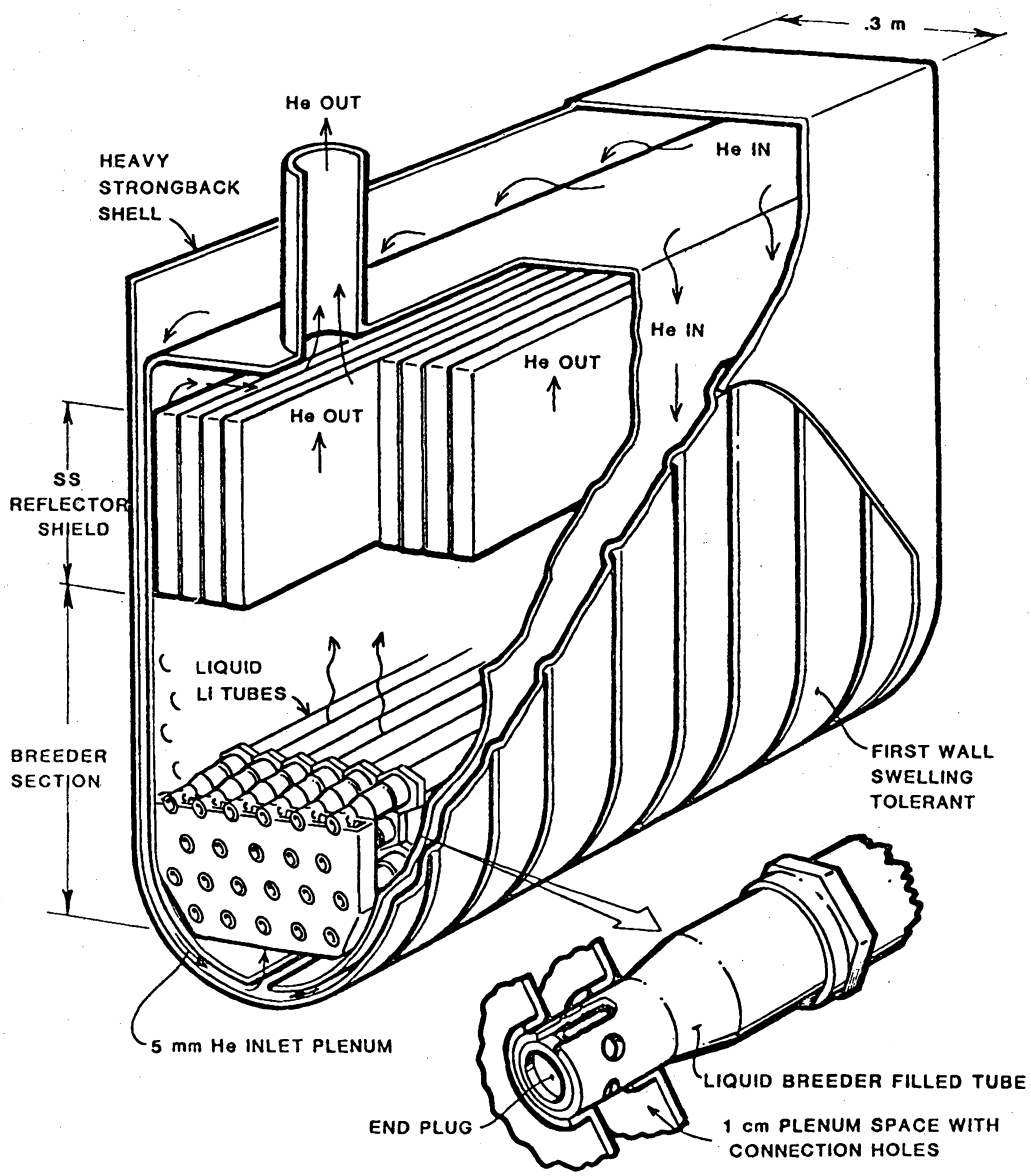

Figure VII.2-14. Helium cooled/liquid lithium breeder blanket module.

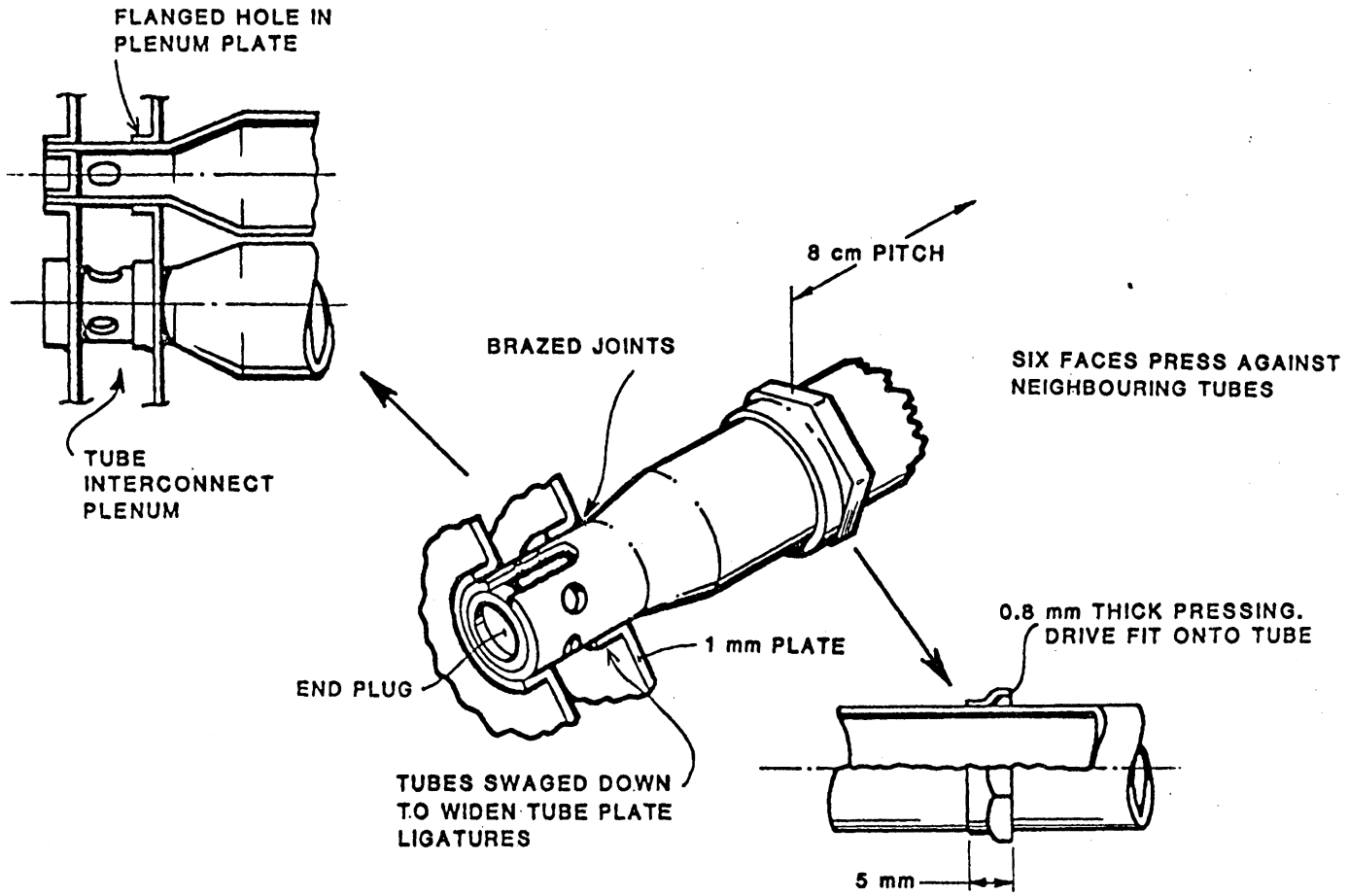

Figure VII.2-15. Liquid metal tube assembly details.

assembly as a whole will be mounted from the plena, but the restraints will be such as to allow some motion of the assembly from thermal or neutronic dimension changes to later place freely.

VII.2.1.5 Thermal-Hydraulics Design

VII.2.1.5.1 General Considerations

The thermal hydraulic design of a gas-cooled reactor system should have high thermal efficiency and low pressure losses. The high efficiency requirement dictates a high coolant outlet temperature, restricted by the maximum operating temperature limits of the reactor materials. The low pressure loss requirement leads to high system operating pressure to obtain high coolant density, a large coolant inlet-to-outlet temperature differential, and restricts the velocities of the coolant in various sections of the coolant loop. On the other hand, the restrictions on material operating temperature limits lead to high coolant velocities to maintain high heat transfer coefficients. During the course of the liquid breeder, helium-cooled blanket thermal-hydraulics design, close interaction was maintained with the mechanical design, neutronics analysis and material selection efforts.

VII.2.1.5.2 Temperature and Pressure Drop Limits

The temperature limits of different materials crucial to the design of the blanket must be established. At the same time, the pressure drop limits for different regions of the blanket need to be defined to establish a basis for the thermal-hydraulic design and analysis. In the blanket region, the crucial materials are the structural material and the fuel materials. In the blanket locations where the material strength is important and radiation levels are high, PCA was recommended to be the structural material. Its maximum allowable temperature is 550°C. Typically, the reactor first wall would experience the highest flux of high energy neutrons, thus this temperature limit would be applicable to the heat transfer analysis of the first wall.

The temperature limits imposed on the present designs, based on preliminary recommendation by the liquid metal corrosion task group, are that the liquid metal/structure interface temperature be less than 450°C and 550°C

for lithium with PCA and HT-9, respectively, and less than 400°C and 450°C for 17Li-83Pb with PCA and HT-9 respectively. These compatibility temperature limits require careful thermal-hydraulics design in order to achieve adequate helium outlet temperatures. The more recent lower temperature limits for 17Li-83Pb with HT-9 would require modifications of the breeder zone thermal-hydraulics design presented below.

Low coolant pressure drop in a power producing machine is important in reducing the power necessary to circulate the helium coolant. The acceptable pressure-drop depends on the overall optimization of the reactor economics. At this stage of the conceptual design, two pressure drop limits can be used. A value of approximately 5% of the thermal power can be used for the pumping power for the complete coolant circuit, which includes the heat exchangers, the blanket, pumps, and piping. The second limit is imposed by the pressure differential capability of the helium circulator. Using a single-stage circulator, a value of $(\Delta P)/(P) < 4.3\%$ can be used for the entire coolant loop.

Experience with helium-cooled nuclear power systems indicates that a helium pressure of 40 to 80 atm will be needed for a good thermal-hydraulic design. Steam-generator design conditions dictate a minimum coolant inlet temperature of about 275°C and a minimum coolant temperature rise of above 100°C. Based on this information, a helium operating pressure of 5.1 MPa (50 atm) and an inlet temperature of 275°C were selected. Helium outlet temperatures of 525°C and 500°C were selected for the Li and 17Li-83Pb blankets, respectively, satisfying the liquid metal/HT-9 interface temperature limits given above, and resulting in a thermal cycle efficiency of about 36.5%.

VII.2.1.5.3 First-Wall Cooling

Thermal-hydraulics calculations were performed on the first wall, that section of the reactor which is closest to the plasma and which has the highest volumetric heat generation and surface heat loading in the range of 0.1 to 1 MW/m^2, the bellows first wall configuration, as illustrated in Fig. VII.2-5, was used for the analysis. This is necessary in order to increase the heat transfer surface area and the heat transfer coefficient. This configuration is also conveniently coupled with the mechanical design requirements as presented in Section VII.2.3.1. The key results of this

analysis are the bellows detailed dimension, coolant heat transfer coefficient, and temperature distribution. These were then used as inputs for the two dimensional first wall thermal mechanical analysis, which is presented in Section VI.2.1.3.2. The equations used to calculate the one-dimensional temperature distribution in the wall were presented in Reference 2. The first wall coolant is separated from the module intervals by a closely attached metal wall in order to maintain high coolant velocity in the first wall region.

Table VII.2-4 gives the parameters for the selected bellows first wall design.

TABLE VII.2-4. PARAMETERS OF THE BELLOWS FIRST WALL DESIGN

Parameter	Values - Units
Neutron wall loading	5 MW/m^2
Volumetric heat generation	50 MW/m^3
Surface heat flux range	0.1 to 1 MW/m^2
Equivalent wall thickness	63 mm (BOL),[a] 5 mm (EOL)
Inside (coolant) groove width	1.2 mm
Outside (plasma side) groove width	2.4 mm
Bellows wall thickness	1.6 mm
Inside groove height	7.2 mm
Outside groove height	9.2 mm (BOL), 7.2 mm (EOL)
Helium pressure	5 MPa (50 atm)
The following are for surface heat wall loading of 1 MW/m^2:	
Helium coolant maximum temperature	322°C
Reynolds number	16,377
Coolant velocity	54 m/sec
Pressure drop	9.2 kPa (1.34 psi)

[a]At the beginning of life (BOL), a 2 mm thick sacrificial layer is added on for erosion.

VII.2.1.5.4 Breeder Zone Thermal-Hydraulics Design

In the breeding zone, the thermal-hydraulics design is guided by liquid metal/structure compatibility concerns. Figure VII.2-1 shows a schematic of

the breeder tube bank arrangement. The equations used in the analysis of cross-flow heat transfer through the tube bank are presented in References 10 and 11. The resultant thermal-hydraulics design characteristics are summarized in Table VII.2-5 for 17Li-83Pb, Li, and Pb-multiplier with Li breeder in HT-9 tubes. Except for the Pb multiplier, these designs all satisfy the preliminary compatibility-limited interface temperature guidelines with low pumping power requirements (0.4% to 0.6%), high breeder volume fractions (> 72%), and reasonable tube sizes. With PCA tubes, the maximum helium outlet temperature would be limited to 425°C with Li and < 400°C with 17Li-83Pb in order stay below the liquid metal/PCA interface temperature limits of 450°C and 400°C. Thus, 17Li-83Pb blankets with PCA tubes cannot meet the compatibility temperature limits due to pinch point constraints on the helium outlet temperature, and lithium breeder blankets with PCA tubes result in low net plant efficiencies (approximately 33%). These difficulties are relieved with the use of ferritic steel tubes. Further improvements are possible by improving the energy split in the breeder zone/reflector regions, and potentially, also by the use of alternative nonstructural materials and perhaps relaxed temperature limits in this nonstructural application.

TABLE VII.2-5. BLANKET BREEDER ZONE THERMAL-HYDRAULICS DESIGN

	Li/HT-9	Pb-Li/HT-9	17Li-83b/HT-9
Helium inlet temperature, °C	275	275	275
Helium outlet temperature, °C	525	525	500
Net plant efficiency, %	36.5	36.5	36.5
Max. blanket He flow, velocity, m/s	26	21	19
Breeder zone pumping power, %	0.53	0.63	0.39
Maximum interface temperature, °C	541	546	487
(Max. allowable interface temp. °C)	(550)	525[a]	(500)
Maximum breeder temperature, °C	565	559	510
Maximum tube inner radius, cm	3.1	1.025	1.0
Tube wall thickness, cm	0.078	0.025	0.025
Pitch, cm	6.75	2.25	2.25
Gap, cm	0.4	0.15	0.2
Number of 4 m tubes for 4000 MW(t)	28,000	150,000	130,000
Breeder zone structure volume fraction	0.039	0.038	0.036
Breeder volume fraction	0.765	0.75	0.72

[a]For static isothermal conditions (assumed same as Li-Pb).

VII.2.1.5.5 Coolant Pressure Drop

Calculations were performed to estimate the total pressure drop of the whole blanket cooling circuit including the steam generators. The pressure losses due to friction, acceleration of flow from density change as a function of temperature, joints, turns, expansions, and contractions are all taken into consideration. Table VII.2-6 summarizes the friction pressure drop from different blanket sections.

TABLE VII.2-6. FRICTION PRESSURE DROP FOR THE DIFFERENT BLANKET SECTIONS

Section	Flow Velocity V (m/s)	Pressure Drop ΔP (kPa)
1. Inlet manifold	55	9.1
2. Distribution channel	32	1.3
3. Side flow path	38	14.7
4. Grooved first wall	54	9.2
5. Breeder tube bank	26	12.8
6. Collection channel	16	1.9
7. Outlet manifold	77	12.0
TOTAL		61.0

The total pressure drops in the blanket and in the primary coolant are given in table VII.2-7.

TABLE VII.2-7. TOTAL PRESSURE DROP IN THE BLANKET

Pressure Drop	ΔP (kPa)	ΔP (%)
Friction	61.0	1.0
Turning, joining, and dividing	45.6	0.9
Expansion/contraction	11.6	0.2
TOTAL	118.2	2.1
Total pressure drop in the primary coolant loop		
Blanket	118.2	2.1
Sector lines, 22.3 Ring ducts, 4.3 Steam generator piping, 7.1 Steam generator, 27.4	61.1	1.2
TOTAL	179.3	3.3
Total pumping power fraction = loop pumping power/reactor thermal power × 100% = 4%.		

It should be noted that both $\Delta P/P$ = 3.3% and pumping fractions of 4% are within the design limits of 4.3% and 5%, respectively, as established in Section VII.2.1.5.2.

VII.2.1.6 Neutronics Design

All neutronic calculations were performed using the one-dimensional transport code, ANISN,[12] with P_3S_8 approximation in cylindrical geometry. The nuclear data library used is the coupled 46 group neutron and 21 group gamma-ray cross section data collapsed from the ORNL processed VITAMIN-C library.[13] The reactor cross sections and kerma factors are produced from the MACK-IV code and are processed into the same 46 group neutron and 21 group gamma-ray group structures.[14,15]

Most of the calculations employed the straigtforward one-dimensional poloidal axis (or minor radius) model, as shown in Fig. VII.2-16. This model treats the first wall blanket and shield layers as annuli of an infinite cylinder with the centerline of the plasma as the axis of the cylinder. For the helium-cooled liquid metal breeder system, the model consists of a 60 mm first wall region, a variable thickness breeding zone and reflector, a 0.22 m gas plenum, and a 0.3 m shield. The first wall region is composed of only 6.6% by volume structural material and balance of helium simulating the homogenized region of the gas-cooled first wall design. The breeding zone consists of 10% structure, 75% breeding material, liquid lithium or 17Li-83Pb, and 15% helium, all be volume. The reflector zone is composed of 85% reflector material and 15% helium. The gas plenum consists of mostly void space for helium coolant to flow. The smeared structure in this zone is only 10% by volume. The 0.3 m shield is included in all calculations to take into account the effect of the entire shield, although there is an albedo boundary condition of 0.3 for all neutron and gamma-ray groups at the right boundary of this problem.

One of the major characteristics of a helium-cooled fusion blanket is that the blanket consists of a substantial amount of space to flow the helium coolant. In the blanket modelled in Fig. VII.2-16, we can easily see that a total linear space of 0.28 cm in the blanket is devoted to first wall and plenum arrangement and more than 90% by volume of these regions is reserved for helium coolant. In the breeding and reflector zones, about 15% by volume

ZONE		RADIUS (m)
	CENTERLINE OF PLASMA	0.0
1	PLASMA	
		2.53
2	VACUUM	
		2.73
3	PCA FIRST WALL (6.6 % DENSE)	
		2.79
4	BREEDING ZONE PCA + BREEDER + HELIUM	
		3.21
5	PCA PLENUM (10% DENSE)	
		3.43
6	STAINLESS STEEL SHIELD	
		3.73

Figure VII.2-16. Schematic of the one-dimensional cylinder plasma centerline axis model for blanket neutronic calculations.

space, is also needed to pass the helium coolant. Therefore, for a total blanket thickness of 0.6 m, the net material which interacts with neutrons in the blanket is reduced to about 65% by volume. Thus, special attention should be paid to coolant plenum and flow distribution design when we design the gas-cooled blanket system that requires limited dimensions. Due to the consideration of the stringent space limitation in the inboard of a tokamak reactor, a major radius torus model was also used in the neutronic calculations when necessary to reveal the flexibility of blanket thickness in the inboard as well as the outboard direction. Figure VII.2-17 describes the schematic of the model used in this study.

The tritium breeding ratio and nuclear heating rates for the liquid lithium and 17Li-83Pb blankets obtained from several calculations using the

ZONE		RADIUS (m)
	CENTERLINE OF PLASMA	0.0
		3.86
1	STAINLESS STEEL SHIELD	
		4.16
2	PCA PLENUM (10% DENSE)	
		4.38
3	BREEDING ZONE PCA + BREEDER + HELIUM	
		4.80
4	PCA FIRST WALL (6.6% DENSE)	
		4.86
5	VACUUM	
		5.06
6	PLASMA	
		9.53
7	VACUUM	
		9.73
8	PCA FIRST WALL (6.6% DENSE)	
		9.79
9	BREEDING ZONE PCA + BREEDER + HELIUM	
		10.21
10	PCA PLENUM (10% DENSE)	
		10.43
11	STAINLESS STEEL SHIELD	
		10.73

Figure VI.2-17. Schematic of the one-dimensional cylinder torus axis model for tokamak reactor calculations.

poloidal axis model are given in Tables VII.2-8 and VII.2-9, respectively. The tritium breeding ratios obtainable from these two blankets are further depicted in Figs. VII.2-18 and VII.2-19 as a function of breeding zone thickness at several ^{6}Li enrichment values in lithium.

For the liquid lithium blankets, the tritium breeding ratio is a sum over two nuclear reactions, namely $^{6}Li(n,t)$ (designated at T_6) and $^{7}Li(n,n't)$ (designated at T_7). The values of $T_6 + T_7$, T_6 and T_7 are given in Fig. VII.2-18 as a function of breeding zone thickness at 7.4%, 15%, and 20% ^{6}Li in lithium. As seen from Fig. VII.2-18, a tritium breeding ratio greater than 1.20 can be obtained for the helium-cooled liquid lithium blanket employing naturally enriched lithium when the breeding zone thickness exceeds 0.54 m (total blanket thickness is about 0.82 m). However, about 80 mm reduction in the breeding zone thickness can be made while maintaining tritium breeding greater than 1.2 if the lithium is enriched to 20% ^{6}Li. An enrichment more than 20% is probably not going to gain any advantage in tritium breeding because of excessive reduction of tritium production in ^{7}Li due to the corresponding decrease of ^{7}Li concentration in lithium. The blanket energy multiplication for the blanket with a tritium breeding ratio greater than 1.2 can be about 1.2 as seen in Table VII.2-8. The ultimate value can be about 1.3 if the nuclear energy deposited in the shield is taken into account.

The tritium breeding ratio obtainable from helium-cooled 17Li-83Pb blankets is primarily contributed by T_6. The contribution from T_7 is, in general, less than 1% when a tritium breeding ratio greater than one is considered. As shown in Fig. VII.2-19, the tritium breeding ratio for the blanket system increases as the breeding zone thickness of 0.42 m (total blanket thickness is 0.7 m) when the ^{6}Li enrichment is 90%, while it is only 0.76 when the naturally enriched lithium (7.4% ^{6}Li in lithium) is employed. Hence, it is desirable to employ 90% ^{6}Li in lithium for this blanket system to obtain a thin breeding zone and low lithium inventory blanket and still meet the tritium breeding requirement. At this enrichment, the tritium breeding ratio will exceed 1.2 if the breeding zone thickness is more than 0.32 m (total blanket thickness is 0.55 m). The blanket energy multiplication is also shown in Table VII.2-9 for an 0.7 m blanket with varying reflector thickness and ^{6}Li enrichment values. The reflector is needed to enhance the blanket otherwise, a substantial amount of the nuclear energy will be

TABLE VII.2-8. TRITIUM BREEDING RATIOS AND NUCLEAR HEATING RATES IN HELIUM-COOLED LIQUID LITHIUM FUSION BLANKETS

	Option 1			Option 2[a]			Option 3
First wall (PCA) zone	4 mm[b] (6 cm, 6.6% dense)			4 mm 6 cm, 6.6% dense)			4 cm (6 cm, 6.6% dense)
Lithium zone	0.42 m			0.52 m			0.42 m
Reflector	None			None			None
PCA plenum	0.22 m (10% dense)			0.22 m (10% dense)			0.22 m (10% dense)
First 0.3 m shield	Stainless Steel			Stainless Steel			Graphite
^{6}Li enrichment (% in Li)	7.42	15	20	7.42	15	20	15
^{6}Li(n,α)	0.702	0.749	0.826	0.768	0.854	0.883	0.770
^{7}Li(n,n'α)[b]	0.383	0.349	0.327	0.408	0.372	0.348	0.350
TBR[b]	1.085	1.143	1.153	1.176	1.226	1.231	1.120
Blanket nuclear heating	15.40	15.58	15.66	16.28	16.42	16.48	15.61
(E/14.1 MeV)	(1.09)	(1.11)	(1.11)	(1.15)	(1.16)	(1.17)	(1.11)

[a]Note: total blanket thickness is 0.8 m.

[b]This was changed to 5 mm from structural requirement at the uneroded condition.

[c]10% reduction in the ^{7}Li(n,n'α) reaction rate was taken into account.

TABLE VII.2-9. TRITIUM BREEDING RATIOS AND NUCLEAR HEATING RATES IN HELIUM COOLED 17Li-83Pb BREEDER FUSION BLANKETS

	Option 1			Option 2			Option 3
First wall (PCA zone)	4 mm[a] (6 cm, 6.6% dense)			4 mm (6 cm, 6.6% dense)			4 mm (6 cm, 6.6% dense)
17Li-83Pb zone	0.42 m			0.30 m			0.20 m
Reflector	None			0.12 m Stainless Steel			0.22 m Stainless Steel
PCA plenum	0.22 m (10% dense)			0.22 m (10% dense)			0.22 m (10% dense)
First 0.3 m shield	Stainless Steel			Stainless Steel			Stainless Steel
^{6}Li enrichment (% in Li)	90	60	7.42	90	60	7.42	90
^{6}Li(n,α)	1.346	1.246	0.636	1.181	1.068	0.485	0.955
^{7}Li(n,n'α)[b]	0.002	0.009	0.020	0.002	0.009	0.020	0.001
TBR[b]	1.348	1.255	0.656	1.183	1.077	0.505	0.968
Blanket nuclear heating (E/14.1 MeV)	15.73 (1.12)	15.56 (1.10)	15.19 (1.08)	16.37 (1.16)	16.45 (1.17)	17.44 (1.24)	17.39 (1.23)

[a]This was changed to 5 mm from structural requirement at the uneroded condition.

[b]10% reduction in the ^{7}Li(n,n'α) reaction rate was taken into account.

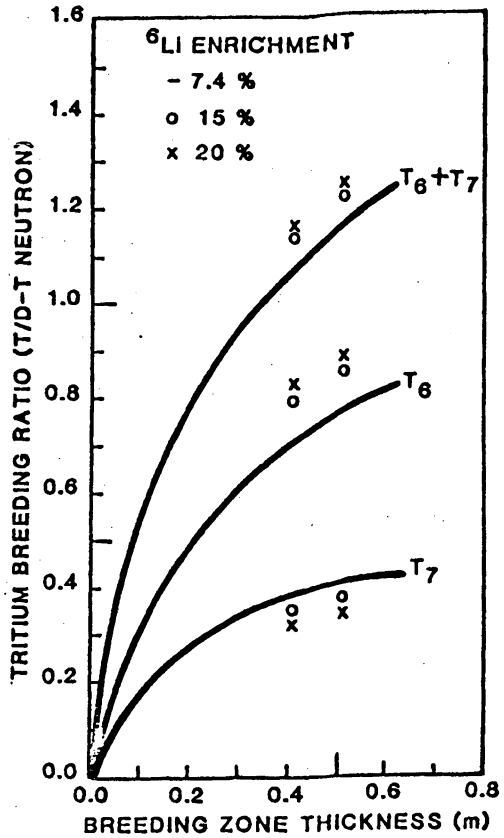

Figure VII.2-18. Tritium breeding ratio for helium-cooled liquid lithium blanket as a function of breeding zone thickness at several ^{6}Li enrichment values in lithium.

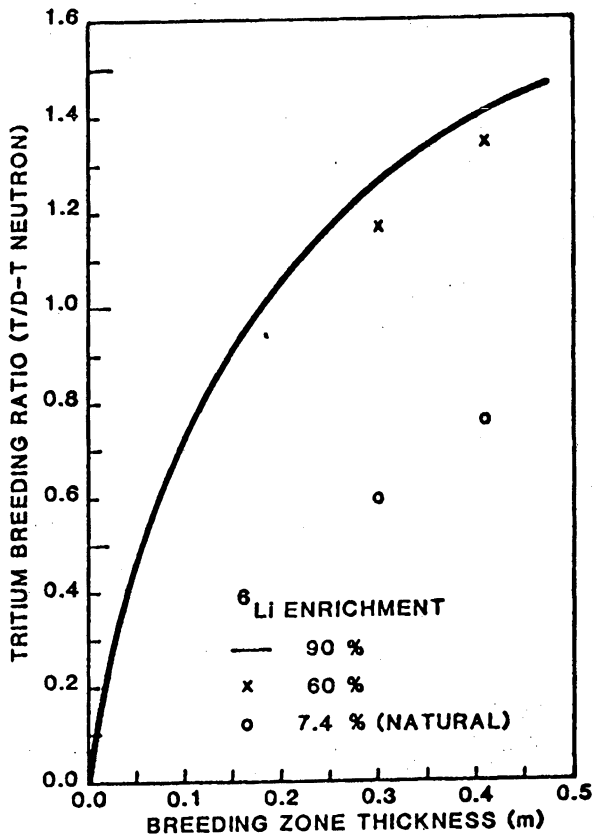

Figure VII.2-19. Tritium breeding ratio for the helium-cooled 17Li-83Pb blanket as a function of breeding zone thickness at 7.4%, 60%, and 90% ^{6}Li in lithium.

deposited in the shield and recovered at low efficiency. The 0.7 m blanket which represents one of the best neutronic designs which gives a high blanket energy multiplication, about 1.16, and an attractive tritium breeding ratio, about 1.2. If the nuclear energy deposited in the shield is taken into account, the blanket energy multiplication can be about 1.3.

Incorporation of a neutron multiplier, either beryllium or lead in a fusion blanket usually results in the reduction of (1) total blanket thickness, (2) lithium inventory, and (3) nuclear energy deposited in the shield and still enjoys attractive tritium breeding ratio and blanket energy multiplication. We have incorporated the lead multiplier in the liquid lithium blanket design. Results of the blanket performance for an 0.7 m blanket are given in Table VII.2-10. It shows in this table that with a 40 to 80 mm lead zone in the blanket, the tritium breeding ratio becomes attractive, i.e., greater than 1.2, and the blanket energy multiplication is about 1.2. These would otherwise be 1.15 and 1.11, respectively, as shown in Table VII.2-8 for a thin blanket with only liquid lithium as the blanket material.

The major radius torus calculations were performed for the liquid lithium and lead multiplier/liquid lithium blankets to reveal the flexibility of the inboard and outboard blanket thickness adjustment. The results show that a tritium breeding ratio of 1.16 will be obtained for the liquid lithium blanket if the inboard blanket is arranged to be 0.5 m thick (corresponding to an 0.22 m breeding zone) and the outboard blanket is extended to 0.9 m thick (breeding zone thickness is 0.62 m) at 20% ^{6}Li in lithium. This arrangement gives a blanket energy multiplication of 1.13.

The results for the lead multiplier/lithium designs are given in Table VII.2-11. Note that in these design arrangements, the 80 mm lead multiplier zone design as shown in Table VII.2-10, Design II, is employed. As can be seen from Table VII.2-11, an attractive tritium breeding ratio greater than 1.2 can be obtained for arrangements where the inboard blanket thickness is equal to or less than 0.5 m and the outboard blanket is fixed at 0.7 m. The blanket energy multiplication for these systems is 1.07 and 1.15, respectively, when the inboard blanket thicknesses are 0.4 and 0.5 m.

TABLE VII.2-10. CHARACTERISTICS OF TWO LEAD MULTIPLIER LITHIUM BLANKETS

Blanket Configuration	Design I	Design II
First wall (PCA)	60 mm (0.066 dense)	60 mm (0.066 dense)
Lead region[a]	40 mm	80 mm
Lithium region[b]	0.3 m	0.16 m
Stainless steel reflector	80 mm	0.18 m
Plenum	0.22 m (0.1 dense)	0.22 m (0.1 dense)
Stainless steel shield	0.3 m	0.3 m
Tritium breeding ratio[c]	1.21	1.20
Nuclear heating (MeV/D-T neutron)		
First wall	0.549	0.582
Lead region	3.087	4.748
Lithium region	12.489	9.422
Reflector	0.616	2.285
Plenum	0.113	0.153
Total blanket nuclear heating	16.84	17.20
First 0.3 m shield	0.661	0.882
Blanket energy multiplication	1.19	1.22

[a]Composition: 75% Pb + 10% PCA + 15% He.

[b]Composition: 35% Li + 50% PCA + 15% He (90% ^{6}Li in Li).

[c]10% reduction in ^{7}Li(n,n'α) reaction rate is taken into consideration.

TABLE VII.2-11. INBOARD BLANKET THICKNESS STUDY FOR LEAD MULTIPLIER/ LITHIUM BREEDER TOKAMAK REACTORS

Thickness (m)		Tritium Breeding Ratio	Blanket Nuclear Heating MeV/D-T Neutron
Inboard	Outboard		
0.5	0.7	1.23 (total) 0.34 (inboard) 0.89 (outboard)	16.2 (1.15)
0.4	0.7	1.21 (total) 0.29 (inboard) 0.92 (outboard)	15.1 (1.07)

VII.2.1.7 Blanket Tritium Handling

A model of the liquid breeder/helium-cooled blanket was developed as shown in Fig. VII.2-20 for the purposes of identifying the tritium release pathways throughout the system and establishing the requirements on the tritium recovery and control systems so as to meet this study's design goals. The model can be described briefly as follows. Tritium is generated within the liquid breeder-containing tubes via neutron capture. The tritium is removed from the tubes by very slow circulation of the liquid breeder to a tritium recovery system and/or via diffusion through the tube walls into the primary helium coolant. The primary loop has a small slipstream which is also routed to a tritium recovery system. Oxygen partial pressure control in the primary helium is assumed to be available for converting tritium in the T_2 form into tritiated water (T_2O). Tritium which is not cleaned up by the tritium recovery systems permeates through the steam generator tube walls and is presumed lost.

The requirements on the tritium management system are established by the safety guidelines adopted by this study. For the present blanket, the goals are to maintain a total tritium inventory less than 1 kg, and tritium losses less than 1 Ci/d. Referring to Fig. VII.2-20, to achieve these goals, the necessary tritium partial pressures throughout the systems can be obtained by controlling:

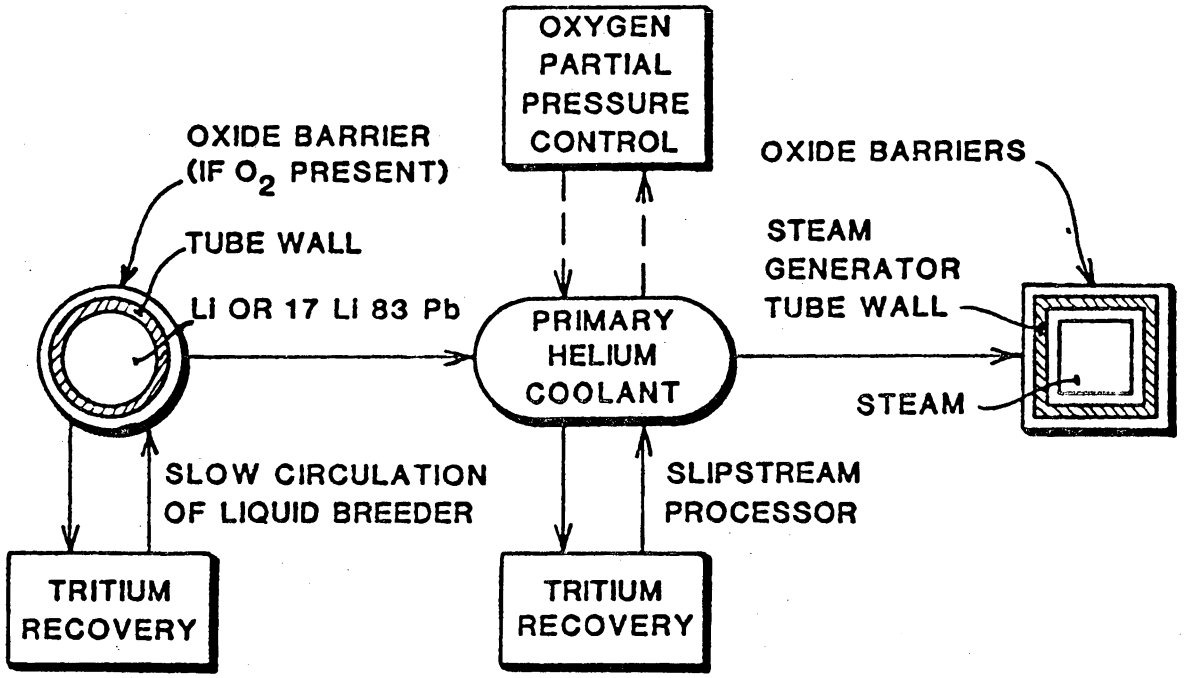

Figure VII.2-20. Schematic representation of blanket tritium management approach.

1. The breeder recirculation rate.
2. The slipstream processing fraction of the main coolant circulation rate.
3. Control of the oxygen partial pressure.

The data used in the calculational model are shown in Table VI.2-12.

TABLE VII.2-12. TRITIUM SYSTEM PARAMETER LIST

	Li	17Li-83Pb
Blanket breeder tube surface area, m^2	2.1×10^4	3.0×10^4
Blanket breeder tube thickness, m	0.00078	0.00025
Liquid breeder inventory, m^3	644	301
Tritium solubility, $g/m^3\ Pa^{1/2}$	2×10^3	4×10^{-2}
Mass of helium in primary loop, moles	5.8×10^6	5.8×10^6
Steam generator surface area, m^2	4.4×10^4	4.4×10^4
Average steam generator tube thickness, m^2	0.002	0.002
Average steam generator temperature, K	800	750
Oxide barrier effectiveness	10	10
Equilibrium constant for reaction $H_2 + 1/2\ O_2 \rightleftarrows H_2O$, $Pa^{-1/2}$	1.4×10^{12}	6.1×10^{10}

The breeder circulation rate is limited by the acceptable MHD pumping power and pressure losses of circulating a liquid metal in a magnetic field. The liquid metal flow in this blanket configuration is for tritium recovery and not heat removal and it was shown previously[10] that in this application the MHD pressure drop within the tubes is more restrictive than pumping power losses. For a comfortable tube pressure drop in the range of 0.6 to 6 MPa, the maximum liquid breeder flow velocity in an assumed 8 T magnetic field is in the range of 0.004 to 0.04 m/sec. This corresponds to acceptable breeder recirculation rates in the range of 0.022 to 0.22 m^3/sec for Li and 0.01 to 0.1 m^3/sec for 17Li-83Pb.

The maximum helium slipstream fraction is set by considerations of the capital cost of the processor. A processor handling 3% of the main helium

flow has previously been proposed[2] and considered feasible. Combining the above features with oxygen partial pressure control in the primary helium, considerable flexibility and diversity is available for achieving the tritium safety goals. The results of the calculations for two possible tritium system designs with Li and 17Li-83Pb breeders are shown in Table VII.2-13.

TABLE VII.2-13. TRITIUM SYSTEMS PERFORMANCE SUMMARY

	Li	17Li-83Pb
Inventory in breeder, g	27[a]	560
Inventory in helium, g	3.1×10^{-9}	41
Partial pressure in breeder, Pa	4.5×10^{-10}[a]	2100
Partial pressure in helium, Pa - T_2	4.5×10^{-10}	4.4×10^{-13}
- T_2O	NA	6.2
- O_2	NA	100
Leakage rate into helium, Ci/d	1[a]	5.5×10^{6}
Leakage rate into HX, Ci/d (Assuming a factor of 10 reduction in T_2 permeation due to oxide barrier)	1[a]	1.7×10^{-2}
Breeder cleanup recirculation rate, m^3/sec	0.15	NA
Helium cleanup slipstream fraction, % of main	NA	1.0

[a]The actual tritium inventory in the lithium blanket is predicted to be an order of magnitude larger than assumed in this calculation. The tritium partial pressures and leakage rates will be correspondingly higher.

Analyses conducted as part of the tritium recovery evaluation indicate that the tritium inventory in the lithium blanket will be about an order of magnitude higher (~ 270 g) than assumed in the calculation here. The tritium partial pressures and tritium leakage rates will be correspondingly higher.

With 17Li-83Pb, recirculation of the breeder is not necessary. Instead, a 1.0% slipstream processor and control of the oxygen partial pressure to 100 Pa are adequate to maintain tritium permeation through the SG to less than 0.02 Ci/day. Due to the formation of an oxide barrier on the outside of the breeder tubes, the tritium partial pressure and thus the inventory is higher

than for Li breeders. The tritium inventory is 560 g in the 17Li-83Pb breeder and 41 g in the helium, for a total inventory less than 1 kg, as desired. The impact of this relatively high tritium pressure on the structural material may be significant and therefore, must be evaluated in more detail.

VII.2.1.8 Safety Considerations

The objectives of this section are to identify and highlight those aspects of the liquid breeder, helium-cooled blankets which are of safety interest, and to indicate how safety is satisfactorily addressed by the present design. Since the structure and breeder source term, risk, occupational exposure, and waste disposal concerns will be addressed as part of future efforts, and tritium inventories and leakage rates were presented in the previous section, this section presents a discussion of the fault tolerance of the present design. Events considered include submodule and/or breeder tube depressurization or leakage, loss of coolant (LOCA), loss of flow (LOFA), and loss of site power (LOSP).

The lobed submodule design of the blanket does not incorporate coolant tubes. Thus, leakage or rupture of the breeder tubes does not result in loss of cooling capability. Since the breeder tubes are pressure balanced to the primary coolant, such leakage would not result in overpressurization of either system. Minor leakage of the liquid breeder from the fuel tube bank into the submodule would be tolerable without shutdown, since the breeder would be swept away from the first wall region by the high velocity helium flow. Operation with minor leakage would than be analogous to that of fission reactors which continue to operate with a certain fraction of failed fuel rods. Minor leakage of the primary helium into the liquid breeder would similary not result in any appreciable level of breeder-coolant interaction due to the low levels of impurities present.

The major accident concern in the present blanket is depressurization of a submodule lobe, possibly as a result of external forces or near-blanket system interaction. It is first noted that the tube bank configuration affords multiple barrier protection to the release of the liquid breeder. Thus, either very specific sequences of events (to be determined) or multiple structural failures would have to be postulated in order to result in a large energy release. The major uncertainty is then the survivability of the

configuration in a depressurization event, and the subsequent thermal response and cooling concerns.

The analysis of a first wall scenario has been directed at bracketing the extent of the problem. Consider first the interconnection of adjacent lobes. Figure VII.2-21 presents a lobe interconnection diagram, representing the volumes and distances available for flow in one meter of adjacent submodule lobes. It can be shown that pressure balancing between the lobes will be rapid, on the order of milliseconds, and thus no domino effect will occur. If it is assumed, however, that the worst case scenario applies and no communication between the lobes exists, the lobe contents can be designed to take the full pressure loading with less than one millimeter distortion in the lobe membranes. This is accomplished by increasing the metal fraction in the tube bank by 1.25% and reacting the load across the failed submodule. The short term creep strength of the breeder tubes is sufficient to prevent bursting for time on the order of days. Thus, no cascading of the failure is foreseen for the present blanket.

The remaining safety concerns addressed here are the survivability of the modules with respect to LOCA, LOFA, and LOSP. Though no transient thermal analyses were performed for the specific blanket configuration presented in this section, valuable insight into the expected temporal temperature behavior can be obtained from recent analyses[9] performed for a very similar blanket.[1] The blanket design of Reference 1 contains the same first wall and breeder tube bank configuration, but operates the 17Li-83Pb breeder at much higher temperature (up to approximately 800°C) with a helium coolant outlet temperature of 700°C. The proposed tube material in that design is Nb-1Zr. The blanket additionally incorporates a nonstructural, SiC high-temperature zone which operates in the 1200°C to 1500°C range. Detailed two-dimensional, finite difference thermal analyses of LOCA, LOFA, and LOSP using temperature dependent correlations for all critical physical properties were performed for that blanket and are summarized below.

In the event of primary coolant system depressurization (LOCA), one of the major advantages of helium cooling is that pumping can be still provided by the main circulators or auxiliary circulators operating at atmospheric condition. The net effect of depressurized cooling is illustrated in Fig. VII.2-22 which shows that the first wall and breeder structure remain below

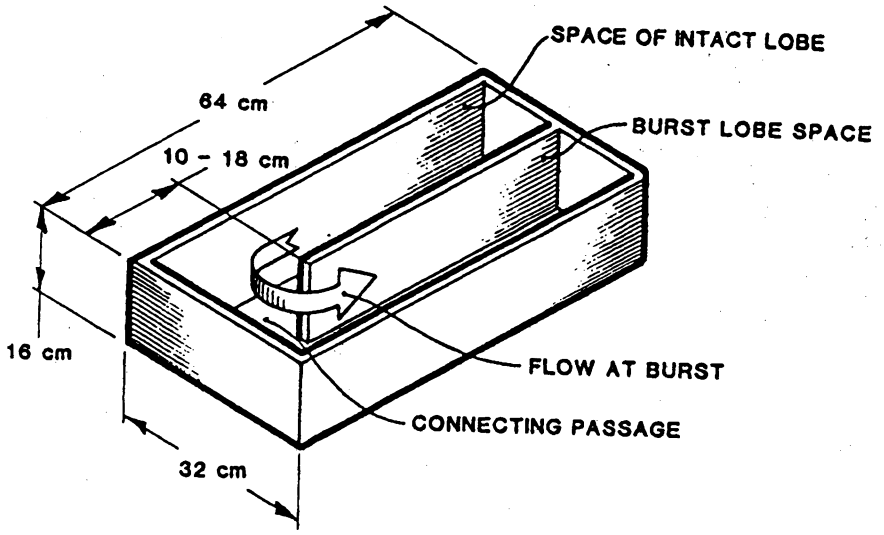

Figure VII.2-21. Lobe convection diagram representing the equivalent volumes and distances for 1 m of two adjacent lobes.

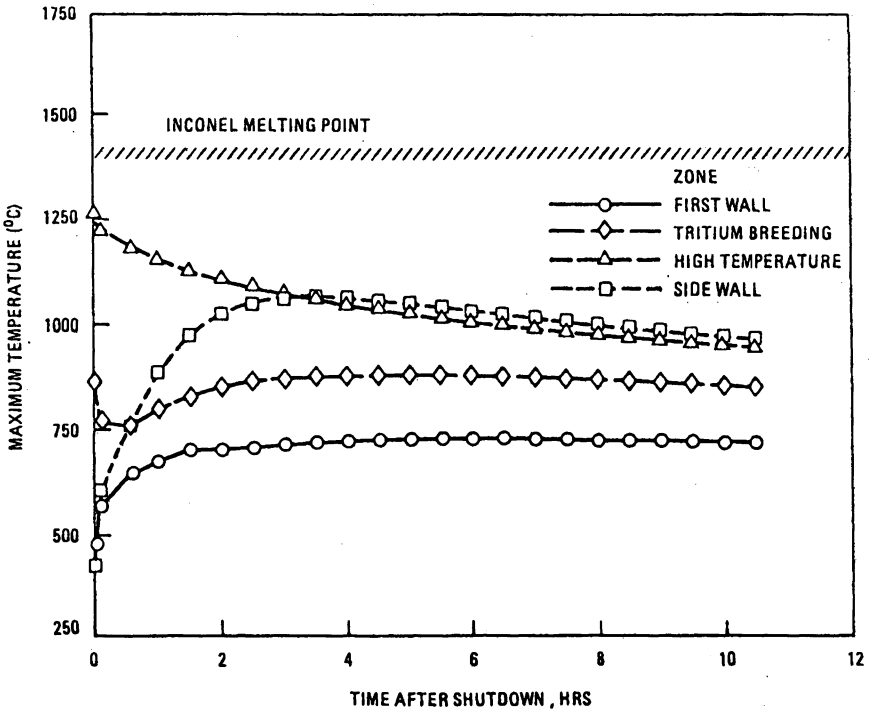

Figure VII.2-22. Fault tolerance to LOCA: blanket temperature response with depressurized cooling (reproduced from Ref. 9).

~ 800°C and may be able to maintain structural integrity. Note that the breeder region in the figure was initially at a maximum temperature of ~ 800°C, whereas the maximum temperature in the present blanket's breeder zone structure is ~ 500°C. Note also that the maximum sidewall temperature in the figure is driven by the high-temperature zone, which is not present in the current design.

A unique feature of liquid breeder designs is that the liquid breeder can be circulated in either LOCA or LOFA situations, providing the inherent feature of a redundant and diverse cooling circuit. This effect is shown in Fig. VII.2-23. The parameter used in the figure is the liquid breeder sink temperature and the breeder flow rate is limited to maintain low MHD and frictional pressure drops. Again, it shows that melting is precluded and module integrity can be attained by proper design.

Under the pressurized conditions that would exist during a LOFA, it has been shown that natural circulation of the pressurized helium can provide adequate passive cooling of the blanket in an HTGR-type of geometry.[16] It is expected that similar advantageous use of geometry in fusion reactor design would allow for similar results. It is noted that minimal diversity and redundancy need to be incorporated into the primary pumping circuitry to minimize the probability of this event.

In the event of LOSP, natural circulation of the pressurized helium may provide adequate cooling as described above. Natural circulation of the liquid breeder may also be possible. If it is further postulated that the primary system depressurizes, it is estimated that the blanket can tolerate total absence of cooling for approximately 7 h without melting, as shown in Fig. VII.2-24. Note that a very small supply of stand-by auxiliary on-site power would provide the circulation requirements under depressurized conditions, further lowering the probabilities of total absence of cooling.

VII.2.1.9 Conclusions and Recommendations

In the reference helium-cooled liquid breeder pressurized module design, an integral first wall is used with full flow of the cool inlet helium directed to the first wall. The helium then turns and flows radially outward through the liquid breeder fuel elements. This arrangement allows all the material temperature limits to be met while still achieving high outlet

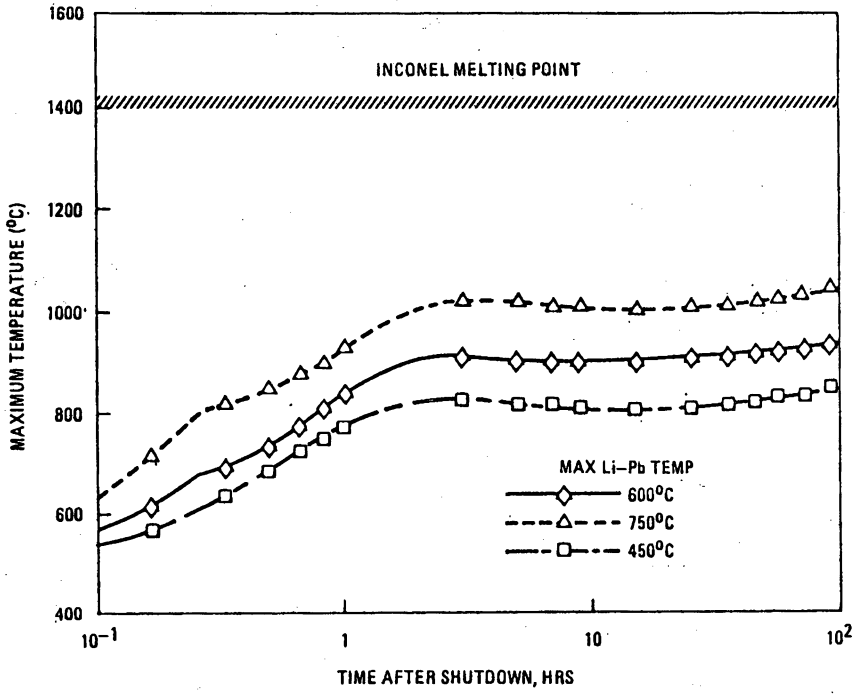

Figure VII.2-23. Fault tolerance to LOCA or LOFA: first-wall temperature response with circulating liquid breeder (reproduced from Reference 9).

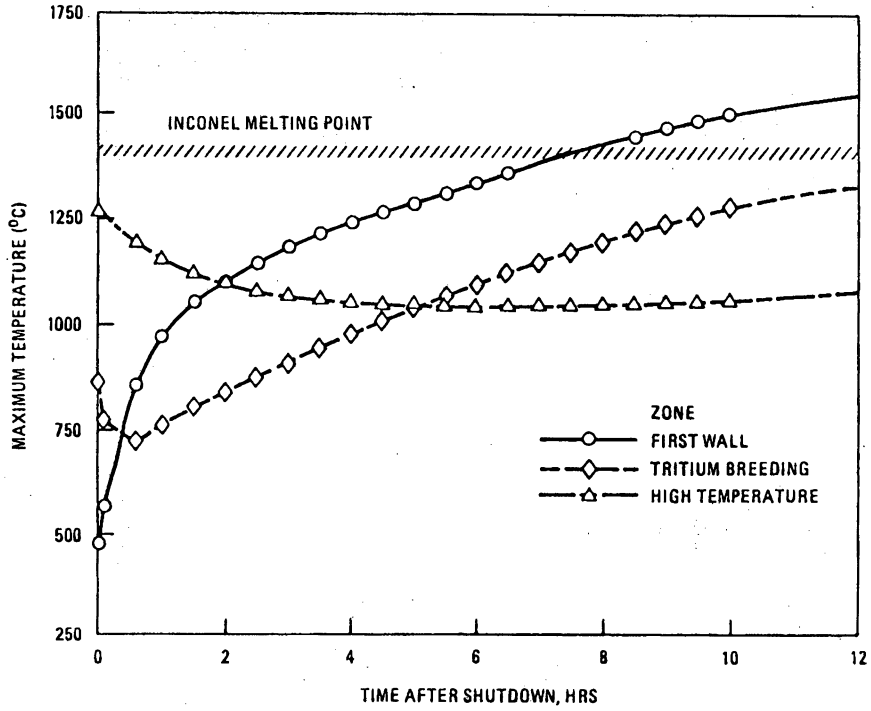

Figure VII.2-24. Fault tolerance to LOSP: blanket temperature response during complete loss of cooling (reproduced from Reference 9).

temperatures (525°C with Li, 500°C with 17Li-83Pb) and high net power conversion efficiency (36.5%)

With the relatively optimistic erosion rate of 1 mm/y, and the restrictive temperature limit of 550°C for PCA (even when used in a nonstructural mode), the bellows first wall can satisfy a surface loading of 0.6 MW/m^2 with a corresponding neutron wall loading of 5 MW/m^2. For the present design, a sacrificial layer of 2 mm of PCA is included on the plasma side of the first wall to give a blanket life time of two years. The bellows configuration of the first wall is designed to accommodate neutron-induced swelling without creating large stresses, while maintaining a thin structural member with extended heat transfer surfaces.

The first wall can be the most critical issue for tokamak blanket designs. Further quantification of the first wall erosion rate and the acceptable range of surface temperature and wall loading at the corresponding neutron wall loading are needed. In the area of thermal-mechanical analysis, the bellows geometry will need to be optimized and the effects of thermal and radiation-induced creep included. The bellows side wall erosion must be quanitified. The erodable layer may need to be grooved in the lobe direction in order to reduce thermal stresses. The manufacturing techniques for the bellows first wall will need to be demonstrated.

Thermal-hydraulics concerns for the concept center mainly on the compatibility-limited breeder-structure interface temperature in the breeding zone, and manifolding. The low volumtric heat capacity of ehlium makes analyses of sensitivity to changes in flow conditions (e.g., flow gap sizes) especially important. The manifold flow pattern selected for the sector and the manifold flow passage requirements also will directly affect blanket thickness. Because of the importance of the inboard blanket thickness in a tokamak, the present flow passage requirement calculation should be verified and optimized.

Based on one-dimensional neutronics calculations, the tritium breeding ratio was calculated to be 1.23 and 1.19 with a 90 cm Li and a 66 cm 17Li-83Pb blanket, respectively. With the selected coolant inlet/outlet temperatures of 275°C/525°C (Li), 275°/500°C (17Li-83Pb), and using helium at 50 atm, after accounting for all the pressure losses in the helium coolant circuit, including the steam generator, the net blanket power conversion efficiency was

calculated to be 36.5%. Tritium inventory and permeation losses are 0.03 kg and 1 Ci/d, and 0.6 kg and 0.02 Ci/d with Li and 17Li-83Pb, respectively.

The present design offers many inherent safety features. In a depressurization event, the design allows for rapid communication between submodules and can withstand the maximum forces expected without failure propagation to adjacent units. With gas cooling, the capability exists to circulated in LOCA or LOFA situatins as a redundant and diverse cooling circuit. Under complete loss of cooling events, natural circulation of pressurized helium and/or the liquid breeder may be adequate for handling afterheat. Total absence of cooling can be tolerated for approximately 7 h without melting. More detailed calculations of the blanket safety system behavior are needed for further quantification of the safety characteristics.

In summary, the helium-cooled liquid breeder blanket designs appear to be quite attractive. The basic design criteria can be satisfied and the blanket tritium breeding and thermal performances appear reasonable. Additional design, analysis, and optimization are needed in several areas to allow the evaluation indices to be determined. The most severe critical issues for this design appear to be the understanding, quantification, and accommodation of plasma erosion effects to the first wall, materials irradiation effects to the structural materials, and liquid metal compatibility with the structural materials.

VII.2.2 Li-Pb/Water Coolant

Pressurized water has been considered by the study as a separate coolant for blankets with 17Li-83Pb breeder. To date, the focus has been on identification of key issues. A first-order investigation has been conducted in the area of tritium permeation into water coolant. Sufficient work has not yet been done to establish the concepts viability nor to permit its evaluation against the project's initial screening criteria. Key issues for the concept will continue to be investigated until a temporary ranking (see Section II.10) can be assigned with confidence.

Water is an excellent coolant with good heat transfer characteristics. By using water as a separate coolant with 17Li-83Pb (Li-Pb), problems associated with MHD, corrosion, and mass transport of corrosion products can be either alleviated or eliminated.

However, the use of high-temperature, high-pressure water coolant with Li-Pb appears to have two serious disadvantages. The first is the possibility of reactor damage resulting from breeder/coolant contact. If water coolant contacts the Li-Pb in a leak situation, pressurization of the module will almost certainly occur. This pulse propagates to the module walls at the sonic velocity for Li-Pb. Unless the module is designed to withstand the full coolant pressure, the result could be a rupture of the module wall with ejection of a large fraction of the contained Li-Pb into the vacuum chamber. This type of accident could perhaps be precluded by use of a bottle or pressurized module concept. The probability of its occurrence in modules not designed to withstand the coolant pressure could be minimized by using a double wall tube construction with an annulus between tubes (e.g., grooves set into one tube surface) for detection of a leak from either the breeder or the coolant. Additional analyses are necessary to properly quantify the results of a water/Li-Pb contact. Engineering tests simulating realistic blanket designs and conditions should also be performed to help determine the validity of the accident scenario.

The second serious disadvantage of the water coolant is the very high level of tritium permeation through single wall tubes into the water. Processing of substantial amounts of tritium from the water coolant may be economically prohibitive. Excessive accumulation of tritium in the water coolant would have important safety implications in the event of a leak. Possible solutions to this problem — double walled coolant tubes with helium purge gas in the annulus, an IHX, or a steam generator with double walled tubes -- will probably result in overall thermal recovery efficiency levels below those achievable with single wall coolant tubes.

The following subsections briefly address the key issues identified for this concept.

VII.2.2.1 Tritium Permeation into Water Coolant

The P-x diagram of tritium in Li-Pb is shown in Fig. VII.2-25. The most probable operating range is a tritium partial pressure of 10^{-2} to 10^{-5} Torr. This high partial pressure will cause a severe problem in tritium confinement. The permeability of tritium through ferritic steel is shown on Fig. VII.2-26. For HT-9, the permeability can be calculated by:

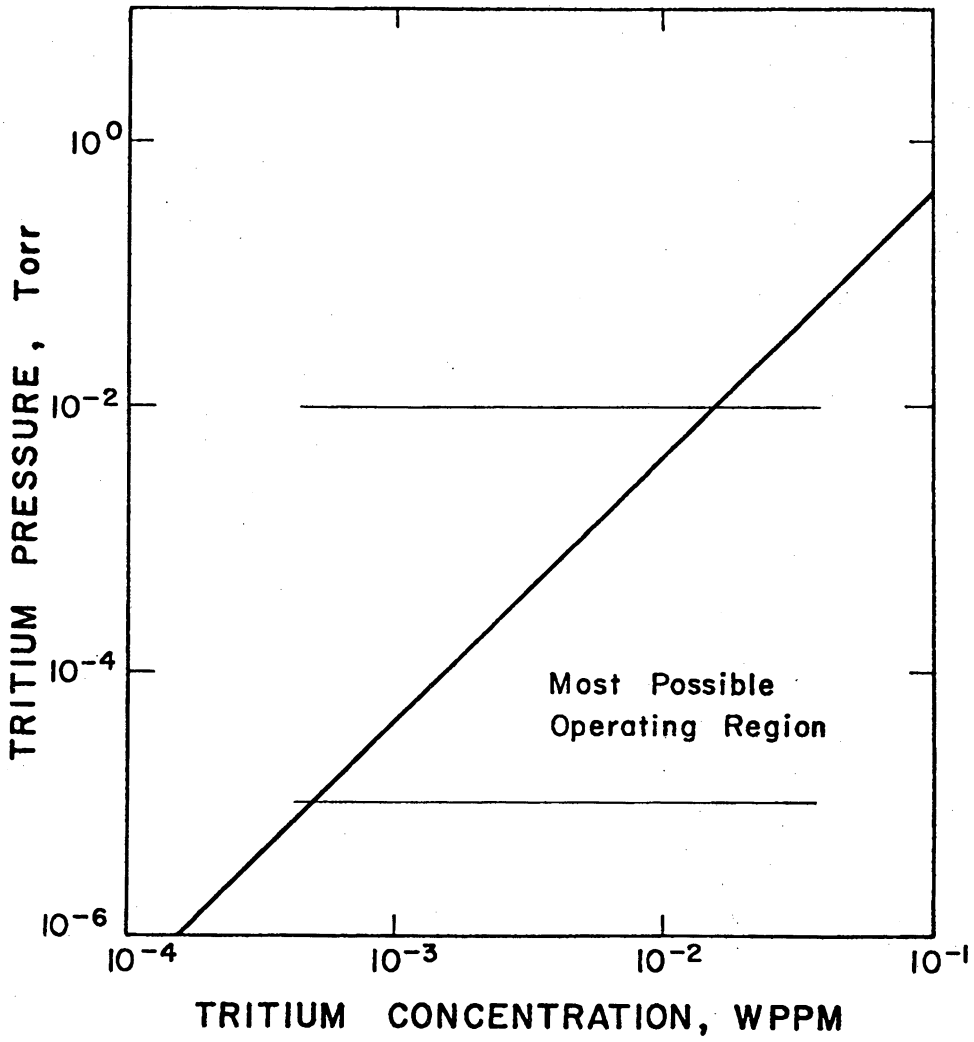

Figure VII.2-25. P-X diagram of tritium in 17Li-83Pb.

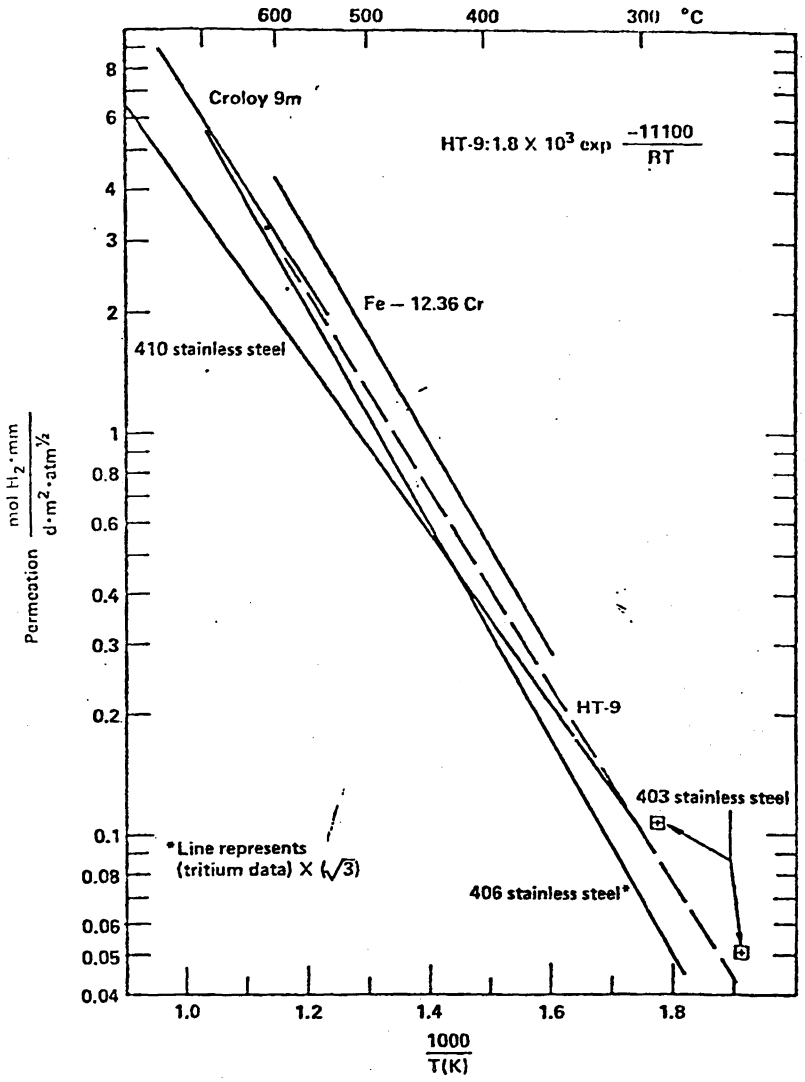

Figure VII.2-26. Hydrogen permeation through chromium ferritic steels.

$$P_m = \frac{1.8 \times 10^3}{\sqrt{3}} \exp\left(-\frac{11100}{RT}\right) \frac{\text{mol } T_2 \times \text{mm}}{d \times m^2 \times \text{atm}^{1/2}}$$

and $$m = P_m \times \left(\frac{tA\sqrt{P}}{x}\right)$$

where

Tritium Pressure	$= 10^{-4}$ Torr
Area	$= 10^4$ m^2
Tube Wall Thickness	= 2 mm
Temperature	= 350°C

For the values assumed, the tritium permeation rate to water coolant is ~ 7 × 10^3 Ci/day. However, an oxide coating will form on the water side which could decrease the permeation rate by a factor of 100. The tritium permeation rate to water is then reduced to 70 Ci/day, which may be economically acceptable. A blanket tritium partial pressure significantly higher than 10^{-4} Torr may require special coolant tube design to reduce the tritium leakage to water.

A possible method to reduce tritium leakage is to use a double walled tube design.[17] Due to the complicated blanket geometry and coolant flow pattern, a double-walled tube with a purge gas in between is more difficult to fabricate than a single wall tube. However, a static helium gas between the tubes with oxygen partial pressure will also provide a significantly larger resistance to tritium permeation than a single walled tube. The combination of the oxide layers formed on the annular surfaces, the oxide layer on the water side tube surface, and the low contact area between tubes (~ 1-2%) could result in tritium permeation resistance factors of ~ 10^3 to 10^4. The effects on blanket tritium partial pressure and Li-Pb circulation rates for tritium recovery need to be examined.

VII.2.2.2 Power Conversion

A typical pressurized water power conversion cycle is presented in the STARFIRE report.[18] The water enters the blanket at 280°C and exits at 320°C. The steam conditions for such a system are 299°C and 6.3 MPa, which results in a gross thermal efficiency of about 35%. The net system efficiency for STARFIRE is about 30%. This is a relatively low efficiency, but is

acceptable. The power cycle is almost identical to that of a PWR and is conventional. An important aspect of the further development of this blanket concept will therefore be determining design solutions to the tritium permeation and accident safety problems that have minimal impact on power conversion efficiency.

VII.2.2.3 Safety

A blanket module filled with Li-Pb with gas or water coolant contained in tubes has a potential safety problem. A shock wave may form when a coolant tube leakage occurs, and the module can be pressurized to the full coolant pressure level. Even higher pressures are possible if chemical interaction occurs between the Li-Pb and the coolant.

VII.2.3 Dual Coolant Design

The use of a separate coolant for the inboard blanket of a tokamka reactor with a self-cooled liquid metal outboard blanket has been investigated to a first-order. The concept examined uses helium coolant in a nonbreeding inboard blanket with 17Li-83Pb as a breeder-coolant in the outboard blanket.One potential problem associated with 17Li-83Pb is its compatibility with steel structure. Ferritic steel permits a higher allowable interface temperature than austenitic stainless steel with 17Li-83Pb because of its low Ni content. However, even for ferritic steel, the recommended maximum interface temperature is ~ 450°C for flowing Li-Pb. For this study, an interface temperature limit of 450°C to 475°C has been imposed, depending on the velocity of Li-Pb. The average bulk coolant exit temperature is probably limited to 450°C due to design details required to accommodate the first wall surface heat load. This coolant temperature will result in a steam temperature around 400°C. Improvement of the steam condition to improve thermal efficiency is desirable.

A T-H diagram of a good steam cycle is shown on Fig. VI.2.-27. The steam condition corresponding to this cycle is 538°C and 16.6 MPa. The gross thermal conversion efficiency of such a cycle is ~ 44%. To obtain 538°C steam, a coolant exit temperature of ~ 580°C is needed which is not available from a 17Li-83Pb/steel blanket. However, the helium coolant for the inboard blanket in the present concept can be used in combination with the 17Li-83Pb

self-cooled outer blanket to achieve a more desirable steam condition then can be achieved with a fully self-cooled Li-Pb/HT-9 blanket.

The elements of this concept are as follows. The outer blanket uses 17Li-83Pb as a breeder/coolant, with inlet and outlet temperatures of 325 and 425°C. (Maximum expected interface temperature for the ferritic steel is 450°C.) The Li-Pb is used in the preheater and boiler part of the steam generator. The nonbreeding inboard blanket is cooled with helium having inlet and outlet temperatures of 400° and 600°C, respectively. A special design is required to obtain the 600°C outlet temperature since this exceeds the maximum allowable HT-9 temperature of 550°C. The helium is used in the superheater part of the steam generator.

The design proposed here separates the functions of the inboard and outboard blankets and, therefore, each zone of the blanket can be designed according to its role. Methods to achieve the 600°C helium outlet temperature while holding structure temperature to 500°C are being investigated. A complete T-H diagram of the steam cycle is shown in Fig. VII.2.-28. Some of the major operating parameters of the blanket are listed in Table VII.2.-14.

A gas cooled blanket will increase the total thickness of the blanket and shield. However, removal of the breeding function from the blanket permits one to design a more efficient shielding blanket. A one dimensional neutronic calculation was carried out to estimate the required total thickness of the blanket and shield for the protection of the magnets. The geometry of the calculation is shown on Fig. VII.2.-29. The blanket thickness x is defined as that within which 95% of the thermal energy is deposited. The shield is divided into three regions, the proportions of which are varied to give the optimum shielding. A 5% void is used in each region to account for helium cooling passages. The 10 cm gap represents helium for a coolant manifold. The neutronic results are shown on Fig. VII.2.-30 and summarized on Table VII.2.-15. The total blanket and shield thickness is 121 cm, comparing to 101 cm for STARFIRE, which was 35 cm tungsten mixture. It is expected that with similar shield design, the blanket and shield thickness required here may be similar to that of STARFIRE.

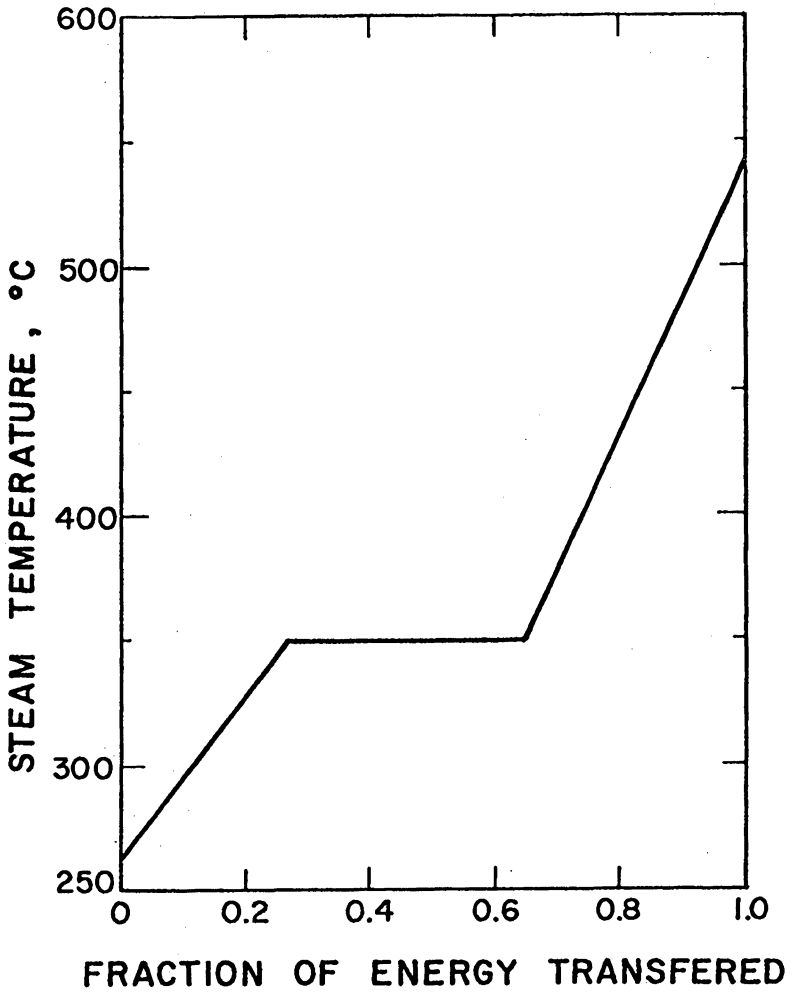

Figure VII.2-27. T-H diagram for a 16.6 MPa, 538°C stem.

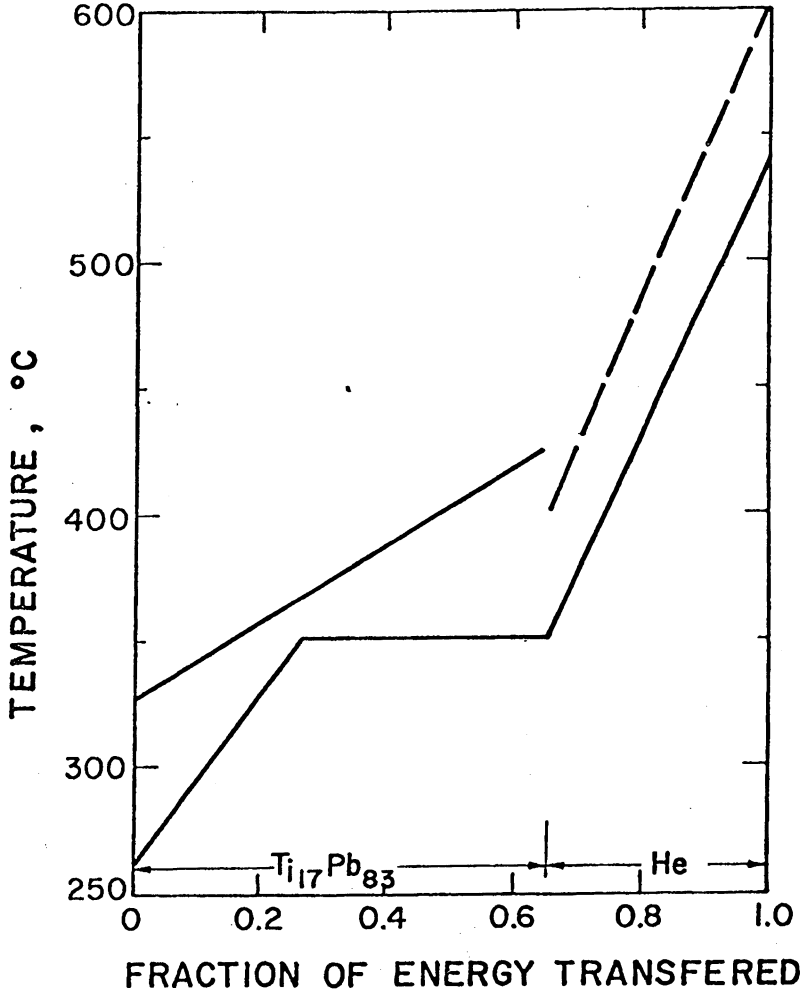

Figure VII.2-28. Proposed T-H diagram for the steam cycle.

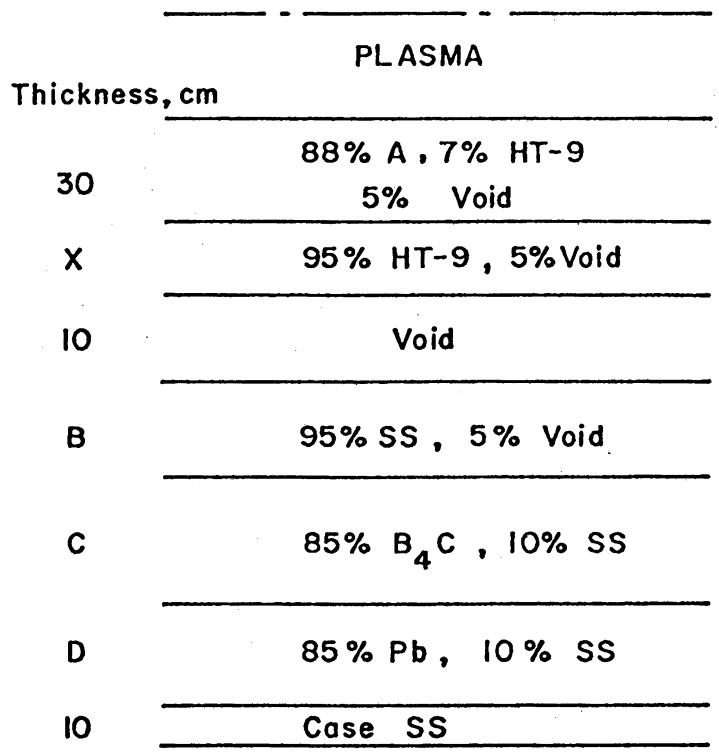

Figure VII.2-29. Model for neutronic shielding calculations.

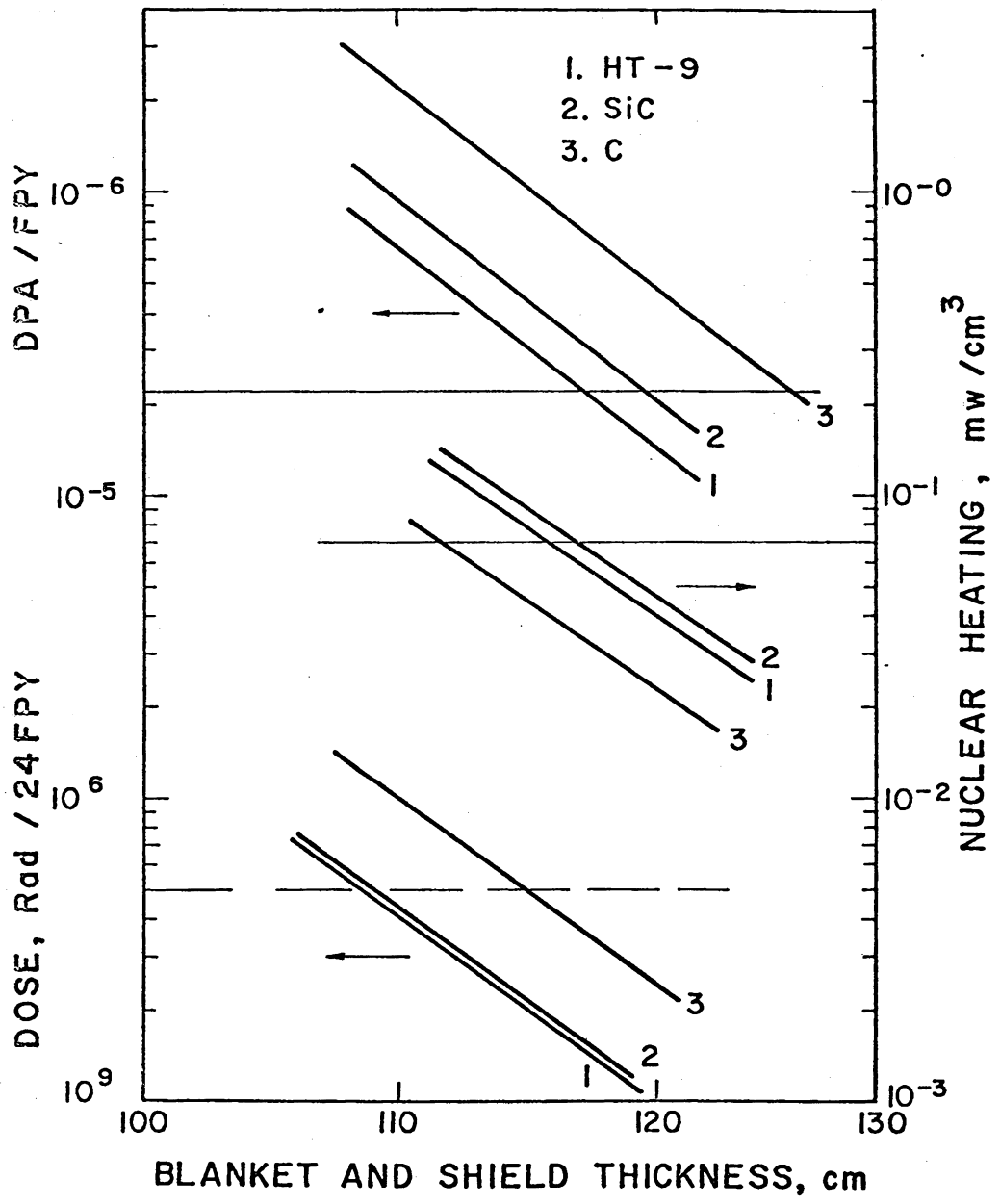

Figure VII.2-30. Results of shielding calculations for a breeding blanket.

TABLE VII.2.-14. PARAMETERS FOR SEPARATE COOLANT DESIGN

Inner Blanket	
Coolant	He
Coolant Pressure	5 MPa
Coolant Inlet - Outlet Temperature	400 - 600°C
Maximum Structural Temperature	~ 500°C
Maximum Blanket Temperature	650°C
Outer Blanket	
Coolant	17Li-83Pb
Coolant Pressure	~ 1 MPa
Coolant Inlet - Outlet Average Temperature	325 - 425°C
Maximum Coolant Temperature (First Wall)	~ 450°C
Power Cycle	
Steam Temperature	538°C
Steam Pressure	16.6 MPa
Preheat Temperature	538°C
Gross Thermal Efficiency	44%

Adequate tritium breeding is difficult to achieve for a partial breeding blanket. For this reason, Li-Pb alloy is very attractive for its excellent neutronic properties. Figure VII.2.-31 shows the one dimensional breeding calculation for Li and 17Li-83Pb. For 90% Li enriched 17Li-83Pb, a local breeding ratio of 1.5 can be achieved with a reasonably thick blanket, ~ 70 cm. Li-Pb may be the only material which will breed adequately with a partial breeding blanket. Li may also produce acceptable breeding with a layer of Be added as a neutron multiplier.

In conclusion, a helium cooled inner blanket and 17Li-83Pb cooled outer blanket will alleviate some of the problems associated with a self-cooled inboard blanket of a tokamak. In particular, it will eliminate the inboard blanket MHD problem. Power cycle thermal efficiency will also be increased. Tritium breeding appears to be adequate by using 90% enriched Li-Pb. The increased thickness for the gas cooled inner blanket and shield will be partially offset by removing the breeding function from the inner blanket.

TABLE VII.2.-15. SUMMARY OF INNER BLANKET/SHIELD NEUTRONIC CALCULATIONS

Item	HT-9	SiC	C	Limits Used
Shield Thickness, cm	62	71	71	
Blanket Thickness,	56	50	56	
Dpa in Cu per FPY	2.2×10^{-5}	2.1×10^{-5}	2.1×10^{-5}	2.2×10^{-5}
Heating in Magnet, mW/cc	0.06	0.024	0.024	0.06
Dose in Insulator Polyimide, Rad/24 FPY	1.0×10^{9}	1.0×10^{9}	1.1×10^{9}	5×10^{9}
Total Heating, Mev/D-T Reaction	21.2	18.1	20	

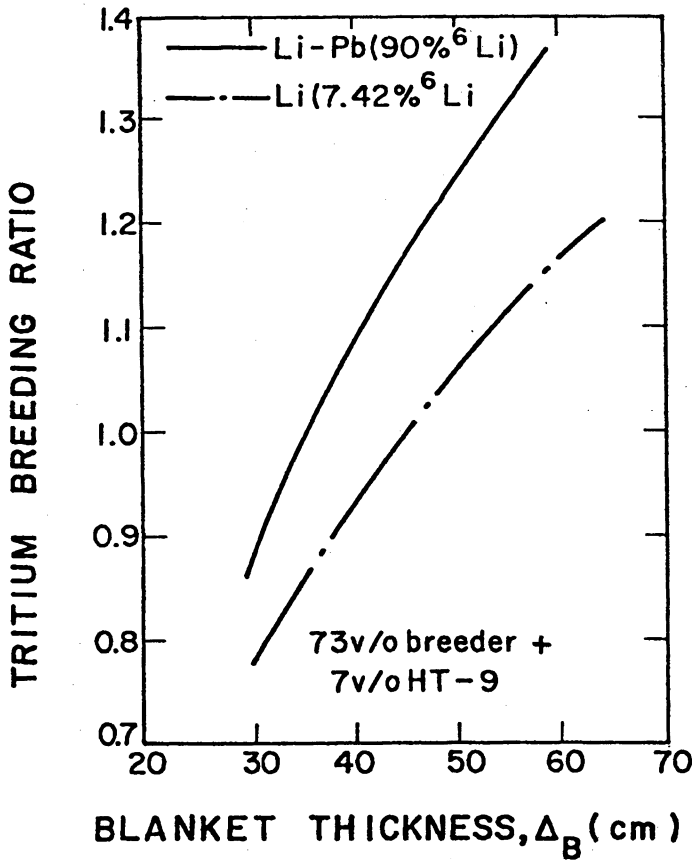

Figure VII.2-31. Tritium breeding calculations for Li and 17Li-83Pb blanket for a TMR with small first wall diameter.

REFERENCES FOR SECTION VII.2

1. I. Maya, et al., "A High-Temperatur Fusion Blanket for Thermochemical Hydrogen Production," Proceedings of the 17th IECEC, August 1982; also GA-A16754, May 1982.

2. D. Kearney, et al., "Doublet Demonstration Fusion Power Reactor Study," GA Technologies Report GA-A14742, July 1978.

3. W. S. Neef, Jr., "Maintenance of a Multi-Cell Field Reversed Mirror Reactor," Third ANS Topical Meeting on Technology of Fusion, May 1978, also UCRL-80863, May 1978.

4. A. Y. Lee, "Thermal and Hydraulic Analysis of a Cylindrical Blanket Module Design for a Tokamak Reactor," Westinghouse Report WFPS-TME-78-103, October 1978.

5. D. Kearney, et al., "Conceptual Design Study of a Noncircular Tokamak Demonstration Fusion Power Reactor," GA Technologies Report GA-A13992, November 1976.

6. J. T. D. Mitchell and J. A. Booth, "Wall Loading Limitations in a Helium-Cooled Fusion Reactor Blanket," UKAEA Research Group, Culham Laboratory, CLM-R126, Paper No. 13 of Workshop of Fusion Reactor Design Problems, February 1974.

7. J. D. Lee, et al., "Feasibility Study of a Fission-Suppressed Tandem Mirror Hybrid Reactor," LLNL Report fUCID-19327, April 1982; also GA Technologies Report GA-C16273, September 1981.

8. D. Steiner, "ORNL Fusion Power Demonstration Study, Interim Report," ORNL/TM-5813, March 1977.

9. I. Maya, et al., "Utility Fusion Synfuel Production System - Final Report," GA Technologies Report GA-A16813, July 1983.

10. R. W. Moir, et al., "Tandem Mirror Hybrid Reactor Design Study Final Report," LLNL Report UCID-18808, September 1980, Chapter 6.

11. R. W. Werner, et al., "Synfuels from Fusion," LLNL Report UCID-19609, November 1982, Chapter 5.

12. C. F. McDonald, et al., "A New HTGR Plant Concept with Inherently Safe Features Aimed at Small Energy User Needs," Proceedings of the Third Japan-U.S. HTGR Safety Technology Seminar, June 1982; also GA Technologies Report GA-A16768, May 1982.

13. R. W. Roussin, et al., "The CTR Processed Multigroup Cross Section Library for Neutronics Studies," Oak Ridge National Laboratory Report, ORNL/RSIC-37 (1977).

14. M. A. Abdou, Y. Gohar, and Q. Wright, "MACK-IV, A New Version of MACK: A Program to Calculate Nuclear Response Functions from Data in ENDF/B Format," Argonne National Laboratory Report, ANL/FPP/TM-75-5 (1978).

15. Y. Gohar and M. A. Abdou, "MACKLIB-IV, A Library of Nuclear Response Functions Generated with the MACK-IV Computer Program for ENDF/B-IV," Argonne National Laboratory Report, ANL/FPP/TM-106 (1978).

16. C F. McDonald, et al., "A New HTGR Plant Concept with Inherently Safe Features Aimed at Small Energy User Needs," Proceedings of the Third Japan-U.S. HTGR Safety Technology Seminar (June 1982); also GA Technologies Report, GA-A16768 (May 1982).

17. J. J. Henry, "Thermal Contact Resistance," AECE Report No. M.I.T. - 2079-2 (1964).

18. C. C. Baker, et al., "STARFIRE - A Commercial Tokamak Fusion Power Plant Study," Argonne National Laboratory report, ANL/FPP-80-1 (September 1980).

U.S. DEPARTMENT OF COMMERCE
National Technical Information Service
Alexandria, VA 22312 703-605-6000

U.S. DEPARTMENT OF COMMERCE
National Technical Information Service
Alexandria, VA 22312 703-605-6000